UNDERSTANDING COMPLEX SYSTEMS

Springer: COMPLEXITY

Thilo Gross
Hiroki Sayama
Editors

Adaptive Networks

Theory, Models and Applications

Springer

NECSI

Springer Complexity

Springer Complexity is an interdisciplinary program publishing the best research and academic-level teaching on both fundamental and applied aspects of complex systems – cutting across all traditional disciplines of the natural and life sciences, engineering, economics, medicine, neuroscience, social and computer science.

Complex Systems are systems that comprise many interacting parts with the ability to generate a new quality of macroscopic collective behavior the manifestations of which are the spontaneous formation of distinctive temporal, spatial or functional structures. Models of such systems can be successfully mapped onto quite diverse "real-life" situations like the climate, the coherent emission of light from lasers, chemical reaction-diffusion systems, biological cellular networks, the dynamics of stock markets and of the internet, earthquake statistics and prediction, freeway traffic, the human brain, or the formation of opinions in social systems, to name just some of the popular applications.

Although their scope and methodologies overlap somewhat, one can distinguish the following main concepts and tools: self-organization, nonlinear dynamics, synergetics, turbulence, dynamical systems, catastrophes, instabilities, stochastic processes, chaos, graphs and networks, cellular automata, adaptive systems, genetic algorithms and computational intelligence.

The two major book publication platforms of the Springer Complexity program are the monograph series "Understanding Complex Systems" focusing on the various applications of complexity, and the "Springer Series in Synergetics", which is devoted to the quantitative theoretical and methodological foundations. In addition to the books in these two core series, the program also incorporates individual titles ranging from textbooks to major reference works.

Understanding Complex Systems

Founding Editor: J.A. Scott Kelso

Future scientific and technological developments in many fields will necessarily depend upon coming to grips with complex systems. Such systems are complex in both their composition – typically many different kinds of components interacting simultaneously and nonlinearly with each other and their environments on multiple levels – and in the rich diversity of behavior of which they are capable.

The Springer Series in Understanding Complex Systems series (UCS) promotes new strategies and paradigms for understanding and realizing applications of complex systems research in a wide variety of fields and endeavors. UCS is explicitly transdisciplinary. It has three main goals: First, to elaborate the concepts, methods and tools of complex systems at all levels of description and in all scientific fields, especially newly emerging areas within the life, social, behavioral, economic, neuro- and cognitive sciences (and derivatives thereof); second, to encourage novel applications of these ideas in various fields of engineering and computation such as robotics, nano-technology and informatics; third, to provide a single forum within which commonalities and differences in the workings of complex systems may be discerned, hence leading to deeper insight and understanding. UCS will publish monographs, lecture notes and selected edited contributions aimed at communicating new findings to a large multidisciplinary audience.

New England Complex Systems Institute Book Series

Series Editor

Dan Braha

New England Complex Systems Institute
24 Mt. Auburn St.
Cambridge, MA 02138, USA

New England Complex Systems Institute Book Series

The world around is full of the wonderful interplay of relationships and emergent behaviors. The beautiful and mysterious way that atoms form biological and social systems inspires us to new efforts in science. As our society becomes more concerned with how people are connected to each other than how they work independently, so science has become interested in the nature of relationships and relatedness. Through relationships elements act together to become systems, and systems achieve function and purpose. The study of complex systems is remarkable in the closeness of basic ideas and practical implications. Advances in our understanding of complex systems give new opportunities for insight in science and improvement of society. This is manifest in the relevance to engineering, medicine, management and education. We devote this book series to the communication of recent advances and reviews of revolutionary ideas and their application to practical concerns.

Thilo Gross · Hiroki Sayama
Editors

Adaptive Networks

Theory, Models and Applications

Editors
Thilo Gross
MPI für Physik Komplexer Systeme
Max-Plack Institute for Physics of Complex Systems
01187 Dresden
Germany
thilo.gross@physics.org

Hiroki Sayama
Binghamton University
State University of New York
Dept. Bioengineering
P.O. Box 6000
Binghamton NY 13902-6000
USA
sayama@binghamton.edu
sayama@necsi.edu

This volume is part of the NECSI Studies on Complexity collection.

ISSN 1860-0832 e-ISSN 1860-0840
ISBN 978-3-642-01283-9 e-ISBN 978-3-642-01284-6
DOI 10.1007/978-3-642-01284-6
Springer Dordrecht Heidelberg London New York

Library of Congress Control Number: 2009927028

Cover design: WMXDesign GmbH Heidelberg

Printed on acid-free paper

Springer is part of Springer Science+Business Media (www.springer.com)

New England Complex Systems Institute

President
Yaneer Bar-Yam
New England Complex Systems Institute
24 Mt. Auburn St.
Cambridge, MA 02138, USA

For over 10 years, The New England Complex Systems Institute (NECSI) has been instrumental in the development of complex systems science and its applications. NECSI conducts research, education, knowledge dissemination, and community development around the world for the promotion of the study of complex systems and its application for the betterment of society.

NECSI was founded by faculty of New England area academic institutions in 1996 to further international research and understanding of complex systems. Complex systems is a growing field of science that aims to understand how parts of a system give rise to the systems collective behaviors, and how it interacts with its environment. These questions can be studied in general, and they are also relevant to all traditional fields of science.

Social systems formed (in part) out of people, the brain formed out of neurons, molecules formed out of atoms, and the weather formed from air flows are all examples of complex systems. The field of complex systems intersects all traditional disciplines of physical, biological and social sciences, as well as engineering, management, and medicine. Advanced education in complex systems attracts professionals, as complex systems science provides practical approaches to health care, social networks, ethnic violence, marketing, military conflict, education, systems engineering, international development and terrorism.

The study of complex systems is about understanding indirect effects. Problems we find difficult to solve have causes and effects that are not obviously related. Pushing on a complex system here often has effects over there because the parts are interdependent. This has become more and more apparent in our efforts to solve societal problems or avoid ecological disasters caused by our own actions. The field of complex systems provides a number of sophisticated tools, some of them conceptual helping us think about these systems, some of them analytical for studying these systems in greater depth, and some of them computer based for describing, modeling or simulating them.

NECSI research develops basic concepts and formal approaches as well as their applications to real world problems. Contributions of NECSI researchers include studies of networks, agent-based modeling, multiscale analysis and complexity, chaos and predictability, evolution, ecology, biodiversity, altruism, systems biology, cellular response, health care, systems engineering, negotiation, military conflict, ethnic violence, and international development.

NECSI uses many modes of education to further the investigation of complex systems. Throughout the year, classes, seminars, conferences and other programs assist

students and professionals alike in their understanding of complex systems. Courses have been taught all over the world: Australia, Canada, China, Colombia, France, Italy, Japan, Korea, Portugal, Russia and many states of the U.S. NECSI also sponsors postdoctoral fellows, provides research resources, and hosts the International Conference on Complex Systems, discussion groups and web resources.

The New England Complex Systems Institute is comprised of a general staff, a faculty of associated professors, students, postdoctoral fellows, a planning board, affiliates and sponsors. Formed to coordinate research programs that transcend departmental and institutional boundaries, NECSI works closely with faculty of MIT, Harvard and Brandeis Universities. Affiliated external faculty teach and work at many other national and international locations. NECSI promotes the international community of researchers and welcomes broad participation in its activities and programs.

Preface

Adding one and one makes two, usually. But sometimes things add up to more than the sum of their parts. This observation, now frequently expressed in the maxim "more is different", is one of the characteristic features of complex systems and, in particular, complex networks. Along with their ubiquity in real world systems, the ability of networks to exhibit emergent dynamics, once they reach a certain size, has rendered them highly attractive targets for research. The resulting network hype has made the word "network" one of the most influential buzzwords seen in almost every corner of science, from physics and biology to economy and social sciences.

The theme of "more is different" appears in a different way in the present volume, from the viewpoint of what we call "adaptive networks." Adaptive networks uniquely combine dynamics on a network with dynamical adaptive changes of the underlying network topology, and thus they link classes of mechanisms that were previously studied in isolation. Here adding one and one certainly does not make two, but gives rise to a number of new phenomena, including highly robust self-organization of topology and dynamics and other remarkably rich dynamical behaviors.

Adaptive networks have for a long time been implicitly contained in models from a wide range of fields including discrete mathematics, computer science, statistical physics, systems biology, social sciences, engineering and medicine. However, only recently research in the different fields has begun to converge on the functioning of the adaptive networks as such. In the different fields, adaptive networks have appeared as a topic of intense research almost at the same time. Consequently, they are currently attacked from many different angles by the tools different disciplines have established.

It is becoming more and more apparent that adaptive networks could hold the key to many phenomena observed in a wide variety of applications. Major breakthroughs have recently been made and common themes now frequently appear across disciplines. A unified theory of adaptive networks seems within reach.

The book you have at hand, "Adaptive Networks: Theory, Models and Applications", is the first edited volume that illustrates the dawn of a new research field on the coevolution of topologies and states of complex networks. It showcases the recent advances in the theory, models and applications of adaptive networks by cutting-edge scientists. We hope that the book will play a role in setting the

scope and directions of this emerging field of research, by raising the researcher's awareness to developments in different fields. It can also act as introductory text for the large group of researchers who presently start working on adaptive networks.

The project about this book started in January 2008 when the first editor (T.G.) invited the second editor (H.S.) as a guest scientist to the Max-Planck Institute for the Physics of Complex Systems in Dresden, Germany. For both of us it was clear that the coevolutionary dynamics of states and topologies in adaptive networks will be *the* next big movement in network research. Fortunately, at that time we had an offer to edit a book in the Springer/NECSI Studies on Complexity Collection; therefore it did not take long to come up with an idea to compile a book that collects the most influential and state-of-the-art in the forefront of adaptive network research. T.G. took the lead of selecting and inviting contributions primarily from statistical physics community, while H.S. invited contributions from empirical network research and computer science communities. All the chapters were included based on invitation only.

The contributors, who collectively represent the cutting edge of the rapidly advancing fields of network research, were enthusiastic about the concept this book aimed to illustrate, and they were extremely cooperative in preparing their chapters on a timely manner following a tight project timeline. We are wholeheartedly thankful for their contribution to and cooperation for this book project, without which it would not have been possible.

We are also very thankful to several people who played key roles in this book project, including: Dan Braha at UMass Dartmouth (Series Editor of the Springer/NECSI Studies on Complexity Collection) and Chris Caron at Springer for inviting us to guest-edit a book; Gabriele Hakuba and Sabine Lehr at Springer for their editorial assistance; Ellen Madison at the Department of Bioengineering at Binghamton University for clerical assistance; and the last but not the least, Cristian Huepe who unconsciously served as a key "hub" in the huge social network that made the two editors get to know each other in the first place and work together for this book. Finally, we thank the Visitor Program of the Max-Planck Institute for the Physics of Complex Systems for financial support.

Dresden, Germany — Thilo Gross
Binghamton, NY — Hiroki Sayama
May 2009

Contents

Contributors

Albert-László Barabási Center for Complex Network Research, Department of Physics, Biology and Computer Science, Northeastern University, Boston, MA 02115, USA, a.barabasi@neu.edu

Yaneer Bar-Yam New England Complex Systems Institute, Cambridge, MA 02138, USA, yaneer@necsi.edu

Daniel P. Bebber Department of Plant Sciences, University of Oxford, Oxford, OX1 3RB UK, dan.bebber@plants.ox.ac.uk

Lynne Boddy Cardiff School of Biosciences, Cardiff University, Cardiff, CF10 3US UK, boddyl@cardiff.ac.uk

Stefan Bornholdt Institute for Theoretical Physics, University of Bremen, Otto-Hahn-Allee, 28359 Bremen, Germany, bornholdt@itp.uni-bremen.de

Dan Braha University of Massachusetts, Dartmouth, MA 02747, USA; New England Complex Systems Institute, Cambridge, MA 02138, USA, braha@necsi.edu

Guido Caldarelli Dipartimento di Fisica Universitá "Sapienza", Centre SMC CNR-INFM, Piazzale A. Moro 5 00185, Roma, Italy, Guido.Caldarelli@cnr.it

Maoyin Chen Tsinghua National Laboratory for Information Science and Technology, Department of Automation, Tsinghua University, Beijing 100084, P. R. China, mychen@mail.tsinghua.edu.cn

Anne-Ly Do Max-Planck-Institute for the Physics of Complex Systems, 01187 Dresden, Germany, ly@mpipks-dresden.mpg.de

Mark D. Fricker Department of Plant Sciences, University of Oxford, Oxford, OX1 3RB, UK, mark.fricker@plants.ox.ac.uk

Diego Garlaschelli Dipartimento di Fisica, Universitá di Siena, Via Roma 56, 53100 Siena, Italy, Garlaschelli@unisi.it

Gourab Ghoshal Department of Physics and Michigan Center for Theoretical Physics, Ann Arbor, MI 48109, USA, gghosal@umich.edu

Thilo Gross Max-Planck-Institute for the Physics of Complex Systems, 01187 Dresden, Germany, thilo.gross@physics.org

Petter Holme Department of Physics, Umeå University, 90187 Umeå, Sweden, petter.holme@physics.umu.se

Junji Ito Theoretical Neuroscience Group, RIKEN Brain Science Institute, 2-1 Hirosawa, Wako, Saitama, 351-0198, Japan, j-ito@brain.riken.jp

Kunihiko Kaneko Department of Basic Science, University of Tokyo and ERATO complex systems biology, Meguro, Tokyo 153-8002, Japan, kaneko@complex.c.u-tokyo.ac.jp

Haruhisa Kurokawa National Institute of Advanced Industrial Science and Technology (AIST), Tsukuba, Ibaraki 305-8564 Japan, kurokawa-h@aist.go.jp

Jürgen Kurths Potsdam Universität, Center for Dynamics of Complex Systems, Am Neuen Palais 10, 14469, Germany, jkurths@gmx.de

Craig Laramee Collective Dynamics of Complex Systems Research Group/Department of Bioengineering, Binghamton University, State University of New York, Binghamton, NY 13902-6000, USA, claramee@binghamton.edu

Satoshi Murata Department of Computational Intelligence and Systems Science, Interdisciplinary Graduate School of Science and Technology, Tokyo Institute of Technology, 4259 Nagatsuda, Midori-ku, Yokohama, 226-8502 Japan, murata@dis.titech.ac.jp

Toshiyuki Nakagaki Research Institute for Electronic Science, Hokkaido University, Sapporo, 060-0812, Japan, nakagaki@es.hokudai.ac.jp

Jorge M. Pacheco ATP-Group and CFTC, Departamento de Física da Faculdade de Ciências, 1649-003 Lisboa, Codex, Portugal, pacheco@cii.fc.ul.pt

Gergely Palla Statistical and Biological Physics Research Group of HAS, 1117 Budapest, Pázmány Pétersétány 1/A, Hungary,pallag@angel.elte.hu

Robin Pemantle Department of Mathematics, University of Pennsylvania, Philadelphia, PA 19104, USA, pemantle@math.upenn.edu

Péter Pollner Statistical and Biological Physics Research Group of HAS, 1117 Budapest, Pázmány Pétersétány 1/A, Hungary, pollner@complex.elte.hu

Thimo Rohlf Max-Planck-Institute for Mathematics in the Sciences, Inselstrasse 22, 04103 Leipzig, Germany, rohlf@mis.mpg.de

Francisco C. Santos Institut de Recherches Interdisciplinaires et de Développements en Intelligence Artificielle (IRIDIA) of the Université Libre de Bruxelles (ULB), 1050 Brussels, Belgium, fsantos@ulb.ac.be

Hiroki Sayama Collective Dynamics of Complex Systems Research Group/Department of Bioengineering, Binghamton University, State University of New York, Binghamton, NY 13902-6000, USA; New England Complex Systems Institute, Cambridge, MA 02138, USA, sayama@binghamton.edu, sayama@necsi.edu

Ira B. Schwartz Plasma Physics Division, Nonlinear Systems Dynamics Section, US Naval Research Laboratory, Code 6792, Washington, DC 20375, USA, ira.schwartz@nrl.navy.mil

Leah B. Shaw Department of Applied Science, College of William and Mary, Williamsburg, VA 23187, USA, lbshaw@wm.edu

Brian Skyrms School of Social Sciences, University of California at Irvine, Irvine, CA 92607, USA, bskyrms@uci.edu

Kohji Tomita National Institute of Advanced Industrial Science and Technology (AIST), 1-2-1 Namiki, Tsukuba, Ibaraki 305-8564, Japan, k.tomita@aist.go.jp

Arne Traulsen Evolutionary Dynamics Group, Max-Planck-Institute for Evolutionary Biology, 24306 Plön, Germany, traulsen@evolbio.mpg.de

Tamás Vicsek Statistical and Biological Physics Research Group of HAS, Department of Biological Physics, Eötvös University, 1117 Budapest, Pázmány Péter sétány 1/A, Hungary, vicsek@angel.elte.hu

Chapter 1
Adaptive Networks

Thilo Gross and Hiroki Sayama

1.1 Introduction

Over the past decades it has become clear that the metaphor of *networks* – ensembles of discrete *nodes* connected by *links* – offers a powerful conceptual framework for the description and analysis of many real world systems [1–5]. The science of networks has grown into a field which is by now firmly established in several disciplines, including mathematics, physics, biology, computer science, economics and the social sciences. Dramatic progress has been made both in the characterization of real world networks and in the study of dynamical models of networks.

It is interesting to note that the notion of *dynamical networks* has so far referred to either one of two distinct concepts. First, the nodes can be individual dynamical systems which are coupled through static links. Second, the pattern of links, i.e. the network *topology*, can evolve dynamically in time. We can thus distinguish between *dynamics ON networks* and *dynamics OF networks*. Combining the two yields an *adasptive network* – a network whose links change *adaptively* with respect to its states, resulting in a dynamical interplay between the state and the topology of the network [6].

Adaptive networks are hardly new. Almost all real world networks are adaptive to some extent. Consequently, examples of adaptive networks occur in many disciplines and can be found in a large number of applied models. What is new, however, is that only over the recent years adaptive networks have come into focus of rigorous investigations that employ simple conceptual models. These investigations have revealed a number of new mechanisms and phenomena: Adaptive networks based on simple local rules can self-organize robustly toward phase transitions [7] and highly non-trivial complex topologies [8]; distinct classes of nodes can emerge spontaneously from an initially homogeneous population [9]; and, complex dynamics can be observed as a consequence of phase transitions [10] and bifurcations [11] that involve topological as well as local degrees of freedom.

T. Gross (✉)
Max-Plack-Institute for Physics of Complex Systems, 01187 Dresden, Germany
e-mail: thilo.gross@physics.org

T. Gross, H. Sayama (eds.), *Adaptive Networks,* Understanding Complex Systems,
DOI 10.1007/978-3-642-01284-6_1,

While the results of the recent surge of activity on adaptive networks have been predominately reported in the statistical physics literature, the investigation of adaptive networks has profited greatly from approaches and insights from other fields of science, most prominently discrete mathematics, nonlinear dynamics, game theory, sociology, and computer science. As a consequence, the questions posed by adaptive networks are currently attacked from many different directions with the tools that the different disciplines have established. Despite the different approaches, common themes frequently emerge in the investigations, and insights of broad importance begin to crystallize. A theory of adaptive networks that provides a unifying framework linking the previously isolated phenomena has come within reach.

The purpose of this book is to provide a broad overview over major insights in the functioning of adaptive networks. We aim on the one hand to provide an accessible introduction for researchers starting to work on adaptive networks, and, on the other hand, to draw the attention of experts to parallel developments outside their own disciplines.

In the remainder of this introductory chapter, we will explain basic concepts and illustrate the origin of adaptive networks in different disciplines. We will start in Sect. 1.2 by introducing some key notions, especially the interplay between state and topology that is the key to many intriguing phenomena observed on adaptive networks. In Sect. 1.3, we will specifically discuss the separation of timescales between the dynamics of states and the evolution of topologies, and several important critical phenomena discovered with models that adopt separable timescales. In Sect. 1.4, we will focus on the formation of self-organized topology in adaptive networks, and discuss some important research agendas. In Sect. 1.5, we will introduce a more complex class of adaptive network models in which the timescales of changes of states and topologies are not separable. Finally, in Sect. 1.6, we will give an overview of the other chapters in this book, where we will highlight how the approaches shed light on adaptive networks from different directions and how these different views could be combined to reveal a coherent picture of this intriguing, rapidly evolving field.

1.2 The Interplay Between State and Topology

What makes dynamics in adaptive networks so different from dynamics *ON* networks or dynamics *OF* networks? To answer this question, we begin by considering dynamics on a static network first.

It is well known that almost all dynamical processes that can be placed on a network are highly sensitive to the network topology. This means that the dynamics explores the network topology and thereby, somehow, "encodes" topological information in the time series of the states of the nodes. A simple example is an infectious disease spreading across the network. Each node is either susceptible to the disease or infected. Susceptible nodes that are linked to infected nodes become infected with a certain rate, while infected nodes recover at a different rate, coming back

to susceptible again. Whether such a disease can persist in the network depends on the rates of infection and recovery, but also on the number of connections per network node, or the *degree* of the nodes. Specifically, it depends on a quantity called *mean excess degree*, which denotes the average number of additional links that one finds connected to a node that is reached by following a random link. In a large connected network in which the excess degree exceeds a certain threshold, the disease can persist indefinitely. In this case, every node will be infected once in a while. Consequently, we can estimate whether the mean excess degree exceeds the threshold (global topological information) just by watching the behavior of a single node (time series of states of an individual node) for a sufficiently long period of time.

The example given above illustrates how topological information could be encoded in the dynamics of every single node. In certain situations, we can use the information that is thus encoded; for instance, it has been proposed to simulate the dynamics of coupled oscillators on a given network in order to detect cliques of closely connected nodes. However, on networks with static topology, the flow of information is a one-way road. The information about the states of nodes cannot feed back to the network topology.

Let us return to the example of the disease spreading, but now we allow the susceptible nodes to cut links to infected neighbors with a certain probability. As a result of this additional rule, a dynamical feedback loop is formed between topologies and states of the network. Namely, the dynamics of the prevalence of the disease depends on the network topology, but the evolution of the network topology also depends on the prevalence of the disease.

1.3 Timescale Separation and Critical Phenomena

The coupling of the topological evolution and the dynamics of states leads to an intriguing interplay. The effect of this interplay can be well understood in systems with timescale separation. A good example that can be seen in our everyday life is a road network. It is apparent that the decision where to build new roads depends on the traffic load on the existing roads, and therefore on the dynamical state of the network. Once a new road is built, it will alter the traffic patterns. However, the two processes – the road construction and the traffic shift in response to it – take place at very different timescales: years compared to days.

From the theory of dynamical systems, it is known that, in systems with timescale separation, the fast processes are governed by the slow processes. For example, if we start our road network in a random initial state, the traffic load will quickly settle down to some pattern. This pattern is a dynamical attractor of the fast system. Only if the network is observed on a much longer timescale, one can notice that the traffic pattern still changes in response to the evolving topology. However, compared to phenomena on the longer timescale, the response of the traffic load to topological changes is so fast that it can be regarded an instantaneous process.

Unless discontinuous dynamical transitions in the dynamics of the fast system take place, it will remain in this *quasi-attractor* all the time. The states visited in this quasi-attractor, i.e., the specific patterns of traffic, are then governed by the network topology.

An important consequence of timescale separation was described in a groundbreaking paper by Bornholdt and Rohlf [7]. Suppose that the dynamics on the network undergoes a *phase transition*, if the topology is altered in a certain way. In the language of statistical physics, this transition is detected by an *order parameter* – a global property of the dynamics. Bornholdt and Rohlf showed that the order parameter is encoded in the dynamics and therefore accessible to every node when the system falls in its quasi-attractor. In the meantime, the topological evolution is assumed to take place a slower timescale, and therefore the information about the order parameter can be extracted and utilized for topological changes. If the topological evolution follows appropriate rules, it is conceivable that this system self-organizes toward a critical state in which the dynamics on the network is exactly in the critical, transitional regime. While this mechanism sounds slightly artificial at first, it turns out that it arises almost automatically if the system is governed by simple natural rules.

Let us return once again to the example of epidemics, but now assume that the nodes are very reluctant to cut links so that the topological dynamics is much slower than the dynamics of the epidemic. If we start the system in the epidemic state, every node will be infected once in a while. On a longer time scale, every node will decide to cut a link once in a while. This decreases the connectivity of the network very slowly, and eventually, the epidemic threshold is reached and the disease becomes extinct, freezing the network exactly at the critical connectivity. Many more realistic examples can be found in the context of regulatory and neural networks.

Critical states have some peculiar dynamical properties. In particular they are frequently linked to the appearance of power-laws in the sizes of avalanches of events. Furthermore, they can give rise to multiple coexisting periodic and quasi-periodic attractors. Several authors have presented evidence that this form of self-organization is present in biological systems at many different scales.

1.4 Self-Organization of Non-trivial Network Topologies

A different form of topological self-organization was first observed in a model by Ito and Kaneko [9]. They describe a system that is initially homogeneous, where every node is connected to every other node and all nodes are in the same state (except for very small perturbations). In their model, the states of the nodes as well as the strength of the links change continuously. A rule is applied that increases the link strength between nodes in similar states but effectively weakens the connection between nodes in different states. This rule leads to the evolution of two distinct classes of nodes: Leaders, which exert a strong influence on other nodes, and followers, which exert little influence on others. Although the topology of the network keeps evolving indefinitely, leaders remain leaders and followers remain followers.

The work of Ito and Kaneko has inspired several subsequent investigations, in particular in the context of game theory. Although the mechanism that drives the spontaneous formation of the distinct classes of nodes is still unclear, an interesting pattern can be observed: All models in which nodes in similar states are linked preferentially lead to the formation of heterogeneous topologies, which either follow a scale-free degree distribution or split into distinct classes of nodes with different mean degrees. By contrast, if the opposite rule is applied so that nodes in different states are linked preferentially, homogeneous topologies that favor synchronization are obtained [12].

Both the self-organized formation of distinct classes of nodes and the ability to communicate topological information seem to be important ingredients for the self-organized formation of global non-random topologies based on local rules. Indeed, the formation of such topologies, although not stationary ones, was first reported by Holme and Ghoshal [8], and later, the self-assembly of adaptive networks was studied by Rosvall and Sneppen [13]. Nevertheless, the formation of distinct topologies in adaptive networks still remains largely unexplored at this point. More work in this direction would be highly desirable as it is likely to reveal the mechanisms that govern structure formation in biological networks and could, in the form of design principles, be utilized in engineering applications.

1.5 Adaptive Networks with Inseparable Timescales

So far we have mainly focused on systems in which the dynamics on the network is faster than the topological evolution. We have seen that, in these networks, the dynamics can be used to communicate topological information among nodes. However, the opposite is also possible: if the topological evolution is much faster than the dynamics on the network then topology can be used as a medium to communicate information on the state of the nodes.

Yet another, particularly interesting situation can arise if the dynamics on the network and the dynamics of the network take place at the same timescale. In such a case, the states and the topology of the network are truly coupled, and the entwined feedback loops between topological and local information may give rise to highly complex outcomes. For instance, it has been shown that the adaptive interplay can give rise to new bifurcations and phase transitions that involve changes in the dynamics of state and the topology of the network [10, 11].

An alternative approach to describing the interplay between states and topologies at the same timescale is the *graph transformation* (also called graph rewriting or graph grammars), which has been studied in discrete mathematics and theoretical computer science for the last couple of decades. While very difficult to treat analytically, the graph transformation is a convenient way to formulate the evolution of networks in both states and topologies algorithmically, using some local rules of substructure rewriting applied to labeled graphs. This kind of formulation is particularly powerful for the description of complex network growth processes, such as morphogenesis and self-replication of biological systems. It is anticipated that the combination these algorithmic approaches

and other statistical-physics-based ones will produce novel research directions on adaptive networks.

1.6 In this Book

This book contains a broad survey of the state-of-the-art in adaptive networks. The individual chapters are contributed by leading researchers from different disciplines. The chapters aim on the one hand to provide first-hand accounts focused on significant insights that have been gained, and on the other hand to provide mini-reviews of selected areas.

The following three chapters of the book focus on empirical investigations of real-world adaptive networks. In Chap. 2, Palla, Pollner, Barabási, and Viscek present an approach to the evolution of communities in social networks. This approach is illustrated by the analysis of social network data which reveals significant differences between small and large communities. Chapter 3 by Braha and Bar-Yam connects almost seamlessly to the first. Here a different approach to the analysis of real-world social networks is proposed by which the role of nodes in the network can be quantified. Again the application to social network data reveal a surprising result; while local hubs are found as expected, who is a hub and who is not changes on short timescales. This result strongly emphasizes the inherent dynamic nature of adaptive networks that has long been neglected in the literature. The theme of the investigation of real world adaptive networks continues in the fourth chapter in an entirely different context. Fricker, Boddy, Nakagaki, and Bebber present data on the growth of fungal mycelial networks. In the forest floor these networks can grow to enormous size and play an important role for forest ecosystems. In the context of this book mycelial networks are interesting as they can be cultured in the lab and thus constitute an example of real-world adaptive networks that can be studied with relative ease.

In the fifth chapter we launch into the theoretical investigation of adaptive networks. In this chapter Rohlf and Bornholdt review their original work on self-organized criticality in adaptive networks as well as several subsequent models inspired by the original paper. The basic mechanism proposed is probably responsible for self-organization of many systems in biology and beyond. The self-organization of adaptive networks with time-scale separation is further illustrated by the work of Caldarelli and Garlaschelli presented in Chap. 6. Here, an adaptive ecological network is considered in which Bak-Sneppen-like dynamics are coupled to topological evolution rules. This model illustrates clearly how the behavior of both the topological model and the Bak-Sneppen-model are significantly altered as they are combined.

The subsequent chapters focus on a different form of self-organization of adaptive networks. In Chap. 7 Ito and Kanako show how distinct classes of nodes can spontaneously emerge in a system of coupled oscillators. While many other models have been used to investigate the emergence of discrete classes, the models reviewed

in this chapter remain, to our knowledge, the only ones that show such an emergence from an initially homogeneous population and use deterministic dynamics. Chapter 8 by Chen and Kurths likewise focuses on systems of coupled oscillators. In contrast to the setting studied by Ito and Kaneko, the aim is to build up not heterogeneous topologies but very homogeneous ones promoting synchronization. The authors discuss different adaptive rewiring rules by which this aim can be achieved.

After networks with weighted links and continuous states have been discussed in Chaps. 7 and 8, we return to the far simpler models with unweighted links and discrete node states. In Chap. 9 Do and Gross review several recent investigations, which apply such models for the study of opinion formation and epidemic spreading on networks of social contacts. The comparison of the different model approaches reveals several interesting parallels and differences. This chapter also introduces the moment closure, an approximation scheme by which the dynamics of an adaptive network can be captured in a low dimensional system of differential equations. This approximation is then used by Shaw and Schwartz in Chap. 10 to analyze a more complex epidemiological model. This chapter also contains an interesting discussion of the effect of noise in adaptive networks.

Another class of systems that can be described by unweighted links and a finite number of node states are discrete games on adaptive networks. In Chap. 11 we return to the formation of complex topologies, but this time consider it from a game theoretical perspective. Skyrms and Pemantle discuss several network formation games of which Rosseau's stag hunt, a coordination game, is the most complex. With great skill and mathematical rigor the authors show that, in the context of adaptive networks, even very simple scenarios can yield interesting results. The subsequent chapter, Chap. 12, connects almost seamlessly with a discussion of slightly more complex games. Traulsen, Santos and Pacheco study three fundamental classes of games using a powerful approximation scheme and numerical simulation. It is shown that adaptive rewiring effectively changes the rules of the game. Thus, the players actually behave as if they were playing a different type of game in a static or well-mixed system. While well studied models from game theory can thus show new types of behavior if considered on an adaptive networks, also entirely new games become possible. In Chap. 13 Holme and Ghoshal propose a game in which the players do not attempt to maximize an abstract payoff, but struggle for an advantageous topological position on the network. The desired position is characterized by low degree and high centrality which presents the nodes with a dilemma and results in interesting dynamics.

The models discussed in Chaps. 9–13 show that even very simple rules can lead to the formation of complex network topologies and non-trivial dynamics. Several graph-transformation-based approaches for the automated discovery of such "interesting" rules have been proposed in the context of computer science. In Chap. 14 Tomita, Kurokawa, and Murata propose a restricted, but very flexible class of adaptive networks for which an exhaustive search for rules and initial network configurations is possible. The authors apply this framework to construct self-replicating networks by evolutionary optimization. Finally in Chap. 15, Sayama and Laramee propose a modeling framework named generative network automata that extends

established methods for the investigation of cellular automata and other discrete dynamical systems to adaptive networks. This formal framework allows for an enumeration of all possible rules and therefore for an exhaustive search, which reveals several distinct classes of dynamical behavior.

References

1. R. Albert, A. Barabasi, Rev. Mod. Phys. **74**(1), 1 (2002)
2. S.N. Dorogovtsev, J.F.F. Mendes, *Evolution of Networks* (Oxford University Press, Oxford, 2003)
3. M.E.J. Newman, SIAM Rev. **45**(2), 167 (2003)
4. S. Boccaletti, V. Latora, Y. Moreno, M. Chavez, D. Hwang, Phys. Reports **424**, 175 (2006)
5. M.E.J. Newman, A. Barabasi, D.J. Watts, *The Structure and Dynamics of Networks* (Princeton University Press, Princeton, 2006)
6. T. Gross, B. Blasius, J. R. Soc. Interface **5**, 259 (2008)
7. S. Bornholdt, T. Rohlf, Phys. Rev. Lett. **84**(26), 6114 (2000)
8. P. Holme, G. Ghoshal, Phys. Rev. Lett. **96**, 908701 (2006).
9. J. Ito, K. Kaneko, Phys. Rev. Lett. **88**(2), 028701 (2002)
10. P. Holme, M.E.J. Newman, Phys. Rev. E **74**, 056108 (2007).
11. T. Gross, C. Dommar D'Lima, B. Blasius, Phys. Rev. Lett. **96**, 208701 (2006)
12. C.S. Zhou, J. Kurths, Phys. Rev. Lett. **96**, 164102 (2006).
13. M. Rosvall, K. Sneppen, Euro. Phys. Lett. **74**(6), 1109 (2006)

Part I
Real-World Examples of Adaptive Networks

Chapter 2
Social Group Dynamics in Networks

Gergely Palla, Péter Pollner, Albert-László Barabási, and Tamás Vicsek

Abstract The rich set of interactions between individuals in the society results in complex community structure, capturing highly connected circles of friends, families, or professional cliques in a social network. Due to the frequent changes in the activity and communication patterns of individuals, the associated social and communication network is subject to constant evolution. The cohesive groups of people in such networks can grow by recruiting new members, or contract by loosing members; two (or more) groups may merge into a single community, while a large enough social group can split into several smaller ones; new communities are born and old ones may disappear. We discuss a new algorithm based on a clique percolation technique, that allows to investigate in detail the time dependence of communities on a large scale and as such, to uncover basic relationships of the statistical features of community evolution. According to the results, the behaviour of smaller collaborative or friendship circles and larger communities, e.g., institutions show significant differences. Social groups containing only a few members persist longer on average when the fluctuations of the members is small. In contrast, we find that the condition for stability for large communities is continuous changes in their membership, allowing for the possibility that after some time practically all members are exchanged.

2.1 Introduction

Mapping social relations between people onto a network has a long tradition in sociology [20, 72, 76]. The standard method for revealing the topology of the connections is to use questionnaires and personal interviews. The advantage of this approach is that it can provide very detailed information about the social ties, e.g., the type of acquaintance behind a given connection, what sort of emotions do the examined pairs of people induce in each other, whether the relation is mutual or

T. Vicsek (✉)
Statistical and Biological Physics Research Group of HAS, Department of Biological Physics, Eötvös University, 1117 Budapest, Pázmány Péter sétány 1/A, Hungary
e-mail: vicsek@angel.elte.hu

T. Gross, H. Sayama (eds.), *Adaptive Networks,* Understanding Complex Systems,
DOI 10.1007/978-3-642-01284-6_2,

not, etc. The drawback of this data collection framework is that the typical size of the examined sample is of the order of $N \approx 10^2$ individuals and the strength associated to the links between people is subjective.

In the last decade a change of paradigm took place due to the rapid development of *complex network theory* [2, 4, 39, 75]. This new interdisciplinary field is devoted to the analysis of the statistical features of systems ranging from protein interaction networks through stock correlation graphs to the Internet. Since the size of the investigated networks can grow up to more than $N \approx 10^6$ nodes, the underlying data must be collected in an automated way, extracting the relevant information from large electronic databases. This approach has been successfully used to create large social networks as well [50, 51, 73]. E-mail databases [10, 12, 13], phone-call records [1, 50, 51] and scientific co-authorship data [5, 22, 23, 42] provide good examples for the starting point of a social network analysis on large scale. Although the range of social interactions that can be detected using data bases of this type is narrow compared to the questionnaires, in some cases the strength of the connections (e.g., the number of phone-calls between two individuals in a certain time period) may be more objectively quantifiable.

In this chapter we present a study concerning the statistical properties of two large social networks of major interest, capturing the collaborations between scientists and the calls between mobile phone users. Our focus is on the *community dynamics*, where the communities (also called as modules, clusters or cohesive groups) can correspond to families, friendship circles, work groups [63, 74], etc. These structural sub-units have no widely accepted unique definition, however we can assume that a community member is usually more tightly connected to its group than to other parts of the network, and that most people in a community know each other [15, 33, 43, 57, 64] (the groups are dense).

Although most empirical studies have focused on snapshots of these communities, thanks to frequent changes in the activity and communication patterns of individuals, the associated social and communication network is subject to constant evolution [5, 11, 31, 38, 47, 70, 78]. Our knowledge of the mechanisms governing the underlying community dynamics is limited, but is essential for a deeper understanding of the development and self-optimisation of the society as a whole [25, 28, 32, 34, 37, 56].

Typically, the communities in a complex system are not isolated from each other, instead, they have overlaps, e.g., people can be members in different social groups at the same time [72]. This observation naturally leads to the definition of the *community graph*: a network representing the connections between the communities, with the nodes referring to communities and links corresponding to shared members between the communities. Accordingly, the community degree d^{com} of a community is given by the number of other communities it overlaps with, and is equal to the degree of the corresponding node in the community graph. So far, in the networks investigated, the community degree distribution was shown to decay exponentially for low and as a power law for higher community degree values. This means that fat tailed degree distributions appear at two levels in the hierarchy of these systems:

both at the level of nodes (the underlying networks are scale free), and at the level of the communities as well.

Preferential attachment is a key concept in the field of scale-free networks. In a wide range of graph models the basic mechanism behind the emerging power law degree distribution is that the new nodes attach to the old ones with probability proportional to their degree [2, 4, 39]. Furthermore, in earlier works the occurrence of preferential attachment was directly demonstrated in several real world networks with scale free degree distribution [5, 41]. The observed fat tails in the degree distribution of the community graphs indicate that the mechanism of preferential attachment could be present *at the level of communities* as well. One of our aims in the present chapter is to examine the attachment statistics of communities in order to clarify this question.

We further develop a new algorithm based on the clique percolation method (CPM) [9, 53], that allows to investigate in detail the time dependence of overlapping communities on a large scale and as such, to uncover basic relationships of the statistical features of community evolution [52, 55]. According to our results, the behaviour of large – and small communities show an interesting difference. We find that large groups persist longer if they are capable of dynamically altering their membership, suggesting that an ability to change the composition results in better adaptability and a longer lifetime for social groups. Remarkably, the behaviour of small groups displays the opposite tendency, the condition for stability being that their composition remains unchanged. We also show that the time commitment of members to a given community can be used for estimating the community's lifetime.

This chapter is organised as follows. We begin with the construction of the investigated networks from the basic data sets in Sect. 2.2. and continue with the main aspects of the CPM in Sect. 2.3. We detail the algorithm for building evolving communities from subsequent snapshots of the community structure in Sect. 2.4. The main results are discussed in Sect. 2.5, whereas the concluding remarks are drawn in Sect. 2.6.

2.2 Construction of the Networks

The data sets we consider contain the monthly roster of articles in the arXiv.org cond-mat archive spanning 142 months, with over 30,000 authors [71], and the complete record of phone-calls between the customers of a mobile phone company spanning 52 weeks (accumulated over two week long periods), and containing the communication patterns of over 4 million users [50, 51]. Both type of collaboration events (a new article or a phone-call) document the presence of social interaction between the involved individuals (nodes), and can be represented as (time-dependent) links. We assumed that in both cases the *social connection* between people had started some time before the collaboration/communication events and lasted for some time after these events as well. (E.g., the submission of an article to

the archive is usually preceded by intense collaboration and reconciliation between the authors, which is in most cases prolonged after the submission as well). Collaboration/communication events between the same people can be repeated from time to time again, and higher frequency of collaboration/communication acts usually indicates closer relationship [58]. Furthermore, weights can be assigned to the collaboration and communication events quite naturally: an article with n authors corresponds to a collaboration act of weight $1/(n-1)$ between every pair of its authors, whereas the cost of the phone-calls provide the weight in case of the phone-call network. Based on this, we define the *link weight* between two nodes a and b at time t as

$$w_{a,b}(t) = \sum_i \left[w_i \Theta(t - t_i) \exp\left(-\lambda_+ (t - t_i)/w_i\right) + w_i \Theta(t_i - t) \exp\left(-\lambda_- (t_i - t)/w_i\right) \right], \tag{2.1}$$

where the summation runs over all collaboration events in which a and b are involved e.g., a phone-call between a and b, and w_i denotes the weight of the event i occurring at t_i. (The constants λ_+ and λ_- are decay time characteristic for the particular social system we study. The function $\Theta(t)$ is the step function taking 0 at negative t values and 1 for positive). Thus, in this approach the time evolution of the network is manifested in the changing of the link weights. However, if the links weaker than a certain threshold w^* are neglected, the network becomes truly restructuring in the sense that links appear only in the vicinity of the events and disappear further away in time (Fig. 2.1). The above method of weighting ties between people is very useful in capturing the continuous time dependence of the strength of connections when the information about them is available only at discrete time steps. Except for our analysis of the preferential attachment of communities (Sect. 2.3.2.) we used symmetric decay characteristics $\lambda_- = \lambda_+$, whereas in Sect. 2.3.2. we applied a special choice corresponding to a simple growing network.

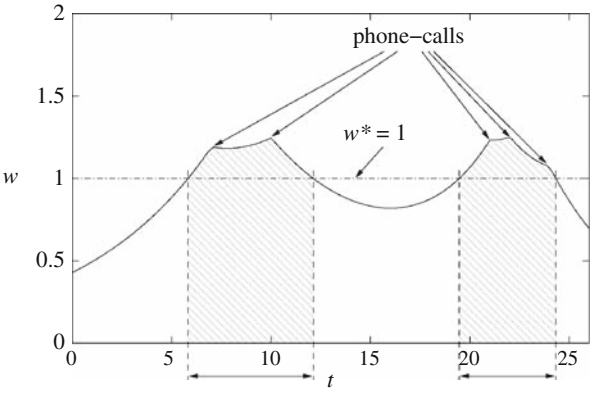

Fig. 2.1 The link-weight as a function of time for a connection in the phone-call network. If a weight threshold of $w^* = 1$ is introduced, the link is absent outside the *shaded intervals*. Here $\lambda_- = \lambda_+$. Figure from the Suppl. of [52]

2.3 Finding Communities

2.3.1 The Clique Percolation Method

The study of the *intermediate-scale* substructures in networks, made up of vertices more densely connected to each other than to the rest of the network, has become one of the most highlighted topic in complex network theory. These structural subunits can correspond to multi-protein functional units in molecular biology [59, 65], a set of tightly coupled stocks or industrial sectors in economy [30, 49], groups of people [52, 63, 74], cooperative players [66, 67, 69], etc. The location of such building blocks can be crucial to the understanding of the structural and functional properties of the systems under investigation. Furthermore, a reliable method to pinpoint such objects has many potential industrial applications, e.g., it can help service providers (phone, banking, Internet, etc.) identify meaningful groups of customers (users), or support biomedical researchers in their search for individual target molecules and novel protein complex targets [3, 35].

Since communities have no widely accepted unique definition, the number of available methods to pinpoint them is vast [15, 16, 19, 24, 26, 27, 33, 40, 43, 53, 54, 60–64]. The majority of these algorithms classify the nodes into disjunct communities, and in most cases a global quantity called *modularity* [44, 45] is used to evaluate the quality of the partitioning. However, as pointed out in [17, 36], the modularity optimisation introduces a resolution limit in the clustering, and communities containing a smaller number of edges than $\sqrt{M}$ (where M is the total number of edges) cannot be resolved.

One of the big advantages of the *clique percolation method* (CPM) is that it provides a *local* algorithm for detecting the communities, and therefore, it does not suffer from resolution problems of this type [9, 53]. In this approach the communities are built up from k-cliques, corresponding to complete (fully connected) sub-graphs of size k. Two k-cliques are said adjacent if they share $k-1$ nodes [6, 9, 14], and a k-clique community corresponds to a set of k-cliques in which all k-cliques can reach each other through chains of k-clique adjacency. In other words, the communities defined in this way are equivalent to k-clique percolation clusters. These objects can be best visualised with the help of k-clique templates (Fig. 2.2), that are objects isomorphic to a complete graph of k vertices. Such a template can be placed onto any k-clique in the graph, and rolled to an adjacent k-clique by relocating one of its vertices and keeping its other $k-1$ vertices fixed. Thus, the k-clique percolation clusters (k-clique communities) of a graph are all those subgraphs that can be fully explored by rolling a k-clique template in them but cannot be left by this template.

The further advantages of the community definition above (beside its locality) are that it is not too restrictive, it is based on the density of the links and it allows *overlaps between the communities*: a node can be part of several k-clique percolation clusters at the same time. Revealing overlaps between communities has obtained a significant attention in the recent literature devoted to community detection [7, 18, 29, 40, 46, 60, 68, 77, 79]. Indeed, communities in real-world

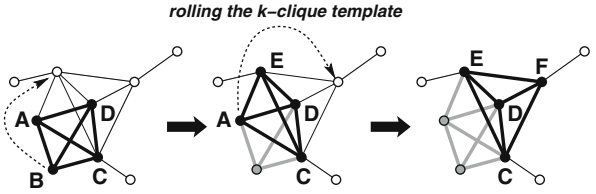

Fig. 2.2 Illustration of k-clique template rolling at $k = 4$. Initially the template is placed on A-B-C-D (*left panel*) and it is "rolled" onto the subgraph A-C-D-E (*middle panel*). The position of the k-clique template is marked with *thick black lines* and *black nodes*, whereas the already visited edges are represented by *thick gray lines* and *gray nodes*. Observe that in each step only one of the nodes is moved and the two 4-cliques (before and after rolling) share $k - 1 = 3$ nodes. At the final step (*right panel*) the template reaches the subgraph C-D-E-F, and the set of nodes visited during the process (A-B-C-D-E-F) are considered as a k-clique percolation cluster

graphs are often inherently overlapping: each person in a social web belongs usually to several groups (family, colleagues, friends, etc.), proteins in a protein interaction network may participate in multiple complexes [29] and a large portion of webpages can be classified under multiple categories. Prohibiting overlaps during module identification strongly increases the percentage of false negative co-classified pairs. As an example, in a social web a group of colleagues might end up in different modules, each corresponding to e.g., their families. In this case, the network module corresponding to their work-group is bound to become lost.

2.3.2 Preferential Attachment at the Level of Communities

In this section we examine whether the fat tails observed earlier in the community distribution could result from preferential attachment mechanisms at the level of communities. The method presented below can be applied in general to any empirical study of an attachment process where the main goal is to decide whether the attachment is uniform or preferential with respect to a certain property (e.g., degree, size, etc.) of the attached objects (e.g., nodes, communities etc.).

2.3.2.1 Method for Detecting Preferential Attachment

If the studied process is uniform with respect to a property ρ, then objects with a given ρ are chosen at a rate given by the distribution of ρ amongst the available objects. However, if the attachment mechanism prefers high (or low) ρ values, then objects with high (or low) ρ are chosen with a higher rate compared to the ρ distribution of the available objects. To monitor this enhancement, one can construct the cumulative ρ distribution $P_t(\rho)$ of the available objects at each time step t, together with the un-normalised cumulative ρ distribution of the objects chosen by the process between t and $t + 1$, denoted by $w_{t\to t+1}(\rho)$. The value of $w_{t\to t+1}(\rho^*)$ at a given ρ^* equals to the number of objects chosen in the process between t and $t + 1$, that had a ρ value larger than ρ^* at t. To detect deviations from uniform attachment, it

is best to accumulate the ratio of $w_{t\to t+1}(\rho)$ and $P_t(\rho)$ during the time evolution to obtain

$$W(\rho) = \sum_{t=0}^{t_{\max}-1} \frac{w_{t\to t+1}(\rho)}{P_t(\rho)}. \tag{2.2}$$

If the attachment is uniform with respect to ρ, then $W(\rho)$ becomes a flat function. However, if $W(\rho)$ is an increasing function, then the objects with large ρ are favoured, if it is a decreasing function, the objects with small ρ are favoured in the attachment process. The advantage of this approach is that the rate-like variable $w_{t\to t+1}(\rho)$ associated to the time step between t and $t+1$ is always compared to the $P_t(\rho)$ distribution at t. Therefore $W(\rho)$ is able to indicate preference (or the absence of preference) even when $P_t(\rho)$ is slowly changing in time (as in the case of the community degree in the co-authorship network under investigation).

We have tested the above method on simulated graphs grown with known attachment mechanisms, (i) uniform attachment (new nodes are attached to a randomly selected old node), (ii) linear preferential attachment (new nodes are attached to old ones with a probability proportional to the degree), (iii) and anti-preferential attachment (new nodes are attached to the old ones with a probability proportional to $\exp(-d)$, where d is the degree). In these cases the degree d of the individual nodes plays the role of the parameter ρ. For each time step, we recorded the cumulative degree distribution of the nodes $P_t(d)$, together with the number of nodes gaining new links with a degree higher than a given d, labelled by $w_{t\to t+1}(d)$. By summing the ratio of these two functions along the time evolution of the system one gets $W(d) = \sum_{t=0}^{t_{\max}-1} w_{t\to t+1}(d)/P_t(d)$. In Fig. 2.3a. we show the empirical results for $W(d)$ obtained for the simulated networks grown with the three different attachment rules. The curves reflect the difference between the three cases very well: for the uniform attachment probability $W(d)$ is flat, for the preferential attachment $W(d)$ is clearly increasing, and for the anti-preferential attachment $W(d)$ is decreasing.

We have also calculated the attachment statistics of the nodes in the studied co-authorship network. In this case we used extremely asymmetric decay characteristics in (2.1): $\lambda_- = \infty$ and $\lambda_+ = 0$. This results in a simply growing network, where every collaboration event gives rise to a set of links between each pair of collaborators at the very moment of the collaboration act, and the strengths of these links remain constant from then on. As it can be seen in Fig. 2.3b., the corresponding $W(d)$ curve is increasing, therefore preferential attachment is present at the level of nodes in the system.

2.3.2.2 Community Growth in the Co-authorship Network

The two properties to be substituted in place of ρ in Eq.(2.2) are the community degree d^{com} and the community size s, therefore, the cumulative community size distribution $P_t(s)$ and the cumulative community degree distribution $P_t(d^{\text{com}})$ were recorded at each time step t. To study the *establishment of the new community links*,

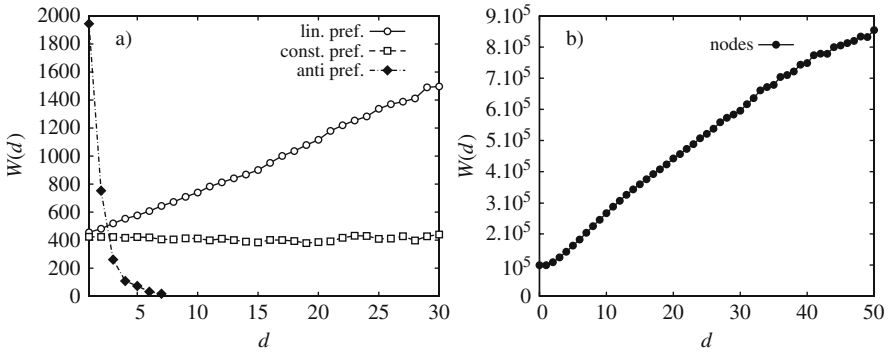

Fig. 2.3 (**a**) The $W(d)$ function for networks grown with known attachment rules: uniform probability (*squares*), linear preferential attachment (*open circles*), and anti preferential attachment (*diamonds*). (**b**) The $W(d)$ function in the co-authorship network of the Los Alamos cond-mat archive. Figure from [56]

we constructed the un-normalised cumulative size distribution $w_{t\to t+1}(s)$ and the un-normalised cumulative degree distribution $w_{t\to t+1}(d^{\rm com})$ of the communities gaining new community links to previously unlinked communities. The value of these distributions at a given s (or given $d^{\rm com}$) is equal to the number of unlinked communities at t that establish a community link between t and $t+1$ with a community larger than s (or having larger degree than $d^{\rm com}$) at t. By accumulating the ratio of the rate-like variables and the corresponding distributions we obtain

$$W(s) = \sum_{t=0}^{t_{\max}-1} \frac{w_{t\to t+1}(s)}{P_t(s)}\,, \qquad W(d^{\rm com}) = \sum_{t=0}^{t_{\max}-1} \frac{w_{t\to t+1}(d^{\rm com})}{P_t(d^{\rm com})}. \quad (2.3)$$

For the investigation of the *appearance of new members* in the communities, we recorded the un-normalised community size distribution $\widehat{w}_{t\to t+1}(s)$ and the un-normalised community degree distribution $\widehat{w}_{t\to t+1}(d^{\rm com})$ of the communities gaining new members (belonging previously to none of the communities) between t and $t+1$. The corresponding distributions that can be used to detect deviations from the uniform attachment are

$$\widehat{W}(s) = \sum_{t=0}^{t_{\max}-1} \frac{\widehat{w}_{t\to t+1}(s)}{P_t(s)}\,, \qquad \widehat{W}(d^{\rm com}) = \sum_{t=0}^{t_{\max}-1} \frac{\widehat{w}_{t\to t+1}(d^{\rm com})}{P_t(d^{\rm com})}. \quad (2.4)$$

In Fig. 2.4a. we show the empirical $W(s)$ and $\widehat{W}(s)$ functions, whereas in Fig. 2.4b. the empirical $W(d^{\rm com})$ and $\widehat{W}(d^{\rm com})$ are displayed. All four functions are clearly increasing, therefore we can draw the following important conclusions:

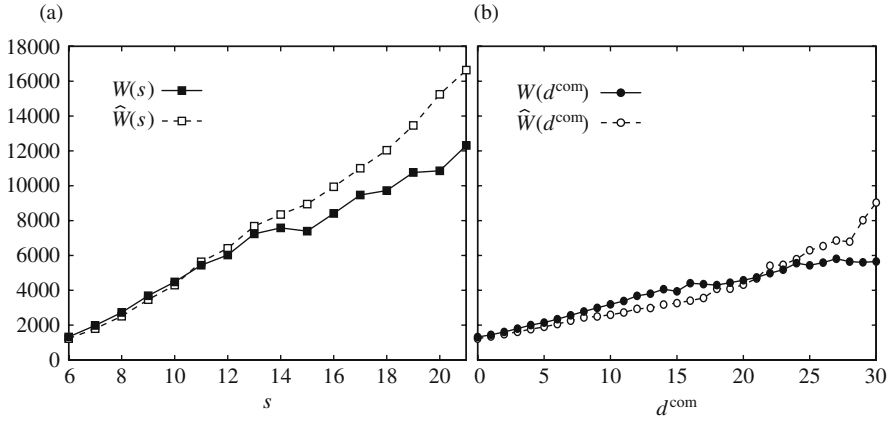

Fig. 2.4 (**a**) The $W(s)$ and $\widehat{W}(s)$ functions for the communities of the co-authorship network of the Los Alamos cond-mat e-print archive. (**b**) The $W(d^{\text{com}})$ and $\widehat{W}(d^{\text{com}})$ functions of the same network. The increasing nature of these functions indicates preferential attachment at the level of communities in the system. Figure from [56]

- When a previously unlinked community establishes a new community link, communities with large size and large degree are selected with enhanced probability from the available other communities.
- When a node previously belonging to none of the communities joins a community, communities with large size and large degree are selected with enhanced probability from the available communities.

2.3.2.3 Model for Growth of Community Network

In this section we outline a simple model for the growth of overlapping communities. Our goal is to demonstrate that preferential attachment of the nodes to communities with the community size, together with minor additional assumptions are enough for the emergence of a community system with a scaling community size and community degree distribution.

In our model the underlying network between the nodes is left unspecified, the focus is on the content of the communities. During the time evolution, similarly to the models published in [28, 48, 58], new members may join the already existing communities, and new communities may emerge as well. The new nodes introduced to the system choose their community preferentially with the community size, therefore the size distribution of the communities is expected to develop into a power-law. The appearance of the new community links originates in new nodes joining several communities at the same time. The detailed rules of the model are the following:

- The initial state of the model is a small set of communities with random size.
- The new nodes are added to the system separately. For each new node i, a membership m_i is drawn from a Poissonean distribution with an expectation value of μ.

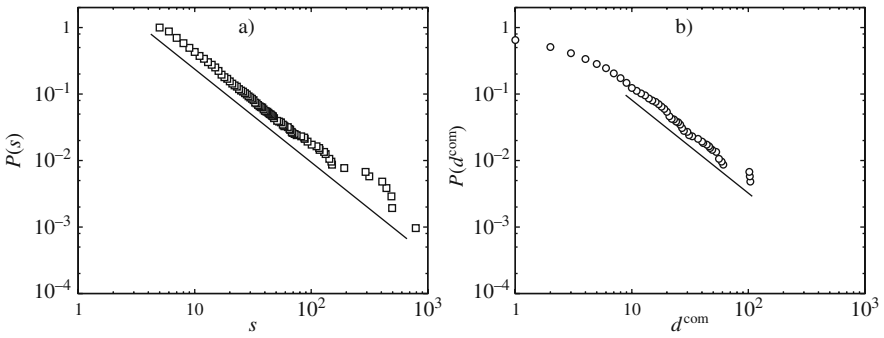

Fig. 2.5 **(a)** the cumulative community size distribution $P(s)$ (*open circles*) in our model at $\mu = 0.6$ follows a power-law with an exponent of -1.4 (*straight line*) (**b**) the cumulative community degree distribution $P(d^{\text{com}})$ (*filled circles*) in our model at the same μ. The tail of this distribution follows the same power-law as the community size distribution (*straight line*), similarly to the communities found in the co-authorship network [53]. Figure from [56]

- If $m_i \geq 1$, communities are subsequently chosen with probabilities proportional to their sizes, until m_i is reached, and the node i joins the chosen communities simultaneously.
- If $m_i = 0$, the node i joins the group of unclassified vertices.
- When the ratio r of the group of unclassified nodes compared to the total number of nodes N exceeds a certain limit r^*, a number of q vertices from the group establish a new community. (Obviously, q must be smaller than Nr even in the initial state).

To be able to compare the results of the model with the community structure of the co-authorship network, the runs were stopped when the number of nodes in the model reached the size of the co-authorship network.

Our experience showed that the model is quite insensitive to changes in r or q, and μ is the only important parameter. For small values ($\mu < 0.3$) the resulting community degree distribution is truncated, whereas when μ is too large ($\mu > 1$), a giant community with abnormally large community degree appears. For intermediate μ values ($0.3 < \mu < 1$), the community size – and community degree distributions become fat tailed, similarly to the co-authorship network. In Fig. 2.5. we show the cumulative community size distribution $P(s)$ and the cumulative community degree distribution $P(d^{\text{com}})$ of the communities obtained in our model at $\mu = 0.6$. (Changes in the parameters r and q only shifts these curves, their shape remains unchanged). Our model grasps the relevant statistical properties of the community structure in the co-authorship network [53] quite well: the community size distribution and the tail of the community degree distribution follow a power-law with the same exponent.

2.3.3 The Static Communities

Turning back to the study of the community evolution (where links corresponding to abandoned social connections may disappear with time, $0 < \lambda_- = \lambda_+ < \infty$),

the communities at each time step were extracted with the CPM for both the co-authorship and the phone-call networks. When applied to weighted networks, the CPM has two parameters: the k-clique size k, (in Fig. 2.6a, b we show the communities for $k = 4$), and the weight threshold w^* (links weaker than w^* are ignored). By increasing k or w^*, the communities start to shrink and fall apart, but at the same time they become also more cohesive. In the opposite case, at low k there is a critical w^*, under which a giant community appears in the system that smears out the details of the community structure by merging (and making invisible) many smaller communities. The criterion used to fix these parameters is based on finding a community structure as highly structured as possible: at the highest k value for which a giant community may emerge, the w^* is decreased just below the critical point. The actual values of these parameters in our studies were $k = 3$, $w^* = 0.1$ in case of the co-authorship network, and $k = 4$, $w^* = 1.0$ in case of the phone-call network.

In Fig. 2.6a, b we show the local structure at a given time step in the two networks in the vicinity of a randomly chosen individual (marked by a black frame). The communities (social groups represented by more densely interconnected parts within a network of social links) are coloured with different shades of gray, so that white nodes (and dashed edges) do not belong to any community, and those that simultaneously belong to two or more communities are shown in black. The two networks have rather different local structure: due to its bipartite nature, the collaboration network is quite dense and the overlap between communities is very significant, whereas in the phone-call network the communities are less interconnected and are often separated by one or more inter-community nodes/edges. Indeed, while the phone record captures the communication between two people, the publication record assigns to all individuals that contribute to a paper a fully connected clique. As a result, the phone data is dominated by single links, while the co-authorship

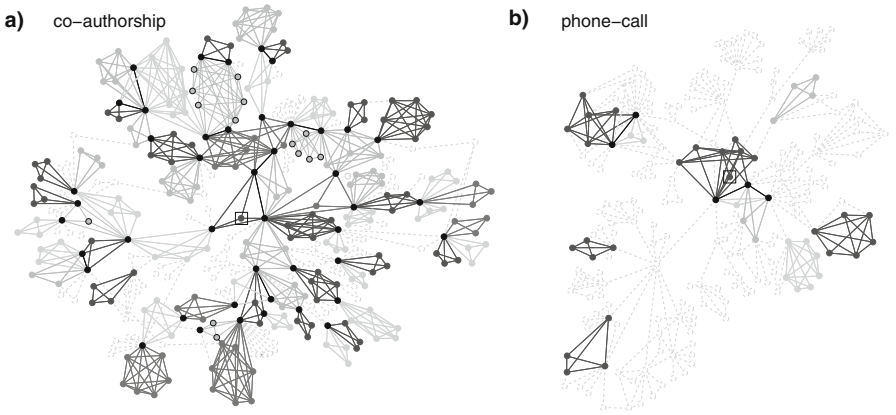

Fig. 2.6 (**a**) The local community structure at a given time step in the vicinity of a randomly selected node in case of the co-authorship network. (**b**) The same picture in the phone-call network. Figure from [52]

data has many dense, highly connected neighbourhoods. Furthermore, the links in the phone network correspond to instant communication events, capturing a relationship as is happens. In contrast, the co-authorship data records the results of a long term collaboration process. These fundamental differences suggest that any potential common features of the community evolution in the two networks potentially, represent generic characteristics of community formation, rather than being rooted in the details of the network representation or data collection process.

2.3.4 Validating the Communities

When validating the found communities, as a first step, it is important to check if the uncovered communities correspond to groups of individuals with a shared common activity pattern. For this purpose we compared the average weight of the links inside communities, w_c, to the average weight of the inter-community links, w_{ic}. For the co-authorship network w_c/w_{ic} is about 2.9, while for the phone-call network the difference is even more significant, since $w_c/w_{ic} \simeq 5.9$, indicating that the intensity of collaboration/communication within a group is significantly higher than with contacts belonging to a different group [8, 21, 50, 51].

While for coauthors the quality of the clustering can be directly tested by studying their publication records in more detail, in the phone-call network personal information is not available. In this case the zip-code and the age of the users provides additional information for checking the homogeneity of the communities. In Fig. 2.7a we show the size of the largest subset of people having the same zip code in the communities, $\langle n_{\text{real}} \rangle$, averaged over the time steps, as the function of the community size s, divided by $\langle n_{\text{rand}} \rangle$, representing the average over random sets of users. The significantly higher number of people with the same zip-code in the CPM

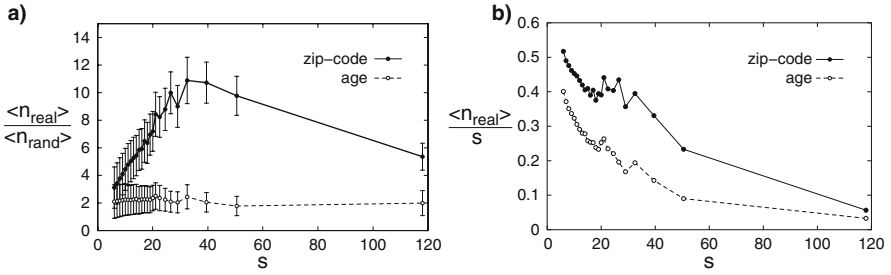

Fig. 2.7 (**a**) The *black symbols* correspond to the average size of the largest subset of members with the same zip-code, $\langle n_{\text{real}} \rangle$, in the phone-call communities divided by the same quantity found in random sets, $\langle n_{\text{rand}} \rangle$, as the function of the community size s. Similarly, the *white symbols* show the average size of the largest subset of community members with an age falling in a three year time window, divided by the same quantity in random sets. The error-bars in both cases correspond to $\langle n_{\text{real}} \rangle / (\langle n_{\text{rand}} \rangle + \sigma_{\text{rand}})$ and $\langle n_{\text{real}} \rangle / (\langle n_{\text{rand}} \rangle - \sigma_{\text{rand}})$, where σ_{rand} is the standard deviation in case of the random sets (**b**) The $\langle n_{\text{real}} \rangle / s$ as a function of s, for both the zip-code (*black symbols*) and the age (*white symbols*). Figure from [52]

communities as compared to random sets indicates that the communities usually correspond to individuals living relatively close to each other. It is of specific interest that $\langle n_{\text{real}} \rangle / \langle n_{\text{rand}} \rangle$ has a prominent peak at $s \simeq 35$, suggesting that communities of this size are geographically the most homogeneous ones. However, as Fig. 2.7b shows, the situation is more complex: on average, the smaller communities are more homogeneous, but there is still a noticeable peak at $s \simeq 30 - 35$. In Fig. 2.7a we also show the average size of the largest subset of members with an age falling into a three years wide time window, divided by the same quantity obtained for randomly selected groups of individuals. The fact that the ratio is larger than one indicates that communities have a tendency to contain people from the same generation, and the $\langle n_{\text{rand}} \rangle / s$ plot indicates that the homogeneity of small groups is on average larger than that of the big groups.

Another interesting feature of Fig. 2.7 is that the difference in the homogeneity of the age is less pronounced than in case of the zip-code. A plausible reason for this effect is that due to the strong social relation between parents and children, many communities contain members coming from different generations. This is supported by the distribution of the age difference in communities, shown in Fig. 2.8a: there is a major peak at zero corresponding to members with the same age, however there is also another peak at 25, corresponding to the typical age difference between parents and children.

Beside the zip-code and the age, the statistics of the *service usage* of the customers supports the validity of the communities as well. In our primary data, the number of times people have used a certain service in one of the two weeks long periods was also available. (There were altogether 34 available services for the customers). However, for most services, the probability for a randomly selected customer using the service at all is very low. For this reason, instead of comparing the average number of members using the same service in communities and random

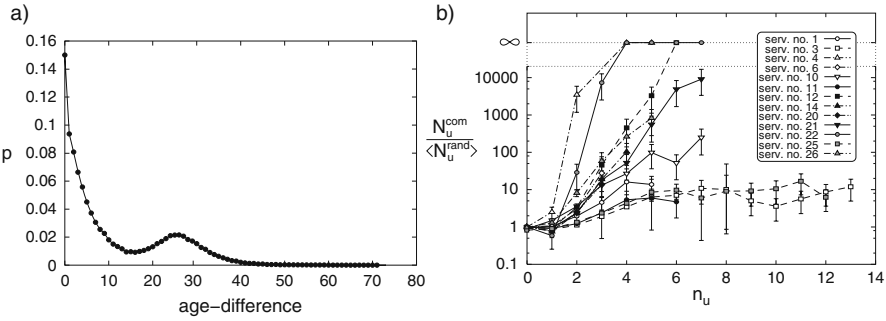

Fig. 2.8 (**a**) The probability distribution of the age difference between community members in the phone-call network. The most probable values are zero and 25, indicating that a pair of members from a community are most likely to be of the same age, or to be a generation apart from each other. (**b**) The number of communities divided by the average number of random sets containing the same n_u number of people using a given service. Each sample of the random sets was prepared with size distribution of the communities determined for the phone-call network. Figure from the Suppl. of [52]

sets, we compared the $N_{\mathrm{u}}^{\mathrm{com}}(n_{\mathrm{u}})$ number of communities having n_{u} members using the same service to the same quantity in random sets, denoted by $N_{\mathrm{u}}^{\mathrm{rand}}(n_{\mathrm{u}})$. For each service, random sets with the same size distribution as the communities were constructed 10,000 times, and $N_{\mathrm{u}}^{\mathrm{rand}}(n_{\mathrm{u}})$ was averaged over the samples. As it can be seen from Fig. 2.8b, for 13 services the $N_{u}^{\mathrm{com}}(n_{u})$ number of communities having n_{u} members using the service is significantly larger than in case of random sets. In fact, the $N_{\mathrm{u}}^{\mathrm{com}}(n_{\mathrm{u}})/N_{\mathrm{u}}^{\mathrm{rand}}(n_{\mathrm{u}})$ ratio in some cases reaches infinity, indicating that there were no random sets at all containing such high number of service users as some communities.

In summary, the phone-call communities uncovered by the CPM tend to contain individuals living in the same neighbourhood, and with comparable age, a homogeneity that supports the validity of the uncovered community structure.

2.4 Evolving Communities

Our focus is on the statistical properties of evolving communities, therefore, we need a reliable method for matching the static "snap-shots" of the community structure at subsequent time steps. The basic events that may occur in the life of a community are shown in Fig. 2.9a: a community can grow by recruiting new members, or contract by loosing members; two (or more) groups may merge into a single community, while a large enough social group can split into several smaller ones; new communities are born and old ones may disappear.

Given the huge number of groups present at each time step, it is a significant algorithmic and computational challenge to match communities uncovered at different time steps. The fact that the communities obtained by the CPM can have overlaps makes the problem even more complicated.

A simple approach would be to match communities from consecutive time steps in descending order of their relative overlap. The relative overlap between communities A and B can be defined as

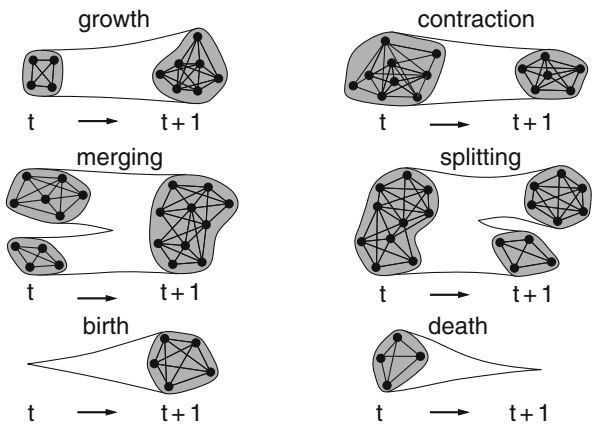

Fig. 2.9 Possible events in the community evolution. When new members are introduced, the community grows, whereas leaving members cause decay in the size. Communities can merge and split, new groups may emerge and old ones can disappear. Figure from [52]

$$C(A, B) \equiv \frac{|A \cap B|}{|A \cup B|}, \tag{2.5}$$

where $|A \cap B|$ is the number of common nodes in A and B, and $|A \cup B|$ is the number of nodes in the union of the two communities. However, the nodes shared between the communities can undermine this type of community conjugation between consecutive time steps: In case a small community A is inflated by large magnitude between time steps t and $t+1$, and at $t+1$ it overlaps with a small static community $B = B_t = B_{t+1}$, then the relative overlap (2.5) between A_{t+1} and B_t can be larger than the relative overlap between A_{t+1} and A_t.

To overcome this difficulty, we refine the identification of communities as shown in Fig. 2.10. For each consecutive time steps t and $t+1$ we construct a joint graph consisting of the union of links from the corresponding two networks, and extract the CPM community structure of this joint network (we thank I. Derényi for pointing out this possibility). When new links are introduced in a network, the CPM communities may remain unchanged, they may grow, or a group of CPM communities may become joined into a single community, however no CPM community may decay by loosing members. From this it follows that if we merge two networks, any CPM community in any of the original networks will be contained in exactly one community in the joined network.

Let us denote the set of communities from t by **A**, the set of communities from $t+1$ by **B**, and the set of communities from the joint network by **V**. For any community

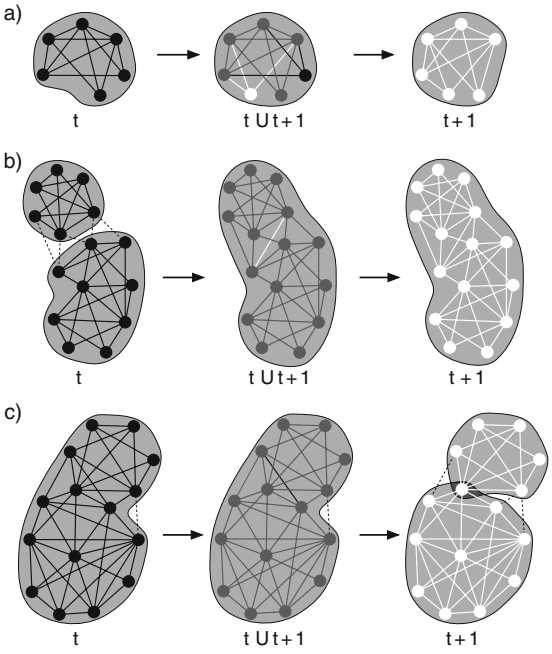

Fig. 2.10 Simple scenarios in the community evolution of the phone-call network for $k = 4$. The communities at t are coloured *black on light gray*, the communities at $t+1$ are coloured *white on light gray*, and the communities in the joint network are coloured *dark gray on light gray*. (**a**) a community simply "propagates", (**b**) the larger community swallows the smaller one, (**c**) a small community is detached from a larger one. Figure from the Suppl. of [52]

$A_i \in \mathbf{A}$ or $B_j \in \mathbf{B}$ we can find exactly one community $V_k \in \mathbf{V}$ containing it. When matching the communities in $\mathbf{A}$ and in $\mathbf{B}$, first for every community $V_k \in \mathbf{V}$ in the joint system we extract the list of communities $A_i^k \in \mathbf{A}$ and $B_j^k \in \mathbf{B}$ that are contained in V_k (this means $A_i^k \subseteq V_k$ and $B_j^k \subseteq V_k$). (Note that either of the lists may be empty). Then the relative overlap between every possible (A_i^k, B_j^k) pairs can be obtained as

$$C_{ij}^k = \frac{\left|A_i^k \cap B_j^k\right|}{\left|A_i^k \cup B_j^k\right|}, \tag{2.6}$$

and we match the pairs of communities in descending order of their relative overlap.

As an illustration of the above process, in Fig. 2.10 we show three simple scenarios occurring in the community evolution of the phone-call network. In Fig. 2.10a both lists A_i^k and B_j^k consist of only a single community, therefore these can be matched right away. However, in Fig. 2.10b the A_i^k list contains two elements, let us denote the smaller community of size $s = 6$ at t by A_1^k and the larger community consisting of nine nodes at t by A_2^k. The corresponding B_j^k list contains a single community B_1^k having 15 members. The relative overlaps between the communities are given as $C_{1,1}^k = 2/5$ and $C_{2,1}^k = 3/5$. Since the $C_{2,1}^k$ relative overlap of the B_1^k community with A_2^k community is larger than the $C_{1,1}^k$ relative overlap with A_1^k, we assign B_1^k to A_2^k. As a consequence the A_1^k community comes to the end of its life at t, and it is swallowed by A_2^k. The opposite process is shown in Fig. 2.10c: in this case the A_i^k list consists of a single community A_1^k of size $s = 15$, whereas the B_j^k list has two elements, the community with six members labelled by B_1^k, whereas and the community containing ten nodes labelled by B_2^k. The relative overlaps are $C_{1,1}^k = 2/5$ and $C_{1,2}^k = 2/3$, therefore the A_1^k is matched to B_2^k, and B_1^k is treated as a new born community. In general, whenever the community V_k contains more communities from $\mathbf{A}$ than from $\mathbf{B}$, the communities A_i^k left with no counterpart from B_j^k finish their life's at t, and when V_k contains more communities from $\mathbf{B}$ than from $\mathbf{A}$, the communities B_j^k left with no counterpart from A_i^k are considered as new born communities.

In some cases we can observe that although a community was disintegrated, after a few steps it suddenly reappears in the network. Our conjecture is that this is more likely to be the consequence of a temporally lower publishing-rate/calling-rate of the people in question than of the real disassembly and re-assembly of the corresponding social community between the people. Therefore, whenever a newborn community includes a formerly disintegrated one, then the last state of the old community is elongated to fill the gap before the reappearance, and the newborn community is treated as the continuation of the old one, as shown in Fig. 2.11.

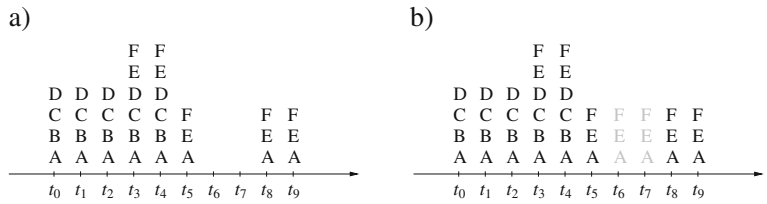

Fig. 2.11 (**a**) A community is disintegrated after step t_5, and it is reborn at step t_8. (**b**) We treat the community as if it was alive at steps t_6 and t_7 too, with the same nodes as at step t_5. Figure from the Suppl. of [52]

2.5 Statistical Properties of the Community Dynamics

2.5.1 Basic Statistics

One of the most basic properties characterising the partitioning of a network is the overall coverage of the community structure, i.e. the ratio of nodes contained in at least one community. In case of the co-authorship network the average value of this ratio was above 59%, which is a reasonable coverage for the CPM. In contrast, we could only achieve a significantly smaller ratio for the phone-call network. At such a large system size, in order to be able to match the communities at subsequent time steps in reasonable time we had to decrease the number of communities by choosing a higher k and w^* parameter ($k = 4$ and $w^* = 1.0$), and keeping only the communities having a size larger or equal to $s = 6$. Therefore, in the end the ratio of nodes contained in at least one community was reduced to 11%. However, this still means more than 400,000 customers in the communities on average, providing a representative sampling of the system. By lowering the k to $k = 3$, the fraction of nodes included in the communities is raised to 43%. Furthermore, a significant number of additional nodes can be also classified into the discovered communities. For example, if a node not yet classified has link(s) only to a single community (and, if it has no links connecting to nodes in any other community) it can be safely added to that community. Carrying out this process iteratively, the fraction of nodes that can be classified into communities increases to 72% for the k = 3 co-authorship network, and to 72% (61%) for the k = 3 (k = 4) mobile phone network, which, in principle, allows us to classify over 2.4 million users into communities.

Another important statistics describing the community system is the community size distribution. In Fig. 2.12a we show the community size distribution in the phone-call network at different time steps. They all resemble to a power-law with a high exponent. In case of $t = 0$, the largest communities are somewhat smaller than in the later time steps. This is due to the fact that the events before the actual time step cannot contribute to the link-weights in case of $t = 0$, whereas they can if $t > 0$. In Fig. 2.12b we can follow the time evolution of the community size distribution in the co-authorship network. In this case $t = 0$ corresponds to the birth of the system itself as well (whereas in case of the phone-calls it does not), therefore the network

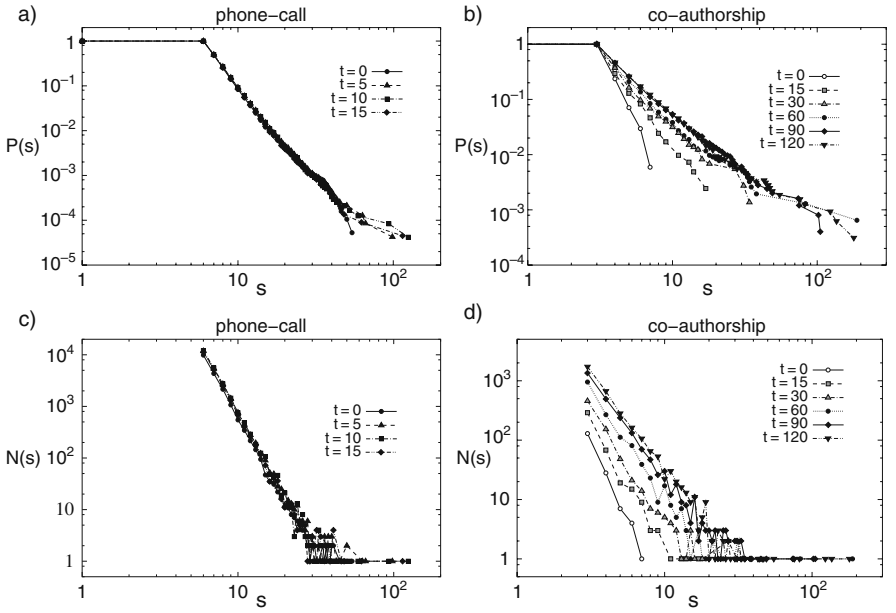

Fig. 2.12 (**a**) The cumulative community size distribution in the phone-call network at different time steps. (**b**) The time evolution of the cumulative community size distribution in the co-authorship network. (**c**) The number of communities of a given size at different time steps in the phone-call network. (**d**) The time evolution of the number of communities with a given size in the co-authorship network. Figure from [55]

and the communities in the network are small in the first few time steps. Later on, the system is enlarged, and the community size distribution is stabilised close to a power-law. In Fig. 2.12c, d we show the number of communities as a function of the community size at different time steps in the examined systems. For the phone-call network (Fig. 2.12c), this distribution is more or less constant in time. In contrast, (due to the growth of the underlying network) we can see an overall growth in the number of communities with time in the co-authorship network (Fig. 2.12d). Since the number of communities drops down to only a few at large community sizes in both systems, we used size binning when calculating the statistics shown in Figs. 2.13, 2.14, and 2.17.

As for evolving communities, we first consider two basic quantities characterising a community: its size s and its age τ, representing the time passed since its birth. s and τ are positively correlated: larger communities are on average older (Fig. 2.13a), which is quite natural, as communities are usually born small, and it takes time to recruit new members to reach a large size.

Next we used the auto-correlation function, $C(t)$, to quantify the relative overlap between two states of the same community $A(t)$ at t time steps apart:

$$C_A(t) \equiv \frac{|A(t_0) \cap A(t_0 + t)|}{|A(t_0) \cup A(t_0 + t)|}, \tag{2.7}$$

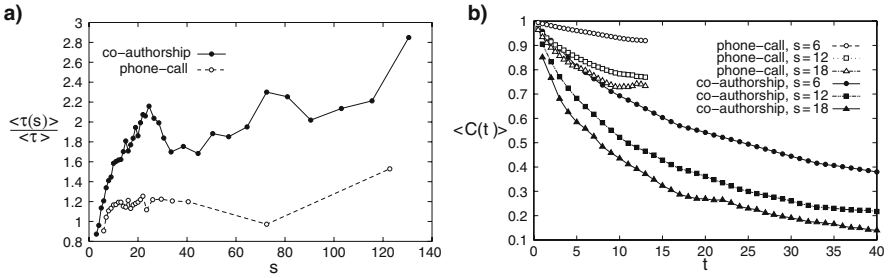

Fig. 2.13 (**a**) The average age τ of communities with a given size (number of people) s, divided by the average age of all communities $\langle\tau\rangle$, as the function of s, indicating that larger communities are on average older. (**b**) The average auto-correlation function $C(t)$ of communities with different sizes (the unit of time, t, is one month). The $C(t)$ of larger communities decays faster. Figure from [52]

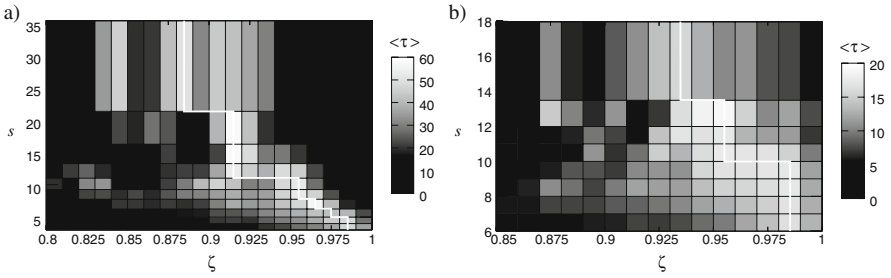

Fig. 2.14 (**a**) The average life-span $\langle\tau^*\rangle$ of the communities as the function of the stationarity ζ and the community size s for the co-authorship network. The peak in $\langle\tau^*\rangle$ is close to $\zeta = 1$ for small sizes, whereas it is shifted towards lower ζ values for large sizes. (**b**) Similar results found in the phone-call network. Figure from [52]

where $|A(t_0) \cap A(t_0 + t)|$ is the number of common nodes (members) in $A(t_0)$ and $A(t_0 + t)$, and $|A(t_0) \cup A(t_0 + t)|$ is the number of nodes in the union of $A(t_0)$ and $A(t_0 + t)$. Figure 2.13b shows the average time dependent auto-correlation function for communities born with different sizes. We find that in both networks, the auto-correlation function decays faster for the larger communities, indicating that the membership of the larger communities is changing at a higher rate. On the contrary, small communities change at a smaller rate, their composition being more or less static.

2.5.2 Stationarity and Lifetime

According to the results of Sect.2.5.1 a difference can be observed in the versatility of small and large communities. To quantify this aspect of community evolution, we define the *stationarity* ζ of a community as the average correlation between subsequent states:

$$\zeta \equiv \frac{\sum_{t=t_0}^{t_{\max}-1} C(t, t+1)}{t_{\max} - t_0 - 1}, \tag{2.8}$$

where t_0 denotes the birth of the community, and $t_{\max}$ is the last step before the extinction of the community. In other words, $1 - \zeta$ represents the average ratio of members changed in one step; larger ζ corresponds to smaller change (more stationary membership).

We observe a very interesting effect when we investigate the relationship between the lifetime τ^* (the number of steps between the birth and disintegration of a community), the stationarity and the community size. The lifetime can be viewed as a simple measure of "fitness": communities having higher fitness have an extended life, while the ones with small fitness quickly disintegrate, or are swallowed by another community. In Fig. 2.14a, b we show the average life-span $\langle \tau^* \rangle$ as a function of the stationarity ζ and the community size s (both s and ζ were binned). In both networks, for small community sizes the highest average life-span is at a stationarity value very close to one, indicating that for small communities it is optimal to have static, time independent membership. On the other hand, the peak in $\langle \tau^* \rangle$ is shifted towards low ζ values for large communities, suggesting that for these the optimal regime is to be dynamic, i.e., a continually changing membership. In fact, large communities with a ζ value equal to the optimal ζ for small communities have a very short life, and similarly, small communities with a low ζ (being optimal at large sizes) are disappearing quickly as well.

To illustrate the difference in the optimal behaviour (a pattern of membership dynamics leading to extended lifetime) of small and large communities, in Fig. 2.15. we show the time evolution of four communities from the co-authorship network. As Fig. 2.15. indicates, a typical small and stationary community undergoes minor changes, but lives for a long time. This is well illustrated by the snapshots of the community structure, showing that the community's stability is conferred by a core of three individuals representing a collaborative group spanning over 52 months. While new co-authors are added occasionally to the group, they come and go. In contrast, a small community with high turnover of its members, (several members abandon the community at the second time step, followed by three new members joining in at time step three) has a lifetime of nine time steps only (Fig. 2.15b). The opposite is seen for large communities: a large stationary community disintegrates after four time steps (Fig. 2.15c). In contrast, a large non-stationary community whose members change dynamically, resulting in significant fluctuations in both size and the composition, has quite extended lifetime (Fig. 2.15d). Indeed, while the community undergoes dramatic changes, gaining (Fig. 2.15e) or loosing a high fraction of its membership, it can easily withstand these changes.

2.5.3 Predicting Community Break Up

The quite different stability rules followed by the small and large communities raise an important question: could an inspection of the community itself predict its future?

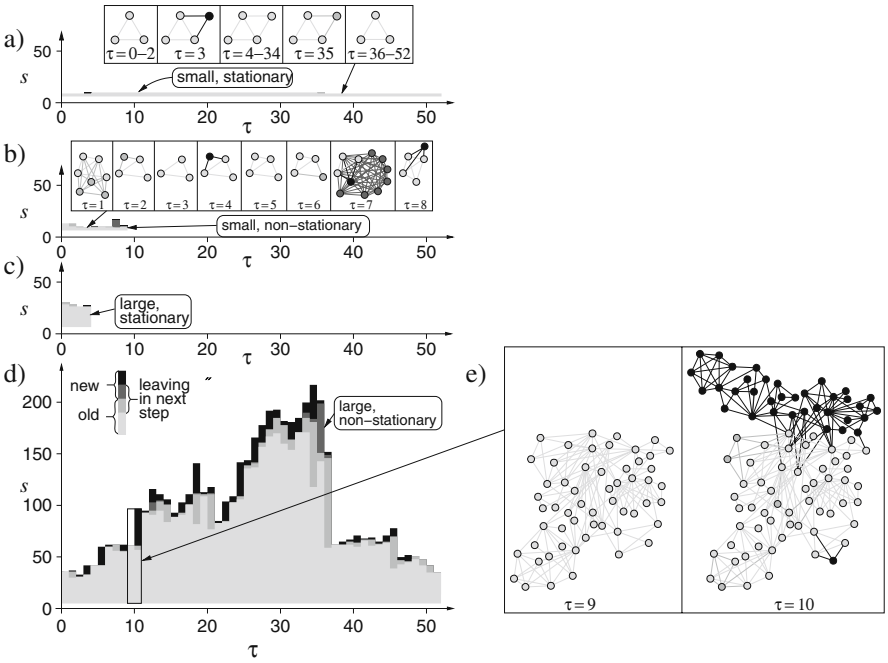

Fig. 2.15 Time evolution of four communities in the co-authorship network. The height of the columns corresponds to the actual community size, and within one column the *light gray colour* indicates the number of "old" nodes (that have been present in the community at least in the previous time step as well), while newcomers are shown with *black*. The members abandoning the community in the next time step are shown with *mid gray colours*, the shade depending on whether they are old or new. (This latter type of member joins the community for only one time step). From *top to bottom*, we show a small and stationary community (**a**), a small and non-stationary community (**b**), a large and stationary community (**c**) and, finally, a large and non-stationary community (**d**). A mainly growing stage (two time steps) in the evolution of the latter community is detailed in panel (**e**). Figure from [52]

To address this question, for each member in a community we measured the total weight of this member's connections to outside of the community (w_{out}) as well as to members belonging to the same community (w_{in}). We then calculated the probability that the member will abandon the community as a function of the $w_{\text{out}}/(w_{\text{in}} + w_{\text{out}})$ ratio. As Fig. 2.16a shows, for both networks this probability increases monotonically, suggesting that if the relative commitment of a user is to individuals outside a given community is higher, then it is more likely that he/she will leave the community.

In parallel, the average time spent in the community by the nodes, $\langle \tau_{\text{n}} \rangle$, is a decreasing function of the above ratio (Fig. 2.16a inset). Individuals that are the most likely to stay are those that commit most of their time to community members, an effect that is particularly prominent for the phone network. As Fig. 2.16a shows, those with the least commitment have a quickly growing likelihood of leaving the community.

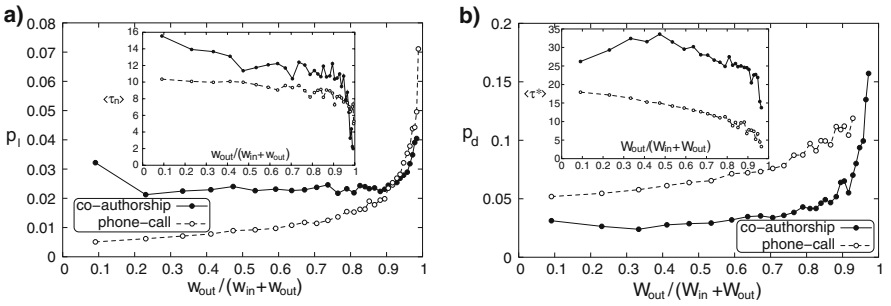

Fig. 2.16 (**a**) The probability p_ℓ for a member to abandon its community in the next step as a function of the ratio of its aggregated link weights to other parts of the network (w_{out}) and its total aggregated link weight ($w_{\text{in}} + w_{\text{out}}$). The *inset* shows the average time spent in the community by the nodes, $\langle \tau_{\text{n}} \rangle$, in function of $w_{\text{out}}/(w_{\text{in}} + w_{\text{out}})$. (**b**) The probability p_{d} for a community to disintegrate in the next step in function of the ratio of the aggregated weights of links from the community to other parts of the network (W_{out}) and the aggregated weights of all links starting from the community ($W_{\text{in}} + W_{\text{out}}$). The *inset* shows the average life time $\langle \tau^* \rangle$ of communities as a function of $W_{\text{out}}/(W_{\text{in}} + W_{\text{out}})$. Figure from [52]

Taking this idea from individuals to communities, we measured for each community the total weight of links (a measure of how much a member is committed) from the members to others, outside of the community (W_{out}), as well as the aggregated link weight inside the community (W_{in}). We find that the probability for a community to disintegrate in the next step increases as a function of $W_{\text{out}}/(W_{\text{in}} + W_{\text{out}})$ (Fig. 2.16b), and the lifetime of a community decreases with the $W_{\text{out}}/(W_{\text{in}} + W_{\text{out}})$ ratio (Fig. 2.16b inset). This indicates that self-focused communities have a significantly longer lifetime than those that are open to the outside world. However, an interesting observation is that, while the lifetime of the phone-call communities for moderate levels is relatively insensitive to outside commitments, the lifetime of the collaboration communities possesses a maximum at intermediate levels of inter-collaborations (collaboration between colleagues who belong to different communities). These results suggest that a tracking of the individual's as well as the community's relative commitment to the other members of the community provides a clue for predicting the community's fate.

2.5.4 Merging of Communities

Finally, we investigate a special aspect of the merging process between communities. During such event, a pair (or a larger group) of initially distinct communities join together and form a single community. A very interesting question connected to this is that can we find a simple relation between the size of a community and the likelihood that it will take part in such process?

To investigate this issue we carried out measurements similar to those in [56] and presented in Sect. 2.3.2.1. The basic idea is that if the merging process is uniform

with respect to the size of the communities s, then communities with a given s are chosen at a rate given by the size distribution of the available communities. However, if the merging mechanism prefers large (or small) sizes, then communities with large (or small) s are chosen with a higher rate compared to the size distribution of the available communities. To monitor this enhancement we used the indicator function, defined in Eq. (2.2), substituting the $\rho = (s_1, s_2)$ size-pair object. At each time step t the cumulative size-pair distribution $P_t(s_1, s_2)$ was recorded. Simultaneously, the un-normalised cumulative size-pair distribution of the communities merging between t and $t+1$ was constructed; we shall denote this distribution by $w_{t\to t+1}(s_1, s_2)$. The value of this rate-like variable $w_{t\to t+1}(s_1^*, s_2^*)$ at a given value of s_1^* and s_2^* is equal to the number of pairs of communities that merged between t and $t+1$ and had sizes $s_1 > s_1^*$ and $s_2 > s_2^*$. Here the resulting indicator function

$$W(s_1, s_2) \equiv \sum_{t=0}^{t_{\max}-1} \frac{w_{t\to t+1}(s_1, s_2)}{P_t(s_1, s_2)} \tag{2.9}$$

is defined on a two dimensional plane. When the merging process is uniform with respect to the community size the $W(s_1, s_2)$ becomes a flat function: on average we see pairs of communities merging with sizes s_1 and s_2 at a rate equal to the probability of finding a pair of communities of these sizes. However, if the merging process prefers large (or small) communities, than pairs with large (or small) sizes merge at a higher rate than the probability of finding such pairs, and $W(s_1, s_2)$ becomes increasing (or decreasing) with the size.

The reason for using un-normalised $w_{t\to t+1}(s_1, s_2)$ distributions is that in this way each merging event contributes to $W(s_1, s_2)$ with equal weight, and the time steps with a lot of merging events count more than those with only a few events. In the opposite case (when $w_{t\to t+1}(s_1, s_2)$ is normalised for each pairs of subsequent time steps $t, t+1$), the merging events occurring between time steps with a lot of other merging events are suppressed compared to the events with only a few other parallel events, as each pairs of consecutive time steps $t, t+1$ contribute to the $W(s_1, s_2)$ function with equal weights. This difference between normalised and un-normalised $w_{t\to t+1}(s_1, s_2)$ becomes important in case of the co-authorship network, where in the beginning the system is small and merging is rare, and later on as the system is developing, merging between communities becomes a regular event.

In Fig. 2.17. we show $W(s_1, s_2)$ for both networks, and the picture suggests that large sizes are preferred in the merging process. This is consistent with our findings that the content of large communities is changing at a faster rate compared to the small ones. Swallowing other communities is an efficient way to bring numerous new members into the community in just one step, therefore taking part in merging is beneficial for large communities following a survival strategy based on constantly changing their members.

Another interesting aspect of the results shown in Fig. 2.17. is that they are analogous to the attachment mechanism of links between already existing nodes in collaboration networks [5]: the probability for a new link to appear between two

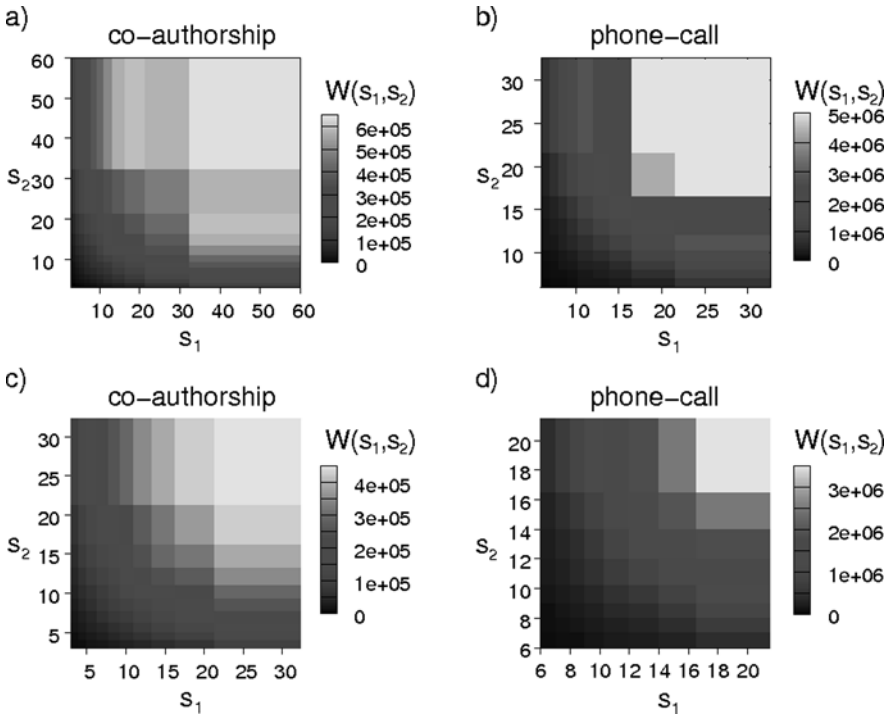

Fig. 2.17 The merging of communities. (**a**) the $W(s_1, s_2)$ function for the co-authorship network, (**b**) the $W(s_1, s_2)$ function for the phone-call network, (**c**) the region with smaller $W(s_1, s_2)$ in (**a**) enlarged, (**d**) the region with smaller $W(s_1, s_2)$ in (**b**) enlarged. Figure from the Suppl. of [52]

nodes with degree d_1 and d_2 is roughly proportional to $d_1 \times d_2$. Similarly, the probability that two communities of sizes s_1 and s_2 will merge is proportional to $s_1 \times s_2$, therefore the large communities attract each other in a similar manner to hubs in collaboration networks.

2.6 Conclusion

In this chapter we investigated the statistical properties of community dynamics in two large social networks. Due to the frequent changes in the communication/collaboration patterns between individuals, the communities corresponding to groups of mobile phone users or collaborating scientists are under constant evolution. In case of a simple growing scenario, we found that similar processes control the development of the system at different levels in the hierarchy, as the growth of the communities, the development of the community graph and the growth of the underlying network are all driven by preferential attachment.

When deletion of the links is taken into account as well, the picture gets more complex. In order to be able to track the intricate merging, splitting, growth, decay,

etc. of the investigated social groups, we developed an algorithm based on the CPM for matching the communities extracted at subsequent time steps. According to our results, a significant difference can be observed between smaller collaborative or friendship circles and institutions when subjected to the processes above. At the heart of small cliques are a few strong relationships, and as long as these persist, the community around them is stable. In other words, small groups can persist for a long time if their membership is constant. It appears to be almost impossible to maintain this strategy for large communities, however. Thus we find that the condition for stability for large communities is continuous changes in their membership, allowing for the possibility that after some time practically all members are exchanged. Such loose, rapidly changing communities are reminiscent of institutions, that can continue to exist even after all members have been replaced by new members. For example, in a few years most members of a school or a company could change, yet the school and the company will be detectable as a distinct community at any time step during its existence.

We also showed that the knowledge of the time commitment of the members to a given community can be used for predicting the community's lifetime. Furthermore, we found that the likelihood of merging between communities is increasing with the community size. These findings offer a new view on the fundamental differences between the dynamics of small groups and large institutions.

References

1. Aiello, W., Chung, F., Lu, L.: A random graph model for massive graphs. In: Proc. 32nd ACM Symp. on the Theory Comput., pp. 171–180, ACM, New York (2000)
2. Albert, R., Barabási, A.L.: Statistical mechanics of complex networks. Rev. Mod. Phys. **74**, 47–97 (2002)
3. Antonov, A.V., Mewes, H.W.: Complex functionality of gene groups identified from high-throughput data. J. Mol. Biol. **363(1)**, 289–296 (2006)
4. Barabási, A.L., Albert, R.: Emergence of scaling in random networks. Science **286**, 509–512 (1999)
5. Barabási, A.L., Jeong, H., Néda, Z., Ravasz, E., Schubert, A., Vicsek, T.: Evolution of the social network of scientific collaborations. Physica A **311**, 590–614 (2002)
6. Batagelj, V., Zaveršnik, M.: Short cycle connectivity. Discrete Math. **307**, 310–318 (2007)
7. Baumes, J., Goldberg, M., Magdon-Ismail, M.: Efficient identification of overlapping communities. Lect. Notes Comput. Sci. **3495**, 27–36 (2005)
8. Csermely, P.: Weak Links. Springer Verlag, Heidelberg, Germany (2006)
9. Derényi, I., Palla, G., Vicsek, T.: Clique percolation in random networks. Phys. Rev. Lett. **94**, 160202 (2005)
10. Dodds, P.S., Muhamad, R., Watts, D.J.: An experimental study of search in global social networks. Science **301**, 827–829 (2003)
11. Ebel, H., Davidsen, J., Bornholdt, S.: Dynamics of social networks. Complexity **8**, 24–27 (2002)
12. Ebel, H., Mielsch, L.I., Bornholdt, S.: Scale-free topology of e-mail networks. Phys. Rev. E **66**, 35103(R) (2002)
13. Eckmann, J.P., Moses, E., Sergi, D.: Entropy of dialogues creates coherent structures in e-mail traffic. Proc. Natl. Acad. Sci. USA **101**, 14333–14337 (2004)
14. Everett, M.G., Borgatti, S.P.: Analyzing clique overlap. Connections **21**, 49–61 (1998)

15. Everitt, B.S.: Cluster Analysis, 3th edn. Edward Arnold, London (1993)
16. Farkas, I.J., Ábel, D., Palla, G., Vicsek, T.: Weighted network modules. New J. Phys. **9**, 180 (2007)
17. Fortunato, S., Barthelemy, M.: Resolution limit in community detection. Proc. Natl. Acad. Sci. USA **104**, 36–41 (2007)
18. Gfeler, D., Chappelier, J.C., Rios, P.D.L.: Finding instabilities in the community structure of complex networks. Phys. Rev. E **72**, 056135 (2005)
19. Girvan, M., Newman, M.E.J.: Community structure in social and biological networks. Proc. Natl. Acad. Sci. USA **99**, 7821–7826 (2002)
20. Granovetter, M.: Decision Making: Alternatives to Rational Choice Models Economic Action and Social Structure: The Problem of Embeddedness. SAGE, Newbury Park, CA (1992)
21. Granovetter, M.S.: The strength of weak ties. Am. J. Sociol. **78**, 1360–1380 (1973)
22. Grossman, J.W.: The evolution of the mathematical research collaboration graph. Congressus Numerantium **158**, 202–212 (2002)
23. Grossman, J.W., Ion, P.D.F.: On a Portion of the well-known collaboration graph. Congressus Numerantium **108**, 129–131 (1995)
24. Guimerà, R., Amaral, L.A.N.: Functional cartography of complex metabolic networks. Nature **433**, 895–900 (2005)
25. Guimerá, R., Danon, L., Diaz-Guilera, A., Giralt, F., Arenas, A.: Self-similar community structure in organisations. Phys. Rev. E **68**, 065103 (2003)
26. Guimerà, R., Mossa, S., Turtschi, A., Amaral, L.A.N.: The worldwide air transportation network: Anomalous centrality, community structure, and cities' global roles. Proc. Natl. Acad. Sci. USA **102**, 7794–7799 (2005)
27. Guimerà, R., Sales-Pardo, M., Amaral, L.A.N.: Module identification in bipartite and directed networks. Phys. Rev. E **76**, 036102 (2007)
28. Guimerá, R., Uzzi, B., Spiro, J., Amaral, L.A.N.: Team assembly mechanisms determine collaboration network structure and team performance. Science **308**, 697–702 (2005)
29. Guldener, U., Munsterkotter, M., Kastenmuller, G., Strack, N., van Helden, J.: CYGD: The comprehensive yeast genome database. Nucl. Acad. Res. **33**, D364–D368 (2005)
30. Heimo, T., Saramäki, J., Onnela, J.P., Kaski, K.: Spectral and network methods in the analysis of correlation matrices of stock returns. Physica A-Statist. Mech. Appl. **383**, 147–151 (2007)
31. Holme, P., Edling, C.R., Liljeros, F.: Structure and time-evolution of an internet dating community. Soc. Networks **26**, 155–174 (2004)
32. Hopcroft, J., Khan, O., Kulis, B., Selman, B.: Tracking evolving communities in large linked networks. Proc. Natl. Acad. Sci. USA **101**, 5249–5253 (2004)
33. Knudsen, S.: A Guide to Analysis of DNA Microarray Data, 2nd edn. Wiley-Liss, New York (2004)
34. Kossinets, G., Watts, D.J.: Empirical analysis of an evolving social network. Science **311**, 88–90 (2006)
35. Krogan, N.J., Cagney, G., Yu, H.Y., Zhong, G.Q., Guo, X.H., Ignatchenko, A., Li, J., Pu, S.Y., Datta, N., Tikuisis, A.P., Punna, T., Peregrin-Alvarez, J.M., Shales, M., Zhang, X., Davey, M., Robinson, M.D., Paccanaro, A., Bray, J.E., Sheung, A., Beattie, B., Richards, D.P., Canadien, V., Lalev, A., Mena, F., Wong, P., Starostine, A., Canete, M.M., Vlasblom, J., Orsi, S.W.C., Collins, S.R., Chandran, S., Haw, R., Rilstone, J.J., Gandi, K., Thompson, N.J., Musso, G., Onge, P.S., Ghanny, S., Lam, M.H.Y., Butland, G., Altaf-Ui, A.M., Kanaya, S., Shilatifard, A., O'Shea, E., Weissman, J.S., Ingles, C.J., Hughes, T.R., Parkinson, J., Gerstein, M., Wodak, S.J., Emili, A., Greenblatt, J.F.: Global landscape of protein complexes in the yeast Saccharomyces cerevisiae. Nature **440**, 637–643 (2006)
36. Kumpula, J.M., Saramäki, J., Kaski, K., Kertész, J.: Limited resolution in complex network community detection with Potts model approach. Eur. Phys. J. B **56**, 41–45 (2007)
37. Li, C., Maini, P.K.: An evolving network model with community structure. J. Phys. A: Math. Gen. **38**, 9741–9749 (2005)

38. Liljeros, F., Edling, C.R., Amaral, L.A.N., Stanley, H.E., Aberg, Y.: The web of human sexual contacts. Nature **411**, 907–908 (2001)
39. Mendes, J.F.F., Dorogovtsev, S.N.: Evolution of networks: From biological nets to the Internet and WWW. Oxford University Press, Oxford (2003)
40. Nepusz, T., Petróczi, A., Négyessy, L., Bazsó, F.: Fuzzy communities and the concept of bridgeness in complex networks. Phys. Rev. E **77**, 016107 (2008)
41. Newman, M.E.J.: Phys. Rev. E **64**, 025102 (2001)
42. Newman, M.E.J.: From the cover: The structure of scientific collaboration networks. Proc. Natl. Acad. Sci. USA **98**, 404–409 (2001)
43. Newman, M.E.J.: Detecting community structure in networks. Eur. Phys. J. B **38**, 321–330 (2004)
44. Newman, M.E.J.: Fast algorithm for detecting community structure in networks. Phys. Rev. E **69**, 066133 (2004)
45. Newman, M.E.J., Girvan, M.: Finding and evaluating community structure in networks. Phys. Rev. E **69**, 026113 (2004)
46. Newman, M.E.J., Leicht, E.A.: Mixture models and exploratory analysis in networks. Proc. Natl. Acad. Sci. USA **104**, 9564–9569 (2007)
47. Newman, M.E.J., Park, J.: Why social networks are different from other types of networks. Phys. Rev. E **68**, 036122 (2003)
48. Noh, J.D., Jeong, H.C., Ahn, Y.Y., Jeong, H.: Growing network model for community with group structure. Phys. Rev. E **71**, 036131 (2005)
49. Onnela, J.P., Chakraborti, A., Kaski, K., Kertész, J., Kanto, A.: Dynamics of market correlations: Taxonomy and portfolio analysis. Phys. Rev. E **68**, 056110 (2003)
50. Onnela, J.P., Saramäki, J., Hyvönen, J., Szabó, G., Lazer, D., Kaski, K., Kertész, J., Barabási, A.L.: Structure and tie strengths in mobile communication networks. Proc. Natl. Acad. Sci. USA **104**, 7332–7336 (2007)
51. Onnela, J.P., Saramäki, J., Hyvönen, J., Szabó, G., de Menezes, M.A., Kaski, K., Barabási, A.L., Kertész, J.: Analysis of a large-scale weighted network of one-to-one human communication. New J. Phys. **9**, 179 (2007)
52. Palla, G., Barabási, A.L., Vicsek, T.: Quantifying social group evolution. Nature **446**, 664–667 (2007)
53. Palla, G., Derényi, I., Farkas, I., Vicsek, T.: Uncovering the overlapping community structure of complex networks in nature and society. Nature **435**, 814–818 (2005)
54. Palla, G., Farkas, I.J., Pollner, P., Derényi, I., Vicsek, T.: Directed network modules. New J. Phys. **9**, 186 (2007)
55. Palla, G., Vicsek, T., Barabási, A.L.: Community dynamics in social networks. Fluctuation and Noise Letters **7**, L273–L287 (2007)
56. Pollner, P., Palla, G., Vicsek, T.: Preferential attachment of communities: The same principle, but a higher level. Europhys. Lett. **73**, 478–484 (2006)
57. Radicchi, F., Castellano, C., Cecconi, F., Loreto, V., parisi, D.: Defining and identifying communities in networks. Proc. Natl. Acad. Sci. USA **101**, 2658–2663 (2004)
58. Ramasco, J.J., Morris, S.A.: Social inertia in collaboration networks. Phys. Rev. E **73**, 016122 (2006)
59. Ravasz, E., Somera, A.L., Mongru, D.A., Oltvai, Z.N., Barabási, A.L.: Hierarchical organization of modularity in metabolic networks. Science **297**, 1551–1555 (2002)
60. Reichardt, J., Bornholdt, S.: Detecting fuzzy community structures in complex networks with a Potts Model. Phys. Rev. Lett. **93**, 218701 (2004)
61. Reichardt, J., Bornholdt, S.: Statistical mechanics of community detection. Phys. Rev. E **74**, 016110 (2006)
62. Rives, A.W., Galitski, T.: Modular organization of cellular networks. Proc. Natl. Acad. Sci. USA **100**, 1128–1133 (2003)
63. Scott, J.: Social Network Analysis: A Handbook, 2nd edn. Sage Publications, London (2000)

64. Shiffrin, R.M., Börner, K.: Mapping knowledge domains. Proc. Natl. Acad. Sci. USA **101**, 5183–5185 (2004)
65. Spirin, V., Mirny, K.A.: Protein complexes and functional modules in molecular networks. Proc. Natl. Acad. Sci. USA **100**, 12123–12128 (2003)
66. Szabó, G., Fáth, G.: Evolutionary games on graphs. Phys. Rep.-Rev. Section Phys. Lett. **446**, 97–216 (2007)
67. Szabó, G., Vukov, J., Szolnoki, A.: Phase diagrams for an evolutionary prisoner's dilemma game on two-dimensional lattices. Phys. Rev. E **72**, 047107 (2005)
68. Vicsek, T.: Phase transitions and overlapping modules in complex networks. Physica A-Statist. Mech. Appl. **378**, 20–32 (2007)
69. Vukov, J., Szabó, G., Szolnoki, A.: Cooperation in the noisy case: Prisoner's dilemma game on two types of regular random graphs. Phys. Rev. E **73**, 067103 (2006)
70. Wagner, C.S., Leydesdorff, L.: Network structure, self-organization, and the growth of international collaboration in science. Res. Policy **34**, 1608–1618 (2005)
71. Warner, S.: E-prints and the open archives initiative. Library Hi Tech **21**, 151–158 (2003)
72. Wasserman, S., Faust, K.: Social network analysis: methods and applications structural analysis in the social sciences. Cambridge University Press, Cambridge (1994)
73. Watts, D.J.: A twenty-first century science. Nature **445**, 489 (2007)
74. Watts, D.J., Dodds, P.S., Newman, M.E.J.: Identity and search in social networks. Science **296**, 1302–1305 (2002)
75. Watts, D.J., Strogatz, S.H.: Collective dynamics of 'small-world' networks. Nature **393**, 440–442 (1998)
76. White, H.C., Boorman, S.A., Breiger, R.R.: Social structure from multiple networks. I. Blockmodels of roles and positions. Am. J. Sociol. **81**, 730–780 (1976)
77. Wilkinson, D.M., Huberman, B.A.: A method for finding communities of related genes. Proc. Natl. Acad. Sci. USA **101**, 5241–5248 (2004)
78. Yeung, Y.Y., Liu, T.C.Y., Ng, P.H.: A social network analysis of research collaboration in physics education. Am. J. Phys. **73**, 145–150 (2005)
79. Zhang, S., Wang, R.S., Zhang, X.S.: Uncovering fuzzy community structure in complex networks. Phys. Rev. E **76**, 046103 (2007)

Chapter 3
Time-Dependent Complex Networks: Dynamic Centrality, Dynamic Motifs, and Cycles of Social Interactions

Dan Braha and Yaneer Bar-Yam

Abstract We develop a new approach to the study of the dynamics of link utilization in complex networks using data of empirical social networks. Counter to the perspective that nodes have particular roles, we find roles change dramatically from day to day. "Local hubs" have a power law degree distribution over time, with no characteristic degree value. We further study the dynamics of local motif structure in time-dependent networks, and find recurrent patterns that might provide empirical evidence for cycles of social interaction. Our results imply a significant reinterpretation of the concept of node centrality and network local structure in complex networks, and among other conclusions suggest that interventions targeting hubs will have significantly less effect than previously thought.

3.1 Dynamic Centrality in Large-Scale Communication Networks

Recent advances have demonstrated that the study of universal properties in physical systems may be extended to complex networks in biological and social systems [1–6]. This has opened the study of such networks to experimental and theoretical characterization of properties and mechanisms of formation. In this chapter we extend the study of complex networks by considering the dynamics of the activity of network connections. Our analysis suggests that fundamentally new insights can be obtained from the dynamical behavior, including a dramatic time dependence of the role of nodes that is not apparent from static (time aggregated) analysis of node connectivity and network topology.

We study the communication between 57,158 e-mail users based on data sampled over a period of 113 days from log files maintained by the email server at a

D. Braha (✉)
University of Massachusetts, Dartmouth, MA 02747, USA; New England Complex Systems Institute, Cambridge, MA 02138, USA
e-mail: braha@necsi.edu

This chapter is an extension of D. Braha and Y. Bar-Yam, "From Centrality to Temporary Fame: Dynamic Centrality in Complex Networks," Complexity, Vol. 12 (2), November/December 2006.

T. Gross, H. Sayama (eds.), *Adaptive Networks,* Understanding Complex Systems,
DOI 10.1007/978-3-642-01284-6_3,

large university [7]. The time when an e-mail link is established between any pair of email addresses is routinely registered in a server, enabling the analysis of the temporal dynamics of the interactions within the network. To consider only emails that reflect the flow of valuable information, spam and bulk mailings were excluded using a prefilter. There were 447,543 messages exchanged by the users during 113 days observation. We report results obtained by treating the communications as an undirected network, where email addresses are regarded as nodes and two nodes are linked if there is an e-mail communication between them. Analysis based upon treating the network with asymmetric links (where a distinction is made between out-going links and incoming links) gave essentially equivalent results. From the temporal connectivity data, a time series of topological networks can be obtained; each represents an aggregation of links over a time scale that is short compared to the duration of observation (113 days). The edges forming each network in the time series thus represent the short time opportunity for communication as detected by the log files of the email server. Unless otherwise indicated, we set the time scale to one day, thus creating 113 consecutive daily networks.

Most studies of large social networks have accumulated data over the entire time of observation, whereas here using the smaller intervals of accumulation we can study how the network interactions change over time. Social network dynamics has historically been of interest, though data was limited [8, 9]. Recent papers have considered the times between communications [10] or the creation of temporally linked structures [11]. In this chapter we study for the first time the dynamics of individual importance and local structure (sub-graphs or motifs) in Dynamic Complex Networks [12].

Our first result is that networks obtained on different days are substantially different from each other. Figure 3.1 shows the correlation between corresponding edges of the 113 daily networks. Surprisingly, we find that all networks are weakly correlated, despite the expected routine nature of the social activity. Correlations between any two networks have a distribution that is approximately normal with a mean $\pm$ standard deviation of 0.15 ± 0.05 (we adopt this notation throughout). The low correlation implies that the existence of a link between two individuals at one time does not make it much more likely that the link will appear at another time. While all networks are weakly correlated, we find that workdays and weekends are more distinct, so that workday networks, and weekend networks are more correlated among themselves (correlations 0.17 ± 0.03 and 0.16 ± 0.05, respectively), than they are with each other (correlation 0.12 ± 0.02). Remarkably, the low correlations increase only very gradually if we form networks using data over multiple days, and never reach a high value even if networks are made from communications over a month or more (Fig. 3.1b).

Using the nodal "degree" (the number of nodes a particular node is connected to) we characterized the centrality of nodes in the daily networks. Each of the daily networks has a distribution of nodal degrees well described by a power-law [13], with exponents in the range . Thus a small number of highly connected nodes have great importance in the connectivity of the network. However, while each daily network has highly connected nodes, we found that they were not the same nodes. The degree of a node varied dramatically over time. For each identified "local hub," we

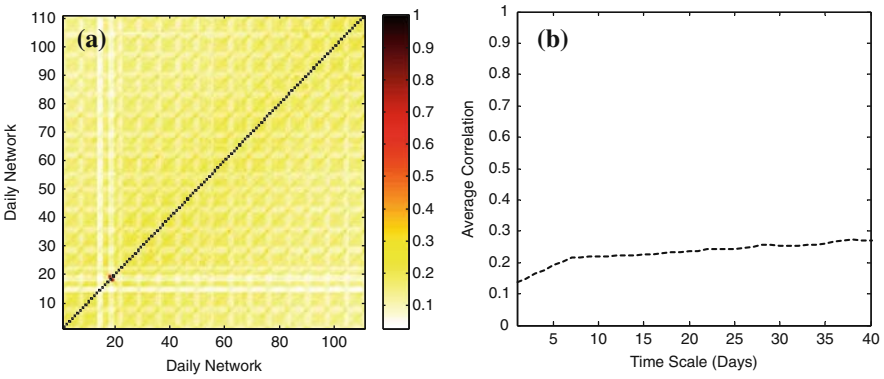

Fig. 3.1 **(a)** Matrix of correlations between pairs of daily networks sampled July 29th, 2001 (Sunday) to November 18th, 2001 (Sunday). Days 55 and 56 were excluded from further analysis due to lack of email communication. **(b)** Correlation between pairs of daily networks aggregated over times ranging from 1 to 40 days

measured its degree from day to day over the duration of observation. Surprisingly, we find that a large number of "local hubs" exhibit a highly fluctuating time-series (Fig. 3.2). The corresponding distribution of degrees over time itself follows a scale-free power-law distribution [13, 23] over two orders of magnitude (Fig. 3.2). The degree distribution of a hub over time implies that the node's degree does not have a characteristic value. The degree is small most of the time, but we only need to wait long enough to encounter degrees of any size.

A broader characterization of which nodes are important on a given day was made by comparing how the nodes were ranked in importance. We identified the top 1000 nodes, about 1.7% of the network according to their degree, for each of the daily networks. We then determined, for each pair of daily networks, the percentage of nodes that appear in both top-ranking lists ("centrality overlap," Fig. 3.3). The centrality overlap between any two networks is small, around 0.27 ± 0.06. When considering separately workday and weekend networks, the overlap values are around 0.33 ± 0.03 and 0.20 ± 0.04, respectively; consistent with the bimodal nature of the social activity. The distinctiveness of the top 1,000 nodes between daily networks is also typical for other top-ranking list sizes. By varying the percentage of nodes in the top-ranking list, it is found that the mean centrality overlap, which is already small for small percentages (0.3), actually decreases to a value of 0.2 at around 4%, before increasing slowly to 1 when the list includes all the nodes. The distributions of ranking overlaps are well behaved, having a standard deviation much smaller than the mean.

We compared daily networks with the aggregate network, as would be considered by other contemporary studies, by aggregating over the entire 113 day observation. Our previous results suggest, and direct analysis confirms, that daily networks deviate significantly from the aggregate network. We determined which nodes in the daily 1,000 top-ranking list also appear in the top-ranking list of the aggregate network, obtaining the binary image in Fig. 3.4a. Though some nodes that are ranked

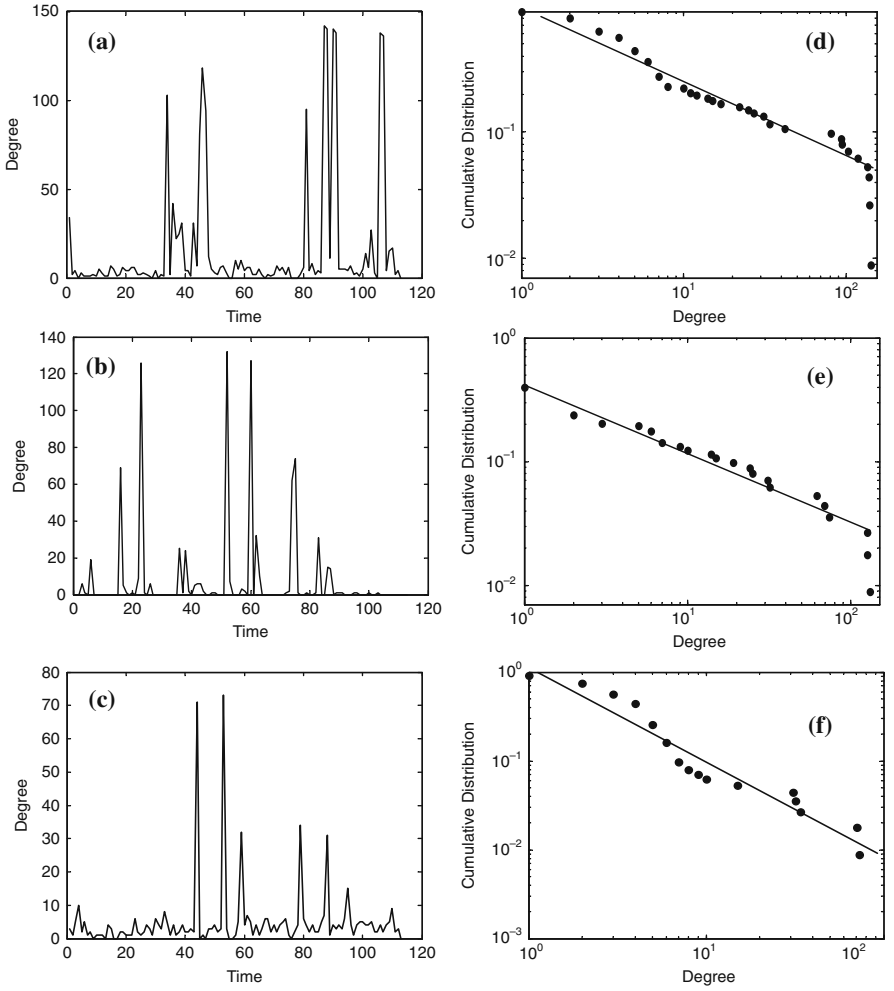

Fig. 3.2 Degree variations over time associated with the most connected node ("local hub") identified for a particular daily network. **(a–c)** Time series of degrees associated with nodes 724 (hub in day 34), 4,631 (hub in day 52), and 450 (hub in day 44), respectively. Small and very large node degrees are observed. **(d–f)** The corresponding log–log plots of the cumulative distributions of degrees over time associated with "local hubs" 724, 4,631, and 450, respectively. The distributions follow a power law ($p < 0.001$)

high in the daily networks are also ranked high in the aggregate network, a significant number are not. In particular, we find that the centrality overlap is 0.41 ± 0.03 and 0.27 ± 0.04, for weekday and weekends respectively. Comparing other sizes of the top ranked nodes gives similar results. Perhaps even more surprisingly, the nodes that are highly ranked in the aggregate network are not even *on-average* important in daily networks. To show this we calculated the average ranking position of the top 1,000 highly connected nodes in the aggregate network for each daily network.

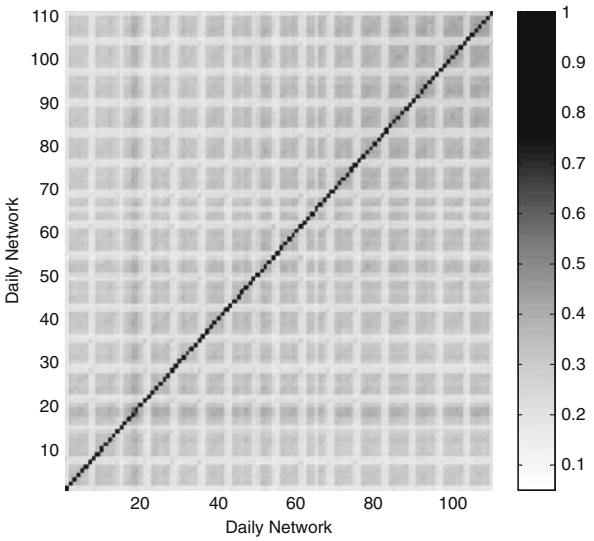

Fig. 3.3 Top-ranking list overlap between pairs of daily networks. For each pair of networks, the color code of the matrix denotes the percentage of nodes that appear in the 1,000 top-ranking list of the networks

The average ranking position over time (normalized to a fraction so that 1 is the highest and 0 is the lowest) exhibits a weekly oscillation from about 0.40 to 0.65. In the aggregate network these nodes have an average ranking of 0.99. This shows that highly connected nodes in the aggregate network only play a moderate role in the daily networks.

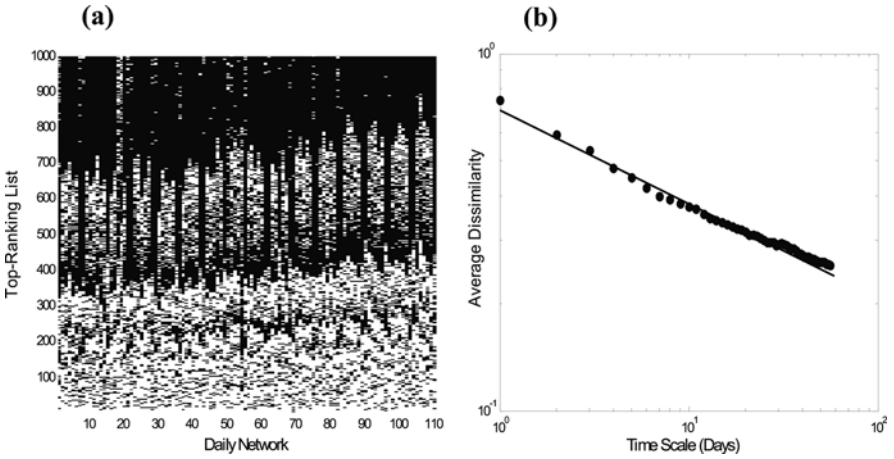

Fig. 3.4 **(a)** Comparison of the aggregate network with daily networks. A binary overlap matrix describing whether a node, included in the 1,000 top-ranking list of a daily network, also appear (*colored white*) in the 1,000 top-ranking list of the aggregate network. **(b)** Average dissimilarity of networks aggregated over times ranging from 1 to 56 days. Dissimilarity is measured as one minus the fractional overlap of the 1,000 top-ranking nodes. The plot follows a power law ($p < 0.001$) indicating that networks formed over longer time periods do not converge to a well-defined structure

Finally, we considered a full range of networks formed by aggregating links over time scales that are longer than a day and shorter than the full time period (Fig. 3.4b). Similar relationships between smaller and larger time scales to those found above are observed. Moreover, the similarity between networks at a particular time scale increases as a power-law, so there is no particular time scale at which a converged structure is achieved. Thus, the network dynamics follows a "multiscale" structure with networks at each scale forming scale-free topologies, but the specific links in existence vary dramatically between observation time scales as well as over time.

3.2 Dynamic Centrality in Spatial Proximity Social Networks

In addition to the e-mail network studied here, we have found similar results when analyzing social network data about interactions found from the spatial proximity of personal Bluetooth wireless devices, recording the interactions between pairs of students over the period of 31 days of October 2004 [12]. The spatial proximity network records dynamic interactions among 80 students who are socially related in some way (students in the same school or class), and thus reliably approximates social ties.

As before, we start our analysis by testing the association between the 31 temporal sequence of networks. We computed the Pearson's correlation coefficients as well as simple matching coefficients between corresponding edges of the 31 data networks. Consistent with the results previously reported in Sect. 3.1, we find that all networks are weakly correlated (see Fig. 3.5) despite the expected routine nature of the social activity. Despite the weak correlations, Fig. 3.5 suggests that neighboring workday networks tend to be more correlated than networks that are far apart in time. We also find that networks representing workday social interactions are significantly more correlated among themselves than they are with networks representing weekend social interactions, indicating a periodicity in the link dynamics. The relatively strong interactions among the workday networks over the fourth week suggest that unique patterns of social interactions might show up over time in response to both internal and external spikes ("external stimuli"). Overall, the above initial analysis implies that a static network analysis, which is based on aggregating the interaction data over all various time periods, will lose a lot of valuable information that is embedded in a dynamic social network.

While the identification of the "most important" nodes in networks has help to understand or predict the behavior of networked systems, it is based on the assumption that node centrality is a time-invariant property. We have demonstrated in Sect. 3.1 that, for a dynamic email network, centrality measures are time-dependent and might fluctuate over time. That is, a highly central node at one time point might be the least central in a different time point. In general, a node centrality index in a dynamic network may be better defined as a probability distribution over the total sampling time of the network. This is in contrast to static network, where node centrality index is a single measure. To illustrate the above argument in the context of the spatial proximity network, we computed the ranking of each node (student) according to its degree for each of the 31 data networks. Figure 3.6 shows that the

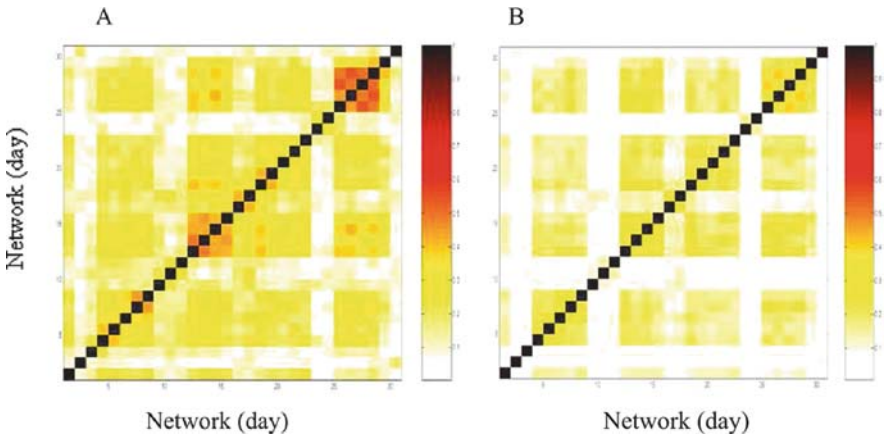

Fig. 3.5 Correlation profiles of the time-series networks sampled over 31 days. **(a)** The Pearson's correlation coefficient between corresponding links of the 31 temporal sequences of networks. **(b)** Correlation based on Jaccard's coefficient of similarity. The Jaccard's coefficient measures the degree of overlap between two networks by computing the ratio of the number of shared links to the number possessed by both networks. The color code of each matrix denotes the degree of correlation shown in the matrix

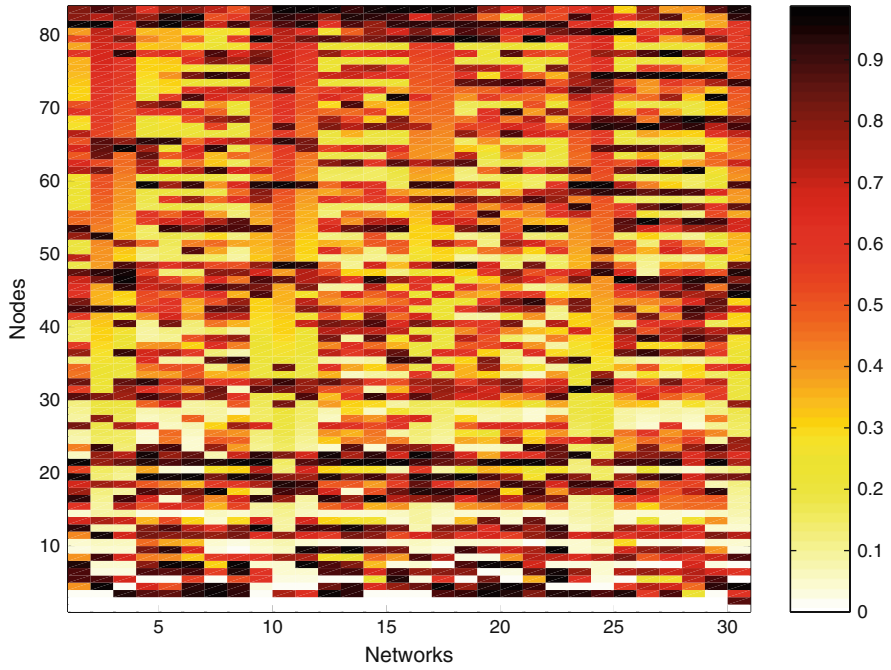

Fig. 3.6 Normalized degree ranking of each actor in each sampled network. The degree ranking is obtained by sorting actors in ascending order by their degree centrality measure. The normalized ranking centrality is the ranking position divided by the number of actors. The color code of the matrix denotes the degree of normalized degree ranking shown in the matrix

prominence of actors is "spread out" quite consistently over time suggesting that the prominence of actors embedded in a network is time-based.

3.3 Dynamic Network Motifs and Cycles of Social Interaction

We have found above that the time-series social networks are weakly correlated (Figs. 3.1 and 3.5). Notwithstanding the weak correlation, it is of interest to analyze and compare the local structure of the various temporal sequence of networks. It has been shown that many complex networks include some sub-graphs (motifs) that are significantly abundant as compared to randomized versions of the same networks, while others are strongly suppressed [14, 15]. The presence or absence of a given sub-graph presumably encapsulate information about the system-level function the network performs [14, 15]. Moreover, *a sub-graph significance profile* – a set of counts of the different kinds of sub-graphs that arise in a real-world network compared to randomized networks – serves as a distinctive signature of the network [14, 15]. For a dynamic network, the local structure is time-dependent and might evolve over time. Analyzing the time-based local structure might provide important information about the dynamics of system-level task and functionality.

We present in Fig. 3.7 the significance profiles of the 6 types of connected tetrads for the different time-series networks. Despite the overall similarity of significance

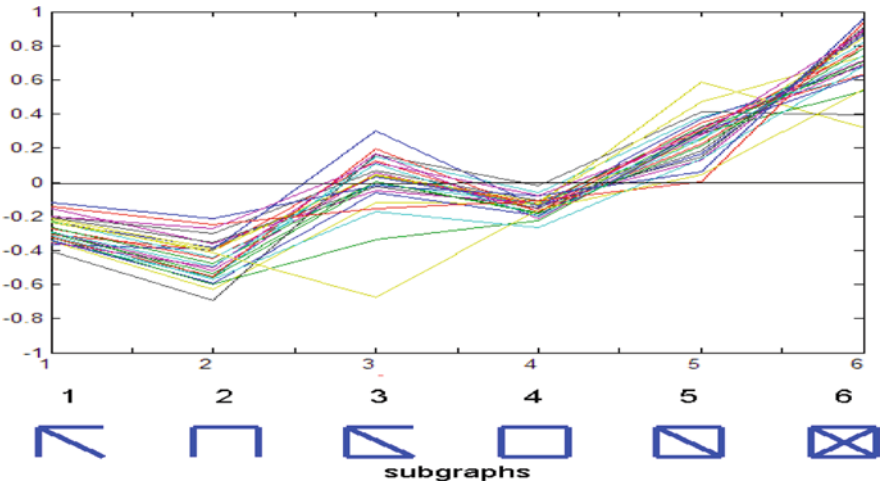

Fig. 3.7 The tetrad significance profile of networks for the different time-series networks. Continuous lines are drawn as guide to the eye. The tetrad significance profile shows the normalized significance level (Z score) for each of the 6 connected tetrads. Tetrad significance (Z score) is the difference between numbers of occurrence in the given network and in an ensemble of randomly rewired surrogate networks with the same degree sequence, divided by the standard deviation. The tetrad significance profile is the normalized vector of tetrad significances (see [14, 15] for details). The wide fluctuations of the network local structure reproduce the dynamic of social interaction at the system level

profiles, the figure indicates a fluctuation of the network local structure over time. To examine for possible cyclic behavior embedded in the time-series networks, we calculated the similarities between them by looking at the correlation between the significance profiles of the 6 types of connected tetrads for the different networks. Next, we applied an average-linkage hierarchical clustering algorithm [16] to the significance profile correlations (Fig. 3.8). Several families of networks – each includes networks separated by time intervals varying 2–20 days – with very similar significance profiles ($c > 0.995$) emerge from this analysis. The relation between the local structures of networks within tightly interconnected families is further visualized in Fig. 3.9, which presents the significance profiles of the 6 types of connected tetrads for several families of networks. The recurrent patterns of network local structure over time might provide empirical evidence for cycles of social interaction despite being only the aggregate of distinctive behaviors and preferences of individuals.

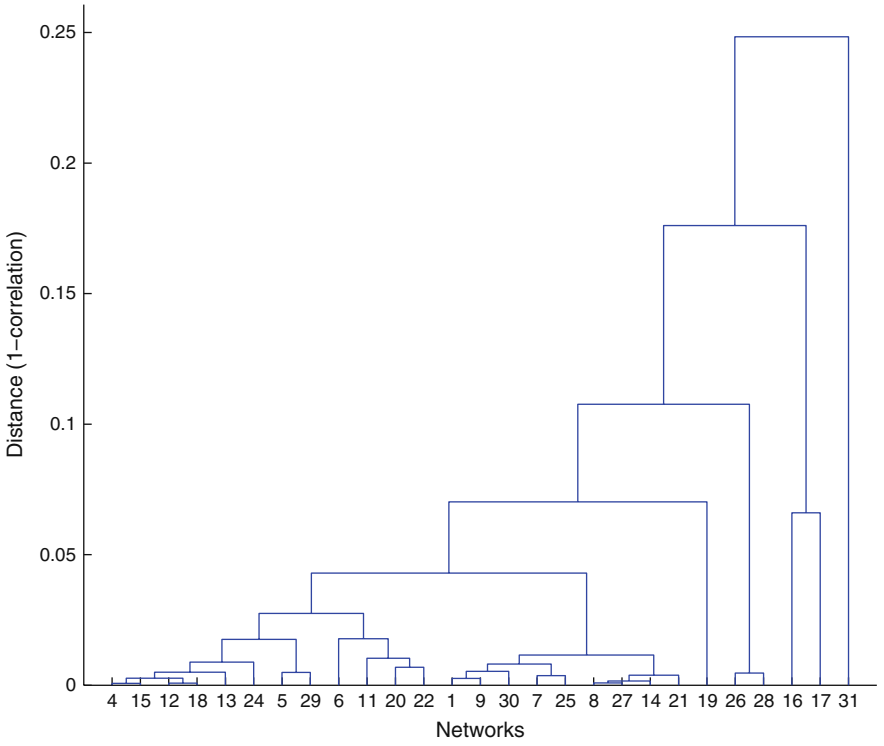

Fig. 3.8 Identifying families of networks over time with similar local structure. The hierarchical cluster tree that quantifies the relation between the different networks, based on the correlation coefficients between the tetrad significance profiles of the temporal sequence of networks

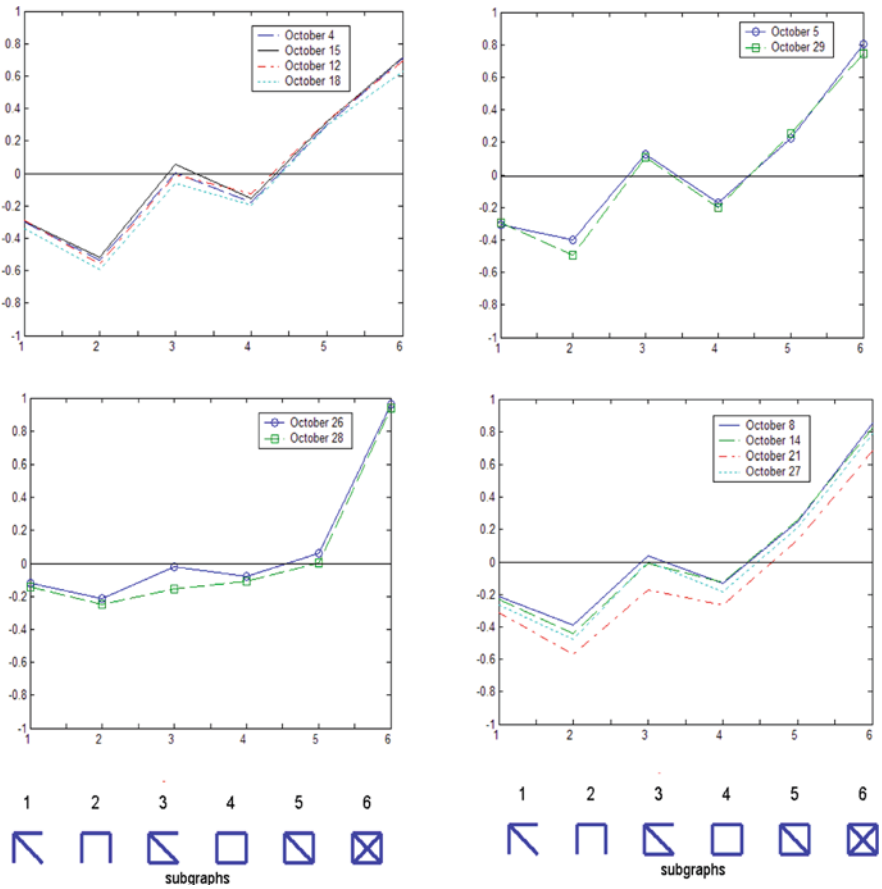

Fig. 3.9 Evidence for cycles of social interaction in dynamic social networks. Families of networks with highly similar local structure are identified, as suggested by the average-linkage hierarchical clustering tree (Fig. 3.8)

3.4 Summary

In summary, we have demonstrated that the static topology does not capture the dynamics of social networks. The prominence of nodes (as measured by degree) within the networks fluctuates widely from day to day, and a high degree in the aggregate network does not predict a high degree for individual days. Our conclusions are in sharp contrast to previous complex network research, which emphasizes the importance of aggregate nodal centrality in a static network topology [1–5, 7, 11, 14, 15, 17–20, 24].

Implications of a dynamic node centrality contrast with existing analyses that consider targeting nodes with the highest degrees to disrupt network communication or transport [25]. Dynamic centrality implies that targeting nodes with the

highest degrees at one time only weakly affects the nodes that are highly connected at another time. The approach of targeting high-degree nodes has been suggested, for example, to be an effective disease and computer virus prevention strategy; i.e. identification and "vaccination" of those nodes, would inhibit the spread of infection or computer viruses [21, 22]. Similarly, popular influencer marketing techniques (closely related to word-of-mouth or viral marketing) are based on the premise that a large number of people are connected to everyone else through a small number of hubs. Thus, identifying and focusing marketing activities around these hubs could increase the likelihood of initiating a cascading adoption of products or services – a type of social epidemic. The perspective of such marketing techniques presupposes that an individual who is an influencer now is likely to be a social hub later. In other words, the topology of a social network is quite static. Our work implies that, at the very least, a more agile strategy of monitoring, vaccinating nodes, or focusing marketing activities based upon centrality over time is necessary. Otherwise a treatment based upon aggregate connectivity information will miss the impact of a node that otherwise has a low connectivity, becoming highly connected. More generally, our findings call for a radical rethink of the mechanisms underlying the processes of link dynamics and diffusion on Dynamic Complex Networks – both experimentally and theoretically.

The type of dynamic analysis of networks we performed is pertinent to a wide range of network types. Whether or not there exists an underlying fixed topological structure, the question of which links are actually used is a relevant one. Thus, actual travel on a transportation network, and actual interactions that occur between molecules that can bind to each other, are both examples of networks that have an underlying structure but whose dynamic structure is relevant to the behavior and functionality of the system over time. This study demonstrated the potential role of time in complex networks. Ultimately our goal is to understand the role of both time and space in complex networks, leading to a Spatio-Temporal Complex Network Theory.

References

1. D. Braha and Y. Bar-Yam, Phys. Rev. E **69**, 016113 (2004).
2. D. Braha and Y. Bar-Yam, Manage. Sci. **53** (No. 7), 1127 (July 2007).
3. R. Albert and A.-L. Barabási, Rev. Mod. Phys. **74**, 47 (2002).
4. L. A. N. Amaral, A. Scala, M. Barthélémy and H. E. Stanley, Proc. Nat. Ac. Sci USA **97**, 11149 (2000).
5. Y. Bar-Yam and I. R. Epstein, Proc. Nat. Ac. Sci USA **101**, 4341 (2004).
6. Y. Bar-Yam, *Dynamics of Complex Systems* (Perseus Books, Reading, 1997).
7. H. Ebel, L.-I. Mielsch and S. Bornholdt, Phys. Rev. E **66**, 035103 (2002).
8. S. Wasserman and K. Faust, *Social Network Analysis* (Cambridge University Press, Cambridge, 1999).
9. P. Doreian and F. N. Stokman (Eds.) *Evolution of Social Networks* (Gordon and Breach, New York, 1997).
10. A.-L. Barabási, Nature **435**, 207 (2005).
11. J. P. Eckmann, E. Moses and D. Sergi, Proc. Natl. Acad. Sci. U.S.A. **101**, 14333 (2004).

12. D. Braha and Y. Bar-Yam, NECSI Technical Report 2005-February-01 (2005). The spatial proximity raw data was collected by the MIT Media Lab.
13. A.-L. Barabási and R. Albert, Science **286**, 509 (1999).
14. R. Milo, S. Shen-Orr, S. Itzkovitz, N. Kashtan, D. Chklovskii and U. Alon, Science **298**, 824 (2002).
15. R. Milo, S. Itzkovitz, N. Kashtan, R. Levitt, S. Shen-Orr, I. Ayzenshtat, M. Sheffer and U. Alon, Science **303**, 1538 (2004).
16. S. C. Johnson, Psychometrika **32**, 241 (1967).
17. H. Jeong, B. Tombor, R. Albert, Z. N. Oltavi and A.-L. Barabási, Nature **407**, 651 (2000).
18. H. Jeong, S. Mason, A.-L. Barabási and Z. N. Oltvai, Nature **411**, 41 (2001).
19. R. Ferrer, C. Janssen and R. V. Solé, Phys. Rev. E **63**, 32767 (2001).
20. R. Guimerà, L. Danon, A. Díaz-Guilera, F. Giralt and A. Arenas, Phys. Rev. E **68**, 65103 (2003).
21. A. L. Lloyd and R. M. May, Science **292**, 1316 (2001).
22. R. Pastor-Satorras and A. Vespignani, Phys. Rev. Lett. **86**, 3200 (2001).
23. D. J. de S. Price, Science **149**, 510 (1965).
24. W. Aiello, F. Chung and L. Lu, Proc. ACM STOC, 171 (2000).
25. R. Albert, H. Jeong and A.-L. Barabási, Nature **406**, 378 (2000).

Chapter 4
Adaptive Biological Networks

Mark D. Fricker, Lynne Boddy, Toshiyuki Nakagaki, and Daniel P. Bebber

Abstract Mycelial fungi and acellular slime molds grow as self-organized networks that explore new territory to search for resources, whilst maintaining an effective internal transport system in the face of continuous attack or random damage. These networks adapt during development by selective reinforcement of major transport routes and recycling of the intervening redundant material to support further extension. In the case of fungi, the predicted transport efficiency of the weighted network is better than evenly weighted networks with the same topology, or standard reference networks. Experimentally, nutrient movement can be mapped using radiotracers and scintillation imaging, and shows more complex transport dynamics, with synchronized oscillations and switching between different pre-existing routes. The significance of such dynamics to the interplay between transport control and topology is not yet known. In a similar manner, the resilience of the network can be tested *in silico* and experimentally using grazing invertebrates. Both approaches suggest that the same structures that confer good transport efficiency also show good resilience, with the persistence of a centrally connected core. The acellular slime mold, *Physarum polycephalum* also forms efficient networks between food sources, with a good balance between total cost, transit distance and fault tolerance. In this case, network formation can be captured by a mathematical model driven by non-linear positive reinforcement of tubes with high flux, and decay of tubes with low flux. We argue that organization of these simple planar networks has been honed by evolution, and they may exemplify potential solutions to real-world compromises between search strategy, transport efficiency, resilience and cost in other domains.

4.1 Introduction

Networks are common within biological systems and have been characterized in a range of different contexts that include metabolism, protein–protein interaction, neural circuits and ecological food webs. Despite the recent progress in biological

M.D. Fricker (✉)
Department of Plant Sciences, University of Oxford, Oxford, OX1 3RB, UK
e-mail: mark.fricker@plants.ox.ac.uk

T. Gross, H. Sayama (eds.), *Adaptive Networks,* Understanding Complex Systems,
DOI 10.1007/978-3-642-01284-6_4, © NECSI Cambridge/Massachusetts 2009

network analysis, one area that has received relatively little attention is the characterization of organisms whose entire growth form is as a network. In particular, both plasmodial slime molds (myxomycetes) and mycelial fungi form elaborate interconnected networks that are highly responsive to local environmental conditions. Unlike the other biological networks described, the network formed by these organisms is not *part* of the organism, it *is* the organism. These networks develop as the organism forages for new resources in a patchy environment and must both transport nutrients between spatially separated source and sink regions, and also maintain their integrity in the face of predation or random damage [4, 5]. The challenges that these conflicting demands place on the network organization have strong parallels with those faced in the design of anthropogenic infrastructure networks. The balance the biological systems have achieved between cost, efficiency and resilience may represent a good compromise to such a combinatorial optimization problem, and may yield useful insights into the design of delocalized, robust infrastructure networks. This presumes that solutions adopted by biological networks will exemplify useful generic theoretical principles, such as persistence, robustness, error-handling or appropriate redundancy, as they have been honed by evolution. The expectation is that the process of Darwinian natural selection based on variation, competition and survival has explored a significant range of possible network organizations and the resulting systems are likely to be well-adapted to survive and reproduce under particular biotic and abiotic conditions to solve certain ecological problems. A range of network architectures, development and dynamics can be found within the fungi and myxomycetes, suggesting a comparative approach may be instructive. However, the constraints imposed by the components used to construct the network (i.e. branching tubes) may have a profound effect on the possible network organization and dynamics, so it is possible that any result can only be generalized to a very limited set of real-world problems.

In this Chapter we focus on recent work describing the structure and function of foraging woodland fungi [3, 33], to illustrate how these essentially planar, weighted spatial networks resolve the conflicting demands of exploration, exploitation, transport and resilience [3]. We provide a brief introduction to network development in Sect. 4.2 then describe predicted transport of such networks in Sect. 4.3 and how it compares with experimentally measured nutrient movement in Sect. 4.4. We further comment on the experimentally observed oscillations and pulsatile transport in Sect. 4.5. Section 4.6 covers both predicted and experimentally determined network robustness. In Sect. 4.7, we compare the results from mycelial fungi with network development in *Physarum*, as a second exemplar of an adaptive biological network, before speculating on the universal features of such biological networks in Sect. 4.8.

4.2 Network Development in Mycelial Fungi

Filamentous fungi grow by apical extension of slender hyphae (Fig. 4.1a) that then branch sub-apically to form a fractal, tree-like mycelium. In ascomycetes and basidiomycetes, tangential hyphal fusions or anastomoses occur as the colony develops to

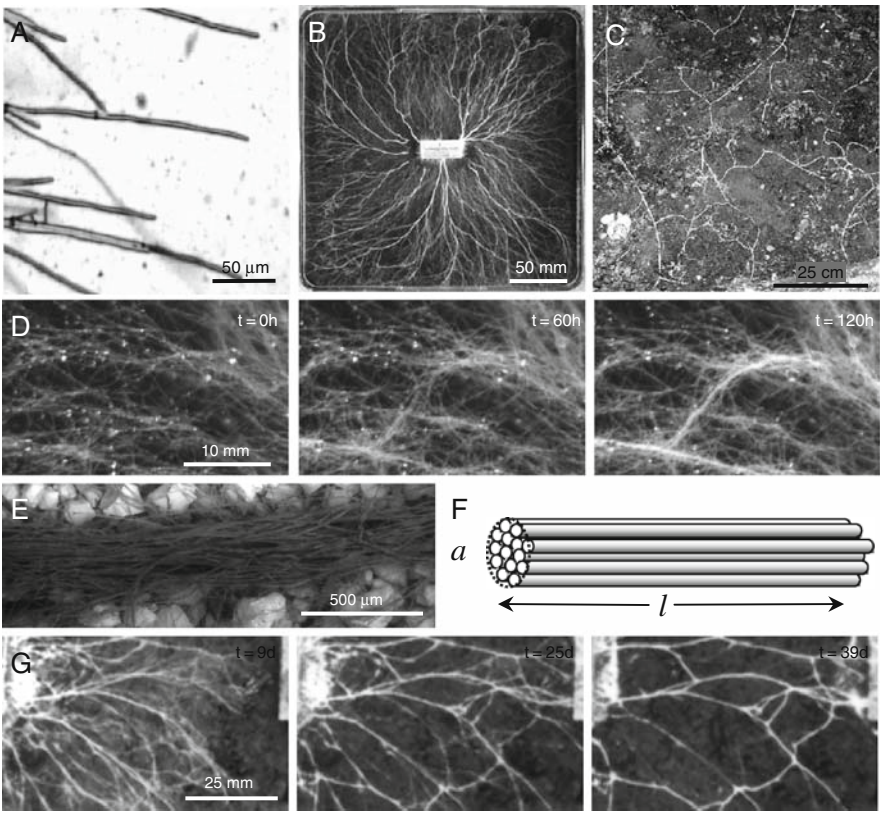

Fig. 4.1 Development of mycelial networks. (**a**) Bright-field image of hyphae of *Phanerochaete velutina* growing across agar. (**b**) Mycelial system of *P. velutina* grown from 4 cm^3 beech wood inocula on a 24 × 24 cm tray of compressed, non-sterile soil after 39 d. (**c**) a 75 × 75 cm portion of an extensive network of the saprotrophic basidiomycete *Megacollybia platyphylla* interconnecting dead wood resources in Wytham Wood, Oxfordshire, UK. (**d**) Time lapse imaging of cord-formation through hyphal aggregation in a growing colony of *P. velutina* on compressed sand/soil. (**e**) Scanning electron micrograph showing the aggregation of hyphae in a cord. (**f**) Schematic representation of a cord illustrating the length (l) and area (a) measures used to weight each link. (**g**) Time lapse imaging of cord-regression and thinning-out of the network in a growing colony of *P. velutina*. Modified from [21]

form an interconnected mycelial network [24, 25, 48, 49]. In the larger, more persistent saprotrophic and ectomycorrhizal basidiomycetes that grow out into soil from colonized food sources, the network architecture develops further with the formation of specialized high-conductivity organs, termed cords or rhizomorphs [12]. These form visible networks interconnecting food resources on a scale of centimetres in laboratory microcosms (Fig. 4.1b) to meters in undisturbed woodland (Fig. 4.1c), through parallel aggregation of many individual hyphae (Fig. 4.1d, e), [18]. Indeed mycelial fungi form the most extensive biological networks so far characterized [16, 33, 52–54], popularly known as the Wood Wide Web [50, 53].

The network topology is defined by classifying junctions (branch-points and anastomoses) as nodes, and the cords between nodes as links. In general, during foraging the number of nodes, number of links and the total material in the network, increase through time. However, the local scale network evolution is also characterized by selective loss of connections and thinning out of the fine mycelium and weaker cords (Fig. 4.1g). This behaviour is also apparent in the box-count mass fractal dimension of these networks, which shows a decrease as the networks thin out [6]. Thus, fungal networks progress from a radial branching tree to a weakly connected lattice-like network behind the growing margin, through a process of fusion and reinforcement to form loops, and selective removal and recycling of excess redundant material [3]. This shift can be quantified by the meshedness or alpha coefficient [11, 26], that gives the number of closed loops or cycles present as a fraction of the maximum possible for a planar network with the same number of nodes. The alpha coefficient measured over the whole colony increased over time from near zero, as expected for a branching tree, to 0.11 ± 0.04 in control systems, and to 0.20 ± 0.05 in systems with an additional wood block resource [3]. The values of the alpha index for *Phanerochaete velutina* were similar to those for networks of tunnels in ant galleries [11], *Physarum polycephalum* (unpublished observations) and street networks in cities [10, 13], suggesting that addition of around 20% of the maximum number of cross-links into a planar network may be sufficient to achieve desirable network properties in a range of different scenarios.

Other topological network measures have not proved to be very informative as they are heavily constrained by the developmental processes of branching and fusion, and crowding effects restricting the maximum number of connections possible in a planar network [2, 3, 3, 19, 29, 33]. Thus, the possible degree (k) of each node is limited to 1 for tips, 3 for branch points or fusion, or occasionally 4 for initially overlapping cords that then fuse. Likewise, the mean clustering coefficient, C [70], is of limited relevance for fungal networks, as their growth habit effectively precludes formation of triads. The frequency distribution of node strength shows more diversity than node degree alone, and follows an approximately log-normal distribution for *P. velutina* networks [3]. However, we have not found evidence for power law relationships that have attracted so much attention in other network analyses.

4.3 Predicted Transport Characteristics of the Mycelial Network

One approach to investigate the transport capacity of the network is to assume that nutrient fluxes will follow the shortest path between pairs of nodes, calculated from the predicted resistance of each link where longer, thinner cords have greater resistance to flow. The changes in thickness of the cords during growth and network re-modeling can be captured by image analysis of the reflected intensity of each cord, with appropriate calibration, to give each link a weight that depends on its length (l) and cross-sectional area (a). Each cord is modeled as a cylinder packed

with identical hyphae (Fig. 4.1f), rather than a single tube that increases in diameter, although the internal structure of cords can be much more complex [62]. An overall measure of transport is the average network efficiency (E), defined as the mean of the reciprocal of shortest path lengths for transport through the network [34, 35].

In isolation, the average efficiency is not useful without some frame of reference. It is not straightforward to generate suitable reference models against which to test the extent that differential cord weighting improves the performance of the network. Indeed elucidation of such biologically-inspired algorithms is a key goal of current research. At present there are no suitable algorithms available to generate weighted planar networks with defined properties. In other areas of network theory, comparisons are typically made with a reference network produced by random rewiring of the links. However, this does not make sense biologically. Likewise, randomly reassigning the weights to different links does not give an intuitively satisfying model to test performance, as it also has no biological basis. We currently use a two stage procedure to evaluate the performance of the fungal networks [3]. In the first step, nodes within the Euclidean fungal network (Fig. 4.2b), were used to construct model networks using well defined neighborhood graphs, including the minimum spanning tree (MST, Fig. 4.2c) as a lower bound giving a low cost, but extremely vulnerable network, the relative neighborhood graph (RNG, Fig. 4.2d), Gabriel graph (GAB, Fig. 4.2e) and the Delaunay triangulation (DT, Fig. 4.2f), giving an upper bound for a well-connected, robust, but rather expensive network [11, 13, 23, 43]. In the second step of analysis, the effect of including a fixed amount of material in the network, equivalent to the total material in the real network (Fig. 4.2a), was examined. Thus, each link in the "uniform" fungal and model networks was allocated a constant weight, such that the total construction cost was the same. Effectively we asked what the consequences for transport would be if the fungus had chosen to allocate the same amount of resource evenly over the existing or model networks, to determine the functional efficiency of the network. This also allowed comparison with the real, differentially weighted network (Fig. 4.2a) as the network measures were in comparable units.

Visual inspection of the resultant networks suggested that the topology of the fungal network had some similarity to the RNG, in terms of the density of cross-linking outside of the inoculum itself (Fig. 4.2d). Quantitatively, the RNGs had an alpha coefficient of $\sim$0.12, slightly lower than the alpha coefficient of the fungal networks. It was also apparent that regression of some links triggered substantial rearrangements in the layout of the model networks, particularly for the MST, which showed dramatic alteration in the connections between neighboring nodes over time (Fig. 4.2c) as the biological network developed.

Perhaps unsurprisingly, the real weighted networks had much shorter physiological paths, especially in the central region, than their corresponding uniform networks [3]. More surprisingly, the weighted fungal network outperformed both the uniform DT and the uniform MST when the predicted transport from just the inoculum to all other nodes was considered (Fig. 4.3). Although very well connected, the DT performed poorly, as distributing material across the large number

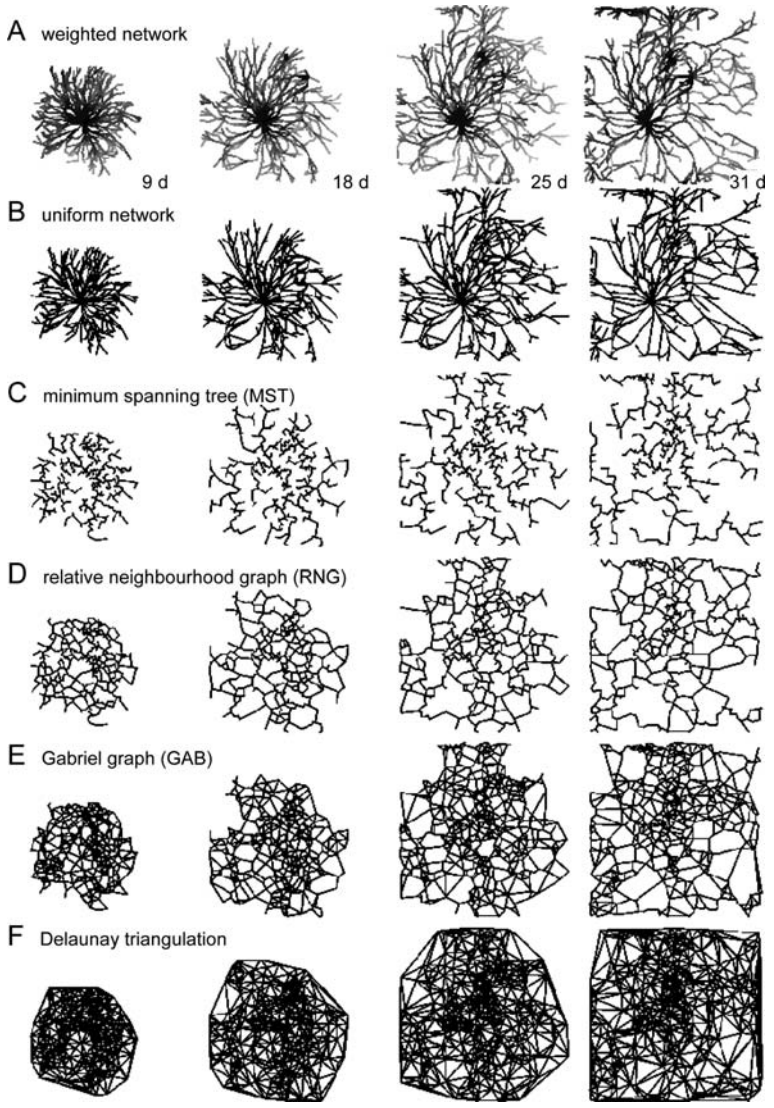

Fig. 4.2 Comparison of weighted fungal networks and neighborhood graphs. *P. velutina* was grown from a wood block inoculum over compressed soil in the presence of an additional wood-block resource, and the weighted network digitized at 9, 18, 25 and 31 d. (**A**) The weighted fungal network, in which line thickness and intensity indicate the relative cross-sectional area of each cord. (**B**) A simplified version of the network that retains nodes arising from branching or fusion, but not nodes simply required to trace the outline of each cord correctly. The amount of material present in the network is distributed evenly across all links to give a uniform network. The nodes present in the simplified graph were then connected according to well-defined rules to give: the minimum spanning tree (**C**); the relative neighborhood graph (**D**); the Gabriel graph (**E**); or the fully connected Delaunay triangulation (**F**). Modified from [21]

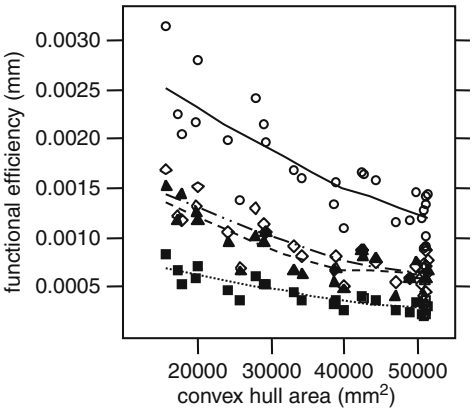

Fig. 4.3 Comparison of transport efficiency between weighted fungal and uniform model networks. The functional efficiency of the fungal network was predicted from the sum of the inverse of the shortest paths from the inoculum to every node as the colony increased in area. The weighted fungal network (○, —) has the highest functional efficiency, in comparison to uniform networks constructed with the same topology (◇, · — · · —), or connected using a Delaunay Triangulation (■, · · ·), or Minimum Spanning Tree (▲, ——). Redrawn from [3]

of links present gave each one low cross-sectional area and consequent high resistance. Conversely, the MST performed better than the DT as it was populated with few, but extremely thick, links. The uniform fungal networks were similar in performance to the MST, although they clearly have a different architecture, but the real weighted fungal network showed the best predicted transport behavior (Fig. 4.3). By normalizing to the DT, the local efficiency (E_{loc}) of the real network, uniform network and MST were calculated as 4.4 ± 0.11, 2.22 ± 0.07 and 2.08 ± 0.12, respectively [3]. Thus, differential weighting of links in the real network gave a > 4 fold improvement in local efficiency in comparison to a fully connected uniform network constructed with the same total cost. The ability of fungal networks to modify link strengths in a dynamic way is, therefore, crucial to achieve high transport capacity.

Subtle shifts in the predicted transport performance of the network as it grows can be identified by which links carry the greatest number of shortest paths and therefore have a high shortest-path betweenness centrality (SPBC) [17, 36]. The relative importance of particular links between the inoculum and added resource, as judged by their SPBC, fluctuate in the early stage of growth with several cords competing before one thickens up sufficiently to achieve dominance [21]. Equally, one of the disadvantages of using shortest path analysis is that comparable parallel pathways that are only marginally longer do not feature prominently in the analysis, but might be expected to participate in transport in a real system. A key area for future development will be to evaluate comparable parallel flow centrality measures.

4.4 Comparison Between Predicted Transport and Experimental Transport

In parallel to the theoretical network analysis, we have developed methods to image nutrient movement directly in these microcosms by mapping the distribution of the amino-acid analogue, ^{14}C-amino isobutyrate (^{14}C-AIB), using photon-counting scintillation imaging (PCSI), [22, 63–66]. ^{14}C-AIB accumulates in the free amino acid pool and is not metabolized in a range of woodland fungi so far examined, as judged by the lack of incorporation of ^{14}C in other metabolites or released as $^{14}CO_2$ [15, 31, 37, 46, 47, 69]. This allows it to be used as a proxy for nitrogen translocation [69] and provides an opportunity to compare the predictions made by the theoretical network analysis to the actual pattern of nutrient movement in the same microcosms [20].

Networks were allowed to develop in microcosms for ~45 d (Fig. 4.4a) and the weighted network digitised (Fig. 4.4b) and analysed to give the link evolution (Fig. 4.4c) and the SPBC (Fig. 4.4d). ^{14}C-AIB was added at the end of the growth period and imaged using photon-counting scintillation imaging (PCSI) to map nutrient movement (Fig. 4.4e). The topological network was then superimposed on the ^{14}C-AIB image to determine the amount of AIB present in each link from the integrated ^{14}C-AIB intensity (Fig. 4.4f). Ideally we would like to calculate the total flux through each link rather than just the integrated amount using knowledge of the amount of ^{14}C-AIB appearing further downstream. However, this is challenging as it requires assumptions about the flow pathway to reallocate the AIB signal correctly. Nevertheless, as a first approximation we have compared ^{14}C-AIB maps with various network parameters such as final link weight (Fig. 4.4g), link evolution (Fig. 4.4h), based on linear regression of the change in link weight with time, and SPBC (Fig. 4.4i). A number of different populations of links were identified. The most prominent were a cluster with high ^{14}C-AIB but low SPBC, corresponding to the tips where the ^{14}C-AIB accumulated. For the other links there was some degree of correlation between the AIB distribution and the network parameter. Equally, the AIB pattern did not always match expectations. For example, there was no obvious reason from the weighted network image why there should be substantial accumulation on the right-hand side of the colony, or little apparent transport to the added resource or beyond (Fig. 4.4e) based on the final link weight (Fig. 4.4b, final panel), link evolution (Fig. 4.4c) or SPBC (Fig. 4.4d). There are clearly additional features governing the control of nutrient distribution that cannot be captured by simple predictions of flow, based solely on network measures or shortest path calculations.

4.5 Oscillations and Pulsatile Transport

In addition to the evolution of the longer term trends described above, a strong pulsatile component was also associated with ^{14}C-AIB transport [22, 64–66]. To characterize this oscillatory behavior, we have analyzed the image-series in the frequency domain and mapped the frequency, phase or magnitude, on a pixel-by-pixel basis as the hue in pseudo-color coded images [22, 64–66]. In single juvenile

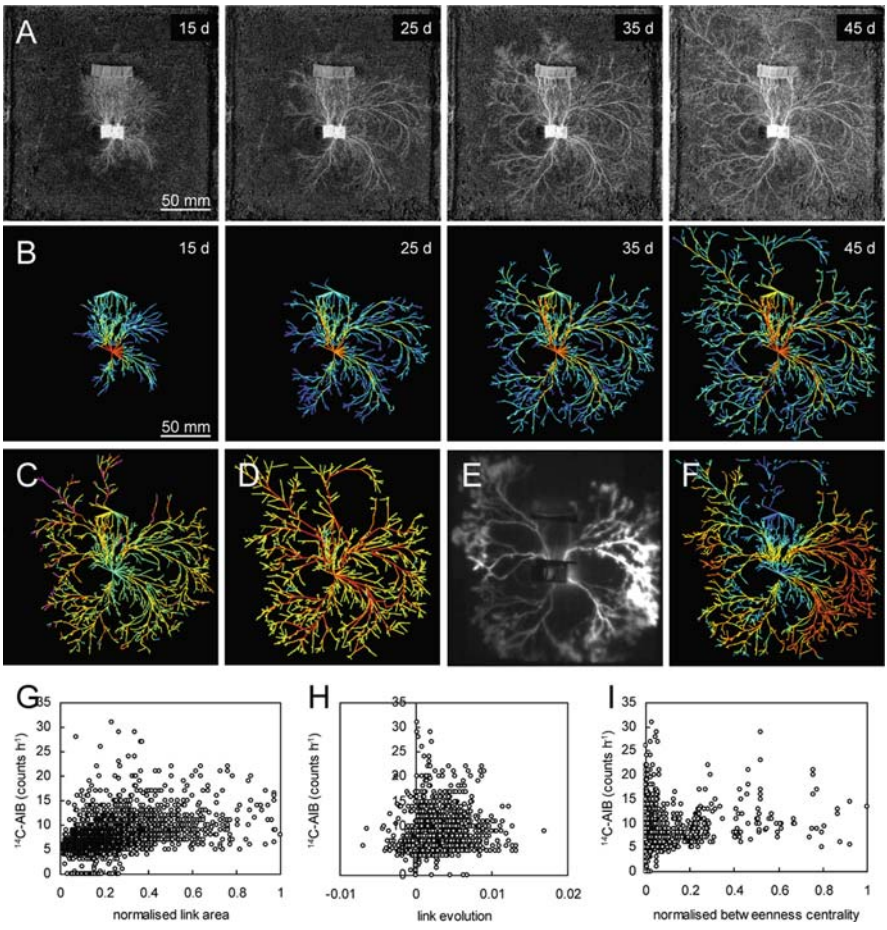

Fig. 4.4 Bright-field images of *P. velutina* growing from a beech wood block inoculum to a set of additional resource wood blocks over compressed soil were obtained at ~3 d intervals for 45 d (**a**). Branch points and anastomoses were manually coded as nodes connected by links, and the cord diameter estimated by image analysis, to give a weighted network (**b**) in which thick cords are represented in red and thin cords in blue, through a rainbow spectrum. Various network parameters were calculated including link evolution (**c**), based on linear regression of the change in link weight with time and color-coded by gradient of the regression equation, and shortest-path betweenness centrality, measured as the number of shortest paths passing through each link (**d**). To compare the predicted transport properties of the network with actual transport, ^{14}C-AIB movement was mapped by photon-counting scintillation imaging (PCSI) at the end of the time-series (**e**) and the amount of AIB present in each link extracted using the digitized network (**f**). The distribution of AIB was then compared with link cross-sectional area at the last time point (**g**), link evolution (**h**) or link betweenness centrality (**i**). Redrawn from [20]

mycelial systems with no additional resource, the mycelium beneath the inoculum and that growing over the screen formed distinct oscillatory domains with the same frequency, but almost 180 degrees out-of-phase with each other [22, 64]. When two colonies were allowed to grow and fuse, the oscillations synchronized between the

two connected inocula but still showed a phase shift with respect to the rest of the colony [22]. Recently we have examined the phase relationships in more complex systems in which arrays of colonies of both compatible and incompatible strains were allowed to grow and fuse. A subset of inocula were labeled and rapid, long-distance transport of ^{14}C-AIB occurred between the connected compatible inocula following fusion, with eventual distribution throughout the super-organism formed

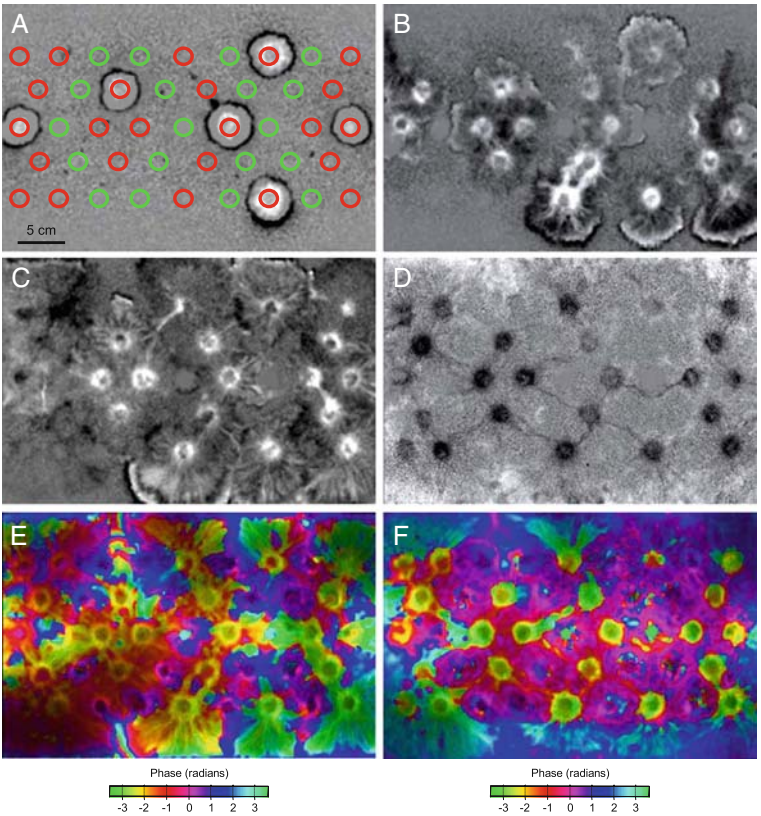

Fig. 4.5 Synchronized oscillations and phase domains in coupled networks. A 9 × 5 array of inocula from two incompatible isolates of *Coniophora puteana* (shown as *red* and *green circles* in panel (**a**) was set up on a scintillation screen. Several inocula were labeled with ^{14}C-AIB and transport imaged using photon-counting scintillation imaging (PCSI) for 12 d. When compatible growing colonies met, they fused and allowed rapid distribution of ^{14}C-AIB throughout the newly inter-connected system. Initially signals from the inoculum and growing mycelium of each colony showed out-of-phase oscillations, which are shown in (**b–d**) as a difference in intensity following subtraction of the long term trend during Fourier analysis. The phase of the oscillations determined from the Fourier analysis on a pixel-by-pixel basis was color-coded (**e** and **f**), in which regions of the same color are oscillating in phase. Before the network was fully connected there was considerable variation in the phase relations across the system (**e**). Following fusion, three domains of synchronized oscillations emerged, that differed in phase (**f**). Thus the interconnected inocula were all synchronized with one phase (*green*), the central domain (*purple*) and the outer, growing margin (*blue*)

(Fig. 4.5a–d). Furthermore, whilst oscillations in the individual colonies were not coupled initially (Fig. 4.5e), they became synchronized following fusion to give a network of linked cords and inocula with one phase, a central mycelial domain within the new super-colony that was phase-shifted by a few hours, and a contiguous foraging margin that was further phase-shifted by a few hours again (Fig. 4.5f). At this stage we do not know what significance to attribute to these oscillating phenomena.

4.6 Network Robustness

High transport capacity and low construction cost could have come at the expense of other network properties, such as robustness to damage, as there is no a priori reason why link weight allocation for one feature necessarily enhances another. This is clearly seen in the improved global transport efficiency of the uniformly weighted MST, even though the MST would be expected to be very vulnerable to disconnection during attack. Robustness to damage, e.g. by physical breakage or grazing by invertebrates [5, 7, 27, 30, 67, 68, 71], is of major significance to long-lived mycelial systems. Having a large number of alternate pathways is important in this context, and the differential strengthening of links not only imparts high transport capacity but also robustness to damage. This can be seen by examining the effects of breaking links in models of the fungal networks in comparison to corresponding uniform networks. We chose to look at link breakage rather than node removal, which is commonly used in other networks, as the cord is the biologically relevant target for attack. Links were broken in order, assuming that the probability of breakage increased with length and decreased with the thickness of the link. That is long, thin links were broken before short, thick ones. Robustness was quantified as the proportion of the total material cost of the network that remained connected to the inoculum. The fungal networks maintained a much greater system connected with the inoculum than did the uniform fungal, DT or MST networks (Fig. 4.6), i.e. the fungal networks were much more robust to damage.

This represents a minimum estimate of the real network resilience in nature, as the network is also able to respond to local damage, by modification of adjacent link strength, and to regrow and reconnect. Thus, for example, local mechanical damage to a small region of the network promoted strengthening of distal circumferential connections (Fig. 4.7a, c). Continuous grazing trimmed the network back to the reinforced core, in support of the *in silico* predictions (Fig. 4.7b), but also promoted an increase in tangential connections (Fig. 4.7d).

4.7 Simple Networks in the Plasmodial Slime Mould *Physarum Polycephalum*

Whilst network analysis of mycelial fungi is in its infancy, considerable progress has already been made in the analysis of simple networks in the plasmodial slime

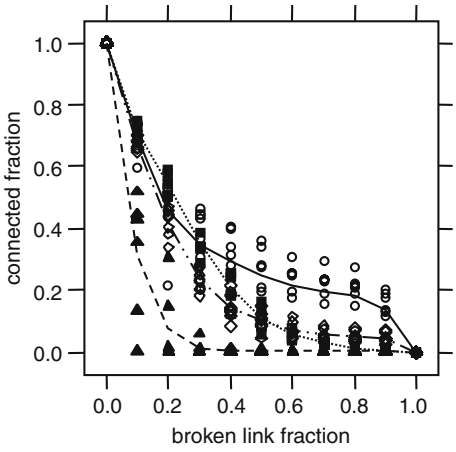

Fig. 4.6 Comparison of network resilience between weighted fungal and uniform model networks. The amount of mycelium remaining connected to the inoculum was measured as an increasing fraction of links were broken. When more than ∼0.3 of the total fraction of the link area was broken, the weighted fungal networks (○, −) maintained a greater connected core than the uniform fungal network (◇, · — · · —), or networks connected using a Delaunay Triangulation (■, · · ·), or Minimum Spanning Tree (▲, ——). Redrawn from [3]

mould *Physarum polycephalum* [32, 38–45, 57–61]. *P. polycephalum* is a large, single-celled amoeboid organism that forages for food resources in a woodland environment. During exploration, it spreads with a relatively contiguous foraging margin to maximize the area searched. However, behind the margin, it resolves this dense structure into a tubular network, interconnecting captured food resources and acting as a supply network to support further exploration.

This natural capacity to construct a transport network can be exploited in experimental microcosms in which food sources (FSs), typically oat flakes, are arranged in specific geometric patterns [39]. As the plasmodium grows, it links each FS encountered in an efficient manner to form a network that includes both direct connections, Steiner points and some additional cross-links that improve both transport efficiency and resilience (Fig. 4.8) [41, 43]. In all cases, the network that is established by the plasmodium has a relatively short total length of interconnecting tubes, but maintains close connections among all the food sources and exhibits a high tolerance to accidental fragmentation.

Growth can also be constrained by physical barriers [44] or influenced by the light regime [40], increasing the opportunity for experimental manipulation to mimic real-world network problems. Thus, for example, *P. polycephalum* can find the shortest path through a maze [40, 44, 45], or connect different arrays of FSs in an efficient manner. For three or more FRs up to about 10, the system strikes a balance between a low total length (TL) of the interconnected network whilst keeping a short connection distance (CD) between any pair of FSs and a high degree of fault tolerance (FT) against accidental disconnection of any tube [41, 43].

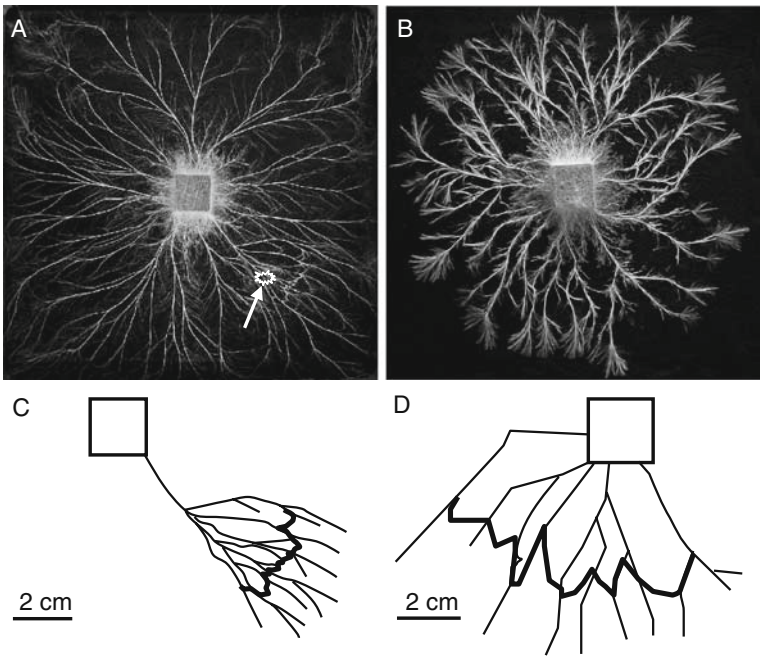

Fig. 4.7 Adaptive network resilience. Colonies of *P. velutina* were grown from 2 × 2 × 2 beech wood blocks over compressed soil in the absence (**a**) or presence (**b**) of grazing by *Folsomia candida*. In (**a**) a localized region of physical damage (indicated by the *arrow*) stimulated a localized increase in tangential connections (**c**). In (**b**) grazing continuously trimmed the finest hyphae, stimulating more local sprouting, and accentuated growth both of the dominant radial cords and also tangential connections (**d**). Redrawn from [19]

The degree of separation is defined as the number of food sources along the shortest path between two food sources. The average separation (AS) is the degree of separation averaged over all pairs of food sources, and decreases as food sources are more closely coupled. To allow comparisons between different arrangements, AS is normalized to the average separation for the minimum spanning tree [41]. The fault tolerance (FT) is the probability that the organism is not fragmented into separate pieces if an accidental breakage occurs at a random point along the tubes. Since the probability of disconnection of a tube is proportional to its length, a longer tube has a higher risk of disconnection. The combined index, FT/TL, can be regarded as a measure of the ratio of benefit to cost. By judicious positioning of food sources, the geometry of the network can be compared to possible theoretical solutions in terms of path length and fault tolerance, such as the minimal spanning tree (MST), the Steiner minimal tree (SMT) and a Delaunay triangulation network (DTN) [41]. Examples are given in Fig. 4.8 for the predicted network with 3 food sources (Fig. 4.8d) and experimental results for 3 food sources (Fig. 4.8e–g), 6 and 7 food sources (Fig. 4.8h, i) with the associated analysis of path length and fault

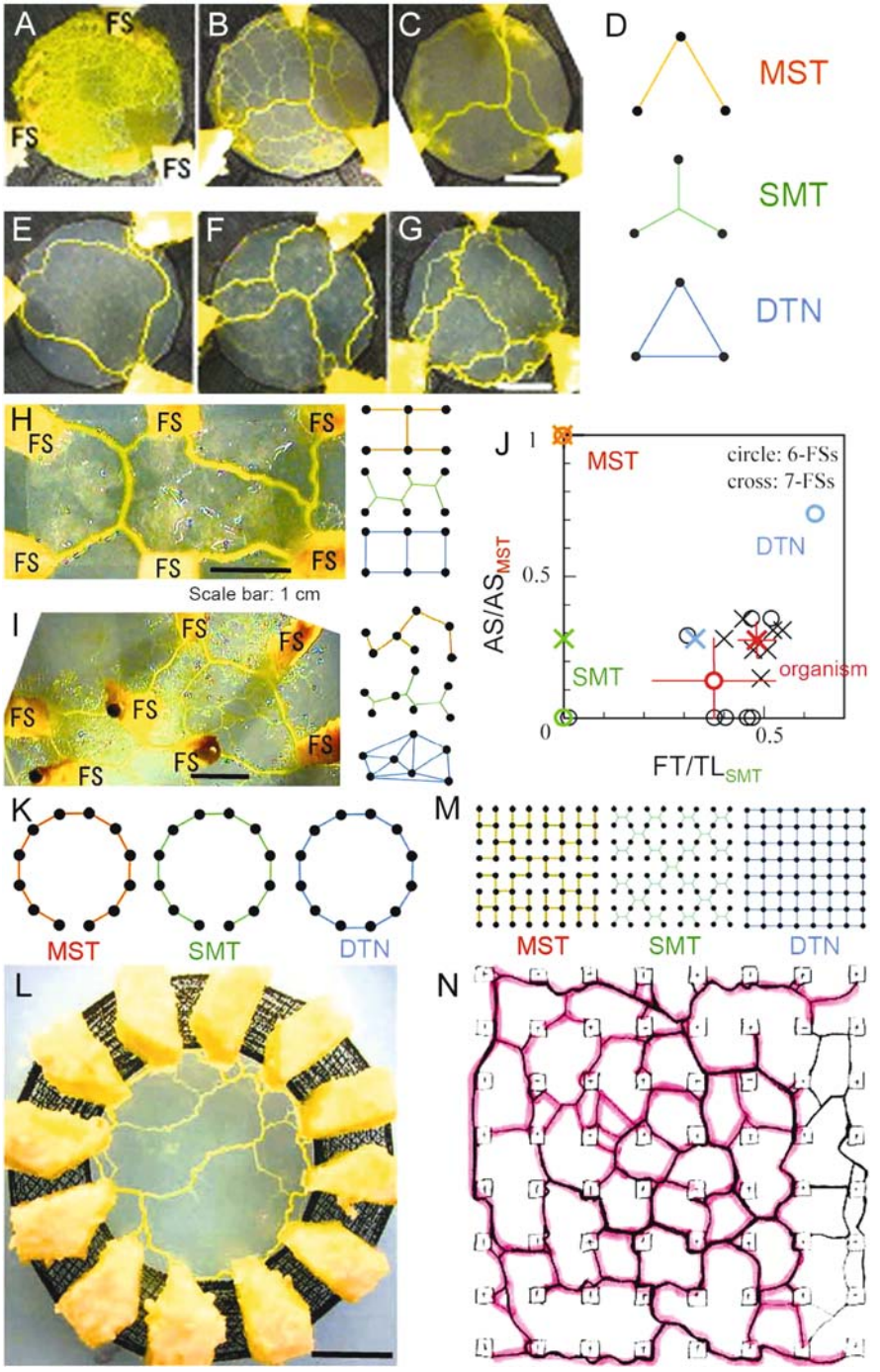

Fig. 4.8 (continued)

tolerance (Fig. 4.8j), rings of 12 food sources (Fig. 4.8k, l) and grids of 64 food sources (Fig. 4.8m, n).

In computational terms, it becomes progressively more challenging to find a good solution to such a combinatorial optimization problem as the number of FSs increases, particularly with the inclusion of Steiner points [61]. It is remarkable, therefore, that solutions reached by *P. polycephalum*, whilst not necessarily optimal individually, cluster around the predicted optimal solution in replicate experiments. Furthermore, the solution is reached rapidly, based only on local information and parallel analogue computing. If it were possible to capture the essence of such a system in simple rules, it might have significant potential to guide de-centralized network development in other domains [39, 42, 58–60].

4.8 Universal Features of Biological Networks?

Characterization of mycelial networks is still in its infancy. However, the network approach provides a way of quantifying and analyzing complex fungal systems for the first time, and also makes it possible to link measurements in microcosms in the laboratory to observations of networks in the field. The simple models predicting transport through such networks, so far based on shortest path considerations through the weighted network, only capture part of the experimentally determined transport behavior. We anticipate that models that include parallel-flow pathways and evolution of the network should improve the match between simulation and experiment, and will benefit from the recent advances in fast algorithms to calculate the necessary metrics. The next conceptual advance will be to identify the rules that allow the network iteratively to refine its structure and transport behavior to yield the network architectures observed. It is conceivable that the identification of such rules will allow development of generic "fungal colony optimization" algorithms

◄

Fig. 4.8 (*Opposite page*) Self-organization of robust network architecture in *Physarum polycephalum*. (a–c) Development of a network between three food sources, starting from a continuous sheet of plasmodium on the surface of agar. Network structure at 0 h (a), 6 h (b) and 36 h (c). Scale bar = 1 cm. (d) Schematic illustration of the arrangement of food sources (*black dots*). The *orange, green* and *blue lines* represent the network of minimum spanning tree (MST), Steiner's minimal tree (SMT) and Delaunay triangulation network (DTN), respectively. (e–g) Three typical networks in ascending order of total length (TL) after 35 h. Scale bar = 1 cm. (h, i) Typical emergent network structure with six (h) and seven (i) food sources (FS) and schematic representation of the corresponding MST (*orange*), SMT (*green*) and DTN (*blue*). (j) Properties of the plasmodial networks, defined by average separation of food sources (AS), normalised to the value for the minimal spanning tree, and benefit to cost ratio, defined as the fault tolerance over the total length (FT/TL). *Black symbols* give the value for each specimen, and *red*, the value of the mean with associated s.e.m. *Orange, green* and *blue symbols* give the values of MST, SMT and DTN respectively. The organism maintains a short total length of tubes with close connections between food sources yet high tolerance of accidental disconnection. (k–n) Network organization with ring (k, l) and grid (m, n) arrangement of food sources. These systems also show robust network architecture, with short path length but high fault tolerance. Redrawn from [43]

similar to those that have evolved from the study of ant colony foraging patterns [14] or based on *P. polycephalum* [40, 41, 58–60].

Even at this stage, some common features of biological network formation seem to emerge. Fungal networks are constructed by local iterative developmental processes rather than predetermined blueprints or centralized control, with growth involving over-production of links and nodes, followed by selective pruning of some links and reinforcement of others. Such a process mimics the process of Darwinian evolution in which natural selection removes less fit offspring. This "Darwinian network model" may be applicable to other biological systems, including foraging ant trails, *P. polycephalum*, axon development and angiogenesis, and may represent a generalized model for growth of physical biological networks. Based on the ant colony and *P. polycephalum* models, we might expect the generic ingredients in such a model will involve a non-linear positive reinforcement term related to the local flux and a linear decay term. Notably this model differs from other models of weighted network evolution that incorporate differential strengthening of links, i.e. "the busiest get busier" [1], rather than differential weakening and loss that is the hallmark of evolution by natural selection. However, the model has parallels with the selective link removal model recently proposed for unweighted networks [51]. In infrastructure networks where costs are associated with creation and maintenance of links, where links differ in some measure of fitness, and where material can be recycled, such a Darwinian model may be applicable. In practical terms such a process may also be witnessed in the evolution of real infrastructure networks, such as British railways following the Beeching reviews in the early '60s [8, 9]. In these reviews, the flux along various routes was measured and routes with too low a level of traffic, mainly branch lines, were targeted for closure. At the same time, major routes were strengthened to cope with the expected source-sink relationships for both passenger and freight traffic. Interestingly, the reports focussed on efficiency rather than any explicit consideration of resilience, which may explain the sensitivity of the current UK rail network to disruption.

A second feature of interest emerging, particularly through consideration of the *P. polycephalum* and fungal networks, is the extent that coupled flows may contain global information. Networks involving physical flows obey continuity equations and are therefore intrinsically coupled across the network. This automatically means that increasing the flow in one part of the network will lead to reductions elsewhere, even though the local conditions in the distal region remain the same. Thus each part of the network is influenced by and can influence the whole network, but without any global assessment of behavior. Useful properties of the network may emerge from the interaction between the local update rules governing topology and flows without the need for long-distance communication or calculation of aggregate properties of the network. It is this coupling in the *P. polycephalum* model that allows the network to resolve from a fine mesh into a quasi-optimal solution [40, 58–60]. Furthermore, the computational overhead for such self-organized networks scales well with the number of additional nodes.

The third general observation on these biological networks is the prevalence of some form of oscillatory process. In *P. polycephalum* it is an actin-myosin contrac-

tion with a short (min) period whilst in the fungal networks it is manifest as a change in the amount of radiolabeled nutrient with a longer (hr to day) period. In both cases the oscillations can synchronize across large regions of the developing system, even if the individual components are asynchronous initially [22, 56, 57]. That the oscillations manage to synchronize is not surprising [55], but the extent that the organisms may be able to interpret and act upon the oscillations is not known. In other contexts, such as supply chains or traffic flow, the existing strategy is to minimize oscillations to achieve maximum throughput [28]. This suggests that either the biological systems lack the additional sensory and feedback systems to suppress oscillations, or that maintaining an oscillatory system is an alternative means to achieve a stable long-term quasi-optimal solution, potentially with less control infrastructure. In *P. polycephalum*, oscillations drive protoplasmic shuttle streaming and generate flows considerably greater than the volume needed simply for extension growth at the margin. It seems likely therefore that the additional energy demands of rhythmic contraction represent the cost of this indirect information transfer. Nevertheless, such a cost is minimal compared to the developmental and behavioral complexity and metabolic cost of the more sophisticated neuron-based sensory systems used by higher organisms.

Acknowledgements Research has been supported by BBSRC (43/P19284), EPSRC (GR/S63090/01), NERC (GR3/12946 and NER/A/S/2002/882), EU Framework 6 (STREP No. 12999), Oxford University Research Infrastructure Fund and the University Dunston Bequest. We thank A. Ashford, K. Burton, P.R. Darrah, D.P. Donnelly, D. Eastwood, J. Efstathiou, J. Hynes, N. Johnson, F. Reed-Tsochas, M. Tlalka, G.M. Tordoff, S.C. Watkinson and members of CABDyN for stimulating discussions.

References

1. Barrat, A., Barthelemy, M., Vespignani, A.: Modeling the evolution of weighted networks. Physical Review E **70**, 066149 (2004)
2. Barrat, A., Barthelemy, M., Vespignani, A.: The effects of spatial constraints on the evolution of weighted complex networks. Journal of Statistical Mechanics p. P05003 (2005)
3. Bebber, D., Hynes, J., Darrah, P., Boddy, L., Fricker, M.: Biological solutions to transport network design. Proceedings of the Royal Society B **274**, 2307–2315 (2007)
4. Bebber, D., Tlalka, M., Hynes, J., Darrah, P., Ashford, A., Watkinson, S., Boddy, L., Fricker, M.: Imaging complex nutrient dynamics in mycelial networks. In: G. Gadd, S. Watkinson, P. Dyer (eds.) Fungi in the Environment, vol. 25, pp. 3–21. Cambridge University Press, Cambridge (2007)
5. Boddy, L., Jones, T.: Mycelial responses in heterogeneous environments: parallels with macroorganisms. In: G. Gadd, S. Watkinson, P. Dyer (eds.) Fungi in the Environment, vol. 25, pp. 112–158. Cambridge University Press, Cambridge (2007)
6. Boddy, L., Wells, J.M., Culshaw, C., Donnelly, D.P.: Fractal analysis in studies of mycelium in soil. Geoderma **88**, 301–328 (1999)
7. Bretherton, S., Tordoff, G.M., Jones, T.H., Boddy, L.: Compensatory growth of *Phanerochaete velutina* mycelial systems grazed by *Folsomia candida* (collembola). FEMS Microbiology Ecology **58**, 33–40 (2006)
8. British Railways Board: The development of the major railway trunk routes (1965)
9. British Transport Commission: The reshaping of british railways - part 1: report (1963)

10. Buhl, J., Gautrais, J., Reeves, N., Sole, R.V., Valverde, S., Kuntz, P., Theraulaz, G.: Topological patterns in street networks of self-organized urban settlements. European Physical Journal B **49**, 513–522 (2006)
11. Buhl, J., Gautrais, J., Sole, R.V., Kuntz, P., Valverde, S., Deneubourg, J.L., Theraulaz, G.: Efficiency and robustness in ant networks of galleries. European Physical Journal B **42**, 123–129 (2004)
12. Cairney, J.W.G.: Basidiomycete mycelia in forest soils: dimensions, dynamics and roles in nutrient distribution. Mycological Research **109**, 7–20 (2005)
13. Cardillo, A., Scellato, S., Latora, V., Porta, S.: Structural properties of planar graphs of urban street patterns. Physical Review E **73**, 066107 (2006)
14. Dorigo, M., Di Caro, G., Gambardella, L.M.: Ant algorithms for discrete optimization. Artificial Life **5**, 137–172 (1999)
15. Elliott, M.L., Watkinson, S.C.: The effect of alpha-aminoisobutyric-acid on wood decay and wood spoilage fungi. International Biodeterioration **25**, 355–371 (1989)
16. Ferguson, B.A., Dreisbach, T.A., Parks, C.G., Filip, G.M., Schmitt, C.L.: Coarse-scale population structure of pathogenic *Armillaria* species in a mixed-conifer forest in the blue mountains of northeast oregon. Canadian Journal of Forest Research **33**, 612–623 (2003)
17. Freeman, L.C.: Set of measures of centrality based on betweenness. Sociometry **40**, 35–41 (1977)
18. Fricker, M., Bebber, D., Boddy, L.: Mycelial networks: structure and dynamics. In: L. Boddy, J. Frankland, P. van West (eds.) Ecology of Saprotrophic Basidiomycetes, vol. 28, pp. 3–18. Academic Press, Amsterdam (2008)
19. Fricker, M., Boddy, L., Bebber, D.: Network organisation of mycelial fungi. In: R. Howard, N. Gow (eds.) The Mycota, vol. VIII, pp. 309–330. Springer-Verlag, Berlin (2007)
20. Fricker, M., Lee, J., Bebber, D., Tlalka, M., Hynes, J., Darrah, P., Watkinson, S., Boddy, L.: Imaging complex nutrient dynamics in mycelial networks. Journal of Microscopy **231**, 299–316 (2008)
21. Fricker, M., Lee, J., Boddy, L., Bebber, D.: The interplay between structure and function in fungal networks. Topologica **1**, 004 (2008)
22. Fricker, M.D., Tlalka, M., Bebber, D., Takagi, S., Watkinson, S.C., Darrah, P.R.: Fourier-based spatial mapping of oscillatory phenomena in fungi. Fungal Genetics and Biology **44**, 1077–1084 (2007)
23. Gastner, M.T., Newman, M.E.J.: Shape and efficiency in spatial distribution networks. Journal of Statistical Mechanics p. P01015 (2006)
24. Glass, N.L., Jacobson, D.J., Shiu, P.K.T.: The genetics of hyphal fusion and vegetative incompatibility in filamentous ascomycete fungi. Annual Review of Genetics **34**, 165–186 (2000)
25. Glass, N.L., Rasmussen, C., Roca, M.G., Read, N.D.: Hyphal homing, fusion and mycelial interconnectedness. Trends in Microbiology **12**, 135–141 (2004)
26. Haggett, P., Chorley, R.: Network Analysis in Geography. Arnold, London (1969)
27. Harold, S., Tordoff, G.M., Jones, T.H., Boddy, L.: Mycelial responses of *Hypholoma fasciculare* to collembola grazing: effect of inoculum age, nutrient status and resource quality. Mycological Research **109**, 927–935 (2005)
28. Helbing, D.: Traffic and related self-driven many-particle systems. Reviews of Modern Physics **73**, 1067–1141 (2001)
29. Hitchcock, D., Glasbey, C.A., Ritz, K.: Image analysis of space-filling by networks: application to a fungal mycelium. Biotechnology Techniques **10**, 205–210 (1996)
30. Kampichler, C., Rolschewski, J., Donnelly, D.P., Boddy, L.: Collembolan grazing affects the growth strategy of the cord-forming fungus *Hypholoma fasciculare*. Soil Biology and Biochemistry **36**, 591–599 (2004)
31. Kim, K.W., Roon, R.J.: Transport and metabolic effects of alpha-aminoisobutyric-acid in *Saccharomyces cerevisiae*. Biochimica et Biophysica Acta **719**, 356–362 (1982)
32. Kobayashi, R., Tero, A., Nakagaki, T.: Mathematical model for rhythmic protoplasmic movement in the true slime mold. Journal of Mathematical Biology **53**, 273–286 (2006)

33. Lamour, A., Termorshuizen, A.J., Volker, D., Jeger, M.J.: Network formation by rhizomorphs of *Armillaria lutea* in natural soil: their description and ecological significance. FEMS Microbiology Ecology **62**, 222–232 (2007)
34. Latora, V., Marchiori, M.: Efficient behavior of small-world networks. Physical Review Letters **87**, 198701 (2001)
35. Latora, V., Marchiori, M.: Economic small-world behavior in weighted networks. European Physical Journal B **32**, 249–263 (2003)
36. Latora, V., Marchiori, M.: A measure of centrality based on network efficiency. New Journal of Physics **9**, 188 (2007)
37. Lilly, W.W., Higgins, S.M., Wallweber, G.J.: Uptake and translocation of 2-aminoisobutyric acid by *Schizophyllum commune*. Experimental Mycology **14**, 169–177 (1990)
38. Nakagaki, T.: Smart behavior of true slime mold in a labyrinth. Research in Microbiology **152**, 767–770 (2001)
39. Nakagaki, T., Guy, R.D.: Intelligent behaviors of amoeboid movement based on complex dynamics of soft matter. Soft Matter **4**, 57–67 (2008)
40. Nakagaki, T., Iima, M., Ueda, T., Nishiura, Y., Saigusa, T., Tero, A., Kobayashi, R., Showalter, K.: Minimum-risk path finding by an adaptive amoebal network. Physical Review Letters **99**, 068104 (2007)
41. Nakagaki, T., Kobayashi, R., Nishiura, Y., Ueda, T.: Obtaining multiple separate food sources: behavioural intelligence in the *Physarum* plasmodium. Proceedings of the Royal Society of London Series B **271**, 2305–2310 (2004)
42. Nakagaki, T., Saigusa, T., Tero, A., Kobayashi, R.: Effects of amount of food on path selection in the transport network of an amoeboid organism. In: Proceedings of the International Symposium on Topological Aspects of Critical Systems and Networks. World Scientific (2007)
43. Nakagaki, T., Yamada, H., Hara, M.: Smart network solutions in an amoeboid organism. Biophysical Chemistry **107**, 1–5 (2004)
44. Nakagaki, T., Yamada, H., Toth, A.: Maze-solving by an amoeboid organism. Nature **407**, 470–470 (2000)
45. Nakagaki, T., Yamada, H., Toth, A.: Path finding by tube morphogenesis in an amoeboid organism. Biophysical Chemistry **92**, 47–52 (2001)
46. Ogilvie-Villa, S., Debusk, R.M., Debusk, A.G.: Characterization of 2-aminoisobutyric acid transport in *Neurospora crassa* – a general amino-acid permease-specific substrate. Journal of Bacteriology **147**, 944–948 (1981)
47. Olsson, S., Gray, S.N.: Patterns and dynamics of ^{32}P-phosphate and labelled 2-aminoisobutyric acid (^{14}C-AIB) translocation in intact basidiomycete mycelia. FEMS Microbiology Ecology **26**, 109–120 (1998)
48. Rayner, A., Griffith, G., Ainsworth, A.: Mycelial interconnectedness. In: N. Gow, G. Gadd (eds.) The Growing Fungus, pp. 21–40. Chapman and Hall, London (1994)
49. Rayner, A., Watkins, Z., Beeching, J.: Self-integration - an emerging concept from the fungal mycelium. In: N. Gow, G. Robson, G. Gadd (eds.) The Fungal Colony, pp. 1–24. Cambridge University Press, Cambridge (1999)
50. Read, D.: Mycorrhizal fungi – the ties that bind. Nature **388**, 517–518 (1997)
51. Salathe, M., May, R.M., Bonhoeffer, S.: The evolution of network topology by selective removal. Journal of the Royal Society Interface **2**, 533–536 (2005)
52. Simard, S.W., Durall, D.M.: Mycorrhizal networks: a review of their extent, function, and importance. Canadian Journal of Botany **82**, 1140–1165 (2004)
53. Simard, S.W., Perry, D.A., Jones, M.D., Myrold, D.D., Durall, D.M., Molina, R.: Net transfer of carbon between ectomycorrhizal tree species in the field. Nature **388**, 579–582 (1997)
54. Smith, M.L., Bruhn, J.N., Anderson, J.B.: The fungus *Armillaria bulbosa* is among the largest and oldest living organisms. Nature **356**, 428–431 (1992)
55. Strogatz, S.H.: From kuramoto to crawford: exploring the onset of synchronization in populations of coupled oscillators. Physica D **143**, 1–20 (2000)

56. Takamatsu, A., Tanaka, R., Yamada, H., Nakagaki, T., Fujii, T., Endo, I.: Spatiotemporal symmetry in rings of coupled biological oscillators of *Physarum* plasmodial slime mold. Physical Review Letters **87**, 078102 (2001)
57. Tero, A., Kobayashi, R., Nakagaki, T.: A coupled-oscillator model with a conservation law for the rhythmic amoeboid movements of plasmodial slime molds. Physica D **205**, 125–135 (2005)
58. Tero, A., Kobayashi, R., Nakagaki, T.: Physarum solver: A biologically inspired method of road-network navigation. Physica A **363**, 115–119 (2006)
59. Tero, A., Kobayashi, R., Nakagaki, T.: A mathematical model for adaptive transport network in path finding by true slime mold. Journal of Theoretical Biology **244**, 553–564 (2007)
60. Tero, A., Nakagaki, T., Toyabe, K., Yumili, K., Kobayashi, R.: A method inspired by physarum for solving the steiner problem. International Journal for Unconventional Computing **in press** (2009)
61. Tero, A., Yumiki, K., Kobayashi, R., Saigusa, T., Nakagaki, T.: Flow-network adaptation in physarum amoebae. Theory in Biosciences **127**, 89–94 (2008)
62. Thompson, W., Rayner, A.D.M.: Structure and development of mycelial cord systems of *Phanerochaete laevis* in soil. Transactions of the British Mycological Society **78**, 193–200 (1982)
63. Tlalka, M., Bebber, D., Darrah, P., Watkinson, S., Fricker, M.: Dynamic resource allocation and foraging strategy in mycelial systems. Fungal Genetics and Biology **45**, 1111–1121 (2008)
64. Tlalka, M., Bebber, D., Darrah, P.R., Watkinson, S.C., Fricker, M.D.: Emergence of self-organised oscillatory domains in fungal mycelia. Fungal Genetics and Biology **44**, 1085–1095 (2007)
65. Tlalka, M., Hensman, D., Darrah, P.R., Watkinson, S.C., Fricker, M.D.: Noncircadian oscillations in amino acid transport have complementary profiles in assimilatory and foraging hyphae of *Phanerochaete velutina*. New Phytologist **158**, 325–335 (2003)
66. Tlalka, M., Watkinson, S.C., Darrah, P.R., Fricker, M.D.: Continuous imaging of amino-acid translocation in intact mycelia of *Phanerochaete velutina* reveals rapid, pulsatile fluxes. New Phytologist **153**, 173–184 (2002)
67. Tordoff, G.M., Boddy, L., Jones, T.H.: Grazing by *Folsomia candida* (collembola) differentially affects mycelial morphology of the cord-forming basidiomycetes *Hypholoma fasciculare*, *Phanerochaete velutina* and *Resinicium bicolor*. Mycological Research **110**, 335–345 (2006)
68. Tordoff, G.M., Boddy, L., Jones, T.H.: Species-specific impacts of collembola grazing on fungal foraging ecology. Soil Biology and Biochemistry **40**, 434–442 (2008)
69. Watkinson, S.C.: Inhibition of growth and development of *Serpula lacrimans* by the non-metabolized amino-acid analog alpha-aminoisobutyric-acid. FEMS Microbiology Letters **24**, 247–250 (1984)
70. Watts, D.J., Strogatz, S.H.: Collective dynamics of 'small-world' networks. Nature **393**, 440–442 (1998)
71. Wood, J., Tordoff, G.M., Jones, T.H., Boddy, L.: Reorganization of mycelial networks of *Phanerochaete velutina* in response to new woody resources and collembola (*Folsomia candida*) grazing. Mycological Research **110**, 985–993 (2006)

Part II
Self-Organization of Adaptive Networks

Chapter 5
Self-Organized Criticality and Adaptation in Discrete Dynamical Networks

Thimo Rohlf and Stefan Bornholdt

Abstract It has been proposed that adaptation in complex systems is optimized at the critical boundary between ordered and disordered dynamical regimes. Here, we review models of evolving dynamical networks that lead to self-organization of network topology based on a local coupling between a dynamical order parameter and rewiring of network connectivity, with convergence towards criticality in the limit of large network size N. In particular, two adaptive schemes are discussed and compared in the context of Boolean Networks and Threshold Networks: (1) Active nodes loose links, frozen nodes aquire new links, (2) Nodes with correlated activity connect, de-correlated nodes disconnect. These simple local adaptive rules lead to co-evolution of network topology and -dynamics. Adaptive networks are strikingly different from random networks: They evolve inhomogeneous topologies and broad plateaus of homeostatic regulation, dynamical activity exhibits $1/f$ noise and attractor periods obey a scale-free distribution. The proposed co-evolutionary mechanism of topological self-organization is robust against noise and does not depend on the details of dynamical transition rules. Using finite-size scaling, it is shown that networks converge to a self-organized critical state in the thermodynamic limit. Finally, we discuss open questions and directions for future research, and outline possible applications of these models to adaptive systems in diverse areas.

5.1 Introduction

Many complex systems in nature, society and economics are organized as networks of many interacting units that collectively process information or the flow of matter and energy through the system; examples are gene regulatory networks, neural networks, food webs in ecology, species relationships in biological evolution, economic interaction and the internet. From an abstract point of view, one can distinguish *network structure*, i.e. the (typically directed) graph that describes the wiring of interactions between the nodes the network is composed of, and *network dynamics*, refer-

T. Rohlf (✉)
Max-Planck-Institute for Mathematics in the Sciences, Inselstrasse 22, 04103 Leipzig, Germany
e-mail: rohlf@mis.mpg.de

T. Gross, H. Sayama (eds.), *Adaptive Networks,* Understanding Complex Systems,
DOI 10.1007/978-3-642-01284-6_5,

ring to certain state variables assigned to the nodes which can change in response to inputs or perturbations from other nodes. In the case of the genome, for example, dynamics of regulatory networks, as captured in changes of gene expression levels, results from repression and -activation of gene transcription controlled by regulatory inputs (transcription factors) from other genes [25].

A main characteristic of all these systems is that they evolve in time, under the continuous pressure of adaptation to highly dynamic environments. Since network topology and dynamics *on* the network are typically tightly interrelated, this implies a co-evolutionary loop between a time-varying network wiring and adaptive changes in the nodes' dynamics. For example, there is evidence from the analysis of gene regulatory networks that interactions between genes can change in response to diverse stimuli [58], leading to changes in network toplogy that can be far greater than what is expected from random mutation. In the case of nervous systems, it is evident that self-organization and adaptation processes have to continue throughout the lifetime of a network, since learning is a major function of such networks. In this context, a major conceptual challenge lies in the fact that, in order to properly function as information processing systems, adaptive networks have to be, on the one hand, highly robust against *random* (or dys-functional) perturbations of wiring and dynamics (noise) [5, 9, 90], and, on the other hand, stay responsive to essential cues (information) from the environment that can change in time. While robustness would clearly favor highly ordered dynamics that is basically insensitive to any perturbation, sensitivity and adaptive pressure tend to favor an ergodic sampling of the accessible state space. The latter comes with the risk of leading network evolution into regimes of chaotic dynamics with large parameter ranges where network dynamics is not easily controlled [63].

Two interesting and interrelated questions arise: First, is there a critical point, given by specific values of order parameters that characterize network toplogy and -dynamics, where adaptive dynamics with its delicate balance between robustness and flexibility is optimized? Second, can we find simple, very general principles of network self-organization from *local* co-evolutionary rules that couple network rewiring and -dynamics such that the network globally evolves to this point?

In the inanimate world, phase transitions from ordered to disordered dynamics at critical values of a system parameter are found in several classes of many particle systems, as for example in ferromagnets, where the system can maintain spontaneous magnetization below the Curie temperature, while above this critical point disorder induced by thermal fluctuations wins. Similar transitions form an organized to a disorganized state also have been observed in living systems, for example in enzyme kinetics [64], growth of bacterial populations [66] and brain activity [43]. Most biological networks are different in many regards from the many particle systems as considered in standard statistical mechanics. In particular, interactions between units are typically asymmetric and directed, such that a Hamiltonian (energy function) does not exist. Furthermore, to make global dynamical properties accessible despite the overall stunning degree of complexity found in these networks, a number of simplifying assumptions have to be made.

In this line, random Boolean networks (RBN) were proposed as simplified model of large gene regulatory networks [39, 88]. In these models, each gene receives a constant number K of regulatory inputs from other genes. Time is assumed to proceed in discrete steps. Each gene i is either "on" or "off", corresponding to a binary state variable $\sigma_i \in \{0, 1\}$, which can change at time t according to a (fixed) Boolean function of its inputs at time $t - 1$ (a more formal definition will be given in Sect. 5.2.2). RBNs can easily be generalized to a variable number of connections per node, and "biased" update rules [1] Despite its simple deterministic update rule, this model exhibits rich dynamical behavior. In particular, RBNs exhibit an order-disorder phase transition when each unit has on average two inputs from other nodes[2] [29].

Combinatorial and statistical methods have provided quite detailed knowledge about properties of RBNs near criticality [3, 4, 11, 12, 16, 17, 23, 24, 30, 32, 35, 40–42, 44, 45, 55–57, 79, 83]. The second class of discrete dynamical networks that we will consider are Random Threshold Networks (RTN) with sparse asymmetric connections (for details, cf. Sect. 5.2.3). Networks of this kind were first studied as diluted, non-symmetric spin glasses [26] and diluted, asymmetric neural networks [28, 47]. For the study of topological questions in networks, a version with discrete connections $c_{ij} = \pm 1$ is convenient and will be considered here. It is a subset of Boolean networks with similar dynamical properties. Random realizations of these networks exhibit complex non-Hamiltonian dynamics including transients and limit cycles [10, 49]. In particular, a phase transition is observed at a critical average connectivity K_c with lengths of transients and attractors (limit cycles) diverging exponentially with system size for an average connectivity larger than K_c. A theoretical analysis is limited by the non-Hamiltonian character of the asymmetric interactions, such that standard tools of statistical mechanics do not apply [28]. However, combinatorial as well as numerical methods provide a quite detailed picture about their dynamical properties and correspondence with Boolean Networks [10, 11, 27, 29, 30, 35, 48, 49, 57, 65, 75, 77, 79].

From the observation that complex dynamical behavior in these simple model systems is primarily found near criticality, Kauffman [39, 40] and other researchers [50, 91] postulated that evolution should drive living systems to this "edge of chaos". Indeed, a number of parameters that are highly relevant for biological systems, as, for example, robustness [40] and basin entropy [46] of attractors (limit cycles), mutual information in the switching dynamics of nodes [55, 73] and information diversity in structure-dynamics relationships [68] are maximized near the order-disorder transition of RBNs, supporting the idea that this point provides unique properties for balancing the conflicting needs of robustness and adaptive flexibility. Today, experimental results provide strong support for the idea that many biological

[1] The bias is typically parameterized in terms of a stochastic control parameter p, which determines the probability that a particular input configuration generates the output "1".

[2] This critical connectivity $K_c = 2$ refers to the simplest case, when all Boolean functions have equal probability to occur. For the case of biased update rules, this generalizes to $K_c = 1/(2p(1-p))$.

systems operate in a regime that shares relevant properties with criticality in random networks. Indications for critical behavior were found, for example, in gene expression dynamics of several organisms [67, 72, 82] and in neuronal networks in the brain [14, 52]. Since, in all these systems, there generally exists no central control that could continuously adjust system parameters to poise dynamics at the critical state, we are *forced* to postulate that there are simple, *local* adaptive mechanisms present that are capable of driving *global* dynamics to a state of *self-organized criticality*. Evolution towards self-organized criticality was established in a number of non-equilibrium systems [6], namely, avalanche models with extremal dynamics [8, 71], multi-agent models of financial markets [59], forest fires [60] and models of biological macroevolution [31]. Still, these approaches are limited in the sense that they consider a fixed or at least pre-structured topology.

Network models of *evolving* topology, in general, have been studied with respect to critical properties earlier in other areas, e.g., in models of macro-evolution [84]. Network evolution with a focus on gene regulation has been studied first for Boolean networks in [20] observing self-organization in network evolution, and for threshold networks in [21]. Combining the evolution of Boolean networks with game theoretical interactions is used for model networks in economics [70].

Christensen et al. [22] introduced a static network with evolving topology of undirected links that explicitly evolves towards a critical connectivity in the largest cluster of the network. In particular they observed for a neighborhood-oriented rewiring rule that the connectivity of the largest cluster evolves towards the critical $K_c = 2$ of a marginally connected network. However, in this model the core characteristics of adaptive networks, a co-evolution between dynamics and topology [37], is hard to establish, since the evolution rule, here chosen according to the Bak-Sneppen model of self-organized criticality [7], does not provide a direct coupling between rewiring of connections and an order parameter of the dynamics *on* the networks.

Keeping the idea of local connectivity adaptations, a different line of research pursues models of adaptive co-evolutionary networks in the context of discrete dynamical networks, in particular based on RBNs and RTNs. The common principle in these models is the coupling of *local* rewiring events to approximate, local measurements of a dynamical order parameter. In the limit of large network sizes N, this principle leads to network evolution towards a *global* self-organized critical state. Bornholdt and Rohlf [19] introduced a topology-evolving rule based on the dynamical activity of nodes in RTNs: Active nodes, whose binary state changes in time, tend to lose links, while inactive (frozen) nodes, whose binary states are fixed, tend to gain new links. In a recent extension [76], also adaptive changes of the nodes' activation thresholds were considered. A very similar co-evolutionary rule was applied to RBNs by Liu and Bassler [53]; besides the case where only the rewired node is assigned a new Boolean function, they also consider "annealed" networks, where each node is assigned a new logical function in each evolutionary time step. Teuscher and Sanchez [87] showed that this adaptive principle can also be applied to turing neural networks. Self-organized critical neural networks with stochastic dynamics and a rewiring rule based on dynamical correlations between

nodes was studied by Bornholdt and Röhl [18], observing robust self-organization of both network toplogy and -dynamics. In the same context, Bertschinger et al. [15] studied a synaptic scaling rule leading to self-organized criticality in recurrent neural networks. A different adaptive scheme, based on a input-dependent disconnection rule and a minimal connectivity in RBNs, was studied by Luque et al. [54]. A perturbation analysisindicates the emergence of self-organized critical behavior.

The remainder of this chapter is organized as follows: in Sect. 5.2, the dynamics of RBNs and RTNs are defined and basic dynamical and statistical properties of these systems are summarized. In particular, central order parameters that are relevant for the definition of adaptive algorithms will be introduced. In Sect. 5.3, we will review different models of adaptive, discrete dynamical networks leading to evolution towards self-organized criticality that have been established in this context so far, with a focus on activity- and correlation-based rewiring rules. Finally, Sect. 5.4 contains a summary and conclusions.

5.2 Dynamics of Random Boolean Networks and Random Threshold Networks

In this section, we provide definitions for the two types of discrete dynamical networks under consideration, Random Boolean Networks and Random Threshold Networks. First, the underlying graph structure that connects dynamical units (automata) is defined, then dynamical update rules are provided. Further, basic dynamical properties of these systems are summarized.

5.2.1 Underlying Graph Structure

Concerning topology, discrete dynamical networks are described by *random directed graphs* $G(N, Z, g)$, where N is the number of nodes, Z the number of edges or links (arrows connecting nodes), and g a function that describes the statistical distribution of the links between nodes. Arrows pointing *at* a node are considered as *inputs*, arrows pointing from this node *to* another node as *outputs*. If, for example, Z links out of the $2N^2$ possible are assigned at random such that the average connectivity $\bar{K} := Z/N$ is fixed at a predefined value and $Z \ll 2N^2$ (sparse network), the resulting statistical distributions of the number k of inputs and outputs follow a Poissonian [34]:

$$P(k) = \frac{\bar{K}^k}{k!} \exp(-\bar{K}). \tag{5.1}$$

A schematic example of interaction graph structure is shown in the left panel of Fig. 5.1.

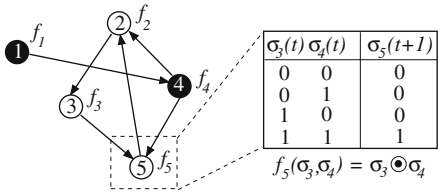

Fig. 5.1 *Left panel*: example of an interaction graph structure for a RBN of size $N = 5$ with average connectivity $\tilde{K} = 6/5$; f_i are individual Boolean functions assigned to each node $i = 1, .., 5$, *black circles* mark $\sigma_i = 1$, *white circles* $\sigma_i = 0$. *Right panel*: example of a Boolean update table assigned to a site (AND function of the site's inputs)

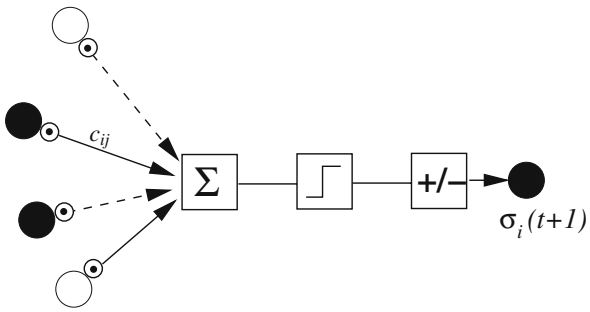

Fig. 5.2 Schematic sketch of a threshold dynamical unit: input states (*circles on the left, black circles* correspond to a state $\sigma_j = +1$, *white circles* to $\sigma_j = -1$) are multiplied ($\odot$) with interaction weights c_{ij} (*lined arrows*: $c_{ij} = +1$, *dashed arrows*: $c_{ij} = -1$); these values are summed (Σ) and added to a threshold. Finally, the output $\sigma_i(t + 1)$ is determined by the sign $(+/-)$ of the resulting signal

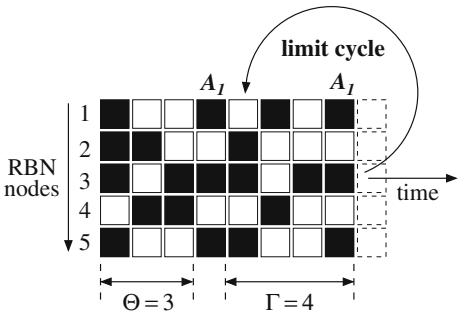

Fig. 5.3 Example of a dynamical trajectory for a $N = 5$ Boolean network, time is running from *left to right*, network nodes are labeled from *top to bottom*. *Black squares* correspond to $\sigma_i = 1$, *white squares* to $\sigma_i = 0$. After a transient of $\Theta = 3$ system states Σ the first state A_1 appears that repeats itself after $\Gamma = 4$ time steps, defining a periodic attractor (limit cycle) with period 4

5.2.2 Random Boolean Networks

A Random Boolean Network (RBN) is a discrete dynamical system composed of N automata. Each automaton is a Boolean variable with two possible states: {0, 1}, and the dynamics is such that

$$\mathbf{F} : \{0, 1\}^N \mapsto \{0, 1\}^N, \tag{5.2}$$

where $\mathbf{F} = (f_1, ..., f_i, ..., f_N)$, and each f_i is represented by a look-up table of K_i inputs randomly chosen from the set of N automata. Initially, K_i neighbors and a look-up table are assigned to each automaton at random.

An automaton state $\sigma_i(t) \in \{0, 1\}$ is updated using its corresponding Boolean function:

$$\sigma_i(t + 1) = f_i(\sigma_{i_1}(t), \sigma_{i_2}(t), ..., \sigma_{i_{K_i}}(t)). \tag{5.3}$$

We randomly initialize the states of the automata (initial condition of the RBN). The N automata are updated synchronously using their corresponding Boolean functions, leading to a new system state $\Sigma := (\sigma_1, ..., \sigma_N)$:

$$\Sigma(t + 1) = \mathbf{F}(\Sigma(t)). \tag{5.4}$$

The right panel of Fig. 5.1 provides an example of an individual update table assigned to a network site.

5.2.3 Random Threshold Networks

A Random Threshold Network (RTN) consists of N randomly interconnected binary sites (spins) with states $\sigma_i = \pm 1$. For each site i, its state at time $t + 1$ is a function of the inputs it receives from other spins at time t:

$$\sigma_i(t + 1) = \mathrm{sgn}\,(f_i(t)) \tag{5.5}$$

with

$$f_i(t) = \sum_{j=1}^{N} c_{ij}\sigma_j(t) + h. \tag{5.6}$$

The N network sites are updated synchronously. In the following discussion the threshold parameter h is set to zero. The interaction weights c_{ij} take discrete values $c_{ij} = +1$ or -1 with equal probability. If i does not receive signals from j, one has $c_{ij} = 0$.

5.2.4 Basic Dynamical Properties of RBNs and RTNs

Let us review a few aspects of the dynamics of Random Boolean Networks and Random Threshold Networks. In fact, they share most basic properties which is closely related to the fact that RTNs are a subset of RBNs.

5.2.4.1 Attractors and Transients

Update dynamics as defined in 5.2.2 and 5.2.3, given the binary state $\sigma_i(t)$ of each node i at time $t-1$, assigns a state vector $\Sigma(t) = (\sigma_1(t), ..., \sigma_N(t))$ to the network at each discrete time step t. The path that $\Sigma(t)$ takes over time t is a dynamical trajectory in the phase space of the system. Since the dynamics is deterministic and the phase space of the system is finite for finite N, all dynamical trajectories eventually become periodic. When we start dynamics from a random initial state, e.g. with each $\sigma_i(0)$, $i = 1...N$ set to 0 or 1 (-1 or $+1$ for RTN, respectively) independent from each other with equal probability $p = 1/2$, the trajectory will pass through Θ transient states before it starts to repeat itself, forming a limit cycles given by

$$\Sigma(t) = \sigma(t + \Gamma). \tag{5.7}$$

The periodic part of the trajectory is the attractor of the dynamics, and the minimum $\Gamma \geq 1$ that satisfies Eq. (5.7) is the *period* of the attractor.

5.2.4.2 Definition of Average Activity and Average Correlation

Let us now define two *local* measures that characterize the typical dynamical behavior of a network site, and the dynamical coordination of pairs of sites.

The *average activity* $A(i)$ of a site i is defined as the average over all states $\sigma_i(t)$ site i takes in dynamical network evolution between two distinct points of time T_1 and T_2:

$$A(i) = \frac{1}{T_2 - T_1 + 1} \sum_{t=T_1}^{T_2} \sigma_i(t) \tag{5.8}$$

"Frozen" sites i which do not change their states between T_1 and T_2 obviously have $|A(i)| = 1$ (or $|A(i)| = 0$, in the case of RBN), whereas sites that occasionally change their state have $0 \leq |A(i)| < 1$. The *average correlation* $\mathrm{Corr}(i, j)$ of a pair (i, j) of sites is defined as the average over the products $\sigma_i(t)\sigma_j(t)$ in dynamical network evolution between two distinct points of time T_1 and T_2:

$$\mathrm{Corr}(i, j) = \frac{1}{T_2 - T_1 + 1} \sum_{t=T_1}^{T_2} \sigma_i(t)\sigma_j(t) \tag{5.9}$$

If the dynamical activity of two sites i and j in RTN is (anti-)correlated, i.e. if σ_i and σ_j always have either the same or the opposite sign, one has $|\mathrm{Corr}(i, j)| = 1$.[3] If the relationship between the signs of σ_i and σ_j occasionally changes, one has $0 \leq |\mathrm{Corr}(i, j)| < 1$.

5.2.4.3 Properties of $A(i)$ and $\mathrm{Corr}(i, j)$ and Their Relation to Criticality

If we consider statistical ensembles of randomly generated networks with sparse wiring ($\bar{K} \ll N$), both $A(i)$ and $\mathrm{Corr}(i, j)$ of RBNs and RTNs exhibit a second order phase transition at a critical average connectivity K_c (averaged over the whole network ensemble). Below K_c, network nodes are typically frozen, above K_c, a finite fraction of nodes is active; this can be clearly appreciated from the behavior of the *frozen component* $C(\bar{K})$, defined as the fraction of nodes that do not change their state along the attractor. The average activity $A(i)$ of a frozen site i thus obeys $|A(i)| = 1$. In the limit of large N, $C(K)$ undergoes a transition at K_c vanishing for larger K. With respect to the average activity of a node, $C(K)$ equals the probability that a random site i in the network has $|A(i)| = 1$. Note that this is the quantity which is checked stochastically by the local rewiring rule that will be discussed in Sect. 5.3.1.2. The frozen component $C(K, N)$ is shown for random networks of two different system sizes N in Fig. 5.4. One finds that $C(K, N)$ can be approximated by

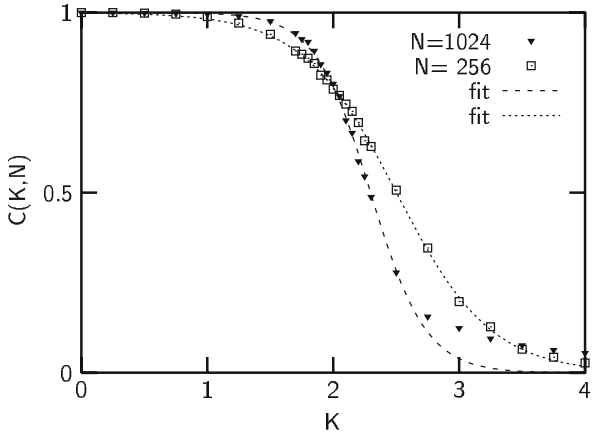

Fig. 5.4 The frozen component $C(K, N)$ of random threshold networks, as a function of the networks' average connectivities K. For both system sizes shown here ($N = 256$ and $N = 1{,}024$) the data were measured along the dynamical attractor reached by the system, averaged over 1,000 random topologies for each value of K. One observes a transition around a value $K = K_0$ approaching $K_c = 2$ for large N. A sigmoid function fit is also shown. To avoid trapping in exponential divergence of attractor periods for $K > 2$, the simulations have been limited to $T_{max} = 10{,}000$. The mismatch of data and fit for $N = 1{,}024$, $K \geq 2.75$ is due to this numerical limitation

[3] In RBN, correlated pairs have $|\mathrm{Corr}(i, j)| = 1$ and anti-correlated pairs $|\mathrm{Corr}(i, j)| = 0$.

$$C(K, N) = \frac{1}{2}\{1 + \tanh[-\alpha(N) \cdot (K - K_0(N))]\}. \tag{5.10}$$

This describes the transition of $C(K, N)$ at an average connectivity $K_0(N)$ which depends only on the system size N. One finds for the finite size scaling of $K_0(N)$ that

$$K_0(N) - 2 = a \cdot N^{-\beta} \tag{5.11}$$

with $a = 3.30 \pm 0.17$ and $\beta = 0.34 \pm 0.01$ (see Fig. 5.5), whereas the parameter α scales with system size as

$$\alpha(N) = b \cdot N^{\gamma} \tag{5.12}$$

with $b = 0.14 \pm 0.016$ and $\gamma = 0.41 \pm 0.01$. This indicates that the transition of $C(K, N)$ exhibits a sharp decay near the critical connectivity K_c when the thermodynamic limit $N \to \infty$ is approached.

The number of frozen nodes is a decisive quantity for the evolution of adaptive networks. If all nodes are frozen ($C = 1$), as it is typically found for networks with very sparse $\bar{K}$, the network is basically irresponsive to signals from the environment and hence can neither process information nor adapt. If, on the other hand, C vanishes, all nodes exhibit more or less chaotic switching behavior – dynamics becomes completely autonomous and hence again useless for information processing. A finite number of frozen nodes, as it is found near K_c, enables adaptive response to environmental signals by assignment of new, functional behavior to previously frozen nodes, and also makes sure that global network dynamics avoids the extremes of overly ordered and chaotic regimes. In the following section, we will discuss models of adaptive network evolution by local dynamical rules that lead to emergence

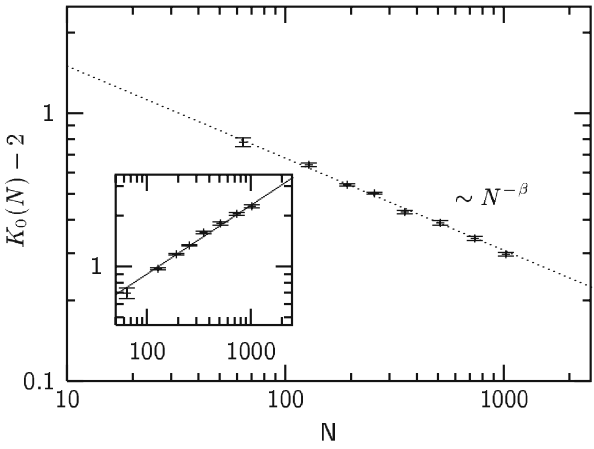

Fig. 5.5 The finite size scaling of the transition value K_0, obtained from sigmoidal fits as shown in Fig. 5.4. K_0 approaches $K_c = 2$ with a scaling law $\sim N^{-\beta}$, $\beta = 0.34 \pm 0.01$. The inset shows the scaling behavior of the parameter $\alpha(N)$; one finds $\alpha(N) \sim N^{\gamma}$, $\gamma = 0.41 \pm 0.014$

of self-organized critical networks, i.e. networks that evolve to the "optimal" point just at the phase transition from ordered to chaotic dynamics.

5.3 Network Self-Organization from Co-evolution of Dynamics and Topology

In this section, we will discuss models of adaptive network self-organization in the context of discrete dynamical networks. The common principle that governs network evolution is a *co-evolution of dynamics and topology from local dynamical rules*: An order parameter of network dynamics is estimated from local measurements (often averaged over a representative number of dynamical update cycles, e.g., over one attractor period of a limit cycle the dynamics converged to, cf. Sect. 5.2.4.1). Based on the measured value of the order parameter, network connectivity and/or the switching behavior of nodes is adapted by local adaptive rules. Usually, there is a time scale separation between frequent dynamical updates and rare rewiring events. After a large number of adaptive cycles, evolution towards a *self-organized critical state* is observed.

5.3.1 Activity-Dependent Rewiring

5.3.1.1 Motivation

Living organisms process their information by dynamical systems at multiple levels, e.g. from gene regulatory networks at the cellular level, to neural networks in the central nervous system of multi-cellular organisms. As *complex adaptive systems*, organisms have to deal with the conflicting needs of flexible response to changing environmental cues, while maintaining a reasonable degree of stability in the dynamical networks that process this information. This led to the idea that these systems may have evolved to the "edge of chaos" between ordered and disordered dynamical regimes [40, 50]. In the following, a simple evolutionary mechanism will be introduced [19], based on a local coupling between a dynamical order parameter – the average activity of dynamical units (sites) in RTNs (Eq. 5.8) – and a topological control parameter – the number of inputs a site receives from other units. In a nutshell, the adaptive rule can be summarized as *frozen nodes grow links, active nodes lose links*. This rule abstracts the need for both flexibility and stability of network dynamics. In a gene regulatory network, for example, a frozen gene cannot respond to different inputs it may receive, and hence is practically dysfunctional; the addition of a new regulatory input potentially assigns a new function to this gene. On the other hand, a very active gene will tend to show chaotic switching behavior and may lead to loss of stability in network dynamics – a reduction in input number reduces the probability of this undesirable behavior [78]. Similar demands for a local, homeostatic regulation of activity and connectivity can be expected in neural networks of the nervous system and are supported by experimental evidence [33].

5.3.1.2 Model

Let us consider a Random Threshold Network of N randomly interconnected binary elements as defined in Sect. 5.2.3. In the beginning, network topology is initialized as a directed, random graph with connectivity distributed according to a Poissonian with average connectivity K_{ini} (cf. Sect. 5.2.1), and $c_{ij} = +1$ or $c_{ij} = -1$ with equal probability for non-vanishing links. While network evolution is insensitive to K_{ini} in general (as will be shown), we choose $0 < K_{ini} < 3$ in simulations to obtain reasonably fast convergence of the evolutionary dynamics. Network dynamics is iterated according to Eq. (5.5) starting from a random initial state vector $\Sigma(0) = (\sigma_1(0), ..., \sigma_N(0))$, with $\sigma_i = +1$ or $\sigma_i = -1$ with equal probability for each i. After T iterations, the dynamical trajectory eventually reaches a periodic attractor (limit cycle or fixed point, compare Sect. 5.2.4.1). Then we apply the following local rewiring rule to a randomly selected node i of the network: **If node i does not change its state during the attractor, it receives a new non-zero link c_{ij} from a random node j. If it changes its state at least once during the attractor, it loses one of its non-zero links c_{ij}.** Iterating this process leads to a self-organization of the average connectivity of the network. The basic idea of this rewiring rule is sketched schematically in Fig. 5.6, a particular algorithmic realization is provided in Box 5.1.

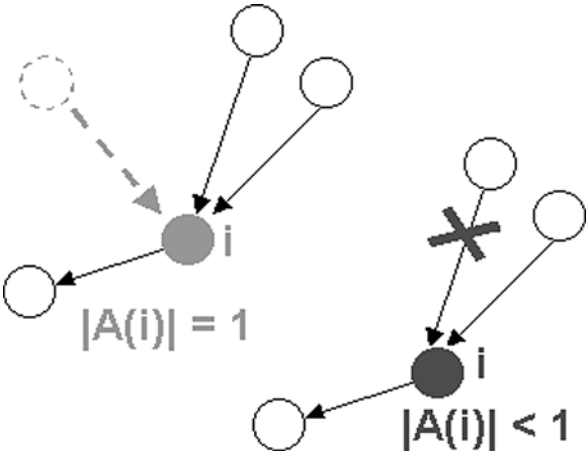

Fig. 5.6 The selective criterion leading to topological self-organization: A dynamically frozen site ($|A(i)| = 1$) receives an additional regulatory input, an active site ($|A(i)| < 1$) looses one of its inputs

Box 5.1 Adaptive algorithm for activity-dependent rewiring

This box gives an example of an adaptive algorithm that realizes the local rewiring rule "frozen nodes grow links, active nodes lose links" [19]:

1. Choose a random network with an average connectivity K_{ini}.
2. Choose a random initial state vector $\Sigma(0) = (\sigma_1(0), ..., \sigma_N(0))$.

3. Calculate the new system states $\Sigma(t)$ according to Eq. (5.2), using parallel update of the N sites.
4. Once a previous state reappears (a dynamical attractor with period Γ is reached) or otherwise after T_{max} updates the simulation is stopped. Then, a site i is chosen at random and its average activity $A(i)$ during the last $T = \Gamma$ time steps is determined (in case no attractor is reached, $T = T_{max}/2$ is chosen).
5. If $|A(i)| = 1$, i receives a new link c_{ij} from a site j selected at random, choosing $c_{ij} = +1$ or -1 with equal probability. If $|A(i)| < 1$, one of the existing non-zero links of site i is set to zero.
6. Finally, one non-zero entry of the connectivity-matrix is selected at random and its sign reversed.
7. Go to step number 2 and iterate.

5.3.1.3 Results

The typical picture arising from the model as defined above is shown in Fig. 5.7 for a system of size $N = 1,024$. Independent of the initial connectivity, the system evolves towards a statistically stationary state with an average connectivity $K_{ev}(N = 1,024) = 2.55 \pm 0.04$. With varying system size we find that with increasing N the average connectivity $\bar{K}$ approaches K_c (which, for threshold $h = 0$ as considered here, is found slightly below $\bar{K} = 2$ [77]), see Fig. 5.8. In particular, one can fit the scaling relationship

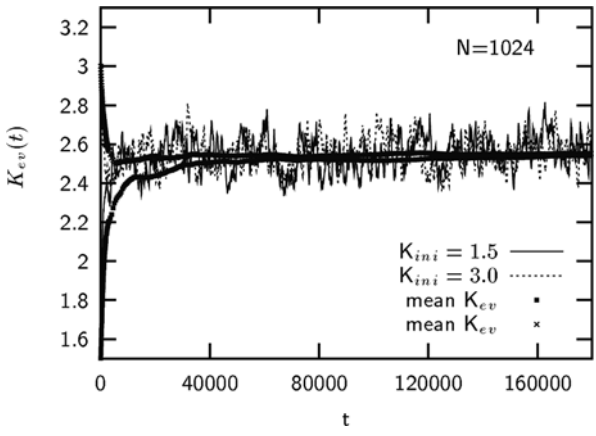

Fig. 5.7 Evolution of the average connectivity of threshold networks rewired according to the rules described in the text, for $N = 1,024$ and two different initial connectivities ($K_{ini} = 1.5$ and $K_{ini} = 3.0$). Independent of the initial conditions chosen at random, the networks evolve to an average connectivity $K_{ev} = 2.55 \pm 0.04$. The plot shows the time series and the corresponding cumulative means for K_{ev}. The evolutionary time t is discrete, each time step representing a dynamical run on the evolved topology. Individual runs were limited to $T_{max} = 1,000$ iterations

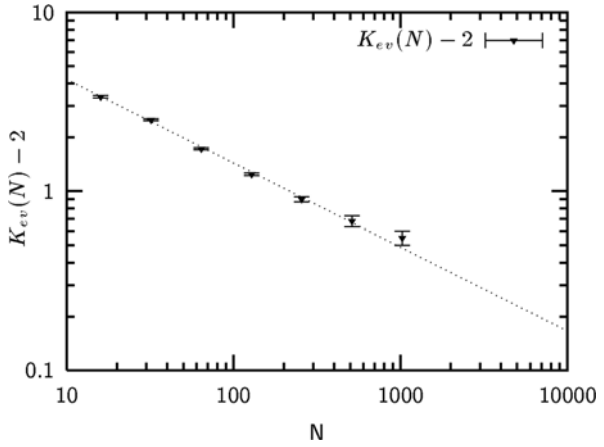

Fig. 5.8 The average connectivity of the evolved networks converges towards K_c with a scaling law $\sim N^{-\delta}$, $\delta = 0.47 \pm 0.01$. For systems with $N \leq 256$ the average was taken over $4 \cdot 10^6$ time steps, for $N = 512$ and $N = 1{,}024$ over $5 \cdot 10^5$ and $2.5 \cdot 10^5$ time steps, respectively. Finite size effects from $T_{max} = 1{,}000$ may overestimate K_{ev} for the largest network shown here

$$K_{ev}(N) - 2 = c \cdot N^{-\delta} \tag{5.13}$$

to the measured connectivity values with $c = 12.4 \pm 0.5$ and $\delta = 0.47 \pm 0.01$. In the evolutionary steady state, the average connectivity $\bar{K}$ of evolving networks exhibits limited fluctuations around the evolutionary mean K_{evo} which are approximately Gaussian distributed, with a variance vanishing $\sim 1/N$ [74].

Going beyond averaged topological quantities, one can also measure the degree distributions of inputs and outputs in evolving networks, and compare it to what is expected for random networks (cf. Sect. 5.2.4.3). In finite size networks, substantial deviations from random graphs are found [78]: While the outdegree distribution stays close to the Poissonian of a random graph, evolved in-degree distributions are considerably flatter. For the averaged statistical distribution $p(K)$ of in-links (Fig. 5.9) of the evolving networks one observes a flat exponential decay

$$p(K) \approx p_0 \cdot \exp[-\alpha K], \tag{5.14}$$

with $p_0, \alpha = \text{const}$. This observation indicates that the self-organized network state, at least for finite N, is substantially different from random networks with the same average connectivity. Since network evolution is based on co-evolutionary adaptation of dynamics and topology by local rewiring rules, this raises the question of whether the evolutionary statistically stationary state exhibits specific characteristics and correlations between dynamical and toplogical order parameters also on the *global scale*. This is indeed the case for finite N: If we compare, for example, the frozen component $C(\bar{K})$ or fraction of "frozen genes" for different values of connectivity fluctuations around the evolutionary mean K_{evo} (Fig. 5.10), we observe that this curve exhibits a broad plateau where activity is stabilized at intermediate values,

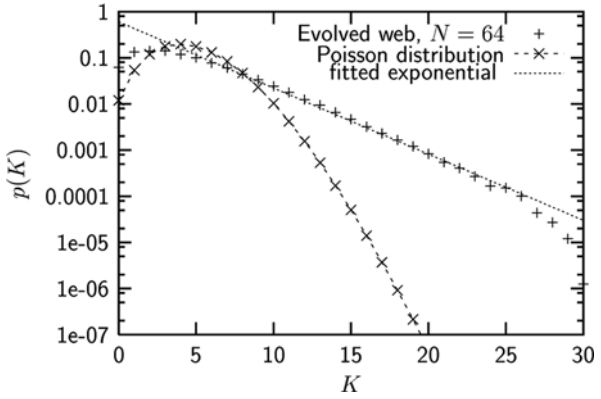

Fig. 5.9 Statistical distribution $p(K)$ of the number of inputs K per node (gene) in the proposed model for a network of size $N = 64$. Compared to the Poisson distribution for random networks with $\bar{K} = 4.46$, it shows a flatter decay $\propto \exp[-K]$

with almost step-like boundaries for small and large $\bar{K}$, whereas the corresponding curve for random networks is much smoother and decays earlier (compare also Sect. 5.2.4.3 for the phase transition observed in ensembles of random networks). This indicates that coevolution of dynamics and topology extends to a global scale, in spite of local rewiring events and a pronounced time scale separation between dynamical and topological updates.[4]

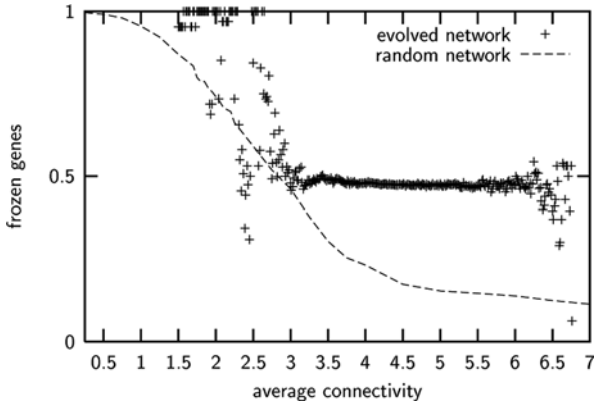

Fig. 5.10 The frozen component C (fraction of frozen genes) as a function of the average connectivity for an evolved network of size $N = 64$ (*crosses*). The *dashed line* shows the corresponding curve for random networks

[4] This time scale separation can be easily identified e.g. from step 4 of the adaptive algorithm summarized in Box 5.1: After T dynamical system updates, one out of N sites is rewired, hence time scale separation is at the order of $T \cdot N$.

Last, let us characterize dynamics *on* the evolving networks, and investigate in how far it may exhibit signatures of self-organized critical behavior even in the finite size networks we studied so far (which, concerning average connectivity, are evidently super-critical). In contrast to random, noise-driven dynamics, where correlations decay fast (typically as an exponential), the self-organized critical state is characterized by non-trivial, long-range correlations in dynamical trajectories. A convenient measure to characterize such long-range correlations is the *power spectrum* of the dynamical time series. Let us consider the autocorrelation function of a time signal $f(t)$, defined by

$$R(\tau) = \int_{-\infty}^{+\infty} f(t) f(t-\tau)\, dt. \tag{5.15}$$

The power spectrum $G(f)$ is the Fourier transform of the autocorrelation function, i.e.

$$G(f) = \int_{-\infty}^{+\infty} R(\tau) e^{-2\pi i f \tau} d\tau. \tag{5.16}$$

In the case of time-discrete systems, the integrals are replaced by the corresponding sums. For strongly (auto-)correlated systems, e.g. near the critical point, we typically expect a flat decay of the power spectrum $G(f) \sim 1/f^{\alpha}$ with $\alpha \approx 1$, while for a random walk, e.g., we would obtain $\alpha = 2$. The dynamical order parameter that we investigate is the *global average activity* at evolutionary time step t:

$$\langle A \rangle(t) = \left| \frac{1}{N} \sum_{i=1}^{N} A_i(t) \right|. \tag{5.17}$$

Figure 5.11 shows a typical snapshot of the time series of $\langle A \rangle$ on evolving networks, the power spectrum is shown in Fig. 5.12. A least squares fit yields $G(f) \sim 1/f^{\alpha}$ with $\alpha = 1.298$ for the global average activity, i.e. a clear indication of long-range correlations in dynamics [74]. Other measures of global dynamics also show evidence for criticality, for example, the statistical distribution of attractor periods is scale-free, as will be discussed in Sect. 5.3.3 for a RBN variant of the model.

The self-organization towards criticality observed in this model is different from other known mechanisms exhibiting the amazingly general phenomenon of self-organized criticality (SOC) [7, 8, 71, 84]. Our model introduces a (new, and interestingly different) type of mechanism by which a system self-organizes towards criticality, here $K \rightarrow K_c$. This class of mechanisms lifts the notions of SOC to a new level. In particular, it exhibits considerable robustness against noise in the system. The main mechanism here is based on a topological phase transition in dynamical networks.

In addition to the rewiring algorithm as described in this chapter, a number of different versions of the model were tested. Including the transient in the measurement

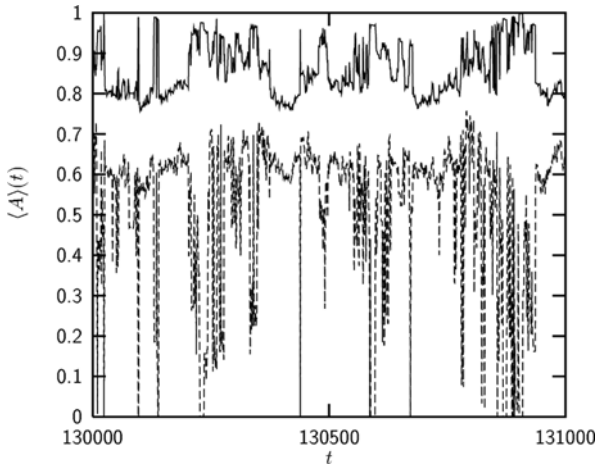

Fig. 5.11 Time series of the global average activity $\langle A \rangle$ (arbitrary time window of the evolutionary process). *Upper curve*: Signal averaged over the whole network, *lower curve*: Signal averaged over non-frozen nodes only

of the average activity $A(i)$ results in a similar overall behavior (where we allowed a few time steps for the transient to decouple from initial conditions). Another version succeeds using the correlation between two sites instead of $A(i)$ as a mutation criterion (this rule could be called "anti-Hebbian" as in the context of neural network learning). In addition, this version was further changed allowing different locations of mutated links, both, between the tested sites or just at one of the nodes. All these different realizations exhibit the same basic behavior as found for the model above.

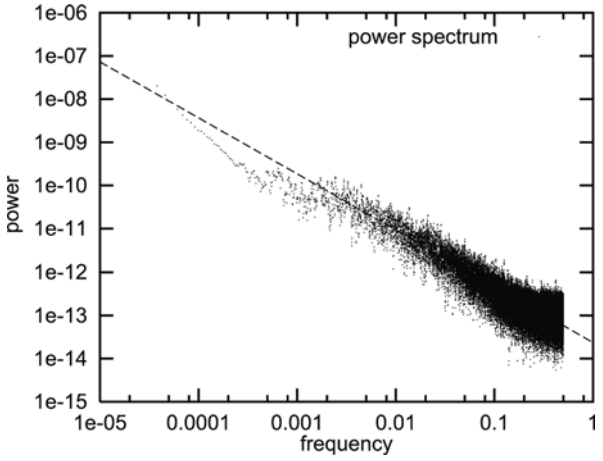

Fig. 5.12 Power spectrum of the global average activity $\langle A \rangle$ over 10^5 evolutionary time steps, averaged over all network sites (compare *upper curve* in Fig. 5.11, double-logarithmic plot. The *dashed line* has slope -1.298

Thus, the proposed mechanism exhibits considerable robustness. Interestingly, it has been shown that this mechanism leads to robust topological and dynamical self-organization also in other classes of dynamical networks. In particular, Teuscher and Sanchez [87] showed that this rule can be generalized to Turing neural networks and drives network evolution to $K_c = 2$ in the limit of large N.

In the next subsection, we will discuss an extension of the model that includes adaptation of thresholds in RTN, in addition to rewiring of links. This extension still exhibits robust self-organization as in the original model, however, exhibits several interesting new features, namely, symmetry breaking of evolutionary attractors, and correlation of dynamical and toplogical diversity.

5.3.2 Adaptive Thresholds – Time Scale Separation Leads to Complex Topologies

So far, we assumed that dynamical units in the networks are homogeneous (identical) with respect to their switching behavior, which for real world networks usually is a quite unrealistic assumption. Furthermore, recent studies have shown that inhomogeneity of thresholds leads to new and unexpected phenomena in RTNs, e.g. an order-disorder transition induced by *correlations* between thresholds and input number of nodes [75]. In the general case of inhomogeneous thresholds, we have to modify Eq. (5.5) such that

$$f_i(t) = \sum_{j=1}^{N} c_{ij}\sigma_j(t) + h_i, \tag{5.18}$$

where the indexed threshold h_i now takes into account that thresholds can vary from node to node. The only restriction we impose is $h_i \leq 0$, to make activation, i.e. $\sigma_i = +1$, more difficult.

We now introduce a minimal model linking regulation of activation thresholds and rewiring of network nodes in RTNs to local measurements of a dynamical order parameter [76]. Adaptation of thresholds opens up for the possibility of units that become heterogeneous with respect to their *dynamical* properties: Nodes with high thresholds are inert and switch their state only for few input configurations (similar to the effect of canalizing functions in RBNs), whereas nodes with low thresholds are more likely to switch. A new control parameter $p \in [0, 1]$ determines the probability of rewiring vs. threshold adaptations. In particular, the activity $A(i)$ of a site i can be controlled in two ways: If i is frozen, it can increase the probability to change its state by either increasing its number of inputs $k_i \rightarrow k_i + 1$, or by making its threshold $h_i \leq 0$ less negative, i.e. $|h_i| \rightarrow |h_i| - 1$. If i is active, it can reduce its activity by adapting either $k_i \rightarrow k_i - 1$ or $|h_i| \rightarrow |h_i| + 1$. To realize this adaptive scheme, we have to modify step 4 in the adaptive algorithm of Box 5.1: **A site i is chosen at random and its average activity $A(i)$ during the last $T = \Gamma$ time steps is determined (in case no attractor is reached, $T = T_{max}/2$ is chosen). If $|A(i)| < 1$, then $k_i \rightarrow k_i - 1$ with probability p (removal of one**

randomly selected input). With probability $1-p$**, adapt** $|h_i| \to |h_i|+1$ **instead. If** $|A(i)| = 1$**, then** $k_i \to k_i + 1$ **with probability** p **(addition of a new input from a randomly selected site). With probability** $1-p$**, adapt** $|h_i| \to |h_i| - 1$ **instead. If** $h_i = 0$**, let its value unchanged.** If the control parameter p takes values $p > 1/2$, rewiring of nodes is favored, whereas for $p < 1/2$ threshold adaptations are more likely. Notice that the model discussed in the last subsection is contained as the limiting case $p = 1$ (rewiring only and $h_i = const. = 0$ for all sites).

Results. After a large number of adaptive cycles, networks self-organize into a *global* evolutionary steady state. An example is shown in Fig. 5.13 for networks with $N = 512$: starting from an initial value $\bar{K}_{ini} = 1$, the networks' average connectivity $\bar{K}$ first increases, and then saturates around a stationary mean value $\bar{K}_{evo}$; similar observations are made for the average threshold $\bar{h}$ (Fig. 5.13, lower panel). The non-equilibrium nature of the system manifests itself in limited fluctuations of both $\bar{K}$ and $\bar{h}$ around $\bar{K}_{evo}$ and $\bar{h}_{evo}$. Regarding the dependence of $\bar{K}$ with respect to p, we make the interesting observation that it changes non-monotonically. Two cases can be distinguished: When $p = 1$, $\bar{K}$ stabilizes at a very sparse mean value $\bar{K}_{evo}$, e.g. for $N = 512$ at $\bar{K}_{evo} = 2.664 \pm 0.005$. When $p < 1$, the symmetry of this evolutionary steady state is broken. Now, $\bar{K}$ converges to a much higher mean value $\bar{K}_{evo} \approx 43.5 \pm 0.3$ (for $N = 512$), however, the particular value which is finally reached is *independent of* p. On the other hand, *convergence times* T_{con} needed to reach the steady state are strongly influenced by p: $T_{con}(p)$ diverges when p

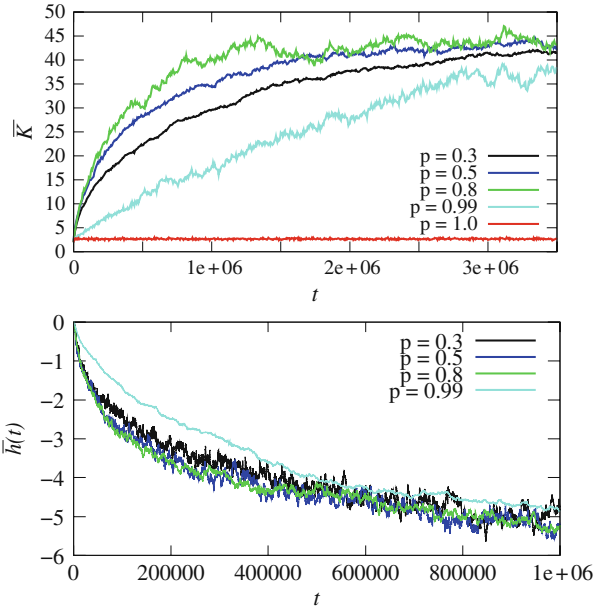

Fig. 5.13 *Upper panel:* Evolution of the average connectivity $\bar{K}$ of threshold networks, using the adaptive algorithm (cf. Fig. 5.1), for $N = 512$ and initial connectivity $\bar{K}_{ini} = 1$. Time series for five different values of p are shown. *Lower panel:* The same for the average threshold $\bar{h}$

approaches 1 (compare Fig. 5.2 for $p = 0.99$). We conclude that p determines the *adaptive time scale*. This is also reflected by the stationary in-degree distributions $p(k_{in})$ that vary considerably with p (Fig. 5.14); when $p \to 1$, these distributions become very broad. The numerical data suggest that a power law

$$\lim_{p \to 1} p(k_{in}) \propto k_{in}^{-\gamma} \tag{5.19}$$

with $\gamma \approx 3/4 \pm 0.03$ is approached in this limit (cf. Fig. 5.4, dashed line). At the same time, it is interesting to notice that the evolved out-degree distributions are much narrower and completely insensitive to p (Fig. 5.14, data points without lines). Hence, we make the interesting observation of a highly robust self-organization and homeostatic regulation of the average wiring density, while, at the same time in the limit $p \to 1$, time scale separation between frequent rewiring and rare threshold adaptation leads to emergence of complex, heterogeneous topologies, as reflected in the broad distribution of input numbers approaching a power law. Obviously, we have a non-trivial coevolutionary dynamics in the limit $p \to 1$ which is significantly different from the limit of small p. This is also indicated by the emergence of strong correlations between input number and thresholds in this limit (see the steep increase of the curves for $p > 0.5$ in Fig. 5.15), while in the limit of small p correlations are weak.

To summarize, we find that coevolution of both rewiring and threshold adaptation with the dynamical activity on RTNs leads to a number of interesting new effects: We find spontaneous symmetry breaking into a new class of adaptive networks that is characterized by increased heterogeneity in wiring topologies and emergence of correlations between thresholds and input numbers. At the same time, we find a highly robust regulation of the average wiring density which is independent of p for any $p < 1$.

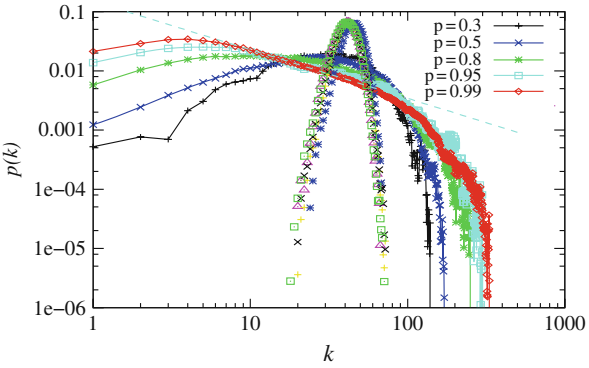

Fig. 5.14 *Line-pointed curves:* in-degree distributions of evolved networks, *data points only:* the corresponding out-degree distributions ((△) $p = 0.3$, (+) $p = 0.5$, (x) $p = 0.8$, (*) $p = 0.95$, (*squares*) $p = 0.99$). Statistics was gathered over 10^6 evolutionary steps, after a transient of $4 \cdot 10^6$ steps. Networks had size $N = 512$. The *dashed line* has slope $-3/4$

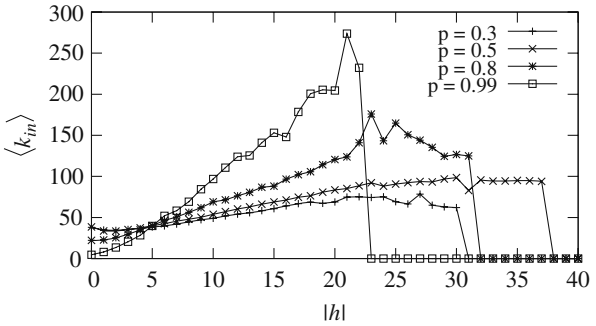

Fig. 5.15 Average number $\langle k_{in} \rangle$ of inputs for a given node in evolving networks, as a function of the respective nodes (absolute) threshold $|h|$. Statistics was taken over 10^6 rewiring steps, after a transient of $4 \cdot 10^6$ steps. For all values $p < 1$, a clear positive correlation between $\bar{k}_{in}$ and $|h|$ is found

In the next subsection, we will discuss another generalization of the adaptive, coevolutionary scheme of activity-dependent rewiring to Random Boolean Networks, which was introduced by Liu and Basler [53].

5.3.3 Extension to Random Boolean Networks

Activity-dependent rewiring was originally introduced for Random Threshold Networks, as discussed in Sect. 5.3.1.2, the basic adaptive scheme, however, can be generalized to other classes of dynamical systems. Since RTN are a subclass of Random Boolean Networks, one possible direction of generalization is to apply this coevolutionary, adaptive rule to RBNs. Compared to RTNs, rewiring by local dynamical rules in RBN comes with an additional complication: While in RTNs the dynamical transition rule is the same for all network sites (the evaluation of the weighted sum of regulatory inputs, cf. Eq. 5.6), switching of network nodes in RBNs is governed by individual logical functions that vary from node to node *and* depend on the input number k. If, for example, we have a node with two inputs and a logical AND function of these two inputs assigned (compare the example in Fig. 5.1), there does not exist a well-defined mapping that would assign a new logical function to this node in the case we change its input number to $k = 1$ or $k = 3$.

Liu and Bassler [53] suggested two variants of activity-dependent rewiring to overcome the problem associated to the reassignment of logical functions: in the first variant, only the node that is rewired at evolutionary time step t is assigned a new logical function which is randomly drawn out of the 2^{2^k} possible Boolean functions of k inputs (where k is the new input number *after* rewiring). The adaptive algorithm that was applied in this study is summarized in Box 5.2.

Box 5.2 Adaptive algorithm for activity-dependent rewiring in RBN

1. Start with a homogeneous RBN, $G(N, K_0)$ with uniform in-degree connectivity $K_i = K_0$ for all N, and generate a random Boolean function f_i for each node i.
2. Choose a random initial system state $\Sigma(0)$. Update the state using Eq. (5.4) and find the dynamical attractor.
3. Choose a node i at random and determine its average activity $A(i)$ over the attractor.
4. Change the network topology by rewiring the connections to the node chosen in the previous step. If it is frozen, then a new incoming link from a randomly selected node j is added to it. If it is active, then one of its existing links is randomly selected and removed.
5. The Boolean functions of network are regenerated. Two different methods have been used:
   - Annealed model: A new Boolean function is generated for every node of the network.
   - Quenched model: A new Boolean function is generated only for the chosen node i, while the others remain what they were previously.
6. Return to step 2.

For simplicity, all random Boolean functions are generated with $p = 1/2$, and therefore all Boolean functions with the same in-degree are equally likely to be generated.

Results. Liu and Bassler show that for both variants of the model, robust self-organization of network topology is found. Independent from the initial network realization, network evolution always converges to a characteristic average connectivity $K_{ev}(N)$. Graph (a) of Fig. 5.16 shows the evolution of the average in-degree connectivity $\overline{K}$ for networks of size $N = 30$ in the annealed variant of the model, with results obtained by beginning with networks with different uniform connectivity $K_0 = 2, 3, 4$, and 5. Each curve is the average of 15000 independent realizations of the network evolution. All curves approach the same final statistical steady state that has an average in-degree connectivity $\langle \overline{K} \rangle = 3.06$. The steady state value of $\langle \overline{K} \rangle$ depends on the size of the system as shown in graph (b) of Fig. 5.16. Starting with networks that all have the same initial uniform connectivity $K_0 = 4$, but which have different size $N = 30, 50$, and 100, one finds that larger networks evolve to steady states with smaller values of $\langle \overline{K} \rangle$.

Given the steady state value $\langle \overline{K} \rangle = 2$ in the large network limit $N \to \infty$, Liu and Bassler also studied the finite-size effects in the model. They found that the values of $\langle \overline{K}(N) \rangle$ for finite N obey the scaling function

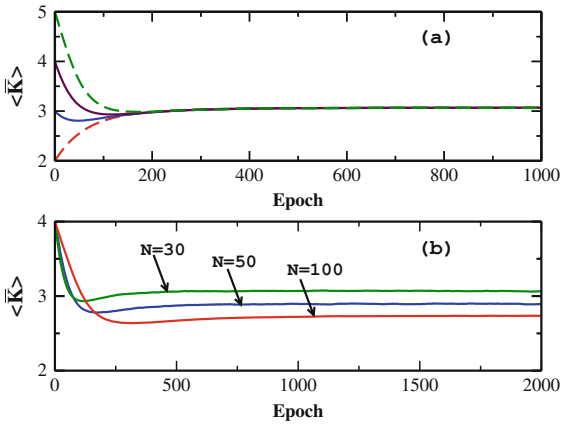

Fig. 5.16 (**a**). Evolution of the ensemble averaged in-degree connectivity in the annealed model, as studied by Liu and Bassler [53], for networks of size $N = 30$. The networks in each ensemble initially start from different uniform connectivity, $K_0 = 2,\ 3, 4$, and 5, but reach a same statistical steady state $\langle \overline{K} \rangle = 3.06$. (**b**). Evolution of ensemble averaged in-degree connectivity for networks of three different size $N = 30, 50$, and 100 in the annealed model

$$\langle \overline{K}(N) \rangle - 2 = c\, N^{-\delta}. \tag{5.20}$$

Fitting the data to this function, we find that the coefficient is $c = 2.50 \pm 0.06$ and the exponent is $\delta = 0.264 \pm 0.005$. Thus the value of $\langle \overline{K}(N) \rangle$ is always larger than 2 for finite N. Note that steady state values of the average connectivity in RTNs have a similar scaling form, but with slightly different values of the scaling parameters (cf. Sect. 5.3.1.3, Eq. 5.13).

In order to probe the dynamical nature of evolved steady states the authors computed the distribution $P(\Gamma)$ of steady state attractor period Γ in the ensemble of RBNs simulated. The distribution has a broad, power-law behavior for both the

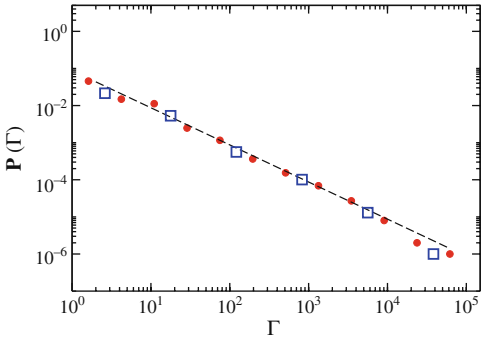

Fig. 5.17 Power law distribution of steady state attractor period Γ in both annealed (*circle*) and quenched (*square*) models as studied by Liu and Bassler [53], for $N = 200$ systems. The *dashed straight line* has a slope of 1.0

annealed and quenched variants of the model. Figure 5.17 shows the results for networks with $N = 200$. A power-law distribution of attractor periods is a typical signature of critical dynamics, hence, similar to the results discussed in Sect. 5.3.1.3 for the self-organization of the global average activity, this finding indicates that *dynamics* exhibits close-to critical behavior already for finite size networks, while *toplogical* criticality is attained in the limit of large N.

To summarize, the results of this study give strong evidence that the local, adaptive coevolutionary principle *frozen nodes grow links, active nodes lose links* leads to robust self-organization not only in RTNs, but also in the more general class of RBNs, and hence has the potential to be generalized to large classes of dynamical systems.

5.3.4 Correlation-Based Rewiring in Neural Networks

In this section, we will review a different adaptive coeveolutionary scheme of network self-organization which is based on the basic paradigm *correlated activity connects, decorrelated activity disconnects.* This local, topology-evolving rule is inspired by the idea of *Hebbian learning* in neural networks [38], and, consequently, was studied first for discrete neural networks with architectural and dynamical constraints motivated by corresponding observations in the brain [18]. In particular, an explicit parameterization of space on a two-dimensional grid is given, and dynamics is not deterministic any more, in contrast to the models discussed in the previous sections. The core result of this study is that network self-organization by correlation-driven rewiring is robust even when spatial constraints are present and dynamics is affected by noise. Correlation-driven rewiring can be considered as a natural extension of the basic, activity-driven rewiring, as it exploits long range correlations naturally emerging near phase transitions, and thereby is particularly suited for neural networks where information processing takes place typically in form of correlated activity. Let us now briefly motivate the correlation based self-organization in the context of neural networks.

Neural networks with asymmetric connectivity patterns often exhibit regimes of chaotic dynamics [63]. In networks whose central function is information transfer, these regimes would instantly render them useless. Consider, for example, model neural networks with asymmetric synaptic couplings, where a percolation transition between regimes of ordered and disordered dynamics is known [48]. In the disordered phase, which occurs for densely connected networks, already small perturbations percolate through the networks.[5] In such networks, developmental processes that change connectivity always face the risk of driving the network into the highly connected regime (where chaotic dynamics prevails), as long as no explicit mechanism is given that controls the global degree of connectivity.

[5] This is reminiscent of avalanche-like propagation of activity in the brain which is observed in some diseases of the central nervous system [81].

In a correlation-based rewiring rule we will exploit that also the average correlation between the activities of two neurons contains information about global order parameter of network dynamics. The network can then use this approximate order parameter to guide the developmental rule. A possible adaptive scheme is that new synaptic connections preferentially grow between correlated neurons, as suggested by the early ideas of Hebb [38] and the observation of activity-dependent neural development [33, 62, 69, 89]. In the remainder of this section let us recapitulate this problem in the framework of a specific toy model [18]. First a neural network model with a simple mechanism of synaptic development is defined. Then, the interplay of dynamics on the network with dynamics of the network topology is modeled. Finally, robustness of self-organizing processes in this model and possible implications for biological systems are discussed.

5.3.4.1 Model

Let us consider a two-dimensional neural network with random asymmetric weights on the lattice. The neighborhood of each neuron is chosen as its Moore neighborhood with eight neighbors.[6] The weights c_{ij} are randomly drawn from a uniform distribution $c_{ij} \in [-1, +1]$ and are nonzero between neighbors, only. Note that weights c_{ij} are asymmetric, i.e., in general, $c_{ij} \neq c_{ji}$. Within the neighborhood of a node, a fraction of its weights c_{ij} may be set to 0. The network consists of N neurons with states $\sigma_i = \pm 1$ which are updated in parallel with a stochastic Little dynamics on the basis of inputs received from the neighbor neurons at the previous time step:

$$\sigma_i(t+1) = \begin{cases} +1 & \text{with probability } g_\beta\left(f_i(t)\right) \\ -1 & \text{with probability } 1 - g_\beta\left(f_i(t)\right) \end{cases} \tag{5.21}$$

where

$$g_\beta(f_i(t)) = \frac{1}{1 + e^{-2\beta f_i(t)}} \tag{5.22}$$

with the inverse temperature β. The transfer function $f_i(t)$ is evaluated according to Eq. 5.18, that defines dynamics of threshold units with individually assigned thresholds. The threshold is chosen here as $h_i = -0.1 + \gamma$ and includes a small random noise term γ from a Gaussian of width ε. This noise term is motivated by the slow fluctuations observed in biological neural systems [1, 2].

---

[6] The choice of the type of neighborhood is not critical, however, here the Moore neighborhood is more convenient than the von Neumann type since, in the latter case, the critical link density (fraction of nonzero weights) at the percolation threshold accidentally coincides with the attractor of the trivial developmental rule of producing a link with $p = 0.5$. In general, also random sparse neighborhoods would work as demonstrated in [21].

The second part of the model is a slow change of the topology of the network by local rewiring of synaptic weights: If the activity of two neighbor neurons is on average highly correlated (or anticorrelated), they will obtain a common link. If their activity on average is less correlated, they will lose their common link. The degree of correlation in the dynamics of pairs of nodes is quantified by the *average correlation*, as defined in Eq. (5.9) in Sect. 5.2.4.2. The full model dynamics is then realized by the algorithm summarized in Box 5.3.

Box 5.3 Adaptive algorithm for correlation-dependent rewiring in neural networks

1. Start with a random network with an average connectivity (number of nonzero weights per neuron) K_{ini} and a random initial state vector $\Sigma(0) = (\sigma_1(0), ..., \sigma_N(0))$.
2. For each neuron i, choose a random threshold h_i from a Gaussian distribution of width ε and mean μ.
3. Starting from the initial state, calculate the new system state applying Eq. (5.21) using parallel update. Iterate this for τ time steps.
4. Randomly choose one neuron i and one of its neighbors j and determine the average correlation according to Eq. (5.8) over the last $\tau/2$ time steps. (Alternatively, the correlation can be obtained from a synaptic variable providing a moving average at any given time).
5. If $|\mathrm{Corr}(i, j)|$ is larger than a given threshold α, i receives a new link c_{ij} from site j with a weight chosen randomly from the interval $c_{ij} \in [-1, 1]$. If $|\mathrm{Corr}(i, j)| \leq \alpha$, the link c_{ij} is set to 0 (if nonzero).
6. Go to step 2 and iterate, using the current state of the network as new initial state.

The dynamics of this network is continuous in time, with neuron update on a fast time scale and topology update of the weights on a well-separated slow "synaptic plasticity" time scale. Note that the topology-changing rule does not involve any global knowledge, e.g., about attractors.

5.3.4.2 Results

Independent of the initial conditions the networks evolve to a specific average connectivity. Parameters are $\beta = 25$, $\epsilon = 0.1$, a correlation cutoff $\alpha = 0.8$, and an averaging time window of $\tau = 200$. One observes that the continuous network dynamics, including the slow local change of the topology, results in a convergence of the average connectivity of the network to a characteristic value which is independent of initial conditions.

Finite size scaling of the resulting average connectivity indicates the convergence towards a characteristic value for large network size N and exhibits the scaling relationship

$$K_{ev}(N) = aN^{-\delta} + b \tag{5.23}$$

with $a = 1.2 \pm 0.4$, $\delta = 0.86 \pm 0.07$, and $b = 2.24 \pm 0.03$. Thus, in the large system size limit $N \to \infty$ the networks evolve towards $K_{ev}^{\infty} = 2.24 \pm 0.03$. The self-organization towards a specific average connectivity is largely insensitive to thermal noise of the network dynamics, up to $\approx 10\%$ of thermal switching errors (or $\beta > 10$) of the neurons. This indicates that the structure of a given dynamical attractor is robust against a large degree of noise. Figure 5.18 shows the evolved average connectivity as a function of the inverse temperature β.

While the stability of dynamical attractors on an intermediate time scale is an important requirement for the local sampling of neural correlation, on the long time scale of global topological changes, switching between attractors is necessary to ensure ergodicity at the attractor sampling level. The second source of noise, the slow random change in neural thresholds as defined in step (2) of the algorithm, is closely related to such transitions between attractors. While, in general, the model converges also when choosing some arbitrary fixed threshold h and omitting step (2) from the algorithm, a small threshold noise facilitates transitions between limit cycle attractors [61] and thus improves sampling over all attractors of a network, resulting in an overall increased speed and robustness of the convergence. An asynchronous change of the threshold h_i, updating one random h_i after completing one sweep (time step) of the network, leads to similar results as the parallel rule defined above.

The basic mechanism of the observed self-organization in this system is the weak coupling of topological change to an order parameter of the global dynamical state of the network, and thus is different from the mechanism of extremal dynamics, underlying many prominent models of self-organized criticality [7, 8]. To illustrate this, let us for a moment consider the absolute average correlation $|\mathrm{Corr}(i, j)|$ of two neurons which is the parameter used as a criterion for the rewiring process. It can be shown that this quantity undergoes a phase transition depending on the average

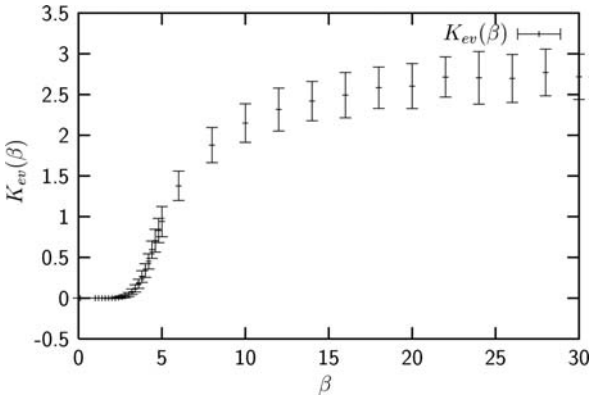

Fig. 5.18 Evolved average connectivity K_{ev} as a function of the inverse temperature β. Each point is averaged over 10^5 time steps in a network of size $N = 64$ and $\alpha = 0.5$. After Bornholdt and Röhl [18]

connectivity $\bar{K}$ which is similar to the transition of the frozen component observed in RTN (Fig. 5.4, cf. Sect. 5.2.4.3). Note that the correlation is large for networks with small connectivity, and small for networks that are densely connected. The rewiring rule balances between these two regimes: For high correlation, it is more likely that a link is created, at low correlation, links are vanishing. The balance is reached most likely in the region of the curve where the slope reaches its maximum, as here the observed correlation reacts most sensitively to connectivity changes. As the steep portion of the correlation curve occurs in a region of small connectivities where also the critical connectivity $K_c \approx 2$ of the network is located, this makes the correlation measure sensitive to the global dynamical state of the network and potentially useful as an approximation of the order parameter. Synaptic development dependent on averaged correlation between neurons can thus obtain approximate information about the global dynamical state of the network as is realized in the above toy model with a simple implementation on the basis of a threshold α. The exact choice of the threshold α is not critical, which can be seen from the histogram of the absolute correlation shown in Fig. 5.19 for a typical run of the model. Correlations appear to cluster near high and near low values such that the cutoff can be placed anywhere in between the two regimes. Even a threshold value close to 1, as compared with the correlation cutoff $\alpha = 0.8$ used in the simulations here, only leads to a minor shift in K_{ev} and does not change the overall behavior.

Up to now we focused on changes of the network structure as a result of the dynamics on the network. A further aspect is how the structural changes affect the dynamics on the network itself. Do also dynamical observables of the networks self-organize as a result of the observed convergence of the network structure? An interesting quantity in this respect is the average length of periodic attractors.

Indeed, this dynamical observable of the network dynamics converges to a specific value independent of the initial network, similarly to the convergence of the structural parameter $\bar{K}$ considered earlier. From the $\bar{K}$ dependency of the neural

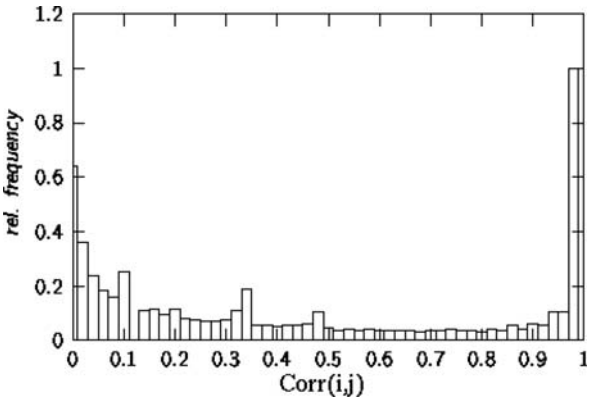

Fig. 5.19 Histogram of Corr(i, j) for a network evolving in time, with $N = 64$ and $\beta = 10$, taken over a run of 4×10^5 time steps, according to the model of Bornholdt and Röhl [18]

pair correlation we have seen above that the rewiring criterion tends to favor connectivities near the critical connectivity of the network. Does also the evolved average attractor length relate to critical properties of the percolation transition? An approximate measure of this aspect is the finite size scaling of the evolved average period.

For static networks we find that the attractor lengths typically scale exponentially with N in the overcritical regime, but less than linearly in the ordered regime. For the evolved connectivity K_{ev} in our model, we observe scaling close to criticality. Large evolved networks exhibit relatively short attractors, which otherwise for random networks in the overcritical regime could only be achieved by fine tuning. The self-organizing model studied here evolves non-chaotic networks without the need for parameter tuning.

In a continuously running network, robust self-organization of the network towards the percolation transition between ordered and disordered dynamics is observed, independent of initial conditions and robust against thermal noise. The basic model is robust against changes in the details of the algorithm. We conclude that a weak coupling of the rewiring process to an approximate measurement of an order parameter of the global dynamics is sufficient for a robust self-organization towards criticality. In particular, the order parameter has been estimated solely from information available on the single synapse level via time averaging of correlated neural activities.

5.4 Summary and Outlook

We reviewed models of topological network self-organization by *local dynamical rules*. Two paradigms of local co-evolutionary adaptation were applied to discrete dynamical networks: The principle of *activity-dependent rewiring* (active nodes lose links, frozen nodes aquire new links), and the principle of *correlation-dependent rewiring* (nodes with correlated activity connect, decorrelated nodes disconnect). Both principles lead to robust self-organization of *global* network topology and – dynamics, without need for parameter tuning. Adaptive networks are strikingly different from random networks: they evolve inhomogeneous topologies and broad plateaus of homeostatic regulation, dynamical activity exhibits $1/f$ noise and attractor periods obey a scale-free distribution. The proposed co-evolutionary mechanism of topological self-organization is robust against noise and does not depend on the details of dynamical transition rules. Using finite-size scaling, it was shown that networks converge to a self-organized critical state in the thermodynamic limit.

The proposed mechanisms of coevolutionary adaptation in dynamical networks are very robust against changes in details of the local rewiring rules – in particular, they only require a local estimate of some dynamical order parameter in order to achieve network adaptation to criticality.

A classical route to self-organized criticality is the feedback of an order parameter onto local dynamics of a system [85]. The local rewiring rules considered here extend this idea to using only approximate local estimates of a global order

parameter. As seen in the examples above, locally measured averages prove to be sufficient for self-organized criticality. In particular, in the presence of a time-scale separation between fast dynamics on the networks and slow topology evolution, the evolutionary steady state naturally provides a quasi-ergodic sampling of the phase space near the critical state, such that accurate order parameter values are not necessary. In the models considered in this review, an estimate of the order parameter is achieved by local averaging over the switching activity of single nodes, or over the dynamical correlation of pairs of nodes.

A number of open questions remains to be addressed in the context of the class of adaptive networks considered here. The robust network self-organization observed in the models, approaching criticality in the limit of large N, is far from being understood in detail. With regard to dynamics, evolving networks exhibit pronounced differences to random networks with comparable connectivity. In particular, the frozen component exhibits for finite N a plateau around the evolutionary mean K_{evo}, with step-like discontinuities when the average wiring density substantially departs from K_{evo} (Fig. 5.10); for comparison, the corresponding curves for random networks show a smooth decay. This may suggest that the self-organized critical state rather exhibits characteristics of a first order phase transition, while order parameters in random discrete dynamical networks typically exhibit second order transitions at K_c. With regard to topology, deviations from random networks become particularly pronounced when dynamical units are allowed to diversify with respect to their switching behavior during evolution, leading to symmetry breaking and emergence of scale-free in-degree distributions; again, these observations are hard to explain in the context of the traditional statistical mechanics approach based on random ensembles of networks.

In the studies reviewed in this chapter, evolving networks were treated as completely autonomous systems, without coupling to an external environment. An important step in future research will be to introduce network-environment interaction and study network evolution under the influence of external signals or perturbations; this also connects to the particularities of information processing in self-organized critical networks, and the idea of optimal adaptation at the "edge of chaos" [15].

Finally, let us widen the scope of these models beyond their theoretical value, and discuss possible applications.

On the one hand, they represent prototypical models of self-organized critical dynamical networks, toy models that demonstrate possible mechanisms for dynamical networks to adapt to criticality. On the other hand, these mechanisms are not limited to the extremely simple toy models discussed here, and may themselves occur in natural systems. They do not depend on fine-tuning of parameters or details of the implementation, and they are robust against noise. This is contrary to standard mechanisms of self-organized criticality [7, 8] which are sensitive to noise [80] and, therefore, not easily applied to natural systems. Network self-organization as reviewed above, however, is itself defined on the basis of stochastic dynamical operations (update of randomly selected links, noisy local measurement of order

parameter, for example). We therefore expect that these mechanisms can occur in natural systems quite easily.

A strong need for adaptive mechanisms is present in nervous systems, where assemblies of neurons need to self-adjust their activity levels, as well as their connectivity structure [13, 36, 86, 89]. The mechanism discussed here is one possible route to adaptivity in natural neural networks. It can serve as the basis for more biologically detailed models [14, 15, 51].

Further applications of the network adaptation models are conceivable, e.g. to socio-economic systems. Network adaptation could in principle occur in adapting social links or economic ties of humans acting as agents in complex social or economic systems.

References

1. Abraham, W.C., Mason-Parker, S.E., Bear, M.F., Webb, S., Tate, W.P.: Heterosynaptic metaplasticity in the hippocampus in vivo: A bcm-like modifiable threshold for ltp. Proc. Natl. Acad. Sci. USA **98**, 10924–10929 (2001). DOI 10.1073/pnas.181342098
2. Abraham, W.C., Tate, W.P.: Metaplasticity: A new vista across the field of synaptic plasticity. Prog. Neurobiol. **52**, 303–323 (1997)
3. Albert, R., Barabasi, A.L.: Dynamics of complex systems: Scaling laws for the period of boolean networks. Phys. Rev. Let. **84**, 5660–5663 (2000)
4. Andrecut, M.: Mean field dynamics of random boolean networks. J. Stat. Mech. (2005). DOI 10.1088/1742-5468/2005/02/P02003
5. Anirvan M. Sengupta, M.D., Shraiman, B.: Specificity and robustness in transcription control networks. Proc. Natl. Acad. Sci. **99**, 2072–2077 (2002)
6. Bak, P.: How Nature Works: The Science of Self-organized Criticality. Copernicus, New York (1996)
7. Bak, P., Sneppen, K.: Punctuated equilibrium and criticality in a simple model of evolution. Phys. Rev. Lett. **71**, 4083–4086 (1993) DOI 10.1103/PhysRevLett.71.4083
8. Bak, P., Tang, C., Wiesenfeld, K.: Self-organized criticality: An explanation of the 1/f noise. Phys. Rev. Lett. **59**, 381–384 (1987)
9. Barkai, N., Leibler, S.: Robustness in simple biochemical networks. Nature **387**, 913–916 (1997)
10. Bastolla, U., Parisi, G.: Closing probabilities in the kauffman model: An annealed computation. Physica D **98**, 1–25 (1996)
11. Bastolla, U., Parisi, G.: Relevant elements, magnetization and dynamical properties in kauffman networks: A numerical study. Physica D **115**, 203–218 (1998)
12. Bastolla, U., Parisi, G.: The modular structure of kauffman networks. Physica D **115**, 219–233 (1998a)
13. Beggs, J.M., Plenz, D. Neuronal avalanches in neocortical circuits. J. Neurosci. **23** 11167 (2003)
14. Beggs, J.M.: The criticality hypothesis: how local cortical networks might optimize information processing. Phil. Trans. Roy. Soc. A **366**(1864), 329–343 (2008). DOI 10.1098/rsta.2007.2092
15. Bertschinger, N., Natschläger, T., Legenstein, R.A.: At the edge of chaos: Real-time computations and self-organized criticality in recurrent neural networks. In: L.K. Saul, Y. Weiss, L. Bottou (eds.) Advances in Neural Information Processing Systems 17, pp. 145–152. MIT Press, Cambridge, MA (2005)

16. Bhattacharjya, A., Liang, S.: Median attractor and transients in random boolean nets. Physica D **95**, 29–34 (1996)
17. Bhattacharjya, A., Liang, S.: Power-law distributions in some random boolean networks. Phys. Rev. Lett. **77**, 1644–1647 (1996)
18. Bornholdt, S., Röhl, T.: Self-organized critical neural networks. Phys. Rev. E **67**, 066 118 (2003). DOI 10.1103/PhysRevE.67.066118
19. Bornholdt, S., Rohlf, T.: Topological evolution of dynamical networks: Global criticality from local dynamics. Phys. Rev. Lett. **84**, 6114–6117 (2000)
20. Bornholdt, S., Sneppen, K.: Neutral mutations and punctuated equilibrium in evolving genetic networks. Phys. Rev. Lett. **81**, 236–239 (1998)
21. Bornholdt, S., Sneppen, K.: Robustness as an evolutionary principle. Proc. R. Soc. Lond. B **267**, 2281–2286 (2000)
22. Christensen, K., Donangelo, R., Koiller, B., Sneppen, K.: Evolution of random networks. Phys. Rev. Lett. **81**, 2380 (1998)
23. Correale, L., Leone, M., Pagnani, A., Weigt, M., Zecchina, R.: The computational core and fixed point organization in boolean networks. J. Stat. Mech. (2006). DOI 10.1088/1742-5468/2006/03/P03002
24. Correale, L., Leone, M., Pagnani, A., Weigt, M., Zecchina, R.: Core percolation and onset of complexity in boolean networks. Phys. Rev. Lett. **96**, 018 101 (2006). DOI 10.1103/PhysRevLett.96.018101
25. Davidson, E.: Genomic Regulatory Systems. Development and Evolution. Academic Press, San Diego, CA (2001)
26. Derrida, B.: Dynamical phase transition in non-symmetric spin glasses. J. Phys. A **20**, 721–725 (1987)
27. Derrida, B., Flyvbjerg, H.: Distribution of local magnetisations in random networks of automata. J. Phys. A **20**, 1107–1112 (1987)
28. Derrida, B., Gardner, E., Zippelius, A.: An exactly solvable asymmetric neural network model. Europhys. Lett. **4**, 167 (1987)
29. Derrida, B., Pomeau, Y.: Random networks of automata: a simple annealed approximation. Europhys. Lett. **1**, 45–49 (1986)
30. Derrida, B., Stauffer, D.: Phase transitions in two-dimensional kauffman cellular automata. Europhys. Lett. **2**, 739ff (1986)
31. Drossel, B.: Extinction events and species lifetimes in a simple ecological model. Phys. Rev. Lett. **81**, 5011 (1998)
32. Drossel, B.: Number of attractors in random boolean networks. Phys. Rev. E **72**(1, Part 2) (2005). DOI 10.1103/PhysRevE.72.016110
33. Engert, F., Bonhoeffer, T.: Dendritic spine changes associated with hippocampal long-term synaptic plasticity. Nature **399**, 66–69 (1999)
34. Erdős, P., Rényi, A.: On the evolution of random graphs. Publ. Math. Inst. Hung. Acad. Sci. **5**, 17–61 (1960)
35. Flyvbjerg, H.: An order parameter for networks of automata. J. Phys. A **21**, L955–L960 (1988)
36. Gireesh, E.D., Plenz, D.: Neuronal avalanches organize as nested theta- and beta/gamma-oscillations during development of cortical layer 2/3. Proc. Natl. Acad. Sci. USA **105**, 7576-7581 (2008).
37. Gross, T., Blasius, B.: Adaptive coevolutionary networks: a review. J. Roy. Soc. Interface **5**, 259–271 (2008). DOI 10.1098/rsif.2007.1229
38. Hebb, D.O.: The Organization of Behavior. Wiley, New York (1949)
39. Kauffman, S.: Metabolic stability and epigenesis in randomly constructed genetic nets. J. Theor. Biol. **22**, 437–467 (1969)
40. Kauffman, S.: The Origins of Order: Self-Organization and Selection in Evolution. Oxford University Press, Oxford (1993)
41. Kaufman, V., Drossel, B.: Relevant components in critical random boolean networks. New J. Phys. **8** (2006). DOI 10.1088/1367-2630/8/10/228

42. Kaufman, V., Mihaljev, T., Drossel, B.: Scaling in critical random boolean networks. Phys. Rev. E **72**, 046 124 (2005). DOI 10.1103/PhysRevE.72.046124
43. Kelso, J.A.S., Bressler, S.L., Buchanan, S., DeGuzman, G.C., Ding, M., et al.: A phase transition in human brain and behavior. Phys. Lett. A **169**, 134–144 (1992)
44. Kesseli, J., Ramo, P., Yli-Harja, O.: Iterated maps for annealed boolean networks. Phys. Rev. E **74**(4, Part 2), 046 104 (2006). DOI 10.1103/PhysRevE.74.046104
45. Klemm, K., Bornholdt, S.: Stable and unstable attractors in boolean networks. Phys. Rev. E **72**(5, Part 2) (2005). DOI 10.1103/PhysRevE.72.055101
46. Krawitz, P., Shmulevich, I.: Basin entropy in boolean network ensembles. Phys. Rev. Lett. **98**(15) (2007). DOI 10.1103/PhysRevLett.98.158701
47. Kree, R., Zippelius, A.: Continuous-time dynamics of asymmetrically diluted neural networks. Phys. Rev. A **36**(9), 4421–4427 (1987). DOI 10.1103/PhysRevA.36.4421
48. Kürten, K.: Critical phenomena in model neural networks. Phys. Lett. A **129**, 156–160 (1988)
49. Kürten, K.: Correspondence between neural threshold networks and kauffman boolean cellular automata. J. Phys. A **21**, L615–L619 (1988b)
50. Langton, C.: Life at the edge of chaos. In: Artificial Life, vol. II, pp. 255–276. Addison-Wesley, Boston, MA (1991)
51. Levina, A., Herrmann, J.M., Geisel, T. Dynamical synapses causing self-organized criticality in neural networks. Nat. Phys. **3** 857–860 (2007)
52. Linkenkaer-Hansen, K., Nikouline, V.V., Palva, J.M., Ilmoniemi, R.J.: Long-range temporal correlations and scaling behavior in human brain oscillations. J. Neurosci. **21**, 1370–1377 (2001)
53. Liu, M., Bassler, K.E.: Emergent criticality from coevolution in random boolean networks. Phys. Rev. E **74**, 041 910 (2006). DOI 10.1103/PhysRevE.74.041910
54. Luque, B., Ballesteros, F.J., Muro, E.M.: Self-organized critical random boolean networks. Phys. Rev. E **63**, 051 913 (2001). DOI 10.1103/PhysRevE.63.051913
55. Luque, B., Ferrera, A.: Measuring mutual information in random boolean networks. Complex Syst. **12**, 241–252 (2000)
56. Luque, B., Sole, R.: Lyapunov exponents in random boolean networks. Physica A **284**(1–4), 33–45 (2000)
57. Luque, B., Sole, R.V.: Phase transitions in random networks: simple analytic determination of critical points. Phys. Rev. E **55**, 257–260 (1996)
58. Luscombe, N.M., et al.: M.M.B.: Genomic analysis of regulatory network dynamics reveals large topological changes. Nature **431**, 308–312 (2004)
59. Lux, T., Marchesi, M.: Scaling and criticality in a stochastic multi-agent model of a financial market. Nature **397**, 498–500 (1999). DOI 10.1038/17290
60. Malamud, B.D., Morein, G., Turcotte, D.L.: Forest fires: An example of self-organized critical behavior. Science **281**, 1840–1842 (1998)
61. McGuire, P.C., Bohr, H., Clark, J.W., Haschke, R., Pershing, C.L., Rafelski, J.: Threshold disorder as a source of diverse and complex behavior in random nets. Neural Networks **15**, 1243–1258 (2002)
62. li Ming, G., Wong, S.T., Henley, J., bing Yuan, X., jun Song, H., Spitzer, N.C., Poo, M.m.: Adaptation in the chemotactic guidance of nerve growth cones. Nature **417**, 411–418 (2002)
63. Molgedey, L., Schuchard, J., Schuster, H.G.: Suppressing chaos in neural networks by noise. Phys. Rev. Lett. **69**, 3717 (1992)
64. Murray, J.: Mathematical Biology. Springer, New York (2002)
65. Nakamura, I.: Dynamics of threshold network on non-trivial distribution degree. Eur. Phys. J. B **40**, 217–221 (2004). DOI 10.1140/epjb/e2004-00260-4
66. Nicolis, G., Prigogine, I.: Self-Organization in Nonequilibrium Systems: From Dissipative Structures to Order Through Fluctuations. Wiley, New York (1977)
67. Nykter, M., Price, N.D., Aldana, M., Ramsey, S.A., Kauffman, S.A., Hood, L.E., Yli-Harja, O., Shmulevich, I.: Gene expression dynamics in the macrophage exhibit criticality. Proc. Natl. Acad. Sci. USA **105**(6), 1897–1900 (2008). DOI 10.1073/pnas.0711525105

68. Nykter, M., Price, N.D., Larjo, A., Aho, T., Kauffman, S.A., Yli-Harja, O., Shmulevich, I.: Critical networks exhibit maximal information diversity in structure-dynamics relationships. Phys. Rev. Lett. **1**(5) (2008). DOI 10.1103/PhysRevLett.100.058702
69. van Ooyen, A.: Competition in the development of nerve connections: a review of models. Network: Computation in Neural Systems **12**, R1–R47 (2001)
70. Paczuski, M., Bassler, K.E., Corral, A.: Self-organized networks of competing boolean agents. Phys. Rev. Lett. **84**, 3185–3188 (2000). DOI 10.1103/PhysRevLett.84.3185
71. Paczuski, M., Maslov, S., Bak, P.: Avalance dynamics in evolution, growth and depinning models. Phys. Rev. E **53**, 414–443 (1996)
72. Rämö, P., Kesseli, J., Yli-Harja, O.: Perturbation avalanches and criticality in gene regulatory networks. J. Theor. Biol. **242**, 164–170 (2006). DOI 10.1016/j.jtbi.2006.02.011
73. Ribeiro, A.S., Kauffman, S.A., Lloyd-Price, J., Samuelsson, B., Socolar, J.E.S.: Mutual information in random boolean models of regulatory networks. Phys. Rev. E **77**(1, Part 1) (2008). DOI 10.1103/PhysRevE.77.011901
74. Rohlf, T.: Networks and Self-Organized Criticality. Master's thesis, Christian-Albrechts-Universität Kiel (Germany) (2000)
75. Rohlf, T.: Critical line in random threshold networks with inhomogeneous thresholds.Phys. Rev. E **78**, 066118 (2008)
76. Rohlf, T.: Self-organization of heterogeneous topology and symmetry breaking in networks with adaptive thresholds and rewiring. Europhys. Lett. **84**, 10004 (2008)
77. Rohlf, T., Bornholdt, S.: Criticality in random threshold networks: Annealed approximation and beyond. Physica A **310**, 245–259 (2002)
78. Rohlf, T., Bornholdt, S.: Gene regulatory networks: A discrete model of dynamics and topological evolution. In: A. Deutsch, J. Howard, M. Falcke, W. Zimmermann (eds.) Function and Regulation of Cellular Systems: Experiments and Models. Birkhäuser Basel (2004)
79. Rohlf, T., Gulbahce, N., Teuscher, C.: Damage spreading and criticality in finite dynamical networks. Phys. Rev. Lett. **99**, 248701 (2007). DOI 10.1103/PhysRevLett.99.248701
80. Schmoltzi, K., Schuster, H.G.: Introducing a real time scale into the Bak-Sneppen model. Phys. Rev. E **52**, 5273–5280 (1995).
81. Schroeder, B.C., Kubisch, C., Stein, V., Jentsch, T.: Moderate loss of function of cyclic-amp-modulated kcnq2/kcnq3 k+ channels causes epilepsy. Nature **396**, 687–690 (1998). DOI 10.1038/25367
82. Shmulevich, I., Kauffman, S.A., Aldana, M.: Eukaryotic cells are dynamically ordered or critical but not chaotic. Proc. Natl. Acad. Sci. USA **102**, 13439–13444 (2005)
83. Sole, R., Luque, B.: Phase transitions and antichaos in generalized kauffman networks. Phys. Lett. A **196**, 331–334 (1995)
84. Sole, R.V., Manrubia, S.C.: Criticality and unpredictability in macroevolution. Phys. Rev. E **55**, 4500–4507 (1997)
85. Sornette, D.: Critical phase transitions made self-organized: a dynamical system feedback mechanism for self-organized criticality. J. Phys. I France **2**, 2065–2073 (1992)
86. Stewart, C.V., Plenz, D. Homeostasis of neuronal avalanches during postnatal cortex development in vitro. J. Neurosci. **169**, 405–416 (2008)
87. Teuscher, C., Sanchez, E.: Self-organizing topology evolution of turing neural networks. Artificial Neural Networks - ICANN 2001, Proceedings **2130**, 820–826 (2001)
88. Thomas, R.: Boolean formalization of genetic control circuits. J. Theor. Biol. **42**, 563–585 (1973)
89. Trachtenberg, J.T., Chen, B.E., Knott, G.W., Feng, G., Sanes, J.R., Walker, E., Svoboda, K.: Long-term in vivo imaging of experience-dependent synaptic plasticity in adult cortex. Nature **420**, 788–794 (2002)
90. Wagner, A.: Robustness against mutations in genetic networks of yeast. Nat. Genet. **24**, 355–361 (2000)
91. Wooters, W.K., Langton, C.G.: Is there a sharp phase transition for deterministic cellular automata? Physica D **45**, 95–104 (1990)

Chapter 6
Self-Organization and Complex Networks

Guido Caldarelli and Diego Garlaschelli

Abstract In this chapter we discuss how the results developed within the theory of fractals and Self-Organized Criticality (SOC) can be fruitfully exploited as ingredients of adaptive network models. In order to maintain the presentation self-contained, we first review the basic ideas behind fractal theory and SOC. We then briefly review some results in the field of complex networks, and some of the models that have been proposed. Finally, we present a self-organized model recently proposed by Garlaschelli et al. (Nat. Phys. 3: 813, 2007) that couples the fitness network model defined by Caldarelli et al. (Phys. Rev. Lett. 89: 258702, 2002) with the evolution model proposed by Bak and Sneppen (Phys. Rev. Lett. 71: 4083, 1993) as a prototype of SOC. Remarkably, we show that the results obtained for the two models separately change dramatically when they are coupled together. This indicates that self-organized networks may represent an entirely novel class of complex systems, whose properties cannot be straightforwardly understood in terms of what we have learnt so far.

6.1 Introduction

Several important results on both the empirical characterization and the theoretical modelling of complex networks have been achieved in the last decade [1–5]. Among the factors that have rendered this fast progress possible, one should surely acknowledge the unprecedented possibility to digitally store, and computationally analyse, huge datasets documenting the large-scale organization of biological, technological, and socio-economic systems. This has determined an empirically well-grounded problem of information extraction from a new form of data, where many units (vertices) are mutually interconnected by links (or edges), requiring novel paradigms for the identification of relevant patterns, and possibly regularities. A second reason is surely the scientific awareness, steadily grown during at least the last three decades, of the ubiquitous presence in nature of collective and emergent phenomena resulting

G. Caldarelli (✉)
Dipartimento di Fisica Università "Sapienza", Centre SMC CNR-INFM,
Piazzale A. Moro 5 00185 Roma, Italy
e-mail: Guido.Caldarelli@cnr.it

T. Gross, H. Sayama (eds.), *Adaptive Networks,* Understanding Complex Systems,
DOI 10.1007/978-3-642-01284-6_6,

from the interaction of many units within a complex system. In particular, the developments achieved within the broad fields of statistical physics, nonlinear dynamics, critical phenomena, fractal geometry, spin glasses, and many-body theory have contributed to the formation of a modern and interdisciplinary perspective, whose major focus is the (often unexpected) role of the interactions between constituents, rather than the individual details of the latter. Within this research field, whose boundaries are rather blurred, a diverse set of tools to handle the complexity of heterogeneous systems was developed. When the empirically-driven pressure towards the understanding of networks built up, the scientific community was faced with the possibility, and the challenge, to apply these tools to a genuinely new problem. As a result, some universal features across different real-world networks were identified, and theoretical models were proposed to reproduce and interpret them. At the same time, the scientific horizon extended even further, since a complete framework was not there to tackle the problem yet. Indeed, a satisfactory and unified approach to complex networks is still lacking, and this exciting field continues to attract the interest of a large community of scientists extending across different disciplines.

Broadly speaking, the main lines of research on networks that have been traced in the last decade are: (i) the definition and the empirical analysis of the static topological properties of networks; (ii) the modelling of (either static or growing) network formation; (iii) the effects that the topology has on various dynamical processes taking place on networks. Some useful references [1–5] present reviews of these results. More recently, a few attempts to provide a unified approach to the problem have been proposed, exploiting the idea that these aspects of networks should in the end be related to each other. In particular, it has been argued that the complexity of real-world networks is in the most general case the result of the interplay between topology and dynamics. While most studies have focused either on the effects that topological properties have on dynamical processes, or on the reverse effects that vertex-specific dynamical variables have on network structure, it has been suggested that one should consider the mutual influence that these processes have on each other. This amounts to relax the (often implicit) hypothesis that dynamical processes and network growth take place at well separated timescales, and that one is therefore allowed to consider the evolution of the fast variables while the slower ones are quenched. Remarkably, one finds that the feedback between topology and dynamics can drive the system to a steady state that differs from the one obtained when the two processes are considered separately [6]. These results imply that adaptive networks generated by this interplay may represent an entirely novel class of complex systems, whose properties cannot be straightforwardly understood in terms of what we have learnt so far.

In what follows we shall review our contribution to this line of research. In particular, we shall present a self-organized model [6] where an otherwise static model of network formation driven by vertex *fitness* [7] is explicitly coupled to an extremal dynamics process [8] providing an evolution rule for the fitness itself. In order to highlight the novel phenomena that originate from the interplay between the two mechanisms, we first review the main properties of the latter when considered separately. In Sect. 6.2 we recall some aspects of scale invariance

and Self-Organized Criticality (SOC), and in particular the biologically-inspired Bak-Sneppen model [8] where the extremal dynamics for the fitness was originally defined on static graphs. In Sect. 6.3 we briefly review complex networks and in particular the so-called fitness model of network formation [7], where the idea that network properties may depend on some fitness parameter associated to each vertex was proposed. Finally, in Sect. 6.4 we present the self-organized model obtained by coupling these mechanisms. The order of the presentation is also meant to highlight the fruitful synthesis that, as we have already mentioned, has originated by the application of ideas inherited by the previous understanding of complex systems to networks.

6.2 Scale Invariance and Self-Organization

Self-similarity, or fractality, is the property of an object whose subparts have the same shape of the whole. At first, self-similarity appeared as a peculiar property of a limited class of objects. Only later, due to the activity of Benoit Mandelbrot [9, 10], it turned out that examples of fractal structures (even if approximate due to natural cutoffs) are actually ubiquitous in nature. Indeed, in an incredible number of situations the objects of interest can be represented by self-similar structures over a large, even if finite, range of scales. Examples include commodity price fluctuations [9], the shape of coastlines [10], the discharge of electric fields [11], the branching of rivers [12], deposition processes [13], the growth of cities [14], fractures [15], and a variety of biological structures [16].

6.2.1 Geometric Fractals

Due to this ubiquity, scientists have tried to understand the possible origins of fractal behaviour. The first preliminary studies have focussed on mathematical functions built by recursion (Koch's snowflake, Sierpiński triangle and carpet, etc.). Based on these examples, where self-similar geometric objects are constructed iteratively, mathematicians introduced quantities in order to distinguish rigorously between fractals and ordinary compact objects.

For instance, one of the simplest fractals defined by recursion is the Sierpinski triangle, named after the Polish mathematician Waclaw Sierpiński who introduced it in 1915 [17]. When the procedure shown in Fig. 6.1 is iterated an infinite number of times, one obtains an object whose empty regions extend at any scale (up to the maximum area delimited by the whole triangle). It is therefore difficult to measure

Fig. 6.1 First steps in the iteration procedure defining the Sierpinski triangle

its area in the usual way, i.e. by comparison with another area chosen as the unit of measure. A way to solve this problem is to consider a limit process not only for the generation of the fractal, but also for the measurement of its area. Note that at the first iteration we only need three triangles of side length $1/2$ to cover the object (while for the whole triangle we would need four of them). At the second iteration we need nine covering triangles of side $1/4$ (while for the whole triangle we would need sixteen of them). In general, for a compact triangle the number of triangles needed grows quadratically as we reduce the size of the covering triangles. The (scale-dependent) number of objects required to cover a fractal is at the basis of the definition of the *fractal dimension* D. Formally, if $N(\varepsilon)$ is the number of D_E-dimensional volumes of linear size ε required to cover an object embedded in a metric space of Euclidean dimension D_E, then the fractal dimension is defined as

$$D = \lim_{\varepsilon \to 0} \frac{\ln N(\varepsilon)}{\ln 1/\varepsilon}, \tag{6.1}$$

which approaches an asymptotic value giving a measure of the region occupied by the fractal.

For a compact object the fractal dimension gives the same value as the Euclidean dimension D_E. Indeed, for the above compact triangle $D = D_E = 2$. To see this, note that at the first iteration the number of necessary triangles is 4 and $1/\varepsilon$ is 2, therefore $D = \frac{\ln 4}{\ln 2} = 2$. At the next iteration $1/\varepsilon$ is 4 and the number of covering triangles is 16 so that again $D = \frac{\ln 16}{\ln 4} = 2$. Clearly, the same value of D is found at all subsequent iterations, and therefore also in the limit $\varepsilon \to 0$. By contrast, for the Sierpiński triangle it is easy to realise that at the k-th iteration the linear size of each covering triangle is $\varepsilon = 2^{-k}$ and that $N = 3^k$ such triangles are needed. This implies

$$D = \lim_{\varepsilon \to 0} \frac{\ln N(\varepsilon)}{\ln 1/\varepsilon} = \frac{\ln 3}{\ln 2} \simeq 1.58496... \tag{6.2}$$

Now we find that $D < D_E = 2$. Therefore the fractal dimension measures the difference between the compactness of a fractal and that of a regular object embedded in a space of equal dimensionality. In the present example, D is lower than 2 because the Sierpinski triangle is less dense than a compact bidimensional triangle. D is also larger than 1 because it is denser than a one-dimensional object (a line). Note that the above formula can be rewritten in the familiar form of a power law by writing, for small ε,

$$N(\varepsilon) \propto \varepsilon^{-D} \tag{6.3}$$

This highlights the correspondence between the geometry of a fractal and scale-invariant laws.

6.2.2 Self-Organized Criticality

Despite their importance in characterizing the geometry of fractals, purely mathematical algorithms are not helpful in order to understand whether a few common mechanisms might be responsible for the fractal behaviour observed in so many different, and seemingly unrelated, real-world situations. This has shifted the interest towards dynamical models. Indeed, open dissipative systems are in many cases associated with fractals for more than one reason. Firstly, attractors in the phase space of a nonlinear dynamical system can have a fractal geometry; secondly, their evolution can proceed by means of scale-invariant bursts of intermittent activity [18] extending over both time and space. In general, these features are obtained when a driving parameter of the nonlinear dynamical system is set to a crossover value at which chaotic behaviour sets on. When this occurs, the nonlinear system is said to be at the "edge of chaos". Another situation where self-similarity is observed is at the critical point of phase transitions. For instance, magnetic systems display a sharp transition from a high-temperature disordered phase, where microscopic spins point in random directions and generate no macroscopic magnetization, to a low-temperature ordered phase where almost all spins point in the same direction, determining a nonzero overall magnetization. Exactly at the critical transition temperature, spins are spatially arranged in aligned domains whose size is power-law distributed. This means that domains of all sizes are present, with a scale-invariant pattern.

In both cases, in order to explain the ubiquity of self-similar systems one should understand why they appear to behave as if their control parameter(s) were systematically fine-tuned to the critical value(s). This point led to the idea that feedback effects might exist, that drive the control parameter to the critical value as a spontaneous outcome of the dynamics. In this scenario, it is the system itself that evolves autonomously towards the critical state, with no need for an external fine-tuning. This paradigm is termed Self-Organized Criticality (SOC) (for a review see [19] and references therein). At a phenomenological level, SOC aims at explaining the tendency of open dissipative system to rearrange themselves in such a way to develop long-range temporal and spatial correlations. Why this happens is still a matter of debate, even if some authors claimed that this behaviour may be based on the minimization of some energy potential [20–22].[1] Also, it has been proposed that a temperature-like parameter can actually be introduced for these systems [24, 25], and shown to lead to SOC only if fine-tuned to zero. This supports the hypothesis that SOC models are closely related to ordinary critical systems, where parameters have to be tuned to their critical value, the fundamental difference being the feasibility of this tuning.

There are several examples of simplified models showing SOC, and most of them have a common structure. In practice, two classes of SOC models attracted many

[1] Interestingly a similar claim has been made for networks as well [23].

studies: the class of sandpile models [26] and the class of models based on extremal dynamics such as the Bak-Sneppen [8] and Invasion Percolation [27] models. In what follows we briefly review these examples.

6.2.2.1 Sandpiles

One prototype is represented by *sandpile* models [26], a class of open dissipative systems defined over a finite box Λ in a d-dimensional hypercubic lattice. In $d = 2$ dimensions, one considers a simple square lattice. Any site i of the lattice is assumed to store an integer amount z_i of sand grains, corresponding to the height reached by the sandpile at that site. At every time step one grain of sand is added on a randomly chosen site i, so that the height z_i is increased by one. As long as z_i remains below a fixed threshold, nothing happens.[2] But as soon as z_i exceeds the threshold, the column of sand becomes unstable and "topples" on its nearest neighbours. Therefore the heights evolve according to

$$z_i \to z_i - \Delta_{ki} \tag{6.4}$$

where

$$\Delta_{ki} = \begin{cases} 2d & k = i \\ -1 & k \quad \text{nearest neighbor of } i \\ 0 & \text{otherwise.} \end{cases} \tag{6.5}$$

This process is called *toppling*. As the neighbouring sites acquire new grains, they may topple in their turn, and this effect can propagate throughout the system until no updated site is active, in which case the procedures starts again with the addition of a new grain. While the amount of sand remains constant when toppling occurs in the bulk, for topplings on the boundary sites ($i \in \partial\Lambda$) some amount of sand falls outside and disappears from the system. In the steady state of the process, this loss balances the continuous random addition of sand.

All the toppling events occurring between two consecutive sand additions are said to form an *avalanche*. One can define both a size and a characteristic time for an avalanche. The size of an avalanche can be defined, for instance, as the total number of toppling sites (one site can topple more than once) or the total number of topplings (it is clear that these two definitions give more and more similar results as the space dimension increases). In order to define the lifetime of an avalanche, one must first define the unit timestep. The latter is the duration of the fundamental event defined by these two processes:

- a set of sites becomes critical due to the previous toppling event;
- all such critical sites undergo a toppling process, and the heights of their neighbours are updated.

[2] Different functions of the height z_i can be defined: for example the height itself, the difference of height between nearest neighbours (first discrete derivative of the height), the discrete Laplacian operator of height (second discrete derivative), and so on.

Then the lifetime of an avalanche can be defined as the number of unit timesteps between two sand additions. The fundamental result of the sandpile model is that at the steady state both the size s and the lifetime t of avalanches are characterized by power law distributions $P(s) \sim s^{-\chi}$, $Q(t) \sim t^{-\xi}$ [26]. Therefore the model succeeds in reproducing the critical behaviour, often associated to phase transitions, with a self-organized mechanism requiring no external fine tuning of the control parameter. Note that the grain addition can be viewed as the action of an external field over the system. Similarly, the avalanche processes can be viewed as the response (relaxation) of the system to this field. The spatial correlations that develop spontaneously at all scales indicate that the system reacts macroscopically even to a microscopic external perturbation, a behaviour reminiscent of the diverging susceptibility characterizing critical phenomena.

6.2.2.2 The Bak-Sneppen Model

A model that attempts to explain some key properties of biological evolution, even if with strong simplifications, is the Bak-Sneppen (BS) model [8, 28]. It is defined by the following steps:

- N species are arranged on the sites of a 1-dimensional lattice (a chain, or a ring if periodic boundary conditions are enforced);
- a *fitness* value x_i (sometimes interpreted as a fitness *barrier*) is assigned to each species i, drawn randomly from a uniform distribution in the interval [0, 1];
- the site with the lowest barrier and its nearest neighbours are updated: new random fitness values, drawn from the same uniform distribution on the unit interval, are assigned them.

The basic idea behind the model is that the species with the lowest fitness is the one that is most likely to go extinct and replaced by a new one. Alternatively, the update is interpreted as a mutation of the least fit species towards an evolved species representing its descendant or offspring. Finally, one can interpret x_i as the barrier against mutation for the genotype of species i: the higher the barrier, the longer the time between two modifications of the genetic code. The species with lowest barrier is therefore the first to evolve. In any case, the reason for updating the nearest neighbours is the same: the mutation of one species changes the state of all the interacting species (for instance, both predator and prey along the food chain). The effect of this change on the fitness of the nearest neighbours is not known a priori (it may be beneficial or not), and is modelled as a random update of their fitness as well.

If the procedure described above is iterated, the system self-organizes to a critical stationary state in which almost all the barriers are uniformly distributed over a certain threshold value $\tau = 0.66702 \pm 0.00008$ [29] (see Fig. 6.2, left panel). In other words, the fitness distribution evolves from a uniform one in the interval [0, 1] to a uniform one in the interval $[\tau, 1]$. In this model an (evolutionary) x-avalanche is defined as a causally connected sequence of mutations of barriers, all below a fixed

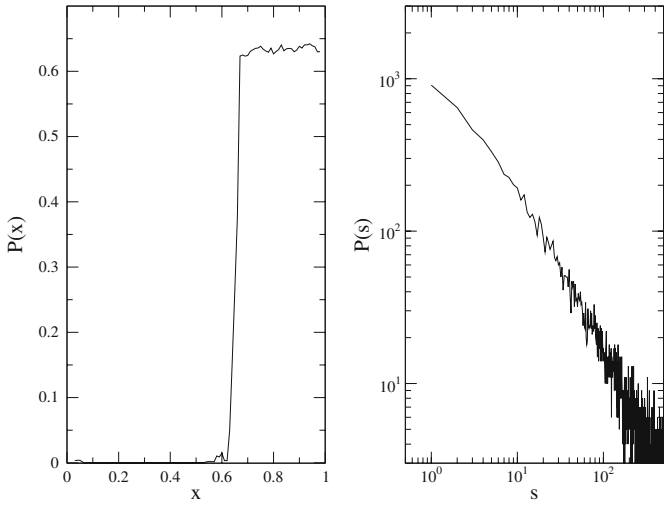

Fig. 6.2 *Left*: plot of the probability distribution of fitness values at the steady state in the Bak-Sneppen model with 500 species. *Right*: the probability distribution $P(s)$ for the size of a critical τ-avalanche

value x. In this way the size of an x-avalanche is uniquely defined as the number of mutations between two consecutive configurations where all barriers are above x. For $x \approx \tau$ the avalanche distribution is a power law $P(s) \propto s^{-\chi}$ with an exponent $\chi = 1.073 \pm 0.003$ [29] (see Fig. 6.2, right panel).

The Bak-Sneppen model is a prototype mechanism generating fractal phenomena as an effect of extremal dynamics [30]. It also provides a possible explanation for the phenomena of mass extinctions observed in the fossil records [31], some analyses of which have indicated that extinction sizes are power-law distributed. Rather than considering large-scale extinctions as triggered by external catastrophic events (such as meteorites or major environmental changes) and small-scale extinctions as caused by evolutionary factors, the model shows that a power-law distribution of extinction events may be interpreted as the outcome of a single internal macroevolutionary process acting at all scales.

The Bak-Sneppen model has been studied within a variety of different frameworks ranging from numerical simulation [29, 32], theoretical analysis [33], renormalization group techniques [34, 35], field theory [36], mean-field approximations [28, 30] and probabilistic approaches (run time statistics) [37, 38]. It has also been defined on higher-dimensional lattices and more general graphs, including complex networks [8, 28, 38–43], which are the subject of the next section. For a recent review on this model see [44] and references therein. Being so well studied, the Bak-Sneppen model is ideal for studying the effects introduced by a feedback mechanism between fitness dynamics and topological restructuring. For this reason, it is at the basis of the adaptive model [6] that we shall present in detail in Section 6.4.

6.3 Complex Networks

Networks are encountered anywhere in nature [1–5]. For example, in biology they describe protein interactions, metabolic reactions, and gene expressions [45–47]. In the different context of ecology, food webs [48, 49] report predator-prey or host-parasite interactions, and taxonomic trees are used to classify different species [50–52]. Socio-economic systems display a strongly networked structure as well, for instance when considering the relationships between firms [53] or trading countries [54]. Technology produces network structures as well, the most striking evidences of which being the Internet and the WWW [55–57]. During the last decade, it has been found that the overwhelming majority of real-world networks is characterized by nontrivial features, leading to the term "complex networks". As for the notion of "complex systems", a rigorous and/or widely accepted definition of network complexity does not exist. Nonetheless, what is generally meant is that many topological properties of real networks are not easily reproduced by simple graph models. Quite surprisingly, these properties are often shared by networks of very different nature, suggesting common organizing mechanisms.

6.3.1 Network Properties

One of the widespread features observed in real networks is a scale-free distribution $P(k) \propto k^{-\gamma}$ for the degree k, representing the number of links emanating from a vertex. More formally, for an undirected network with N vertices, the degree of each vertex i can be expressed as

$$k_i \equiv \sum_j a_{ij} \tag{6.6}$$

where $a_{ij} = 1$ if a link between i and j is there, and $a_{ij} = 0$ otherwise. The empirical finding that k_i is power-law distributed indicates that even if the majority of vertices has a small number of neighbours, some of them (the "hubs") are connected to many vertices.

Another nontrivial property is the (anti)correlation between degrees of neighbouring vertices: vertices with a large value of the degree tend either to "attract" or to "repel" vertices with similar degree, a property known as *assortativity* or *disassortativity* respectively [1, 4]. This can be quantified by measuring the average degree of the nearest neighbours of a vertex i, defined as

$$k_i^{nn} \equiv \frac{\sum_j a_{ij} k_j}{k_i} = \frac{\sum_{jk} a_{ij} a_{jk}}{\sum_j a_{ij}} \tag{6.7}$$

and plotting it versus k_i. Assortative mixing corresponds to an increasing trend, while disassortative mixing corresponds to a decreasing trend of the resulting curve. In absence of correlations, a flat behaviour would be observed.

Another observed tendency is the presence of many more triangles (fully connected triples of vertices) than expected by chance, a feature denoted *clustering* [1, 4]. For each vertex i, the clustering coefficient c_i is defined as the fraction of links existing among its neighbours:

$$c_i \equiv \frac{\sum_{jk} a_{ij} a_{jk} a_{ki}}{k_i(k_i - 1)/2} = \frac{\sum_{jk} a_{ij} a_{jk} a_{ki}}{\sum_{jk} a_{ij} a_{ki}} \tag{6.8}$$

When plotted against k_i, for most real networks c_i displays a decreasing trend, indicating the presence of *hierarchy*. Unstructured networks would instead display a flat behaviour. An average of c_i over all vertices measures the overall probability that two vertices, both joined to a third one, are also connected to each other. This average clustering is found to be much larger than expected by chance.

High clustering is often combined with a small value of the average distance between pairs of vertices, and the term *small world effect* is used to describe this combination [5]. Another property of interest is the existence in large networks of (sometimes overlapping) communities, modules, and "rich clubs" [1, 2]. Besides their structural importance, these topological properties have a deep effect on the dynamical processes that take place on networks. Examples of processes whose dependence on the underlying network structure has been studied in detail include the spreading of epidemics [58], percolation [4], critical phenomena [59], the exchange of wealth [60, 61], and the sandpile [62] and Bak-Sneppen models themselves [8, 28, 38–43].

6.3.2 Network Models

All these interesting properties are detected by comparing the topology, or the dynamical performance, of a network with a null model providing a randomized version of it. Graph models are therefore important benchmarks for understanding complex networks. Moreover, they are also used to test candidate mechanisms believed to be responsible for the onset of a particular topological feature, thus providing an insight into realistic network formation processes. The vast majority of theoretical models can be grouped in two broad classes. On one hand, one has static models with a fixed number of links and specified connection probabilities between them. This generates an ensemble of networks whose expected topological properties can be obtained analytically. The prototype of all static models is the random graph, that we shall briefly review in Sect. 6.3.2.1. On the other hand, one has evolving models with a variable number of vertices and links, that grow under specified stochastic rules. The earliest example of these models is the one proposed by Barabási and Albert [63], and we shall present it in Sect. 6.3.2.2. Most models proposed in the last decade are (often nontrivial) modifications of these two simple ones. For instance, in Sect. 6.3.2.3 we briefly review the fitness model, where the idea that the connection probability depends on some vertex-specific fitness has

been introduced. As we have anticipated in the Introduction, besides these two well established frameworks a third, more recent approach focuses on networks shaped by the interplay between dynamical processes defined on them and the readjustment of topology. Our main focus is exactly an example of such adaptive models, which shall be presented in detail separately in Sect. 6.4.

6.3.2.1 The Random Graph Model

For an undirected network with N vertices, the maximum possible number of edges (excluding self-loops) one can draw is given by $L_{max} = N(N-1)/2$. If all these edges are present, the graph is said to be "complete". At the opposite limit, if no edge is present, the graph is said to be "empty". In between these two extremes, one can form instances of more or less dense networks by drawing each of the possible edges independently with a probability p. This defines the random graph model [5], whose only parameter (besides N) is p. The case $p = 0$ recovers the empty graph, while the case $p = 1$ yields the complete one. The expected number (average $\langle \cdots \rangle$ over the ensemble of possible realisations) of edges in a random graph with probability p is given by

$$\langle L \rangle = p\frac{N(N-1)}{2} \tag{6.9}$$

and the expected degree, which is the same for all vertices, is

$$\langle k \rangle = p(N-1) \approx pN. \tag{6.10}$$

For N large the correlations between the various degrees can be neglected (degrees are not independent in a finite graph), and the degree distribution $P(k)$ can be approximated by the probability that a single vertex has degree k. To obtain a vertex with degree k, we must have k times a successful event whose probability is p, and $(N-1-k)$ times an unsuccessful event whose probability is $(1-p)$. Since this can happen in

$$\binom{N-1}{k} = \frac{(N-1)!}{(N-1-k)!k!} \tag{6.11}$$

combinations, we have

$$P(k) = \binom{N-1}{k} p^k (1-p)^{N-1-k} \tag{6.12}$$

The distribution is automatically normalized since

$$\sum_{k=0}^{N-1} P(k) = [p + (1-p)]^{N-1} = 1. \tag{6.13}$$

The above binomial distribution is well approximated by a Poisson distribution in the limit $N \to \infty$ and $p \to 0$ (with Np kept constant):

$$P(k) \approx \frac{(Np)^k e^{-pN}}{k!} = \frac{\langle k \rangle^k e^{-\langle k \rangle}}{k!}. \tag{6.14}$$

where we have used Eq. (6.10). Thus the degree distribution of the random graph decays exponentially, and is well concentrated about the average value $\langle k \rangle$. This is in stark contrast with the scale-free behaviour of most real networks, characterized by the power-law tail of $P(k)$.

The expected value of the average nearest neighbours degree defined in Eq. (6.7) is the same for all vertices as well, and equals the average degree:

$$\langle k^{nn} \rangle = \frac{p^2(N-1)^2}{p(N-1)} = p(N-1) \tag{6.15}$$

This means that, as expected, in the random graph no (dis)assortative mixing is present, and the degrees of neighbouring vertices are uncorrelated.

Similarly, for the expected value of the clustering coefficient defined in Eq. (6.8) one finds

$$\langle c \rangle = \frac{p^3(N-1)(N-2)}{p^2(N-1)(N-2)} = p \tag{6.16}$$

so that no hierarchical structure is present. Moreover, if the value of p is chosen in such a way that the expected number of links in Eq. (6.9) matches the empirically observed one, then the resulting value of $\langle c \rangle$ is much smaller that the observed average clustering coefficient.

One can also derive an upper bound for the average distance, by considering the *diameter* D (defined as the maximum distance between pairs of vertices). Exploring the graph as in a breadth first search algorithm, one finds that if the number of first neighbours of a vertex is $\langle k \rangle$, and if the network is connected, then the number of vertices visited after d steps must be approximately $\langle k \rangle^d$. The total number N of vertices is reached in at most D steps, so that

$$N \gtrsim \langle k \rangle^D \quad \Rightarrow \quad D \lesssim \frac{\ln N}{\ln \langle k \rangle}. \tag{6.17}$$

Therefore the average distance scales at most logarithmically with N, a feature which is consistent with the small values observed.

In summary, for random graphs

- no scale-free degree distribution is present;
- degrees of neighbouring vertices are uncorrelated;
- the clustering is too weak and not hierarchical;
- no small world effect is present, even if the average distance is small.

6.3.2.2 The Barabási-Albert Model

The Barabási-Albert model [63] is the prototype of evolving network models, where it is assumed that the system grows at any time step. Both the number of vertices and the number of edges increase with time, since new vertices enter the network and are assumed to connect to the pre-existing ones with a probability proportional to the degree of the latter (*rich-get-richer* mechanisms). This implies that newcomers establish their connections preferentially with vertices that already have a large degree. It is then clear that the two novel ingredients in this model of network formation are *growth* and *preferential attachment*. The main success of the model is that these two simple rules produce naturally scale-free networks with degree distribution $P(k) \propto k^{-\gamma}$ (where $\gamma = 3$).

In order to derive this result, we rephrase the model quantitatively. The initial ($t = 0$) state consists of N_0 vertices and no link. At each timestep t a new vertex attached to m_0 new edges enters the system. The loose ends of these m_0 edges connect to m_0 pre-existing vertices, chosen with a probability $\Pi(k_i, t)$ proportional to their degree at time t:

$$\Pi(k_i, t) = \frac{k_i(t)}{\sum_j k_j(t)} \tag{6.18}$$

This directly implies that the numbers of vertices and edges at time t are given by

$$\begin{aligned} N(t) &= N_0 + t \\ m(t) &= \frac{1}{2}\sum_j k_i(t) = m_0 t. \end{aligned} \tag{6.19}$$

Using a continuous-time approximation, one can write the time evolution of the degree k_i by noting that its rate of increase is

$$\frac{\partial k_i}{\partial t} = m_0 \Pi(k_i, t) = m_0 \frac{k_i(t)}{\sum_j k_j(t)} = \frac{m_0 k_i(t)}{2 m_0 t} = \frac{k_i(t)}{2t} \tag{6.20}$$

The above differential equation can be solved using the initial condition $k(t_i) = m_0$, where t_i is the time when vertex i entered the network. The solution is

$$k_i(t) = m_0 \left(\frac{t}{t_i}\right)^{1/2} \tag{6.21}$$

showing that the degree grows with the square root of time. This relation allows us to compute the exponent of the degree distribution. The probability $P(k_i < k)$ that a vertex has a degree smaller than k is $P(k_i < k) = P\left(t_i > \frac{m_0^2 t}{k^2}\right)$. Since vertices enter at a constant rate, the distribution of their injection times is uniform between the initial time $t_i = 0$ and the current time $t_i = t$. In this interval, $P(t_i) = 1/N(t) =$

$1/(N_0 + t)$. This implies

$$P\left(t_i > \frac{m_0^2 t}{k^2}\right) = 1 - P\left(t_i \leq \frac{m_0^2 t}{k^2}\right) = 1 - \frac{m_0^2 t}{k^2}\frac{1}{(N_0 + t)} \tag{6.22}$$

from which we have

$$P(k) = \frac{\partial P(k_i < k)}{\partial k} = \frac{2m_0^2 t}{(N_0 + t)}\frac{1}{k^3} \propto k^{-3} \tag{6.23}$$

Therefore, we find that the degree distribution is a power law with a value of the exponent $\gamma = 3$.

This derivation highlights the difficulty, as compared with static models, of deriving exact results for growing networks, which are therefore often explored by means of numerical simulations. Despite this difficulty, a series of results have been derived for the model. We only list some of them by reporting that networks generated by the Barabási-Albert model

- have power-law distributed degrees (as shown above);
- have no correlations between degrees of neighbouring vertices [4];
- show a clustering larger than the random graph case [64, 65];
- display the small-world effect [66].

6.3.2.3 The Fitness Model

A completely different approach to obtain self-similar networks is to extend in a suitable way the random graph model defined in Sect. 6.3.2.1. In the latter, all vertices are assumed to be statistically equivalent, so unsurprisingly no heterogeneity emerges. By contrast, one can define a static model where heterogeneity is explicitly introduced at the level of vertices. In particular, Caldarelli et al. [7] have proposed a model where each vertex i ($i = 1, \ldots, N$) is assigned a *fitness* x_i drawn from a specified distribution $\rho(x)$. Then, each pair of vertices i and j is sampled, and a link is drawn between them with a fitness-dependent probability $p_{ij} = f(x_i, x_j)$. The expected topological properties of the network can be easily computed in terms of $\rho(x)$ and $f(x, y)$ [7, 67, 68]. For instance, the expected degree of vertex i is

$$\langle k_i \rangle = \sum_j p_{ij} = \sum_j f(x_i, x_j) \tag{6.24}$$

For N large, the discrete sum can be approximated by an integral. Thus the expected degree of a vertex with fitness x is

$$k(x) = N \int f(x, y)\rho(y)dy \tag{6.25}$$

where the integration extends over the support of $\rho(x)$. If one consider the cumulative fitness distribution and the cumulative degree distribution defined as

$$\rho_>(x) \equiv \int_x^{+\infty} \rho(x')dx' \qquad P_>(k) \equiv \int_k^{+\infty} P(k')dk' \tag{6.26}$$

then the latter can be easily obtained in terms of the former as

$$P_>(k) = \rho_>[x(k)] \tag{6.27}$$

where $x(k)$ is the inverse of the function $k(x)$ defined in Eq. (6.25).

Similarly, the expected value of the average nearest neighbours degree defined in Eq. (6.7) is

$$\langle k_i^{nn} \rangle = \frac{\sum_j p_{ij} \langle k_j \rangle}{\langle k_i \rangle} = \frac{\sum_{jk} p_{ij} p_{jk}}{\sum_j p_{ij}} \tag{6.28}$$

and the expected value of the clustering coefficient defined in Eq. (6.8) is

$$\langle c_i \rangle = \frac{\sum_{jk} p_{ij} p_{jk} p_{ki}}{\langle k_i \rangle (\langle k_i \rangle - 1)/2} = \frac{\sum_{jk} p_{ij} p_{jk} p_{ki}}{\sum_{jk} p_{ij} p_{ki}} \tag{6.29}$$

As for Eq. (6.24), the above expressions can be easily rephrased in terms of integrals involving only the functions $f(x, y)$ and $\rho(x)$, upon which all the results depend.

The constant choice $f(x, y) = p$ is the trivial case corresponding to a random graph, irrespectively of the form of $\rho(x)$. The simplest nontrivial choice can be obtained requiring that the fitness-dependent network has no degree correlations other that those introduced by the local properties alone. It can be shown that this requirement leads to the form [69, 70]

$$f(x, y) = \frac{zxy}{1 + zxy} \tag{6.30}$$

where z is a positive parameter controlling the number of links. Apart for the so-called *structural correlations* induced by the degree sequence [69, 70], higher-order properties are completely random, as in the *configuration model* [4, 71]. When $z << 1$, the above connection probability reduces to the bilinear choice

$$f(x, y) = zxy \tag{6.31}$$

In this case, a sparse graph is obtained where structural correlations disappear. Also, from Eq. (6.24) one finds that $\langle k_i \rangle \propto x_i$. If one chooses a power-law fitness distribution $\rho(x) \propto x^{-\gamma}$, it is therefore clear that the degree distribution will have exactly the same shape: $P(k) \propto k^{-\gamma}$. In the more general case corresponding to

Eq. (6.30), the same choice for $\rho(x)$ yields again a power-law degree distribution, with a cut-off at large degree values that correctly takes into account the requirement $k \leq N$ for dense networks. Equation (6.30) also generates disassortativity and hierarchically distributed clustering, both arising as structural correlations imposed by the local constraints. For sparse networks, corresponding to Eq. (6.31), these correlations disappear.

Another interesting choice is given by

$$f(x, y) = \Theta(x + y - z) \qquad \rho(x) = e^{-x} \tag{6.32}$$

where z, which again controls the number of links, now plays the role of a positive threshold. This choice yields again a power-law degree distribution $P(k) \propto k^{-\gamma}$ (where now $\gamma = 2$), anticorrelated degrees with $k^{nn}(k) \propto k^{-1}$, and hierarchically distributed clustering $c(k) \propto k^{-2}$ (times logarithmic corrections) [7, 67, 68]. Remarkably, it has been shown that both Eqs. (6.30) and (6.32) are particular cases of a more general expression obtained by introducing a temperature-like parameter [72]. Equation (6.30), with $\rho(x) \propto x^{-\gamma}$, corresponds to the finite-temperature regime, where the temperature can be reabsorbed in a redefinition of x and z. By contrast, Eq. (6.32) corresponds to the zero-temperature regime where the graph reaches a sort of "optimized" topology [72]. In all these cases, the average distance is small. In summary, for a series of reasonable choices the networks generated by the fitness model display

- a scale-invariant degree distribution;
- correlations between neighbouring degrees;
- hierarchically distributed clustering;
- a small-world effect.

6.4 A Self-Organized Network Model

As we have anticipated in the Introduction and in Sect. 6.3.2, more recent approaches to the modelling of complex networks have considered the idea that the topology evolves under a feedback with some dynamical process taking place on the network itself (see for instance [6, 48, 73–80]). Among the various contributions, some groups have considered a possible connection with Self-Organized Criticality [6, 74–77]. A first such set of results is reviewed in the chapter by Rohlf and Bornholdt in this issue [74]. Another review of the results obtained for a model inspired by solar processes can be found in [75]. In what follows, we review a different set of models inspired by the sandpile and Bak-Sneppen dynamical rules recalled in Sects. 6.2.2.1 and 6.2.2.2.

Bianconi and Marsili [76] have defined a model where slow network growth, defined as the gradual addition of links between randomly chosen vertices, is combined to fast relaxation, defined as the random rewiring of links connected to congested (toppling) vertices. To avoid the collapse to a complete graph, dissipation is

also introduced, allowing toppling nodes to lose all their links at a given rate. The outcomes of the model depend on the dissipation rate and on the probability density function for the toppling probabilities to be assigned at each vertex. A particular choice of these quantities drives the system to a stationary state characterized by a scale-free topology and a power-law distribution for toppling avalanches.

Fronczak et al. [77] have proposed a model where no parameter choice is required in order to drive the system to the critical region. They considered the sandpile dynamics defined in Sect. 6.2.2.1, but where each vertex has a different critical height equal to its degree, as in other previous studies [62]. In addition, they assumed that after an avalanche of size A, the A ends of links in the network that have not been rewired for the longest time are rewired to the initiator of the avalanche. In this way, the avalanche area distribution and the degree distribution evolve in time, and at the stationary state become very similar and scale-free.

Garlaschelli et al. [6] have introduced another fully self-organized model where the Bak-Sneppen dynamics defined in Sect. 6.2.2.2 takes place on a network whose topology is in turn continuously shaped by the fitness model presented in Sect. 6.3.2.3. Remarkably, they find that the mutual interplay between topology and dynamics drives the system to a state characterized by scale-free distributions for both the degrees and the fitness values. These unexpected properties differ from what is obtained when the two models are considered separately. The rest of the chapter is devoted to a detailed description of this model.

6.4.1 Motivation

We have already mentioned that the topology of a network affects dramatically the outcomes of dynamical processes taking place on it [1, 2, 4, 5]. On the other hand, the idea behind the fitness model presented in Sect. 6.3.2.3 captures the empirically observed result [53, 54, 81] that the topology of many real networks is strongly dependent on some vertex-specific quantity. Clearly, these results imply that in general one should consider the mutual effects that dynamics and topology have on each other. Unfortunately, the overwhelming majority of studies have instead considered the two processes separately, by postulating either a scenario where the topology evolves over a much longer timescale than the dynamics, or the opposite situation where the dynamical variables evolve much more slowly than the topology (and are therefore assumed fixed as in the fitness model itself). In cases when there is indeed such a sharp separation of timescales, these approaches are helpful. But in many cases the topological evolution and the dynamics may occur at comparable rates, and the decoupled approach gives no insight into the real process. Moreover, even when the timescales are indeed well separated, it is clear that the variables involved in the slower of the two processes must be specified as external parameters, and *ad hoc* assumptions must therefore be made. For instance, when considering the spreading of epidemics on a network one should assume an arbitrary fixed topology. Similarly, when a network is formed according to the fitness model, one should assume an arbitrary distribution for the fitness variables.

These motivations lead Garlaschelli et al. [6] to define a self-organized model where *ad hoc* specifications of any fixed structure, either in the topology or in the dynamical variables, are unnecessary. Rather, it is the interplay between dynamics and topology that autonomously drives the system to a stationary state. The choice of both the dynamical rule and the graph formation process was driven by the interest to highlight the novel effects arising uniquely by the feedback introduced between them. Therefore, two extremely well understood models where chosen. On one hand, the extremal fitness dynamics of the Bak-Sneppen model (see Sect. 6.2.2.2), and on the other hand the fitness network model (see Sect. 6.3.2.3). As we have shown in Sect. 6.3.2.3, the topology generated by the fitness model can be completely calculated for any distribution of the fitness values. Similarly, the outcomes of the Bak-Sneppen model on several static networks are well studied [8, 28, 38–43]. On a generic graph, each of the N vertices is assigned a fitness value x_i, initially drawn from a uniform distribution between 0 and 1, as in the one-dimensional case. At each timestep the species i with lowest fitness and all its k_i neighbours undergo a mutation, and $k_i + 1$ new fitness values (drawn from the same uniform distribution) are assigned them. On regular lattices [8, 39], random graphs [28], small-world [40] and scale-free [41–43] networks it has been shown that, as for the one-dimensional model, at the stationary state the fitness values are uniformly distributed above a critical threshold τ. The only dependence on the particular topology is the value of τ [8, 28, 39–43]. In particular, τ vanishes for scale-free degree distributions with diverging second moment [41–43].

While these more complicated networks are closer to realistic food webs [49], as long as the graph is static the model leads to the ecological paradox that, after a mutation, the evolved species inherits the same connections of the previous species. By contrast, macroevolution is believed to be at the same time the cause and the effect of food web dynamics [48]. In particular, after a mutation, a species is expected to develop a new set of interactions with the other species.

6.4.2 Definition

In order to overcome this problem, Garlaschelli et al. assumed that the Bak-Sneppen dynamics is combined with a fitness-driven link updating. At the initial state the network is generated as in the fitness model, and between all pairs of vertices i and j a link is drawn with probability $f(x_i, x_j)$ (where the x_i's are the initial fitness values). Then, whenever a species i is assigned a new fitness x_i', all the set of connections between i and the other vertices $j \neq i$ are drawn anew with updated probability $f(x_i', x_j)$. This automatically implies that major mutations (a large change in x_i) are associated with very different connection probabilities, while little changes lead to almost equiprobable interactions. An example of this evolution rule is depicted in Fig. 6.3.

Two possible choices for updating the fitness of a mutating vertex where proposed. In the original paper [6], the usual prescription was adopted: each neighbour

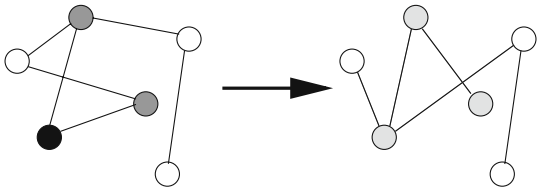

Fig. 6.3 Example of graph evolution in the self-organized model. The minimum-fitness vertex (*black*) and its two neighbours (*grey*) undergo a mutation: three new fitness values are assigned them (*light grey*), and new links are drawn between them and all the other vertices

j of the minimum-fitness vertex receives a fitness drawn anew from the uniform distribution on the unit interval. This means

$$x_j(t+1) = \eta \tag{6.33}$$

where η is uniformly distributed between 0 and 1. Therefore, x_j is completely updated, independently of its degree k_j. In another study [82], a weaker rule was assumed. In particular, the fitness of each neighbour j is assumed to change only by an amount proportional to $1/k_j$:

$$x_j(t+1) = \frac{1}{k_j}\eta + \frac{k_j - 1}{k_j}x_j(t) \tag{6.34}$$

where again η is a random number uniformly distributed between 0 and 1. Under this second assumption, x_j is completely modified if the only neighbour of j is the minimum-fitness vertex, in which case $k_j = 1$. If j has $k_j - 1$ additional neighbours, a share $(k_j - 1)/k_j$ of x_j is unchanged, and the remaining fraction x_j/k_j is updated to η/k_j. This makes hubs affected less than small-degree vertices. Clearly, it also implies that the probability of connection to all other vertices varies by a smaller amount. In what follows we shall present both analytical and numerical results derived under the first choice [6]. Numerical simulations of the model under the second rule are reported in [82].

6.4.3 Analytical Solution

Remarkably, the model is exactly solvable for any choice of the connection probability $f(x, y)$ [6]. Indeed, one can write down a master equation for the fitness distribution $\rho(x, t)$ at time t:

$$\frac{\partial \rho(x,t)}{\partial t} = r^{in}(x,t) - r^{out}(x,t) \tag{6.35}$$

where $r^{in}(x, t)$ and $r^{out}(x, t)$ are the fractions of vertices with fitness x entering and exiting the system at time t respectively. If a stationary (time-independent) distribu-

tion $\rho(x)$ exists, it is found by requiring

$$\frac{\partial \rho(x,t)}{\partial t} = 0 \quad \Rightarrow \quad r^{in}(x) = r^{out}(x) \tag{6.36}$$

where at the stationary state the quantities no longer depend on time. If one manages to write down $r^{in}(x)$ and $r^{out}(x)$ in terms of $f(x, y)$ and $\rho(x)$, then the above condition will give the stationary form of $\rho(x)$ for any choice of $f(x, y)$.

To this end, it is useful to introduce the distribution $q(m)$ of the minimum fitness $m \equiv x_{min}$. For x small enough, $\rho(x)$ must be very close to $q(x)/N$ (the distribution of all fitness values must be approximated by the correctly renormalized distribution of the minimum). The range where $\rho(x) \approx q(x)/N$ holds can be defined more formally by introducing the fitness value τ such that

$$\lim_{N\to\infty} \frac{N\rho(x)}{q(x)} \begin{cases} = 1 & x \leq \tau \\ > 1 & x > \tau \end{cases} \tag{6.37}$$

This means that in the large size limit the fitness distribution for $x < \tau$ is determined by the distribution of the minimum. After an expression for $\rho(x)$ is derived, the value of τ can be determined by the normalization condition

$$\int_0^1 \rho(x)dx = 1 \tag{6.38}$$

as we show below. Note that we are not assuming from the beginning that $\tau > 0$ as is observed for the Bak-Sneppen model on other networks. It may well be that for a particular choice of $f(x, y)$ Eq. (6.38) yields $\tau = 0$, signalling the absence of a nonzero threshold. Also, note that $\lim_{N\to\infty} q(x) = 0$ for $x > \tau$, since Eq. (6.37) implies that the minimum is surely below τ. Thus the normalization condition for $q(x)$ reads $\int_0^\tau q(x)dx = 1$ as $N \to \infty$.

The knowledge of $q(m)$ allows one to rewrite $r^{in}(x)$ and $r^{out}(x)$ as $r^{in}(x) = \int q(m)r^{in}(x|m)dm$ and $r^{out}(x) = \int q(m)r^{out}(x|m)dm$, where $r^{in}(x|m)$, $r^{out}(x|m)$ are conditional probabilities corresponding to the fractions of vertices with fitness x which are added and removed when the value of the minimum fitness is m. Let us consider $r^{in}(x)$ first. If the minimum fitness is m, then $1 + k(m)$ new fitness values are updated, where $k(m)$ is the expected degree of the minimum-fitness vertex. Since each of these $1 + k(m)$ values is uniformly drawn between 0 and 1, one has

$$r^{in}(x|m) = \frac{1 + k(m)}{N} \tag{6.39}$$

independently of x. This directly implies

$$r^{in}(x) = \int_0^\tau q(m)r^{in}(x|m)dm = \frac{1 + \langle k_{min}\rangle}{N} \tag{6.40}$$

where $\langle k_{min} \rangle \equiv \int_0^\tau q(m)k(m)dm$ is the average degree of the vertex with minimum fitness, a quantity that can be derived independently of $k(m)$ as we show below. Now consider $r^{out}(x)$, for which the independence on x does not hold. For $x < \tau$, $r^{out}(x|m) = 1/N$ if $x = m$ since the minimum is surely replaced. For $x > \tau$, the fraction of vertices with fitness x that are removed equals $\rho(x)$ times the probability that a vertex with fitness x is connected to the vertex with minimum fitness m. This probability depends on the fitness values x' and m' that the vertices currently having fitness x and m had at the most recent update of the link connecting them, and simply equals $f(x', m')$ [6]. This means

$$r^{out}(x|m) = \Theta(\tau - x)\frac{\delta(x-m)}{N} + \Theta(x-\tau)\rho(x)f(x,m) \tag{6.41}$$

where $\Theta(x) = 1$ if $x > 0$ and $\Theta(x) = 0$ otherwise, and $\delta(x)$ is the Dirac delta function. An integration over $q(m)dm$ yields

$$\begin{aligned} r^{out}(x) &= \int_0^\tau q(m)r^{in}(x|m)dm \\ &= \begin{cases} q(x)/N & x < \tau \\ \rho(x)\int_0^\tau q(m)f(x,m)dm & x > \tau \end{cases} \end{aligned} \tag{6.42}$$

Finally, one can impose Eq. (6.36) at the stationary state. If $x < \tau$, this yields $q(x) = 1 + \langle k_{min} \rangle$ independently of x. Combining this result with $q(x) = 0$ for $x > \tau$ as $N \to \infty$, one finds that the distribution of the minimum fitness m is uniform between 0 and τ:

$$q(m) = (1 + \langle k_{min} \rangle)\Theta(\tau - m) \tag{6.43}$$

Requiring that $q(m)$ is normalized yields

$$\langle k_{min} \rangle = \frac{1-\tau}{\tau} \tag{6.44}$$

Therefore Eq. (6.40) can be written as

$$r^{in}(x) = \frac{1}{\tau N} \qquad \forall x \tag{6.45}$$

If $x > \tau$, Eq. (6.36) implies

$$\begin{aligned}\rho(x) &= \frac{r^{out}(x)}{\int_0^\tau q(m)f(x,m)dm} \\ &= \frac{r^{in}(x)}{\int_0^\tau q(m)f(x,m)dm} \\ &= \frac{1}{\tau N \int_0^\tau q(m)f(x,m)dm} \\ &= \frac{1}{N \int_0^\tau f(x,m)dm}\end{aligned} \tag{6.46}$$

which must be equal to $\rho(x) = q(x)/N = (\tau N)^{-1}$ for $x < \tau$. Using this relation, the exact solution for $\rho(x)$ at the stationary state is found [6]:

$$\rho(x) = \begin{cases} (\tau N)^{-1} & x < \tau \\ \dfrac{1}{N \int_0^\tau f(x,m)dm} & x > \tau \end{cases} \tag{6.47}$$

where τ is determined using Eq. (6.38), that reads

$$\int_\tau^1 \frac{dx}{\int_0^\tau f(x,m)dm} = N - 1 \tag{6.48}$$

The above analytical solution holds for any form of $f(x, y)$. As a strikingly novel result, one finds that $\rho(x)$ is in general no longer uniform for $x > \tau$. This unexpected result, which contrasts with the outcomes of the Bak-Sneppen model on any static network, is solely due to the feedback between topology and dynamics. At the stationary state the fitness values and the network topology continue to evolve, but the knowledge of $\rho(x)$ allows to compute the expected topological properties as shown in Sect. 6.3.2.3 for the static fitness model.

6.4.4 Particular Cases

In what follows we consider specific choices of the connection probability $f(x, y)$. In particular, we consider two forms already presented in Sect. 6.3.2.3. Once a choice for $f(x, y)$ is made, one can also confirm the theoretical results with numerical simulations. As we show below, the agreement is excellent.

6.4.4.1 The Random Neighbour Model

As we have noted, the trivial choice for the fitness model is $f(x, y) = p$, which is equivalent to the random graph model. When the Bak-Sneppen dynamics takes place on the network, this choice removes the feedback with the topology, since the evolution of the fitness does not influences the connection probability. Indeed,

this choice is asymptotically equivalent to the so-called *random neighbour* variant [28] of the Bak-Sneppen model. In this variant each vertex has exactly d neighbours, which are uniformly chosen anew at each timestep. Here, we know that for a random graph the degree is well peaked about the average value $p(N-1)$ (see Sect. 6.3.2.1), thus we expect to recover the same results found for $d = p(N-1)$ in the random neighbour model. Indeed, Eq. (6.47) leads to

$$\rho(x) = \begin{cases} (\tau N)^{-1} & x < \tau \\ (p\tau N)^{-1} & x > \tau \end{cases} \tag{6.49}$$

and Eq. (6.48) yields

$$\tau = \frac{1}{1+pN} \to \begin{cases} 1 & pN \to 0 \\ (1+d)^{-1} & pN = d \\ 0 & pN \to \infty \end{cases} \tag{6.50}$$

The reason for the onset of these three dynamical regimes must be searched for in the topological phases of the underlying network. For p large, there is one large connected component that spans almost all vertices. As p decreases, this *giant cluster* becomes smaller, and several separate clusters form. Below the critical *percolation threshold* $p_c \approx 1/N$ [4, 5], the graph is split into many small clusters. Exactly at the percolation threshold p_c, the sizes of clusters are power-law distributed according to $P(s) \propto s^{-\alpha}$ with $\alpha = 2.5$ [4]. Here we find that the dense regime $pN \to \infty$ is qualitatively similar to a complete graph, where many fitness values are continuously updated and therefore $\tau \to 0$ as in the initial state (thus $\rho(x)$ is not step-like). In the sparse case where $pN = d$ with finite $d > 1$ as $N \to \infty$, then each vertex has a finite number of neighbours exactly as in the random neighbour model, and one correctly recovers the finite value $\tau = (1+d)^{-1}$ found in [28]. The subcritical case when p falls faster than $1/N$ yields a fragmented graph below the percolation threshold. This is qualitatively similar to a set of N isolated vertices, for which $\tau \to 1$. It is instructive to notice from Eq. (6.47) that the choice $f(x, y) = p$ is the only one for which $\rho(x)$ is still uniform. This confirms that, as soon as the feedback is removed, the novel effects disappear.

6.4.4.2 The Self-Organized Configuration Model

Following the considerations in Sect. 6.3.2.3, the simplest nontrivial choice for $f(x, y)$ is given by Eq. (6.30). For a fixed $\rho(x)$, this choice generates a fitness-dependent version of the *configuration model* [4, 71], where all graphs with the same degree sequence are equiprobable. All higher-order properties besides the structural correlations induced by the degree sequence are completely random [69, 70]. In this self-organized case, the degree sequence is not specified *a priori* and is determined by the fitness distribution at the stationary state. Inserting Eq. (6.30) into Eq. (6.47) one finds a solution that for $N \to \infty$ is equivalent to [6]

$$\rho(x) = \begin{cases} (\tau N)^{-1} & x < \tau \\ (\tau N)^{-1} + 2/(zN\tau^2 x) & x > \tau \end{cases} \tag{6.51}$$

where τ, again obtained using eq.(6.48), is

$$\tau = \sqrt{\frac{\phi(zN)}{zN}} \to \begin{cases} 1 & zN \to 0 \\ \sqrt{\phi(d)/d} & zN = d \\ 0 & zN \to \infty \end{cases} \tag{6.52}$$

Here $\phi(x)$ denotes the ProductLog function, defined as the solution of $\phi e^{\phi} = x$. Again, the above dynamical regimes are related to three (subcritical, sparse and dense) underlying topological phases. This can be ascertained by monitoring the cluster size distribution $P(s)$. It is found that $P(s)$ develops a power-law shape $P(s) \propto s^{-\alpha}$ (with $\alpha = 2.45 \pm 0.05$) when $d \equiv zN$ is set to the critical value $d_c = 1.32 \pm 0.05$ [6] (see Fig. 6.4), which therefore represents the percolation threshold. This behaviour can also be explored by measuring the fraction of vertices spanned by the giant cluster as a function of d (see Fig. 6.5). This quantity is negligible for $d < d_c$, while for $d > d_c$ it takes increasing finite values. Also, one can plot the average size fraction of non-giant components. As shown in the inset of Fig. 6.5, this quantity diverges at the critical point where $P(s)$ is a power law.

The analytical results in Eq. (6.51) mean that $\rho(x)$ is the superposition of a uniform distribution and a power-law with exponent -1. The decay of $\rho(x)$ for $x > \tau$ is entirely due to the coupling between extremal dynamics and topological restructuring. It originates from the fact that at any time the fittest species is also the most likely to be selected for mutation, since it has the largest probability to be connected to the least fit species. This is opposite to what happens on fixed networks. The theoretical predictions in Eqs. (6.51) and (6.52) can be confirmed by

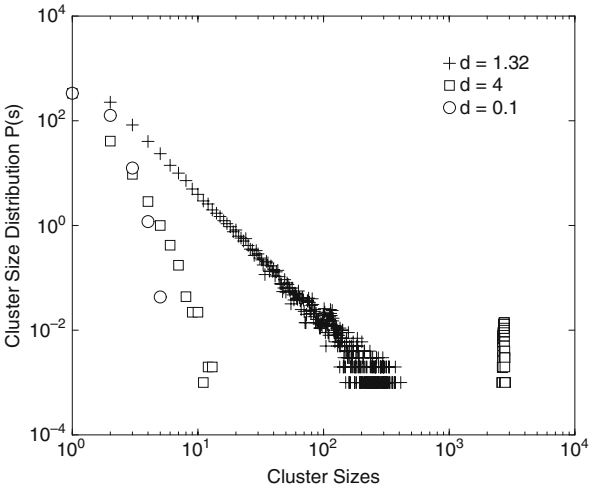

Fig. 6.4 Cluster size distribution. Far from the critical threshold ($d = 0.1$ and $d = 4$), $P(s)$ is well peaked. At $d_c = 1.32$, $P(s) \propto s^{-\alpha}$ with $\alpha = 2.45 \pm 0.05$. Here $N = 3,200$. (After [6])

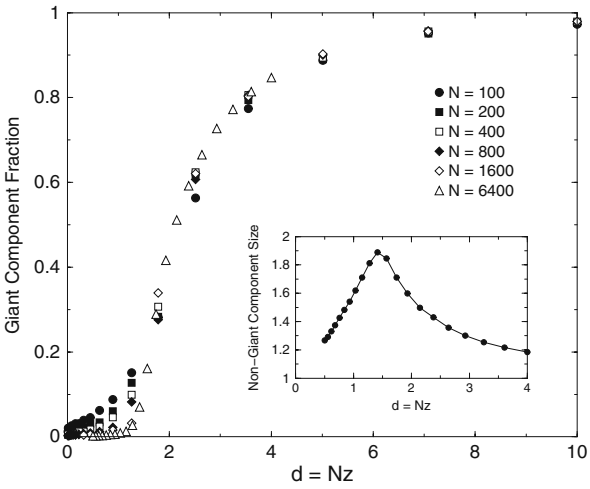

Fig. 6.5 Main panel: the fraction of nodes in the giant component for different network sizes as a function of d. Inset: the non-giant component average size as a function of d for $N = 6,400$. (After [6])

large numerical simulations. This is shown in Fig. 6.6, where the cumulative fitness distribution $\rho_>(x)$ defined in Eq. (6.26) and the behaviour of $\tau(zN)$ are plotted. Indeed, the simulations are in very good accordance with the analytical solution. Note that, as we have discussed in Sect. 6.3.2.3, in the sparse regime $z \ll 1$ one has $f(x, y) \approx zxy$. Here, this implies a purely power-law behaviour $\rho(x) \propto x^{-1}$ for $x > \tau$. Therefore $\rho_>(x)$ is a logarithmic curve that looks like a straight line in log-linear axes. In the dense regime obtained for large z, the uniform part gives instead a significant deviation from the power-law trend. This shows one effect of structural correlations.

Other effects are evident when considering the degree distribution $P(k)$. Using Eq. (6.25) one can obtain the analytic expression of the expected degree $k(x)$ of a vertex with fitness x:

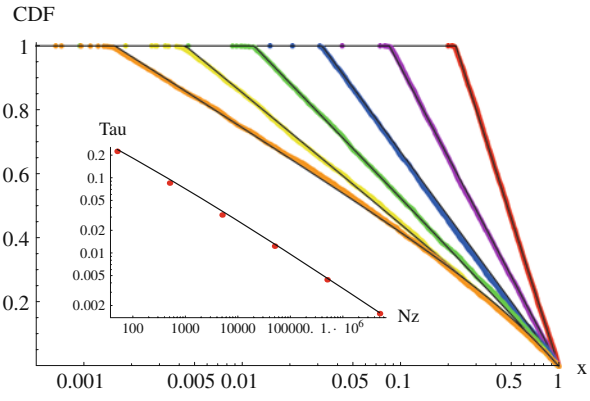

Fig. 6.6 *Main panel*: cumulative density function $\rho_>(x)$ in log-linear axes. From right to left, $z = 0.01$, $z = 0.1$, $z = 1$, $z = 10$, $z = 100$, $z = 1,000$ ($N = 5,000$). *Inset*: log-log plot of $\tau(zN)$. *Solid lines*: theoretical curves, *points*: simulation results. (After [6])

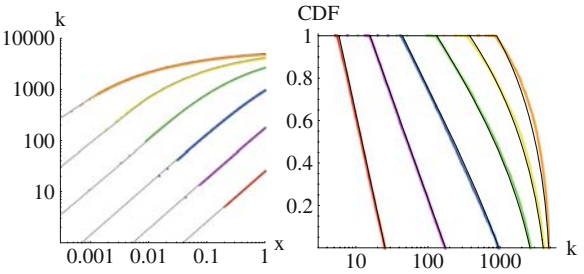

Fig. 6.7 *Left*: $k(x)$ ($N = 5,000$; from right to left, $z = 0.01$, $z = 0.1$, $z = 1$, $z = 10$, $z = 100$, $z = 1,000$). *Right*: $P_>(k)$ (same parameter values, inverse order from left to right). *Solid lines*: theoretical curves, points: simulation results. (After [6])

$$k(x) = \frac{2}{z\tau^2} \ln \frac{1 + zx}{1 + z\tau x} + \frac{zx - \ln(1 + zx)}{z\tau x} \tag{6.53}$$

Computing the inverse function $x(k)$ and plugging it into Eq. (6.27) allows to obtain the cumulative degree distribution $P_>(k)$. Both quantities are shown in Fig. 6.7, and again the agreement between theory and simulations is excellent. For small z, $k(x)$ is linear, while for large z a saturation to the maximum value $k_{max} = k(1)$ takes place. As discussed in Sect. 6.3.2.3, this implies that in the sparse regime $P(k)$ has the same shape as $\rho(x)$. Another difference from static networks is that here τ remains finite even if $P(k) \propto k^{-\gamma}$ with $\gamma < 3$ [41–43]. For large z the presence of structural correlations introduces a sharp cut-off for $P(k)$.

6.5 Conclusions

We have presented a brief, and by no means complete, summary of the ideas that inspired much of the research on scale-invariance and self-similarity, from the early discovery of fractal behaviour to the more recent study of scale-free networks. We have highlighted the importance of understanding the emergence of the ubiquitously observed patterns in terms of dynamical models. In particular, the framework of Self-Organized Criticality succeeds in explaining the onset of fractal behaviour without external fine-tuning. According to the SOC paradigm, open dissipative systems appear to evolve spontaneously to a state where the response to an infinitesimal perturbation is characterized by avalanches of all sizes. We have emphasized the importance of introducing similar mechanisms in the study of networks. In particular, we have argued that in many cases of interest it is not justified to decouple the formation of a network from the dynamics taking place on it. In both cases, one is forced to introduce ad hoc specifications for the process assumed to be slower. Indeed, by presenting an extensive study of a self-organized network model, we have shown that if the feedback between topology and dynamics is restored, novel and unexpected results are found. This indicates that adaptive networks provide a more complete explanation for the spontaneous emergence of complex topological properties in real networks.

References

1. Caldarelli G., Scale-Free Networks, Oxford University Press, Oxford (2007).
2. Caldarelli G., Vespignani A. (eds), Large Scale Structure and Dynamics of Complex Networks (World Scientific Press, Singapore 2007).
3. Dorogovtsev S.N., Mendes J.F.F., Evolution of Networks: From Biological Nets to the Internet and WWW, Oxford University Press, Oxford (2003).
4. Newman M.E.J., SIAM Rev. **45**, 167 (2003).
5. Albert R., Barabási A.-L., Rev. Mod. Phys., **74**, 47–97 (2001).
6. Garlaschelli D., Capocci A., Caldarelli G., Nature Phys., **3** 813–817 (2007).
7. Caldarelli G., Capocci A., De Los Rios P., Muñoz M. A., Phys. Rev. Lett., **89**, (2002) 258702.
8. Bak P., Sneppen K., Phys. Rev. Lett., **71**, 4083–4086 (1993).
9. Mandelbrot B.B., The variation of certain speculative prices. J. Business **36** 394–419, (1963).
10. Mandelbrot B.B., How long is the coast of britain? statistical self-similarity and fractional dimension. Science **156**, 636–638 (1967).
11. Niemeyer L., Pietronero L., Wiesmann H.J., Fractal dimension of dielectric breakdown, Phys. Rev. Lett. **52**, 1033 (1984)
12. Rodriguez-Iturbe, I., Rinaldo A., Fractal River Networks: Chance and Self-Organization, Cambridge University Press, New York (1997).
13. Brady R.M., Ball, R.C., Fractal growth of Copper electrodeposits Nature **309**, 225 (1984).
14. Batty M., Longley P.A., Fractal Cities: a Geometry of Form and Functions, Academic Press, San Diego (1994)
15. Mandelbrot B.B., Passoja D.E., Paullay A.J., Fractal character of fracture surface in metals, Nature **308**, 721 (1984).
16. Brown J.H., West G.B. (eds.), Scaling in Biology Oxford University Press Oxford (2000).
17. Sierpiński W., Sur une courbe dont tout point est un point de ramification, C. R. Acad. Sci. Paris **160**, 302–305 (1915).
18. Eldredge N., Gould S.J., Punctuated equilibria: an alternative to phyletic gradualism, In T.J.M. Schopf, ed., Models in Paleobiology. Freeman Cooper, San Francisco pp. 82–115 (1972). Reprinted in N. Eldredge Time frames. Princeton University Press (1985) Princeton.
19. Jensen H. J., Self-Organized Criticality Cambridge University Press, Cambridge (1998).
20. Rigon R., Rodríguez-Iturbe I., Rinaldo A., Feasible optimality implies Hack's law, Water Res. Res., **34**, 3181–3190 (1998).
21. Marani M., Maritan A., Caldarelli G., Banavar J.A., Rinaldo A., Stationary self-organized fractal structures in potential force fields, J. Phys. A **31**, 337–343 (1998).
22. Caylor K.K., Scanlon T.M. Rodríguez-Iturbe I., Feasible optimality of vegetation patterns in river basins, Geoph. Res. Lett., **31**, L13502 (2004).
23. Ferrer i Cancho R. and Solé R.V., Optimisation in complex networks, Lect. Notes Phys., **625**, 114-126, (2003)
24. Caldarelli G., Maritan A., Vendruscolo M., Hot sandpiles, Europhys. Lett. **35** 481–486 (1996).
25. Caldarelli G., Mean Field Theory for Ordinary and Hot sandpiles, Physica A, **252**, 295–307 (1998).
26. Bak P., Tang C., Weisenfeld K., Phys. Rev. Lett. **59**, 381 (1987).
27. Wilkinson D. Willemsen J.F., Invasion Percolation: A new form of Percolation Theory, J. Phys. A **16**, 3365–3376 (1983).
28. Flyvbjerg H., Sneppen K., Bak P., Phys. Rev. Lett. **71**, 4087 (1993).
29. Grassberger P., Phys. Lett. A **200**, 277 (1995).
30. Dickman R., Muñoz M.A., Vespignani A., Zapperi S., Braz. J. Phys. **30**, 27 (2000).
31. Benton M.J., The Fossil Record 2, Chapman and Hall, London. (1993).
32. De Los Rios P., Marsili M., Vendruscolo M., Phys. Rev. Lett. **80**, 5746 (1998).
33. Dorogovtsev S.N., Mendes J.F.F., Pogorelov Y.G., Phys. Rev. E **62**, 295 (2000).
34. Marsili M., Europhys. Lett. **28**, 385 (1994).
35. Mikeska B., Phys. Rev. E **55**, 3708 (1997).

36. Paczuski M., Maslov S., Bak P., Europhys. Lett. **27**, 97 (1994).
37. Caldarelli G., Felici M., Gabrielli A., Pietronero L., Phys. Rev. E **65** 046101 (2002).
38. Felici M., Caldarelli G., Gabrielli A., Pietronero L., Phys. Rev. Lett., **86**, 1896–1899 (2001).
39. De Los Rios, P., Marsili M., Vendruscolo, M., Phys. Rev. Lett., **80**, 5746–5749 (1998).
40. Kulkarni R.V., Almaas E., Stroud D., Evolutionary dynamics in the Bak–Sneppen model on small–world networks. *ArXiv:cond-mat/9905066*.
41. Moreno Y., Vazquez A., The Bak–Sneppen model on scale–free networks. Europhys. Lett. **57**(5), 765–771 (2002).
42. Lee S., Kim Y., Coevolutionary dynamics on scale-free networks. Phys. Rev. *E* **71**, 057102 (2005).
43. Masuda N., Goh K.-I., Kahng B., Extremal dynamics on complex networks: Analytic solutions. Phys. Rev. *E* **72**, 066106 (2005).
44. Garcia G.J.M., Dickman R., Asymmetric dynamics and critical behavior in the Bak-Sneppen model, Physica A **342**, 516–528 (2004).
45. Middendorf M., Ziv E., Wiggins C.H., Inferring network mechanisms: The Drosophila melanogaster protein interaction network, Proc. Nat. Acad. Sci. **102**, 3192–3197 (2005).
46. Giot L et al., A protein interaction map of Drosophila melanogaster, Science **302** 1727–1736 (2003).
47. Jeong H., Tombor B., Albert R., Oltvai Z.N., Barabási A.-L., The large-scale organization of metabolic networks, Nature **407**, 651 (2000).
48. Caldarelli G., Higgs P.G., McKane A.J., J. Theor. Biol. **193**, (1998) 345.
49. Garlaschelli D., Caldarelli G. Pietronero L., Universal scaling relations in food webs, Nature **423**, 165–168 (2003).
50. Burlando B., J. Theor. Biol. **146** 99–114 (1990).
51. Burlando B., J. Theor. Biol. **163** 161–172 (1993).
52. Caretta Cartozo C., Garlaschelli D., Ricotta C., Barthélemy M., Caldarelli G.J., Phys. A: Math. Theor. **41**, 224012 (2008).
53. Garlaschelli D., Battiston S., Castri M., Servedio V.D.P., Caldarelli G., Phys. A **350**, (2005) 491–499.
54. Garlaschelli D., Loffredo M.I., Phys. Rev. Lett. **93**, (2004) 188701.
55. Faloutsos M., Faloutsos P., Faloutsos C., On Power-law relationships of the Internet topology, Proc. ACM SIGCOMM, Comp. Comm. Rev., **29**, 251–262 (1999).
56. Adamic L.A. Huberman B.A, Power-law distribution of the World Wide Web, Science **287**, 2115 (2000).
57. Caldarelli G., R. Marchetti R., and Pietronero L., Europhys. Lett. **52**, 386 (2000).
58. Pastor-Satorras R., Vespignani A., Phys. Rev. Lett. **86**, 3200 (2001).
59. Dorogovtsev S.N., Goltsev A.V., Mendes J.F.F., Critical phenomena in complex networks, arXiv:0705.0010v6.
60. Garlaschelli D., Loffredo M.I., Physica A **338**(1–2), 113–118 (2004).
61. Garlaschelli D., Loffredo M.I., J. Phys. A: Math. Theor. **41**, 224018 (2008).
62. Goh K.-I., Lee D.-S., Kahng B., Kim D., Phys. Rev. Lett. **91**, 148701 (2003).
63. Barabási A.-L., Albert R. Emergence of scaling in random networks, Science **286**, 509–512 (1999).
64. Fronczak A., Fronczak P., Holyst J.A., Mean-Field theory for clustering coefficient in Barabási-Albert networks, Phys. Rev. E, **68**, 046126 (2003).
65. Barrat A., Pastor-Satorras R., Rate equation approach for correlations in growing network models, Phys. Rev. E, **71**, 036127 (2005).
66. Bollobás B., Riordan O., The diameter of a scale-free random graph, Combinatorica, **24**, 5–34 (2004).
67. Boguñá M., Pastor-Satorras R., Phys. Rev. E **68**, 036112 (2003).
68. Servedio V.D.P., Caldarelli G., Buttà P., Phys. Rev. E **70** 056126 (2004).
69. Park J., Newman M.E.J., Phys. Rev. E **68**, 026112 (2003).
70. Garlaschelli D., Loffredo M.I., Phys. Rev. E **78**, 015101(R) (2008).

71. Maslov S., Sneppen K., Zaliznyak A., Physica A **333**, (2004) 529.
72. Garlaschelli D., Ahnert S.E., Fink T.M.A., Caldarelli G., ArXiv:cond-mat/0606805v1.
73. Jain, S., Krishna, S. Autocatalytic Sets and the Growth of Complexity in an Evolutionary Model. Phys. Rev. Lett. **81**, 5684–5687 (1998).
74. Rohlf T., Bornholdt S., This issue.
75. Paczuski M., ArXiv:physics/0502028v1.
76. Bianconi G., Marsili M., Clogging and self–organized criticality in complex networks. Phys. Rev. E **70**, 035105(R) (2004).
77. Fronczak P., Fronczak A. Holyst J.A. Self–organized criticality and coevolution of network structure and dynamics. Phys. Rev. E **73**, 046117 (2006).
78. Zanette D.H., Gil, S. Opinion spreading and agent segregation on evolving networks. Physica *D* **224**(1–2), 156–165 (2006).
79. Santos F.C., Pacheco J.M. Lenaerts T., Cooperation prevails when individuals adjust their social ties. PLoS Comput. Biol. **2**(10), e140 (2006).
80. Kozma B., Barrat A., Phys. Rev. E **77**, 016102 (2008).
81. Balcan D. Erzan A., Content-based networks: A pedagogical overview. CHAOS **17**, 026108 (2007).
82. Caldarelli G., Capocci A., Garlaschelli D., A Self–organized model for network evolution. Eur. Phys. J. B **64**, 585-591 (2008).

Chapter 7
Self-Organization of Network Structure in Coupled-Map Systems

Junji Ito and Kunihiko Kaneko

Abstract Coupled map models with variable connection weights between the units are studied. A generally observed feature in this type of model is the appearance of the units with massive outgoing connections. Such structure formation is the consequence of the feedback between unit and connection dynamics.

7.1 Introduction

Unveiling network structure is often important in studying biological and social systems. Universal topological properties of network structure have been found in a variety of natural and artificial networks [1–3]. Some of those properties such as scale-free or small-world structures have been shown to emerge from simple construction rules or by evolution of networks to achieve some function [4, 5]. Since the main interest in these early studies of complex networks was in the structure of networks, the dynamics of the constituent units were largely ignored.

Recently, more and more studies on complex networks have taken into account the activity of nodes and/or the flow through links, since they are often primary determinants of network growth or structure formation. For example, the relationship between abundances of chemicals on nodes in a chemical-reaction network has been studied from the viewpoint of the optimization of metabolic flow through the network [6, 7]. In these studies, each unit (i.e., chemical concentration) on a node is in a stationary state and therefore the interplay between the dynamics of the units and the network structure is not considered. This aspect is sought in another line of studies where behaviors of coupled dynamical systems in a network of units with non-trivial dynamics are extensively investigated. Some of those studies searched for the synchronization condition for oscillatory elements in a network and examined how it depends on network topology [5, 8–10], while others focused on dynamical systems of chaotic elements on a network interacting through links, which show

J. Ito (✉)
Theoretical Neuroscience Group, RIKEN Brain Science Institute, 2-1 Hirosawa, Wako, Saitama 351-0198, Japan
e-mail: j-ito@brain.riken.jp

T. Gross, H. Sayama (eds.), *Adaptive Networks,* Understanding Complex Systems,
DOI 10.1007/978-3-642-01284-6_7,

synchronization, clustering, and chaotic itinerancy [11–15]. In these studies, though the units on the network showed rich dynamics, the network structure itself was not dynamic: once initially given, it did not change in time. Following these previous studies, the next step should be to seek common principles in systems with an interplay between the network structure formation and dynamical systems on the network [16–21].

Adaptive network is the term given to the types of network whose structure varies depending on the dynamics of the units on the nodes [22]. The aim of the present study is to discover the generic features in the dynamics and the structure of adaptive networks. We adopt the system of coupled maps with variable connection weights as our tool to explore a class of models for adaptive networks, as coupled map dynamics have been thoroughly investigated for cases with various forms of fixed regular couplings [23–27]. We mainly focus on how non-trivial dynamic structure emerges from homogeneous populations of units and connections, and try to extract the underlying mechanisms of such structure formation.

We review three types of coupled map models, following our earlier studies [16–18]: the first one is coupled logistic maps, the second one is coupled circle maps, and the last one is coupled circle maps with external input. For all these three models, coupling strengths between nodes change according to the correlation between the values on the nodes. For the first model, an exhaustive analysis of unit and connection dynamics is given in Sect. 7.2. To avoid redundant description on similar behaviors in different models, only the characteristic behaviors specific to the latter two models are described in Sects. 7.3 and 7.4. The last section is a summary and discussion on our findings.

7.2 Adaptive Network of Logistic-Map Units

Throughout the present review we discuss a system of coupled maps on a network. Each node in the network is assigned with map dynamics which depend on the instantaneous state of the node as well as on those of the other nodes that are linked to it. This sort of dynamical system is known as *coupled maps* and has been extensively studied over decades. In particular, coupled map lattices with nearest neighbor couplings on a regular lattice [23, 24] and globally coupled maps (GCM) with all-to-all coupling of equal weight [25] are two standard models. Here we adopt the coupled map approach, but instead of fixed global or nearest-neighbor couplings a time-varying connection weight is introduced in our models.

In this section, we consider the model of coupled logistic maps. Logistic map is a nonlinear map from x_n to x_{n+1} with one parameter a representing its nonlinearity, defined as:

$$x_{n+1} = ax_n(1 - x_n). \tag{7.1}$$

Successive application of this mapping yields, depending on the value of the parameter a, oscillatory dynamics with arbitrary period as well as chaotic dynamics.

Owing to this variety in dynamics, one network of logistic-map units can represent a wide range of networks with various kinds of unit dynamics. For this reason, this type of network is of primary and special interest in our study.

7.2.1 Model Formulation

Our coupled map model is defined as follows. Suppose we have a network of N units, each of which has its own time-dependent internal state. Let x_n^i denote the state variable of the i-th unit ($1 \leq i \leq N$) at the n-th time step. Connectivity between these units is given by the connection matrix w_n^{ij} which represents the weight (or strength) of the connection from unit j to unit i at the n-th time step. To introduce dynamics to the network, we install the following two functions into our model. One is the function f that defines the mapping from x_n^i to x_{n+1}^i, in other words, the dynamics of the units. The other is the function g that represents the rule of connection change. For simplicity, we assume that the range of g is between 0 and 1, and g depends only on the two state variables of the units at the both ends of the connection. With this setup, our model is described by the following set of equations:

$$x_{n+1}^i = (1-c) f(x_n^i) + c \sum_j w_n^{ij} f(x_n^j), \tag{7.2}$$

$$w_{n+1}^{ij} = \frac{[1 + \delta g(x_n^i, x_n^j)] w_n^{ij}}{\sum_j [1 + \delta g(x_n^i, x_n^j)] w_n^{ij}}, \tag{7.3}$$

where c ($0 \leq c \leq 1$) is the parameter that represents the strength of the interaction between units and δ ($0 \leq \delta \leq 1$) is the parameter that represents the degree of plasticity of connections. The normalization of incoming connection weights in Eq. (7.3) is introduced in order to avoid the divergence of connection weights in the case where the steady state of unit dynamics satisfies strengthening condition of the connection change, which could lead to endless growing of the connection weights. This normalization also imposes competition among incoming connections of a unit. When $\delta = 0$, this model reduces to the standard GCM.

By choosing appropriate functions for f and g, Eqs. (7.2) and (7.3) can model various types of adaptive networks. This choice would depend on the purpose of modeling. For example, connection dynamics that strengthen the connections between units in different dynamical states would lead to global synchronization of the whole system. This type of rewiring rule is introduced by Chen and Kurth to a coupled phase oscillator model and described in detail in the subsequent chapter. In this study, however, we focus on the opposite type of connection dynamics, i.e., "Hebbian" type dynamics, which is characterized by the strengthening of connections between units in a similar state. This type of dynamics is called Hebbian because it can be considered as a natural extension of the Hebb rule, which is widely used as a synaptic update rule in neural network studies and considered as the

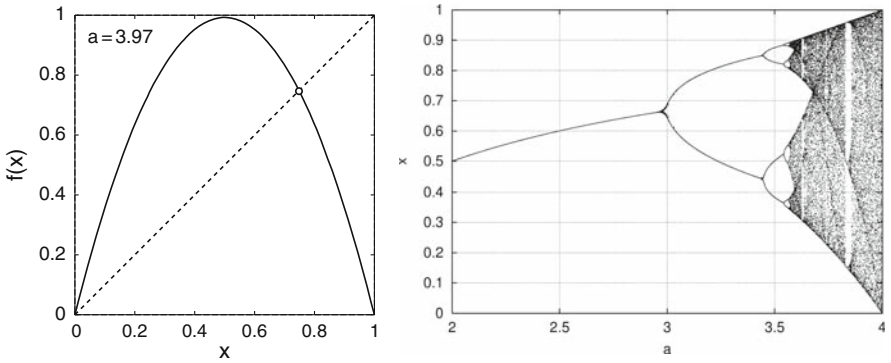

Fig. 7.1 The logistic map and its bifurcation diagram. (*Left*) The mapping function $f(x) = ax(1 - x)$; $a = 3.97$. The *open circle* in the graph represents the unstable fixed point of the dynamics generated by this map. (*Right*) The bifurcation diagram of logistic map. Asymptotic values of x are plotted for each value of the parameter a. This map generates chaotic dynamics for values of a larger than about 3.57

fundamental principle of structure formation in neural networks, to systems with continuous state variables. The function that we use in practice for the connection dynamics in our simulations is $g(x^i, x^j) = 1 - 2|x^i - x^j|$, but any other function which monotonically decreases with the difference between its two arguments gives essentially identical results. For unit dynamics, as mentioned above, we adopt the logistic map: $f(x^i) = ax^i(1 - x^i)$. Figure 7.1 shows the graph of this mapping function and how the unit dynamics depend on the value of the parameter a.

To this end, our model possesses three parameters: a for the nonlinearity of unit dynamics, c for the strength of interaction between units, and δ for the plasticity of connection. In this section, δ is set to 0.1, though a wide range of δ values give similar results [17].

In the following, we study the dynamics of the networks described by Eqs. (7.2) and (7.3) using numerical simulations. In most of the simulations, we use the following initial condition. First, the initial value of self-connection w_0^{ii} is set to 0 for all i. This assures that the self-connections (besides the term $(1 - c) f(x_n^i)$) are 0 at any time step n. Second, all the remaining connection weights are set to be identical. This means that, at the initial step, every unit in the system uniformly connects to all the other units. Due to the normalization of incoming connections, the initial connection weight is determined to be $1/(N - 1)$. Finally, x_0^i are randomly chosen from the uniform distribution between 0 and 1.

7.2.2 Unit Dynamics

We start our analysis from studying the dependence of unit dynamics on the values of the parameters a and c. It is known that the dynamics of coupled map systems are characterized by the formation of synchronized clusters of units. In Fig. 7.2,

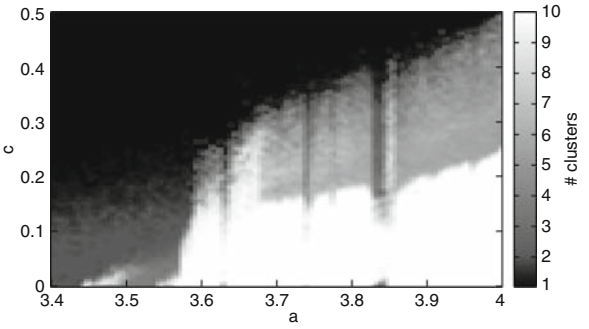

Fig. 7.2 The number of clusters plotted against the parameters a and c, obtained from the numerical simulations of our model composed of 10 units. The number of clusters is counted after 5,000 steps of transient period and averaged over 100 simulations starting from random initial conditions

the number of clusters observed in our model is plotted against the parameters a and c. Basically, the number of clusters increases as a gets larger or c gets smaller, which is consistent with the previous studies of GCM [25] where the connection weights are constant over elements and time. A novel dynamical feature induced by the introduction of connection change is the appearance of a large regime of $N/2$-cluster state in the (a, c)-space. In this state, every unit forms a pair with another unit and the state variables of the units in a pair are synchronized, resulting in $N/2$ clusters in the system. Destabilization of this pair (by increase of a or decrease of c) immediately results in the total absence of synchronized clusters, because all the units in our model have the same set of parameter values, and therefore, once a pair is destabilized, so are all the other pairs as well. This means that there is hardly any set of parameter values that allows an intermediate number of clusters between $N/2$ and N.

In the following, we give a more detailed description for the three representative states of unit dynamics observed in our model.

Synchronized state: For small a and large c values, all the units in the system are synchronized. The dynamics of the units are either periodic or chaotic, depending on the value of a (Fig. 7.3a). The connection weights do not change in this state, because in our model, connection dynamics are driven by the difference between the state variables, and all the state variables have an identical value in the synchronized state. Due to this lack of connection dynamics, the system is essentially identical to the standard GCM. The stability of the synchronized state in the standard GCM can be estimated using the tangential Lyapunov exponent, or split exponent [25], defined as follows for our model:

$$\lambda_{\mathrm{spl}}(a, c) = \ln\left(1 - \frac{N}{N-1}c\right) + \lambda_0(a), \tag{7.4}$$

where λ_0 represents the Lyapnov exponent of, in our case, the logistic map with parameter value a. With this quantity, the stability condition for the synchronized state is written as $\lambda_{\mathrm{spl}}(a, c) < 0$, and hence the boundary of the region (in (a, c)-space) where a synchronized state is allowed is given by:

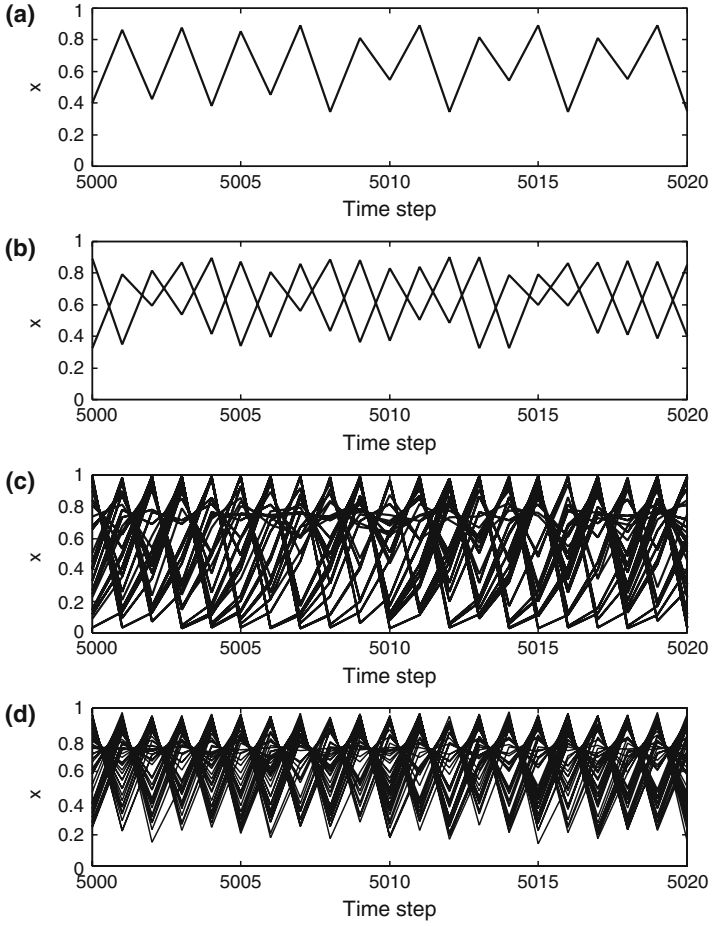

Fig. 7.3 Time series of x_n^i $(1 \leq i \leq N, N = 50)$. Traces for all state variables are superimposed. (**a**) coherent state. $a = 3.6, c = 0.3$. (**b**) ordered state with two clusters. $a = 3.6, c = 0.2$. (**c**) ordered state with N/2 clusters. $a = 3.97, c = 0.3$. (**d**) desynchronized state. $a = 3.97, c = 0.125$

$$\ln\left(1 - \frac{N}{N-1}c\right) + \lambda_0(a) = 0. \tag{7.5}$$

Desynchronized state: For large a and small c values, unit dynamics are not synchronized between any pair of units. Each unit shows chaotic dynamics (Fig. 7.3d). Due to the difference between the state variables, connection weights show temporal change, which can lead to self-organization of network structure. The interaction between unit and connection dynamics will be discussed later in detail.

Clustered state: For intermediate values of a and c, units spontaneously form clusters, within which units oscillate synchronously. The dynamics of the units are either periodic or chaotic, depending on the value of a (Fig. 7.3b, c). The con-

nection weights between the units in the same cluster do not vary in time, while the connection between units in different clusters can have temporal change. The number of the clusters is 2 near the boundary with the synchronized state region. As a gets larger or c gets smaller, the number increases to reach the maximum number $N/2$ at the boundary against the desynchronized state. As mentioned above, in an $N/2$-cluster state, every unit forms a pair and the two units in a pair synchronize to each other. The stability of the $N/2$-cluster state can be evaluated again with the split exponent according to the following argument. Due to the increase in connection strength between the units forming a pair (and the normalization of incoming connections), the connection between the units in different pairs vanishes. In this state, a unit in a pair interacts only with its partner and therefore the system can be regarded as a collection of GCM of 2 units. Hence, the estimation of the stability of this state is reduced to that of a small GCM system. The split exponent of GCM of 2 units is obtained by substituting 2 to N in Eq. (7.4), resulting in $\lambda_{\rm spl}(a, c) = \ln(1 - 2c) + \lambda_0(a)$. Thus, the boundary between the region of the $N/2$-cluster state and that of the desynchronized state is given by:

$$\ln(1 - 2c) + \lambda_0(a) = 0. \tag{7.6}$$

According to Eqs. (7.5) and (7.6), we define in the (a, c)-space the following three phases, named after those in GCM system [25]: (I) *coherent phase*, which is above Eq. (7.5), (II) *ordered phase*, which is between Eqs. (7.5) and (7.6), and (III) *desynchronized phase*, which is below Eq. (7.6).

7.2.3 Connection Dynamics

We proceed to study connection dynamics, which are largely influenced by the unit dynamics discussed above. It is intuitively expected that connection weights would be kept constant in the coherent and ordered phases and that they would show active dynamics in the desynchronized phase. To confirm this in a quantitative manner, we define a measure of the network activity, which represents the intensity of temporal change in connection weights, as follows:

$$A = \frac{1}{(N-1)^2} \sum_{i \neq j} \langle |w_n^{ij} - w_{n-1}^{ij}| \rangle, \tag{7.7}$$

where $\langle \cdot \rangle$ stands for temporal average taken after an appropriate transient period. This is the connection change in one time step averaged over time and over connections. Figure 7.4(top) is the plot of A against the parameters a and c. As expected, It can be seen that A is zero in the coherent and the ordered phases and that finite values of A are observed only within the desynchronized phase. An interesting point is that there are regions in the desynchronized phase where A takes extremely small

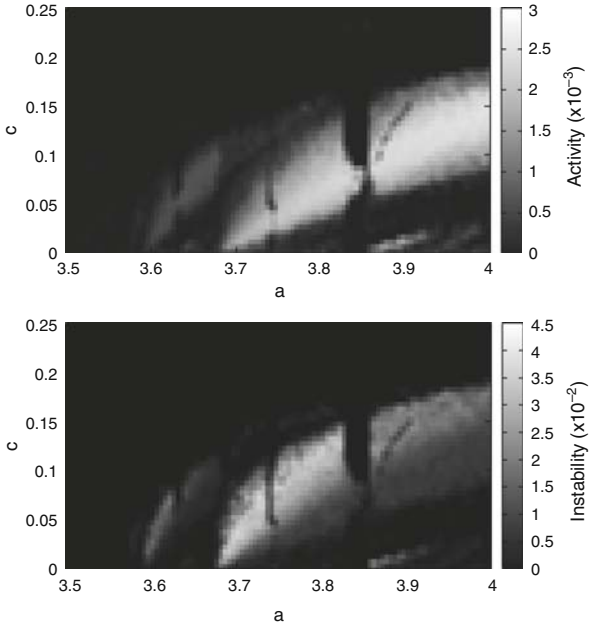

Fig. 7.4 Plot of the activity A (*top panel*) and the instability I (*bottom panel*) of the network against the parameters a and c, obtained from the numerical simulation of our model composed of 10 units. The values of A and I are calculated from w_n^{ij} values during the 1,000 steps after 100,000 steps of transient period. The network activity A represents the intensity of connection change and the network instability I represents the fragility of network structure. See the main text for their definitions

values, and that the region of large A values forms a complex structure in (a,c)-space.

Vanishing values of A reflect diminishing connection change, which means the appearance of long-lasting structure in the network. From Fig. 7.4(top), it is expected that such network structures are present in the coherent and the ordered phases, and also in a part of the desynchronized phase where A shows extremely small values. On the other hand, large values of A reflect active connection dynamics. Under such situation, it seems impossible for a stable structure to survive in the network. However, there is a possibility that the change in connection weights is due to fluctuations around some fixed values, which are kept stable over time. In such a case, the network activity A takes a non-zero value but some stable structure is preserved in the network. To check for this possibility, we define a measure for the instability of network structure using the temporal variance of connection weight around its mean as follows:

$$I = \frac{1}{(N-1)^2} \sum_{i \neq j} \left(\langle {w_n^{ij}}^2 \rangle - \langle w_n^{ij} \rangle^2 \right), \tag{7.8}$$

where $\langle \cdot \rangle$ is the temporal average as in Eq. (7.7). Large I values reflect that connection weights have large fluctuations and are not fixed in time so that the network structure is unstable. Figure 7.4(bottom) is the plot of I against the parameters a and c. By definition, $I = 0$ in the area where $A = 0$, which corresponds to the trivial fact that if there is no connection change, network structure is maximally stable. An

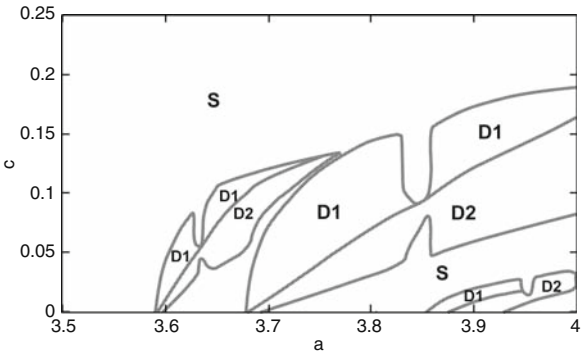

Fig. 7.5 A rough phase diagram illustrating the regions in the desynchronized phase. Letters in the panel stand for static region (S), where static networks are observed, dynamic region I (D1), where dynamic and unstable networks are observed, and dynamic region II (D2), where dynamic and stable networks are observed. See the main text for the definition of the regions

interesting observation is that the high activity region in Fig. 7.4(top) seems to be separated into two subregions; one with large I values and the other with moderate, namely ~ 0.01, I values. For example, at $a = 3.8$, the intervals $0.03 < c < 0.07$ and $0.07 < c < 0.13$ seem to belong to the moderate I and the large I subregions, respectively. This implies the possibility that dynamic but structured networks are allowed to exist in certain parts of the desynchronized phase.

Based on these observations, we separate the desynchronized phase into three regions (Fig. 7.5): (i) static region, characterized by extremely small A values, (ii) dynamic region I, characterized by large A values and large I values, and (iii) dynamic region II, characterized by large A values and moderate I values.

7.2.4 Network Structure

As mentioned above, in the beginning of the numerical simulations, connection in the network is uniform and all-to-all. From this initial condition, the system develops to various kinds of structured network, depending on the type of unit dynamics. Here we run through the phases and the regions and see what type of network structure is formed in each of the phases (regions) by examining the connection matrix w^{ij}.

(I) *Coherent phase*: A snapshot of the connection matrix in this phase is shown in Fig. 7.6a. In this phase, all-to-all connection is preserved as in the initial state. Connection weights are, however, distributed around the initial values due to the connection change during the transient to the asymptotic state, i.e., synchrony among all the units. Once the synchronization is achieved, no further connection change occurs.

(II) *Ordered phase*: Snapshots of the connection matrix in this phase are shown in Fig. 7.6b, c. In this phase, network structure depends on the clustering of units. Once the clusters are formed, connections within a cluster are strengthened and ones across clusters are weakened, resulting in vanishing connection weights between clusters. In the case of a 2-cluster state, the network separates into two almost independent sub-networks, within which units are connected in all-to-all fashion

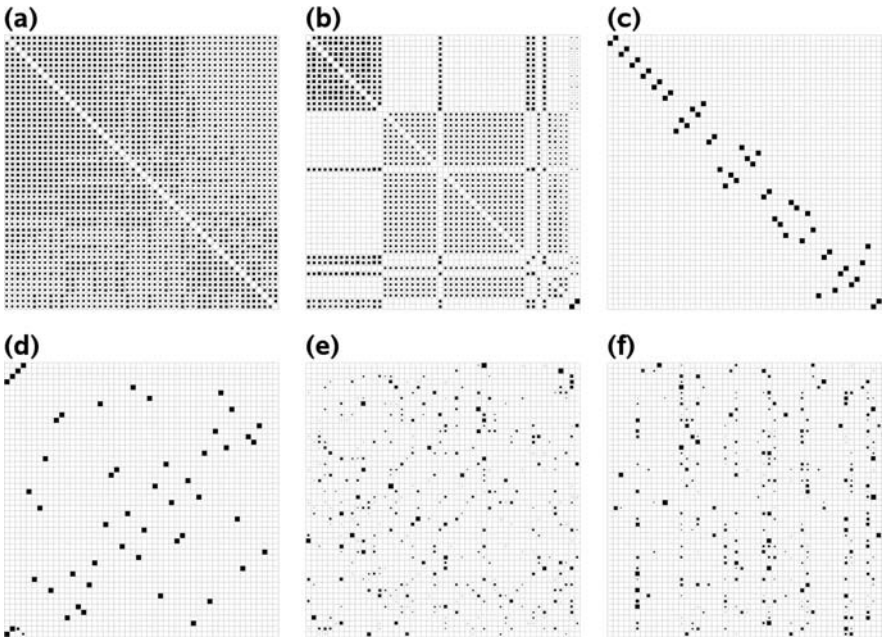

Fig. 7.6 Snapshots of the connection matrix w^{ij} in different phases/regions. The value of w^{ij} is indicated by the size of the filled square at the i-th row and the j-th column. (**a**) Coherent phase. $a = 3.6, c = 0.3$. (**b**) Ordered state with two clusters. $a = 3.6, c = 0.2$. (**c**) Ordered state with N/2 clusters. $a = 3.97, c = 0.3$. (**d**) Static region in desynchronized state. $a = 3.97, c = 0.2$ (**e**) Dynamic region I in desynchronized state. $a = 3.97, c = 0.15$. (**f**) Dynamic region II in desynchronized state. $a = 3.97, c = 0.125$

(Fig. 7.6b). As mentioned above, the maximum number of clusters is $N/2$. In an $N/2$-cluster state, units form pairs and have connections only within the pairs (Fig. 7.6c).

(III) *Desynchronized phase*: This phase is separated into three regions.

(i) *Static region*: A snapshot of the connection matrix in this region is shown in Fig. 7.6d. This region is characterized by low network activity A. In this region, most units make pairs and each unit is connected only with its partner. Although their connection strengths hardly change over time, decomposition and recomposition of pairs occasionally occurs. Besides those units forming pairs, a few units that do not form pairs remain. Their connection weights show rapid changes over time. The dynamics of units forming a pair are not synchronized, but highly correlated, while there is almost no correlation between units that belong to different pairs.

(ii) *Dynamic region I*: A snapshot of the connection matrix in this region is shown in Fig. 7.6e. This region is characterized by high network activity A and high structural instability I. There is no synchronization between any two units, and the correlation between units is very weak for any pair of units. Due to these disordered unit dynamics, connection weights change intensely, and the network structure seems to be random.

(iii) *Dynamic region II*: A snapshot of the connection matrix in this region is shown in Fig. 7.6f. This region is characterized by high network activity A and moderate structural instability I. Similarly to the dynamic region I, there is neither synchronization nor a significant correlation between any two units. Here the network seems to possess a certain structure which is characterized by the concentration of outgoing connection weights to a small fraction of units, although the connection weights change as intensely as in dynamic region I.

In the rest of this section, we focus on the dynamic networks observed in the desynchronized phase and study their structure and dynamics in detail.

7.2.5 Dynamic Networks in the Desynchronized Phase

In this part, we focus on the networks observed in dynamic regions I and II, and study the difference between the two networks in both structural and dynamical aspects. Here, we use the parameter values $(a, c) = (3.97, 0.15)$ for dynamic region I and $(a, c) = (3.97, 0.125)$ for dynamic region II.

7.2.5.1 Network Structure and Its Stability

To compare the structural properties of the networks in a quantitative manner, we characterize their structure from the values of w^{ij}. First, we look at the distribution of w^{ij} values. Figure 7.7a shows the distributions calculated for the networks from dynamic region I and II. Though larger values are observed slightly more often in dynamic region II, the distribution of w_{ij} values has quite similar shape in both of the regions, meaning that the apparent difference in the network structure seen in Fig. 7.6d, f is not due to the difference in the connection weights but based solely on

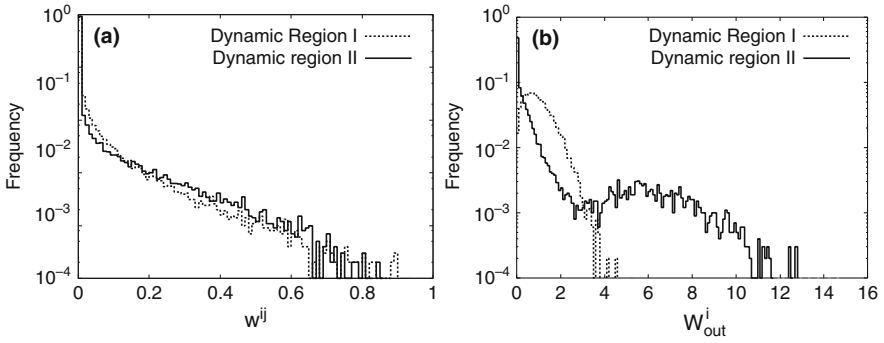

Fig. 7.7 Distributions of the values of connection matrix w^{ij} and those of the total weight of outgoing connection weights ${W_{\text{out}}}^i$ in dynamic region I and II. (**a**) Distribution of w^{ij} in dynamic region I and II. Values of w^{ij} at the 500,000th step are collected from 10 simulations. (**b**) Distribution of ${W_{\text{out}}}^i$ in dynamic region I and II. Values of ${W_{\text{out}}}^i$ at the 500,000th step are collected from 100 simulations

the manner in which they connect the units. Next, to assess how the distribution of the connections differs across units, we look at the distribution of the sum of outgoing connection weights $W_{\text{out}}{}_n^i = \sum_j w_n^{ji}$. Figure 7.7b shows the distribution of $W_{\text{out}}{}^i$ values for the networks from dynamic region I and II. The distributions are clearly different. In dynamic region I, the distribution is unimodal with the peak at around 0.7 and shows exponential (or even faster) decay for large values. In dynamic region II, there are two peaks in the distribution: the main peak is at 0 and the distribution shows exponential (or slower) decay, while the other peak is at around 6, suggesting the existence of a small group of units that have very large $W_{\text{out}}{}^i$ values.

As these distributions are calculated from the instantaneous values of w^{ij}, they tell us nothing about how the network changes its structure in time. To illustrate the temporal evolution of network structure, time series of $W_{\text{out}}{}^i$ for the network in dynamic region II is plotted for all i in Fig. 7.8. In this plot, units are separated into two groups according to the $W_{\text{out}}{}^i$ value at the 10^7th step: units that have $W_{\text{out}}{}^i$ values larger than 2 are plotted in gray, and the others are plotted in black. By retrospectively tracing the $W_{\text{out}}{}^i$ values of each of the groups, it is confirmed that the separation of units into the two groups is already evident at a very early stage of the temporal evolution, namely at the 2.0×10^6th step or even earlier. The moderate value of the network instability I in dynamic region II reflects this stable separation of units into large and small $W_{\text{out}}{}^i$ groups.

To assess this separation in a quantitative manner, we define an autocorrelation function regarding the separation of units in the following way. First, as a preparation step, we define a membership function μ as follows:

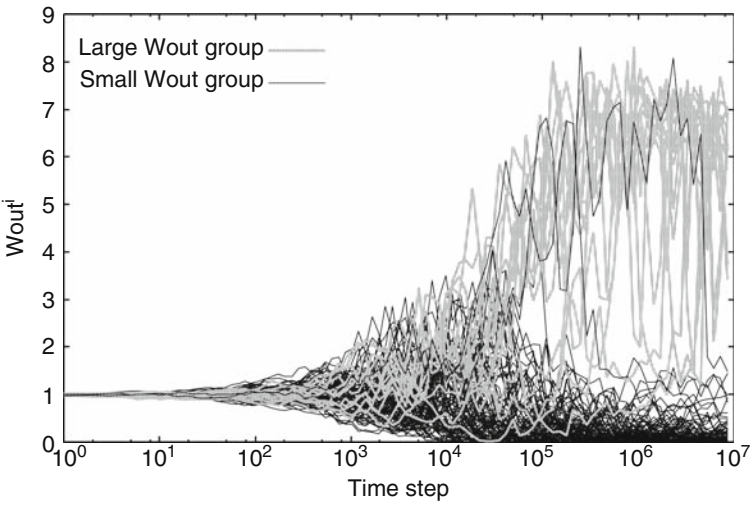

Fig. 7.8 Temporal evolution of $W_{\text{out}}{}^i$ in a network observed in dynamic region II. The values of $W_{\text{out}}{}^i$ at each 10^4 steps are plotted. Traces for all units are superimposed. The colors indicate the value of $W_{\text{out}}{}^i$ at the 10^7th step: units with a $W_{\text{out}}{}^i$ value larger than 2 are plotted in *gray*, and the others in *black*. $N = 100$

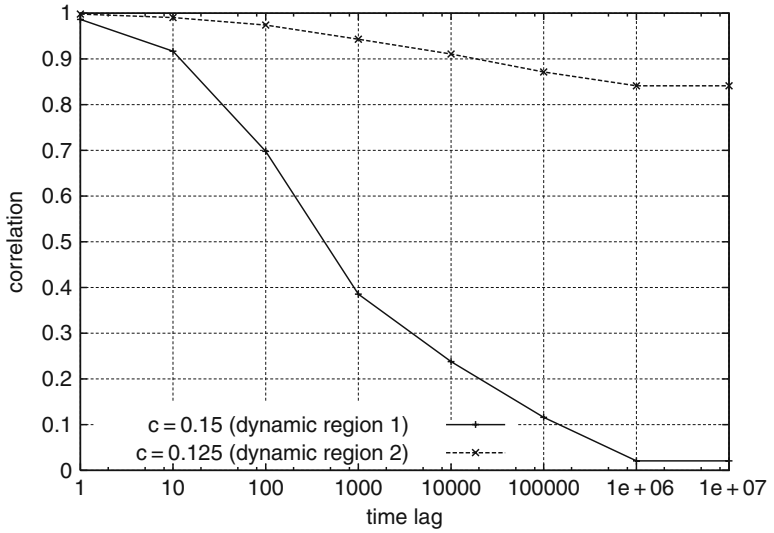

Fig. 7.9 The temporal autocorrelation $C_{\text{sep}}(\tau_l)$ regarding the separation of units, plotted for different values of τ_l. See the main text for the definition of $C_{\text{sep}}(\tau_l)$

$$\mu({W_{\text{out}}}^i) = \begin{cases} 1 & ({W_{\text{out}}}^i \geq 1.0) \\ -1 & ({W_{\text{out}}}^i < 1.0) \end{cases} \tag{7.9}$$

This function indicates whether unit i belongs to the large or small ${W_{\text{out}}}^i$ group. The threshold value 1.0 used here is the average of the total outgoing connection weight of a unit. With this function, we define the temporal autocorrelation C_{sep} regarding the separation as follows:

$$C_{\text{sep}}(\tau_l) = \frac{1}{N} \sum_i \langle \mu({W_{\text{out}}}_n^i) \mu({W_{\text{out}}}_{n+\tau_l}^i) \rangle, \tag{7.10}$$

where $\langle \cdot \rangle$ is the temporal average as in Eq. (7.7). We measure the stability of the separation by computing the decay of C_{sep} with the increase of τ_l. A plot of C_{sep} for different values of τ_l is shown in Fig. 7.9. In dynamic region II, the correlation decays very slowly and remains as large as 0.84 even for a lag of 10^7 steps, while in dynamic region I, the correlation decays to almost zero within 10^6 steps. This shows that the separation of the units into the high and low ${W_{\text{out}}}^i$ groups is highly stable in dynamic region II, while the separation is unstable, or never appears, in dynamic region I.

7.2.5.2 Mechanism of Structure Formation

In this section, we study the relationship between unit dynamics and the change in network structure to reveal the mechanism of the structure formation.

In the dynamic regions, each unit is connected to many other units in a complex manner. To gain an intuition about how the units interact with each other during the course of structure formation, we examine the dynamics of the correlations between a given unit and the others, by calculating the correlations during a short time period, namely ten steps, and observing their temporal evolution.

In Fig. 7.10 (bottom), the time series of x^1 in a simulation of a network in dynamic region I and the correlations between x^1 and the other x^is are shown. The temporal dynamics of the correlations have the following characteristics: (1) strong positive or negative correlation lasts for a certain number of steps, followed by a short period with weak correlation; (2) after this period, the sign of the correlation reverses in most cases. The unit dynamics in dynamic region II also show the same characteristics, though the interval between the succeeding weak correlation periods is much longer than in dynamic region I.

The period of weak correlation sometimes appears simultaneously for all units. Note that this simultaneous appearance of the weak correlation period coincides with the approach of x^1 to the unstable fixed point ($x = 0.748\ldots$), which is typically accompanied by a reduced oscillation amplitude (Fig. 7.10 (top)). The dynamics of the logistic map here is dominated by the oscillation around the unstable fixed point: the state variables take values larger or smaller than this fixed point alternately. According to the phase of this oscillation, units are naturally separated

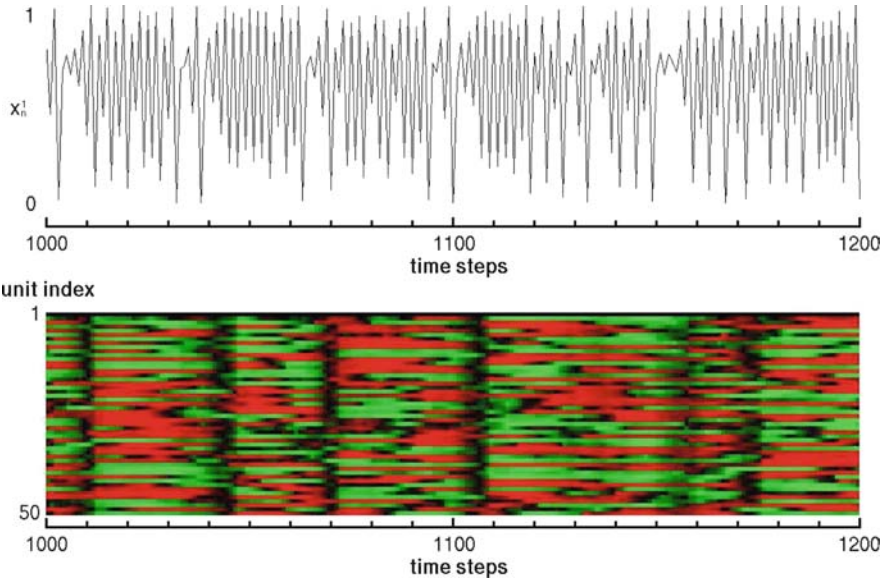

Fig. 7.10 Time series of x^1 in a simulation (*top*) and temporal evolution of the instantaneous correlations (for 10 steps) between unit 1 and the others (*bottom*), obtained from a simulation of the network in dynamic region I. The correlations are plotted in a color scale, where *green or red* represents positive or negative correlation, respectively, and the brightness of the colors indicates the magnitude of correlation

into two groups: when the units of one group take large values, the others take small values, and vice versa. This separation is not fixed over time. Indeed, each unit sometimes fails to jump over the fixed point, which reverses the phase of the oscillation. As a unit moves across the groups, the sign of the correlations to the other units changes at once, because the phase relationships to the other units are flipped to the opposite simultaneously. The periods with weak correlation seen in Fig. 7.10 correspond to the occurrences of this movement of units from one group to the other. We call this motion across the groups trans-group hopping (TGH). TGH is closely related to the temporal change in correlations between units. Hence, the dynamics of TGH are expected to have a strong influence on the formation of network structures.

To uncover the interaction between the dynamics of TGH and structure formation in the network, we study how the interval between two succeeding TGHs is related to the process of the network structure formation. The TGH interval is measured with the following method. After a transient period of τ_f steps, we fix the connection weights and only allow for the evolution of the state variables. Then we measure the TGH intervals for a certain time period and compute the average interval, separately for each of the units. In this way we estimate the expected TGH interval at an arbitrary stage in the process of the structure formation.

In Fig. 7.11, we plot the average TGH intervals of units against ${W_{\text{out}}}^i$ for several different values of τ_f, i.e., at several different stages of network structure formation. Initially, TGH intervals are almost same for all units (Fig. 7.11a). Then, the intervals

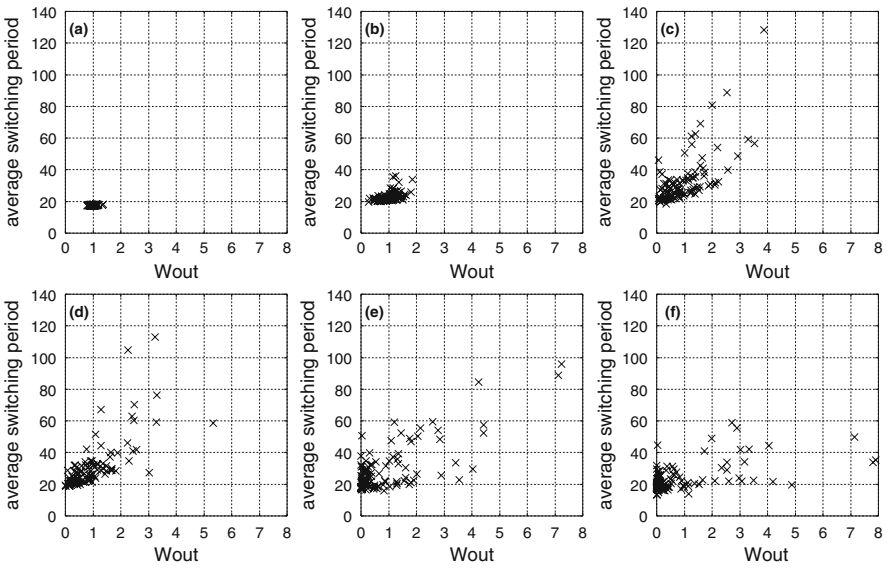

Fig. 7.11 Average TGH interval of units plotted against ${W_{\text{out}}}^i$ values. The intervals are calculated with connection weights fixed after τ_f steps of connection dynamics. (**a**) $\tau_f = 100$. (**b**) $\tau_f = 1,000$. (**c**) $\tau_f = 5,000$. (**d**) $\tau_f = 10,000$. (**e**) $\tau_f = 50,000$. (**f**) $\tau_f = 100,000$

become diverse among units (Figs. 7.11b–d). During these stages, TGH intervals are positively correlated to ${W_{\text{out}}}^i$, meaning that a unit with a larger ${W_{\text{out}}}^i$ value has a long TGH interval. Finally, at later stages, the correlation between TGH interval and ${W_{\text{out}}}^i$ gets weaker (Figs. 7.11e, f), but the separation of units into the large and small ${W_{\text{out}}}^i$ groups remains. This observation tells us that during the process of network structure formation, variety in the values of ${W_{\text{out}}}^i$ among units is positively reflected in TGH interval of the units: a unit with a large ${W_{\text{out}}}^i$ value has a long TGH interval (or a low TGH rate).

Next, we consider the opposite relationship, i.e., the influence of unit dynamics on the formation of the network structure. Here we study how the TGH interval is related to the correlation between units, which is directly reflected in the strengthening or weakening of connections. We measure the average correlation C^i of unit i to all the other units, defined as follows:

$$C^i = \frac{1}{N-1} \sum_{j \neq i} \frac{|\langle x_n^i x_n^j \rangle - \langle x_n^i \rangle \langle x_n^j \rangle|}{\sqrt{\langle {x_n^i}^2 \rangle - \langle x_n^i \rangle^2} \sqrt{\langle {x_n^j}^2 \rangle - \langle x_n^j \rangle^2}}. \tag{7.11}$$

In Fig. 7.12, the average correlation C^i, calculated in the network structure at the 10,000th step, is plotted against the average interval of TGH. A simple relationship can be recognized between C^i and TGH interval. A unit with a longer TGH interval has a stronger average correlation. Since C^i gives a measure of the degree of the increase in connections between unit i and the other units, this result suggests that a unit with a longer TGH interval is more likely to strengthen its connections.

Combining the influences from unit to connection dynamics and the other way around, the mechanism of network structure formation can now be understood as follows. A unit with a lower TGH rate grows its connections more rapidly than the others, and a unit with stronger outgoing connections decreases its rate of TGH. This mutual enhancement amplifies the difference in the outgoing connection weights

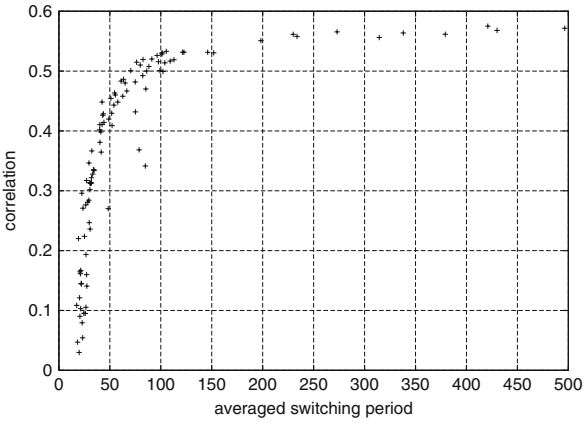

Fig. 7.12 The average correlation C^i of units plotted against the average TGH interval. The correlations are calculated with connection weights fixed after 10,000 steps of connection dynamics. See the main text for the definition of C^i

among units. The consequence of this amplification is the separation of units into the large and the small ${W_{\text{out}}}^i$ groups observed in dynamic region II.

7.3 Adaptive Network of Bursting Units

In the dynamics of the logistic map, oscillation around the unstable fixed point is dominant. Indeed, the mechanism of the network structure formation revealed in the previous section is closely related to this type of oscillatory dynamics. Hence, in order to infer the generality of such self-organization of network structure, it is necessary to check whether a similar kind of structure formation is observed in models with other unit dynamics. For this purpose, in this section, we consider a coupled-map model which is composed of circle-map units.

7.3.1 Model Formulation

The circle map, which is obtained by the discretization of a nonlinear phase oscillator, is defined as follows:

$$x_{n+1} = x_n + \omega + \frac{K}{2\pi} \sin 2\pi x_n \bmod 1, \tag{7.12}$$

where ω is the characteristic angular velocity and K represents the nonlinearity of the map. As the parameter K gets larger, this map yields more complex dynamics and finally gains the property of excitability, characterized by highly nonlinear responses to external perturbations due to the closely located stable and unstable fixed points, as shown in Fig. 7.13. Here we use the parameter values corresponding to Fig. 7.13, so that each unit is an excitable system from a stable fixed point. We

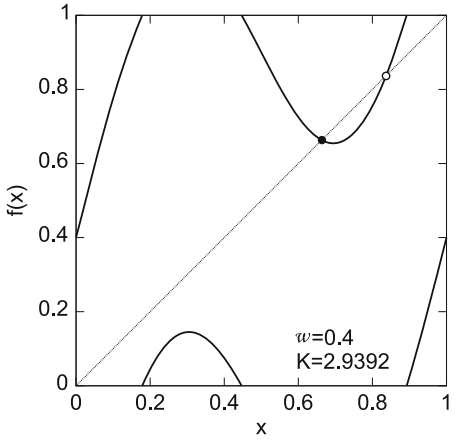

Fig. 7.13 The mapping function of the circle map. $f(x) = x + \omega + \frac{K}{2\pi} \sin 2\pi x \bmod 1$. $\omega = 0.4$, $K = 2.9392$. The *filled* and the *open circles* in the graph represent the stable and the unstable fixed points of the dynamics generated by this map

consider a network of circle-map units, defined as follows:

$$x_{n+1}^i = f(x_n^i + c \sum_{i \neq j} w_n^{ij} x_n^j) \tag{7.13}$$

where f is the mapping function of circle map, i.e., $f(x) = x + \omega + \frac{K}{2\pi} \sin 2\pi x \bmod 1$ and c represents the strength of the interaction between units as in the previous model. The dynamics of connection weights w_n^{ij} are the same as in the previous model (Eq. (7.3)).

Besides showing synchronization/desynchronization and clustering as in the previous model, this model exhibits a novel kind of collective dynamics, i.e. synchronized intermittent bursting. In this section, we focus on the structure formation related to this type of dynamics; parameter values are set to $(\omega, k, c, \delta) = (0.4, 2.9392, 0.1, 0.01)$. The initial conditions in simulations are same as in the previous section: uniform, all-to-all coupling and random state variables.

7.3.2 Unit Dynamics

As mentioned above, our model shows synchronized bursting for the parameter values we use here. Figure 7.14 (top) shows the temporal evolution of state variables around the beginning of a simulation. For most of the time, units stay near the stable fixed point, the value of which is represented by the brightest color in the gray scale. From time to time, units simultaneously show excursions from the fixed point, indicated by the simultaneous appearance of darker colors for all the units. This excursion does not last so long: most of the units return to the position near the fixed point within a few steps.

We refer to the state where most of the units stay around the fixed point as the resting state, and the state where most of the units show excursion dynamics as the bursting state. The transition between the resting and bursting states is captured by computing the dynamics of the mean of the state variables, or the mean field X_n defined as $X_n = \frac{1}{N} \sum_i x_n^i$. The time series of the mean field corresponding to the unit dynamics shown in Fig. 7.14 (top) is plotted in Fig. 7.14 (bottom). The resting state is represented by periods of almost constant mean field, while the bursting state is characterized by fluctuating mean field dynamics with a large amplitude.

This amplitude gets smaller as simulation time elapses. Figure 7.15a is the time series of the mean field during 37,000–38,000 steps. The resting and bursting states cannot be clearly distinguished as in the early stage. This seems to indicate that the bursts of units get less synchronized. However, although system-wide synchronized bursting no longer exists, synchrony within subgroups of units is still preserved. Figure 7.15b–d are the mean fields of three subgroups of units. Transition between the resting and bursting states can be observed in these mean fields, indicating synchronous bursting of units within each of the subgroups. These subgroups show

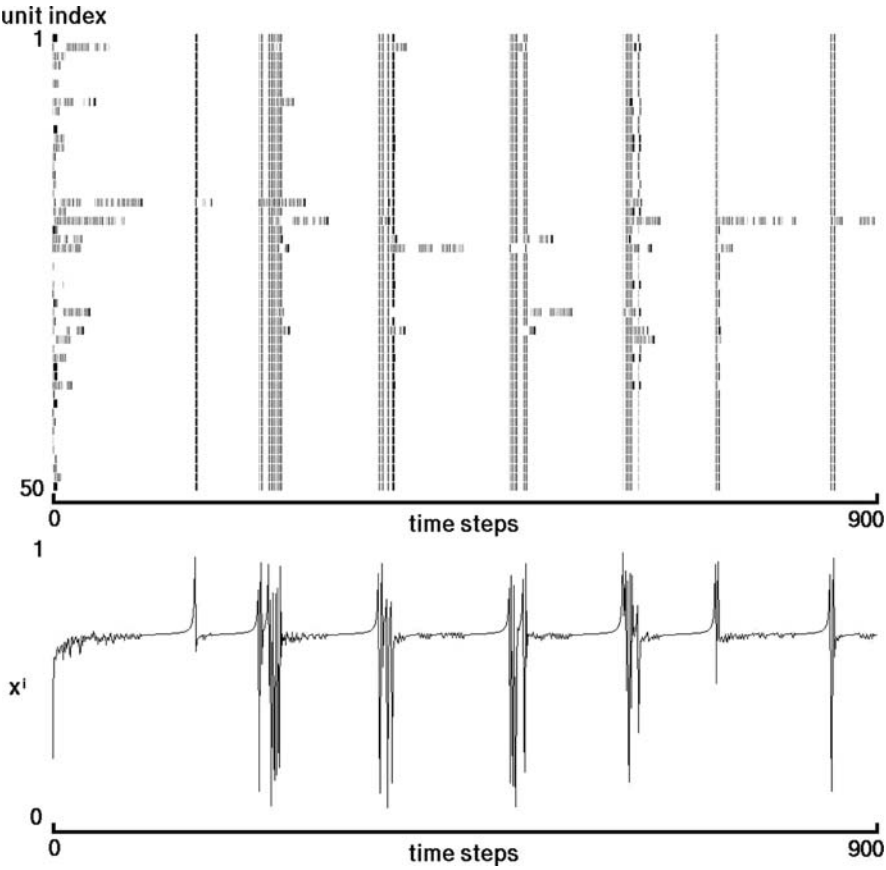

Fig. 7.14 Synchronized intermittent bursting of units in the model of coupled circle maps, observed at the beginning of a simulation. (*top*) Time series of the state variables x_n^i. Values of x_n^i are plotted in a gray scale, where the brightest color is assigned to the stable fixed point of unit dynamics. The color gets darker as x_n^i takes more distant values from the fixed point. (*bottom*) Time series of the corresponding mean field

bursting with different timings, which leads to the diminished fluctuation in the grand mean field shown in Fig. 7.15a. Such separation of units into synchronizing subgroups is achieved via the interaction between unit and connection dynamics. Indeed, the synchronized subgroups can easily be identified by looking at the connection matrix.

7.3.3 Connection Dynamics

Figure 7.16 is the connection matrix at the 37,000-th step of the simulation shown in Fig. 7.15. Units are clearly partitioned into three groups, each of which having

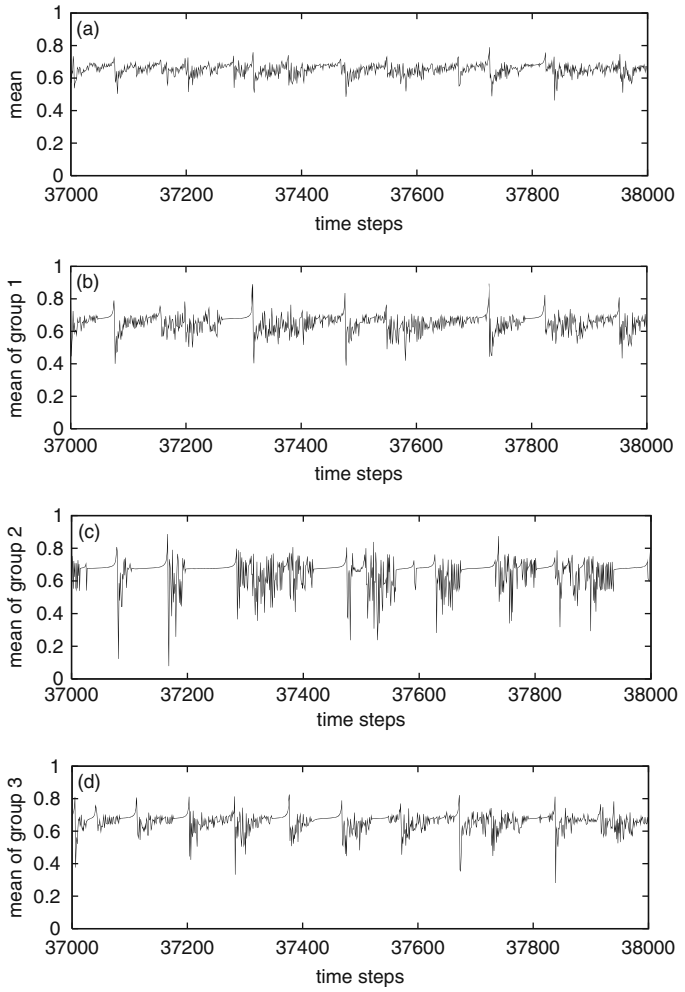

Fig. 7.15 Time series of the mean field, observed after 37,000 steps of temporal evolution. (**a**) The mean field of the whole system. (**b–d**) The mean fields of three subgroups in the system. These subgroups are identified from the connection matrix shown in Fig. 7.16. The groups shown in (**b**), (**c**) and (**d**) are the ones driven by the pacemakers 1, 2 and 3 shown in Fig. 7.16, respectively

a single unit with massive outgoing connections. We call such units pacemakers, because the synchronized bursting of the units within a group is achieved in the form that the group's pacemaker drives the other units to burst. Note that the synchronized bursting in the early time steps is mediated by uniform, all-to-all connection, meaning that the mechanism of the synchronized bursting is different in the early and the later stage of temporal evolution.

To illustrate the process of the formation of pacemakers, we plot the time series of $W_{\text{out}}{}^{i}$ values in Fig. 7.17. As mentioned above, there is no pacemaker at the

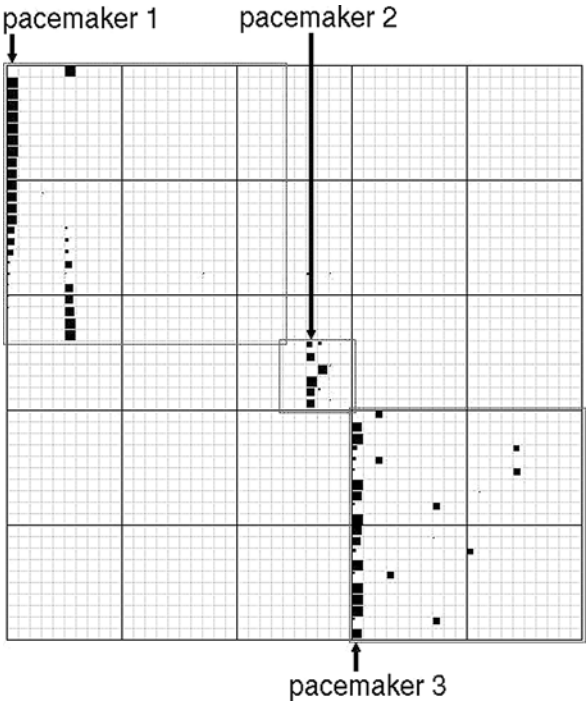

Fig. 7.16 Connection matrix at the 37,000th step of the simulation trial shown in Fig. 7.15. Pacemakers are indicated by the *arrows*. The range of the units driven by each of the pacemakers are indicated by the *square*. Note that, in the group of pacemaker 1, a new pacemaker (the 6th unit) which is still mutually coupled with pacemaker 1 is being formed

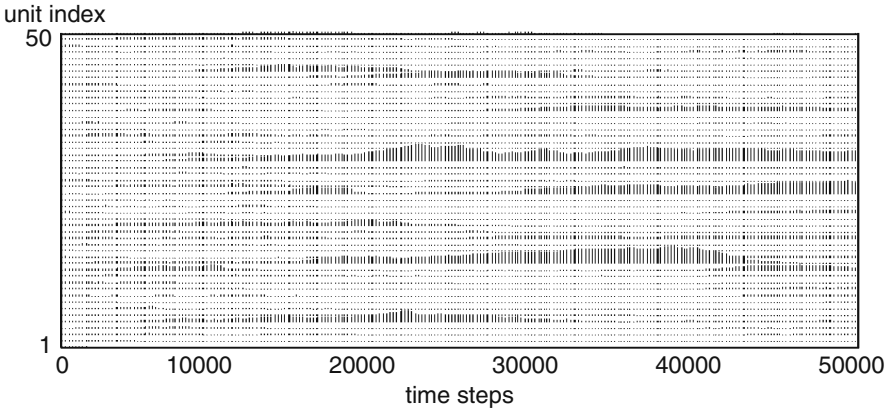

Fig. 7.17 Time series of $W_{\text{out}}{}^{i}$. The length of vertical tics represent the values of $W_{\text{out}}{}^{i}$. This is the same simulation trial as shown in Fig. 7.15

beginning of the simulation. As time elapses, the distribution of $W_{\text{out}}{}^{i}$ values starts to show a bias. By the 20,000th step of the simulation shown in Fig. 7.17, a few units have gained extremely large $W_{\text{out}}{}^{i}$ values compared to the others. These units work as the pacemakers. The separation of units into pacemakers and the rest is not stable over time. Indeed, births and deaths of pacemakers can be seen in Fig.7.17, and this process is accompanied by the reorganization of the groups of synchronously bursting units.

7.3.4 Mechanism of Structure Formation

In this model, the formation of network structure is closely related to the transition between the resting and the bursting states. Noting that connection change hardly occurs during the resting state, where all the state variables take similar values, we can focus our attention on the connection change during the bursting state. As seen in Fig. 7.14, the onset of bursts is highly synchronized among units in the early time steps. However, the timing of the burst offsets is quite diverse among units: some units take much longer time steps to return to the resting state. It is highly likely that such units rapidly lose their outgoing connection weights to most of the other units, which are already in the resting state and whose state variables have quite similar values. This can be stated in the opposite way: the units that return to the resting state earlier than the other units are likely to grow their outgoing connection weights.

Based on this consideration, the mechanism of structure formation in this model can be summarized as follows. At the beginning, all units have the same amount of outgoing connection weights. Through the temporal evolution, more and more units lose their outgoing connection weight by failing to return quickly to the resting state after each burst. This process leads to the concentration of outgoing connection weights to a small fraction of units. Such units work as pacemakers and drive the other units to burst synchronously. Once a group of synchronously bursting units is formed, the connection between the units in different groups is weakened, because they burst with different timings. Thus, groups are separated and gain a certain degree of stability.

7.4 Formation of Hierarchical Network Structure Triggered by External Input

So far, we have considered the models composed of identical units and studied how heterogeneous network structure emerges from the homogeneous condition. However, it would also be of general interest to study how externally induced heterogeneity influences the formation of network structure. Here we briefly review the study of a model where the application of external input to a part of the system triggers the self-organization of a nontrivial network structure [18].

The model is formulated as follows:

$$x_{n+1}^{i} = x_n^i + \omega + \frac{K}{2\pi}\sin 2\pi x_n^i + \frac{c}{2\pi}\sum_j w_n^{ij}\sin 2\pi x_n^j + I^i, \tag{7.14}$$

where I^i is the external input to unit i. This model is essentially same as the one in the previous section, except for the slight difference in the manner of coupling. The dynamics of connection weights w_n^{ij} are same as in the previous models (Eq. (7.3)).

For appropriate sets of parameter values (for example, (ω, K, c, δ)=(0,4.1,1.0,0.1), which is used in the simulations shown below) in the desynchronized phase, this system shows self-organization into a nontrivial network structure upon the application of a constant external input to an arbitrary unit in the system. In this study, network structure is examined after mapping the network to a graph using digitization of connections, i.e. considering only the connections having a large weight, namely larger than 1.0, and ignoring weak ones. In order to examine the network structure using the obtained graph, a proper measure that extracts a salient network structure is necessary. By examining the connection matrix, we found that the generated network structure is characterized by "layers" of nodes. Layers in the network are defined as follows: first, we define the root node, which is the only node that belongs to the first layer, and then, define the subsequent layers as the group of the units that receives direct link from a unit in the previous layer.

In Fig. 7.18, the graph of the network generated under the application of an external input to a single unit (unit 00 in the figure) is illustrated by using this digitization,

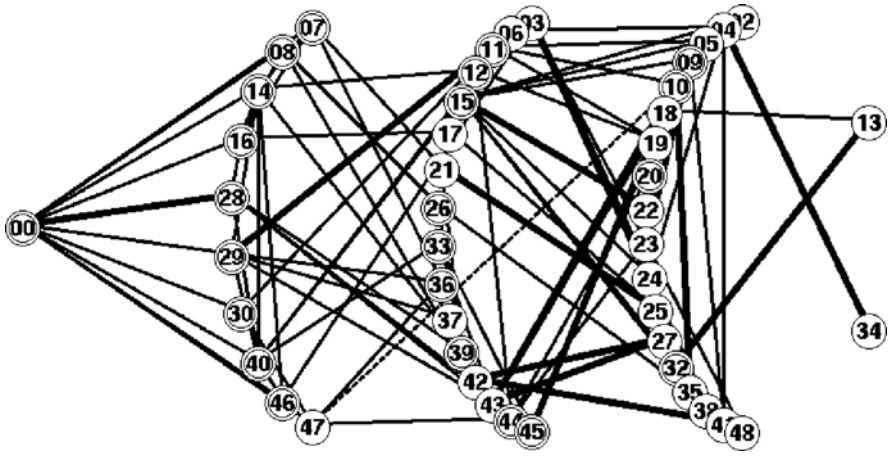

Fig. 7.18 The graph obtained from the connection matrix by digitalizing connections with a certain threshold. *Circles* represent units and the numbers inside are the unit IDs. Only unit 00 is supplied with external input, and this unit is the only constituent of the 1st layer. The arc of the units next to unit 00 is the 2nd layer, and the arc next to it is the 3rd layer, ... and so forth. The lines between *circles* are the links of the graph. *Thin lines* are the links directed from left to right and *thick lines* are bidirectional links. *Dashed lines* represent NLSC, i.e., the links between distant layers

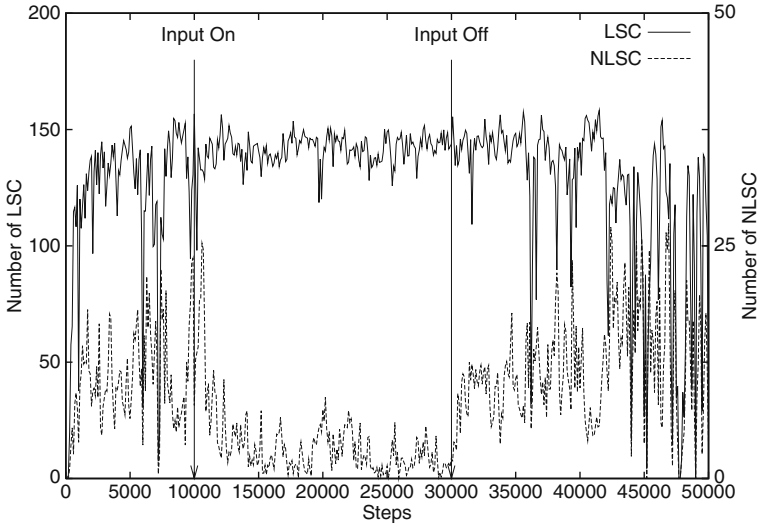

Fig. 7.19 Time series of the numbers of LSC and NLSC. The onset and the offset of external input are indicated by the arrows in the graph. See the main text for the definitions of LSC and NLSC

where layers are organized with the input unit at the root. Five layers are recognized in this case. A surprising finding about the networks self-organized in this model is that the most of connections are between neighbouring layers or within a layer, and that only little fraction of connections are between distant layers. Indeed, in Fig. 7.18, all the connections but one, which is drawn with dashed line, are between neighbouring layers or within a layer.

Here, we denote the connections between neighbouring layer or within a layer as layer structural connections (LSC) and the connections between distant layers as non-layer structural connections (NLSC). In Fig. 7.19, the numbers of LSC and NLSC are plotted in time. Note that the external input is applied only between 10,000th and 30,000th steps. After the application of input at 10,000th step, the number of NLSC shows a substantial decrease. Moreover, immediately after the cut-off of the input, the number of NLSC recovers to the same level as before the application of the input. This result clearly shows that the formation of the layered structure is dependent on the application of external input.

Some interesting dynamical properties such as a power law distribution of the lifetime of unit in a layer have been observed in this model, but the mechanism for this type of structure formation has not yet been uncovered.

7.5 Summary and Discussion

To summarize, we have introduced three types of coupled map models in order to study the self-organization of network structure in adaptive networks. First we

have shown the result of a coupled logistic-map system with Hebbian connection dynamics. In this system, we found spontaneous separation of units into two groups, one consisting of units with strong outgoing connections and the other consisting of units with weak outgoing connections. Only a small fraction of units belongs to the former group, and the rest of the units belonging to the latter are just driven by the dynamics of the former. Thus, the units with strong outgoing connections have more influence on the dynamics of the other units. In this sense, the emergence of a group of units with strong outgoing connections can be interpreted as the emergence of leadership in a population.

A similar self-organized network structure was observed in the second type of model, i.e., a coupled circle-map system. In this model, units self-organize into some synchronously bursting groups, and each group has a pacemaker unit which has strong outgoing connections and drives the dynamics of the other units. Though this model shows quite different unit dynamics from the logistic map model, its self-organized network structure is similar to that of the logistic map model in the point that only a small fraction of units attain the influential positions. This suggests that the emergence of leadership may be a general phenomenon in some class of adaptive networks.

It should be stressed that in these models all units are identical and the initial network structure is uniform, all-to-all connection. This means that the leaders emerge spontaneously from a homogeneous population, without any individual differences among units. In the third model, where external input is applied to only one unit in the system, units are not homogeneous. The self-organized structure in this system is more complex than in the other models: units self-organize into a hierarchical structure, where the unit with external input is located at the root and the other unit form several layers with decreasing centricity from the root node. There is a rule in the connectivity between the units in different layers, i.e. connections between distant layers are avoided. Thus, application of input to only one unit causes global reorganization of connection structure. This might be regarded as another example of the emergence of a leader which has strong influence on the behavior of the whole system.

We studied the mechanism of structure formation for the first model in detail, and extracted the steps of the process. First, variability among units is created by unit dynamics (the variability in the TGH interval is created by the chaotic dynamics). Then, in the next step, this variability is imprinted in connection weights (there is a simple relationship between TGH interval and the average correlation of units, which is directly reflected in the connection change). Finally, the connection structure influences the unit dynamics (we confirmed that units with strong outgoing connections have long TGH interval, resulting in the amplification of the variability in TGH interval). Thus, a closed loop of the interaction between unit dynamics and connection changes is formed. This results in a stable growth of network structure.

Such a feedback process is not properly at work in the second model, which might be the reason for the weaker stability of the structure in this model. There, the timing of returning to the resting state after bursts is distributed, and this variation is reflected in the outgoing connection strength. Up to here, the process is quite

similar to that in the first model. However, the last step is missing in the second model, and hence the feedback loop is not closed. If there were a process that makes pacemakers return quickly to the resting state, the network structure in this model should be stable. Instead, this model has a process such that a stronger outgoing connection enhances the burst synchrony within a group, which only weakens the connections between units in different groups.

We expect that the mechanism of the structure formation we have found here is rather general in adaptive networks with mutual feedback between chaotic dynamics and coupling with Hebbian-type dynamics. These three steps for the structure formation clarified above will be discovered in other class of models of adaptive networks where the emergence of leadership (or strong heterogeneity) is observed, or, conversely, it will be possible to design a system to form leaders spontaneously from a homogeneous population by implementing these three steps in the system's dynamics.

Acknowledgements The authors thank Dr. Abigail Morrison for her careful reading of the manuscript.

References

1. R. Albert and A. -L. Barabási, Rev. Mod. Phys. **74**, 47 (2002).
2. S. N. Dorogovtsev and J. F. F. Mendes, *Evolution of Networks* (Oxford University Press, Oxford, 2003).
3. M. E. J. Newman, A. -L. Barabási and D. J. Watts, *The structure and dynamics of networks* (Princeton University Press, Princeton, 2006).
4. A. -L. Barabási and R. Albert, Science **286**, 509 (1999).
5. D. J. Watts, *Small World* (Princeton University Press, Princeton, 1999).
6. E. Almaas, B. Kovács, T. Vicsek, Z. N. Oltvai and A.-L. Barabási, Nature **427**, 839 (2004).
7. C. Furusawa and K. Kaneko, Phys. Rev. E **73**, 011912 (2006).
8. M. Barahona and L. M. Pecora, Phys. Rev. Lett. **89** 054101 (2002).
9. T. Nishikawa, A. E. Motter, Y. C. Lai, and F. C. Hoppensteadt, Phys. Rev. Lett. **91**, 014101 (2003).
10. H. Kori and A. S. Mikhailov, Phys. Rev. E **74**, 066115 (2006).
11. S. C. Manrubia and A. S. Mikhailov, Phys. Rev. E **60**, 1579 (1999).
12. J. Jost and M. P. Joy, Phys. Rev. E **65**, 016201 (2002).
13. W. L. Lu, F. M. Atay and J. Jost, Eur. Phys. J. B (2008) doi: 10.1140/epjb/e2008-00023-3.
14. F. H. Willeboordse Phys. Rev. Lett. **96**, 018702 (2006).
15. R. E. Amritkar and S. Jalan, Physica A **321**, 220 (2003).
16. J. Ito and K. Kaneko, Phys. Rev. Lett. **88**, 028701 (2002).
17. J. Ito and K. Kaneko, Phys. Rev. E **67**, 046226 (2003).
18. J. Ito and K. Kaneko, Neural Netw. **13**, 275 (2000).
19. J. Ito and T. Ohira, Phys. Rev. E **64**, 066205 (2001).
20. P. Gong and C. van Leeuwen, Europhys. Lett. **67**, 328 (2004).
21. C. S. Zhou and J. Kurths, Phys. Rev. Lett. **96**, 164102 (2006).
22. T. Gross and B Blasius, J. R. Soc. Interface **5**, 259 (2008).

23. K. Kaneko, Prog. Theor. Phys. **72**, 480 (1984).
24. K. Kaneko, Physica D **34**, 1 (1989).
25. K. Kaneko, Physica D **41**, 137 (1990).
26. K. Kaneko and I. Tsuda, *Complex Systems: Chaos and Beyond* (Springer, Berlin, 2000).
27. K. Kaneko, Physica D **75**, 55 (1994).

Chapter 8
Dynamical Optimization and Synchronization in Adaptive Complex Networks

Maoyin Chen and Jürgen Kurths

Abstract We introduce two dynamical optimization coupling mechanisms for achieving different kinds of synchronization in adaptive complex networks. At each node in the network there is an oscillator, and the ensemble of oscillators can be either identical or non-identical. For each oscillator, we adjust only one incoming link's strength in each time interval while the other incoming links' strengths remain constant. The dynamical optimization coupling mechanisms are in effect "winner-take-all" strategies. If one incoming link for each oscillator has the maximal competitive ability in different time intervals, its strength increases by a small value. This way, we realize different kinds of synchronization in adaptive complex networks with instantaneous or delayed couplings, as well as ensure that all oscillators have uniform intensities during the transition to synchronization. We also enhance the synchronizability in complex networks with identical oscillators.

8.1 Introduction

Real-world complex networks (CNs) consist of dynamical entities with an interplay between dynamical states and interaction patterns. While topological studies have revealed important organization principles in the structures [1–6], a more complete understanding would require characterizations beyond the topology. There are recently several approaches in this direction. Especially, one approach is to investigate the synchronization dynamics in oscillatory networks [7–21]. However, most of these works consider networks with fixed topology. Another approach is to study the coevolution of dynamical states and network structures [22–36]. Models of adaptive complex networks (ACNs) have been proposed, e.g., evolving of oscillators due to fitness in interacting species [10], reinforcement of connection strength [11] or rewiring of links [12] due to payoffs among agents playing games; or adaptive

M. Chen (✉)
Tsinghua National Laboratory for Information Science and Technology,
Department of Automation, Tsinghua University, Beijing 100084, P. R. China
e-mail: mychen@mail.tsinghua.edu.cn

T. Gross, H. Sayama (eds.), *Adaptive Networks,* Understanding Complex Systems,
DOI 10.1007/978-3-642-01284-6_8,

changes of coupling strength according to the state distance in globally coupled chaotic maps [13] in a desynchronized regime.

ACNs appear in many biological applications. They combine topological evolution of the network with dynamics in the network oscillators. Recently, Gross and Blasius provided a survey on adaptive coevolutionary networks [15]. According to this survey, the majority of recent studies on the dynamics of networks in general revolve around two key questions corresponding to two distinct lines of research: (i) *what are the values of important topological properties of a network that is evolving in time* and, (ii) *how does the functioning of the network depend on these properties*? The first line of research is concerned with *the dynamics of networks* [15]. Here the topology of the network itself is regarded as a dynamical system. It changes in time according to specific, often local, rules. Investigations in this area have revealed that certain evolution rules give rise to peculiar network topologies with special properties. The second major line of network research focuses on *the dynamics on networks* [15]. Here each oscillator of the network represents a dynamical system. The individual systems are coupled according to the network topology. Thus, the topology of the network remains static, while the states of the oscillators change dynamically. Important processes that are studied within this framework include synchronization of the individual dynamical systems [7–21, 26, 28–36], and contact processes, such as opinion formation and epidemic spreading [37–39].

As a typical dynamical process on networks, synchronization, especially the ability of networks to obtain synchronization (synchronizability), attracts lots of attention [8–16, 18–21, 26, 28–36]. Complete synchronization (CS) in networks of identical oscillators [30–33] and phase synchronization (PS) in networks of non-identical oscillators [28, 29] can be ensured by introducing adaptive local couplings between connected oscillators, or adaptive global couplings in the entire networks. Since these networks combine local dynamics and topological evolution, they can be considered as ACNs. Based on the local dynamical neighborhood information in networks with identical oscillators, Zhou and Kurths introduced an adaptive coupling scheme [30]. For simplicity, this method is called the Zhou–Kurths method. Consequently, the adaptive self-organization by the Zhou–Kurths method drives the network into the direction of a more homogeneous topology, ongoing with an enhanced ability for synchronization. Hence it is possible to synchronize networks that exceed by several orders of magnitude, the size of the largest comparable random graph that is still synchronisable [27].

However, there are some shortcomings in these studies on ACNs, where the local or global couplings are changed adaptively. The first one is that these works can not ensure that all oscillators have uniform intensities during the transition to synchronization. The intensity S_i for oscillator is defined by the sum of the couplings for oscillator i. From the works on synchronizability in networks with a given topology, the synchronizability becomes optimal when the intensities become uniform in networks. This can be verified by the load [18, 19] and degree [20] based weighted networks. For both weighted and unweighted networks with sufficiently random topology, the synchronizability is controlled by $S_{\max}/S_{\min}$, where $S_{\max}$ and $S_{\min}$ are the maximum and minimum of intensities S_i [15]. For scale-free (SF) networks

[15], one gets $S_{\max}/S_{\min} = k_{\max}/k_{\min} \sim N^{1/2}$, where $k_{\max}$ and $k_{\min}$ are the maximal and minimal degree, respectively. For a fixed network topology, the synchronizability can be enhanced if the intensities become more homogeneous. The second shortcoming of the approach is that these methods can not be effectively applied to networks with delayed couplings. For example, for networks with identical chaotic oscillators, the non-uniformity of intensities does not ensure the existence of a synchronous manifold in networks with delayed couplings. Further, there exists no unifying adaptive coupling scheme to get different kinds of synchronization. The scheme for PS in the Kuramoto model can not be effectively applied to PS in networks with non-identical chaotic oscillators and CS in networks with identical chaotic oscillators. The scheme for CS in networks with identical chaotic oscillators can not be effectively applied to PS in networks with non-identical oscillators.

In this chapter we develop two adaptive coupling schemes to get different kinds of synchronization in networks, as well as to ensure that all oscillators have uniform intensities during the transition to synchronization. This chapter is organized as follows. In the next section, we consider PS in the famous Kuramoto model with delayed couplings and external noises. By adaptively adjusting the couplings according to the *dynamical gradient network* (DGN) approach [29], we ensure PS in different variants of the Kuramoto model while maintaining uniform intensities. This approach can be also applied to networks with non-identical oscillators, provided that the "phase" is well-defined. Furthermore, this approach can be extended to CS in networks with identical oscillators. In Sect. 8.3, we further propose another more effective coupling mechanism, the *dynamical optimization* (DO) mechanism [35, 36], for realizing CS in networks with identical oscillators. Though there exist delayed couplings in networks, uniform intensities are maintained while CS is effectively realized. We also discuss the enhanced synchronizability in scale-free (SF) networks and small-world (SW) networks, due to the DO mechanism. This approach is also applicable to PS in networks with non-identical oscillators. In the last section we draw up our conclusion.

8.2 Phase Synchronization in the Kuramoto Model

Among the many models that have been proposed to address synchronization phenomena, one of the most successful models is the Kuramoto model [7, 40, 41]. It can be used to understand the emergence of synchronization in networks of oscillators. In particular, this model presents a second-order phase transition from incoherence to synchronization. For synchronization in the Kuramoto model, many works assumed that the couplings between connected oscillators are constant [12–14]. Recently, some works introduced adaptive couplings in this model. Maistrenko et al. introduced the mechanism of plasticity to study multistability, and assumed that the couplings are varied in accordance with the spike timing-dependent plasticity [42]. Ren and Zhao proposed continuous adaptive couplings rules that

enhance the synchronization in the Kuramoto model. In this scheme, the couplings grow stronger for pairs which have larger phase incoherence [28].

In this chapter we propose a DGN approach to achieve synchronization in the Kuramoto model with adaptive couplings. This study is motivated in part by the work [43, 44], where the concept of gradient networks is introduced. Gradient networks are directed subnetworks of an undirected "substrate" network in which each oscillator has an associated scalar potential and one outlink that points to the oscillator with the smallest (or largest) potential in the reunion of itself and its neighbors on the substrate network. The existence of gradients has been shown to play an important role in biological transport processes, such as cell migration: chemotaxis, haptotaxis, and galvanotaxis. Naturally, the same mechanism will generate flows in complex networks as well [44]. In addition, gradient networks have been already utilized to enhance synchronization in networks [11]. A general weighted asymmetrical network is regarded as a superposition of a weighted symmetrical network and a weighted gradient network. Depending on the degrees of oscillators, a weighted coupling scheme is proposed to enhance the synchronizability in networks. However, the proposed gradient network is static, i.e., its structure is time independent. Differing from the static gradient networks in [11], gradient networks developed in this section are dynamical, which implies that the gradient networks in different time intervals are different.

Here the Kuramoto model consists of a population of N coupled oscillators where the phase $\theta_i(t)$ of the i-th oscillator evolves in time according to

$$\frac{d\theta_i}{dt} = w_i + \sum_j W_{ij} A_{ij} \sin(\theta_j - \theta_i),\ i = 1, 2, \cdots, N, \tag{8.1}$$

where w_i are natural frequencies distributed with a given probability density $g(w)$, A_{ij} is the binary, and potentially asymmetric connection matrix. Further, $W_{ij} \geq 0$ is the coupling strength of the incoming link (i, j) pointing from oscillator j to oscillator i if they are connected. Let K_i be the index set of neighbors of oscillator i.

The Kuramoto model (8.1) can be solved in terms of the order parameter $r(t)$ that measures the extent of synchronization as

$$r(t)\mathrm{e}^{\zeta\Psi(t)} = \frac{1}{N}\sum_{j=1}^{N} \mathrm{e}^{\zeta\theta_j(t)}, \tag{8.2}$$

where $\zeta^2 = -1$, $\Psi(t)$ stands for an average phase, and the parameter $0 \leq r(t) \leq 1$. Obviously, if $r(t) = 1$, PS in the Kuramoto model (8.1) is realized. The parameter $r(t)$ given by Eq. (8.2) has been widely used [7, 13, 28, 40, 41].

We first introduce adaptive couplings into the Kuramoto model (8.1). In order to do so, we segment the time interval $[t_0, +\infty)$ into

$$[t_0, +\infty) = \bigcup_{n\geq 1}[t_{n-1}, t_n), \tag{8.3}$$

where $t_n = t_0 + nT$, t_0 is the transient time, T is the suitably chosen time interval. For the parameter $r(t)$, we define one local order parameter for oscillator i in the interval $[t_{n-1}, t_n)$:

$$r^{i,n} = \frac{1}{T}\int_{t_{n-1}}^{t_n} r_i(t)dt, \tag{8.4}$$

with

$$r_i(t)\mathrm{e}^{\zeta\Psi_i(t)} = \frac{1}{k_i+1}\sum_{j\in K_i\cup\{i\}}\mathrm{e}^{\zeta\theta_j(t)},$$

where k_i is the degree of oscillator i. The parameter $r^{i,n}$ can measure the local synchronization extent among oscillator i and its neighbors. If $r^{i,n_0} = 1$ for certain n_0, oscillator i and its neighbors are locally synchronized in the interval $[t_{n_0-1}, t_{n_0})$.

For the network of oscillators, the extent of synchronization is to choose the order parameter $r_0(n)$:

$$r_0(n) := \frac{1}{T}\int_{t_{n-1}}^{t_n} r(t)dt. \tag{8.5}$$

If there is a n_0 such that $r(n_0) = 1$, we conclude that synchronization in the network is realized effectively.

Now we introduce an adaptive coupling scheme into the Kuramoto model. Our idea to adjust the coupling W_{ij} in the interval $[t_n, t_{n+1})$ is based on the concept of gradient networks [43, 44]. To define a gradient network at the instant $t = t_n$, we consider a network denoted by $\Sigma = (V, E_n)$, where V stands for the set of oscillators, and E_n denotes the set of links at the instant $t = t_n$. Consider a field denoted by $h^n = \{h_1^n, \cdots, h_N^n\}$ at the instant $t = t_n$, where h_i^n is the scalar assigned to oscillator i. We define the gradient $\nabla_{h_i^n}$ of the field h_i^n in oscillator i to be the directed link $\nabla_{h_i^n} = (i, \mu_i^n)$, where $\mu_i^n \in K_i$ represents one neighbor of oscillator i. At the instant $t = t_n$, the network $\Sigma_g = (V, \nabla_n)$, where ∇_n is the set of the gradients $\nabla_{h_i^n}$, is called a gradient network. Note that at different time instants the gradient networks can be different. In this section, this kind of gradient networks is called DGNs. In the gradient network Σ_g, the directed link (i, μ_i^n) points from oscillator μ_i^n, at which the scalar field has the minimum (or maximum) value in oscillator $\mu_i^n \in K_i$, i.e. [44]

$$\mu_i^n = \arg\max_{j\in K_i}\{-h_j^n\} \tag{8.6}$$

to oscillator i. If several neighbors have the same scalar field, we choose only one randomly. For oscillator i in the Kuramoto model (8.1), we choose the scalar field h_i^n as

$$h_i^n = r^{i,n}. \tag{8.7}$$

Denote the coupling W_{ij} in the interval $[t_{n-1}, t_n)$ as W_{ij}^n. In the gradient network, we adjust the coupling $W_{i\mu_i^n}$ of the incoming link (i, μ_i^n) pointing from oscillator μ_i^n to oscillator i. In the interval $[t_n, t_{n+1})$, we adaptively adjust the coupling $W_{i\mu_i^n}$ of the incoming link (i, μ_i^n) in the gradient network $\Sigma_g = (V, \nabla_n)$ by

$$W_{i\mu_i^n}^{n+1} := W_{i\mu_i^n}^n + \varepsilon\,, \tag{8.8}$$

where $\varepsilon > 0$ is an arbitrary small incremental coupling. When the link (i, j) does not belong to the gradient network Σ_g, its coupling satisfies

$$W_{ij}^{n+1} := W_{ij}^n\,. \tag{8.9}$$

From Eqs. (8.6), (8.7), (8.8), and (8.9), the DGN approach is also a dynamical optimization coupling scheme. It reflects the "winner-take-all" strategy in the sense of scalar fields. For oscillator i, the incoming link to be adjusted is always chosen as the one pointing from one neighborhood oscillator with the minimal (or maximal) field to itself. Further, we only adjust one incoming link's strength in different time intervals while the other incoming links' strengths remain constant. Here we define the intensity S_i for oscillator i as $S_i = \sum_{j\in K_i} W_{ij} A_{ij}$. Note that the intensities of all oscillators in networks are uniform, since at each step the intensity of each oscillator increases by the same amount ε.

Now we analyze the feasibility of the above coupling scheme by the linearized dynamics of the Kuramoto model (8.1). When the Kuramoto dynamics is close to the attractor, the phase differences are small, and then the sine coupling function can be approximated linearly. Therefore, in the interval $[t_n, t_{n+1})$, the linearized dynamics of oscillator i can be written in the form

$$\tfrac{d\theta_i}{dt} = \sum_j W_{ij}^n A_{ij}(\theta_j - \theta_i) + \varepsilon(\theta_{\mu_i^n} - \theta_i)\,. \tag{8.10}$$

In the above equation the last term $\varepsilon(\theta_{\mu_i^n} - \theta_i)$ is equivalent to the term $-\varepsilon(\theta_i - \theta_{\mu_i^n})$, which can be regarded as a negative feedback term for the unidirectional synchronization from oscillator μ_i^n to oscillator i. This decreases the phase difference between oscillator i and its neighbor μ_i^n and can therefore lead to synchronization.

The adaptive scheme (8.6), (8.7), (8.8), and (8.9) can be easily extended to Kuramoto models with delayed couplings and external noise. One case is the Kuramoto model described by [12, 41]

$$\frac{d\theta_i}{dt} = w_i + \sum_j W_{ij} A_{ij} \sin(\theta_j - \theta_i) + \xi_i(t),\ i = 1, 2, \cdots, N, \tag{8.11}$$

where $\xi_i(t)$ is white noise due to some complicated environment with expectation and variance

$$< \xi_i(t) >= 0,\ < \xi_i(t)\xi_j(t') >= 2\delta_{ij}\delta(t - t').$$

Another case is the Kuramoto model given by [41]

$$\frac{d\theta_i}{dt} = w_i + \sum_j W_{ij} A_{ij} \sin(\theta_{j,\tau} - \theta_i) + \xi_i(t),\ i = 1, 2, \cdots, N, \tag{8.12}$$

where the term $\theta_{j,\tau}$ represents the delayed phase $\theta_j(t - \tau)$, and τ is a constant time delay.

Our simulations are based on SF and SW networks. SF networks are generated by the Barabási-Albert model [2], where the initial network is a fully connected network with M oscillators, labeled by $i = 1, \cdots, M$. A new oscillator is iteratively added to be connected to M existing oscillators. The probability that a new oscillator is connected to oscillator i depends on the degree k_i of oscillator i, namely $\Pi_i = k_i / \sum_j k_j$. After repeating for $N - M$ times, a SF network has a degree distribution $P(k) \sim k^{-3}$ and the minimal degree $k_{\min} = M$. SW networks are generated by the Newman-Watts model [45]. The initial network is a $K-$nearest-neighbor coupled network consisting of N oscillators arranged in a ring, with each oscillator i being adjacent to its neighbor oscillators $i \pm 1, \cdots, i \pm K/2$, and with K being even. Then one adds with probability p a connection between a pair of oscillators.

In our simulations in this section, the initial couplings for all incoming links for each oscillator are zero, the natural frequencies of the oscillators are uniformly distributed in the interval $[-1, 1]$, the transient time is $t_0 = 100\,\text{s}$, the length of intervals is $T = 1\,\text{s}$, and the incremental coupling is $\varepsilon = 0.01$. The solution of networks is resolved using the Euler method and the step time $h = 0.02\,\text{s}$, and the ending condition for our scheme is $|r(n_0) - 1| < 10^{-2}$ for certain n_0.

We first simulate SF networks with $N = 1{,}000$ and SW networks with $N = 1{,}000$ and $p = 0.03$ in the absence of noise. We plot the local order parameter r_0 as a function of the adjustment time n (Fig. 8.1a), and the global order parameter r as a function of the step m $(= n/h)$ for solving the Kuramoto model (Fig. 8.1b). Obviously, due to our coupling scheme (8.8) and (8.9), the Kuramoto model (8.1) reaches a synchronized regime after several hundreds of adjustment steps. In every time interval, only one incoming link's coupling for each oscillator is adjusted by the same small incremental coupling, and the other incoming links' couplings remain constant. Hence the intensities S_i for all oscillators are identical during the transition to synchronization. From Fig. 8.1a, b, the extent of synchronization in the Kuramoto model increases with increasing of the intensity S given by $S = S_i = n\varepsilon$. In our coupling scheme, the intensity S is a good indicator for synchronization in

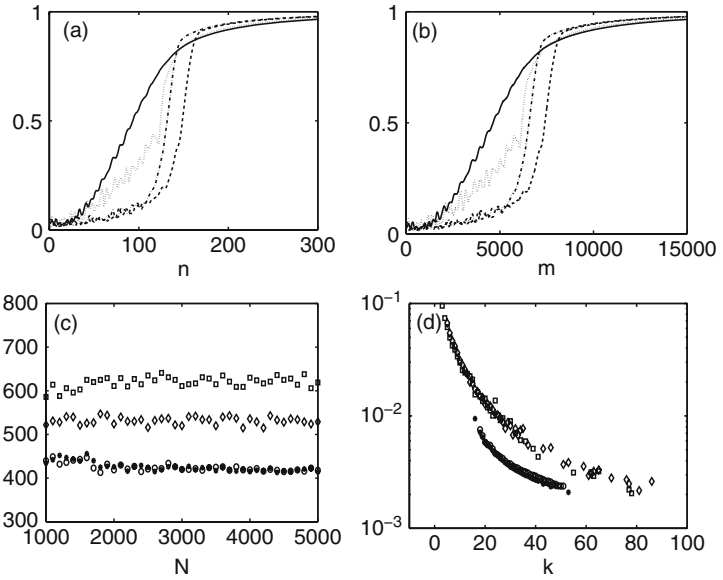

Fig. 8.1 Simulation results in the Kuramoto model (8.1) without noise. The parameter $r_0(n)$ as a function of the adjustment step n (**a**), and the parameter $r(t)$ as a function of the step m for solving the Kuramoto models (**b**), in SF networks (*solid line*: $M = 3$; *dotted line*: $M = 5$) and SW networks (*dashdot line*: $K = 2$, $p = 0.03$; *dashed line*: $K = 4$, $p = 0.03$). The adjustment step n as a function of the size N in networks (**c**), and standard deviation $E_{\text{av}}(k)$ as a function of degree k in SF and SW networks with $N = 1{,}000$ (*square*: $M = 3$; *diamond*: $M = 5$; *star*: $K = 2$, $p = 0.03$; *circle*: $K = 4$, $p = 0.03$). All estimates are the results of averaging over 50 realizations

the Kuramoto model. At about $n = 300$, namely $S = 3$, the Kuramoto model (8.1) is practically in a synchronized state. However, equal intensities cannot be ensured by other known adaptive coupling schemes [28, 30]. The intensities in [30] strongly depend on heterogeneous degrees in SF networks. The larger the degree of an oscillator is, the larger its intensity is.

We also discuss the synchronization in SF and SW networks with different size. Under the same ending condition, we observe that the adjustment steps needed to synchronize SF networks with the same M are almost identical (Fig. 8.1c). It further means that the time $(n_0 T)$ needed to synchronize SF networks with the same M is almost equal. We also obtain similar results in SW networks with the same K and p. The steps in SW networks with the same p and a small K are almost identical while the steps in SF networks with different M are also different. This can be in part explained by the average degree $< k > \approx 2M$ in SF networks and $< k > \approx K + (N-1)p/2$ in SW networks. When the average degree of networks is smaller, it requires a longer time to synchronize networks.

After the ending of our scheme (8.8) and (8.9), we also analyze the relationship between the normalized coupling matrix $G = (G_{ij})$ with $G_{ij} = W_{ij}^{n_0} A_{ij}/n_0\varepsilon$ and the coupling matrix $G_0 = (W'_{ij} A_{ij})$ with $W'_{ij} = 1/k_i$. We compute the average error

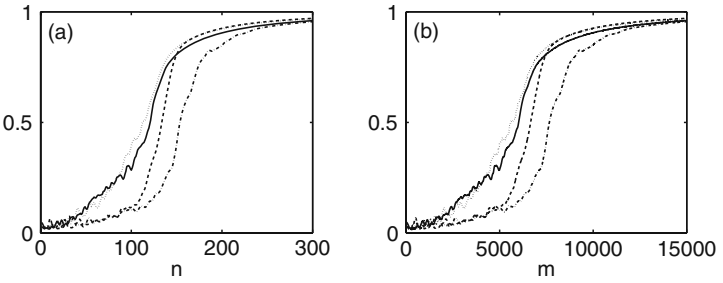

Fig. 8.2 Simulation results in the Kuramoto model (8.1) with noise. The parameter $r_0(n)$ as a function of n (**a**), and the parameter $r(t)$ as a function of m (**b**), in SF networks (*solid line*: $M = 4$; *dotted line*: $M = 6$) and SW networks (*dashdot line*: $K = 6$, $p = 0.01$; *dashed line*: $K = 8$, $p = 0.01$). All estimates are the results of averaging over 50 realizations

$E_{\mathrm{av}}(k) = \frac{1}{\gamma_k}\sum_{q=1}^{\gamma_k} E_q$ between G and G_0, where γ_k is the number of oscillators with the same degree k, and $E_q = \sqrt{\sum_{j\neq i}(G_{ij} - 1/k_i)^2}/k_i$ if $k_i = k$. We show that G_{ij} is almost identical to the value $1/k_i$ (or $G_{ij} \sim k_i^{-1}$) (Fig. 8.1d). After the ending of our scheme, the couplings $W_{ij}^{n_0}$ for the incoming links of oscillator i are approximately $n_0\varepsilon/k_i$. Therefore, for SF networks with the same M and SW networks with the same K and p, the maximal coupling relies on the minimal degree in networks. The larger the degree of oscillator i is, the smaller the coupling $W_{ij}^{n_0}$ is.

Even under the influence of noise in the Kuramoto model (8.1), we can also obtain similar results in SF networks with different M and SW networks with different K and p (Fig. 8.2). For the Kuramoto model (8.12) with delayed couplings, simulation results are plotted in Fig. 8.3 ($\tau = 1$) and Fig. 8.4 ($\tau = 3$). Here we only plot figures on the parameters r_0 and r. From these figures, synchronization can be realized effectively.

Note that there are two parameters T and ε in our scheme. Due to the weak coupling for synchronization in the Kuramoto model, ε can not be large, but the

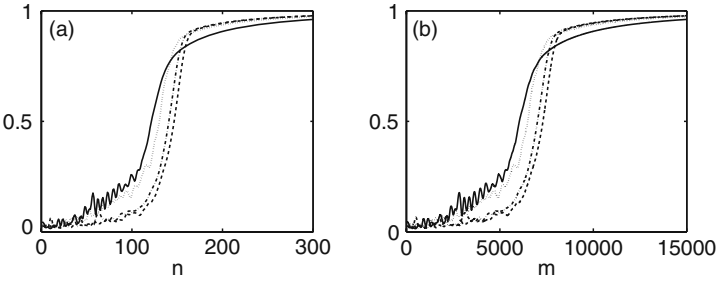

Fig. 8.3 Simulation results in the Kuramoto model (8.12) without noise. The parameter $r_0(n)$ as a function of n (**a**), and the parameter $r(t)$ as a function of m (**b**), in SF network (*solid line*: $M = 4$; *dotted line*: $M = 7$) and SW network (*dashdot line*: $K = 6$, $p = 0.02$; *dashed line*: $K = 8$, $p = 0.02$). All estimates are the results of averaging over 50 realizations

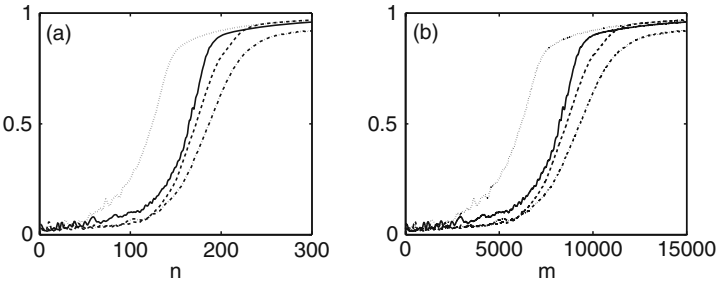

Fig. 8.4 Simulation results in the Kuramoto model (8.12) with noise. The parameter $r_0(n)$ as a function of n (**a**), and the parameter $r(t)$ as a function of m (**b**), in SF network (*solid line*: $M = 4$; *dotted line*: $M = 6$) and SW network (*dashdot line*: $K = 6$, $p = 0.01$; *dashed line*: $K = 8$, $p = 0.01$). All estimates are the results of averaging over 50 realizations

length T of the intervals can be arbitrarily large. In our simulations ε can be chosen in the interval [0.0001,0.02]. For different values of T and ε, we obtain similar results.

Remarks. Gómez-Gardeñes et al. proposed another order parameter r_{link} to measure the extent of synchronization [14], where

$$r_{\text{link}} = \frac{1}{2N_{\text{link}}} \sum_i \sum_{j \in K_i} | \lim_{\Delta_t \to \infty} \frac{1}{\Delta_t} \int_{t_r}^{t_r + \Delta_t} e^{\zeta[\theta_i(t) - \theta_j(t)]} dt |, \tag{8.13}$$

where N_{link} is the number of links, t_r is a large time. The averaging time Δ_t is taken large enough to obtain good measures of the degree of coherence between each pair of physically connected oscillators. Equations (8.4), (8.5), (8.7) in our scheme can be replaced by

$$r_{\text{link}}^{i,n} = \frac{1}{k_i} \sum_{j \in K_i} | \frac{1}{T} \int_{t_{n-1}}^{t_n} e^{\zeta[\theta_i(t) - \theta_j(t)]} dt |, \tag{8.14}$$

$$r'_{\text{link}}(n) = \frac{1}{2N_{\text{link}}} \sum_i \sum_{j \in K_i} | \frac{1}{T} \int_{t_{n-1}}^{t_n} e^{\zeta[\theta_i(t) - \theta_j(t)]} dt |, \tag{8.15}$$

and

$$h_i^n = r_{\text{link}}^{i,n}, \tag{8.16}$$

respectively. One ending condition is $|r'_{\text{link}}(n_0) - 1| < 10^{-2}$ for certain n_0. Since numerical results are very similar to those with respect to the parameters $r^{i,n}$ and $r_0(n)$ (Figs. 8.1, 8.2, 8.3 and 8.4), we omit corresponding figures.

The DGN approach can also be applied to CS in networks with identical oscillators, whose state is represented by $\mathbf{x}_i$. In this case, we should assign a suitable scale

field to oscillator i. Equations (8.4), (8.5), and (8.7) in our scheme can be replaced by

$$r_{\text{link}}^{i,n} = -\frac{1}{k_i} \sum_{j \in K_i} \frac{1}{T} \int_{t_{n-1}}^{t_n} ||\mathbf{x}_i - \mathbf{x}_j|| dt, \tag{8.17}$$

$$r'_{\text{link}}(n) = \frac{1}{2N_{\text{link}}} \sum_i \sum_{j \in K_i} \frac{1}{T} \int_{t_{n-1}}^{t_n} ||\mathbf{x}_i - \mathbf{x}_j|| dt, \tag{8.18}$$

and

$$h_i^n = r_{\text{link}}^{i,n}, \tag{8.19}$$

respectively. One ending condition is $r'_{\text{link}}(n_0) < \varepsilon$ for certain n_0, and ε is arbitrary small.

8.3 Complete Synchronization and Enhanced Synchronizability in Adaptive Complex Networks

In this section, inspired by the DGN approach, we develop another more effective optimization coupling mechanism: the DO coupling mechanism. It does not only realize different kinds of synchronization in networks but also leads to enhanced synchronizability in SF and SW networks. In this section, we first consider CS in networks with instantaneous or delayed couplings. Then we study how to enhance the synchronizability in SF and SW networks.

8.3.1 Complete Synchronization in Adaptive Complex Networks

Our general model for networks consisting of N coupled identical chaotic oscillators with a time-varying coupling matrix is given by

$$\dot{\mathbf{x}}_i = \mathbf{F}(\mathbf{x}_i) + \sum_{j=1}^{N} G_{ij} \mathbf{H}(\mathbf{x}_j, \mathbf{x}_i), \tag{8.20}$$

where $\mathbf{x}_i$ is the state, $\mathbf{F}(\mathbf{x}_i)$ is the dynamics of the individual oscillator $\mathbf{x}_i$, $\mathbf{H}(\mathbf{x}_j, \mathbf{x}_i)$ is the inner coupling function, $G = (G_{ij})$ is the outer coupling matrix. $G_{ij} = W_{ij} A_{ij}$, where $A = (A_{ij})$ is the binary adjacency matrix, W_{ij} is the coupling strength of the incoming link (i, j) pointing from oscillator j to oscillator i if they are connected, $G_{ii} = -\sum_{j \in K_i} A_{ij} W_{ij}$, K_i is the neighbor set of oscillator i.

In this section we consider CS in network (8.20) in two cases. (i) One case is the network (8.20) with instantaneous couplings, where the function $\mathbf{H}(\mathbf{x}_j, \mathbf{x}_i) = \mathbf{H}_0(\mathbf{x}_j) - \mathbf{H}_0(\mathbf{x}_i)$, and $\mathbf{H}_0$ is the output function for each oscillator. (ii) The other

case is the network (8.20) with delayed couplings, in which the function $\mathbf{H}(\mathbf{x}_j, \mathbf{x}_i) = \mathbf{H}_0(\mathbf{x}_j(t-\tau)) - \mathbf{H}_0(\mathbf{x}_i(t))$ with a time delay $\tau > 0$.

In the above section, we have proposed a DGN approach to realize PS in the Kuramoto model, and this approach can be also applied to CS in networks with identical oscillators. However, the DGN approach is very special in two aspects. One is that it should assign a scale potential to each oscillator within any time interval, which depends on the extent of the local synchronization among itself and its neighbor oscillators. The other is that the incoming link to be adjusted by the DGN approach is often not mostly effective. Inspired by the idea of the DGN approach [29], we have further introduced a DO mechanism to SF networks [35]. It also reflects the "winner-take-all" strategy, where the incoming link to be adjusted is always chosen as a pair of oscillators with the weakest synchronization. This means that the DO mechanism is much more effective than the DGN approach.

We first introduce the idea of the DO mechanism. In the interval $[t_n, t_{n+1})$, the choice of the incoming link for oscillator i is based on the maximal accumulated synchronization error in its neighborhood, rather than depending on the scalar fields of oscillators [29]. The DO mechanism is introduced as follows:

(i) For the incoming link (i, j) of oscillator i, we accumulate the synchronization errors by the integral function

$$E_n(i, j) = \int_{t_{n-1}}^{t_n} \boldsymbol{\phi}(\mathbf{x}_i, \mathbf{x}_j)dt, \tag{8.21}$$

where $\boldsymbol{\phi}$ is the error function relying on different kinds of synchronization in networks.

(ii) By the optimization in the neighborhood of oscillator i, we identify the incoming link $(i, j^n_{\max})$ with the index

$$j^n_{\max} = \arg \max_{j \in K_i} E_n(i, j). \tag{8.22}$$

(iii) We adjust the coupling strength W_{ij} adaptively by

$$\begin{cases} W^{n+1}_{ij^n_{\max}} := W^n_{ij^n_{\max}} + \varepsilon \\ W^{n+1}_{ij} = W^n_{ij},\ j \neq j^n_{\max} \end{cases} \tag{8.23}$$

Compared with the incoming link generated by the optimization scheme (8.6) and (8.7), namely the DGN approach, the incoming link generated by the DO mechanism is much more effective. Further, there is one common point: the intensities of the oscillators in the networks are also uniform, since at each step the intensity of each oscillator increases by the same amount ε during the transition to synchronization.

Our simulations in this section are also based on SF networks generated by the Barabási-Albert model [2] and SW networks generated by the Newman-Watts

model [45]. In the following, network (8.1) is a network of Rössler oscillators: $\mathbf{x}_i = (x_i, y_i, z_i)$, $\mathbf{F}(\mathbf{x}_i) = (-0.97y_i - z_i, 0.97x_i + 0.15y_i, z_i(x_i - 8.5) + 0.4)$, the function $\mathbf{H}_0(\mathbf{x}_i) = (x_i, 0, 0)$, and the error function

$$\boldsymbol{\phi}(\mathbf{x}_i, \mathbf{x}_j) = |x_i - x_j| + |y_i - y_j| + |z_i - z_j|.$$

In order to verify CS, we define the average synchronization error as

$$E = \frac{1}{N} \sum_{i=1}^{N} ||\mathbf{x}_i - \bar{\mathbf{x}}||,$$

where $\bar{\mathbf{x}} = (\bar{x}, \bar{y}, \bar{z})$ is the mean-field of all $\mathbf{x}_i$. In our simulations, the initial coupling strengths for all incoming links are zero, the transient time is $t_0 = 100$ s, the length of time intervals is $T = 1$ s, and $\varepsilon = 0.001$. Further, initial conditions for all oscillators are randomly chosen from the chaotic attractor. The solution of network (8.20) is solved by using the Euler method with the time step $h = 0.01$ s, and our ending condition for the DO mechanism is $E < 10^{-5}$.

For network (8.20) with instantaneous couplings, CS is realized effectively (Fig. 8.5). From Eqs. (8.22) and (8.23), all oscillators have uniform intensities during the transition to synchronization, regardless of heterogeneous degrees. But this is totally different from adaptive networks [28, 30]. The average intensity $S(k)$ over oscillators with degree k increases as $S(k) \sim k^{\beta}$ with $\beta \sim 0.5$ [30].

After the adaptation, network (20) with instantaneous couplings can be rewritten as $\dot{\mathbf{x}}_i \approx \mathbf{F}(\mathbf{x}_i) + S_0[\mathbf{H}_0(\bar{\mathbf{x}}_i) - \mathbf{H}_0(\mathbf{x}_i)]$, where $S_0 = \varepsilon n_0$ is the ultimate intensity, n_0 is the ending adjustment step, and $\bar{\mathbf{x}}_i = (1/k_i) \sum_{j \in K_i} \mathbf{x}_j$ is the local mean field of neighbors [15]. In sufficiently random networks the local mean field $\bar{\mathbf{x}}_i$ of oscillators with $k_i \gg 1$ can be approximated by the global mean field $\bar{\mathbf{x}}_i = \bar{\mathbf{x}}$. Hence we get $\dot{\mathbf{x}}_i \approx \mathbf{F}(\mathbf{x}_i) + S_0[\mathbf{H}_0(\bar{\mathbf{x}}) - \mathbf{H}_0(\mathbf{x}_i)]$. Hence all oscillators are forced by a common mean field signal $\mathbf{H}_0(\bar{\mathbf{x}})$ with the same forcing strength S_0, and all oscillators synchronize at a similar speed to the mean activity $\bar{\mathbf{x}}$. The speed only depends on the

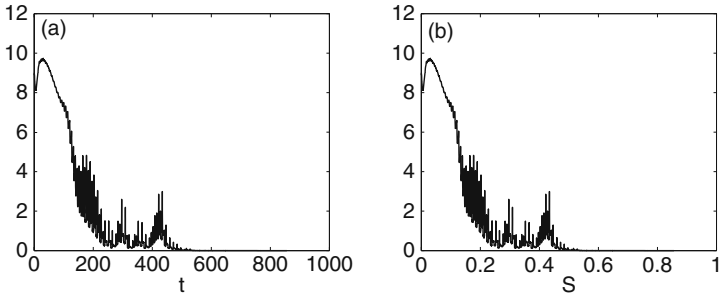

Fig. 8.5 The average synchronization error E in SF networks with instantaneous couplings as a function of (**a**) time t, and (**b**) intensity S, by the DO mechanism. The parameters are $N = 1{,}000$, $M = 5$, $T = 1$ s, $\varepsilon = 0.001$ and $\sigma = 1.5$

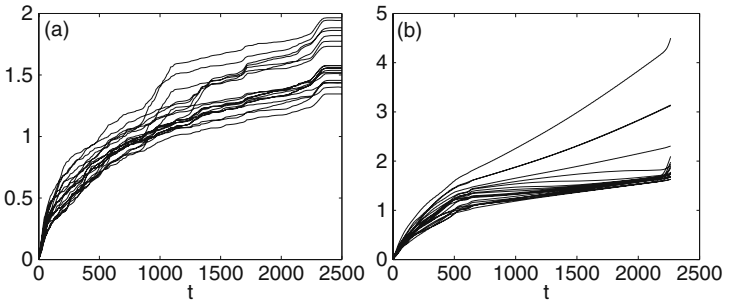

Fig. 8.6 The intensities S_i as a function of time t for arbitrarily 20 oscillators in SW networks with instantaneous couplings (**a**), or delayed couplings (**b**), by the Zhou–Kurths method. The parameters are $N = 500$, $K = 4$, $p = 0.003$, $\gamma = 0.002$, $\tau = 0.01$ s

same intensity (i.e. the sum of input signals each oscillator receives), regardless of the network size. The independence of the network size is not satisfied in [28, 30], where the speed strongly relies on heterogeneous intensities.

For the network (8.20) with instantaneous couplings, the adaptive strategies can realize CS both in SF networks with instantaneous couplings and in SW networks with instantaneous couplings [36]. However, even for SW networks with homogeneous degrees, the adaptive strategies cannot ensure uniform intensities if all oscillators have different initial conditions. We plot the intensities S_i (i.e. $S_i = \sum_{j \in K_i} G_{ij}$), for 20 arbitrarily chosen oscillators in SW networks according to the Zhou–Kurths method (Fig. 8.6a). When the adaptation parameter is chosen as $\gamma = 0.002$, we find that the Zhou–Kurths method can not ensure uniform intensities during or after the adaptation. Based on the DO mechanism, synchronization in SW networks is realized effectively (Fig. 8.7a), and the intensities are always uniform during the transition to synchronization. From Fig. 8.7b, the intensity $S = S_i$ is also a good indicator for synchronization in networks. As S increases to a critical value, a network becomes synchronous.

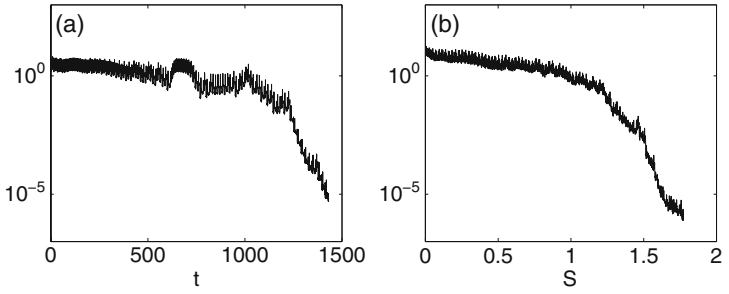

Fig. 8.7 The average synchronization error E in SW networks with instantaneous couplings as a function of (**a**) time t, and (**b**) intensity S, by the DO mechanism. The parameters are $N = 500$, $K = 4$, $p = 0.003$, $T = 1$ s, $\varepsilon = 0.001$

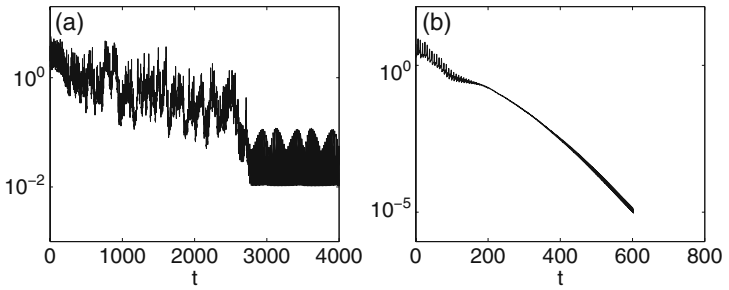

Fig. 8.8 The average synchronization error E in SW networks with delayed couplings as a function of time t. (**a**) the Zhou–Kurths method ($\tau = 0.01$ s). (**b**) the DO mechanism ($\tau = 2$ s). The parameters $N = 500$, $p = 0.003$, $\gamma = 0.002$, $T = 1$ s, $\varepsilon = 0.001$

For the network (8.20) with delayed couplings, even for a small time delay τ (such as $\tau = 0.01$ s), the Zhou–Kurths method can not realize synchronization in SW networks (Fig. 8.8a). The synchronization error between two connected oscillators is about $10^{-2} \times 500 = 5$ for networks with $N = 500$. Due to the DO mechanism, synchronization can be realized effectively when the time delay $\tau = 2$ s (Fig. 8.8b). The synchronization error is about $10^{-5} \times 500 = 0.005$. Hence the DO mechanism is much more effective than the Zhou–Kurths method. The main reason is that the DO mechanism ensures that the intensities are always uniform during the transition to synchronization. But the Zhou–Kurths method can not ensure uniform intensities even for a small time delay (Fig. 8.6b). Though the difference of intensities between oscillators is small initially, it becomes large as time increases. The uniformity of intensities is a necessary condition for the existence of a synchronous manifold in NW networks with delayed couplings. After the adaptation, the synchronous manifold is given by $\{\mathbf{x}_i(t) = \mathbf{x}_0(t),\ i = 1, \cdots, N\}$, where $\mathbf{x}_0(t)$ is the solution of the isolated dynamics

$$\dot{\mathbf{x}}_0(t) = \mathbf{F}(\mathbf{x}_0(t)) + S_0(\mathbf{H}_0(\mathbf{x}_0(t-\tau)) - \mathbf{H}_0(\mathbf{x}_0(t))).$$

Remarks. The DO mechanism can be also applied to PS in networks with nonidentical oscillators, provided that the phase in networks of oscillators is well-defined [6]. For the Kuramoto model, the accumulated synchronization error (8.21) is defined by

$$E_n(i,\, j) = \frac{1}{T}\int_{t_{n-1}}^{t_n} [1 - r_n(i,\, j)]dt \tag{8.24}$$

with $r_n(i,\, j)\mathrm{e}^{\zeta \Psi_n(i,j)} = (\mathrm{e}^{\zeta\theta_j} + \mathrm{e}^{\zeta\theta_i})/2$, where $0 \le r_n(i,\, j) \le 1$ measures the extent of synchronization of oscillators i, j, and $\Psi_n(i,\, j)$ stands for an average phase.

For the networks $\dot{\mathbf{x}}_i = \tau_j \mathbf{F}_i(\mathbf{x}_i) + \sum_{j=1}^{N} G_{ij}\mathbf{H}(\mathbf{x}_j, \mathbf{x}_i)$, where the parameter τ_j is distributed uniformly in an interval $[1 - \triangle\tau,\, 1 + \triangle\tau]$ with the parameter $\triangle\tau = 0.1$,

the accumulated synchronization error (8.21) is defined by

$$E_n(i,\, j) = \frac{1}{T}\int_{t_{n-1}}^{t_n} [1 - r_n(i,\, j)]dt, \tag{8.25}$$

where $r_n(i,\, j)e^{\zeta\Psi_n(i,j)} = (e^{\zeta\vartheta_j} + e^{\zeta\vartheta_i})/2$, the phase ϑ_i can be simply defined by $\vartheta_i = \arctan(y_i/x_i)$ [6]. Of course, for the above two cases, we should choose suitable ending conditions (such as Eq. (8.15) and $|r'_{\text{link}}(n_0) - 1| < 10^{-2}$).

Note that the DGN approach can be also applied to PS in networks with much more complex non-identical oscillators, such as the networks of Rössler oscillators. In this case, the order parameters $r(t)$, $r_i(t)$, r_{link}, $r^{i,n}_{\text{link}}$ are defined according to the phase ϑ_i.

8.3.2 Enhanced Synchronizability in Adaptive Complex Networks

We first briefly review the stability of networks with time-invariant topology:

$$\dot{\mathbf{x}}_i = \mathbf{F}(\mathbf{x}_i) + \sigma\sum_{j=1}^{N} G^0_{ij}\mathbf{H}_0(\mathbf{x}_j),\ \ 1 \le i \le N, \tag{8.26}$$

where σ is the overall strength, $\mathbf{F}(\mathbf{x}_i)$ is the dynamics of individual oscillator, $\mathbf{H}_0(\mathbf{x}_j)$ is the output function. For a generally asymmetric matrix $G^0 = (G^0_{ij})$ with $G^0_{ij} = W^0_{ij}A_{ij}$, the variational equation for the synchronous state $\{\mathbf{x}_i = \mathbf{s},\ \forall\, i\}$ is

$$\dot{\xi}_i = [D\mathbf{F}_0(\mathbf{s}) - \sigma\lambda_l D\mathbf{H}_0(\mathbf{s})]\xi_i, \tag{8.27}$$

where D is the Jacobian operator, λ_l are the complex eigenvalues of the Laplacian matrix $L\ (= -G^0)$, satisfying $\text{Re}(\lambda_1) \le \text{Re}(\lambda_2) \le \cdots \le \text{Re}(\lambda_N)$. The largest Lyapunov exponent (LLE), $\Lambda(\alpha, \beta)$, of

$$\dot{\eta} = [D\mathbf{F}_0(\mathbf{s}) - (\alpha + i\beta)D\mathbf{H}_0(\mathbf{s})]\eta \tag{8.28}$$

is a function of α and β. This function is the master stability function (MSF) [8, 9]. Let $\mathcal{R}$ be the region in the complex plane where the MSF provides a negative LLE. The condition for CS in network (8.26) is that the set $\{\sigma\lambda_l,\ \forall\, l\}$ is entirely contained in $\mathcal{R}$ [8]. Here we only consider the case where the region $\mathcal{R}$ is bounded. Then, a better synchronizability is achieved if simultaneously the ratio $\text{Re}(\lambda_N)/\text{Re}(\lambda_2)$ and $\max|\text{Im}(\lambda_i)|$ are minimized [16, 19].

For SF networks, the DO mechanism realizes CS in network (8.20) effectively. During the transition to synchronization in network (8.20), the ratio $\text{Re}(\lambda_N)/\text{Re}(\lambda_2)$ in network (8.26) with $G^0 = G$ approaches the optimal synchronizability $R_{\text{opt}} = 3.8$ (Fig. 8.9). The value R_{opt} is determined by the coupling matrix $G'(\alpha) = (G'_{ij}(\alpha))$

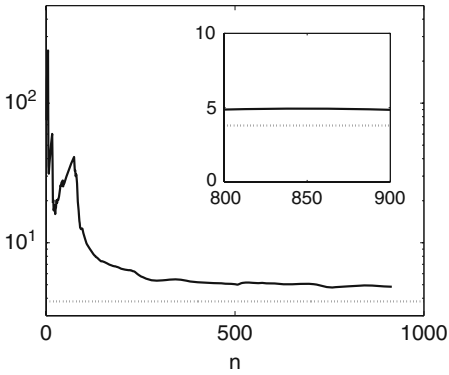

Fig. 8.9 The ratio $\mathrm{Re}(\lambda_N)/\mathrm{Re}(\lambda_2)$ as a function of the adjustment step n in SF networks. *Solid line*: CS in network (8.26) with $G^0 = G$; *dotted line*: R_{opt}. Inset: the stationary ratio. The parameters are $N = 1,000$, $M = 5$, $T = 1$ s and $\varepsilon = 0.001$

with $G'_{ij}(\alpha) = (k_i k_j)^\alpha / \sum_{j\in K_i}(k_i k_j)^\alpha$ and $G'_{ii}(\alpha) = -1$, which extends the couplings in networks [20]. When $\alpha = 0$, the eigenratio of the Laplacian matrix of $G'(0)$ is minimal and the synchronizability in network (8.26) with $G^0 = G'(0)$ is optimal [20]. From Eqs. (8.21), (8.22), and (8.23), the incoming link to be adjusted for each oscillator is always chosen to be the pair of oscillators with the maximal synchronization difference in the previous time interval, which substantially decreases the ratio $\mathrm{Re}(\lambda_N)/\mathrm{Re}(\lambda_2)$. From Fig. 8.9, this is a dynamical process towards the optimal synchronizability R_{opt}.

Here we assign the coupling matrix G^0 in network (8.26) by

$$G^0 = G_{\mathrm{norm}} = G_{\mathrm{end}}/S, \tag{8.29}$$

where G_{end} is the coupling matrix of network (8.20) after the adaptation. Since all oscillators have uniform intensities, the Laplacian matrices of G_{norm} and G_{end} have equal ratios $\mathrm{Re}(\lambda_N)/\mathrm{Re}(\lambda_2)$. The ratio $\mathrm{Re}(\lambda_N)/\mathrm{Re}(\lambda_2)$ in network (8.26) with $G^0 = G_{\mathrm{norm}}$ is shown by the stationary value (Fig. 8.9: Inset). When $\sigma = 1.5$, all nonzero eigenvalues of the Laplacian matrix of σG_{norm} are located in a very narrow region around the real axes in the region $\mathcal{R}$, and the absolute values of imaginary parts are sufficiently small (Fig. 8.10). Hence the ratio $\mathrm{Re}(\lambda_N)/\mathrm{Re}(\lambda_2)$ is a good indicator for the synchronizability in network (8.26). In this section the synchronizability in network (8.26) with $G^0 = G_{\mathrm{norm}}$ is quasi-optimal, compared with the optimal synchronizability [20].

We discuss the effect of the parameters T and ε on the synchronizability in network (8.26) with $G^0 = G_{\mathrm{norm}}$ (Fig. 8.11). The value ε can be chosen in a wide range, and the length T can be arbitrary large. In our simulations ε is from [0.0001,0.005]. From Fig. 8.11, the ratio $\mathrm{Re}(\lambda_N)/\mathrm{Re}(\lambda_2)$ is almost independent of the values of T and ε.

The ratio $\mathrm{Re}(\lambda_N)/\mathrm{Re}(\lambda_2)$ in network (8.26) with $G^0 = G_{\mathrm{norm}}$ increases slightly with increasing network size N, and can be well-fitted by a power-law dependence,

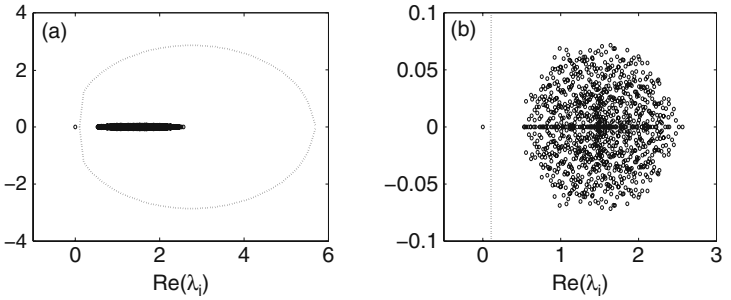

Fig. 8.10 (**a, b**) Distribution of eigenvalues of the Laplacian matrix of σG_{norm} in SF networks. *Circle*: CS in network (8.26) with $G^0 = G_{\text{norm}}$; *solid line*: the region $\mathcal{R}$. The parameters are $N = 1{,}000$, $M = 5$, $T = 1$ s, $\varepsilon = 0.001$ and $\sigma = 1.5$

i.e. the synchronizability decreases slightly (Fig. 8.12). From the fitting, we find that the network (8.26) is still synchronizable till $N \approx 10^{11}$. The size of the network (8.26) that is synchronizable exceeds by several orders of magnitude the size of unweighted networks ($\approx 10^3$) and networks with adaptive couplings ($\approx 8 \times 10^5$) [30]. Obviously, this is a great enhancement of the synchronizability in networks, compared with unweighted networks and other adaptive coupling schemes [30]. It should be pointed out that for different size of networks, $\max |\text{Im}(\lambda_i)|$ is sufficiently small (the maximal value is less than 0.06).

The above result can be ensured by the Gerschgorin disk theorem [46]. For the coupling matrix $G^0 = G_{\text{norm}}$, all eigenvalues are fully contained within the unit circle centered at 1. So $0 \leq \text{Re}(\lambda_l) \leq 2$, $|\text{Im}(\lambda_l)| \leq 1$, and the largest $\text{Re}(\lambda_N)$ will never diverge, independently of the network size N [19]. During the transition to synchronization in network (8.20), $S_{\max}/S_{\min}$ always equals to 1. In [15, 30], the synchronizability decreases with the increasing of $S_{\max}/S_{\min}$, but $S_{\max}/S_{\min}$ increases with the increasing of the size N. Hence the synchronizability here is better than

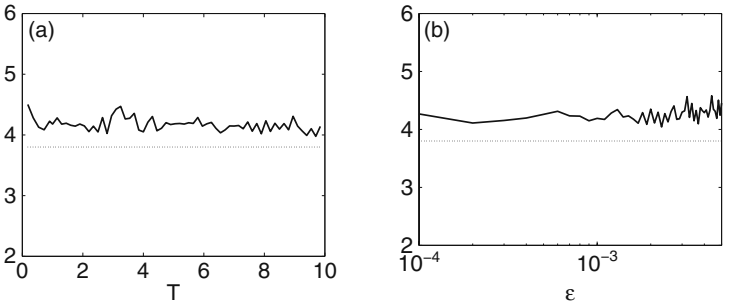

Fig. 8.11 (**a, b**) The ratio $\text{Re}(\lambda_N)/\text{Re}(\lambda_2)$ for different T (**a**) and ε (**b**), in SF networks with $N = 1{,}000$, $M = 5$. *Solid line*: CS in network (8.26) with $G^0 = G_{\text{norm}}$; *dotted line*: R_{opt}. All the estimates are averaged over 20 realizations of networks

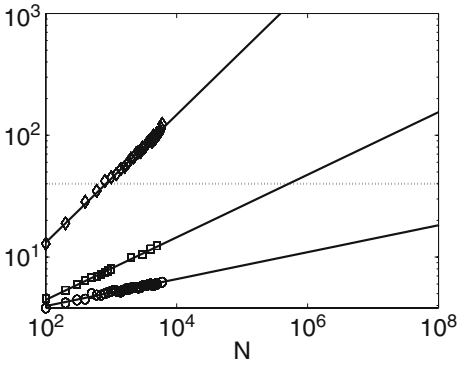

Fig. 8.12 The ratio $\mathrm{Re}(\lambda_N)/\mathrm{Re}(\lambda_2)$ for different size of SF network (8.26) with $M = 5$, $\tau = 1$, $\varepsilon = 0.001$. *Diamond*: unweighted networks; *square*: networks with adaptive couplings [8]; *circle*: CS; fitting: *solid line; dotted line*: $R_\varepsilon = 40$ (the maximal ratio $\mathrm{Re}(\lambda_N)/\mathrm{Re}(\lambda_2)$ in the region $\mathcal{R}$). All the estimates are averaged over 20 realizations of networks

the synchronizability in [30], whose main aim is to reduce the heterogeneity of intensities adaptively.

From the above analysis, we find that the DO mechanism results in a better synchronizability in SF networks, compared with unweighted networks and adaptive networks. Now we also discuss the synchronizability in SW networks due to the DO mechanism.

Obviously, the synchronization in SW networks can be realized by the DO mechanism. Similarly, we assign the coupling matrix G^0 in SW networks by Eq. (8.29), after the adaptation. In order to enhance synchronizability in SW networks, we compare the synchronizability in the unweighted network (8.26) (type I network: $W_{ij}^0 = 1$), the degree based weighted network (8.26) (type II network: $W_{ij}^0 = 1/k_i$), network (8.26) with adaptive couplings by the Zhou–Kurths method (type III network), and network (8.26) with the coupling matrix being designed by network (8.20) with instantaneous couplings (type IV networks).

We find that for a fixed small probability p (such as $p = 0.003$) for adding long-range connections, the synchronizability in type III networks is better than that in type I networks, but it is worse than that in type II networks, no matter how large the size N of the networks is (Fig. 8.13a). However, we find that type IV networks have a better synchronizability than both type II and type III networks when the size is not too large. Of course, the smaller the probability p is, the larger is the size of type IV networks with better synchronizability than both type II and type III networks. For the fixed size $N = 500$, we observe similar results in a certain range of the probability p (Fig. 8.13b). From Fig. 8.13, we see that the synchronizability in type IV networks is better than those in type II networks and type III networks in some cases. It is reasonable that type IV networks have better synchronizability than type III networks. This is because the DO mechanism ensures uniform intensities of all oscillators in type IV networks. Now we further analyze the reason why type IV networks have better synchronizability than type II networks in a certain range of the probability p.

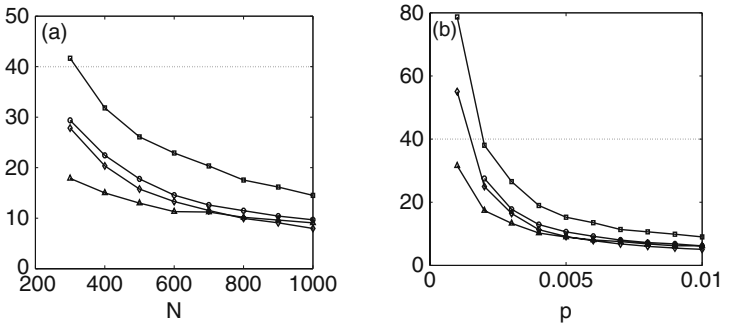

Fig. 8.13 For SW networks, the ratio $\mathrm{Re}(\lambda_N)/\mathrm{Re}(\lambda_2)$ as a function of the network size N for a fixed probability $p = 0.003$ (**a**), and the probability p for a fixed size $N = 500$ (**b**). *Square*: type I networks; *diamond*: type II networks; *circle*: type III networks; *big triangle up*: type IV networks; *dashed line*: the maximal ratio $\frac{\mathrm{Re}(\lambda_N)}{\mathrm{Re}(\lambda_2)}$ in the region $\mathcal{R}$. The parameters are $K = 4$, $\gamma = 0.002$, $T = 1$ s, $\varepsilon = 0.001$. All the estimates are averaged over 20 realizations of networks

In order to do so, we slightly modify SW networks. The initial network is a $K-$nearest-neighbor coupled network consisting of N oscillators arranged in a ring, with each oscillator i being adjacent to its K neighbor oscillators $i \pm 1, \cdots, i \pm K/2$, and with K being even. Then one adds with probability p a long-range connection between a pair of oscillators with indices satisfying

$$n_1 \leq \min\{|i-j|,\ N-|i-j|\} \leq n_2, \tag{8.30}$$

where $0 \leq n_1,\ n_2 \leq N/2$ are two positive integers. This kind of networks is called type V networks. Based on type V networks, we adjust the coupling strengths by the DO mechanism. After the adaptation, we define the average coupling strength $\langle W_v \rangle$ over the k_W links having the same $v = \min\{|i-j|,\ N-|i-j|\}$:

$$\langle W_v \rangle = \frac{1}{k_W} \sum G_{ij}. \tag{8.31}$$

Further, for unweighted type V networks, the average load $\langle L_v \rangle$ over the k_L links having the same v is given by

$$\langle L_v \rangle = \frac{1}{k_L} \sum L_{ij}, \tag{8.32}$$

where the load L_{ij} of the link connecting oscillators i and j quantifies the traffic of the shortest paths passing that link. Here the size of type V networks is $N = 300$ and the probability $p = 0.2$. For different n_1 and n_2, we plot the relationship between $\langle W_v \rangle$ and v (Fig. 8.14a, d, g), and the relationship between $\langle L_v \rangle$ and v (Fig. 8.14b, e, h), respectively. From these subfigures, we conclude that $\langle W_v \rangle$ has a similar dependence on v as $\langle L_v \rangle$, which is further verified by the relationship $\langle W_v \rangle \sim \langle L_v \rangle$ (Fig. 8.14c, f, i). This implies that the adaptation due to the DO mechanism may

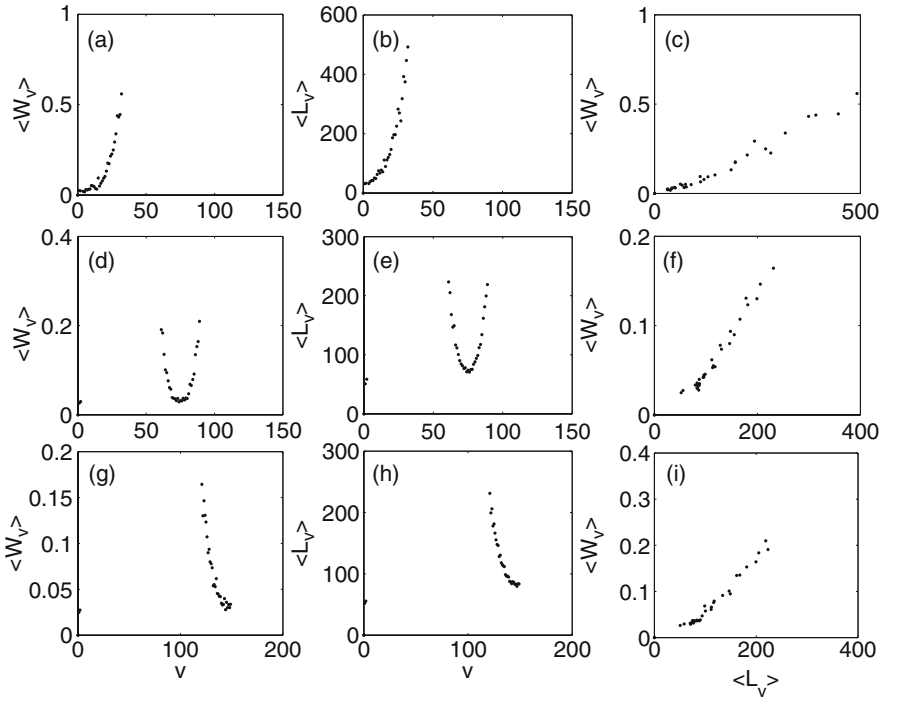

Fig. 8.14 The dependence of $\langle W_v \rangle$ on v in (**a, d, g**), of $\langle L_v \rangle$ on v in (**b, e, h**), and the relationship between $\langle W_v \rangle$ and $\langle L_v \rangle$ in (***c, f, i***), respectively. $n_1 = 0$, $n_2 = 30$ (**a, b, c**); $n_1 = 60$, $n_2 = 90$ (**d, e, f**); $n_1 = 120$, $n_2 = 150$ (**g, h, i**). The parameters in type V networks are $N = 300$, $K = 4$, $p = 0.2$, $T = 1$ s, $\varepsilon = 0.001$

lead to a similar synchronizability as the load based weighted networks. This may in part explain why type IV networks have a better synchronizability than type II networks in a certain range of the probability p for adding long-range connections.

Remarks. From the above subsection, we can extend the DO mechanism to CS in network (8.20) with the coupling function $\mathbf{H}(\mathbf{x}_j, \mathbf{x}_i) = \mathbf{H}(\mathbf{x}_j(t - \tau_0)) - \mathbf{H}(\mathbf{x}_i)$ and a small delay time τ_0 (such as $\tau_0 \leq 2$). The DO mechanism ensures that all oscillators have uniform intensities, which leads to the existence of a synchronous manifold in network (8.20). However, it can not be realized by the dynamical mechanism proposed in [30]. Due to the DO mechanism, we can also obtain a better synchronizability in SF and SW networks due to CS in networks with delayed couplings. Here we omit the corresponding results.

From the DGN approach and the DO mechanism, the two coupling schemes are "winner-take-all" strategies. This implies that the intensity S_i for oscillator i increases to infinity as the adjustment time n tends to infinity. Hence there is one shortcoming: we should choose suitable conditions to end the adaptation of the above two mechanisms. In fact, this shortcoming can be overcome by slightly modifying the adjustment (8.8) and (8.9) for the DGN approach and the adjustment (8.23)

for the DO mechanism. Here the adjustment of couplings for the incoming link with the maximal competitive ability is modified as follows:

$$W_{i\mu_i^n}^{n+1} := W_{i\mu_i^n}^{n} + \varepsilon \mathrm{e}^{-n/k_0} \tag{8.33}$$

for the DGN approach, and

$$W_{ij_{\max}^n}^{n+1} = W_{ij_{\max}^n}^{n} + \varepsilon \mathrm{e}^{-n/k_0} \tag{8.34}$$

for the DO mechanism, where k_0 is a suitable positive integer. From Eqs. (8.33) and (8.34), the intensity S_i still increases, and all oscillators have uniform intensities. However, the intensity S_i for each oscillator can not increase to infinity, and can be bounded by the limit $\bar{S} = \lim_{n\to\infty} S_i$ for all oscillators, where

$$\bar{S} = \varepsilon \mathrm{e}^{-1/k_0}/(1 - \mathrm{e}^{-1/k_0}). \tag{8.35}$$

Obviously, we can adjust the ultimate intensity for all oscillators by a suitable parameter k_0. When k_0 is larger, the intensity $\bar{S}$ is larger; when k_0 is smaller, the intensity $\bar{S}$ is also smaller. It should be noted that we obtain similar results if we choose the parameters $k_0 = 500$, $\varepsilon = 0.01$ for PS in the Kuramoto models and $k_0 = 1{,}000$, $\varepsilon = 0.001$ for CS in networks of Rössler oscillators, respectively.

8.4 Conclusions

In this chapter, we introduce two dynamical optimization coupling mechanisms for getting different kinds of synchronization in adaptive complex networks, whose oscillators could be either identical or non-identical. For each oscillator, we adjust only one incoming link's strength in different time intervals while the other incoming links' strengths remain constant. The dynamical optimization coupling mechanisms are in effect "winner-take-all" strategies. If one incoming link for each oscillator has the maximal competitive ability in its neighborhood in different time intervals, its strength increases by a small value. We realize different kinds of synchronization in adaptive complex networks with instantaneous or delayed couplings, as well as ensure that all oscillators have uniform intensities during the transition to synchronization. We also enhance the synchronizability in complex networks with identical oscillators.

Acknowledgements M.C. was supported by the Alexander von Humboldt Foundation, NSFC project under Grant No. 60804046, and Special Doctoral Fund at Tsinghua University by Ministry of Education under Grant. No. 20070003129. J.K. was supported by SFB 555 (DFG) and BRACCIA (EU).

References

1. Watts, D.J., Strogatz, S.H.: Collective dynamics of 'small world' networks. Nature (London) **393**, 440–442 (1998).
2. Barabasi, A.L., Albert, R.: Emergence of scaling in random networks. Science **286**, 509–512 (1999).
3. Strogatz, S.H.: Exploring complex networks. Nature (London) **410**, 268–276 (2001).
4. Albert, R., Barabasi, A.L.: Statistical mechanics of complex networks. Rev. Mod. Phys. **74**, 47–97 (2002).
5. Boccaletti, S., Latorab, V., Morenod, Y., Chavez, M., Hwang, D.U.: Complex networks: structure and dynamics. Phys. Rep. **424**, 175–308 (2006).
6. Osipov, G., Kurths, J., Zhou, C.S.: Synchronization in Oscillatory Networks. Springer-Verlag, Heidelberg (2007).
7. Strogatz, S.H.: From Kuramoto to Crawford: exploring the onset of synchronization in populations of coupled oscillators. Physica D **143**, 1–20 (2000).
8. Pecora, L.M., Carroll, T.L.: Master stability functions for synchronized coupled systems. Phys. Rev. Lett. **80**, 2109–2112 (1998).
9. Barahona, M., Pecora, L.M.: Synchronization in small-world systems. Phys. Rev. Lett. **89**, 054101 (2002).
10. Nishikawa, T., Motter, A.E., Lai, Y.C., Hoppensteadt, F.C.: Heterogeneity in oscillator networks: are smaller worlds easier to synchronize? Phys. Rev. Lett. **91**, 014101 (2003).
11. Wang, X., Lai, Y.C., Lai, C.H.: Enhancing synchronization based on complex gradient networks. Phys. Rev. E **75**, 056205 (2007).
12. Moreno, Y., Pacheco, A.F.: Synchronization of Kuramoto oscillators in scale-free networks. Europhys. Lett. **68**, 603–609 (2004).
13. Arenas, A., Díaz-Guilera, A., Pérez-Vicente, J.C.: Synchronization reveals topological scales in complex networks. Phys. Rev. Lett. **96**, 114102 (2006).
14. Gómez-Gardeñes, J., Moreno, Y., Arenas, A.: Paths to synchronization on complex networks. Phys. Rev. Lett. **98**, 034101 (2007).
15. Zhou, C., Motter, A.E., Kurths, J.: Universality in the synchronization of weighted random networks. Phys. Rev. Lett. **96**, 034101 (2006).
16. Huang, D., Chavez, M., Amann, A., Boccaletti1, S.: Synchronization in complex networks with age ordering. Phys. Rev. Lett. **94**, 138701 (2005).
17. Radicchi, F., Meyer-Ortmanns, H.: Reentrant synchronization and pattern formation in pacemaker-entrained Kuramoto oscillators. Phys. Rev. E **74**, 026203 (2006).
18. Chavez, M., Hwang, D.U., Amann, A., Hentschel, H.G.E., Boccaletti, S.: Synchronization is enhanced in weighted complex networks. Phys. Rev. Lett. **94**, 218701 (2005).
19. Chavez, M., Hwang, D.U., Amann, A., Boccaletti, S.: Synchronizing weighted complex networks. Chaos **16**, 015106 (2006).
20. Motter, A.E., Zhou, C.S., Kurths, J.: Network synchronization, diffusion, and the paradox of heterogeneity. Phys. Rev. E **71**, 016116 (2005).
21. Nishikawa, T., Motter, A.E.: Synchronization is optimal in nondiagonalizable networks. Phys. Rev. E **73**, 065106 (2006).
22. Jain, S., Krishna, S.: A model for the emergence of cooperation, interdependence, and structure in evolving networks. Proc. Natl. Acad. Sci. U.S.A. **98**, 543–547 (2001).
23. Skyrms, B., Pemantle, R.: A dynamic model of social network formation. Proc. Natl. Acad. Sci. U.S.A. **97**, 9340–9346 (2000).
24. Zimmermann, M.G., Eguíluz, V.M., Miguel, M.S.: Coevolution of dynamical states and interactions in dynamic networks. Phys. Rev. E **69**, 065102 (2004).
25. Ito, J., Kaneko, K.: Spontaneous structure formation in a network of chaotic units with variable connection strengths. Phys. Rev. Lett. **88**, 028701 (2002).
26. Gleiser, P.M., Zanette, D.H.: Synchronization and structure in an adaptive oscillator network. Eur. Phys. J. B 53, 233–238 (2006).

27. Gross, T., Blasius, B.: Adaptive coevolutionary networks: a review. J. R. Soc. Interface **5**, 259–271 (2008).
28. Ren, Q., Zhao, J.: Adaptive coupling and enhanced synchronization in coupled phase oscillators. Phys. Rev. E **76**, 016207 (2007).
29. Chen, M., Shang, Y., Zou, Y., Kurths, J.: Synchronization in the Kuramoto model: a dynamical gradient network approach. Phys. Rev. E. **77**, 027101 (2008).
30. Zhou, C., Kurths, J.: Dynamical weights and enhanced synchronization in adaptive complex networks. Phys. Rev. Lett. **96**, 164102 (2006).
31. Lu, W.L.: Adaptive dynamical networks via neighborhood information: synchronization and pinning control. Chaos **17**, 023122 (2007).
32. Huang, D.B.: Synchronization in adaptive weighted networks. Phys. Rev. E **74**, 046208, (2006).
33. Sorrentino, F., Ott, E.: Adaptive synchronization of dynamics on evolving complex networks. arXiv:0802.1241v1 [cond-mat.dis-nn] 10 Feb 2008.
34. Frasca, M., Buscarino, A., Rizzo, A., Fortuna, L., Boccaletti, S.: Synchronization of moving chaotic agents. Phys. Rev. Lett. **100**, 044102 (2008).
35. Chen, M., Shang, Y., Zhou, C.S., Wu, Y., Kurths, J.: Enhanced synchronizability in scale-free networks. Chaos 19, 013105 (2009)
36. Wu, Y., Shang, Y., Chen, M., Zhou, C.S., kurths, J.: synchronization in small-worked networks. Chaos 18, 037111 (2008).
37. Kozma, B., Barrat, A.: Consensus formation on adaptive networks. arXiv:0707.4416v1 [physics.soc-ph] 30 Jul 2007.
38. Gross, T., Dommar D'Lima, C., Blasius, B.: Epidemic dynamics on an adaptive network. Phys. Rev. Lett. **96**, 208701 (2006).
39. Shaw, L.B., Schwartz, I.B.: Fluctuating epidemics on adaptive networks. Phys. Rev. E **77**, 066101 (2008).
40. Kuramoto, Y.: Chemical Oscillations, Waves, and Turbulence. Springer, Berlin (1984).
41. Acebron, J., Bonilla, L.L., Vicente, C.J.P., Ritort, F., Spigler, R.: The Kuramoto model: a simple paradigm for synchronization phenomena. Rev. Mod. Phys. **77**, 137–185 (2005).
42. Maistrenko, Y.L., Lysyansky, B., Hauptmann, C., Burylko, O., Tass, P.A.: Multistability in the Kuramoto model with synaptic plasticity. Phys. Rev. E **75**, 066207 (2007).
43. Park, K., Lai, Y.C., Zhao, L., Ye, N.: Jamming in complex gradient networks. Phys. Rev. E **71**, 065105(R) (2005).
44. Toroczkai, Z., Bassler, K.E.: Jamming is limited in scale-free systems. Nature **428**, 716–716 (2004).
45. Newman, M.E.J., Watts, D.J.: Renormalization group analysis of the small-world network model. Phys. Lett. A **263**, 341–346 (1999).
46. Varga, R.S.: Gersgorin and his Circles. Springer-Verlag, Heidelberg (2004).

Part III
Contact Processes and Epidemiology on Adaptive Networks

Chapter 9
Contact Processes and Moment Closure on Adaptive Networks

Anne-Ly Do and Thilo Gross

Abstract Contact processes describe the transmission of distinct properties of nodes via the links of a network. They provide a simple framework for many phenomena, such as epidemic spreading and opinion formation. Combining contact processes with rules for topological evolution yields an adaptive network in which the states of the nodes can interact dynamically with the topological degrees of freedom. By moment-closure approximation it is possible to derive low-dimensional systems of ordinary differential equations that describe the dynamics of the adaptive network on a coarse-grained level. In this chapter we discuss the approximation technique itself as well as its applications to adaptive networks. Thus, it can serve both as a tutorial as well as a review of recent results.

9.1 Introduction

Contact processes are based on an elementary observation: Individuals are altered and shaped through interaction with others. Equally basic is the observation that individuals can often decide with whom to interact. Both of these observations can be modeled by a single network, in which nodes correspond to individuals while links correspond to interpersonal connections. The dynamics of this network is governed by two processes: Topology-dependent transmission of dynamical states of individuals, and state-selective evolution of the links. Hence, the combination of the two gives rise to an adaptive network [9].

Within the framework of contact processes on adaptive networks, attention has focused particularly on opinion formation [2, 4, 6, 7, 12, 14–16, 24] and epidemic spreading [8, 10, 11, 20, 21, 23, 25].

Comparing the models studied in the context of the different applications reveals many similarities and some distinct differences. Similarities are found mainly in the general set-up of the models. First, the transmission of states is strictly limited to the neighborhood of a node. Second, to account for differences among individuals

A.-L. Do (✉)
Max-Planck-Institute for the Physics of Complex Systems, 01187 Dresden, Germany
e-mail: ly@mpipks-dresden.mpg.de

T. Gross, H. Sayama (eds.), *Adaptive Networks,* Understanding Complex Systems,
DOI 10.1007/978-3-642-01284-6_9,

and to facilitate computation, the processes in the model are in general defined stochastically. Third, concerning the topological evolution, the vast majority of models allows only for rewiring of links. In contrast to other processes, rewiring conserves the number of nodes and links, which is advantageous for numerical simulation. Finally, all numerical models discussed in this chapter apply an asynchronous update procedure, in which a randomly selected node is updated in any one step. This is believed to yield the best approximation to a continuous time system [3].

The differences between models of epidemics and models of opinion formation arise mainly from differences in the physics of the underlying real-world processes: In epidemics, there is an objective difference between infected and healthy individuals, and the processes are inherently state-specific: The infection can be transmitted along the links, while it is obvious that the same is not possible for the healthy state. By contrast, in models of opinion formation the different opinions are in general treated equally and therefore appear symmetrically in the model. One important consequence of the state-dependence of epidemic processes is that additional processes have to be introduced in the model if the number of states is increased. Indeed, many models of epidemics extend the scenario of healthy and infected individuals by additional states to model distinct temporal phases of the infection. If for instance a state is introduced, which corresponds to individuals that have recovered from the disease, new processes have to be formulated that govern transitions to and from this state. Conversely, the symmetry of state-dependence in opinion-formation processes enables us to increase the number of states without increasing the number of processes in the system. On the one hand this means that a system with a small number of opinions greater than two will behave very similarly to a system with just two opinions [16]. On the other hand it allows to consider systems in which infinitely many opinions compete based on a finite number of processes.

Regardless of the model, the investigation of contact processes on adaptive networks poses characteristic difficulties. Full agent-based simulations are fundamentally inefficient. In order to determine the long-term behavior of the system we have to simulate for a long time. During this time the simulation produces information, namely a dynamical trajectory, which comes at a computational cost although it is generally not used in the analysis of the system. By contrast, the theory of dynamical systems offers many tools, such as Newton's Method and bifurcation analysis, that enable us to determine the long-term behavior of the system directly. In order to apply these methods the adaptive network needs to be described in terms of emergent variables, governed by differential equations or discrete time maps. For contact processes, convenient variables are the densities of certain subgraphs called network moments. A *moment expansion* of the dynamics results in an infinite cascade of differential equations. This cascade can be truncated by a *moment-closure approximation* which is explained below. In practice, it is often sufficient to approximate the network by a small number of differential equations (e.g. 3), which allows for analytical treatment of the system.

In this chapter, we aim to provide an overview of recent studies concerned with contact processes on adaptive networks. Throughout these studies certain system level phenomena, like the emergence of state homogeneous subpopulations, are

found to recur. The underlying mechanisms of these phenomena are addressed and compared. In Sect. 9.2 various papers are reviewed which treat opinion formation by means of different models. A comparison of these models provides insights into the topic *per se* and, moreover, into the relation between the microscopic rules and the system level behavior. Section 9.3 focuses on models of epidemic spreading. The application of a moment closure approximation is demonstrated by means of the adaptive SIS-model. Thereafter we launch into a more general discussion of moment closures. In particular we emphasize that the adaptivity of the network improves the efficiency of this tool.

9.2 Opinion Formation – Theme and Variations

Models of opinion formation explore the spreading of opinions in social networks. Current models assume that this spreading is governed by two competing processes: social adjustment and social segregation. The former means that connected individuals adjust their views, the latter that individuals maintain contacts preferentially to like-minded individuals. In general, both processes reduce the number of links between nodes with conflicting opinions and lead to the formation of homogeneous social communities holding a uniform opinion. A network which is entirely composed of such *consensus communities* is said to be in the *consensus state*. While almost all models ultimately reach a consensus state, the convergence time τ_c and the distribution of community sizes P_s can differ markedly depending on the relative rate of the competing processes.

As interpersonal interactions are highly complex and difficult to capture in models, a variety of different modeling approaches have been proposed. This diversity provides the opportunity to investigate which details of the microscopic description affect the system level properties. Below, models of opinion formation are compared that differ mainly in the three aspects subsequently described.

The first aspect concerns the number of opinions in the model. As we have mentioned above, essentially two cases have to be distinguished: Models in which only two alternative opinions exist, and those in which individuals can choose from a continuous spectrum of opinions. The first, so-called *voter-like* approach models typical electoral decisions, where the number of choices is limited by the number of candidates. The second approach applies to opinions such as religious belief, where in principle an infinite number of choices exists.

The second aspect in which models differ is the treatment of social segregation. A link that connects individuals with conflicting opinions can either be rewired or broken entirely. In the first case the number of links is conserved, and therefore the process is reversible. In the second case the number of links is decreased, therefore the process is irreversible unless it is counteracted by another process in which new links are created. So far, the creation of links has hardly been considered in models of opinion formation as it causes numerical difficulties and introduces additional complexities.

Another difference between the models is how the symmetry of social interactions is broken. In almost all models of opinion formation adjustment of views is conceived as an asymmetric act. However, in the absence of a parameter that measures the persuasive power or the social influence of an individual, the implementation of asymmetry between interacting nodes is arbitrary: If we first randomly chose a node i and subsequently randomly chose one of its neighbors j, then i might either adopt the opinion of j or vice versa. The first option defines a so-called *reverse*, the second a so-called *direct update rule*. It is known that both rules result in qualitatively different behavior [16].

In the following we discuss four major contributions to the subject of opinion formation on adaptive networks. Section 9.2.1 focuses on a model by Holme and Newman, which features a continuous spectrum of opinions [12]. Social segregation is modeled through rewiring and social adjustment through a reverse opinion update. The model which will be discussed in Sect. 9.2.2 can be considered as opposite approach: In [6] Gil and Zanette investigate a voter-like model, in which social segregation is modeled through deletion of links. The model by Kozma and Barrat [14], which is discussed in Sect. 9.2.3, again considers the choice between infinitely many opinions. The main difference to [12] is that social segregation and social adjustment are restricted by an additional parameter, which can be interpreted as bounded tolerance. In Sect. 9.2.4 a paper of Nardini et al. is addressed that compares two voter-like models, both of which use identical rewiring rules but differ with respect to the direct/reverse implementation of the asymmetric adjustment process [16].

9.2.1 Continuous Opinions

Holme and Newman were the first to report that the diversity of opinions sustained in a society undergoes a phase transition if the relative rate of social adjustment and social segregation crosses a critical threshold [12]. In their paper, they consider the case of opinions which are in principle unlimited in number. A node n is initially assigned an opinion g_n at random. In each timestep, a node i is randomly chosen and updated in one of two ways: With probability $1-\phi$, i is convinced by one of his neighbors j and g_i is set to equal g_j. With probability ϕ, node i randomly selects one of its links and reconnects it to a node with opinion g_i.

Note that this parameterization in terms of ϕ is advantageous as only the relative rate of the two processes is important. Rescaling the sum of the rates of the two processes to one normalizes the frequency of events to one per update and thus effects an optimization of simulation time. Although this is rarely spelled out this parameterization is indeed an event-driven simulation of the two competing processes following the Gillespie algorithm.

In simulations, the system ultimately approaches a consensus state, in which all individuals in the same connected component hold the same opinion. As mentioned above, there is no objective difference between different opinions. Thus, in analyz-

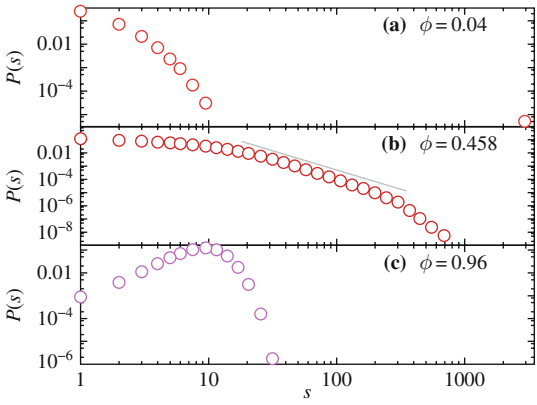

Fig. 9.1 Distribution of community sizes in the consensus state for ϕ below (a), at (b) and above the critical point (c). Numerical data are averaged over 10^4 realizations for each value of ϕ. $N = 3{,}200$, $\bar{k} = 4$. Figure extracted from [12]

ing the consensus state it is not of interest which particular opinions survive, but how many and how the followers are distributed. This information is captured by the component-size distribution P_s.

Figure 9.1 summarizes the dependence of P_s on ϕ. For $\phi = 0$, no connections are rewired, so the component-size distribution of the initial random graph is conserved. In a random graph with mean degree $\langle k \rangle > 1$ there is one giant component of the size $O(N)$ and $O(N)$ small components of size $O(1)$ (see Fig. 9.1a). We therefore find a large majority holding one opinion and many small groups holding different opinions. For $\phi = 1$, opinions never change, so the final cluster-size distribution equals the initial distribution of opinions. In particular the giant component splits into fragments of finite size (see Fig. 9.1c).

Applying a finite-size scaling analysis, Holme and Newman are able to show that a critical parameter value $\phi_c \approx 0.458$ exists, at which a continuous phase transition takes place. At this transition the distribution of followers P_s approaches a power-law (Fig. 9.1b).

The convergence time τ_c needed to reach the consensus state is shown to scale differently in the regimes to both sides of the phase transition. For $\phi = 1$ τ_c scales as N and for $\phi = 0$ as $\log(N)$. For $\phi \approx \phi_c$, τ_c obeys a scaling relation of the form $N^{-\gamma}$ with the critical exponent $\gamma = 0.61 \pm 0.15$ based on numerical simulations.

9.2.2 Two-Valued Choice and Irreversible Discord

The scenario that Gil and Zanette discuss in [6, 24] deviates in two respects from the one investigated above. Firstly, the regarded model is voter-like which means that choices are two-valued. Secondly, disagreeing neighbors break contact irrevocably. Starting from a fully connected network with randomly distributed opinions, conflicts are settled by convincing neighbors or cutting links. As above, rates of both processes are subsumed under one parameter q, which is defined as the probability of opinion transmission.

The dependence of the community-size distribution on q described by Gil and Zanette matches the results of Holme and Newman. Differences in the set-up are solely mirrored by "boundary effects": In the absence of topological evolution the number of opinions in the final state equals the number of initially disconnected communities, which is one in the case under consideration and greater than one in [12]. In the opposite limit, i.e., without contact interactions, the number of disconnected communities in the final state equals the number of initial opinions, which is two in the model of Gil and Zanette and greater than two in that of Holme and Newman. For intermediate values of q (ϕ respectively), the mean of the distribution P_s shifts in both models from smaller to larger s as contact interactions gain influence.

Let us now discuss the underlying mechanisms that lead to the formation of similar community-size distributions in the two different models. In both models, the processes of social adjustment and social segregation occur only on links between disagreeing neighbors, which we therefore call *active links*. The consensus state is reached when all of these active links have vanished. Although segregation is modeled by rewiring in [12] and by cutting links in [6] the effect is in both cases a reduction of active links. Social adjustment results in both models either in an activation or a deactivation of links. Note however, that in voter-like models adjustment reverses the state of all links connecting to the target node. By contrast, in models with continuous opinions, active links connecting to the target node may remain active. Nevertheless, we know that both models eventually reach consensus even without segregation, therefore social adjustment has to decrease the number of active links *in average*.

While the effect of both, adjustment and segregation, is in the long run a reduction of active links, both processes have a different impact on the consensus time τ_c. As we have seen above, consensus through social adjustment requires a convergence time which scales like N. Social segregation significantly accelerates consensus but separates neighbors, whose opinions could in the long term have converged through social adjustment. Thus, increased segregation leads to increased fragmentation, which explains the segregation-rate dependent changes of the distribution P_s as well as their independence of the differences between [12] and [6].

The link-deletion process in the model of Gil and Zanette reveals a phenomenon, which is not obvious in the model of Holme and Newman. Even though the number $\tau_c(q)$ of events necessary to reach consensus decreases with decreasing q, the number of segregation events $(1-q)\tau_c(q)$ depends non-monotonically on q. As shown in Fig. 9.2, a critical parameter value q_{min} exists, at which the fraction r of remaining links in the consensus state is minimized, i.e. at which a maximum number of deletion events occur. This can be understood intuitively: The fraction of remaining links r is minimized if between two subsequent opinion flips the majority of active links is deleted but no consensus communities are isolated. In such a situation an opinion flip almost exclusively activates links, the majority of which will in turn be deleted. If less than the critical number of active links are deleted, the opinion flip not only activates but also inactivates links. These inactive links, unless reactivated later, are not available for deletion, and thus r increases. If on the other hand more than the critical number of active links are deleted, the probability increases that

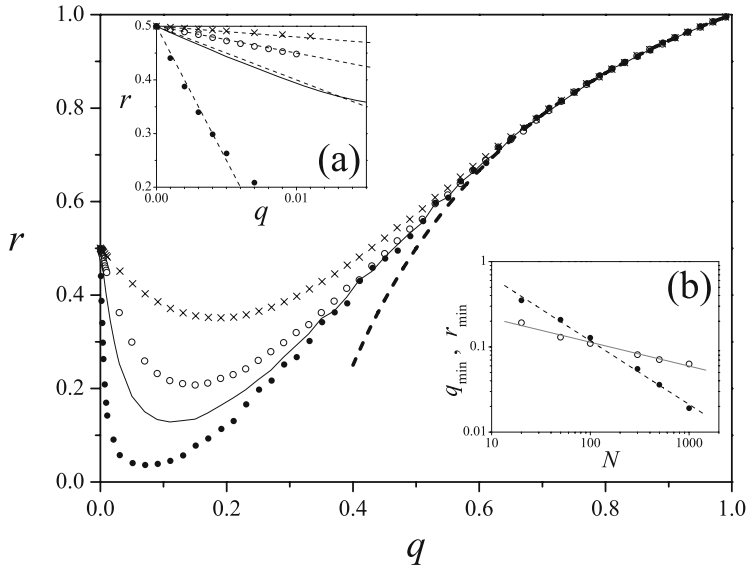

Fig. 9.2 Fraction r of remaining links as a function of the parameter q. Different symbols correspond to different system sizes, $N = 20$ (×), 50 (○), 100 (−) and 500 (•). The *dashed line* represents the analytical approximation for large N. *Inset (a)*: detailed view of the same data for small q. *Inset (b)*: Position q_{min} (○) and depth r_{min} (•) of the minimum of r as a function of N. Figure extracted from [6]

consensus communities are isolated. Internal links of such communities can not be activated in subsequent adjustment events, increasing r.

Based on the similarity of the two compared models, it is arguable whether the critical parameter ϕ_c in [12] corresponds to the same phase transition as q_{min} in [6]. Encouraging in this regard are recent findings of Vazquez et al. that indicate the existence of a generic fragmentation transition for different voter-like models [22]. One may argue that the critical parameter ϕ_c is independent of the system size while q_{min} decreases with growing N (cf. Fig. 9.2b). However, the N-dependence of q_{min} is only a result of the initial conditions chosen in [6]: As the initial graph is fully connected, an opinion-flip event affects $O(N)$ links, whereas a link-deletion event affects one link regardless of the system size. The relative rate of adjustment and segregation events, which minimizes the fraction of remaining links, therefore approaches zero if N goes to infinity.

9.2.3 The Influence of Bounded Tolerance

The influence of tolerance on opinion formation is investigated in [14, 15]. In these papers, Kozma and Barrat consider a scenario where opinions can take continuous values. A global parameter d is introduced describing the tolerance range of individuals. If opinions of neighbors are closer than the tolerance range, i.e., if

$|g_i - g_j| < d$, both adopt the mean opinion with probability $1 - w$. If opinions of neighbors differ more than the tolerance range, i rewires with probability w to a randomly chosen node k.

If defined in this way, bounded tolerance has two different effects: On the one hand it reduces the selectivity of social segregation. On the other hand it enhances selectivity of social adjustment. To illustrate these points let us first consider the effect of bounded tolerance in the absence of segregation. In this case a consensus opinion in a component is only reached if tolerance intervals of neighbors overlap. Otherwise "tolerance patches" may form in which nodes are locally in consensus but do not communicate with nodes outside the patch. In these tolerance patches conflicting opinions can survive indefinitely and thus the equivalence of topological components and consensus communities in the final state is broken. However, to describe the final state we stick with the terminology, which was introduced above, and only adapt the meaning of the term "consensus community" slightly: Used in the present context, it refers to communities of like-minded individuals that are necessarily connected among themselves but not necessarily isolated from individuals of other communities. Kozma and Barrat show that, in the absence of segregation, three parameter regimes can be identified (cf. Fig. 9.3): For large tolerance d, the set-up matches the $\phi = 0$ case in [12]. Consequently, the system reaches a state where nearly all nodes belong to a single community of like-minded individuals. Only when d falls below a critical value $d_c \approx 0.256$, the enhanced selectivity of social adjustment is noticeable. Then, the final state becomes polarized, i.e. two

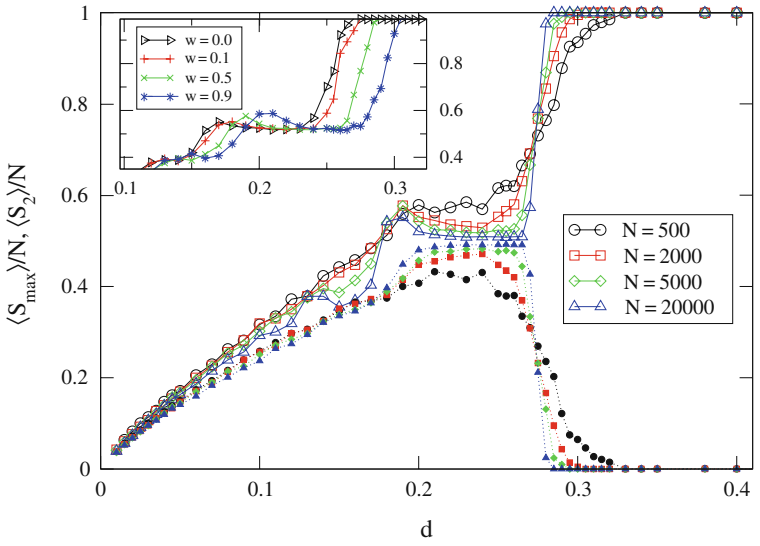

Fig. 9.3 Size of the largest (*open symbols*) and second largest (*filled symbols*) homogeneous opinion cluster as a function of the tolerance d. The color coding for the system size is the same for the largest and second largest cluster. *Inset*: Size of the largest opinion cluster as a function of d for different rewiring rates w. Figure extracted from [14]

macroscopic communities are observed to coexist with a number of finite size communities. Finally, for very small d, an extensive number of small communities form a fragmented final state.

The onset of rewiring is found to have different effects in the different parameter regimes. On the one hand, it impedes complete consensus: the larger the rewiring rate, the larger tolerance values are necessary to reach complete consensus (cf. inset Fig. 9.3). On the other hand, in the fragmented regime, it leads to an enlargement of the consensus-community sizes. This can be explained as follows: For large tolerance, neighbors with overlapping tolerance intervals prevail. Opinions of neighbors that differ more than d are altered through interaction with other neighboring nodes and eventually become closer than d. Hence, the key to the formation of extended communities lies in the possibility of repeated contact interactions. As in the previously studied models, rewiring disconnects communities prematurely and thereby impedes complete consensus. For small tolerance, the limiting factor for the size of consensus communities is the small number of neighbors with overlapping tolerance intervals. In this situation, rewiring allows each node to find those nodes it can communicate with and thus facilitates the merging of small groups.

Indeed, the two different effects of rewiring can also be seen in the model of Holme and Newman. The initial giant component is split due to rewiring. The initial components of finite size, which corresponds to the limit of small tolerance, gain size (cf. Fig. 9.1).

9.2.4 Asymmetric Insertion of Influence

All models presented so far feature asymmetric interactions between a randomly chosen node and a random neighbor. In contrast to a randomly chosen node a random neighbor is not drawn in an unbiased way – it is reached by following a link and therefore nodes with higher degree are preferentially selected as random neighbors. The symmetry of node and neighbor in the rules of the model is in some cases broken by definition of the contact process [6, 12], and in others by the definition of the rewiring mechanism [12, 14]. The effect of the asymmetry of the interactions is studied by Nardini et al. [16] via a mean field analysis. Nardini et al. show that, in case of inhomogeneous networks, the implementation of the asymmetry may decisively influence the behavior of the system. They compare two voter-like models that differ with respect to the asymmetry of the opinion updates. In both models each timestep begins with choosing an individual i and one of its neighbors j at random. If i disagrees with j, it cuts the link and establishes a new link to a randomly chosen node k with probability ϕ. With probability $1-\phi$, one of the two convinces the other of its opinion. The difference in the models lies in the node that is convinced. The first alternative is a reverse voter-like model (rVM), in which i is convinced by j. The second alternative is the direct voter-like model (dVM), in which j is convinced by i.

Simulations show that in both models nodes of the majority opinion have a higher average degree than nodes of the minority opinion. Nodes with high degree, however, are preferentially selected as random neighbors j [1, 17], and hence, the random neighbor j is likely to hold the majority opinion. That is, of two dissenting neighbors, a random node i and its random neighbor j, i probably holds the minority and j the majority opinion. In the rVM the majority opinion reproduces itself as j convinces i. Thus, once a disparity between both opinions emerges it increases. By contrast, in the dVM the majority opinion is repressed as j is convinced by i. Any disparity in the opinion distribution will therefore undergo damping.

In summary, adaptivity generates a positive feedback in case of the rVM impelling the system toward an accelerated consensus. In case of the dVM the generated feedback is negative resulting in a dynamical state where both opinions are in average equally represented. For the parameter values chosen in the paper no consensus is reached in the latter case. Nevertheless, small networks fluctuations may still take the system eventually to an absorbing state in which one opinion vanishes. The different routes to consensus are reflected in the specific convergence time $\tau_c(N)$ observed in numerical simulations (see Fig. 9.4). For the rVM, τ_c displays a logarithmic scaling behavior $\tau_c(N) \propto \ln(N)$ while for the dVM, $\tau_c(N)$ grows exponentially with the system size.

Remarkably, the qualitative differences between the dVM and the rVM are settled if an additional neutral state is introduced, which is the case in the so-called naming game. In this scenario, change of opinion is impeded in the sense that individuals have to pass a transient state before defecting to the opposite view. As long as an individual is in this state, it is accessible for convincing attempts from representatives of both opinions. To model the naming game Nardini et al. choose the following implementation: The competing opinions are assigned with the values $+1$ and -1 and the additional neutral state is denoted by 0. Contact interactions between disagreeing neighbors alter the state of the passive node by ± 1, whereby the sign depends on the state of the active node. If the active individual is in the neutral state, it chooses to represent one of the opinions $+1$ or -1 at random. In analogy to the

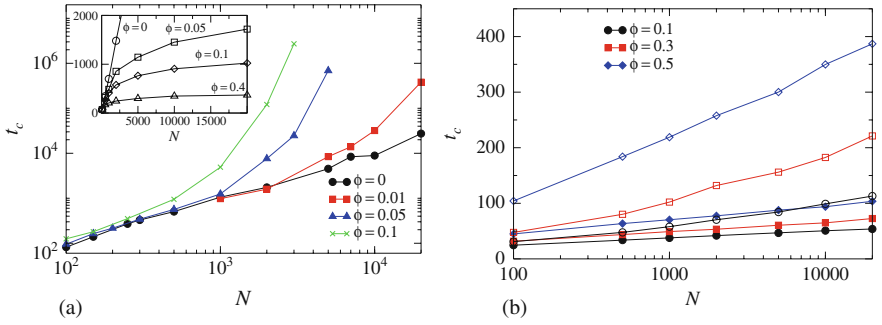

Fig. 9.4 (**a**) Convergence time for the reverse voter-like model as a function of the system size for various rewiring rates. *Inset*: same for the direct voter-like model. (**b**) Convergence time for the direct (*filled symbols*) and reverse naming game. For each parameter set, data are averaged over 100 realizations of the system. Figure extracted from [16]

direct and reverse voter-like models, a distinction can be made between the direct and reverse naming game depending on whether the random node or the random neighbor takes the active part.

On a static network the consensus time τ_c in naming games is known to scale like $\ln(N)$. Simulations yield that in the adaptive case $\tau_c(N)$ remains logarithmic irrespective of the chosen modality of asymmetric opinion update (cf. Fig. 9.4b). This deviation from the behavior of voter-like models is elegantly explained by Nardini et al.: Interactions via links between followers of the competing opinions comply with the dynamics of the dVM (rVM respectively) and exhibit the characteristic negative (resp. positive) dynamical feedback. However, interactions with neutral nodes exert a positive feedback regardless of whether the direct or reverse rule is used. As links to neutral nodes are far more common than links to nodes of the opposing opinion, these links dominate the behavior and hence in total a positive feedback is observed.

9.2.5 Other Approaches

A slightly different setup for the contact process is explored by Benczik et al. [2], Grabowski and Kosiński [7] and Erhardt et al. [4]. Instead of occasional interactions between two randomly chosen neighbors, they consider situations where a node is updated by evaluation of all influences from its entire neighborhood. All three models capture various additional properties. Thus, besides internal state dynamics Ehrhardt et al. include adjustable link creation and removal processes as well as sophisticated partner selection mechanisms. Equally elaborated are the topological evolution rules Grabowski and Kosiński use: the idea of bounded tolerance is combined with a set of parameters that model individually distinct sociability. Furthermore, some links, which represent basic connections like family ties, are excluded from the topological changes. Finally, Benczik et al. investigate a topological evolution rule in which a continuous parameter captures the individuals' tendency to rather avoid or seek contact with dissenting individuals. For more details we refer to the original publications.

An interesting enhancement of the concept of bounded tolerance is discussed in [5]. In this paper, Gargiulo and Mazzoni replace the global tolerance parameter d by state dependent tolerance. The underlying hypothesis is that in realistic systems tolerance decreases if opinions get extreme. Regrettably, the approach is so far only explored in simulations in which tolerance-dependent segregation and tolerance-dependent adjustment occur in consecutive temporal phases of the evolution. So, an exploration in the context of adaptive networks remains to be done.

9.3 Epidemic Spreading and Moment Closure

Subsequently, we focus on models of epidemic spreading, the second intensively studied topic in the class of contact processes. Though both, models of epidemic spreading and models of opinion formation, base on the concept of locally

transmitted properties, epidemiological models are essentially distinguished from those discussed in Sect. 9.2. In epidemiological models, different single node states signify different stages of a disease. This interpretation imposes far-reaching restrictions on the processes modeling the transitions between the states. Construing states as stages of a disease directly attaches a meaning to the transitions between states. Thus, transitions can only occur between appointed states, which reminds of the naming game but differs from the scenario reviewed in Sect. 9.2.1. Moreover, the asymmetry of the contact process is determined by the qualitative differences of the states: Via a link between an infected and a healthy individual, only the infected state can be spread. This is contrary to models of opinion formation where the asymmetry of the convincing act was implemented arbitrarily. Hence, for each state in an epidemiological model we have to formulate specific processes that govern transitions to and from this state. In practice, the transmission of the disease is the only real contact process, while all other processes describe the subsequent progression through epidemic stages which happen only locally.

While models of opinion formation were shown to vary with respect to the implementation of asymmetry, the number of states, and the topological evolution rules, models of epidemic spreading do not exhibit any variations with respect to the implementation of asymmetry. Variations in the number of single-node states are impeded as the introduction of new states necessitates the introduction of new processes. Variations of the topological evolution rules are discussed, however to a minor extend.

The substantial coherence among different adaptive-network models of epidemiological processes allows us to focus exemplarily on the adaptive SIS-model, which features only two states called S, for susceptible, and I, for infected. By means of this simple model, we illustrate the conceptual and methodical framework likewise applying for more complicated scenarios (Sect. 9.3.1). In particular, we demonstrate the use and handling of *moment-closure approximations*, a common tool in epidemiology [13, 18, 19]. Section 9.3.2 launches variations and extensions of the basic SIS model, that aim for more realism [21, 23, 25].

9.3.1 The Adaptive SIS Model

The simplest model, in which epidemic dynamics and topological evolution can be combined is the SIS model. It describes a scenario in which each individual within a social network is either susceptible (S) to the disease under consideration or infected (I). Contacts between individuals are denoted as SS-links, SI-links, and II-links according to the states of the individuals they connect. Susceptible individuals can become infected if they are in contact with an infected individual. The transmission of the disease along a given SI-link is assumed to occur at a rate p. Once an individual has been infected she has a chance to recover, which happens at a rate r and immediately returns the individual to the susceptible state. In the adaptive SIS model proposed by Gross et al. [11] another process completes the circle of infection and

recovery: If a susceptible individual is connected to an infected individual she may want to break the link and instead establish a new link to another susceptible. On a given SI-link this rewiring occurs at a rate w.

Note that the rewiring process has been introduced "optimistically": Only susceptible nodes rewire, and they manage unerringly to rewire to a node that is also susceptible. Under these conditions rewiring always reduces the number of links that are accessible for epidemic spreading and therefore the *prevalence* of the disease, i.e., the density of infected, is always reduced by this form of rewiring behavior. Less optimistic rewiring rules have been explored by Zanette [23], and Zanette and Risau-Gusmán [20, 25] and will be addressed in Sect. 9.3.2.

Let us now study the dynamics of the adaptive SIS model with the tools of nonlinear dynamics. For this purpose we need to derive a low-dimensional emergent-level description of the system. Convenient observables, so-called moments, are given through the densities of certain subgraphs. The number of links contained in such a subgraph is called the order of the respective moment. Dynamical properties of the moments, averaged over many realizations of the stochastic process, can be summarized in a system of ODEs. Due to the contact process, however, dynamics of moments of order n essentially depend on moments of order $n+1$, resulting in an infinite cascade of differential equations. Its truncation necessitates an approximation of higher order moments in terms of lower order moments, the so-called moment closure approximation.

Below, we will derive an emergent-level description of the adaptive SIS model using moment closure approximation. In the SIS model, the moments of zeroth order are the densities of infected and susceptibles, $[I]$ and $[S]$. First order moments are the per-capita densities of SS-, SI- and II-links, $[SS]$, $[SI]$ and $[II]$, and second order moments the densities of triplets $[ABC]$ with a given sequence of states $A, B, C \in \{I, S\}$. Due to the conservation relations $S + I = 1$ and $[SS] + [SI] + [II] = \langle k \rangle$ the dynamics of the zeroth and first order moments are entirely captured by the balance equations for $[I]$, $[SS]$, and $[II]$. A further advantage of the normalization relations is that we can write all subsequent equations as if we were dealing with a number of individual nodes and links instead of densities.

Let us start by writing a balance equation for the density of infected nodes. Infection events occur at the rate $p[SI]$ increasing the number of infected nodes by one; Recovery events occur at a rate $r[I]$ and reduce the number of infected nodes by one. This leads to

$$\frac{\mathrm{d}}{\mathrm{dt}}[I] = p[SI] - r[I]. \tag{9.1}$$

The equation contains the (presently unknown) variable $[SI]$ and therefore does not yet constitute a closed model. One way to close the model were a mean field approximation, in which the density of SI-Links is approximated by $[SI] \approx \langle k \rangle [S][I]$. However, in the present case this procedure is not feasible: Rewiring does not alter the number of infected and hence does not show up in Eq. (9.1). Thus the mean-field approximation is not able to capture the effect of rewiring. Instead, we will

treat $[SI]$, $[SS]$, and $[II]$ as dynamical variables and capture their dynamics by additional balance equations. This approach is often called moment expansion as the link densities can be thought of as the first moments of the network.

As stated above, it suffices to derive balance equations for the densities of SS- and II-links. The density of SI-links can then be obtained from the conservation relation. First the II-links: A recovery event can destroys II-links if the recovering node was part of such links. The expected number of II-links in which a given infected node is involved is $2[II]/[I]$. (Here, the two appears since a single II-link connects to two infected nodes.) Taking the rate of recovery events into account, the total rate at which II-links are destroyed is simply $2r[II]$.

To derive the rate at which II-links are created is only slightly more involved. In an infection event the infection spreads across a link, converting the respective link into an II-link. Therefore every infection event will create at least one II-link. However, additional II-links may be created if the newly infected node has other infected neighbors in addition to the infecting node. In this case the newly infected node was previously the susceptible node in one or more ISI-triplets. Thus, we can write the number of II-links that are created in an infection event as $1+[ISI]/[SI]$. In this expression the "1" represents the link over which the infection spreads while the second term counts the number of ISI-triplets that run through this link. Given this relation we can write the total rate at which II-links are created as $p[SI](1 + [ISI]/[SI]) = p([SI] + [ISI])$.

Now the SS-links: Following a similar reasoning as above we find that infection destroys SS-links at the rate $p[SSI]$. Likewise SS-links are created by recovery at the rate $r[SI]$. In addition SS-links can also be created by rewiring of SI-links. Since rewiring events occur at a rate $w[SI]$ and every rewiring event gives rise to exactly one SS-link the total rate at which rewiring creates SS-links is simply $w[SI]$.

Summing all the terms, the dynamics of the first moments can be described by the balance equations

$$\frac{\mathrm{d}}{\mathrm{dt}}[SS] = (r + w)[SI] - p[SSI] \tag{9.2}$$

$$\frac{\mathrm{d}}{\mathrm{dt}}[II] = p([SI] + [ISI]) - 2r[II]. \tag{9.3}$$

Again, these equations do not yet constitute a closed model, but depend on the unknown second moments $[SSI]$ and $[ISI]$. However, the first order-moment expansion captures the effect of rewiring. While we will return to the equation above later, a feasible way of closing the system is to approximate the second moments by a mean-field-like approximation: the *pair approximation*.

Let us start by approximating $[ISI]$. One half of the ISI-triplet is actually an SI-link, which we know occurs at the density $[SI]$. In order to approximate the number of ISI-triplets running through a given link we have to calculate the expectation value of the number of *additional* infected nodes that are connected to the susceptible node. For this purpose let us assume that the susceptible node of the given SI-link has an expected number of $\langle q \rangle$ links in addition to the one that is

already occupied in the SI-link. Every one of these links is an SI-link with probability $[SI]/(\langle k\rangle S)$. (Here, we have neglected the fact that we have already used up one of the total number of SI-links. This assumption is good if the number of SI-links is reasonably large.) Taking the density of SI-links and the probability that they connect to additional SI-links into account we obtain

$$[ISI] = \kappa \frac{[SI]^2}{[S]} \tag{9.4}$$

where $\kappa = \langle q\rangle/\langle k\rangle$ remains to be determined. The quantity $\langle q\rangle$ that appears in κ is the so-called *mean excess degree*. Precisely speaking it denotes the expected number of additional links that are found by following a random link.

Subsequently we will assume that $\kappa = 1$. This assumption is substantiated in the reasoning of [8]. Here, we only state that it allows us to approximate the density of triplets by $[ISI] = [SI]^2/S$, and following a similar argumentation $[SSI] = 2[SS][SI]/[S]$. Substituting these relations into the balance equations we obtain a closed system of differential equations

$$\frac{\mathrm{d}}{\mathrm{dt}}[I] = p[SI] - r[I] \tag{9.5}$$

$$\frac{\mathrm{d}}{\mathrm{dt}}[SS] = (r+w)[SI] - 2p[SI]\frac{[SS]}{[S]} \tag{9.6}$$

$$\frac{\mathrm{d}}{\mathrm{dt}}[II] = p[SI]\Big(1 + \frac{[SI]}{[S]}\Big) - 2r[II]. \tag{9.7}$$

The system of differential equations can now be studied with the tools of dynamical systems theory. Gross et al. compare the analytical results thus obtained with detailed-level simulations of the full model and find both in very good agreement [11]. This indicates a high accuracy of the emergent-level description (9.5), (9.6), and (9.7).

In contrast to the models of opinion formation, which have been discussed in Sect. 9.2, the adaptive SIS model features three instead of two processes. Therefore the dynamics in the SIS-model depends on two free parameters. Figure 9.5 shows the two parameter bifurcation diagram which results from the analysis of Eqs. (9.5), (9.6), and (9.7). In the white and light gray regions there is only a single attractor, which is a healthy state in the white region and an endemic state in the light gray region. In the medium gray region both of these states are stable. Another smaller region of bistability is shown in dark gray. Here, a stable healthy state coexists with a stable epidemic cycle. The transition lines between these regions correspond to saddle-node (dashed), Hopf (continuous), and cycle fold (dotted) bifurcations. The dash-dotted line marks a transcritical bifurcation that corresponds to the threshold at which epidemics can invade the disease free system.

Although the SIS-model, at first glance, differs strongly from the models of opinion formation, some interesting parallels appear. As in the models of opinion formation high rewiring rates break the network into “consensus” communities in

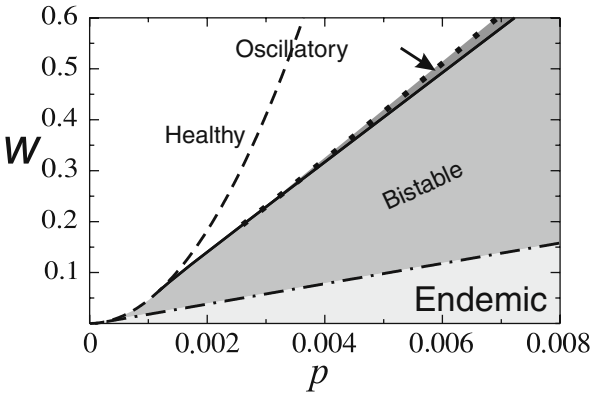

Fig. 9.5 Two parameter bifurcation diagram showing the dependence on the rewiring rate w and the infection probability p at fixed recovery rate $r = 0.002$. Figure extracted from [11]

which all nodes are either susceptible or infected. In this way the contact process, infection, is impeded. This is for instance reflected in a strong increase of the invasion threshold (dash-dotted) with increasing rewiring rate. However, in contrast to the models of opinion formation, the dynamics does not freeze in the consensus state as recovery can still take place.

Another feature of the epidemic model that is not observed in the models of opinion formation is the bistable region. In this region an established epidemic can survive at high prevalence, while epidemics cannot invade a disease-free network. This region appears since the disease suppressing effect of segregation becomes weaker at high prevalence: In contrast to opinion formation models in which both opinions are treated equally, a small community of infected can be more easily isolated than a small community of susceptibles. This asymmetry arises as the links are always rewired into the susceptible community, which is irrelevant if the susceptibles are in the majority, but leads to a sharp rise in the connectivity of susceptibles if they are in the minority. However, high connectivity of susceptibles speeds up the infection process which competes with segregation. Under certain conditions the competition of the two effects can lead to oscillatory dynamics. Both the appearance of bistability and oscillations can therefore be linked directly to the explicit asymmetry that is introduced in the epidemic model.

9.3.2 Other Approaches

Variants of the adaptive SIS model, in which not only susceptible but also infected individuals may rewire their links, have been explored by Zanette and Risau-Gusmán [20, 25]. In these works, the authors prove that rewiring remains advantageous for suppressing the disease even if the isolation of infected agents is modeled to be less effective than in [11].

In [10] Gross and Kevrekidis consider an adaptive SIS model in which the effectivity of rewiring increases with increasing prevalence of the disease. In this case

oscillations can be observed in a much larger parameter range and with significantly increased amplitude.

Models with additional epidemic states have been studied by Shaw and Schwartz [21] and Risau-Gusmán and Zanette [20]. Moreover, Shaw and Schwartz also investigate the effect of noise on the system. This work is reviewed in the subsequent chapter.

9.4 Summary and Outlook

In this chapter, we have reviewed a selection of recent papers concerned with opinion formation and epidemic spreading on adaptive networks.

Comparing the reviewed approaches, we have focused on three major aspects in which models differ: First the number of single-node states a model captures, second the topological evolution rules, and third the way in which the symmetry of interactions is broken. In models of opinion formation, differences in the most subtle aspect, namely the direct or reverse implementation of the opinion update, have crucial impact on the system's behavior. By contrast differences in the two other aspects lead only to minor changes.

In models of epidemic spreading, the asymmetry of interaction is inherent in the modeled situation and can therefore not be modified. We have argued that this intrinsic asymmetry is directly linked to the appearence of bistability and oscillations observed in the epidemic model.

In all reviewed models, rewiring or cutting links lead to the formation of state-homogeneous subpopulations, providing an example for the appearance of global structure from local rules. The subpopulations exhibit different degree distributions if the rewiring rule is sensitive to differences between states, either externally imposed as in the epidemic model, or self-organized as in the models of opinion formation.

The coupling of state-specific degree distributions and asymmetric exertion of influence can stabilize the system in a state in which two states survive at finite density. This can be observed both in the direct voter model and in the adaptive SIS model. In the latter case the dynamics go on indefinitely as no absorbing state can be reached at finite density of infected because of the local processes, i.e. recovery.

A central theme of this book, which appears clearly in this chapter, is that in the investigation of adaptive networks common themes are frequently found in models from very different backgrounds. This shows that adaptive networks, which have emerged from many different disciplines almost at the same time, start to grow together. Certainly more investigations are necessary, but the goal of a unifying theory of adaptive networks, is slowly emerging. In the future steps toward this goal, analytical approximations such as the moment closure approximation described here, will be of central importance, as they allow for a rigorous mathematical treatment and generalization of the observed phenomena.

References

1. Albert, R., Barabàsi, A.: Statistical mechanics of complex networks. Rev. Mod. Phys. **74**(1), 1–54 (2002)
2. Benczik, I.J., Benczik, S.Z., Schmittmann, B., Zia, R.K.P.: Lack of consensus in social systems. Euro. Phys. Lett. **82** 480061–5 (2008)
3. Durrett, R., Levin, S.A.: Stochastic spatial models: A user's guide to ecological applications. Philos. T. R. Soc. B **343**, 329–50 (1994)
4. Ehrhardt, G.C.M.A., Marsili, M., Vega-Redondo, F.: Phenomenological models of socioeconomic network dynamics. Phys. Rev. E **74**, 0361061–11 (2006)
5. Gargiulo, F., Mazzoni, A.: Can extremism guarantee pluralism? arXiv:0803.3879 (2008)
6. Gil, S., Zanette, D.H.: Coevolution of agents and networks: Opinion spreading and community disconnection. Phys. Lett. A **356**, 89–95 (2006)
7. Grabowsi, A., Kosiński, R.A.: Evolution of a social network: The role of cultural diversity. Phys. Rev. E **73**, 0161351–7 (2006)
8. Gross, T.: The interplay of network state and topology in epidemic dynamics. In: Boccaletti, S., Latora, V., Moreno, Y. (Eds.) Handbook of Biological Networks. World Scientific, Singapore, to appear in 2009
9. Gross, T., Blasius, B.: Adaptive coevolutionary networks – A review. JRS Interface **5**, 259–71 (2008)
10. Gross, T., Kevrekidis, I.G.: Coarse-graining adaptive coevolutionary network dynamics via automated moment closure. Europhys. Lett. **82**, 380041–6 (2008)
11. Gross, T., Dommar D'Lima, C., Blasius B.: Epidemic dynamics on an adaptive network. Phys. Rev. Lett. **96**, 208701–4 (2006)
12. Holme, P., Newman, M.E.J.: Nonequilibrium phase transition in the coevolution of networks and opinions. Phys. Rev. E **74**, 0561081–5 (2007)
13. Keeling, M.J., Rand, D.A., Morris, A.: Dyad models for childhood epidemics. Proc. R. Soc. B **264**, 1149–56 (1997)
14. Kozma, B., Barrat, A.: Consensus formation on adaptive networks. Phys. Rev. E **77**, 0161021–10 (2008)
15. Kozma, B., Barrat, A.: Consensus formation on coevolving networks: groups' formation and structure. J. Phys. A **41**, 2240201–8 (2008)
16. Nardini, C., Kozma, B., Barrat, A.: Who's talking first? Consensus or lack thereof in coevolving opinion formation models. Phys. Rev. Lett. **100**, 1587011–4 (2008)
17. Newman, M.E.J.: The structure and function of complex networks. SIAM Rev. **45**(2), 167–256 (2003)
18. Parham, P.E., Singh, B.K., Ferguson, N.M.: Analytical approximation of spatial epidemic models of foot and mouth disease. Theor. Popul. Bio. **73**, 349–68 (2008)
19. Peyrard, N., Dieckmann, U., Franc, A.: Long-range correlations improve understanding of the influence of network structure on contact dynamics. Theor. Popul. Bio. **73**, 383–94 (2008)
20. Risau-Gusmán , S., Zanette, D.H.: Contact switching as a control strategy for epidemic outbreaks. arXiv:0806.1872 (2008)
21. Shaw, L.B., Schwartz, I.B.: Fluctuating epidemics on adaptive networks. Phys. Rev. E **77**, 0661011–10 (2008)
22. Vazquez, F., Eguíluz, V.M., San Miguel, M.: Generic absorbing transition in coevolution dynamics. Phys. Rev. Lett. **100**, 1087021–4 (2008)
23. Zanette, D.H.: Coevolution of agents and networks in an epidemiological model. arXiv:0707.1249 (2007)
24. Zanette, D.H., Gil, S.: Opinion spreading and agent segregation on evolving networks. Physica D **224**, 156–65 (2006)
25. Zanette, D.H., Risau-Gusmán , S.: Infection spreading in a population with evolving contacts. J. Biol. Phys. (2008) doi: 10.1007/s1086700890609

Chapter 10
Noise Induced Dynamics in Adaptive Networks with Applications to Epidemiology

Leah B. Shaw and Ira B. Schwartz

Abstract Recent work in modeling the coupling between disease dynamics and dynamic social network geometry has led to the examination of how human interactions force a rewiring of connections in a population. Rewiring of the network may be considered an adaptive response to social forces due to disease spread, which in turn feeds back to the disease dynamics. Such epidemic models, called adaptive networks, have led to new dynamical instabilities along with the creation of multiple attracting states. The co-existence of several attractors is sensitive to internal and external fluctuations, which lead to enhanced stochastic oscillatory outbreaks and disease extinction. The aim of this chapter is to explore the bifurcations of adaptive network models in the presence of fluctuations and to review some of the new fluctuation phenomena induced in adaptive networks.

10.1 Introduction

In recent years, researchers have used a network approach in studying many systems, from networks of social contacts to the US power grid to the world wide web [3], and a wide variety of mathematical tools have been developed to analyze static networks [8, 26]. However, many natural systems are more complex than static network models. Both the properties of individuals (e.g., neurons, humans) and the connections between them change over time. Examples of networks where the links evolve dynamically occur in simple two state models, such as two player game theory [27, 30] and opinion dynamics [12, 32], as we will describe below.

Static network models fail to capture systems in which dynamical properties are important. A new class of models, adaptive networks, has been introduced recently to address more fully the complexity of many physical systems [18]. In an adaptive network, the network geometry changes dynamically in response to the node characteristics, and these changes in geometry then alter the subsequent dynamics of the nodes.

L.B. Shaw (✉)
Department of Applied Science, College of William and Mary, Williamsburg, VA 23187, USA
e-mail: lbshaw@wm.edu

T. Gross, H. Sayama (eds.), *Adaptive Networks,* Understanding Complex Systems,
DOI 10.1007/978-3-642-01284-6_10,

Many studies of adaptive networks have focused on steady state behavior, and rich new phenomena have been discovered in that context. However, the key aspect of an adaptive network is the interplay of node dynamics and network topology, which generally means that the nodes and links are evolving in time even if a steady state is reached. (Exceptions are cases where the network is evolved to a frozen state, as in, for example, [4, 14].) In this chapter, we consider the role of fluctuations in adaptive network models.

One property that frequently occurs in adaptive networks is self organized criticality, a topic that is discussed in more detail in the chapters of Rohlf and Bornholdt and of Caldarelli and Garlaschelli. Because each node in the network receives dynamical information that depends on the connectivity of the entire network, this can provide global information to individual nodes and cause the system to organize itself. As a result, criticality and scale free behavior are often observed. In the first adaptive network model, that of Christensen et al., adding and removing links to match a node's degree to the local average connectivity led to the network self organizing to a critical average connectivity, with a power law distribution of cluster sizes [7]. In a model by Bornholdt and Röhl motivated by neural networks, the network again organized to a critical average connectivity, balancing the addition of new links when nodes are correlated and the removal of links when nodes are uncorrelated [5]. Fan and Chen studied a growing network of chaotic maps, in which new nodes were linked to the most active previous nodes, and obtained scale free degree distributions [13]. Zhou and Kurths also obtained scale free distributions of connection weights for a network of chaotic oscillators in which the weights were evolved to increase synchrony [34]. Extensions to the latter two models are described in the chapter by Chen and Kurths.

None of the above-mentioned studies looked at fluctuations, but scale free effects on fluctuations have been observed previously. Bornholdt and Sneppen studied an evolving Boolean network, representing a genetic network, in which neutral mutations of the couplings, those that do not affect the network attractor, accumulate over time [6]. The average connectivity of the network was monitored, and long periods of stasis in connectivity were interrupted by bursts of connectivity change. The stasis times followed a scale free distribution. In a model for an evolving network of chemical species, in which species that do not multiply as quickly are replaced by new random species, Jain and Krishna observed similar fluctuations in the number of populated species [25]. In the long time limit, all species are usually populated, but this value is punctuated by drop-out times due to the disruption of autocatalytic sets. Jain and Krishna did not do a statistical analysis of this effect, but their time series are reminiscent of punctuated equilibria.

In evolutionary game theory models with perturbations, scale free distributions have been observed for the sizes of avalanches (number of nodes involved) as the system moves between stationary states (e.g., [11, 28]). A model by Holme and Ghoshal for nodes that rewire the network to maximize their social influence and change their rewiring strategies adaptively also displayed avalanches in strategy changes, but statistics were not collected on the scaling of the avalanche size [20].

The degrees and cluster sizes in this model also fluctuated significantly. This model is discussed in detail in the chapter by Holme and Ghoshal.

Another effect that is observed in adaptive network models for opinion formation in social networks is the existence of metastable states. Ehrhardt and Marsili studied a model in which new links were generated preferentially between nodes with a similar "opinion" or property, and the opinions were influenced by neighbor nodes [12]. In the limit where the nodes were at zero temperature (but links were added and removed stochastically), the system eventually approached one large connected component with uniform opinion, but it spent time in metastable states with multiple components, each with different opinion. The lifetimes of the metastable states could be understood analytically through an exact solution and stability analysis of the zero temperature case.

Holme and Newman developed a model for opinion dynamics in which a parameter governed the relative frequencies of rewiring to new neighbors with identical opinions versus convincing one's neighbors to share one's opinion [21]. The system evolved to a frozen state containing one or more communities, where the number of communities depended on whether the parameter favored convincing or rewiring. The parameter controlled a continuous phase transition, and at the critical value the system exhibited a power law distribution in community sizes and large fluctuations in the time required to converge to the final state. The nature of the phase transition was further explained analytically by Vazquez et al. for a simpler model with only two opinion states [31]. A variety of models of opinion formation are described in detail in the chapter by Do and Gross.

Other adaptive network models have considered synchrony of a network of coupled oscillators while adjusting the network connections adaptively [15, 16, 23, 24, 34]. Gong and Leeuwen studied networks of coupled chaotic maps and added connections between correlated oscillators [16]. They found that the system formed a small world network with intermittent switching in the number of coherent clusters. Ito and Kaneko studied weighted networks of coupled maps and also strengthened the coupling between correlated oscillators [23, 24]. Here they considered in detail the role of the feedback mechanism between node and network dynamics. The model is also discussed in the chapter by Ito and Kaneko. They computed average weight matrices to determine whether there were stable structures in the network and found several phases, including a phase that was desynchronized but had a temporarily stable network structure, and a desynchronized phase with a disordered, rapidly changing network structure [24]. In the disordered network structure, the degree of individual nodes changed almost randomly. However, in the networks with temporarily stable structure, the nodes separated into two groups, controllers with high outdegree and others with low outdegree. The group in which a given node resided remained relatively stable over time. The node dynamics in the desynchronized phase was characterized by hopping between two groups whose dynamics were a half cycle out of phase from each other. In a feedback loop between the network geometry and node dynamics, nodes that hopped more slowly between groups tended to accumulate more connections, which led to further slowing of the

hopping rate. This feedback loop was responsible for the splitting of the nodes into high outdegree and low outdegree groups.

Effects such as self organized criticality, metastable states, and fluctuations in synchrony have been observed in adaptive networks. Thus far, these effects have mainly been quantified through simple network metrics such as time series of the average connectivity or clustering coefficient, or the average node properties may be tracked over time as will be discussed later in this chapter. When the network forms distinct clusters, tracking the number of clusters is also an option. However, higher order network structures are often difficult to track in a time-varying network, and it is not yet clear what are the key network properties to measure for an adaptive network. Also, in many cases the effects that have been observed have not yet been explained analytically. Further study of the fluctuations in adaptive networks is needed.

In this chapter, we focus on fluctuations in a model for an epidemic spreading on an adaptive network. Epidemics have been briefly mentioned in the previous chapter. Some of the results in the present chapter have been published elsewhere [29]. The layout of the paper is as follows: We describe the model and summarize key aspects of its bifurcation structure in Sects. 10.2 and 10.3. Many properties can be predicted from a much lower dimensional mean field model. In Sect. 10.4, we focus particularly on fluctuations in the number of infection cases in the system, which is a physically important quantity. We present some additional results for phase relationships between node and link variables and for scaling of the epidemic lifetime in Sects. 10.5 and 10.6. The dynamic network structure is more difficult to capture, but in Sect. 10.7 we discuss fluctuations in the degree of individual nodes in the system.

10.2 Model

Gross et al. have introduced a susceptible-infected-susceptible (SIS) model on an adaptive network [19], and Zanette and Gusmán have also studied an SIS model on an adaptive network [33]. We have extended this work to a susceptible-infected-recovered-susceptible (SIRS) model [29]. Although we have not chosen parameters corresponding to a particular real disease, tuning the average time a node spends in the recovered class allows us to adjust the average number of infections at the endemic steady state. Although some diseases in the past, such as plague, have eliminated as much as 50% of a worldwide population, many infectious viral diseases, such as measles, mumps, and rubella, infect only 10% or less of a population at a given time [1], depending on epidemiological and social factors. Noise effects are expected to be especially prominent when the infection occurs at low levels. However, in this particular study, we restrict our attention to cases where the minimum endemic steady states are on the order of 10–40% of the population.

Our model is constructed as an extension to that of Gross et al. [19] but includes the addition of a recovered class. The rate for a susceptible node to become infected is $pN_{I,\mathrm{nbr}}$, where $N_{I,\mathrm{nbr}}$ is the number of infected neighbors the node has. The

recovery rate for an infected node is r. We fix $r = 0.002$ throughout this chapter. A recovered node becomes susceptible again with rate q, the resusceptibility rate.

Since the mean time spent in the recovered state is $1/q$, there is a natural limiting case for the SIRS model. Using the recovery rate, r, as a natural time scale, as the ratio q/r becomes sufficiently large, nodes spend less time in the recovered state. In the limit $q/r \to \infty$, the model thus approaches the SIS model. The study of the stochastic dynamics of the SIRS model may then be examined with respect to changes in q.

Rewiring of the network occurs as the epidemic spreads. If a link connects an infected node to a non-infected node, the link is rewired with rate w. The connection to the infected node is broken, and the original non-infected node is now connected to another non-infected node which is randomly selected out of all candidates in the network (excluding self links and multiple links between nodes). This rewiring rule is that of Gross et al. [19] (we treat the recovered nodes in the same manner as susceptibles for rewiring purposes), in contrast to the rewiring scheme of Zanette and Gusmán [33], which allows susceptible nodes to connect to infectives.

We performed Monte Carlo simulations of this model for a system with N nodes and K links, where K/N was fixed at 10. Details of the simulation procedure can be found in [29]. Random sequential updating was used, and each node and eligible link had an opportunity to transition on average once per Monte Carlo step (MCS).

As in [19], we developed a corresponding mean field model using a moment closure approximation to track the dynamics of nodes and links. P_A denotes the probability for a node to be in state A, and P_{AB} denotes the probability for a link to connect a node in state A to a node in state B. For higher order correlations, we assume $P_{ABC} \approx P_{AB}P_{BC}/P_B$. The time evolution of the node states is described by:

$$\dot{P}_S = q\,P_R - p\tfrac{K}{N}P_{SI} \tag{10.1}$$

$$\dot{P}_I = p\tfrac{K}{N}P_{SI} - r\,P_I \tag{10.2}$$

$$\dot{P}_R = r\,P_I - q\,P_R \tag{10.3}$$

The time evolution of the links is described by:

$$\dot{P}_{SS} = q\,P_{SR} + w\tfrac{P_S}{P_S+P_R}P_{SI} - 2p\tfrac{K}{N}\tfrac{P_{SS}P_{SI}}{P_S} \tag{10.4}$$

$$\begin{aligned}\dot{P}_{SI} = {} & 2p\tfrac{K}{N}\tfrac{P_{SS}P_{SI}}{P_S} + q\,P_{IR} - r\,P_{SI} - w\,P_{SI} \\ & -p\left(P_{SI} + \tfrac{K}{N}\tfrac{P_{SI}^2}{P_S}\right)\end{aligned} \tag{10.5}$$

$$\dot{P}_{II} = p\left(P_{SI} + \tfrac{K}{N}\tfrac{P_{SI}^2}{P_S}\right) - 2r\,P_{II} \tag{10.6}$$

$$\begin{aligned}\dot{P}_{SR} = {} & r\,P_{SI} + w\tfrac{P_R}{P_S+P_R}P_{SI} + 2q\,P_{RR} - q\,P_{SR} \\ & -p\tfrac{K}{N}\tfrac{P_{SI}P_{SR}}{P_S} + w\tfrac{P_S}{P_S+P_R}P_{IR}\end{aligned} \tag{10.7}$$

$$\dot{P}_{IR} = 2r P_{II} + p\frac{K}{N}\frac{P_{SI}P_{SR}}{P_S} - q P_{IR} - r P_{IR} - w P_{IR} \tag{10.8}$$

$$\dot{P}_{RR} = r P_{IR} - 2q P_{RR} + w\frac{P_R}{P_S+P_R} P_{IR} \tag{10.9}$$

We integrated the mean field equations numerically and tracked their steady states using a continuation package [9]. We have also considered a stochastic mean field system with internal fluctuations, modeled by multiplicative noise, or with external fluctuations, modeled by additive noise. The stochastic mean field system was studied using a fourth order Runge-Kutta solver.

10.3 Bifurcation Structure

In [29], we considered the bifurcation structure of the mean field for q small and mapped the regions of stability for infectives as a functions of the parameters w and p. We discovered and reported that there were regions of q in which different bifurcation scenarios existed, as well as regions of bistability. In the first case, the value of $q = 0.0064$, the disease free equilibrium became unstable as the infection rate p was increased, and through a transcritical bifurcation was connected to the unstable branch of endemic states. A stable branch of endemic states was then connected to the unstable branch via a saddle-node bifurcation. However, in the second case, that of $q = 0.0016$, there is no saddle-node bifurcation. Instead there exists a saddle-saddle connection. In this case, the unstable endemic state emanating from the disease free state has a one-dimensional unstable manifold. This branch is connected via a turning point to an unstable endemic branch having a two-dimensional unstable manifold, which in turn becomes stable through a Hopf bifurcation.

The bifurcation diagram for this case is reproduced here for clarity of discussion in Fig. 10.1. For the saddle-saddle case, the lower (upper) branch has a one (two) dimensional unstable manifold. The upper branch then undergoes a reverse Hopf bifurcation. The connecting branch of periodic orbits (not shown) is unstable and sub-critical. These orbits have very long periods and large swings in amplitudes of infectives.

Recalling that q controls the resusceptibility rate and w the rewiring rate, we examine the structure of the bifurcation onset of attracting endemic states while holding the other parameters fixed. The onset of Hopf bifurcation points in two parameters was computed, and is shown in Fig. 10.2, for both the mean field model and the full system. Bifurcation points in the full system were estimated as the largest w value for which a single run started near the probable endemic steady state remained near that state for 10^5 MCS without dying out. The region below the curve contains stable endemic branches, while the region above contains unstable endemic states and/or stable disease free equilibria. The same trends are observed in both the mean field and the full system. Notice that for q greater than approximately 0.3, the value of w for the Hopf bifurcation does not change much. In addition, the infective fraction is also approximately independent of q for q sufficiently large,

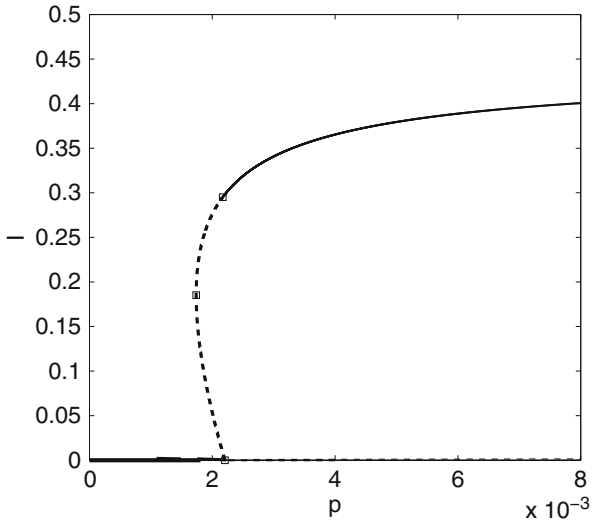

Fig. 10.1 A bifurcation diagram of the infective fraction as a function of p, with $w = 0.04$, $r = 0.002$, $q = 0.0016$. The *squares* denote the saddle–saddle point and transcritical point. *Dashed lines* are unstable branches. As p is decreased, the endemic state loses stability in a Hopf bifurcation

signifying that the model is approaching the SIS model. One would typically expect that as the resusceptibility rate q increases, the number of nodes that are in the recovered state and thus protected from infection will decrease, and the infection will spread more easily. Therefore, a faster rewiring rate (larger w) will be needed to suppress the infection. Indeed, this is the trend observed in Fig. 10.2 for small

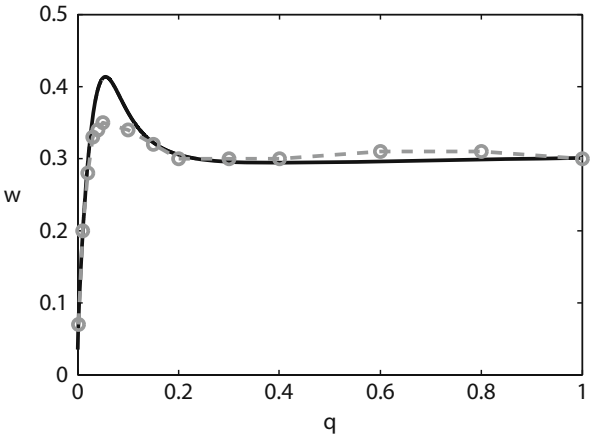

Fig. 10.2 A two parameter diagram of the Hopf bifurcation points as a function of q and w. *Solid curve*: mean field model; *points* and *dashed curve*: full system. Parameters used are $r = 0.002$, $p = 0.004$

and large q. However, the w value for the bifurcation decreases with increasing q between about 0.1 and 0.2. This nonmonotonic shift in the bifurcation point in Fig. 10.2 is a nonlinear effect which has not yet been explained.

In later sections we will explore the fluctuations of the SIRS model for values of q between the values 0 and 1. Effects on the fluctuations of the nonmonotonic bifurcation curve in Fig. 10.2 have not been observed.

We remark that a direct comparison in [29] of the infective fraction between the mean field model and Monte Carlo simulation of the full system showed excellent agreement along the attracting branches. The discrepancies occurred near the bifurcation point where the endemic state loses stability, partly because the actual location of the instability in the full stochastic system was difficult to detect accurately in Monte Carlo simulations and partly due to inaccuracies in the mean field approximation. However, the scaling results near the bifurcation, which we present in the next section, are generally consistent between the mean field model and the full system.

10.4 Effect of Recovered Class on Fluctuations

We have observed that the amplitude of fluctuations in the number of infectives is generally larger in the SIRS model than the SIS model. In the SIS system, links between two infectives are not broken because rewiring operates only on SI links. Thus when an infective becomes susceptible again, the newly formed susceptible may be connected to other infectives that it retained as neighbors while previously infected and can immediately become reinfected. This situation tends to suppress fluctuations, because small decreases in the total number of infectives correspond exactly to increases in the number of susceptibles, and rapid reinfection of the susceptibles can occur, preventing the number of infectives from dropping significantly. In the SIRS model, on the other hand, the recovered compartment introduces an effective time delay from recovery to possible reinfection and allows infective levels to fluctuate more.

Figure 10.3 compares the scaling of fluctuations near the bifurcation point for two different values of the resusceptibility rate q. In the top panels $q = 0.0016$, the rate used in [29]. In the bottom panels $q = 1$, effectively approximating the SIS case, since individuals spend very little time in the recovered class and much less than 1% of the population is in the recovered class at a given time. Fluctuations in the infectives (measured as the standard deviation divided by mean for long Monte Carlo simulations) are plotted as a function of p, the infection rate, as p is swept towards the bifurcation point. Results were computed from 5×10^5 MCS time series sampled every 10 MCS. The magnitude of the fluctuations is greater for the SIRS case (Fig. 10.3a) than for the SIS case (Fig. 10.3c). Notice that the increase in fluctuations is almost an order of magnitude.

The fluctuations exhibit power law scaling, shown in the log–log plots in Fig. 10.3b, d. On the horizontal axis, we plot $\ln(p - p_c)$, where p_c is the critical point at which the endemic state loses stability. The bifurcation points are not known

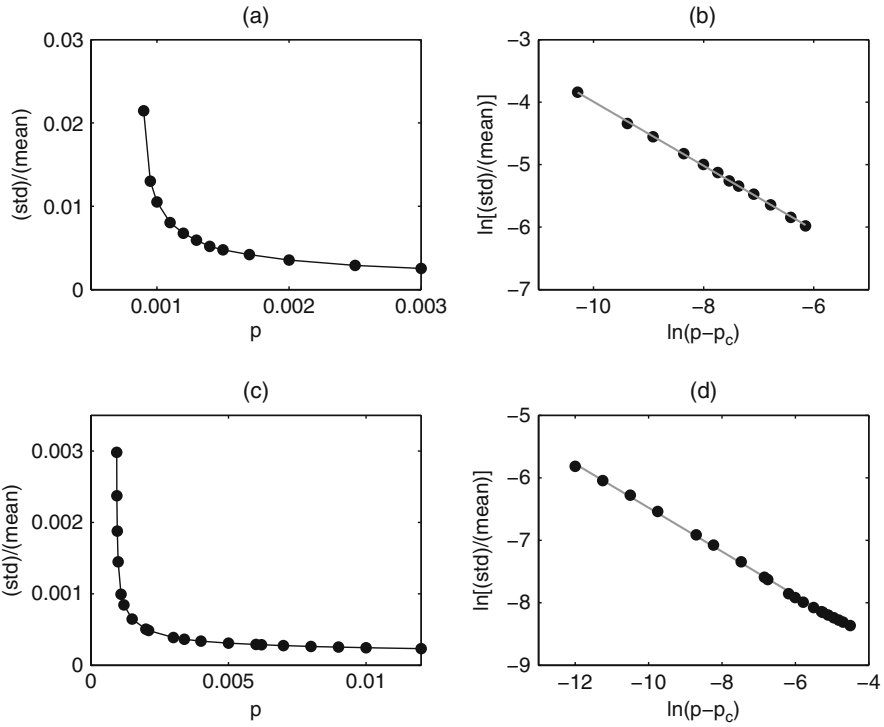

Fig. 10.3 Fluctuations in infectives (standard deviation divided by mean) vs. infection rate p near the bifurcation point, from Monte Carlo simulations: (**a**) $q = 0.0016$ (SIRS case), (**c**) $q = 1$ (approximately SIS case). *Curves* are to guide the eye. Log–log plots (data points with best fit lines) show power law scaling for both $q = 0.0016$ (**b**) and $q = 1$ (**d**). Other parameters: $w = 0.04$, $r = 0.002$. Parts (**a**) and (**b**) are reprinted from [29]

exactly, so we approximate p_c by the value that produces the most linear plot in each case. For the data of Fig. 10.3, the scaling exponents are similar (-0.59 versus -0.51 for $q = 0.0016$ and 1 respectively), so it is not clear that the resusceptibility rate has a significant effect on how the fluctuations scale with p.

The power law scaling of the fluctuations can be understood by considering the scaling near a generic bifurcation point. From our mean field analysis, we expect the bifurcation point where the endemic steady state loses stability to be either a saddle-node bifurcation point or a Hopf point. A generic saddle-node bifurcation exhibits power law scaling of fluctuations near the bifurcation point, as we show in Fig. 10.4 and explain in the discussion below. A Hopf bifurcation can also appear locally to have power law scaling of fluctuations, although the scaling may be over a smaller range of parameters. For a given standard deviation, the probability density function near a Hopf bifurcation is given by [2]:

$$p_{hb}(\beta, r, \sigma, R) = Nr^{\frac{\beta}{\sigma^2}} e^{-\frac{Rr^2}{\sigma^2}} \sigma^{-2} \left[\Gamma\left(1 + 1/2\,\frac{\beta}{\sigma^2}\right) \right]^{-1} \tag{10.10}$$

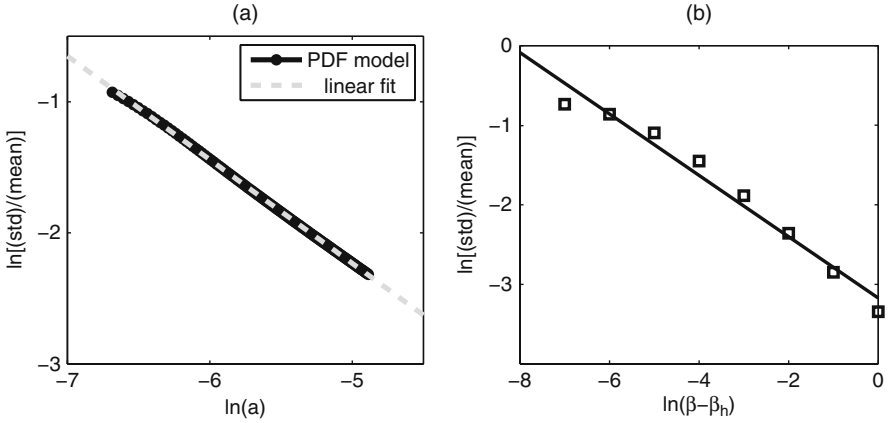

Fig. 10.4 (**a**) Fluctuation size of a generic saddle-node bifurcation as a function of bifurcation parameter a near the bifurcation point using the probability density function in Eq. (10.12). Noise amplitude is $\sigma = 0.005$. (**b**) Fluctuation size of a generic Hopf bifurcation as a function of bifurcation parameter β near the bifurcation point using the PDF in Eq. (10.10) (*squares*). The *line* is a best linear fit. Noise amplitude is $\sigma = 0.05$.

where the state space variable is a radial coordinate r, β is the distance from the Hopf bifurcation point, parameter $R = 0.5$ is fixed, Γ is the gamma function, and N is a normalization constant. An example of the fluctuations using Eq. (10.10), where we have computed the first and second order moments to find the ratio of the standard deviation to the mean, is shown in Fig. 10.4b. The data for the fluctuation size deviates from a power law scaling, as exhibited in the figure. However, there is a monotonic relationship in the fluctuations as measured by σ/μ as a function of the distance to the Hopf bifurcation. Therefore, we expect the fluctuation characteristics of the SIS and SIRS models to hold near bifurcation points regardless of whether the statistics are measured with respect to a Hopf or saddle-node bifurcation.

Since the power law scaling is observed near either a saddle-node or Hopf bifurcation point, it may be understood by considering the local dynamics. For example, near the saddle-node, a center manifold reduction would reduce the study of the vector field to a system with a one-dimensional unstable manifold. Therefore, the power law scaling of the fluctuations can be motivated by considering the following simple stochastic differential equation

$$dx_t = (a - x_t^2)dt + \sigma * dW_t \tag{10.11}$$

for a one dimensional saddle-node bifurcation, where a is the bifurcation parameter, dW/dt is a white noise term, and dW is a Brownian increment. In general, noise can cause a shift in the location of the saddle-node bifurcation, so we assume that the noise is sufficiently small that the location is fixed.

By assuming we are always near the attracting branch of the saddle-node or Hopf bifurcation, we are in a near equilibrium setting driven by noise. Such an

assumption allows us to examine the stationary probability density function (PDF) of the stochastic dynamics by employing the Fokker-Planck equation near steady state. For the stochastic differential equation, Eq. (10.11), the PDF is well known [22] and is given by

$$p(a, x, \sigma) = Ne^{2(ax - x^3/3)/\sigma^2}. \tag{10.12}$$

Here N is a normalization constant. From Eq. (10.12), we compute the first and second order moments to find the ratio of the standard deviation to the mean. We examine the fluctuations in the neighborhood of $a = 0$, which is the location of the saddle-node point. The results display power law scaling, as depicted in Fig. 10.4a.

To further examine the differences in fluctuations between the SIS and SIRS adaptive network models, we perform the following experiment. As discussed above, we can examine the fluctuation sizes as a function of resusceptibility rate q to see how the fluctuation sizes compare between the two model classes. The other variable which controls the recovered, as well as the infected, populations is the rewiring rate, w. It has a significant effect on the fluctuations, since the degree of infectives is dramatically reduced by the rewiring. We examine the interplay between q and w and their effect on fluctuation sizes. Here we turn to a stochastic version of the mean field model. We have shown previously that the scaling behavior of the mean field model is typically similar to that of the full network system [29].

We use additive noise to model fluctuations near the endemic equilibrium state. Details may be found in [29]. The stochastic mean field model has the following form:

$$\mathbf{X}' = \mathbf{F}(\mathbf{X}) + \varepsilon\eta(\mathbf{t}), \tag{10.13}$$

where $\mathbf{F}(\mathbf{X})$ is the mean field system in Eqs. (10.1)–(10.9), $\eta(\mathbf{t})$ is a noise term with $\langle\eta(\mathbf{t})\eta(\mathbf{t}')\rangle = \delta(\mathbf{t} - \mathbf{t}')$, and ε is the noise amplitude. Fluctuations are computed by averaging the standard deviation over mean results for time series starting from 10 random initial conditions near steady state. The runs were computed for 5×10^7 steps using a step length of 0.001, and transients were removed after 10^6 steps.

A typical example of the fluctuations as w is varied is shown in Fig. 10.5b. Similar linear log–log behavior is observed in other stochastic simulations for other values of q. In Fig. 10.5b, w_h denotes the location of the Hopf bifurcation branch. The Hopf bifurcation occurs for all values of q considered here. A typical bifurcation plot is shown in Fig. 10.5a for $q = 0.1$. Attracting states are solid curves, while unstable states are dashed and dotted curves. The Hopf bifurcation point is on the upper branch separating the stable and unstable steady states.

Because of the power law scaling of the fluctuations, as in Fig. 10.5b, we expect a functional relationship of the form

$$\sigma(q)/\mu(q) \propto [w_h(q) - w]^{m(q)} \tag{10.14}$$

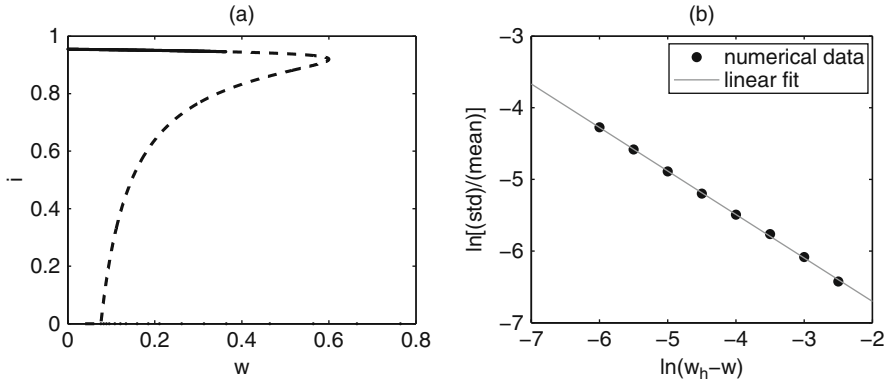

Fig. 10.5 (**a**) A bifurcation plot of the mean field model without noise. Plotted is the fraction infected as a function of w. Parameters are $r = 0.002, p = 0.004, q = 0.1$. (**b**) Plot of the fluctuation sizes as a function of rewiring rate, w. The fixed parameters used are $r = 0.002,\ p = 0.004,\ K/N = 10,\ q = 0.01, \varepsilon = 0.0001$

where $m(q)$ is the average slope of the log–log plots. We can now examine how the average rate of change of fluctuations varies as a function of q. The results are shown in Fig. 10.6. At smaller q values, the fluctuations increase more quickly with w than they do in the large q limit. Therefore, the fluctuations are more sensitive with respect to w in the SIRS model than in the SIS model.

We attempted to confirm this mean field result for the slopes using the full model, but in the case of the full model, the exact locations of bifurcation points are unknown. It is difficult to estimate where the endemic state loses stability from time series because one cannot always distinguish a metastable state from a stable state in the presence of fluctuations. We can approximate the bifurcation point by the value that gives the most linear plot (largest R value) for fluctuations vs. the

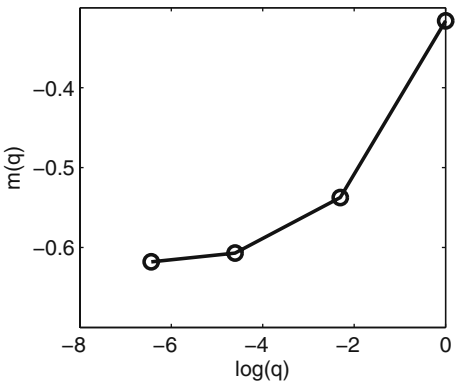

Fig. 10.6 A plot of the slope $m(q)$ as a function of q. See text for details. Parameters used are $r = 0.002, p = 0.004, \varepsilon = 0.0001$

bifurcation parameter as in Fig. 10.3, but this approach is unreliable if the scaling deviates from a power law, as occurs in Fig. 10.4b for a generic Hopf bifurcation. The best fit slope depends sensitively on the estimate for the bifurcation point, so we were not able to obtain robust results for the full system.

10.5 Delayed Outbreaks

We have also considered phase relationships between the fluctuating node and link variables. At each time point in our simulations, we tracked the number of infected nodes as well as the number of non-infected neighbors of infected nodes (which corresponds to the number of SI and IR links). The rewiring causes the fluctuations in the number of infectives to lag behind fluctuations in the number of infective neighbors, as shown in Fig. 10.7a. This effect was observed both in the mean field model (data not shown, see [29]) and in Monte Carlo simulations of the full system.

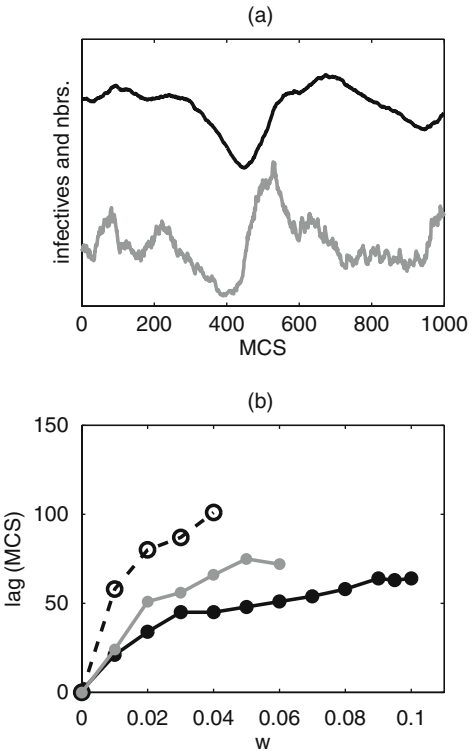

Fig. 10.7 Delayed outbreaks due to rewiring. (**a**) Monte Carlo time series. *Black*: infectives; *gray*: neighbors of infectives. *Curves* are scaled in arbitrary units for comparison of peak times. $p = 0.0065, w = 0.09, q = 0.0016, r = 0.002$. Reprinted from [29]. (**b**) Time in MCS by which infectives lag behind infective neighbors vs. rewiring rate. *Solid black*: $q = 0.0016$; *gray*: $q = 0.001$; *dashed black*: $q = 0.0005$. Other parameters: $p = 0.0065, r = 0.002$

We studied the dependence of this phase lag on both the rewiring rate w and the resusceptibility rate q when the system was fluctuating around the endemic steady state. Monte Carlo simulations were sampled every 1 MCS for 3×10^4 MCS after discarding transients. We computed cross correlations between the infectives and the infective neighbors for varying phase shifts between the two time series and identified the lag maximizing the cross correlation. Figure 10.7b shows results for three different q values. (Note: Curves for smaller q terminate at lower w values because the endemic steady state becomes unstable, as in Fig. 10.2.) In each case, the lag increases with increasing rewiring rate. This effect does not have a simple explanation, but since it is also observed in mean field simulations, it depends on node and link dynamics primarily, rather than higher order geometries.

Further, the lag time increases as the resusceptibility rate q decreases. This occurs because the recovered class introduces an effective delay in the system. When a node becomes at risk because its neighbor is infected, it cannot itself become infected until it is susceptible. As q is lowered, the fraction of infective neighbors that are recovered and have to wait to become susceptible again increases, and the average wait time also increases, so it is expected that the infective fluctuations will lag further behind.

It should be noted that when $q = 1$ and the system approximates the SIS model, the number of infectives and non-infected neighbors of infectives (i.e., SI links) are poorly correlated for any shift between time series. Therefore, the lags discussed here are not observed in the SIS model.

10.6 Lifetime of the Endemic Steady State

Another effect we consider, which depends on fluctuations in the system, is the lifetime of the endemic steady state. Because the system is stochastic and the disease free state is absorbing, the disease will die out in the infinite time limit for any set of parameters. For a generic saddle-node bifurcation in one dimension, the scaling of the lifetime is expected to obey

$$\ln T \propto (p - p_0)^{3/2}, \tag{10.15}$$

where T is the mean dwell time or lifetime of the steady state, p is the bifurcation parameter, and p_0 is the location of the bifurcation point [10, 17]. Using the computational methods in [29], we show preliminary results for the dependence of the lifetime on the infection rate p in Fig. 10.8. The bifurcation point p_0 was estimated by the value that gave the most linear plot for $\ln T$ vs. $(p-p_0)^{3/2}$. The scaling results appear consistent with expectations, but further study is needed. In contrast to the mean field model, because the exact location of bifurcation points is not known for the full system, details such as slopes and scaling exponents can be very much dependent on estimates for the bifurcation point.

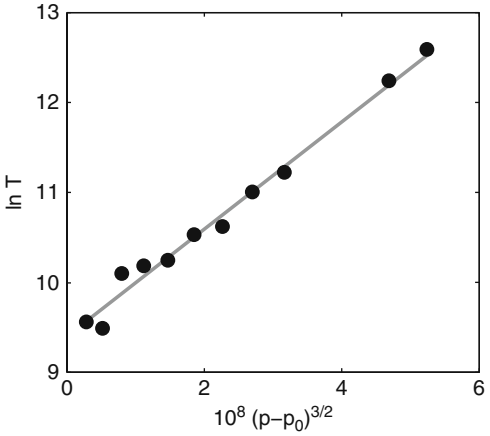

Fig. 10.8 Dependence of endemic state average lifetimes T on infection rate p. *Points*: Monte Carlo simulations; *line*: best fit line. $q = 0.0016$, $r = 0.002$, $w = 0.04$, $N = 4 \times 10^4$, $K = 4 \times 10^5$. (Reprinted from [29].)

10.7 Network Geometry

Defining appropriate statistics to capture a fluctuating network geometry is difficult. Here, the network does not display community structure nor is governed by an underlying spatial structure. Links are rewired to any acceptable target nodes, regardless of distance away. Because the mean field theory for nodes and links captures the dynamics of the system fairly well, higher order correlations involving three or more nodes do not have a large impact on the dynamics. The network may be fairly unstructured at the higher levels.

To demonstrate the role of fluctuations in the network geometry on the scale of individual nodes and links, we show in Fig. 10.9 the time-varying degree of a single arbitrarily chosen node. When the node becomes infected, its non-infected neighbors quickly rewire away from it (dashed gray curves). Because infected neighbors do not rewire away, the degree may not drop all the way to zero before pausing. If the infected node remains infected for sufficiently long, its neighbors will recover and then rewire away, further decreasing the degree. Once the node recovers, other S and R nodes in the system may rewire to it, and its degree begins to climb (black curves). When the node becomes susceptible, the degree continues increasing (solid light gray curves) until the node again becomes infected, and the cycle repeats.

It is not yet known how to predict the degree distributions from first principles [29], but if one assumes that the degree distributions are already known for each node class, the fluctuations in the degree of a single node can be easily understood. Figure 10.10 shows the statistics of the local maxima and minima of the degree time series for a single node. Results are computed for a 4×10^6 MCS time series, which contains approximately 2,000 SIRS transition cycles (and thus approximately

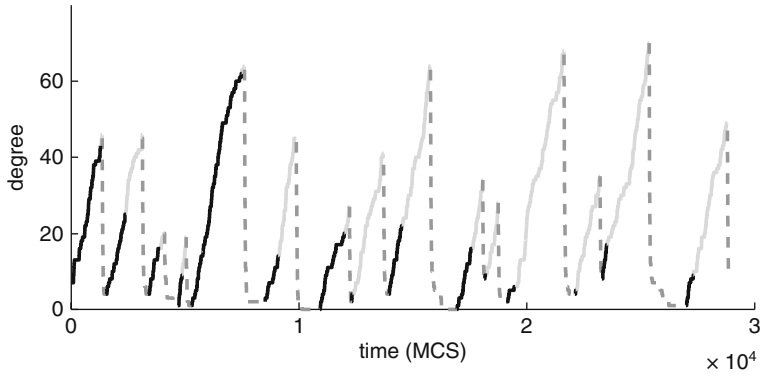

Fig. 10.9 Degree of a single node versus time. *Curves* indicate the node's disease status: *black*: recovered; *light gray*: susceptible; *dashed medium gray*: infected. Parameters: $p = 0.002$, $q = 0.0016$, $r = 0.002$, $w = 0.04$

2,000 maxima and minima). Frequency distributions for the maxima (Fig. 10.10a) and minima (Fig. 10.10b) are shown.

The minima can be most easily understood. Minima occur when an infective recovers. Recovery is governed by the rate r and is equally likely to occur for any infective, regardless of the degree. Therefore, the distribution for the degree minima is the same as the degree distribution for infectives. Figure 10.10b shows good agreement between the observed distribution of minima and that expected from the infective degree distribution (which was found from Monte Carlo simulations in [29]).

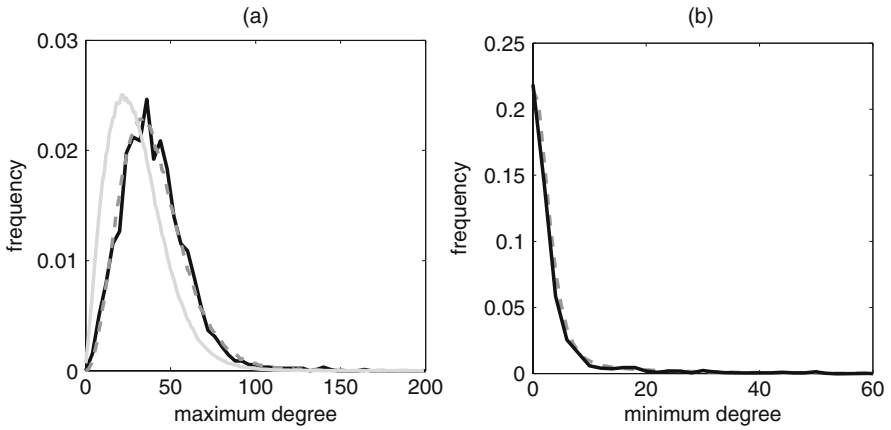

Fig. 10.10 Statistics for degree time series. *Black curves*: observed distributions; *dashed gray curves*: expected distributions. (**a**) Distribution of local maximum degrees. The degree distribution for susceptibles is shown in *light gray* for reference. (**b**) Distribution of local minimum degrees. Parameters: $p = 0.002$, $q = 0.0016$, $r = 0.002$, $w = 0.04$

Degree maxima occur immediately before a susceptible becomes infected. The infection rate depends on the number of infected neighbors a susceptible node has, which is almost directly proportional to its degree. (See [29] for details.) Letting d represent the degree of a susceptible and P_d the degree distribution for susceptibles, we thus expect the infection rate to be proportional to d and the distribution of degree maxima to be proportional to dP_d. This expected distribution is shown in Fig. 10.10a, and there is again good agreement with the observed distribution of maxima and the expected values. The degree distribution for susceptibles is shown for reference. The distribution of maxima is skewed to higher degrees because of the dependence of the infection process on node degree.

To develop a complete understanding of these processes, a theory to predict the degree distributions from first principles is needed. Such a theory must account for correlations between the infection status of an infective and its neighbors, as explained in [29].

10.8 Conclusions and Discussion

In this chapter, we considered a model of an adaptive network and its fluctuations. We introduced a model based on an SIRS epidemic structure which included transition probabilities between node states as well as link dynamics. In this model, the link dynamics are a function of the state variables, and since the state variables depend on the links, it forms a closed feedback system between nodes and links. The model is an extension of, and contains in the limit of large resusceptibility rate q, the SIS model studied in [19]. The fluctuations of the model were simulated in two ways: The full system was studied via Monte Carlo simulation on a finite population. In addition, a low dimensional approximation was studied using a Langevin simulation with an additive noise term to the mean field equations.

Quantifying where the system is most sensitive to fluctuations required an examination of the bifurcation structure of the deterministic mean field equations. For the steady states of the mean field equations, we examined the locations of both Hopf bifurcations and saddle-node points. We saw that as the resusceptibility rate q changes, the type of bifurcation changes. In general, for large q, we have a generic saddle-node bifurcation, while for small q we have a saddle-saddle bifurcation giving rise to a Hopf bifurcation.

Fluctuations were examined with respect to these bifurcations, and particular attention was paid to the large and small q cases. This led us to examine the specific role of the recovered class in the SIRS model as compared with the limiting case of the SIS model. In the SIS case, we found that without the recovery class, newly created susceptibles may be still connected to another infective, and thus may become reinfected immediately. This mechanism led to a reduction in the fluctuations of infectives. On the other hand, the inclusion of the recovery class introduced a mean delay time prior to potential reinfection, thereby increasing infective fluctuations.

By examining the fluctuation sizes near the bifurcation points, we found the existence of scaling laws in both the mean field model and the full system. Comparing

the stochastic dynamics of SIRS and SIS cases, we examined the effect of the rewiring rate w and resusceptibility rate q on the fluctuations. For a large range of q values, we showed the existence of a scaling law near the Hopf bifurcation, which includes the fluctuations for the limiting SIS case. We found that for small q values, the fluctuations change more rapidly with rewiring rate w than they do for the SIS model, making fluctuations more sensitive with respect to parameters in the SIRS case. Other effects, such as latency, or delay, between infective nodes and non-infected neighbors occur in the SIRS model but not the SIS model.

The degree fluctuations are still difficult to predict, although some of these phenomena can be understood in certain cases. However, much work still is required to understand the fluctuations of the network geometry. Current tools for the analysis of static networks are insufficient to make predictions about adaptive networks. A complete understanding of the dynamics, fluctuations, and geometry in the future requires tools which incorporate topology, stochastic dynamics, and time dependent graph theory.

Because adaptive networks based on epidemiology contain many of the features of adaptive networks in general, we expect them to continue to reveal new and interesting dynamic phenomena as they are extended for more detailed modeling of social situations, including and beyond those of infectious disease spread.

Acknowledgements This work was supported by the Office of Naval Research and the Armed Forces Medical Intelligence Center. LBS was supported by the Jeffress Memorial Trust.

References

1. R. M. Anderson and R. M. May. *Infectious Diseases of Humans.* Oxford University Press, Oxford, 1991.
2. L. Arnold. *Random Dynamical Systems*. Springer, New York, 2001.
3. A. Barabási and R. Albert. Emergence of scaling in random networks. *Science*, 286(5439):509–512, 1999.
4. I. J. Benczik, S. Z. Benczik, B. Schmittmann, and R. K. P. Zia. Lack of consensus in social systems. http://arxiv.org/abs/0709.4042, 2007.
5. S. Bornholdt and T. Röhl. Self-organized critical neural networks. *Physical Review E*, 67(6):066118, 2003.
6. S. Bornholdt and K. Sneppen. Neutral mutations and punctuated equilibrium in evolving genetic networks. *Physical Review Letters*, 81(1):236–239, 1998.
7. K. Christensen, R. Donangelo, B. Koiller, and K. Sneppen. Evolution of random networks. *Physical Review Letters*, 81(11):2380, 1998.
8. L. D. Costa, F. A. Rodrigues, G. Travieso, and P. R. V. Boas. Characterization of complex networks: A survey of measurements. *Advances in Physics*, 56:167–242, 2007.
9. E. J. Doedel, R. Paffenroth, A. Champnets, T. Fairgrieve, Y. A. Kuznetsov, B. Sandstede, and X. Wang. *AUTO: Software for continuation and bifurcation for ordinary differential equations*, 2001.
10. M. I. Dykman and M. A. Krivoglaz. Fluctuations in non-linear systems near bifurcations corresponding to the appearance of new stable states. *Physica A*, 104(3):480–494, 1980.
11. H. Ebel and S. Bornholdt. Coevolutionary games on networks. *Physical Review E*, 66(5): 056118, 2002.

12. G. C. M. A. Ehrhardt, M. Marsili, and F. V. Redondo. Phenomenological models of socioeconomic network dynamics. *Physical Review E*, 74(3):036106, 2006.
13. Z. Fan and G. Chen. Evolving networks driven by node dynamics. *International. Journal of Modern Physics B*, 18:2540–2546, 2004.
14. S. Gil and D. H. Zanette. Coevolution of agents and networks: Opinion spreading and community disconnection. *Physics Letters A*, 356(2):89–94, 2006.
15. P. M. Gleiser and D. H. Zanette. Synchronization and structure in an adaptive oscillator network. *European Physics Journal B*, 53:233–238, 2006.
16. P. Gong and C. van Leeuwen. Evolution to a small-world network with chaotic units. *Europhysical Letters*, 67:328–333, 2004.
17. R. Graham and T. Tél. Nonequilibrium potentials for local codimension-2 bifurcations of dissipative flows. *Physical Review A*, 35(3):1328–1349, 1987.
18. T. Gross and B. Blasius. Adaptive coevolutionary networks: a review. *Journal of the Royal Society Interface*, 2007. DOI: 10.1098/rsif.2007.1229.
19. T. Gross, C. J. D. D'Lima, and B. Blasius. Epidemic dynamics on an adaptive network. *Physical Review Letters*, 96:208701, 2006.
20. P. Holme and G. Ghoshal. Dynamics of networking agents competing for high centrality and low degree. *Physical Review Letters*, 96(9):098701, 2006.
21. P. Holme and M. E. J. Newman. Nonequilibrium phase transition in the coevolution of networks and opinions. *Physical Review E*, 74(5):056108, 2006.
22. W. Horsthemke and R. Lefever. *Noise-Induced Transitions: Theory and Applications in Physics, Chemistry, and Biology*. Springer Series in Synergetics , Vol. 15, 1983.
23. J. Ito and K. Kaneko. Spontaneous structure formation in a network of chaotic units with variable connection strengths. *Physical Review Letters*, 88(2):028701, 2002.
24. J. Ito and K. Kaneko. Spontaneous structure formation in a network of dynamic elements. *Physical Review E*, 67(4):046226, 2003.
25. S. Jain and S. Krishna. A model for the emergence of cooperation, interdependence, and structure in evolving networks. *Proceedings of the National Academy of Science*, 98: 543–547, 2001.
26. M. E. J. Newman. The structure and function of complex networks. *SIAM Review*, 45(2): 167–256, 2003.
27. J. M. Pacheco, A. Traulsen, and M. A. Nowak. Coevolution of strategy and structure in complex networks with dynamical linking. *Physical Review Letters*, 97:258103, 2006.
28. J. C. Scholz and M. O. W. Greiner. Topology control with ipd network creation games. *New Journal of Physics*, 8:185–199, 2007.
29. L. B. Shaw and I. B. Schwartz. Fluctuating epidemics on adaptive networks. *Physical Review E*, 77:066101, 2008.
30. B. Skyrms and R. Pemantle. A dynamic model of social network formation. *Proceedings of the National Academy of Sciences*, 97:9340–9346, 2000.
31. F. Vazquez, V. M. Eguíluz, and M. San Miguel. Generic absorbing transition in coevolution dynamics. *Physical Review Letters*, 100(10):108702, 2008.
32. D. H. Zanette and S. Gil. Opinion spreading and agent segregation on evolving networks. *Physica D*, 224:156–165, 2006.
33. D. H. Zanette and S. R. Gusman. Infection spreading in a population with evolving contacts. http://arxiv.org/abs/0711.0874, 2007.
34. C. Zhou and J. Kurths. Dynamical weights and enhanced synchronization in adaptive complex networks. *Physical Review Letters*, 96(16):164102, 2006.

Part IV
Social Games on Adaptive Networks

Chapter 11
A Dynamic Model of Social Network Formation

Brian Skyrms and Robin Pemantle

Abstract We consider a dynamic social network model in which agents play repeated games in pairings determined by a stochastically evolving social network. Individual agents begin to interact at random, with the interactions modeled as games. The game payoffs determine which interactions are reinforced, and the network structure emerges as a consequence of the dynamics of the agents' learning behavior. We study this in a variety of game-theoretic conditions and show that the behavior is complex and sometimes dissimilar to behavior in the absence of structural dynamics. We argue that modeling network structure as dynamic increases realism without rendering the problem of analysis intractable.

11.1 Introduction

Pairs from among a population of ten individuals interact repeatedly. Perhaps they are cooperating to hunt stags and rabbits, or coordinating on which concert to attend together; perhaps they are involved in the somewhat more antagonistic situation of bargaining to split a fixed payoff, or attempting to escape the undesirable but compelling equilibrium of a Prisoner's Dilemma. As time progresses, the players adapt their strategies, perhaps incorporating randomness in their decision rules, to suit their environment. But they may also exert control over their environment. The players may have choice over the pairings, though not perfect information about the other players. They may improve their lot in two different ways. A child who is being bullied either learns to fight better, or to run away. Similarly, a player who obtains unsatisfactory results may choose either to change strategies or to change associates. Regardless of whether the interactions are mostly cooperative or mostly antagonistic, it is natural and desirable to allow evolution of the social network (the propensity for each pair to interact) as well as the individuals' strategies.

B. Skyrms (✉)
School of Social Sciences, University of California at Irvine, Irvine, CA 92607, USA
e-mail: bskyrms@uci.edu

This chapter is based on B. Skyrms and R. Pemantle, "A Dynamic Model of Social Network Formation" PNAS 97 (16), 9340-9346 (2000).

T. Gross, H. Sayama (eds.), *Adaptive Networks,* Understanding Complex Systems,
DOI 10.1007/978-3-642-01284-6_11, © NECSI Cambridge/Massachusetts 2009

We build a model that incorporates both of these modes of evolution. The idea is simple.

(*)
Individual agents begin to interact at random. The interactions are modeled as games. The game payoffs determine which interactions are reinforced, and the social network structure emerges as a consequence of the dynamics of the agents' learning behavior.

As the details of the specific game and the reinforcement dynamics vary, we then obtain a class of models. In this paper we treat some simple reinforcement dynamics, which may serve as a base for future investigation.

The idea of simultaneous evolution of strategy and social network appears to be almost completely unexplored. Indeed, the most thoroughly studied models of evolutionary game theory assume *mean-field* interactions, where each individual is always equally likely to interact with each other. Standard treatments of evolutionary game dynamics [1, 2] operate entirely in this paradigm. This is due, to a large extent, to considerations of theoretical tractability of the model. Models have been introduced that allow the agents some control over their choice of partner [3], but the control is still exerted in a mean-field setting: one chooses between the present partner and a new pick at random from the whole population.

Evolutionary biologists know that evolutionary dynamics can be affected by non-random encounters or population structure, as in Sewall Wright's models of assortative mating [4]. Wright [5] already realized that positive correlation of encounters could provide an account of evolution of altruism. Thus the need for social network models has been long recognized.

When the social network is modeled, it is almost always static.[1] Interactions, for example, may be posited to occur only between players whose locations are close, according to some given spatial data. Biological models in which encounters are governed by spatial structure have become increasingly frequent in the 1990s; see for example the work of Durrett, Levin and Neuhauser [7–9]. A similar hypothesis of spatial structure, in a game theory context, arises in [10]. Here, technology from statistical mechanics is adapted to the analysis of games whose interactions take place between neighbors in a grid.

A number of recent investigations by game theorists, some directly inspired by biological models, have shown that the dynamics of strategic interaction can be strikingly different if interaction is governed by some spatial structure, or more generally, some graph structure [11–13]. For instance, one-shot Prisoner's Dilemma games played with neighbors on a circle or torus allows cooperation to evolve in a way that the random encounter model does not. The spatial or graph structure can be important in determining which equilibria are possible, whether repeated interactions can be expected to converge to equilibrium, and if so, how quickly convergence takes place [14].

Since the outcome of a repeated game may vary with the choice of network model, it is important to get the network model right. Further progress in the theory

[1] An exception, perhaps, is a preprint we have recently encountered by Jackson and Watts [6]

of games and adaptive strategies would be greatly enhanced by a theory of networks of social interaction. In particular, it would be desirable to have a framework within which models may be developed that are both tractable, and plausible as a mechanism governing interactions among a population of agents seeking to improve their lot.

When the network changes much more slowly than do the strategies of individuals, it is reasonable to model the social network by a structure which is fixed, though possibly random. The question of realistically modeling the randomness in such a case is taken up in a number of papers, of which a recent and well known example is the "small world" model [15]. In the other extreme [16–18] evolution of social structure is modeled by agents moving on a fixed graph in the absence of strategy dynamics.

In the general case, however, interaction structures are fluid and evolve in tandem with strategy. What is required here is a dynamics of interaction structure to model how social networks are formed and modified. We distinguish this *structure dynamics* from the *strategic dynamics* by which individuals change their individual behaviors or strategies.

In this paper we introduce a simple, additive model for structure dynamics, and explore the resulting system under several conditions: with or without discounting of the past, with or without added noise, and in the presence or absence of strategic dynamics. Common to all our models is a stochastic evolution from a (usually symmetric) initial state. Individuals in a population start out choosing whom to interact with at random, then modify their choices according to how their choice is reinforced, and the process is repeated. An infinite variety of such models is possible. We will consider only a few basic models, meant to illustrate that rigorous results on structure dynamics are not out of reach, and that further inquiry will be profitable.

We first consider a baseline case of uniform reinforcement. Here, any choice of partner is reinforced as strongly as any alternative choice would have been. In other words, the interaction game between any pair of players always produces a constant reward or punishment. One might expect that such cases would not lead to interesting dynamics, but that is far from the truth. We show both by computer simulation and analytically how structure emerges spontaneously even in these cases. Since the strategic dynamics here are trivial, the baseline case is intended mostly as a building block on which more interesting strategic dynamics are to be grafted. We note, however, that the constant reward game is not completely unreasonable. Studies have shown that in the absence of other environmental attributes, sheer familiarity brings about positive attitudinal change [19]. In fact, an abstract model of network evolution under uniform positive re-weighting has appeared before under the name of "Reinforced Random Walk" [20].

Next, we move to the case where players of different types play a non-trivial game and are reinforced by the payoffs of the game. Here, we examine the co-evolution of behavior and structure when the structural dynamics and strategic dynamics are both operative. The relative speeds of structural dynamics and strategic dynamics affect which equilibrium is selected in the game. In particular, this can determine whether the risk-dominant or payoff-dominant equilibrium is selected.

11.2 Making Friends: A Baseline Model of Uniform Reinforcement

11.2.1 Friends I: Asymmetric Weights

Each morning, each agent goes out to visit some other agent. The choice of whom to visit is made by chance, with the chances being determined by the relative *weights* each agent has assigned to the others. For this purpose, agent number i has a vector of weights $\langle w_{i1}, \ldots, w_{in} \rangle$ that she assigns to other players (assume $w_{ii} = 0$). Then she visits agent j with probability

$$\text{Prob}(\text{agent } i \text{ visits } j) = \frac{w_{ij}}{\sum_k w_{ik}}. \tag{11.1}$$

Here we are interested in a symmetric baseline model, so we will assume that all initial weights are 1. Initially, for all agents, all possible visits are equiprobable.

Every agent is treated nicely on her visit and all are treated equally nicely. They each get a reinforcement of 1. Each agent then updates her weight vector by adding 1 to the weight associated with the agent that she visited. Her probabilities for the next round of visits are modified accordingly. At each stage we have a matrix p_{ij} of probabilities for i to visit j. Do these probabilities converge, and if so to what?

Given all the symmetry built into the starting point and the reinforcement, it is perhaps surprising that all sorts of structure emerge. Here is a description of a simulated sample run of length 1,000. The probabilities, to two decimal places, seem to converge after a few hundred rounds of visits, to a matrix that is anything but uniform (and to a different matrix each time the process is run from the initial, symmetric weights). There is one agent, A, who visits another agent, B, more than half the time. There is no reciprocation, so this has no bearing on how often B visits A, and in fact most agents will not visit any one agent more than a third of the time.

In the analysis section, we show that this outcome is typical.

Theorem 1. *The probability matrix for Friends I with n players will converge to a random limit p as time goes to infinity. The distribution of the limit is that the rows of p are independent, each having Dirichlet distribution (ignoring the zero entry on the diagonal) whose parameters are* $n - 1$ *ones.*

Thus we see spontaneous emergence of structure. This type of simple model has been used before in the economics literature to explain the stabilization of market shares at seemingly random equilibria, due to random reinforcement in the early phases of growth of an industry [21]. We remark that the choices made by each agent are independent of the choices made by each other agent, so the social aspect of the model is somewhat degenerate and the model may be viewed as a model of individual choice. Nevertheless, it fits our definition of social network model in that it gives a probabilistic structure to interactions; one may then extend the model so the interactions are nontrivial games.

11.2.2 Friends II: Symmetrized Reinforcement

Suppose now that the interaction is as pleasant to the host as the visitor. Thus when agent i visits agent j, we add 1 to both w_{ij} and w_{ji}. A typical outcome for 10 agents after 1,000 rounds of visits looks similar to the table for Friends I, except that the entries are nearly symmetric. There are, however, subtle differences that may cause the two models to act very differently when strategic dynamics are introduced. To see these differences, we describe what is typically observed after 10 runs of a simulation of Friends II to time 1,000 for a set of three agents, this being the minimum population size for which structural dynamics are interesting. What we see typically is one or two runs in which each players visits are split evenly (to two decimal places) between the others. We see another several runs that are close to this. We see one run or so in which two agents nearly always visit the third agent, which splits its time among the other two. The remaining runs give something between these extreme outcomes.

What may not be apparent from such data is that the limiting weights for Friends II are always $1/2$. Only a small fraction of sample outcomes decisively exhibit the proven limiting behavior. The data, in other words, show that after 1,000 iterations, the weights may still be far from their limiting values; when this is the case, one of the three agents is largely ignored by the other two, and visits each of the other two herself equally often. Since the lifetime of many adaptive games is 1,000 rounds or fewer, we see that limiting behavior may not be a good guide to behavior of the system on time scales we are interested in. The analysis section discusses both limiting results for this model and finite time behavior. When the population size is more than 3, the weights will always converge, but the limit is random and restricted to the subspace of symmetric matrices. Again, convergence of the weights to their limiting values is slower than in the non-reciprocal game of Friends I.

Theorem 2. *The probability matrix p_{ij} for Friends II with n players converges to random limit p as time goes to infinity. If $n = 3$, the limit is the matrix all of whose off-diagonal entries are $1/2$. In general, the limit may be any symmetric matrix whose rows sum to 1; that is, the closed support of the random limit is the entire subspace of symmetric stochastic matrices.*

11.2.3 Analysis of Friends I and II

To fit this in the framework of $(*)$, construct the following degenerate games. Each of the two players has only one strategy, and the payoff matrix is as follows.

Friends I	Host
Visitor	(1, 0)

Friends II	Host
Visitor	(1, 1)

The weights w_{ij} are initialized to 1 for $i \neq j$, and are then updated according to

$$w_{ij}(t+1) = w_{ij}(t) + u(i, j; t) \tag{11.2}$$

where $w_{ij}(t)$ is the weight agent i gives to agent j at time t and $u(i, j; t)$ is the payoff of the game played at time t between visitor i and host j (and zero if this visit did not occur at time t). This, together with specification of the visitation probabilities in Eq. (11.1), defines the model. Changing the initial weights does not affect the qualitative behavior of any model, so there is no need to vary the initialization.

For Friends I, the updating of the weights for any one agent is the same as a Pólya urn process [22]. Each agent can be thought of as having an urn with balls of $n - 1$ colors, one color representing each other agent. Initially there is one ball of each color in the urn. The agent picks a ball at random, indicating whom she should visit, then returns it to the urn along with an extra ball of the same color. The urns belonging to different agents are statistically independent.

The analysis of this process is well known ([23], Chap. 4). It is easy to show that the sequence of draws for each agent is *exchangeable*, that is, permuting a sequence does not change its probability. Hence by the de Finetti representation theorem, the random sequence of draws from an urn is equivalent to a mixture of multinomial processes, that is, of sequences of independent draws. The mixing measure is easily seen to be Dirichlet. Consequently, the visiting probabilities converge with probability one, but they can converge to anything. That they converge to the uniform vector, where each agent has equal probability to visit each other, has prior probability zero.

Furthermore, convergence to the limiting probability matrix is quite rapid. Let $p(t)$ denote the matrix whose (i, j)-entry is $p_{ij}(t)$. Then exchangeability implies that, conditional on the limit matrix $p = \lim_{t\to\infty} p(t)$, the sequence of visits is a sequence of independent, identically distributed draws from the limit distribution. Thus at time t, the central limit theorem implies that $p(t) - p$ is $t^{-1/2}$ times a multivariate normal.

For Friends II, exchangeability fails. This is not surprising, since the property of exchangeability is not very robust. More surprising, however, is that the sequence of probability matrices $p(t)$ does not form a martingale. To explain this terminology, let $\mathbf{E}_t$ denote the expectation conditioned on the values at time t. A simple computation shows that for Friends I, the expected value of $p_{ij}(t + 1)$ conditioned on the time t value is equal to $p_{ij}(t)$: since w_{ij} increases only when i visits j, we have

$$\begin{aligned}\mathbf{E}_t\, p_{ij}(t+1) &= \mathbf{E}_t \sum_{k=1}^{n} p_{ik}(t)\frac{w_{ij} + \delta_{jk}}{1 + \sum_{l=1}^{n} w_{il}(t)} \\ &= \frac{w_{ij}(t) + p_{ij}(t)}{1 + \sum_{l=1}^{n} w_{il}(t)} \\ &= p_{ij}(t).\end{aligned}$$

Even without exchangeability, the martingale convergence theorem ([24], Sect. 4.2) implies convergence of the quantities p_{ij}, though it says very little about the limit.

For Friends II the complete analysis may be found in [25]. Here is an outline of what is found there. A computation similar to the one for Friends I shows that

$$\mathbf{E}_t\, p(t+1) = p(t) + \frac{1}{t}F(p(t))$$

where F is a certain function on symmetric n by n matrices. In other words, the random sequence of matrices $\{p(t) : t = 1, 2, \ldots\}$ is a *stochastic approximation* in the sense of Robbins and Monro [26], driven by the vector field F. General results of [27] and [28] now imply that $p(t)$ converges to the set where F vanishes. To show that $p(t)$ always converges to a single point, Pemantle and Skyrms [25] compute a Lyapunov function for F, that is, a function V for which $\nabla V \cdot F < 0$ with equality only when $F = 0$. This, together with an efficiency inequality (bounding the angle between f and ∇V away from ninety degrees), establish convergence of p. The remainder of Theorem 2 is then established by showing the only stable zeros of the vector field F are the symmetric matrices with row sums all equal to 1, and that the possible limit points of $p(t)$ are exactly the stable equilibria of the flow determined by F.

Determination of the rate of convergence of $p(t)$ to its limit is somewhat different in this case. Due to the presence of unstable equilibria from the flow determined by F, there is a possibility of being stuck near one of these equilibria for a long time before eventually following the flow to one of the stable equilibria. For the three player game, the unstable equilibria are the following three matrices:

$$\begin{pmatrix} 0 & \frac{1}{2} & \frac{1}{2} \\ 0 & 0 & 1 \\ 0 & 1 & 0 \end{pmatrix} \qquad \begin{pmatrix} 0 & 0 & 1 \\ \frac{1}{2} & 0 & \frac{1}{2} \\ 1 & 0 & 0 \end{pmatrix} \qquad \begin{pmatrix} 0 & 1 & 0 \\ 1 & 0 & 0 \\ \frac{1}{2} & \frac{1}{2} & 0 \end{pmatrix}.$$

These correspond to cases where one of the three agents is entirely ignored, and splits her visits equally between the other two. The probability that $p(t)$ is within ε of one of these traps is roughly $3\varepsilon t^{-1/3}$, so with $t = 1,000$ we find a reasonably high probability that $p(1000)$ is not near the uniform probability matrix but is instead still near one of the unstable equilibria. This persists with reasonable probability well beyond $t = 10^6$. For greater population sizes similar phenomena apply. Convergence to the invariant set is relatively slow. However, for large populations, say 20 or more, another phenomenon takes place. The portion of the space of possible p matrices that are within ε of the possible limits goes to 1; this is known as the concentration of measure phenomenon [29]. Thus it becomes very unlikely to get stuck initially far away from the limit, simply because the initial randomness will very likely lead to a point very near a possible limit. Thus for large populations, the dynamics appear very similar to the dynamics for Friends I.

11.3 Making Enemies

Let us change the "Making Friends" model in just one way. Instead of being rewarded, agents are punished; instead of uniformly positive interactions, we have uniformly negative ones:

Enemies I	Host
Visitor	$(-1, 0)$

Enemies II	Host
Visitor	$(-1, -1)$

Instead of interactions being reinforcing, we take them as inhibiting. The dynamics of inhibition might be modeled in a number of ways. Continuing to use the update Eq. (11.2) will not work because the weights will end up becoming negative and the visitation probabilities in Eq. (11.1) will be meaningless. In this section we explore two other possible rules for updating the weights so as to inhibit past behavior. With negative reinforcement, it is easy to predict what will happen: the social network always becomes uniform, and the dynamics are not sensitive to the particular updating mechanism. Indeed this is what happens. Since there are no surprises, and since this model is just a building block for a model with both structural and strategic dynamics, we keep the discussion brief.

11.3.1 The Transfer Model

Consider a three player model with the following update rule on the weights. Initial weights are all positive integers. When i visits j, the weight w_{ij} is diminished by 1 and the weight w_{ik}, $k \neq i, j$, is increased by 1. This is equivalent to the Ehrenfest model of heat exchange between two bodies [30]. In the original Ehrenfest model there are two urns. A ball is drawn at random from among all balls in both urns and transferred to the other urn. The distribution of balls tends to the binomial distribution, where each ball is independently equally likely to be in either urn. In Making Enemies, with transfer dynamics and three players, each player may be thought of as having such a pair of urns. The urns are independent.

Since the number of balls is fixed, an Ehrenfest urn is a Markov chain with a finite number of states, where the states consist of distributions over the two urns. For example, if there are only two balls, then there are three states, $S1$, $S2$ and $S3$, corresponding to urn cardinalities of $(2, 0)$, $(1, 1)$ and $(0, 2)$. The transition matrix for this Markov chain is

$$\begin{pmatrix} 0 & 1 & 0 \\ \frac{1}{2} & 0 & \frac{1}{2} \\ 0 & 1 & 0 \end{pmatrix}$$

and the unique stationary vector is $(1/4, 1/2, 1/4)$. In contrast to the Pólya urn, we do not have convergence of the conditional probabilities of visits at each stage given the present: at any time, given the present composition, the probability of a given visit may be 0, $1/2$ or 1, depending on the composition of the urns belonging to the visitor. However, if the number of balls, N is large, approximately equal visiting probabilities are very likely in the following sense. The invariant distribution is binomial, which is concentrated around nearly even distributions when the number of balls is large. Thus with high probability, no matter what the initial state, after roughly $N \log N/2$ steps [31], the composition of an urn with N balls will be close to a draw from a binomial distribution. The conditional probability of either of the two possible visits, will therefore be close to $1/2$, and will tend to remain there with high probability. Kac [32] uses these properties to resolve the apparent paradoxes that beset Bolzmann's discussion of irreversibility in statistical mechanics.

11.3.2 The Resistance Model

The transfer model allows for a finite cumulative amount of negative reinforcement, and indeed yields a finite Markov chain. Let us explore a rather different model, termed the *resistance model*, in which negative payoffs generate resistance. Initially every choice has resistance 1. The magnitude of a negative payoff is added to its associated resistance, so the Eq. (11.2) becomes

$$w_{ij}(t+1) = w_{ij}(t) + |u(i, j; t)|.$$

In the case at hand, when all payoffs are negative, the probability of i visiting j is proportional to the reciprocal of the resistance:

$$p_{ij} = \text{Prob(agent } i \text{ visits } j) = \frac{1/w_{ij}}{\sum_{k=1}^{n} 1/w_{ik}}$$

with $1/w_{ii} = 0$ by convention. The dynamics of Enemies I and Enemies II under resistance dynamics are easy to describe.

Theorem 3. *For Enemies I or Enemies II, from any initial conditions, the probability matrix $p(t)$ converges to the uniform probability matrix $\overline{p}$ where $\overline{p}_{ij} = 1/(n-1)$ for any $i \neq j$. The of convergence is rapid: of order $N \log N$ if the initial resistances are of order N. The deviations from uniform obey a central limit theorem:*

$$t^{1/2}(p - \overline{p}) \to X$$

where X is a multivariate normal with covariance matrix of rank $n(n-1)$ in Enemies I and $n(n-1)/2$ in Enemies II. In other words, deviations from uniformity are independent normals, subject to the constraints of adding up to zero for each individual and, in the case of Enemies II, the constraints of symmetry.

The central limit theorem may be derived from a stronger, functional central limit theorem, linearizing the system near the uniform probability to see that the paths

$$t \mapsto N^{-1/2}(p(Nt) - \overline{p})$$

converge in distribution as $N \to \infty$ to a multivariate Ornstein-Uhlenbeck process. The rate of convergence follows from standard coupling arguments.

While uniform positive reinforcement breeds structure from unstructured initial conditions, uniform negative reinforcement evidently breeds uniformity even from structured initial conditions. It would appear, therefore, that the customary random encounter (mean-field) model is more suitable for Making Enemies than Making Friends.

11.3.3 A Better Model?

We would like a model that allows for both positive and negative reinforcement. A natural choice is to let w_{ij} keep track of the log-likelihood for i to visit j, so that probability of i visiting j is given by

$$p_{ij} = \text{Prob(agent } i \text{ visits } j) = \frac{\exp(w_{ij})}{\sum_{k=1}^{n} \exp(w_{ik})} . \tag{11.3}$$

In the next section we will see a property this rule has in common with rules that discount the past, namely that it leads to being trapped in a deterministic state where i always visits the same j.

Question 1. Is there a model incorporating both positive and negative reinforcement, that is realistic, tractable, and non-trapping?

11.4 Perturbations of the Models

In this section we add two features, noise and discounting, commonly used to create more realistic models. We examine the effects on social structure. In particular, these lead to varying degrees of subgroup formation.

11.4.1 Discounting the Past

In the foregoing models, a positive (or negative) payoff in the distant past contributes equally to the weight (or resistance) assigned to an edge as does a like payoff in the immediate past. This is implausible, both psychologically and methodologically. As a matter of psychology, memories fade. From the standpoint of inductive logic, it is not at all certain that the learner is dealing with stationary probabilities – indeed, in cases of prime interest she is not. For this reason, recent experience may have a better chance of being a relevant guide to future action than the remote past.

A simple and standard way to modify the models to reflect this concern is to introduce discounting of the past. We will concentrate here on the models of Making Friends. After each interaction we will now multiply the weights of the previous stage by a discount factor, d, between 0 and 1. The we add the undiscounted payoffs from the present interaction to get new weights. The modification of the dynamics has a dramatic effect on the Making Friends models.

For Friends I, it is immediately evident from simulations with $d = 0.9$, say, and ten players, that the probabilities p_{ij} converge to 0 or 1. In other words, each individual ends up always visiting the same other individual.

In Friends II, simulations show the group breaking into pairs, with each member of a pair always visiting his or her "partner". Which pairs form depends on the randomness in the early rounds of visits, but pairs always form. In fact there are other possible limit states, but their frequency is low except at more extreme discount

rates. The set of possible limit states may be described as follows. Some agents are grouped in pairs, each member of a pair always visiting the other. Other agents are grouped in *stars*. These are clusters of size at least three, in which one agent, called the *center*, visits each of the others with positive frequency, while the others always visit the center.

11.4.2 Analysis of Discounting the Past

It is worth giving a rigorous derivation of the above behavior, since it will shed some light on a defect in the most obvious log-likelihood model to incorporate positive and negative reinforcement. Our derivation highlights this, although the results for discounted Friends I may also be derived from a theorem of H. Rubin ([33], p. 227).

Theorem 4. *In Friends II with discount rate $d < 1$, there is always a partition into pairs and stars and a random time after which each member of a pair visits only the other member of the pair and each non-central member of a star visits only the center. In Friends I, there is a random function f and a random time after which each player i always visits $f(i)$.*

Sketch of Proof : The analysis for Friends I is similar but easier, so we prove the statement only for Friends II. With each probability matrix p we associate a graph $G(p)$ as follows. The edge (i, j) is in the graph G if the probability $p_{ij} > \varepsilon$, where $\varepsilon < 1/(2n)$ is some fixed positive number. Among those graphs having at least one edge incident to each vertex, let S denote the minimal such graphs, that is, ones for which deleting any edge results in an isolated vertex. It is easy to see that S is the set $G(p)$ for all p satisfying the conclusion of the theorem.

The principle behind the analysis of discounted Friends is that the future behavior of p is largely determined by the present $G(p)$. In particular, we find a $\delta > 0$ such that from any state p, for each subgraph H of $G(p)$ such that $H \in S$, there is a probability at least δ^2 that for all sufficiently large t, $G(p(t)) = H$. We show this in two steps: (1) with probability at least δ, there is some t for which $G(p(t)) = H$; (2) from any state p such that $G(p) = H$, there is probability at least δ that $G(p(t))$ is equal to H for all later times, t.

To see why (1) is true, for $H \in S$, let f_H be any function on vertices of H for which each value $f(i)$ is a neighbor if i. Observe that there is a number k such that from any state p with $H \subseteq G(p)$, if each vertex i visits $f(i)$ for the next k rounds, then $G(p(k)) = H$. For each round of visits, this probability is at least ε^n, where n is the number of vertices, so taking $\delta \leq \varepsilon^{kn}$ establishes (1). For (2), it suffices to show that with probability δ each agent visits a neighbor in H at all later times. For each agent i, the sum over j not neighboring i in H of p_{ij} is at most $n\varepsilon < 1/2$ by the definition of $G(p) = H$. After k rounds of visits where agents only visit their neighbors in H, this must decrease to at most $(1/2)d^k$. Thus the probability of N rounds of visits only to neighbors in H is at least

$$\prod_{k=0}^{N-1}\left(1-\frac{1}{2}d^k\right)^n.$$

Sending N to infinity yields a convergent infinite product, since $(1/2)d^k$ is summable. Taking δ to be less than the infinite product proves (2).

With (1) and (2), the rest is a standard tail argument. The constraints on evolution are such that $G(p(t))$ always contains at least one graph in S. As long as it contains more than one graph in S, there is always a probability of at least δ of permanently settling into each one. Thus, with probability 1, eventually $G(p(t))$ is equal to some $H \in S$ for all future times. This is equivalent to the conclusion of the theorem. QED

Remark 1. It is actually shown that in (2), if we choose ε sufficiently small, we can choose δ arbitrarily close to 1.

We now also see why the log-likelihood rule (3) leads to fixation of a degenerate structure. Under these dynamics, an equivalent phenomenon occurs to (1) in the proof of Theorem 4. For a pair (i, j) whose interaction has a positive mean, if the pair plays repeatedly, we will see $w_{ij}(t)/t \to \mu > 0$. The probability the i will ever switch partners, once having tried j a few times is at most on the order of $\sum_{k=0}^{\infty} B\exp(-k\mu)$, where $B = \exp(\sum_{l\neq j} w_{il})$. From here it is easy to construct an argument parallel to the proof of Theorem 4, to show that in presence of a game with positive mean payoff, discounted structural dynamics lead with probability 1 to fixation at a pairing.

11.4.3 Introduction of Noise

A common feature in models of adaptation is the introduction of noise: a small chance of a behavior other than the one chosen by the dynamical equation for the model. This may stem from an agent's uncertainty, from agent error, or from circumstances beyond an agent's control. Alternatively, an agent may purposefully add noise to her strategy in order to avoid becoming wedded to a less than optimally efficient strategy or structure.

From a methodological point of view, noise that does not go to zero with time transforms the model into an ergodic Markov chain. No state is then trapping. To the extent that the trapping states produced by discounting or linear log-likelihood are unrealistic, we may hope to mitigate the problem by adding a noise component. Since dynamics with a noise term do not lead to a single state, the outcome is usually phrased in terms of *stochastically stable states* [34]. A state is termed stochastically stable if the chance of finding the system near that state does not go to zero as the magnitude of the noise term goes to zero.

Neither discounting nor noise will affect the limiting behavior of Making Enemies. For Making Friends, let us modify the probability rule (1) so that in the n-player game, the probability of i visiting j is now some fixed positive number $\varepsilon/(n-1)$, plus $(1-\varepsilon)$ times what it was before:

$$p_{ij} = \frac{\varepsilon}{n-1} + (1-\varepsilon)\frac{w_{ij}}{\sum_k w_{ik}}.$$

The effect of this is to push the system by ε toward the uniform point $\overline{p}$. Neither Friends I nor Friends II is now a martingale, and the stable set of each is reduced to the single point $\overline{p}$. Since this is true at any noise level $\varepsilon > 0$, we see that there is only one asymptotically stable point. Since the qualitative outcome is sensitive to the existence of a noise term, it is incumbent to ask with regard to specific models whether a noise term is natural and realistic.

11.4.4 Noise and Discounting

In the presence of a discount $d < 1$ and a noise term $\varepsilon > 0$, if $1-d$ is much smaller than ε then the discount is so low that the noise term wipes out any effect the discounting might have had. In the other case, where d is held fixed and ε tends to zero, we may ask about the asymptotically stable states of system with past discounting dynamics. For Friends I, nothing much interesting happens: discounting causes the limiting state to be degenerate; with noise, the system may jump from one such state to the other, which does not change which states are stochastically stable.

For Friends II, as long as the number of players n is at least 4, the introduction of noise does indeed change the set of stochastically stable states: it gets rid of stars. Simulations show that pairings are by far the most prevalent states in discounted Friends II, with a star of size 3 forming when necessitated by an odd number of players. We now show that states with more than one star, or a star of size greater than 3, are not stochastically stable.

Theorem 5. *In Friends II, with discounting, with n players, and with noise tending to zero, the stochastically stable states are those that are either unions of pairs (if n is even) or pairs plus a single star of size 3 (if n is odd).*

Sketch of Proof : Let S denote the graphs corresponding to possible limit states as in the proof of Theorem 4, and let $S_0 \subseteq S$ denote those graphs with no stars (perfect pairings) or with a single star of size 3. The important features of the relation of S to S_0 are as follows. (1) if G is the result of adding a single edge to a graph in S_0, then G contains no graph in $S \setminus S_0$. (2) for any $G \in S$ there is a chain $G = G_1, G_2, \ldots, G_k$ leading to S_0, where each G_{j+1} may be obtained from G_j be adding an edge and then deleting two edges. Property (1) is apparent. To verify (2), note that if $H \in S$ and i and j are non-central vertices in stars of H, and they are not both in the same star of size 3, then adding the edge between i and j and removing the two edges previously incident to i and j produces a new graph in S. Iterating this procedure starting from $H = G_1$ leads in finite time (since the number of edges decreases each time) to an element of S_0.

We now follow the usual method for determining stochastic stability [35]. Let the probability ρ of disobeying the structural dynamics equation (11.1) be very small. If ε (in the definition of S) is very small, then a state p with $G(p) = G \in S$

will have $G(p(t)) = G$ for all later times with high probability, until there is a disobeying move. After a single disobedience, the graph $G(p)$ will be the union of G with one extra edge. By the remark after the proof of Theorem 4, we see that after a disobedience, the graph will then relax to some subgraph in S. By property (1), if $G \in S_0$ then this subgraph is again in S_0. Thus a single disobedience followed by relaxation back to S will never escape S_0. Hence the probability of jumping to $S \setminus S_0$ is of order ρ^2, which implies that states in S_0 stay in S_0 for time at least ρ^{-2}. On the other hand, by property (2), from any state in $S \setminus S_0$, there is a chain of single disobediences, such that allowing the system to relax after each may with positive probability land you back in S_0. Thus the expected time spent in $S \setminus S_0$ before returning to S_0 is at most of order ρ. Thus the process spends $(1 - \rho)$ portion of the time in S_0, and sending ρ to zero, we see that only states in S_0 are stochastically stable. It is easy to see that all of these are indeed stochastically stable. QED

11.5 Reinforcement by Games of Nontrivial Strategy

So far we have only considered a baseline model of uniform reinforcement, which turned out still to have nontrivial structural behavior. Now we examine a reinforcement scheme resulting from the payoff of a nontrivial game. We will consider the case where evolution of strategy is slower than evolution of structure. Thus, we will consider the agents as divided into types, each type always playing a fixed strategy, and see what sort of interaction structure emerges. We then extend this by allowing strategic switching of types. We find that coordination of strategy occurs, though whether players coordinate on the risk-dominant or payoff-dominant strategy depends on parameters of the model such as the rate of strategic evolution. Depending on conditions of the model, the social network may or may not split up into pairs.

11.5.1 Rousseau's Stag Hunt

Consider a two-player version of Rousseau's *Stag Hunt* [36]. The choices are either to hunt stag or to hunt rabbit (hare, in the original). It takes two person cooperating to effectively hunt a stag, while one person acting independently can hunt a rabbit. Bagging a stag brings a greater payoff.

	Hunt Stag	Hunt Rabbit
Hunt Stag	(1, 1)	(0, 0.75)
Hunt Rabbit	(0.75, 0)	(0.75, 0.75)

There are two equilibria in this game: both hunt stag, and both hunt rabbit. The first carries the higher payoff and is said to be *payoff dominant*; the second carries the least risk and is said to be *risk dominant* [37]. In models without structural dynamics, Kandori et al. [38] have shown that only the risk dominant equilibrium of

a two player coordination game is stochastically stable. In the presence of structural dynamics, we will describe a more optimistic conclusion.

Theorem 6. *Suppose Stag Hunt is played by* $2n$ *players, with structural dynamics given by equation (2) and cumulative weighting dynamics (1) with no noise or discounting. Then in the limit, stag hunters always visit stag hunters and rabbit hunters visit rabbit hunters.*

Sketch of Proof : First note that no visit of a stag hunter to a rabbit hunter is ever reinforced. Thus $w_{ij}(t) = 1$ for all t if i is a stag hunter and j is a rabbit hunter. Observing that the weights $w_{ij}(t)$ go to infinity when i and j are both stag hunters, we see that the probability of a stag hunter visiting a rabbit hunter goes to zero.

Next consider the subpopulation of rabbit hunters, call it A. For $i \in A$, let

$$Z(i,t) = \frac{\sum_{j \notin A} w_{ij}}{\sum_{j=1}^{n} w_{ij}}$$

denote the probability of visiting a given rabbit hunter visiting a stag hunter on the next turn. The expected value of $Z(i, t+1)$ changes according to the formula

$$\mathbf{E}(Z(i,t+1)|Z(i,t)) = Z(i,t) + t^{-1}Y(i,t)$$

where $Y(i,t)$ is the proportion of increase in expected weight w_{ij} due to $j \notin A$:

$$Y(i,t) = \frac{\sum_{j \notin A} p_{ij} + p_{ji}}{\sum_{j=1}^{n} p_{ij} + p_{ji}}.$$

Ignoring the terms p_{ji} in both the numerator and denominator of the above expression would lead to exactly $Z(i,t)$. The terms p_{ji} for $j \notin A$ are known to be small, while the total from the terms p_{ji} for $j \in A$ cannot be small. Consequently, $Y(i,t) < (1-\varepsilon)Z(i,t)$ for some $\varepsilon > 0$, whence

$$\mathbf{E}(Z(i,t+1) - Z(i,t)|Z(i,t)) \leq -\frac{\varepsilon Z(i,t)}{t}.$$

Since the increments in $Z(i,t)$ are bounded by C/t, there are a $\lambda, \mu > 0$ for which $\exp(\lambda Z(i,t) + \mu \log t)$ is a supermartingale, which implies that $Z(i,t)$ converges to zero exponentially fast in $\log t$. QED.

Introduction of a discount rate changes this outcome. Stag hunters still end up visiting stag hunters, since even discounted reinforcement beats a reinforcement of zero, but now rabbit hunters will get locked either into pairs and stars as in Making Friends, or into repeated visits to a single stag hunter. These limit states are all invariant under introduction of noise. When a rabbit hunter visits a stag hunter the loss to society is the 0.75 that another rabbit hunter would have profited from the visit. The model is evidently weak here, since it allows only one visit *by* each agent

but any number of visits *to* each agent in a round of visits. That is, a more realistic loss would be the stag hunter's wasted time when visited by the rabbit hunter.

It should be noted that although the stochastically stable states include ones that are not optimally efficient, the optimally efficient states (those states where rabbit hunters visit rabbit hunters) will have an edge. Due to the possibility of reciprocal reinforcement, it will be easier for a rabbit hunter to switch from visiting a stag hunter to visiting a rabbit hunter, than *vice versa*. Secondly, when the discount rate is near 1, the model behaves like the undiscounted model for a long enough time that it is very unlikely for a rabbit hunter to get locked into visiting a stag hunter in the first place. Simulations of Stag Hunting with ten players and $d = 0.9$, seem to show that rabbit hunters "always" visit rabbit hunters. Due to both of the effects mentioned above, the system is nearly always found in an optimally efficient state, even though there are stochastically stable states that are not optimally efficient.

11.5.2 Co-evolution of Structure and Strategy

To the previous model, we now add the possibility of an agent switching states: a stag hunter may decide to become a rabbit hunter, or a rabbit hunter may become bold and hunt stag. When this kind of strategic evolution is faster than the structural evolution, we know from studies of random encounter models that the risk dominant equilibrium of everyone hunting rabbits will be arrived at while the network is still near its initial state of uniform visitation probabilities.

Whether strategic dynamics are faster or slower than structural dynamics depends, of course, on the activity being modeled; sometimes interaction structure is externally imposed, while sometimes it is more easily modified than strategy or character. Let us suppose that the investment in re-training as a different kind of hunter is great, so between each round of visits there is only a small chance that one of the hunters will change types. Then we have seen that hunters always (with no noise or discounting) or nearly always (in discounted models) hunt with others of like type. This eliminates the risk inherent in random encounters, and allows hunters to profit from switching to stag hunting after an initial period where they find another stag hunter. Slow strategic adaptation gradually converts rabbit hunters to stag hunters and the payoff dominant strategy dominates.

We describe here the results of simulations of Stag Hunting for 1,000 time steps, where with some probability q at any given time, an individual changes type to whichever type was most successful in the previous round. When $q = 0.1$, we found that in 22% of the cases all hunters ended up hunting stag, while in 78% of the cases, all hunters hunted rabbit. Thus there was perfect coordination, but usually not to the most efficient equilibrium. On the other hand, when $q = 0.01$, the majority (71%) of the cases ended in the optimal state of all hunting stag, while 29% ended up all hunting rabbit. Increasing the initial edge weights made it far less likely to reach the stag hunting equilibrium, since stag hunters took a long time to perfectly align, and without alignment, the previous round's best strategy was almost always rabbit hunting. For instance, if the initial weights were 1,000 for each visit, under 1% of the cases ended up all stag hunting, whether q was 0.1 or 0.01.

Once hunters largely cease to visit hunters of opposite type, the structural evolution within each of the two subpopulations is a version of Friends II. The resulting social structure will not be a perfect pairing, but will have each rabbit (stag) hunter visiting each other rabbit (stag) hunter, but with varying probabilities.

11.6 Conclusion

We have taken some basic steps in exploring dynamics of evolution of interaction structures and co-evolution of structure and strategy. The ultimate goals are to create models that are more true to life, and to find theoretical bases for observed behaviors of systems, including prediction of selection between multiple equilibria.

The particular dynamics we use here are only examples, but it turns out that the simplest of these may deliver interesting and surprising results. Even in baseline models where the game being played is degenerate, we find spontaneous emergence of structure from uniformity and spontaneous emergence of uniformity from structure. We find processes with extremely long transient modes, where limiting behavior is not a good guide for predicting behavior after thousands of trials.

The social interaction structures that emerge tend to separate the population into small interaction groups within which there is coordination of strategy. This separation may be complete, as in discounted Friends II, or may be only a tendency, as in the non-discounted versions of Friends and Stag Hunting.

When we combine structure and strategy dynamics for a non-trivial game, the Stag Hunt, we find that the probable outcomes depend on the timing. Where structure is frozen in a random encounter configuration we get the expected risk-dominant equilibrium outcome. But when structure is fluid relative to strategy, structural adaptation neutralizes the risk and we get the socially efficient payoff dominant equilibrium. Varying between these extremes can give one or the other result with different probabilities – or may leave the group in a state where both strategies are used. We expect to see structure dynamics making a difference in other games as well. Indeed, we have some preliminary simulation evidence showing this to be true for a bargaining game ("split the dollar"), and for a simple coordination game.

There are many more avenues to pursue. As mentioned in Sect. 11.3, it would be desirable to find a model in which positive and negative reinforcement are present, but trapping does not occur. We have not modeled any interaction among three or more players. We also have yet to model any explicit interaction between strategy and structure: the choice of a partner to play with and a strategy to play against that partner need not be independent.

One could continue adding complexity so as to allow information to affect structural evolution, to include communication between players, and so forth. Our main point is this. Structural change is a common feature of the real world. A theory of strategic interaction must take account of it. There is a mathematically rich theory which develops relevant tools. We believe that explicit modeling of structural dynamics, and the interaction of structure and strategy, will generate new insights for the theory of adaptive behavior.

Acknowledgements We wish to thank Persi Diaconis, Joel Sobel and Glenn Ellison, for bringing us together, for helpful discussions, and for greatly improving our awareness of the relevant literature.

References

1. Hofbauer, J. and Sigmund, K. (1988). *The theory of evolution and dynamical systems* (Cambridge University Press: Cambridge).
2. Weibull, J. (1997). *Evolutionary game theory* (MIT Press: Cambridge, MA).
3. Feldman, M. and Thomas, E. (1987). Behavior-dependent contexts for repeated player of the Prisoner's Dilemma II: Dynamical aspects of the evolution of cooperation. *J. Theor. Biol.* **128**, 297–315.
4. Wright, S. (1921). Systems of mating III: assortative mating based on somatic resemblance. *Genetics* **6**, 144–161.
5. Wright, S. (1945). Tempo and mode in evolution: a critical review. *Ecology* **26**, 415–419.
6. Jackson, M. and Watts, A. (1999). On the formation of interaction networks in social coordination games. *Working paper.*
7. Durrett, R. and Neuhauser, C. (1997). Coexistence results for some competition models. *Ann. Appl. Prob.* **7**, 10–45.
8. Kang, H.-C., Krone, S. and Neuhauser, C. (1995). Stepping stone models with extinction and recolonization. *Ann. Appl. Prob.* **5**, 1025–1060.
9. Durrett, R. and Levin, S. (1994). The importance of being discrete (and spatial). *Theor. Pop. Biol.* **46**, 363–394.
10. Blume, L. (1993). The statistical mechanics of strategic interaction. *Games Econ. Behav.* **5**, 387–423.
11. Pollack, G. B. (1989). Evolutionary stability on a viscous lattice. *Soc. Networks* **11**, 175–212.
12. Lindgren, K. and Nordahl, M. (1994). Evolutionary dynamics and spatial games. *Physica D* **75**, 292–309.
13. Anderlini, L. and Ianni, A. (1997). Learning on a torus. In: *The dynamics of norms*, ed. C. Bicchieri, R. Jeffrey, and B. Skyrms (Cambridge University Press: Cambridge) 87–107.
14. Ellison, G. (1993). Learning, local interaction, and coordination. *Econometrica* **61**, 1047–1071.
15. Watts, D. and Strogatz, S. (1998) Collective dynamics of "small-world" networks. *Nature* **393**, 440–442.
16. Schelling, T. (1969) Models of Segregation. *Am. Eco. Rev., Papers Proc*. **59**, 488–493.
17. Schelling, T. (1971). Dynamic models of Segregation. *J. Math. Sociol.* **1**, 143–86.
18. Epstein, J. and Axtell, R. (1996). *Growing Artificial Societies* (MIT/Brookings: Cambridge, MA).
19. Zajonc, R.B. (1968). Attitudinal effects of mere exposure. *J. Personality Social Psychol. Monogr.* **9**, 1–28.
20. Coppersmith, D. and Diaconis, P. (1987). Reinforced Random Walk. *Unpublished manuscript.*
21. Arthur, W. B. (1989). Competing technologies, increasing returns, and lock-in by historical events. *Econ. J.* **99**, 116–131.
22. Eggenberger, F. and Pólya, G. (1923). Über die Statistik verketter Vorgange. *Zeit. Angew. Math. Mech.* **3**, 279–289.
23. Johnson, N. and Kotz, S. (1977). *Urn models and their application* (John Wiley & Sons: New York).
24. Durrett, R. (1996). *Probability: Theory and examples, 2nd edition* (Duxbury Press, Wadsworth Publishing Company: Belmont, CA).
25. Pemantle, R. and Skyrms, B. (2000). Reinforcement schemes may take a long time to exhibit limiting behavior. *In Preparation.*

26. Robbins, H. and Monro, S. (1951). A stochastic approximation method. *Ann. Math. Statist.* **22**, 400–407.
27. Pemantle, R. (1990). Nonconvergence to unstable points in urn models and stochastic approximations. *Ann. Probab.* **18**, 698–712.
28. Benaïm, M. and Hirsch, M. (1995). Dynamics of Morse-Smale urn processes. *Ergodic Theor. Dyn. Syst.* **15**, 1005–1030.
29. Talagrand, M. (1995). Concentration of measure and isoperimetric inequalities in product spaces. *IHES Publ. Math.* **81**, 73–205.
30. Ehrenfest, P. and Ehrenfest, T. (1907). Über zwei bekannte Einwande gegen das Bolzmannshe H-Theorem. *Phys. Zeit.* **8**, 311–314.
31. Diaconis, P. and Stroock, D. (1991). Geometric bounds for eigenvalues of Markov chains. *Ann. Appl. Prob.* **1**, 39–61.
32. Kac, M. (1947). Random walk and the theory of Brownian motion. *Am. Math. Monthly* **54**, 369–391.
33. Davis, B. (1990). Reinforced random walk. *Prob. Theor. Rel. Fields* **84**, 203–229.
34. Foster, D. and Young, H. P. (1990). Stochastic evolutionary game theory. *Theor. Pop. Biol.* **38**, 219–232.
35. Ellison, G. (2000). Basins of attraction, long run stochastic stability, and the speed of step-by-step evolution. *Rev. Econ. Studies,* **67** (1), 17–45.
36. Rousseau, J.-J. (1984). *A discourse on inequality*. Tr. Maurice Cranston (Penguin Books: London).
37. Harsanyi, J. and Selten, R. (1988). *A general theory of equilibrium in games* (MIT Press: Cambridge, MA).
38. Kandori, M., Mailath, G. and Rob, R. (1993). Learning, mutation, and long run equilibria in games. *Econometrica* **61**, 29–56.

Postscript to: *A Dynamic Model of Social Network Formation*

At about the same time as our paper was originally published, several economists initiated a somewhat different account of network formation. [3, 8, 20.] They view network links as all-or-none, whereas we view them as stochastic. Thus, for them a network is a graph or a directed graph, while for us it is a random graph. They imbed the network in a game – a game, where the players acts are choosing to make or break links, and the graph structure determines the players payoffs. We embed the games in an evolving network, with the games being played across links. The network dynamics considered in these three papers is one of *best-response with inertia*. At a random time, a player looks at the network structure and chooses a best response, which may consist of making or breaking links or both. Updating times are independent across players, so updating is asynchronous, which avoids cycles. This line of research can be thought of as complementary to that which we and others to be discussed here have pursued.

We emphasized stochastic networks that evolve as low-rationality agents update their probabilities by reinforcement learning or imitation or both. Deterministic networks might or might not crystallize out, depending of the learning dynamics used and the kind of interaction being modeled. Our point of view is thus close to that expressed by Kirman [9]. Bonacich and Liggett [4] and Liggett and Rolles, [10] work in a closely related model. Our baseline interactions, Friends I and II

always reinforced the visitor, or both the visitor and the host respectively. These papers consider the case where the host alone is reinforced as a model of gift-giving – the visitor takes a gift to the host. They also use reinforcement learning as a dynamics, but the kind of reinforcement learning is different. It derives from Bush and Mosteller rather than from Herrnstein, Roth and Erev, and it generates a Markov chain rather than a reinforcement process. [See Pemantle [13], for a survey of reinforcement processes. See Argiento et al. [2] for application of our kind of reinforcement learning to a signaling game.] As Bonacich and Liggett remark, their dynamics tends to freeze into the same sort of structures as our Friends II model where reinforcement is modified by discounting the past. From the viewpoint of stochastic approximation theory, such discounting converts a process with diminishing step size of order (1/time) to one of constant step size. Individuals then have a tendency to "freeze" into deterministic relationships.

In Pemantle and Skyrms [14, 15] we analyze clique formation in a 3-person "friends" game, *Three's Company*, and in a 3-person version of the Stag Hunt, where the learning is Herrnstein-Roth-Erev reinforcement with discounting the past. It is proved that cliques always form in the limit. However, extensive simulations only show reliable clique formation when the discounting is substantial. It is shown that for small discounting, long-run limiting results are a poor guide to medium-run behavior. Rather the medium run should be expected to approximate the limiting behavior of undiscounted learning. In the 3-person Stag Hunt, in contrast with this slow clique formation, Stag Hunters learn to visit each other rapidly, and thus the positive results for social cooperation of our original paper are preserved.

The structure dynamics, the strategy revision dynamics, and the embedded game may be varied. Skyrms [17, 18] and Skyrms and Pemantle [19] consider various combinations of structure and strategy dynamics. In double reinforcement dynamics both network structure and strategy played evolve by reinforcement, but at different rates Double reinforcement dynamics in the Stag Hunt agrees with the general principle that fast evolution of network structure favors cooperation. But if strategy revision dynamics is changed to best response in the Stag Hunt, individuals may freeze into two social classes – cooperators and loners.

Coevolution of network structure and strategy is also studied by Zimmerman et al. [21], and by Santos et al. [16], who also find a positive effect on evolution of cooperative behavior. Goyal and Vega-Redondo [5] study a model of co-evolution of structure and strategy where link formation is costly. In their model, high costs of link formation favor cooperation in the Stag Hunt game. A model with imitate-the-best strategy revision and with deterministic costly links that require mutual consent, and are driven by cost-benefit analysis, is analyzed in Hanaki et al. [7]. Pacheco et al. [11] and Pacheco et al. [12] interpret fast evolution of network structure as a way of transforming the payoffs of the embedded game. In this way, a Prisoner's Dilemma can be transformed into a Stag Hunt. This is quite consonant with view taken in Skyrms [17]. In both these papers relative rates of network and strategy revision dynamics again play a key role in evolution of cooperation.

Alexander's [1] book systematically compares coevolution of structure and strategy with evolution on fixed structures across a range of games. In addition to the

usual social dilemmas, he also examines bargaining games. There is a comprehensive review across fields of adaptive social networks in Gross and Blasius [6].

Acknowledgements Research supported in part by National Science Foundation grant # DMS 9803249. This chapter is based on B. Skyrms and R. Pemantle, "A Dynamic Model of Social Network Formation," PNAS 97 (16), 9340-9346 (2000).

References

1. Alexander, J. McKenzie (2007) *The Structural Evolution of Morality*. Cambridge: Cambridge University Press.
2. Argiento, R., Pemantle, R., Skyrms, B. and Volkov, S. (forthcoming) Learning to Signal: Analysis of a Micro-Level Reinforcement Model. *Stochastic Processes and their Applications.*
3. Bala, V. and Goyal, S. (2000) A Non-Cooperative Model of Network Formation. *Econometrica* 68: 1181–1229.
4. Bonacich. P. and Liggett, T. (2003) Asymptotics of a Matrix-Valued Markov Chain Arising in Sociology. *Stochastic Processes and their Applications* 104: 155–171.
5. Goyal, S. and Vega-Redondo, F. (2005) Network Formation and Social Co-ordination. *Games and Economic Behavior* 50: 178–207.
6. Gross, T. and Blasius, B. (2008) Adaptive Coevolutionary Networks: A Review. *Journal of the Royal Society Interface* 5: 259–271.
7. Hanaki, N., Peterhansl, A., Dodds, P. S., and Watts, D. (2007) Cooperation in Evolving Social Networks. *Management Science* 53: 1036–1050.
8. Jackson, M. and Watts, A. (2002) On the Formation of Interaction Networks in Social Coordination Games. *Games and Economic Behavior* 41: 265–291.
9. Kirman, A, (1997) The Economy as an Evolving Network. *Journal of Evolutionary Economics* 7: 339–353.
10. Liggett, T. M. and Rolles, S. (2004) An Infinite Stochastic Model of Social Network Formation. *Stochastic Processes and their Applications* 113: 65–80.
11. Pacheco, J. M., Traulsen, A. and Nowak, M. A. (2006) Coevolution of Structure and Strategy in Complex Networks with Dynamic Linking. *Physical Review Letters* 97: 258103.
12. Pacheco, J. M., Traulsen, A., Ohtsuki, H. and Nowak, M. A. (2008) Repeated Games and Direct Reciprocity Under Active Linking. *Journal of Theoretical Biology* 250: 723–731.
13. Pemantle, R. (2007) A Survey of Random Processes with Reinforcement. *Probability Surveys* 4: 1–79.
14. Pemantle, R. and Skyrms, B. (2004a) Time to Absorption in Discounted Reinforcement Models. *Stochastic Processes and their Applications* 109: 1–12.
15. Pemantle, R. and Skyrms, B. (2004b) Network Formation by Reinforcement Learning: The Long and the Medium Run. *Mathematical Social Sciences* 48: 315–327.
16. Santos, F. C., J. M. Pacheco and T. Lenaerts (2006) Cooperation Prevails when Individual Adjust their Social Ties. *PloS Computational Biology* 2: 1284–1291.
17. Skyrms, B. (2004) *The Stag Hunt and the Evolution of Social Structure*. Cambridge: Cambridge University Press.
18. Skyrms, B. (2009) Groups and Networks: Their Role in the Evolution of Cooperation. In *Groups, Games and the Global Good*. Ed. Simon Levin. Berlin: Springer Verlag.
19. Skyrms, B. and R. Pemantle (forthcoming) Learning to Network. In *Probability in Science*. Ed. E. Eells and J. Fetzer. Open Court Publishing.
20. Watts, A. (2001) A Dynamic Model of Network Formation. *Games and Economic Behavior* 34: 331–341.
21. Zimmerman, M. G., Eguiluz, V. M., San Miguel, M. (2004) Coevolution of Dynamical States and Interactions in Dynamic Networks. *Physical Review E* 69: 065102.

Chapter 12
Evolutionary Games in Self-Organizing Populations

Arne Traulsen, Francisco C. Santos, and Jorge M. Pacheco

Abstract Social networks are dynamic: We make new friends and lose touch with old ones, depending on the interactions with them. Most analytic studies of social networks assume that links remain unchanged at all times. In this case, individuals have no control over the number, frequency or duration of their interactions with others. Here, we discuss analytical and numerical models in which individuals can break links and create new ones. Interactions are modeled as general symmetric two-player games. Once a link between two individuals has formed, the productivity of that link is evaluated. Links can be broken off at different rates. In the limiting cases where linking dynamics is much faster than evolutionary dynamics or vice-versa, the system can be tackled analytically for non-local linking dynamics. We show how the individual capacity of forming new links or severing inconvenient ones can change the nature of the game. If the linking rules are local, numerical simulations show that the resulting networks capture some of the features characteristic of real-world social networks.

12.1 Evolutionary Game Dynamics

Game theory describes systems in which the success of an individual depends on the actions of others. The classical approach focused on the determination of optimal strategic behavior of rational individuals in such a static setting [1]. Evolutionary game theory places this framework into a dynamical context by looking at the evolutionary dynamics in a population of players [2]. Successful behaviors spread in such a population. The expected payoff from the game is a function of the frequencies of all strategies. There are two interpretations of evolutionary game theory: In the conventional setting, the payoff is interpreted as biological fitness. Individuals

A. Traulsen (✉)
Evolutionary Dynamics Group, Max-Planck-Institute for Evolutionary Biology, 24306 Plön, Germany
e-mail: traulsen@evolbio.mpg.de

T. Gross, H. Sayama (eds.), *Adaptive Networks,* Understanding Complex Systems,
DOI 10.1007/978-3-642-01284-6_12,

reproduce proportional to their fitness and successful strategies spread by genetical reproduction. A second interpretation is the basis for cultural evolution in social systems: Successful behaviors are imitated with a higher probability. They spread by social learning instead of genetical reproduction. Both frameworks are captured by the same mathematical approach: The generic mathematical description of evolutionary game dynamics is the replicator equation [3–5]. This system of nonlinear ordinary differential equations describes how the relative abundances (frequencies) of strategies change over time. The assumption underlying the replicator equation is that individuals meet each other at random in infinitely large, well-mixed populations. But it also emerges in other cases, e.g. if the interaction rates between individuals are not random [6] or from a large-population approximation of evolutionary game dynamics in finite populations [7].

However, in reality the probability to interact with someone else is not the same across a population or social community. Interactions occur on social networks which define the underlying topology of such cultural dynamics. Initially, this line of research has focused on regular lattices [8–12]. More recently, more complex topologies derived from lattices [13, 14] and general networks have been considered in great detail [15–20]. While the theoretical advances in this field are tremendous, there is so far a lack of experimental data. Designing and implementing such experiments has proven difficult and, so far, only general statements as "the probability to be generous is correlated with the number of social links of an individual" can be made [21]. This statement corresponds perfectly with observations of the evolutionary dynamics in theoretical models of social network dynamics [18, 20].

Observing such data from real-world systems is also problematic. One important property of social networks that is seldom addressed in theoretical studies is that real world social networks are not static. Instead, we make new friends and lose touch with old ones, depending on the kind of interaction we have with them. This makes social networks an example of an adaptive network. The basic idea is that interactions which benefit both partners last longer than interactions where one partner is exploited by the other. Here, we discuss such an approach, which leads to analytical results in certain limits. These serve as important starting points for further developments.

12.2 Active Linking

We break down the model into two parts: Evolutionary dynamics of strategies (or behaviors) of the agents associated with nodes in a network whose links describe social interactions. The adaptive nature of the social interactions leads to a network linking dynamics. We consider a game between two strategies, A and B. The network is of constant size with N nodes. The number of links, however, is not constant and changes over time. There are N_A individuals who use strategy A and N_B individuals who use strategy B. We have $N = N_A + N_B$.

12.2.1 Linking Dynamics

An interaction between two players occurs if there is a link between these players. Links are formed at certain rates and have specific life-times. We denote by $X(t)$ the number of AA links at time t. Similarly, $Y(t)$ and $Z(t)$ are the number of AB and BB links at time t. The maximum possible number of AA, AB and BB links is respectively given by

$$\begin{aligned} X_m &= N_A(N_A-1)/2 \\ Y_m &= N_A N_B \\ Z_m &= N_B(N_B-1)/2. \end{aligned}$$

Suppose A players form new links at rate α_A and B players form new links at rate α_B. Thus, AA links are formed at a rate α_A^2, AB links are formed at a rate $\alpha_A\alpha_B$ and BB links are formed at a rate α_B^2. The death rates of AA, AB and BB links are given by γ_{AA}, γ_{AB} and γ_{BB}, respectively. If the number of nodes and links is large, we can model the dynamics of links by differential equations. We obtain a system of three ordinary differential equations for the number of links

$$\begin{aligned} \dot{X} &= \alpha_A^2(X_m - X) - \gamma_{AA}X \\ \dot{Y} &= \alpha_A\alpha_B(Y_m - Y) - \gamma_{AB}Y \\ \dot{Z} &= \alpha_B^2(Z_m - Z) - \gamma_{BB}Z. \end{aligned}$$

For $\alpha^2 \gg \gamma$, the network is almost complete, which recovers the results for well-mixed populations. For $\alpha^2 \ll \gamma$, the network is sparse with few links. The most interesting case we discuss below is $\alpha^2 \approx \gamma$, where the system has fixed points with intermediate ranges of X, Y and Z. Rescaling α and γ in an appropriate way (note that the equation contains squares of α and linear terms of γ) does not change the fixed points of the system, but affects the overall timescale of active linking. When this process is coupled with strategy dynamics, such changes can be crucial.

While the above is probably the simplest possibility to model linking dynamics, more sophisticated choices are possible, for example taking the number of existing links of a node into account. However, to address some general properties of the coevolution between links and strategies, we concentrate on the simplest choice first. In the steady state, the number of links of the three different types is given by

$$\begin{aligned} X^* &= X_m \frac{\alpha_A^2}{\alpha_A^2 + \gamma_{AA}} = X_m \phi_{AA} \\ Y^* &= Y_m \frac{\alpha_A\alpha_B}{\alpha_A\alpha_B + \gamma_{AB}} = Y_m \phi_{AB} \\ Z^* &= Z_m \frac{\alpha_B^2}{\alpha_B^2 + \gamma_{BB}} = Z_m \phi_{BB}. \end{aligned}$$

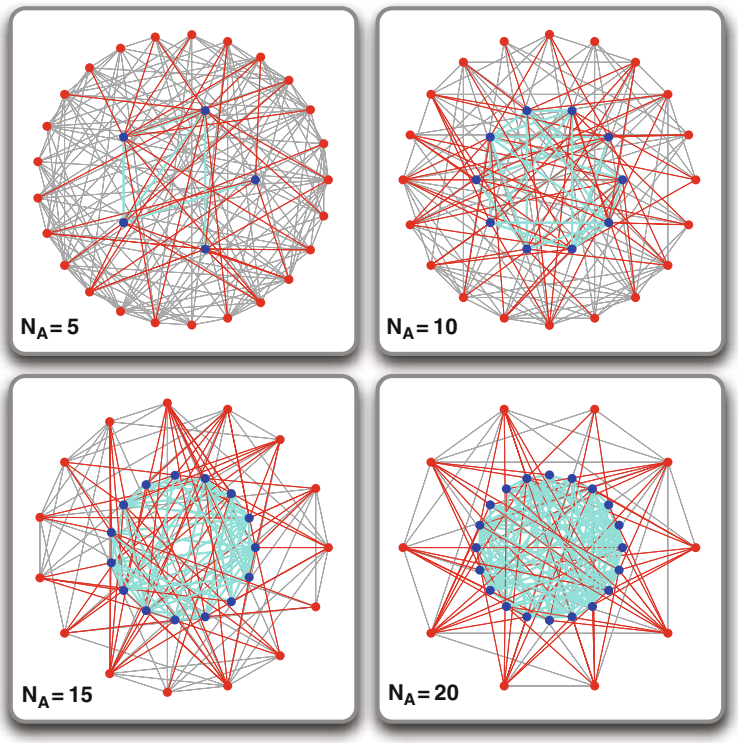

Fig. 12.1 Frequency dependent steady state dynamics. Results of active linking dynamics for a population size of $N = 30$ individuals. A-players are located in the "inner-rim", and are represented by *blue circles*, whereas B-players are located in the "outer-rim", and are represented by *red circles*. In this way, AA-links (*solid cyan lines*) live only within the "inner-rim", whereas AB-links (*solid red lines*) occupy the space between the rims while BB-links (*solid grey lines*) cross the entire region of the figure. Each panel depicts a snapshot in the steady state of the active-linking dynamics, associated with a different (and fixed) frequency of A and B players. The parameters determining the active linking dynamics are: $\alpha_A = \alpha_B = 0.5$, $\gamma_{AA} = 0.5$, $\gamma_{AB} = 0.25$ and $\gamma_{BB} = 0.5$

Here, ϕ_{AA}, ϕ_{AB}, and ϕ_{BB} are the fractions of active AA, AB and BB links in the steady states. Examples of population structures attained under steady-state dynamics for three different combinations of (N_A, N_B) are shown in Fig. 12.1.

12.2.2 Strategy Dynamics

Next, we address the dynamics of the strategies at the nodes. We consider the stochastic dynamics of a finite population, i.e. we restrict ourselves to finite networks. We consider a game between A and B given by the payoff matrix

$$\begin{array}{c} \\ A \\ B \end{array} \begin{array}{c} \begin{array}{cc} A & B \end{array} \\ \begin{pmatrix} a & b \\ c & d \end{pmatrix} \end{array}. \tag{12.1}$$

Thus, an A individual interacting with another A obtains the payoff a. A against B obtains b, whereas the B individual obtains c in such an interaction. Finally, B individuals obtain d from interactions with other B individuals.

We have to distinguish three generic cases of 2×2 games:

- Dominance. If $a > c$ and $b > d$, strategy B is dominated by strategy A. Thus, strategy A always obtains a higher payoff. The outcome does not have to be a social optimum: For $a < d$, the individuals playing strategy A end up with a non-optimum payoff. Similarly, B dominates A for $c > a$ and $d > b$.
- Coordination games: $a > c$ and $b < d$ leads to coordination games, in which it is always good to follow the strategy of the majority in the population. In the generic case, one strategy has a larger basin of attraction. This strategy is called risk dominant strategy. For $a + b > c + d$, strategy A is risk dominant.
- Coexistence games: In the case of $a < c$ and $b > d$, a small minority is favored. This means that the ultimate outcome in a population of players is a mixture of strategies A and B.

From the payoff matrix, we can calculate the payoffs of the individuals, depending on the number of interactions they have with the different types. On a complete network, the payoffs are

$$\pi_A = a(N_A - 1) + bN_B \tag{12.2}$$

and

$$\pi_B = cN_A + d(N_B - 1). \tag{12.3}$$

Often, the payoffs are scaled by $1/(N-1)$, such that the payoffs do not increase with the population size. For the strategy update process defined below, this corresponds simply to a rescaling of the intensity of selection, i.e. changing the noise intensity, if all individuals have the same number of interactions. If the number of interactions is not the same for all players, the heterogeneity between players can lead to new effects [20, 22].

Reproduction can be interpreted as genetic or cultural. We adopt the pairwise comparison rule [11, 23], which has been recently shown to provide a convenient framework of game dynamics at all intensities of selection [24, 25]. According to this rule, two individuals from the population, A and B are randomly selected for update (only the selection of mixed pairs can change the composition of the population). The strategy of A will replace that of B with a probability given by the Fermi function

$$p = \frac{1}{1 + e^{-\beta(\pi_A - \pi_B)}}. \tag{12.4}$$

The reverse will happen with probability $1-p$. The quantity β, which in physics corresponds to an inverse temperature, controls the intensity of selection. For $\beta \ll 1$, we recover the weak selection limit of the frequency dependent Moran process, which can be viewed as a high temperature expansion of the dynamics [24, 26]. For $\beta \gg 1$, we recover imitation dynamics, which corresponds to a low temperature limit [24, 25]: In the limit $\beta \to \infty$, the individual with the lower payoff will always adopt the strategy of the other individual.

The quantity of interest in finite population dynamics is the fixation probability ρ, which is the probability that a single mutant individual of type A takes over a resident population with $N - 1$ individuals of type B.

12.2.3 Separation of Timescales

The system of coevolving strategies and links is characterized by two timescales: One describing the linking dynamics (τ_a), the second one describing strategy dynamics (τ_e). We can obtain analytical results in two limits, where both timescales are separated. Defining the ratio $W = \tau_e/\tau_a$, separation of time scales will occur for $W \ll 1$ and $W \gg 1$.

12.2.3.1 Fast Strategy Dynamics

In this case, active linking does not affect strategy dynamics. Thus, the dynamics is identical to the evolutionary game dynamics on a fixed network. Such systems have been tackled by many authors for a long time [8–20]. The difficulty of an analytical solution for such systems is determined by the topology of the network, which corresponds to an initial condition in our case. Analytical solutions are feasible only for few topologies. One important limiting case leading to analytical solutions is given by complete networks corresponding to well-mixed systems. In this case, the fixation probability can be approximated by

$$\rho_A = \frac{\mathrm{erf}\,[\xi_1] - \mathrm{erf}\,[\xi_0]}{\mathrm{erf}\,[\xi_N] - \mathrm{erf}\,[\xi_0]}, \tag{12.5}$$

where $\mathrm{erf}(x)$ is the error function and $\xi_k = \sqrt{\frac{\beta}{u}}\,(ku + v)$ [25]. We have $2u = a - b - c + d$ and $2v = -a + bN - cN + c$. For $u = 0$, this simplifies to

$$\rho_A = \frac{1 - e^{-2\beta v}}{1 - e^{-2\beta vN}}. \tag{12.6}$$

A second example are Cayleigh trees. In this case, analytical solutions are only possible for weak selection, $\beta \ll 1$. For example, the fixation probability of a single

A individual under death-birth update can be calculated. For this update process, one individual selected at random is removed (death) and one of its neighbors is selected proportional to payoff to fill the empty space (birth). The fixation probability then reads [19]

$$\rho_A = \frac{1}{N} + \eta \frac{N-1}{N}\left[\frac{\mu}{N} + \mu + 3\eta\right], \tag{12.7}$$

where the parameters are $\mu = (k+1)(k-1)(a-b-c+d)$, $\eta = (k+1)a + (k^2 - k - 1)b - c - (k^2-1)d$ and k is the degree of the homogeneous graph.

Consequently, whenever $W \ll 1$ the linking dynamics only becomes relevant in states where the system can no longer evolve from strategy dynamics alone, but changing the topology allows to escape from these states.

12.2.3.2 Fast Linking Dynamics

Whenever $W \gg 1$, linking dynamics is fast enough to ensure that the network will reach a steady state before the next strategy update takes place. At the steady state of the linking dynamics, the average payoffs of *A* and *B* individuals are given by

$$\pi_A = a\phi_{AA}(N_A - 1) + b\phi_{AB}N_B \tag{12.8}$$

and

$$\pi_B = c\phi_{AB}N_A + d\phi_{BB}(N_B - 1). \tag{12.9}$$

Note that the effective number of interactions of an *A* player and a *B* player can become very different if $\phi_{AA} \gg \phi_{BB}$ or vice versa. Comparing Eqs. (12.8) and (12.9) to Eqs. (12.2) and (12.3) suggests that the linking dynamics introduces a simple transformation of the payoff matrix. We can study standard evolutionary game dynamics using the modified payoff matrix

$$\begin{array}{c} \\ A \\ B \end{array}\!\!\begin{array}{c} \begin{array}{cc} A & B \end{array} \\ \begin{pmatrix} a\phi_{AA} & b\phi_{AB} \\ c\phi_{AB} & d\phi_{BB} \end{pmatrix} \end{array} = \begin{array}{c} \\ A \\ B \end{array}\!\!\begin{array}{c} \begin{array}{cc} A & B \end{array} \\ \begin{pmatrix} a' & b' \\ c' & d' \end{pmatrix} \end{array}. \tag{12.10}$$

This is an important observation: Linking dynamics can change the nature of the game [27]. So far, we have only shown this in the limit where linking dynamics is much faster than strategy dynamics ($W \gg 1$). However, the result is expected to hold even when the two time scales are comparable (see below and also [27, 28]. In general, all generic transformations are possible:

- A dominance game with $a > c$ and $b > d$ can change into a coordination game with $a' > c'$ and $b' < d'$ or into a coexistence game with $a' < c'$ and $b' > d'$.

- A coordination game with $a > c$ and $b < d$ can be transformed into a dominance game with $a' < c'$ and $b' < d'$ (or $a' > c'$ and $b' > d'$) or into a coexistence game with $a' < c'$ and $b' > d'$.
- A coexistence game with $a < c$ and $b > d$ can be transformed into a dominance game with $a' < c'$ and $b' < d'$ (or $a' > c'$ and $b' > d'$) or into a coordination game with $a' > c'$ and $b' < d'$.

The transition points can be determined as follows: Strategy A is a Nash equilibrium for $a > c$. This property changes to $a' < c'$ when

$$\frac{a}{c} < \frac{\phi_{AB}}{\phi_{AA}} = \frac{\alpha_B}{\alpha_A} \frac{\alpha_A^2 + \gamma_{AA}}{\alpha_A \alpha_B + \gamma_{AB}}. \tag{12.11}$$

For example, ϕ_{AB} can be increased by reducing the death rate of AB links, γ_{AB}. With increasing ϕ_{AB}, the condition is fulfilled at some point. At the transition point, A is either transformed into a Nash equilibrium or loses this property. An equivalent transition for B is given by the condition

$$\frac{d}{b} < \frac{\phi_{AB}}{\phi_{BB}} = \frac{\alpha_A}{\alpha_B} \frac{\alpha_B^2 + \gamma_{BB}}{\alpha_A \alpha_B + \gamma_{AB}}. \tag{12.12}$$

However, the conditions are not entirely independent, since at least two parameters have to be varied. Usually, it is enough to vary the three link-death rates γ and fix the link-birth rates α to observe these transitions. It is also worth mentioning that, in coordination games, the transformation can change the risk-dominant strategy, that is, the strategy with the larger basin of attraction.

12.2.4 Effects of Active Linking

As we have shown, active linking can lead to a wide range of scenarios that effectively change the character of the game. However, the analytical results have been obtained assuming time scale separation. Figure 12.2 shows the results of numerical simulations for a gradual change of the time scale ratio. Deviations from the analytical predictions are limited to a single order of magnitude. In other words, the time scale separation is not a very strong assumption and remains valid for a much wider range of parameters than expected. Even for moderate active linking, our analytical results are recovered. Thus, self-organising network structures and the evolutionary game dynamics on the network are intimately entangled. Having identified the relevance of time scale separation in a minimal model of linking dynamics, we now turn to more complex linking dynamics based on local rules.

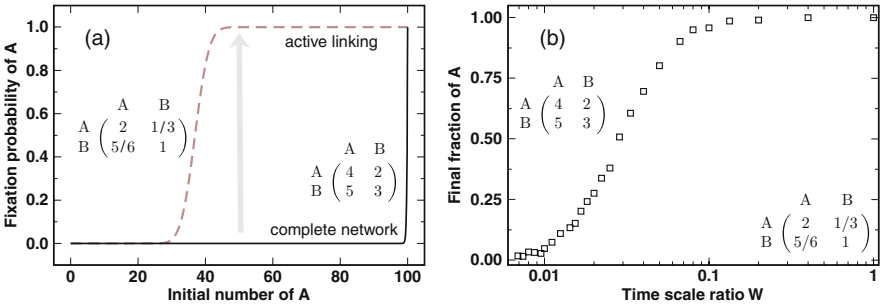

Fig. 12.2 Active linking effectively changes the payoff matrix and the nature of the game. (**a**) We start from a complete network without structure dynamics ($W = 0$) and a game in which strategy B dominates A. In this case, the fixation probability of A (*full line*) is essentially zero for all initial numbers of A. With active linking (*dashed line*), the game turns into a coordination game. In this case, A becomes risk dominant and the fixation probability of A exceeds 0.5 if the initial number of A individuals is larger than 36. (**b**) Numerical simulations reveal the range of validity of our analytical approximations. We start from 50% A individuals. For small W, A individuals never reach fixation. But already for $W = 0.1$, their fixation probability is close to one. Thus, moderate active linking is sufficient to make A the dominant strategy here (averages over 100 realizations, population size $N = 100$, intensity of selection $\beta = 0.05$, $\alpha_A = \alpha_B = 0.4$, $\gamma_{AA} = 0.16$, $\gamma_{AB} = 0.80$ and $\gamma_{BB} = 0.32$.)

12.3 Individual Based Linking Dynamics

In the model discussed in Sect. 12.2, we have a fluctuating number of links and analytical results in the two limits where the time scale of linking dynamics and strategy dynamics are well separated, allowing for the mean-field treatment considered. We now introduce an alternative description in which the number of links is conserved, but in which decision to maintain or rewire a link results both from individual preference in the choice of partners and negotiation between individuals linked [29]. Such an individual based decision making cannot be dealt with at a mean-field level and calls for a numerical implementation.

12.3.1 Specification of the Linking Dynamics

To reduce the number of parameters, let us start by restricting the space of possible games by fixing $a = 1$ and $d = 0$, while $-1 \leq b \leq 1$ and $0 \leq c \leq 2$.

$$\begin{array}{c} \\ A \\ B \end{array} \begin{array}{c} \begin{array}{cc} A & B \end{array} \\ \begin{pmatrix} 1 & b \\ c & 0 \end{pmatrix} \end{array}. \tag{12.13}$$

This spans the four dynamical outcomes introduced before: (a) dominance of A over B ($b > 0$ and $c < 1$); (b) coexistence game ($b > 0$ and $c > 1$); (c) coordination

game ($b < 0$ and $c < 1$) and (d) dominance of B over A ($b < 0$ and $c > 1$) (see Sect. 12.2.2).

Because $b \leq 1$ and $c \geq 0$, the payoff against an A individual is always higher than the payoff against a B individual, cf. Eq. (12.13). Thus, interacting with an A-player is always the best possible option. Consequently, every individual will be satisfied when connected to a A and dissatisfied otherwise. Keeping the total number of links constant, all individuals are now able to decide, on an equal footing, those ties that they want to maintain and those they want to change. The co-evolution between strategy and network structure is therefore shaped by individual preferences towards interacting with one of the two strategies [29]. Figure 12.3 illustrates the process. If Q is satisfied, she will decide to maintain the link. If dissatisfied, then she may compete with R to rewire the link (see Fig. 12.3), rewiring being attempted to a random neighbor of R. The intuition behind this reasoning relies on the fact that agents, equipped with limited knowledge and scope, look for new social ties by proxy [30]. Such a procedure can only be treated numerically and does no longer lead to a simple rescaling of a payoff matrix as the mechanism discussed in Sect. 12.2. On the other hand, it introduces some features characteristic of realistic social networks.

The fact that all individuals naturally seek to establish links with individuals with strategy A, creates possible conflicts of interests as illustrated in Fig. 12.3. For instance, R is satisfied, because it can profit from Q. Obviously, Q is not satisfied and would prefer to seek for a individual A. Decision is contingent on the payoff π_Q and π_R of Q and R, respectively. With the probability $p = [1 + e^{-\beta[\pi_Q - \pi_R]}]^{-1}$

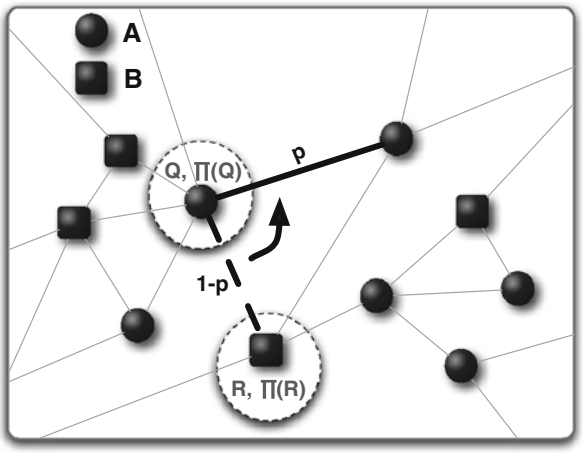

Fig. 12.3 Readjusting social ties. A and B individuals interact via the links of a network. R (B) is satisfied, since Q has strategy A ($c > 0$). On the other hand, Q is unsatisfied with this situation ($b < 1$). Therefore, Q wants to change the link whereas R does not. The action taken is contingent on the fitness π_Q and π_R of Q and R, respectively. With probability p (see Eq. (12.4)), Q redirects the link to a random neighbor of R. With probability $1 - p$, Q stays linked to R. Finally, if both players are dissatisfied, the same methodology is used to decide who keeps the connection

(also used in the strategy update, cf. Eq. (12.4)), Q redirects the link to a random neighbor of R. With probability $1 - p$, Q stays linked to R. Whenever both Q and R are satisfied nothing happens. When both Q and R are unsatisfied, rewiring takes place such that the new link keeps attached to Q with probability p and attached to R with probability $1 - p$. Thus, the more successful individual keeps the link with higher probability.

12.3.2 Numerical Results

As previously, this model establishes a coupling between individual strategy dynamics and population structure dynamics. This leads necessarily to a time scale associated with strategy evolution, τ_e and a second associated with structure evolution, τ_a. When the ratio $W = \tau_e/\tau_a$ equals 0 we recover the fast strategy dynamics of Sect. 12.2.3.1. On the other hand, with increasing W, individuals become apt to adapt their ties with increasing efficiency.

The contour plots in Fig. 12.4 illustrate the final fraction of individuals which adopt strategy A for different values of the ratio W in networks with average connectivity $z = 30$ (this value reflects the mean value of the average connectivities reported in [31] for socials networks). We plot the fraction of A individuals who survive evolution, averaged over 100 independent realizations for the same values of the game payoff entries (b, c) and the time scale ratio W. For $W = 0$ the results reproduce, as expected [20], the predictions for finite, well-mixed populations. Yet, with increasing W, A individuals gain an advantage, as they can terminate their undesireable interactions with B individuals. Rewiring changes the strategy dynamics and paves the way for a radically distinct evolutionary outcome in which A players are now able to dominate for the entire range of games. Under structural dynamics, A individuals can cut their links to B individuals, which gives them an advantage compared to the situation on a static network. The swifter the response of individuals to the nature of their ties, the easier it gets for A players to wipe out B players. Note further that A already dominates B for $W = 4$, corresponding to a situation far from the time-scale separation conditions defined in Sect. 12.2.3.

Additional insight is provided in Fig. 12.5 (left panel), where we show how A dominates B as a function of W when $c = 2$ and $b = -1$ (lower right corner of the panels in Fig. 12.4), which represents the most challenging case for the A individuals. Different values of the average connectivity z are shown. For small W, A individuals have no chance. Their fate changes as W approaches a critical value $W_{critical}$ – which increases monotonically with connectivity z – A players wiping out B players above $W_{critical}$ (the increase of $W_{critical}$ with z is expected, since there are more links to be rewired; in practice, $W_{critical}$ is determined as the value of W at which the frequency of As crosses 50%). Thus, the evolutionary outcome and effective game at stake relies on the capacity of individuals to adjust to adverse ties.

Figure 12.5 also provides evidence of the detailed interplay between strategy and structure. On one hand, strategy updating promotes a local assortment of strategies, since A individuals *breed* A individuals and B individuals *breed* B individuals.

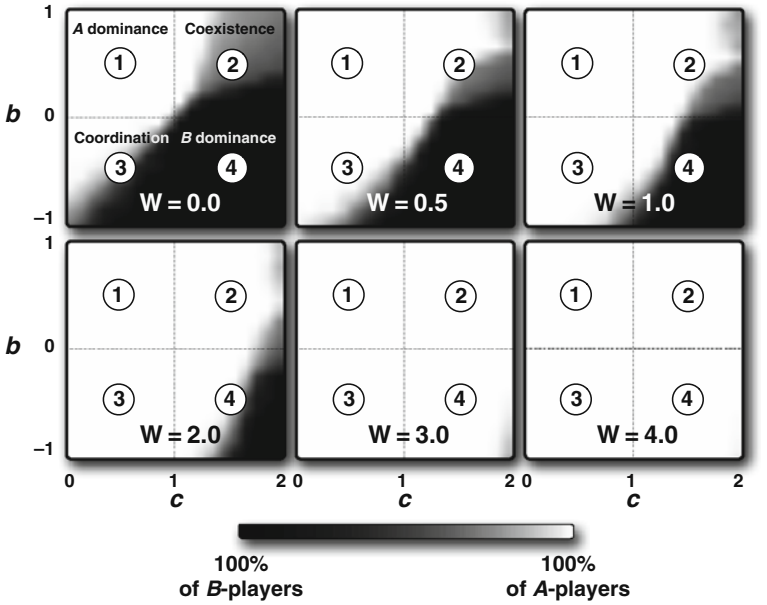

Fig. 12.4 Final frequency of strategy A in all games for different time-scale ratios between strategy and structure dynamics. Results for the fraction of successful evolutionary runs ending in 100% of individuals with strategy A for different values of the time scale ratio W, starting from 50% of each strategy. We study the four different games in the area $2 \geq c \geq 0$ and $1 \geq b \geq -1$: (1) A dominates B; (2) coexistence game; (3) coordination game; (4) B dominates A (see Sect. 12.2.2). For $W = 0$ ($N = 10^3$, $z = 30$ and $\beta = 0.005$), the results fit the predictions from well-mixed populations, although individuals only interact with a small subset of the population. With increasing W (faster structure dynamics), the rate at which individuals readjust their ties increases, and so does the viability of strategy A. Above a critical value $W_{critical} \sim 4.0$ (see also Fig. 12.5), individuals with a strategy A efficiently wipe out Bs. For the strategy evolution dynamics adopted here (pairwise comparison, see Sect. 12.2.2), and according to [19], A would never be favored in static networks

On the other hand, under structural updating, one is promoting local assortative interactions between A-players (that is, AA-links) and disassortative interactions between B and A-players (that is, AB-links), which constitute *favorable steps* from an individual point of view. Clearly, when simultaneously active, strategy update will reinforce assortativity among As, but will inhibit disassortativity between B and A-players, which overall will promote the dominance of A over B.

12.3.3 Graph Structures Under Individual Based Linking Dynamics

For any $W > 0$, individual choices lead to heterogeneous graphs in which some individuals interact more, and more often than, others. The overall onset of increase of heterogeneity qualitatively follows the wave of A dominance shown in Fig. 12.4 [29].

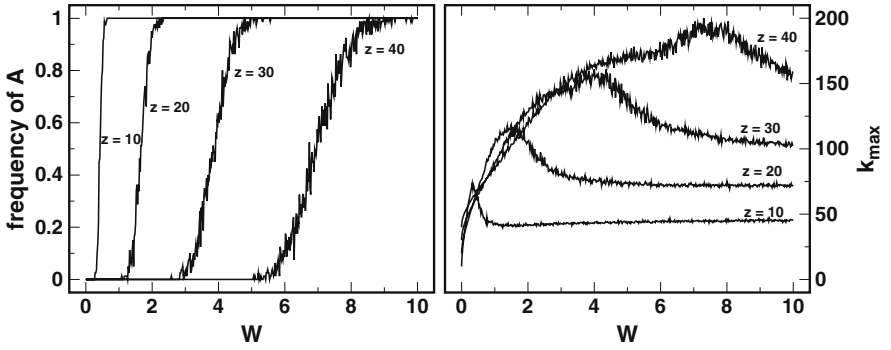

Fig. 12.5 Co-evolution of strategies and links in the game region in which B should dominate for different time-scales. *Left panel*: Final frequency of A strategy at end as a function of W for different average connectivity z. For each average connectivity z, there is a critical value of the time scale ratio $W - W_{critical}$ – above which A-players wipe out B-players. *Right panel*: Connectivity k_{max} of the largest hub in the network, as a function of the time scale ratio W. With increasing z, $W_{critical}$ increases. In all cases, the heterogeneity of the associated network becomes maximal at $W_{critical}$. For higher values of W, the heterogeneity decreases again when type B decreases in frequency. For high values of W, type B is wiped out and only the heterogeneity generated by the rewiring mechanism in a neutral system prevails (Payoffs: $a = 1$, $c = 2$, $b = -1$ and $d = 0$; Intensity of selection $\beta = 0.005$.)

In fact, the overall heterogeneity of the graph increases as W increases reaching a maximum at $W_{critical}$, above which heterogeneity decreases again down to a stationary value determined by neutral dynamics in a system with one strategy only [29]. The results shown suggest that the adaptive dynamics of social ties introduced here coupled with social dilemmas accounts for the heterogeneities observed in realistic social networks [32].

12.4 Discussion

Our analysis has been limited to one-shot games. In other words, individuals interact once during the lifetime of a link as if they have never met before. But in repeated interactions, more possibilities exist. If I only take into account your behavior in the last interaction, there are already $2^2 = 4$ strategies. Since the number of strategies grows rapidly with memory [33, 34], one often considers so called trigger strategies in which individuals keep their behavior unchanged until they are faced with an unsatisfactory partner for the first time. Such strategies can be implemented into our active linking framework, assuming that individuals act repeatedly as long as a link between them is present. This procedure leads to analytical results for evolutionary stability under active linking even in the context of repeated games [35].

Other studies have shown numerically that network dynamics can significantly help dominated strategies. Even if only the dominant strategy can locally affect the network structure, this can help the dominated strategy under certain linking

rules that put restrictions on mutual interactions of the dominant strategy [36, 37]. A recent study for growing networks has shown that the dominant strategy has an advantage as long as a network is growing by preferential attachment. Once network growth is stopped, the dominated strategy increases in frequency [38].

A different approach for self organizating population structures determined by game theoretic interactions has been proposed in computer science [39, 40]. There, agents aim to minimize their linking costs in a network by establishing links that minimize the path to all other nodes. This selfish optimization leads to networks distinct from the social optimum. The performance of such systems is measured in terms of the ratio of the optimal cost for links divided by the linking cost in the worst case Nash equilibrium. This ratio has been referred to as "price of anarchy". Since this quantity is not independent of the cost function and the parameters, it is problematic to transfer it to evolutionary games on networks.

To sum up, by equipping individuals with the capacity to control the number, nature and duration of their interactions with others, we introduce an adaptive network dynamics. This leads to surprising and diverse new game dynamics and realistic social structures. We have presented two approaches how to implement this network dynamics. The first one, active linking, allows to define differential equations for the numbers of links, which leads to analytical results. The second approach, individual based linking dynamics, is implemented numerically and leads to network features of empirical social networks.

The consideration of adaptive social networks is an important step towards more realistic models of social interactions in structured populations. Coupling the dynamics *on* networks with the dynamics *of* networks leads to emergent new phenomena outside the classical considerations of social dynamics on static networks.

Acknowledgements We thank Martin A. Nowak, who was involved in the development of the active linking model. Financial support by the Emmy-Noether program of the DFG, Germany (A.T.), the Fonds de la Recherche Scientifique, Belgium (F.C.S.) and FCT, Portugal (J.M.P.) is gratefully acknowledged.

References

1. J. von Neumann, O. Morgenstern, *Theory of Games and Economic Behavior* (Princeton University Press, Princeton, 1944)
2. J. Maynard Smith, *Evolution and the Theory of Games* (Cambridge University Press, Cambridge, 1982)
3. P.D. Taylor, L. Jonker, Math. Biosci. **40**, 145 (1978)
4. J. Hofbauer, K. Sigmund, *Evolutionary Games and Population Dynamics* (Cambridge University Press, Cambridge, 1998)
5. E.C. Zeeman, Lect. Notes Math. p. 819 (1980)
6. C. Taylor, M.A. Nowak, Theor. Popul. Biol. **69**, 243 (2006)
7. A. Traulsen, J.C. Claussen, C. Hauert, Phys. Rev. Lett. **95**, 238701 (2005)
8. M.A. Nowak, R.M. May, Nature **359**, 826 (1992)
9. A.V.M. Herz, J. Theor. Biol. **169**, 65 (1994)
10. K. Lindgren, M.G. Nordahl, Physica D **75**, 292 (1994)

11. G. Szabó, C. Tőke, Phys. Rev. E **58**, 69 (1998)
12. C. Hauert, Int. J. Bifurcation and Chaos Appl. Sci. Eng. **12**, 1531 (2002)
13. M.H. Vainstein, J.J. Arenzon, Phys. Rev. E **64**, 051905 (2001)
14. G. Szabó, J. Vukov, Phys. Rev. E **69**, 036107 (2004)
15. G. Abramson, M. Kuperman, Phys. Rev. E **63**, 030901(R) (2001)
16. H. Ebel, S. Bornholdt, Phys. Rev. E **66**, 056118 (2002)
17. P. Holme, A. Trusina, B.J. Kim, P. Minnhagen, Phys. Rev. E **68**, 030901(R) (2003)
18. F.C. Santos, J.M. Pacheco, Phys. Rev. Lett. **95**, 098104 (2005)
19. H. Ohtsuki, C. Hauert, E. Lieberman, M.A. Nowak, Nature **441**, 502 (2006)
20. F.C. Santos, J.M. Pacheco, T. Lenaerts, Proc. Natl. Acad. Sci. U.S.A. **103**, 3490 (2006)
21. P. Branas-Garza, R. Cobo-Reyes, M.P. Espinosa, N. Jiménez, G. Ponti, working paper, available at EconPapers (2007)
22. F.C. Santos, J.M. Pacheco, Jour. Evol. Biol. **19**, 726 (2006)
23. L.E. Blume, Games and Economic Behavior **4**, 387 (1993)
24. A. Traulsen, J.M. Pacheco, M.A. Nowak, J. Theor. Biol. **246**, 522 (2007)
25. A. Traulsen, M.A. Nowak, J.M. Pacheco, Phys. Rev. E **74**, 11909 (2006)
26. M.A. Nowak, A. Sasaki, C. Taylor, D. Fudenberg, Nature **428**, 646 (2004)
27. J.M. Pacheco, A. Traulsen, M.A. Nowak, Phys. Rev. Lett. **97**, 258103 (2006)
28. J.M. Pacheco, A. Traulsen, M.A. Nowak, Jour. Theor. Biol. **243**, 437 (2006)
29. F.C. Santos, J.M. Pacheco, T. Lenaerts, PLoS Comput. Biol. **2**, 1284 (2006)
30. G. Kossinets, D.J. Watts, Phys. Rev. Lett. **311** (2006)
31. S. Dorogotsev, J. Mendes, *Evolution of networks: From biological nets to the Internet and WWW* (Oxford University Press, Oxford, 2003)
32. L.A.N. Amaral, A. Scala, M. Barthélémy, H.E. Stanley, Proc. Natl. Acad. Sci. U.S.A. **97**(21), 11149 (2000)
33. K. Lindgren, in *Artificial Life II. SFI Studies in the Science of Complexity Vol. X*, ed. by C.G. Langton, C. Taylor, J.D. Farmer, S. Rasmussen (Addison-Wesley, Redwood City, 1991), pp. 295–312
34. H. Ebel, S. Bornholdt, cond-mat/0211666 (2002)
35. J.M. Pacheco, A. Traulsen, H. Ohtsuki, M.A. Nowak, J. Theor. Biol. **250**, 723 (2008)
36. M.G. Zimmermann, V.M. Eguíluz, M. San Miguel, Am. J. Soc. **110**, 977 (2005)
37. M.G. Zimmermann, V.M. Eguíluz, Phys. Rev. E **72**, 056118 (2005)
38. J. Poncela, J. Gómez-Gardeñes, L.A. Floría, A. Sánchez, Y. Moreno, PLoS One **3**, e2449 (2008)
39. E. Koutsopias, C.H. Papadimitriou, Lect. Notes Comput. Sci. **1563**, 404 (1999)
40. A. Fabrikant, A. Luthra, E. Maneva, C.H. Papadimitriou, S. Shenker, in *Proceedings of the Symposium on Principles of Distributed Computing* (2003), pp. 347–351

Chapter 13
The Diplomat's Dilemma: Maximal Power for Minimal Effort in Social Networks

Petter Holme and Gourab Ghoshal

Abstract Closeness is a global measure of centrality in networks, and a proxy for how influential actors are in social networks. In most network models, and many empirical networks, closeness is strongly correlated with degree. However, in social networks there is a cost of maintaining social ties. This leads to a situation (that can occur in the professional social networks of executives, lobbyists, diplomats and so on) where agents have the conflicting objectives of aiming for centrality while simultaneously keeping the degree low. We investigate this situation in an adaptive network-evolution model where agents optimize their positions in the network following individual strategies, and using only local information. The strategies are also optimized, based on the success of the agent and its neighbors. We measure and describe the time evolution of the network and the agents' strategies.

13.1 Introduction

To increase or maintain power, or position of influence, is a goal of many professionals. Many definitions of power recognize that it is not an inherent attribute of an actor,[1] but a result of the interaction between agents. One well-known definition by Max Weber reads [27]:

> 'Power' is the probability that one actor within a social relationship will be in position to carry out his own will despite resistance, regardless of the basis on which this probability rests.

Definitions like this suggest that there is a link between the power of an actor and its position in the network of social relationships. Thus, by examining a social network, one should be able to say something about the power of the agents. A major theme in social network studies has been to infer the power structures in

P. Holme (✉)
Department of Physics, Umeå University, 90187 Umeå, Sweden
e-mail: petter.holme@physics.umu.se

[1] A person, or other well-defined social unit, in the context of our model; we will use the term *agent*.

T. Gross, H. Sayama (eds.), *Adaptive Networks,* Understanding Complex Systems,
DOI 10.1007/978-3-642-01284-6_13,

organizations based on the contact patterns of their members [16]. In undirected networks of actors, coupled pairwise by their social ties, one idea of measuring, or defining power, is to say that an actor that is close to others has more power, than a more peripheral actor does [24]. This can be turned into a network measure called *closeness centrality* (which will be defined explicitly in the next section). Naively, a way to achieve power would then be to position oneself as close to everyone else in the network as possible, i.e. to have a social tie to each one of the network's actors. In practice, to make, and maintain, a social tie requires the actor to invest time and other resources. To have a direct tie to a significant fraction of the network is thus neither feasible, nor desirable. We call this situation of two contrasting interests – to maximize power (in terms of being central), while at the same time keeping the number of social ties to a minimum – the *diplomat's dilemma*. Economists have studied similar trade-off games under other names (e.g. [3, 14]), typically investigating Nash equilibria in small networks rather than emergent patterns in large scale systems as the focus of this paper.

The diplomat's dilemma can also be motivated from a more academic perspective. Fueled by the increased availability of large-scale network datasets, there is a wave of interest in analyzing and modeling systems as graphs. One theme within this field of *complex-network theory* [1, 5, 19] has been to study systems where the network is formed by strategic decisions by the agents (i.e., situations where the success of the agents depend on the choice of other agents). This problem has been traditionally been analyzed from a *game theory* perspective. Some of the most interesting game-theoretical problems have been inspired by situations where the agents have conflicting objectives. In, for example, the iterated prisoner's dilemma [2], agents have to choose between trying to achieve short-time benefits by exploiting other agents, and trying to optimize their long-term profit by building a relationship of mutual trust, but at the same time making them vulnerable to exploitation. In most real complex networks, and network models, there is a strong positive correlation between different centrality measures [18] such as the local degree centrality (the number of neighbors of a vertex), and closeness centrality. However, one must note that the correlation between these quantities, though mathematically possible – high centrality and low degree (and vice versa) – is not strictly necessary. A potentially interesting question in the interface between complex networks and game theory would then be "How can agents simultaneously maximize their centrality and minimize their degree?". Another interesting aspect of this problem, in a more model-theoretic sense, is that the success of the agents can be estimated from their network positions alone. In most models of adaptive, coevolutionary networks [9], the score of the agents is related to some additional traits of the agents themselves and their interaction. Our model differs from this approach in the sense that the success of agents can be measured from the topological features of the graph itself, rather than some *extremal* attribute artificially ascribed to the agents.

In this chapter, we will discuss how this problem, the diplomat's dilemma, can be phrased in more mathematical terms. We will analyze a model of adaptive agents that try to solve this problem as the network evolves [11]. We will also, discuss the output of this model, both the evolution of the network and the evolution of strategies of the agents.

13.2 Definition of the Model

13.2.1 Preliminaries

The framework of our study is a graph $G(t) = \{V(t), E(t)\}$ of N vertices V and $M(t)$ edges $E(t)$. The vertex set V is fixed, but the edge set $E(t)$ varies (both its content and size) with time. A vertex marks the position of an agent in a social network of edges representing social ties. We will henceforth also assume the graph to be simple, i.e. no multiple- or self-edges are allowed. Let $d(i, j)$ denote the *distance* between i and j. Technically we define $d(i, j)$ as the smallest number of edges in any path (sequence of adjacent edges) connecting i and j. Then, for a connected graph G, the closeness centrality [24] is defined as:

$$c_C(i) = \frac{N-1}{\sum_{j \in G \setminus \{i\}} d(i, j)}. \tag{13.1}$$

The score function, that the agents seek to optimize, should increase with closeness centrality and decrease with degree. A simple choice for such a function is $c_C(i)/k_i$ (where k_i is the degree of i). However, we do not want to restrict ourselves to connected networks. If the network is disconnected, we make the assumption that being a part of a large component should contribute to a larger centrality. One way of modifying closeness centrality to incorporate both these aspects (short distances and being a part of a large component implies centrality), is to define the centrality $c(i)$ as

$$c(i) = \sum_{j \in H(i) \setminus \{i\}} \frac{1}{d(i, j)}, \tag{13.2}$$

where $H(i)$ is the connected subgraph i belongs to and $d(i, j)$ is the graph distance between i and j. The number of elements in the sum of Eq. (13.2) is proportional to the number of vertices of i's connected component which gives a positive contribution from large components. To obtain this property, we use the average reciprocal distance, rather than the reciprocal average distance (as in the original definition of closeness centrality). This adjusted definition gives a higher weight on the count of closer vertices, but captures similar features as closeness does.

With the definitions established above, we are now ready to state the score function:

$$s(i) = \begin{cases} c(i)/k_i & \text{if } k_i > 0 \\ 0 & \text{if } k_i = 0 \end{cases}. \tag{13.3}$$

For the purpose of our simulations, the networks we consider will have a initial configuration similar to Erdős-Rényi networks [7] with M_0 number of edges. In other words, the network is generated by adding M_0 edges one-by-one to N (isolated) vertices such that no multiple- or self-edge is formed.

13.2.2 Moves

We have outlined so far the basic setup for the game – the underlying graph representing the actors and their social network, and the score function that the agents want to optimize. However, to go from this point to a sensible simulation scheme, we need to determine how an agent can update its connections. A first, very common assumption, is that the agents are *myopic* – that they can receive information from, and affect others in the network only within a certain radius from itself. This assumption lies behind so much of social network studies that one may argue that in situations where the myopic assumption is not needed, so agents can see, and manipulate the network at large distances, the representation of the social network as a simple graph is not appropriate. In our case, we assume that an agent i can change its connections (affect the network) within the second neighborhood $\Gamma_2 = \{j \in V : d(i, j) \leq 2\}$, and that i can see the score $s(j)$, centrality $c(j)$ and degree k_j of vertices in Γ_2. (Since s and c are global quantities, some global information reach i indirectly. Nevertheless, since the actual contact network cannot be inferred from this information, we still consider the agents myopic.)

The simulations proceed iteratively where, each time step, every vertex can update its network position by adding an edge to a vertex in Γ_2 and delete an edge to a neighbor. An illustration of the possible moves can be found in Fig. 13.1.

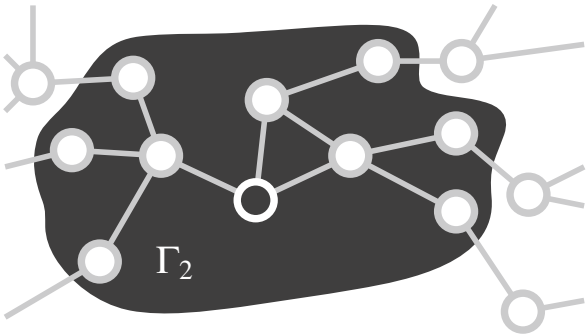

Fig. 13.1 An illustration of the myopia (the restricted knowledge about the network). The agents are assumed to have knowledge of, and be able to affect the second neighborhood Γ_2 (*shaded* in the figure). The agent knows the centrality and degree of the neighbors and their accumulated score the last t_{strat} time steps. Based on this information the agents can, during a time step, based on their strategies, decide to delete the edge to a neighbor, and reconnect to a vertex two steps away

13.2.3 Strategies

Ideally one would provide the agents with some intelligence and use no further restrictions for how they update their positions to increase their scores. This is not as

easy one can imagine and, for simplification, one would like to reduce the capability of the agents further. To do this, we assume that an agent i updates its position (either by deleting or attaching an edge), by applying a sequence of tie-breaking *actions*.

- **MAXD** Choose vertices with maximal degree.
- **MIND** Choose vertices with minimal degree.
- **MAXC** Choose vertices with maximal centrality in the sense of Eq. (13.2).
- **MINC** Choose vertices with minimal centrality.
- **RND** Pick a vertex at random.
- **NO** Do not add (or remove) any edge.

The sequences of actions define the *strategies* of the agents. The strategy of an agent i can be stored in two six-tuples $\mathbf{s}_{\text{add}} = (s_1^{\text{add}}, \cdots, s_6^{\text{add}})$ and $\mathbf{s}_{\text{del}}$ representing a priority ordering of the addition and deletion actions respectively. If $\mathbf{s}_{\text{add}}(i) =$ (MAXD, MINC, NO, RND, MIND, MAXC) then i tries at first to attach an edge to the vertex in $\Gamma_2(i)$ with highest degree. If more than one vertex has the highest degree, then one of these is selected by the MINC strategy. If still no unique vertex is found, nothing is done (by application of the NO strategy). Note that such a vertex is always found after strategies NO or RND are applied. If $X = \varnothing$ no edge is added (or deleted). An illustration of the strategies can be found in Fig. 13.2

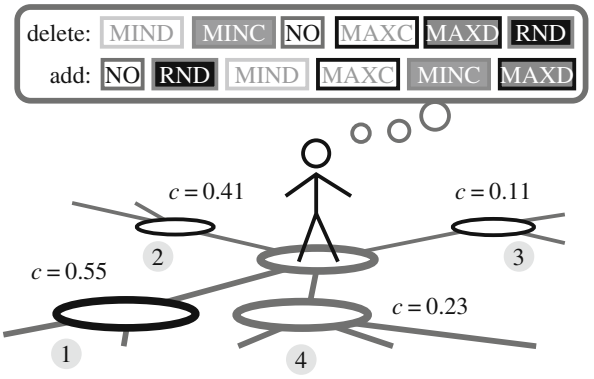

Fig. 13.2 An illustration of the strategies of the agents. At a time step, the agent can delete one edge and add another in order to improve its score. The way to select a neighbor to delete an edge to (or a next-nearest neighbor to attach an edge to) is to consecutively omit possibilities by applying "actions" in a "strategy vector". This agent's leading deletion strategy is MIND, meaning it looks for neighbors with as low degree as possible in the first place, to delete the edge to. In this example there are three neighbors with degree three (*marked with black*). To further eliminate neighbors the agent applies the MINC strategy (ranking the neighbors in order of minimum centrality c). In this case vertex 1 is the unanimously least central neighbor. So, at this time step, the agent will delete the edge to 1. As for addition of edges the leading action is NO, meaning no edge will be added

13.2.4 Strategy Updates and Stochastic Rewiring

The strategy vectors are initialized to random permutations of the six actions. Every t_{strat}'th time step an agent i updates its strategy vectors by finding the vertex in $\Gamma_i = \{j : d(i, j) \leq 1\}$ with highest accumulated score since the last strategy update. This practice of letting the agent mimic the best-performing neighbor is common in spatial games [21], and is closely related to the bounded rationality paradigm of economics [15]. When updating the strategy, i copies the parts of $\mathbf{s}_{\text{add}}(j)$ and $\mathbf{s}_{\text{del}}(j)$ that j used the last time step, and let the remaining actions come in the same order as the strategy vectors prior to the update. For the purposes of making the set of strategy vectors ergodic, driving the strategy optimization [17, 20], and modeling irrational moves by the agents [15]; we swap, with probability p_s, two random elements of $\mathbf{s}_{\text{add}}(j)$ and $\mathbf{s}_{\text{del}}(j)$ every strategy vector update. In addition to the strategy space we also would like to impose ergodicity in the network space (i.e. the game can generate all N-vertex graphs from any initial configuration). In order to ensure this, disconnected clusters should have the ability to reconnect to the graph. We allow this by letting a vertex i attach to any random vertex of V with probability p_r every t_{rnd}'th time step. This is not unreasonable as even in real social systems, edges may form between agents out of sight from each other in the social network. In fact some authors have pointed out, that in addition to information spreading processes, there are other factors that lead to the evolution of the social networks (cf. [26]).

13.2.5 The Entire Algorithm

To summarize, the algorithm works as follows:

1. Initialize the network to a Erdős-Rényi network with N vertices and M_0 edges.
2. For all agents, start with random permutations of the six actions as strategy vectors $\mathbf{s}_{\text{add}}$ and $\mathbf{s}_{\text{del}}$.
3. Calculate the score for all agents.
4. Update the agents synchronously by adding and deleting edges as selected by the strategy vectors. With probability p_r, add an edge to a random vertex instead of a neighbor's neighbor.
5. Every t_{strat}'th time step, update the strategy vectors. For each agent, with probability p_s, swap two elements in it's strategy vector.
6. Increment the simulation time t. If $t < t_{\text{tot}}$, go to step 3.

The parameter n_{avg}, averages over different realizations of the algorithm are performed. We will primarily use the parameter values $M_0 = 3N/2$, $p_s = 0.005$, $t_{\text{strat}} = 10$, $t_{\text{tot}} = 10^5$ and $n_{\text{avg}} = 100$.

13.3 Numerical Results

13.3.1 Time Evolution

To get a feeling for the time evolution, we start by plotting quantities characterizing the strategies of the agents and the network structure. The most important parts of the strategy vectors are the first positions s_1^{add} and s_1^{del}. In practice, $\sim$ 90% of the decisions whether or not to add (or delete) a specific edge do not pass this first tiebreaker. In Fig. 13.3a, b we can see how complex the time-evolution of s_1^{add} and s_1^{del} can be. Each sector of the plot corresponds to a leading addition (or deletion) action, and they have a size in the y-direction proportional to the fraction of vertices having that leading action value. The time evolution is complex, having sudden cascades of strategy changes and quasi-stable periods. Cascades in the leading addition action seem to be accompanied by cascades in the leading deletion action. The particular time-window shown in Fig. 13.3 was chosen to highlight such cascades. For the parameter values of Fig. 13.3, cascades involving more than 75% of the vertices happens about once every 10^5 time steps.

In Fig. 13.3c we measure the average score function $\langle s \rangle$. Being a non-zero-sum game, the value of $\langle s \rangle$ can vary significantly, a fact which can be seen upon examining the figure. Most of the time, the system is close to the observed maximum $\langle s \rangle \approx 80$. One reason for lower scores can be seen in Fig. 13.3d where we plot the average degree $\langle k \rangle$. For some time steps, the network becomes very dense with an average degree of almost 20. As high degree is not desirable, the average score is low during this period. This rise in degree has, naturally, a corresponding peak in the leading deletion action NO. Another reason of the occasional dips in the average score can be seen in Fig. 13.3e where we plot the fraction n_1 that belongs to the largest connected component. This quantity is usually close to one, meaning that all agents are connected (directly or indirectly), but sometimes this fraction becomes very low. It is harder (than for the high-degree peaks) to see the corresponding strategic cause for these fragmented states. There are usually peaks corresponding to NO as the leading addition action, but these are also accompanied by peaks corresponding to NO as the leading deletion action. As we will see, this feature becomes less pronounced as the system size increases.

13.3.2 Example Networks

In light of the complex time evolution of the system, it is not surprising that the system attains a great variety of network topologies as time progresses. In Fig. 13.4 we show four snapshots of the system for a run with the same parameter values as in Fig. 13.3. In Fig. 13.4a the network comes from the most common strategy configuration where both the leading deletion and addition actions are MAXC for a majority of the agents (in this situation, we call the actions *dominating*). In this configuration the network is centered around two indirectly connected hubs. The

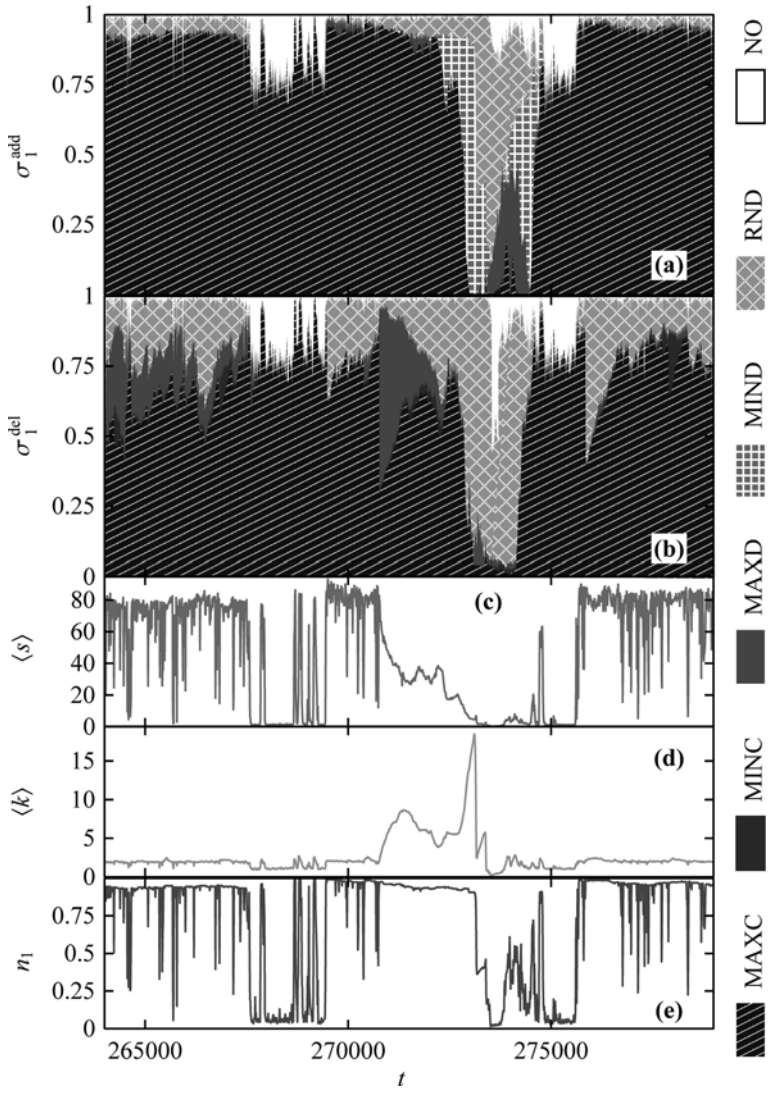

Fig. 13.3 Output from an example run of a $N = 200$ system with $p_r = 0.012$. (**a**) and (**b**) show the fraction of vertices having a certain leading action for addition σ_1^{add} (**a**) and deletion σ_1^{add} (**b**) respectively. (**c**) shows the average score $\langle s \rangle$, (**d**) the average degree k and (**e**) the fraction of vertices in the largest connected component n_1

vertices between these two hubs have the highest centrality, and since they are within the second neighborhood of most vertices in the network, and most agents have $\sigma_1^{\text{add}} = \text{MAXC}$, these vertices will get an edge from the majority of agents (thus becoming hubs in the next time-step). There are 18 isolates with $\sigma_1^{\text{add}} = \text{NO}$. These will stay isolates until their strategy vectors are mutated, which occurs (on average) every $t_{\text{strat}}/p_s = 2,000$'th time step. Figure 13.4b shows a rather similar

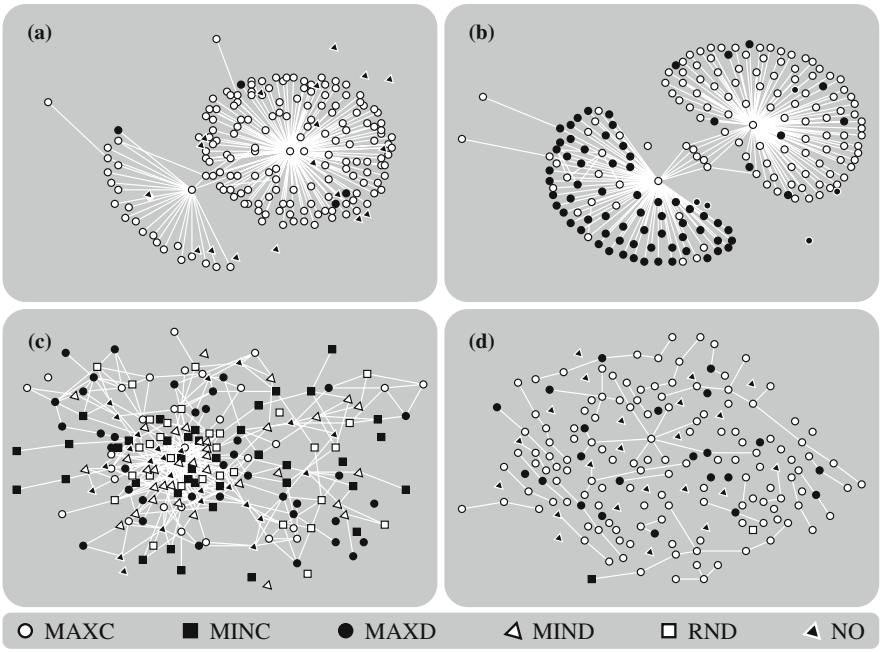

Fig. 13.4 Four different example networks from a run with the same parameter values as in Fig. 13.3. The symbols indicate the leading addition action. (**a**) shows the common situation where MAXC is the leading addition action. σ_1^{del} is MAXC for almost all agents. (**b**) shows a transition stage between σ_1^{add} being mostly MAXD to σ_1^{add} being primarily MAXC. (**c**) shows another transient configuration where a large number of different addition strategies coexist. (**d**) shows the addition strategies in a fragmented state

network topology with the difference that a majority of the vertices have MAXD as their leading addition action (almost all vertices have $\sigma_1^{\text{del}} = \text{MAXC}$). For this configuration, the MAXC vertices will move their edges to the most central vertices whereas the MAXD vertices will not move their edge. In Fig. 13.4c we show a more rare, high-$\langle k \rangle$ configuration ($t \approx 273,545$ in Fig. 13.3). Here the leading deletion action is NO for about one fourth of the vertices, and the system is rapidly accumulating edges. In Fig. 13.3d we show a fragmented state, where a number of vertices have the leading addition action NO. The vertices with $\sigma_1^{\text{add}} = \text{NO}$ that are not isolates have $\sigma_1^{\text{del}} = \text{NO}$ so they will not fragment the network further. On the other hand, the vertices with $\sigma_1^{\text{add,del}} = \text{MAXC}$ and $\sigma_1^{\text{add,del}} = \text{MAXD}$ *can* fragment the network.

13.3.3 Effects of Strategies on the Network Topology

We are now in a position to examine in detail the network topologies that arise from different dominating addition and deletion actions. First, we plot histograms (rescaled to show the probability density functions) of the network structural

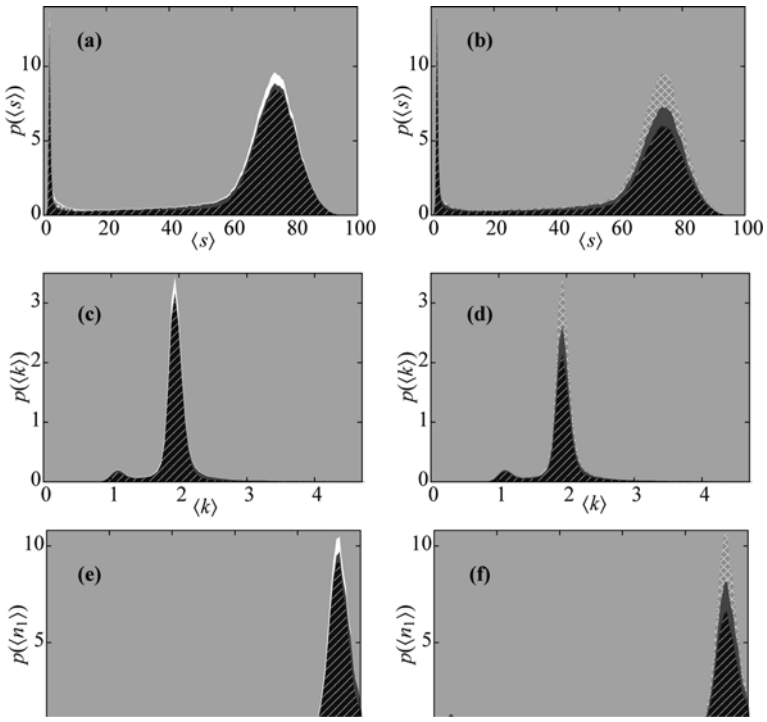

Fig. 13.5 The probability density function of average scores (**a**), (**b**), average degrees (**c**), (**d**), and relative sizes of the largest connected component (**e**), (**f**). The different fields represent different leading addition actions (**a**), (**c**), (**e**), and different leading deletion actions (**b**), (**d**), (**f**). The vertical size of a field gives the probability density function conditioned to that leading action. The *curves* are averages over ten runs of 10^5 timesteps with the same parameter values as in Fig. 13.3. The color codes of the actions are the same as in Fig. 13.3

quantities shown in Figs. 13.3c–e and 13.5. These diagrams all have two peaks – one with low $\langle s \rangle$, $\langle k \rangle$ and $\langle n_1 \rangle$ values (where the network is fragmented, the number of edges small and the scores low), and another broader peak corresponding to a connected network with higher scores and more edges. Interestingly, the different leading actions are not completely localized to different peaks but spread out over the whole range. Another counter-intuitive observation is that there seems to be more agents with $\sigma_1^{\text{add}} = \text{NO}$ in the more dense peaks. These vertices (with $\sigma_1^{\text{add}} = \text{NO}$) seem to be primarily isolated and do not affect the majority of vertices (connected in the largest component). They will therefore stay isolated until their strategies have changed or they have been connected to the rest of the network by random connections. We also observe that there is a larger variety of leading addition actions than leading deletion actions. A possible interpretation of this is that the fitness of agents is more dependent on the leading addition action. This seems natural in a situation where it is disadvantageous to connect to a majority of agents (so the choice of neighbor to disconnect is not important), however it is beneficial to connect to to a minority of well established agents.

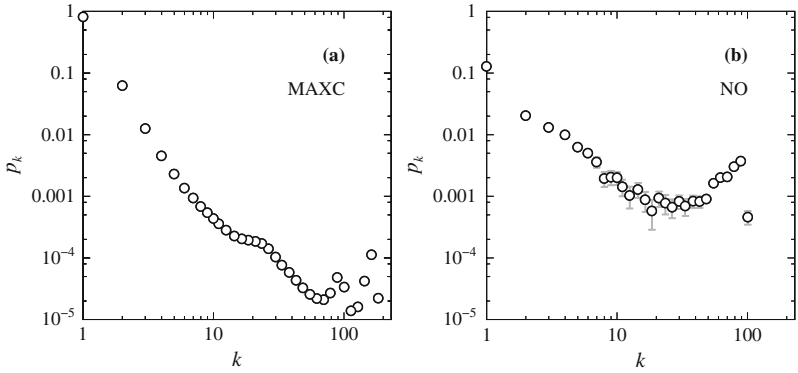

Fig. 13.6 The degree distribution for systems with the same parameter values as in Fig. 13.3. Panel (**a**) shows the averaged degree distribution when more than half of the agents have MAXC as their leading addition actions. Panel (**b**) displays the corresponding plot for the leading addition action NO

One of the most widely studied and revealing metrics of network structure, is the degree distribution – the probability mass function of the degrees of vertices. In Fig. 13.6 we plot the degree distribution for dominating actions $\sigma_1^{\text{add}} = \text{MAXC}$ (a) and $\sigma_1^{\text{add}} = \text{NO}$ (b). The $\sigma_1^{\text{add}} = \text{MAXC}$ graph has two high-k peaks, corresponding to the hubs in the network. The existence of two broad peaks as opposed to only one is strange, and the reasons for this is not immediately apparent. The $\sigma_1^{\text{add}} = \text{NO}$ graphs (whose degree distribution are shown in (b)) are more dense, as expected. However, they also have a large-k peak, which is probably related to, either the strategies of other agents, or a residue from the preceding period (remember that the periods of dominating $\sigma_1^{\text{add}} = \text{NO}$ is very short compared with the $\sigma_1^{\text{add}} = \text{MAXC}$ periods). This implies that one can separate system-wide effects of some strategy driving the decisions of the majority, but there will also be other effects present in the network. Note that, while many studies have focused on the emergent properties of degree distributions as $N \to \infty$, the interesting features of our model occurs for smaller system sizes, consequently we believe this limit is not interesting or relevant to our study and we do not consider it.

We now proceed to look at four other measures of different network structures and how they depend on the dominating addition and deletion actions. The first two measures we consider are the degree k and score s. In Fig. 13.7a, b we plot the average values of these quantities (averaged over all vertices, regardless of strategy, and averaged over all samples with a particular dominating strategy). This plot is based on ten runs for 10^5 time steps, with network quantities measured every tenth time step. During these runs, the two leading actions – $\sigma_1^{\text{add}} = \text{MINC}$ and $\sigma_1^{\text{del}} = \text{MIND}$ were never employed. We note that the most common leading actions (for both addition and deletion) MAXC and MAXD gives the highest average score. This does not mean that all agents have a high score in these situations – from Figs. 13.4a, b we know that the score can differ much from one agent to another. The degrees are low for these strategies, which is a necessary (but not sufficient) condition for a

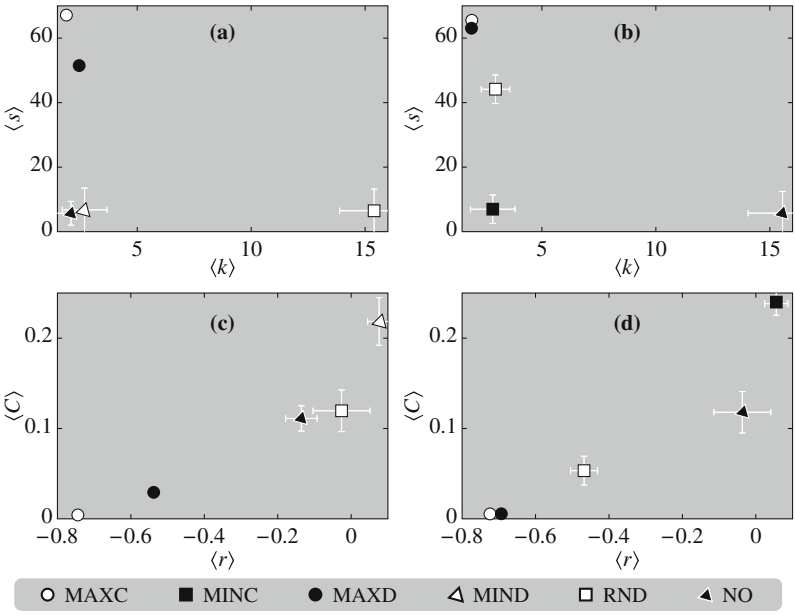

Fig. 13.7 Average values of four different network structural quantities for different dominating addition and deletion actions (i.e. that more than half of the agents have a specific σ_1^{add}, or σ_1^{del}). (**a**) shows the average score as a function of degree for different dominating σ_1^{add}. (**b**) is the corresponding plot for σ_1^{del}. (**c**) displays the clustering coefficient as a function of assortativity for different dominating σ_1^{add}. (**d**) is the corresponding plot for different σ_1^{del}. The *bars* indicate standard errors. The data comes from simulation of ten runs (different random number generator seeds) of 10^5 time steps. Two actions were never attained during these runs: $\sigma_1^{\text{add}} = \text{MINC}$ and $\sigma_1^{\text{del}} = \text{MIND}$

low score. For $\sigma_1^{\text{add}} = \text{NO}$ the average degree is also low, but the score is much lower than for $\sigma_1^{\text{add}} = \text{MAXC}$ and MAXD. The reason, as pointed out above, is that the network can become heavily fragmented for this leading addition action. The σ_1^{add} corresponding to the highest degree is RND, this might seem strange, but during these runs (which is also visible in Fig. 13.3) $\sigma_1^{\text{add}} = \text{RND}$ is correlated with $\sigma_1^{\text{del}} = \text{NO}$ which is a state naturally leading to a comparatively dense network. The other leading actions $\sigma_1^{\text{add}} = \text{MIND}$ and $\sigma_1^{\text{del}} = \text{MINC}$ result in low scores and sparse networks.

The other two measures we examine are the *assortativity* and *clustering coefficient*. Before discussing our results, let us first define these quantities in detail. The average degree tells us if the network is sparse or dense. The degree distribution gives a more nuanced picture of how homogeneous the set of vertices are with respect to the number of neighbors. The next level of complexity in describing the network with respect to the agents' degree, is to measure the correlations between the degrees of vertices at either side of an edge. In particular, one can determine if high-degree vertices are primarily connected to similar high degree vertices, or instead are linked to low-degree vertices. The assortativity r is a measure of vertices' tendency to connect to other vertices of similar type, in this case those with

similar degree [19]. In technical terms, r is the Pearson correlation coefficient of the degrees at either side of an edge. There is an additional caveat that we need to consider; since the edges in our networks are undirected, r has to be symmetric with respect to edge-reversal (i.e. replacing (i, j) by (j, i)). However the standard definition of the Pearson correlation coefficient does not account for this symmetry. The way to fix this problem is to let one edge contribute twice to r, i.e. to represent an undirected edge by two directed edges pointing in opposite directions. If one employs an edge list representation internally (i.e., if edges are stored in an array of ordered pairs $(i_1, j_1), \cdots, (i_M, j_M)$) then we can write the adjusted r as,

$$r = \frac{4\langle k_1 k_2\rangle - \langle k_1 + k_2\rangle^2}{2\langle k_1^2 + k_2^2\rangle - \langle k_1 + k_2\rangle^2}, \tag{13.4}$$

where, for a given edge (i, j), k_1 is the degree of the first argument (i.e., the degree of i), k_2 is the degree of the second argument and the brackets $\langle \cdots \rangle$ denote averaging. The range of r is $[-1, 1]$ where negative values indicate a preference for highly connected vertices to attach to low-degree vertices, and positive values imply that vertices tend to be attached to other vertices with degrees of similar magnitudes.

The clustering coefficient, on the other hand, is a measure of transitivity in the network. In other words it checks whether neighbors of a node are also connected to each other (thus forming triangles). It is a well known empirical fact that social acquaintance networks have a strong tendency to form triangles [10] and it is therefore a worthwhile exercise to examine whether the networks generated by our model display this feature. There is in principle, more than one way to define the clustering coefficient. Here we employ the most commonly used one [4],

$$C = 3n_{\text{triangle}} \Big/ n_{\text{triple}}, \tag{13.5}$$

where n_{triangle} is the number of triangles and n_{triple} is the number of connected triples (subgraphs consisting of three vertices and two or three edges). The factor of three is included to normalize the quantity to the interval [0, 1].

Now that we have defined these quantities we refer back to Fig. 13.7. We note that the most common leading actions $\sigma_1^{\text{add,del}} = \text{MAXC}$ and MAXD have the lowest $\langle C\rangle$ and $\langle r\rangle$ values. A possible explanation for this could be the following. Consider a triangle, a subgraph of three vertices connected by three edges. The graph will be connected even if one of these edges is deleted. In a situation where edges are expensive, this kind of redundancy is not desired. For this reason, it seems natural that, on average, the most successful strategies MAXC and MAXD have few triangles. The negative assortativity of these situations are also conspicuous features of the examples shown in Figs. 13.4a, b (most vertices there are only connected to the two hubs, but the hubs are not connected to each other). For networks with a broad spectrum of degrees, it is known that $\langle C\rangle$ and $\langle r\rangle$ are relatively strongly correlated [13]. This is also true in Figs. 13.7c, d where the relationship between $\langle C\rangle$ and $\langle r\rangle$ is monotonically increasing. The network configurations with highest $\langle C\rangle$ and $\langle r\rangle$ are the ones with $\sigma_1^{\text{add}} = \text{MIND}$ and $\sigma_1^{\text{del}} = \text{MINC}$. Since these networks are both

sparse and fragmented, some components must have a large number of triangles (probably close to being fully connected). The denser states, with $\sigma_1^{\text{add}} = \text{RND}$ and $\sigma_1^{\text{del}} = \text{NO}$, have intermediate $\langle C \rangle$- and $\langle r \rangle$-values, meaning that the edges are more homogeneously spread out, similar to the network in Fig. 13.4c.

13.3.4 Transition Probabilities

From Fig. 13.3 it seems likely that the ability of one leading action to grow in the population depends on the other predominant strategies in the system. For example, $\sigma_1^{\text{add}} = \text{RND}$ dominates after a period of many agents employing $\sigma_1^{\text{add}} = \text{MIND}$ as the leading strategy. Consequently, it is worth asking the question: How does the probability of one leading action depend on the configuration at earlier time steps?

We investigate this qualitatively by calculating the "transition matrix" $\mathbf{T}'$ with elements $T'(s_1, s_1')$ giving the probability of a vertex with the leading action s_1 to have the leading action s_1' at the next time step. However, note that the dynamics is not fully determined by $\mathbf{T}'$, and is thus not a transition matrix in the sense of other physical models. If that were the case (i.e. the current strategy is independent of the strategy adopted in the previous time step) we would have the relation $T'_{ij} = \sqrt{T'_i T'_j}$. To study the deviation from this null-model, we assume the diagonal (i.e. the frequencies of the strategies) given, and calculate $\mathbf{T}$ defined by,

$$T_{ij} = T'_{ij} / \sqrt{T'_i T'_j}. \tag{13.6}$$

The values of $\mathbf{T}$ for the parameters defined in Fig. 13.3 are displayed in Tables 13.1 and 13.2. The off-diagonal elements have much lower values than 1 (the average off-diagonal Θ values are 0.014 for addition strategies and 0.010 for deletion). This reflects the contiguous periods of one dominating action. Note that transitions between MAXC and RND are over-represented: $T'^{\text{del}}_{\text{MAXC,RND}} \approx T'^{\text{del}}_{\text{RND,MAXC}} \approx 0.027$, which is more than twice the value of any other off-diagonal element involving MAXC or RND. As another token of the problem's complexity, the matrix is not completely symmetric $T'^{\text{del}}_{\text{RND,NO}}$ is twice (~ 3 s.d.) as large as $T'^{\text{del}}_{\text{NO,RND}}$ meaning

Table 13.1 Values for the $\mathbf{T}$ matrices for addition. (T_{ij} is the deviation from the expected value in a model of random transitions given the diagonal values.) The values are averaged over 100 realizations of the algorithm. All digits are significant to one s.d. The parameter values are the same as in Fig. 13.3. Numbers in parentheses are the standard errors in units of the last decimal

	MAXC	MINC	MAXD	MIND	RND	NO
MAXC	1	0.0164(3)	0.0088(2)	0.0107(4)	0.0151(5)	0.0010(0)
MINC	0.0169(3)	1	0.0113(6)	0.036(2)	0.025(2)	0.0017(3)
MAXD	0.0093(3)	0.0104(7)	1	0.0103(6)	0.0206(9)	0.0003(0)
MIND	0.0115(4)	0.030(2)	0.0130(7)	1	0.059(5)	0.0020(2)
RND	0.0157(5)	0.024(2)	0.020(1)	0.064(5)	1	0.0023(5)
NO	0.0007(0)	0.0031(2)	0.0009(0)	0.0036(2)	0.0042(4)	1

Table 13.2 Same as in Table 13.1 but for deletion, instead of addition, strategies

	MAXC	MINC	MAXD	MIND	RND	NO
MAXC	1	0.0100(2)	0.0131(4)	0.0094(2)	0.0266(3)	0.0126(3)
MINC	0.0098(2)	1	0.0070(3)	0.010(1)	0.0105(4)	0.0050(3)
MAXD	0.0133(4)	0.0067(3)	1	0.0055(2)	0.0124(3)	0.0062(2)
MIND	0.0087(2)	0.011(1)	0.0054(2)	1	0.0101(2)	0.0055(3)
RND	0.0269(3)	0.0094(4)	0.0128(3)	0.0083(2)	1	0.0072(3)
NO	0.0097(3)	0.0076(3)	0.0053(2)	0.0078(3)	0.0131(3)	1

that it is easier for RND to invade a population with NO as a leading deletion action, than vice versa.

13.3.5 Dependence on System Size and Noise

So far we have focused on one set of parameter values. In this section we investigate how the system behavior depends on the number of agents and the noise level in the deletion and attachment mechanism. In Fig. 13.8, we tune the noise level (fraction of random attachments) p_r for three system sizes. In panels (a)–(c) we show the fraction of leading addition actions among the agents $\langle \Sigma_1^{\text{add}} \rangle$ (averaged over ~ 100 runs and 10^5 time steps). The quantities $\Sigma_1^{\text{add,del}}$ denotes the fraction of agents having a specific $\sigma_1^{\text{add,del}}$. As observed in Fig. 13.3a the leading action is MAXC followed by MAXD and RND. The leading deletion actions, as seen in panels (d)–(f), are ranked similarly except that MAXD has a larger (and increasing) presence. If $p_r = 1$, then all actions are equally likely (they do not have any meaning – all strategies will result in random moves equal to $s_1^{\text{add}} = s_1^{\text{del}} = \text{RND}$). There are trends in the p_r-dependences of $\langle \sigma_1^{\text{add}} \rangle$, but apparently no emerging discontinuity. This observation, (which also seems to hold for the p_s-scaling), that there is no phase transition for any parameter value governing the probability of random permutations in the strategy vectors, is an indication that the results above can be generalized to a large parameter range. We also note that, although the system has the opportunity to be passive (i.e. agents having $s_1^{\text{add}} = s_1^{\text{del}} = \text{NO}$), this does not happen. This situation is reminiscent of the "Red Queen hypothesis" of evolution [25] – organisms need to keep evolving to maintain their fitness.

Next we look at the dependence of the network structure on the number of agents and the noise level. The average degree, plotted in Fig. 13.3g is monotonously increasing with p_r. There is, however, a qualitative difference in the size scaling – for $p_r \lesssim 0.12$ the average degree increases with N, for $p_r \gtrsim 0.12$ this situation is reversed. In Fig. 13.3h we plot the average largest-component size as a function of p_r for different system sizes. The behavior is monotonous in both p_r and N – larger p_r, or a larger system size, means higher $\langle n_1 \rangle$. In all network models we are aware of (allowing fragmented networks), a decreasing average degree implies a smaller giant component. For $p_r \gtrsim 0.12$, in our model the picture is the opposite – as the system grows the giant component spans an increasing fraction of the network. This

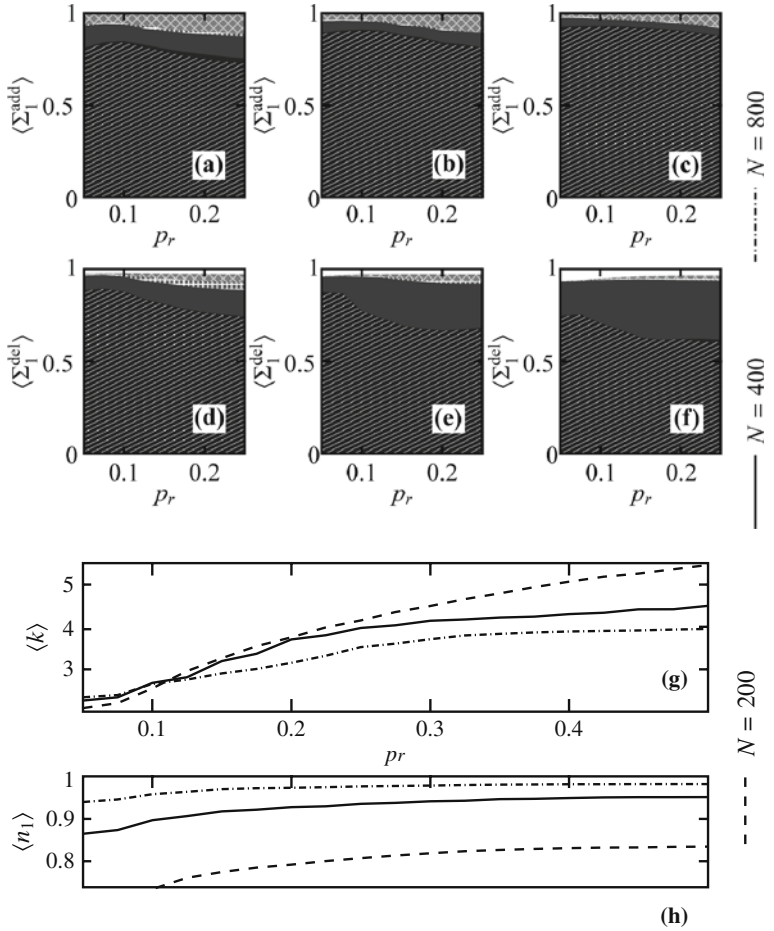

Fig. 13.8 The system's dependence on the topological noise level (via the fraction of random rewirings p_r) for different system sizes N. Panels (**a**), (**b**) and (**c**) show the fraction $\langle \Sigma_1^{\text{add}} \rangle$ of leading addition actions σ_1^{add} for systems of $N = 200$, 400 and 800. Panels (**d**), (**e**) and (**f**) show the fraction of preferred deletion actions for the same three system sizes, while (g) shows the average degree and (**h**) the average size of the largest connected component $\langle n_1 \rangle$

also means that the agents, on average, reach the twin goals of keeping the degree low and the graph connected.

13.4 Discussion

We have presented a general game theoretic network problem, the diplomat's dilemma – how can an agent in a network simultaneously maximize closeness centrality and minimize degree. The motivation for this problem comes in part from

a type of social optimization situation where agents seek to gain power (via closeness centrality) and keep the cost (degree) low. It can also be motivated from a more academic point of view – interesting dynamics often comes from when agents simultaneously try to optimize conflicting objectives. The diplomat's dilemma is one of the simplest such situations in a networked system, because the score function does not depend on any additional variable, or trait, of the vertices, only the vertex' position in the network.

We devise an iterative simulation where at every time step, an agent can delete its connection to a neighbor and add an edge to a second neighbor, based on the information it possesses about the network characteristics of vertices within its local neighborhood (upto second neighbors). The agents use strategies that they update by imitating the best performing neighbor within this information horizon. The dynamics are driven by occasional random moves and random permutations of the vectors encoding the strategies of the agents. For the sake of flexibility, the definition of the problem as stated in this chapter, is deliberately vague. To turn it into a mathematically well-defined problem, one has to specify how the agents can affect their position in the network and what information they can use for this objective. There are of course many choices for how to do this. Although we believe our formulation is natural, it would be very interesting to rephrase these assumptions. A future enhancement would be to equip the agents with methods from the machine learning community to optimize their position, and to tune the amount of information accessible to the agents. A mathematical simplification of the problem would be to let all agents know the precise network topology at all times (this may however lead to some conceptual problems – if the information about the network is obtained via the network, it would be strange if the picture of the network close to an agent would not be more accurate than the picture of more remote sections of the network). Another interesting version of the problem would be to require an edge to represent an agreement between both vertices, so that an agent i cannot add an edge (i, j) unless j finds this profitable.

Nevertheless, despite the simplicity of our model, the time evolution of the simulation is strikingly complex, with quasi-stable states, trends, spikes and cascades of strategies among the agents. This complex dynamics is also captured in various metrics measuring different levels of network structure. Furthermore, the network structure and the agents' strategies directly influence one another. If the agents stop deleting edges, the average degree of the network will grow rapidly, which may benefit a strategy aiming to lower the degree of the agents. This feedback from network structure, to the agents and their decisions about how to update their networks is a central theme in the field of adaptive, coevolutionary networks [9]. We believe that all forms of social optimization involve such feedback loops, which is a strong motivation for studying adaptive networks. The complexity of the time-evolution, especially in the network structural dynamics is more striking for intermediate system sizes. Indeed, many interesting features of our simulation are not emergent in the large-system limit, but rather present only for small sizes. Models in theoretical physics have traditionally focused on properties of the system as $N \to \infty$. In models of social systems however, extrapolating to infinite size is not necessarily a

natural limit in the same way (it will of course be interesting to examine the limiting behavior of such models). We believe this is a good example of the dangers of taking the large-size limit by routine – the most interesting relevant features of the model may be neglected.

In a majority of the cases in our simulations, most of the agents use a strategy where they both delete, and attach to vertices according to the MAXC action. This implies that the agent first deletes the edge to the most central vertex in the second neighborhood (in the sense of a modified closeness centrality), and then reattaches to the most central vertex two steps away (before the deletion). In practice this means that an agent typically transfers an edge from its most central immediate neighbor to its most central neighbor two steps away. This strategy makes the agent move towards the center without increasing its degree, which clearly seems like a reasonable procedure in the diplomat's dilemma. However, this strategy is not evolutionary stable in the presence of noise (hence the complex time evolution). This strategy creates networks with low clustering coefficients, i.e., there are a comparatively small number of triangles. Since forming a triangle introduces an extra edge, which is expensive, without changing the size of connected component, one can understand why agents are reluctant to form these triangles per se in our formulation of the problem.

Different strategies have different ability to invade one another. To test this we measure the deviation from random transitions from one dominating action to another (given the frequency of particular strategies), concluding for example that it is about twice as easy for RND to invade NO as a leading deletion action. Another interesting aspect is that (for some noise levels), as the system size increases, the network becomes both more connected (the relative fraction of vertices in the largest connected component increases), and more sparse (the average degree decreases). This is in sharp contrast to all other generative network models that we are aware of, but definitely consistent with the objectives of the general problem (where large connected components and low degrees are desired).

What does this result tell us about the real professional life of diplomats? Maybe that they can, by selfishly optimizing their positions in the network, self-organize to a connected business network where they need only a few business contacts, without knowing more about the network than the second neighborhood. However to make a stronger and more conclusive statement about the optimal strategy, more results are needed. This is something we hope to gather from future studies.

One of the problems facing this type of mechanistic modeling of social information processes [6, 8, 12, 22, 23], is that they are very hard to validate. Information spreading in social systems is neither routed from agent to agent like the information packets in the Internet, nor do they spread in the same fashion as epidemics. Instead the spreading dynamics is content dependent. Different types of information may be spreading over different social networks, following different dynamic rules. There are some promising datasets for studying social information spreading. For example, networks of blogs, Internet communities, or social networking sites generate large amounts of potentially valuable data, although these data sets are not necessarily conducive to the questions that adaptive models such as the one described in this

chapter seek to address. In the near future, we hope mechanistic modeling of social information processes will be more data driven, asking questions that can actually be validated through empirical study.

Acknowledgements P.H. acknowledges support from the Swedish Foundation for Strategic Research. G.G. thanks the James S. McDonnell foundation for support. The authors thank Matteo Marsili and David Kempe for comments.

References

1. Albert R, Barabási A-L (2002) Statistical mechanics of complex networks. Rev Mod Phys 74:47–98
2. Axelrod R (1984) The Evolution of Cooperation. Basic Books, New York.
3. Bala V, Goyal S (2000) A noncooperative model of network formation. Econometrica 68: 1181–1229
4. Barrat A, Weigt M (2000) On the properties of small-world network models. Eur Phys J B 13:547–560
5. Dorogovtsev SN, Mendes JFF (2003) Evolution of Networks: From Biological Nets to the Internet and WWW. Oxford University Press, Oxford
6. Ehrhardt G, Marsili M, Vega-Redondo F (2006) Diffusion and growth in an evolving network. Int J Game Theory 34:383–397
7. Erdős P, Rényi A (1959) On random graphs I. Publ Math Debrecen 6:290–297
8. Gila S, Zanette DH (2006) Coevolution of agents and networks: Opinion spreading and community disconnection. Phys Lett A 356:89–94
9. Gross T, Blasius B (2008) Adaptive coevolutionary networks: a review. J Roy Soc Interface 5:259–271
10. Holland PW, Leinhardt S (1972) Some evidence on the transitivity of positive interpersonal sentiment. Am J Sociol 72:1205–1209
11. Holme P, Ghoshal G (2006) Dynamics of networking agents competing for high centrality and low degree. Phys Rev Lett 96:098701
12. Holme P, Newman MEJ (2006) Nonequilibrium phase transition in the coevolution of networks and opinions. Phys Rev E 74:056108
13. Holme P, Zhao J (2007) Exploring the assortativity-clustering space of a network's degree sequence. Phys Rev E 75:046111
14. Jackson MO, Wolinsky A (1996) A strategic model of social and economic networks. J Eco Theory 71:44–74
15. Kahneman D (2003) Maps of bounded rationality: psychology for behavioral economics. The Am Eco Rev 93:1449–1475
16. Knoke D (1990) Political Networks: The Structural Perspective. Cambridge University Press, Cambridge
17. Lindgren K, Nordahl MG (1994) Evolutionary dynamics of spatial games. Physica D 75: 292–309
18. Nakao K (1990) Distribution of measures of centrality: Enumerated distributions of freeman's graph centrality measures. Connections 13:10–22
19. Newman MEJ (2003) The structure and function of complex networks. SIAM Rev 45: 167–256
20. Nowak M, Sigmund K (1992) A strategy of win-stay, lose-shift that outperforms tit-for-tat in the prisoner's dilemma game. Nature 364:56–58
21. Nowak MA, May RM (1992) Evolutionary games and spatial chaos. Nature 359:826–829

22. Rosvall M, Sneppen K (2003) Modelling dynamics of information networks. Phys Rev Lett 91:178701
23. Rosvall M, Sneppen K (2006) Modeling self-organization of communication and topology in social networks. Phys Rev E 74:016108
24. Sabidussi G (1966) The centrality index of a graph. Psychometrika 31:581–603
25. van Valen LM (1973) A new evolutionary law. Evol Theory 1:1–30
26. Watts DJ, Strogatz SH (1998) Collective dynamics of 'small-world' networks. Nature 393:440–442
27. Weber M (1947) The Theory of Social and Economic Organization. Oxford University Press, New York

Part V
Graph-Rewriting-Based Approaches

Chapter 14
Graph-Rewriting Automata as a Natural Extension of Cellular Automata

Kohji Tomita, Haruhisa Kurokawa, and Satoshi Murata

Abstract We introduce a framework called graph-rewriting automata to model evolution processes of networks. It is a natural extension of cellular automata in the sense that a fixed lattice space of cellular automata is extended to a dynamic graph structure by introducing local graph-rewriting rules. We consider three different constructions of rule sets to show that various network evolution is possible: hand-coding, evolutionary generation, and exhaustive search. Graph-rewriting automata provide a new tool to describe various complex systems and to approach many scientific problems.

14.1 Introduction

In modeling, analyzing or designing systems comprising many elements in full detail, it is important to clarify the dynamics of each element and the relations among elements. In most cases, structures and states are coupled critically in the sense that the global structure constrains the behavior of each element and is generated as a result of behavior of the elements. From such interaction, unpredicted behavior called emergence arises, which is difficult to describe at the level of elements. Recently, co-evolution of topology (network) and states has been studied in various contexts such as complex networks [3].

Graph rewriting, a method to model such a dynamic structure, has been studied in computer science as graph grammar [13]. Many studies specifically examine general properties or computational aspects such as termination of the processes or recognition of the configuration, and dynamic behavior of rewriting processes is not emphasized. We are instead interested in dynamic behavior of graph development by interplay between structure and states.

The L-system [9, 12] is an early study of structurally varying dynamical systems. Recent studies of this kind are aimed at a general representation of such

K. Tomita (✉)
National Institute of Advanced Industrial Science and Technology (AIST), 1-2-1 Namiki, Tsukuba, Ibaraki 305-8564, Japan
e-mail: k.tomita@aist.go.jp

T. Gross, H. Sayama (eds.), *Adaptive Networks,* Understanding Complex Systems,
DOI 10.1007/978-3-642-01284-6_14,

graph evolution. Salzberg et al. considers graph constructing graphs [14]; graphs are treated as active objects that manipulate other graphs and also as passive objects that are manipulated. Smith et al. proposed network automata, where graph evolution is studied based on adjacency matrices [17]. Sayama proposed generative network automata [15], using local graph replacement in a general framework. Other studies include those using blob machines by Gruau et al. [4], and MGS by Giavitto and Spicher [2] for spatial computing.

In this chapter, we specifically examine a particular class of graph dynamics called graph-rewriting automata, keeping a close relation with cellular automata [6, 24]. Cellular automata is a simple model of discrete symbol dynamics on a fixed topology. Because of its simple framework, with only the state transition of cells on a fixed lattice, it has been applied in various fields. Extension of cellular automata for varying topologies has been studied in, for example, structurally dynamic cellular automata [7]. In this system, the connection change among cells is particularly emphasized; the number of cells is unchanged.

We try to extend cellular automata more naturally to graph structures. As in cellular automata, the number of neighbors of each cell is unchanged. In our framework, we treat three-regular graphs. Local graph-rewriting rules are introduced for structural change. Graphs are rewritten locally according to a given rule set. In spite of this regularity, our framework is sufficiently general to represent various behaviors of network evolution such as self-organization or self-reconfiguration including self-replication. Network evolution using similar rewriting rules is discussed by Wolfram in connection with fundamental physics [25]. In his system, nodes have no states; global or rather arbitrary rule application is treated. We concentrate mainly on deterministic processes using internal states of the nodes.

In the following, we introduce the framework and show simple examples in the next section. Three different constructions of rule sets are in sequence to show that various network evolution is possible: hand-coding, evolutionary generation, and exhaustive search. Each includes self-replicating graphs with different features. Finally, the conclusion follows.

14.2 Formulation

In cellular automata, cells with discrete states are arranged to form a lattice; the transition of each cell's state is determined by the states of its neighbors. For this state transition, a globally homogeneous lattice structure is unnecessary: a locally regular structure is sufficient such that each cell has a certain constant number of neighbors. In our graph-rewriting automata, all cells (hereinafter nodes) have three neighbors. Multiple links between the same two nodes and self-links (loops) are allowed. We consider only a class of graphs that can be projected onto a plane. These constraints of three-regularity and planarity can be satisfied by, e.g., an endless planar honeycomb, a tetrahedron, a cube, a dodecahedron, and a Fullerene. Three-neighbor connectivity is the minimum that can generate non-trivial graphs; more importantly,

it is invariant under the following graph rewriting operations. (A modified system with four links and simple rewriting rules is presented by Kataoka [8].)

We define finite states on nodes that are taken from an arbitrary finite set of symbols. Three links of each node have a cyclic order. Rotation directions of all nodes are identical when the graph is embedded in a plane. The graph rewriting rules are designed so that the graph is always kept planar and the directions of the cyclic orders are conserved.

The constant number of neighbors enables us to write rules in a regular form: each rule is described by a rule name and at most five symbols as its arguments, which is greatly advantageous when we design a large complex system. For instance, the same rule can be reused in different situations. A rule can trigger a cascade of other rules by stacking rules as a subroutine.

Formally, it is definable as follows.

Definition 1. Let S be a finite set of states. Base graph G_S is a quadruple $\langle V, E, \xi, \eta \rangle$, where V is a (possibly empty) set of nodes, E is a set of links, $\xi : V \to S$ is a function that assigns a state to each node, and $\eta : V \times \{0, 1, 2\} \to E$ is a function that specifies three incident links of each node with cyclic order. More precisely, η satisfies $|\{\langle v, d \rangle : \eta(v, d) = e, \text{ where } v \in V \text{ and } d \in \{0, 1, 2\}\}| = 2$ for every $e \in E$.

Hereinafter, base graphs are called graphs for simplicity if no confusion exists.

14.2.1 Rules of Graph-Rewriting Automata

We first give rules of graph-rewriting automata and describe the effect when each rule is applied. There are four rules: one state transition rule and three structural rewriting rules (Fig. 14.1). The state transition rule changes the state of nodes; the structural rewriting rules change the structure of the graph in a local manner. These rules are represented as follows.

State transition rule:

$$\text{trans } m_0(n_1, n_2, n_3) \to m_1, \qquad \text{(state transition)},$$

Structural rewriting rules:

$$\begin{array}{ll} \text{div } m_0(n_1, n_2, n_3) \to m_1, & \text{(division)}, \\ \text{com } (n_1, n_2), & \text{(commutation)}, \\ \text{anh } (n_1, n_2), & \text{(annihilation)}. \end{array}$$

In the first two rules (trans and div), classified as node rules hereinafter, m_0 denotes the current state of the node, and n_1, n_2, n_3 are states of its neighbor nodes in this order. States of the neighbors are matched with the condition part by shifting them in the cyclic order. Therefore, (n_1, n_2, n_3), (n_2, n_3, n_1), and (n_3, n_1, n_2) describe the same condition, but (n_3, n_2, n_1) is not the same. In the latter two rules

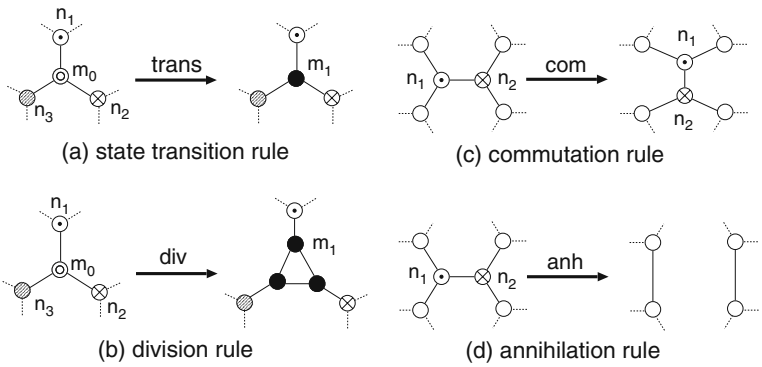

Fig. 14.1 Four rules of graph-rewriting automata: (**a**) state transition, (**b**) division, (**c**) commutation, and (**d**) annihilation. Symbols denote states of the nodes, not the identifiers

(com and anh), classified as link rules hereinafter, n_1 and n_2 are the states of its incident nodes. Exchange of the states is allowed in matching.

The state transition rule simply changes the state of the node when the condition is satisfied (Fig. 14.1a). The division rule divides a node into three nodes with the identical state and generates three new links (Fig. 14.1b). The cyclic orders at the new nodes inherit the previous order.

The commutation rule rearranges the local connective situation including two adjacent nodes (Fig. 14.1c). It can be regarded as a quarter rotation of a pair of adjacent nodes. The commutation direction is defined as the same direction of the cyclic link order. This commutation is realized by reconnection of links. The node states are unchanged. The annihilation rule removes a pair of nodes and a link between them (Fig. 14.1d).

These rules were introduced so that they are universal in the sense that they can rewrite any planar three-regular graph with at least four nodes of different states to any such graph, according to the following update scheme.

14.2.2 Update Procedure

This section presents a description of how the rules are applied to the whole system and updates the graphs. We assume the time step of integers. An initial base graph and a rule set are given. The rule set is a list of rules; the graph is updated at each time step.

To update the graphs, we apply only node rules (trans and div) at even time steps, and link rules (com and anh) at odd time steps. Rules are executed synchronously for all nodes or links. We assume that all conditions of the rules in a rule set are different, and that no ambiguity of rule choice exists. Applying either commutation or annihilation to adjacent links engenders inconsistency. Therefore, all such applications are suppressed. This lateral inhibition is realized in several ways in a local manner.

One is to see a wider area covering the second nearest neighbors to confirm that neighboring links do not satisfy the condition of any rule. Another is to execute the process in two steps. First, each link raises a flag if a rule condition is satisfied; then, if any of the four neighboring links does not raise a flag, the link actually executes the rule. Because of these restrictions, the updating process becomes completely deterministic.

A development process of an initial graph based on a rule set, i.e., a set of instances of the four kinds of graph-rewriting rules, is defined in the following.

Definition 2. Let G and R respectively represent a graph and a rule set. A graph obtained from G by node rules in R, denoted by $R_{\mathrm{N}}(G)$, is a graph that is obtained by application of node rules of R to all matching nodes in G. A graph obtained from G by link rules in R, denoted by $R_{\mathrm{L}}(G)$, is a graph that is obtained by application of link rules of R to every matching link whose neighbor links match no link rules in R.

Definition 3. Let G_0 and R respectively represent a graph and a rule set. A rewriting sequence of graph G_0 by R is the sequence $G_0, G_1, G_2, \ldots$, where $G_{2i+1} = R_{\mathrm{N}}(G_{2i})$ and $G_{2(i+1)} = R_{\mathrm{L}}(G_{2i+1})$ for each i.

Figure 14.2 portrays the rewriting steps beginning with a four-node graph. At time 0, rule A is applied: the node with state 1 is divided into three nodes with the same state. Then, at time 1, rules B and C are applied. No rule is applied at time 2. At time 3, rule C is applied, but rule B is not applied because of lateral inhibition.

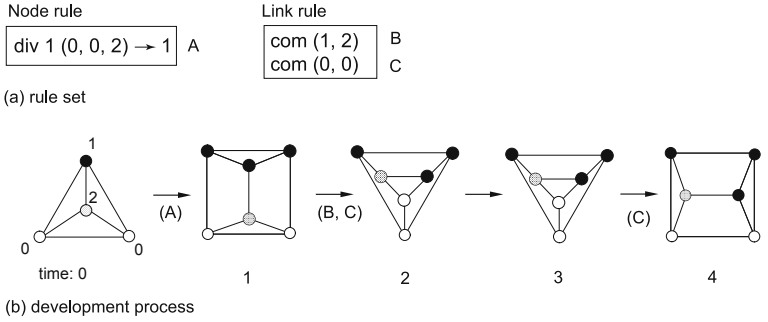

Fig. 14.2 Example of simple rewriting steps: (**a**) rule set, (**b**) development steps

14.2.3 Simulation of Graph-Rewriting Automata

Some interface to visualize the development processes is necessary when we are to design or verify the elaborate graph structures and rule sets. It is also useful to see the development processes when rule sets are generated mechanically. For this purpose, we developed a visual simulator.

In this simulator, the graphs are embedded in three-dimensional Euclidean space and are drawn as wire frames. For simplicity, a link is assumed to be a spring with

a damping characteristic. By applying appropriate force, natural wire frame shapes can be generated according to the development process, as shown later, for example in Fig. 14.4a.

14.2.4 Examples

Here, simple examples are presented to explain the potential of graph-rewriting automata.

14.2.4.1 Flexible Resolution

A uniform honeycomb lattice with arbitrary resolution is obtained when division and commutation are alternately applied using two states and three rules (Fig. 14.3).

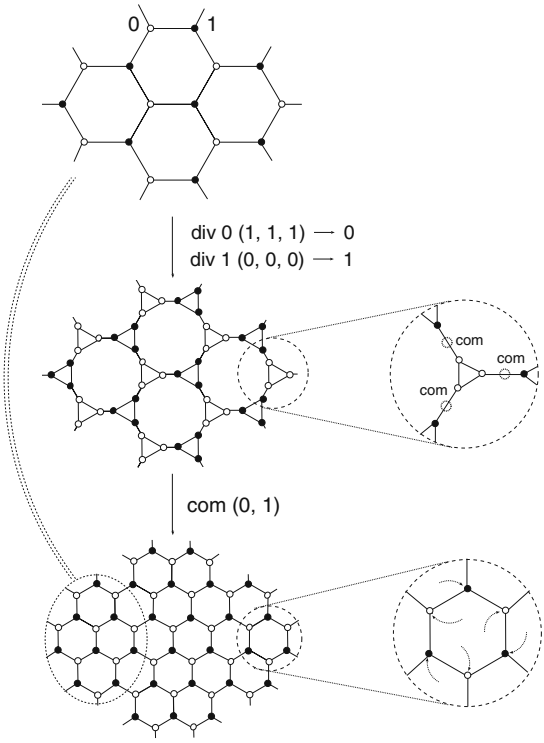

Fig. 14.3 Flexible resolution

14.2.4.2 Generation of a Repetitive Structure

From a heterogeneous tetrahedron (in which all the nodes have different states: 0, 1, 2, and 3), a globular graph is generated using a rule set similar to that described

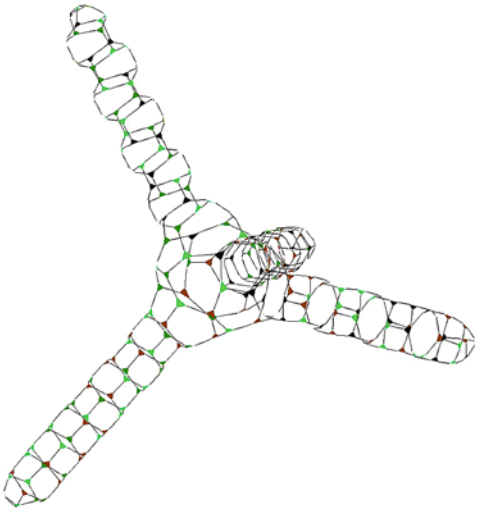

(a)

(b)

div 0 (1, 2, 3) → 0
div 1 (2, 0, 3) → 1
div 2 (3, 0, 1) → 2
div 3 (2, 1, 0) → 3
div 0 (1, 1, 2) → 0
div 1 (0, 0, 3) → 1
div 2 (0, 0, 1) → 2
div 3 (0, 0, 2) → 3
div 0 (2, 2, 3) → 0
div 0 (3, 3, 1) → 0
div 1 (3, 3, 2) → 1
div 1 (2, 2, 0) → 1
div 2 (1, 1, 3) → 2
div 2 (3, 3, 0) → 2
div 3 (2, 2, 1) → 3
div 3 (1, 1, 0) → 3
com (0, 1)
com (0, 2)
com (0, 3)
com (1, 2)
com (1, 3)
com (2, 3)

Fig. 14.4 Generation of repetitive structure: (**a**) structure, (**b**) rule set

in Sect. 14.2.4.1. Then it continues to extend four arms with a repetitive structure (Fig. 14.4a). The process is described by 22 rules (Fig. 14.4b).

14.2.4.3 Simple Self-replication

A rule set for self-replication of a heterogeneous tetrahedron (in which all nodes have different states) is designed (Fig. 14.5a). It requires two additional intermediate states and 19 rules (Fig. 14.5b). The whole structure and internal states of the nodes are replicated after the eighth step. (No rule was applied at time steps 0, 3, or 5.) This replication process is repeated arbitrarily many times.

14.3 Rule Design by Hand-Coding

In this section, we show how a larger rule set can be designed on this framework. As an example, we design self-replication of graphs. Self-replication has been studied after von Neumann's seminal work [23]. Most such studies are based on two-dimensional cellular automata, as reviewed in [16], but it is realized naturally and simply using graph-rewriting automata. For instance, a self-replicating Turing machine that requires complicated steps in cellular automata can be represented concisely using graph-rewriting automata. (Another self-replication of von Neumann style based on translation/transcription is explained in the literature [20] using an additional graph rewriting rule.)

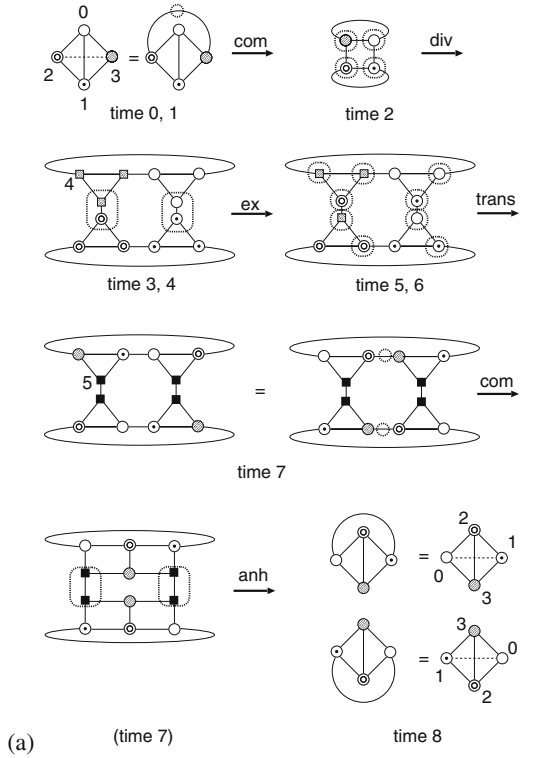

(b)

com $(2, 3)$
div 0 $(1, 3, 3) \to 0$
div 1 $(0, 2, 2) \to 1$
div 3 $(0, 0, 2) \to 4$
div 2 $(1, 1, 3) \to 2$
trans 0 $(0, 0, 1) \to 1$
trans 1 $(1, 1, 0) \to 0$
trans 4 $(4, 4, 2) \to 2$
trans 2 $(2, 2, 4) \to 4$
trans 4 $(4, 0, 2) \to 3$
trans 4 $(4, 2, 0) \to 1$
trans 0 $(0, 1, 4) \to 2$
trans 2 $(4, 4, 4) \to 5$
trans 4 $(2, 2, 2) \to 5$
trans 1 $(0, 0, 0) \to 5$
trans 0 $(1, 1, 1) \to 5$
trans 2 $(2, 1, 4) \to 0$
trans 1 $(1, 2, 0) \to 3$
anh $(5, 5)$

Fig. 14.5 Simple self-replication: (**a**) replication steps, where "ex" denotes exchange of states by simultaneous execution of state transition by two nodes; (**b**) rule set

14.3.1 Design of Self-replicating Turing Machine

A Turing machine is a mathematical model of computation [22] that comprises a one-dimensional tape of infinite length and a moving head. The tape is divided into squares and each square contains a symbol from a finite set. At any time, the head is located at one of the squares; it can read/write only on the square. The Turing machine has an internal state chosen from a finite set. From its internal state and a symbol on the head location, it decides its operation to write a new symbol, move the head to the left or right for one square, and change its internal state. This rewriting process corresponds to computation. It is an extremely simple model, but it can compute any computable function according to Church's thesis [1].

In graph-rewriting automata, the Turing machine can be modeled by a simple ladder structure (Fig. 14.6a). The upper nodes of the ladder correspond to squares of the tape, and one node in the lower row plays the role of the head. Both ends of the ladder (called Ends of Tape (EOTs)) are connected to form a ring to satisfy the three-neighbor constraint. Although the tape is finite, the structure can be extended to arbitrary length by division of EOT if necessary. Each operation of a Turing machine

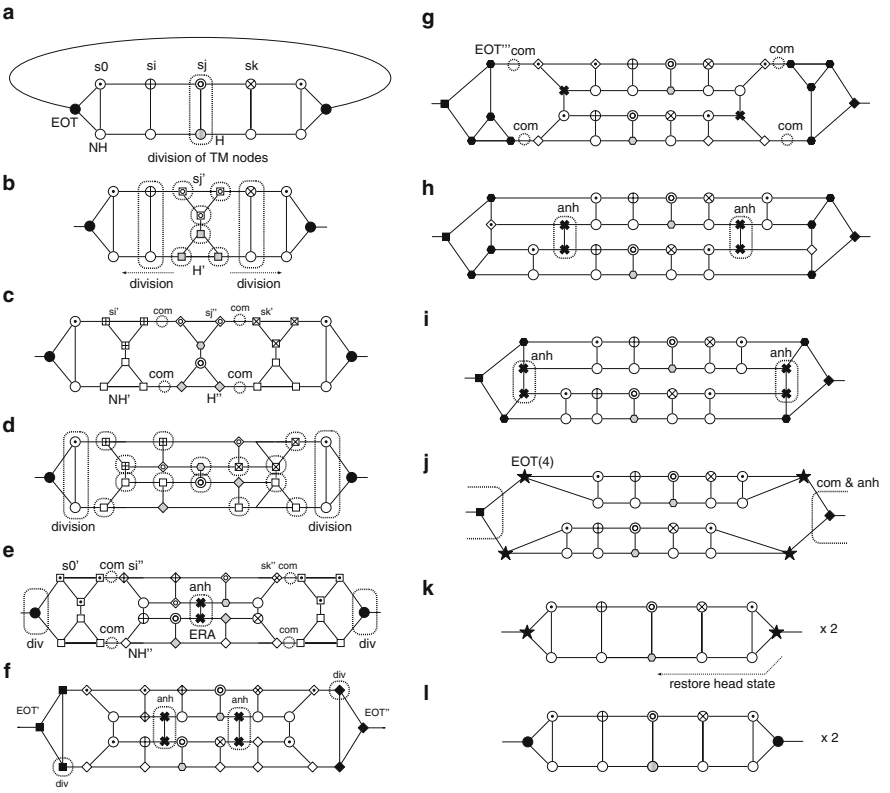

Fig. 14.6 Self-replicating steps of a Turing machine

is realized by several rules in graph-rewriting automata. Writing operation of a new symbol on the tape is realized simply by the state transition because the node is adjacent to the head node. The head moving operation requires two consecutive steps, as described below, because the node at the new location cannot refer to the symbol on the head: First, the head node becomes a state that represents the new internal state and the moving direction. Then, one adjacent node changes its state to the new internal state. Precise steps and rule construction are presented in [18].

The self-replicating process of the Turing machine can be expressed naturally within the framework of graph-rewriting automata (Fig. 14.6). Activation of the replication process begins at the location of the head, which causes a chain reaction of activation, and the activated region is controlled to be only part of the system. After the propagation of the activated region from the head position to both EOTs, the structure is duplicated and separated into two ladders. In the replication process design, we assume that the process begins when the head becomes a special internal state. The outline is as follows.

Step (1) The entire self-replication process is triggered when the head becomes a special state. First, the head node and the corresponding tape node are divided (Fig. 14.6a,14.6b).

Step (2) The nodes are also divided if a neighboring head node or tape node is divided (Fig. 14.6b,14.6c).

Step (3) By commuting the links, a new ladder structure is constructed (Fig. 14.6c,14.6d).

Step (4) By exchanging the information, tape and node information is placed in appropriate positions. Then, unnecessary nodes and links are annihilated to separate the two ladders (Fig. 14.6c,14.6f).

Step (5) Steps (2–4) above are repeated from the head position to both EOTs. Some rules are provided to cope with the special conditions around the EOTs (Fig. 14.6e,14.6j).

Step (6) The EOTs are commuted and then annihilated when the processes in both directions are finished. This produces two identical ladder structures (Fig. 14.6j,14.6k).

Step (7) The original state is restored (Fig. 14.6k,14.6l).

The whole replication process can be repeated. The detailed set of rules are given in [18]. Both the necessary number of states and rules depend on the type of Turing machine. For two symbol Turing machines, the process requires 20 states (including five in the initial state) and 257 rules. No restrictions apply to the tape length: the same rule set is applicable for any sequence of symbols.

It is also possible to realize self-replication of a universal Turing machine. For instance, we can embed Minsky's "small" universal Turing machine [11]. In this case, 30 states and 955 rules are necessary for the replication process. In addition, 23 states and 745 rules are required for computation as a universal Turing machine.

14.4 Rule Search by Evolutionary Computation

This section shows that evolutionary computation is applicable to automatic rule generation of graph-rewriting automata. We conducted an evolutionary search to identify self-replicating behavior as a preliminary trial. This suggests that generating various self-replications is possible in this framework.

14.4.1 Evolutionary Computation

Evolutionary computation is a search method inspired by the evolution of living things [5]. In this method, the goal is to determine a set of parameters with the highest fitness in a search space. A search is performed using a population of individuals: each represents one point in the search space. Updating the generations of population according to the fitness, usually by mutation and crossover, gradually improves the fitness of the population.

We seek a self-replicating system, i.e., a pair of a graph and a rule set. Finding them together simultaneously requires complicated coding. Therefore, we instead fix an initial graph as a four-node complete graph with different states (initial graph in Fig. 14.5) and search only for a rule set such that the development process of

the initial graph by the rule set includes self-replicating behavior. This development process stops when the number of nodes or steps exceeds some predetermined limit.

As described in Sect. 14.2, the rules of graph-rewriting automata are uniform. Therefore, it is easy to encode a rule set into an individual.

14.4.1.1 Representation

One individual corresponds to one rule set, which comprises node rules and link rules. Here we use a fixed number of rules: 80 node rules and 20 link rules. These are represented as

$$\text{n-rule } n_0\ n_1\ n_2\ n_3\ n_4, \qquad \text{and} \qquad \text{l-rule } n_0\ n_1,$$

respectively, where n-rule $\in$ {trans, div}, l-rule $\in$ {com, anh}, and $n_i \in [0..9]$.

14.4.1.2 Structural Development Diagram

In graph-rewriting automata, processes of development (and separation) of graphs begin from one connected graph. At some time, it might be divided into graphs by appropriate application of the annihilation rule. Then, this process is repeated for each. A diagram characterizes this process – a *structural development diagram* – in Fig. 14.7. In the figure, each dot represents one (connected) graph. Arrows indicate rewriting between these graphs. Each rectangle shows that graphs in it are changed, but they remain connected. We connect graphs with an upstream arrow when a new graph coincides with one already generated elsewhere in its ancestor. By examining this diagram, we can determine whether this process includes self-replication as follows.

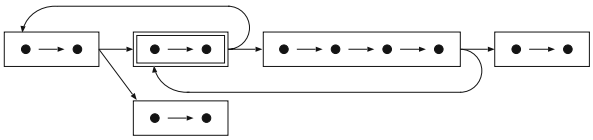

Fig. 14.7 Structural development diagram

Self-replicating systems have several types. A simple one was described in Sect. 14.2.4.3, in which a graph is separated into two identical children. In general, self-replication can be characterized by two (or more) upstream arrows over a rectangle in a structural development diagram. For example, Fig. 14.7 presents self-replication of graphs in the double-squared rectangle. In this process, some structures that are unrelated to self-replication are cut off.

14.4.1.3 Fitness Function

In using the evolutionary computation, defining the fitness function is important but difficult in many cases. As described above, we fix an initial graph and search

for a rule set that realizes self-replication. Based on this line, a fitness function is chosen so that the following three criteria are met: (1) existence of self-replicating systems according to the examination of structural development diagrams, as in Sect. 14.4.1.2; (2) the distance measure from a dead-end graph (where no more rule is applied) to the graphs of its ancestor; and (3) breadth of the search. Of them, (1) is the most important, but we must guide the search to obtain such systems. Details of the condition are found in [19].

14.4.2 Simulation Results

We conducted simulations. The execution is aborted if the number of nodes in one of the connected graphs becomes greater than 1,000 during this process.

First, 100 runs were conducted with 100 individuals and for 1,000 generations. Among them, 83 runs revealed some self-replicating systems. We conducted random searches for the same number (10,000,000 individuals) and found no self-replicating system. Taking after Lohn and Reggia [10], according to Fisher's Exact Test, if we obtain more than five trials, it is a statistically significant result. We infer that ours is significant.

Subsequently, we specifically examined direct self-replicating systems in which a structure generates multiple identical structures as its (direct) children. Among the 83 runs mentioned above, 82 runs generated 99 direct self-replicating systems.

We classify them by the number of nodes and the number of states used in the structure, as shown in Fig. 14.8. This figure shows that, as the number of states increases, it becomes difficult to find self-replicating graphs with a small number of nodes as long as one assumes this simple fitness function. In particular, no graph with more than four states was found.

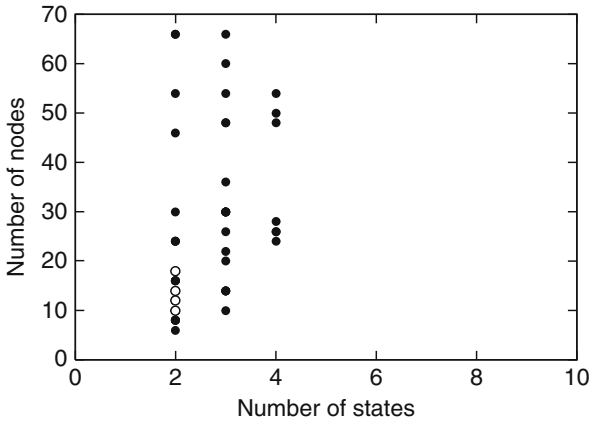

Fig. 14.8 Relationship between the number of states and nodes of the resultant self-replicating graphs. *White circles* denote the four most frequent graphs

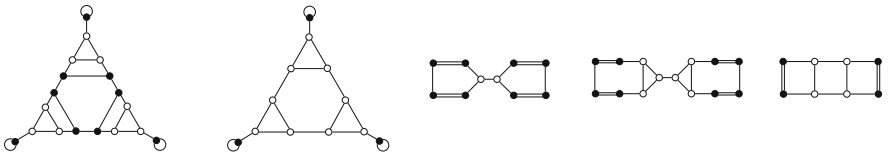

Fig. 14.9 Five typical self-replicating graphs obtained through evolutionary computation

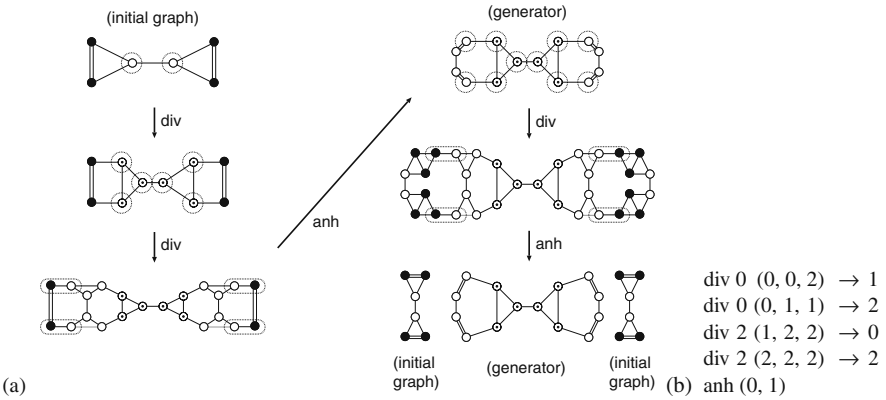

Fig. 14.10 An example of the obtained self-replicating system. (**a**) replication steps, (**b**) rule set

Many obtained graphs are symmetric and include multiple links or loops. No restrictions pertain to our fitness function. Therefore, easily replicated graphs, which have a self-similar nature, are generated. Figure 14.9 exhibits the five most frequently found self-replicating graphs. An example of a self-replication process with different features is displayed in Fig. 14.10. The upper right graph acts as a generator of two initial graphs; the initial graph grows to the generator itself.

14.5 Exhaustive Trial

In the previous section, we saw that various self-replicating systems are generated by graph-rewriting automata based on a particular search method. The space of the possible rule sets was explored only in part. This space is too huge to explore for all rule sets when the number of states is large. In this section, we instead limit the space of rule sets by restricting the states to be in $\{0, 1\}$. Then we investigate the behavior of graph developments for several simple initial graphs by application of all the rules. This is important for evaluating qualitatively how likely self-replication and other behaviors happen in this framework. Although this investigation remains in a preliminary stage, some results are described in this section.

14.5.1 Rule Representation

We conduct a simulation for all possible rules with two states to examine the resulting development processes. We denote each rule as an 11-digit number. The initial eight digits are for the node rules and remaining three are for the link rules. The value of each digit represents a rule for specific conditions determined according to the digit position. For node rules, values 0 and 1 mean that the rule is a state transition rule resulting in states 0 and 1, respectively; values 2 and 3 mean that the rule is a division rule and the resulting states are, respectively, 0 and 1. For link rules, 0, 1, and 2 represent that the corresponding rule is none, com, and anh. This is summarized in Fig. 14.11. Consequently, the total number of possible rules for two states are $4^8 \times 3^3 = 1,769,472$. For instance "01223110201" represents a rule set "trans 0 (0, 0, 0) → 0, tans 0 (0, 0, 1) → 1, div 0 (0, 1, 1) → 0, div 0 (1, 1, 1) → 0, div 1 (0, 0, 0) → 1, div 1 (0, 0, 1) → 1, trans 1 (0, 1, 1)→ 1, trans 1(1, 1, 1) → 0, anh (0, 0), com (1, 1)". Among 27 possible cases for link rules, 17 are the same because of the lateral inhibition.

Corresponding rule condition to each digit: 8 digits for node rules and 3 digits for link rules

0(0,0,0)	0(0,0,1)	0(0,1,1)	0(1,1,1)	1(0,0,0)	1(0,0,1)	1(0,1,1)	1(1,1,1)	0,0	0,1	1,1

Value of digits for node rules

value	rule
0	trans ( ) → 0
1	trans ( ) → 1
2	div ( ) → 0
3	div ( ) → 1

Value of digits for link rules

value	rule
0	none
1	com
2	anh

Fig. 14.11 Rule representation

14.5.2 Results

We chose five initial graphs in Fig. 14.12, and conducted a simulation for 80 steps, until the 1,000 node limit was reached. The results are roughly classifiable as shown in Fig. 14.13, which shows the following characteristic: S0 is the simplest initial structure. That result can be analyzed: 9/16 cases grow to the node limit, 3/8 cases halt, and 1/16 cases reach the limit cycle. Other cases are not so simple. Cases of about 90% grow until the node limit or halt when no rule is applicable. Some examples are presented respectively in Figs. 14.14 and 14.15. Some cases of limit cycles (about 3–10%), and cases in which the graphs are separated (about 0.2–2% except S0) exist.

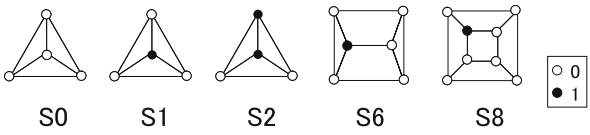

Fig. 14.12 Five initial graphs for the exhaustive trial

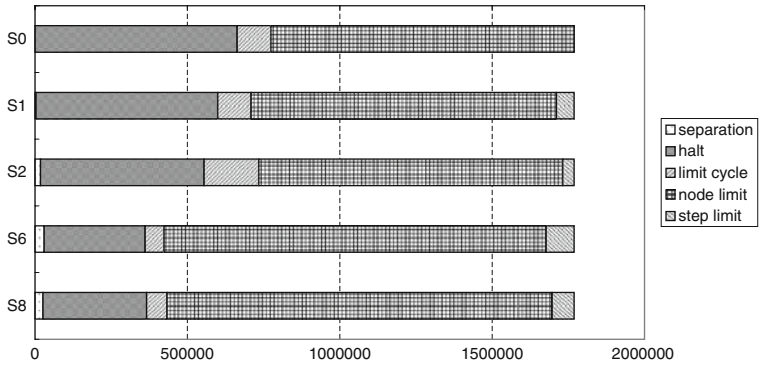

Fig. 14.13 Rough classification of graph development with two states

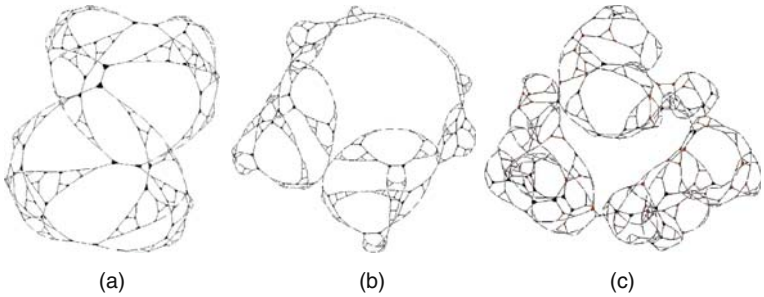

Fig. 14.14 Examples of graph evolution that reach the node limit

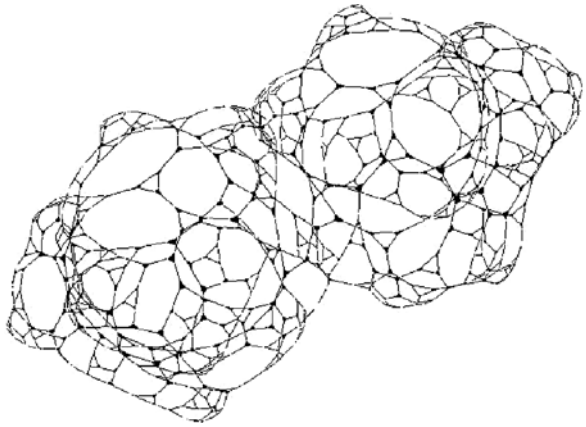

Fig. 14.15 An example of graph evolution halted at 612 nodes. Rule is 00230302 010 S2

Cases of separation are further investigated. The results are portrayed in Fig. 14.16. Again, about 70% cases grow up to the node limit. In some cases (about 3–15%) the processes include self-replication, many of which have nearly linear structures. Figure 14.17 presents typical examples of such self-replication processes.

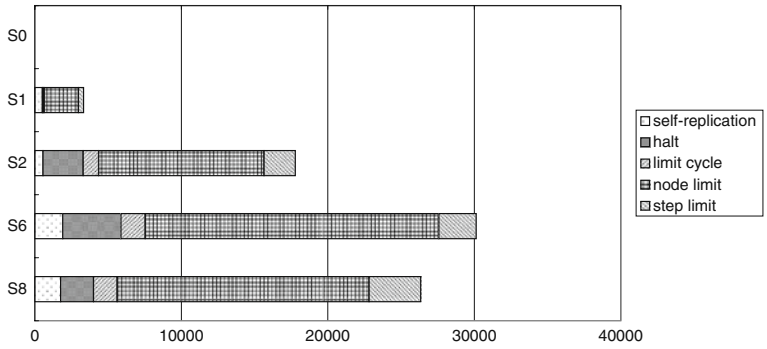

Fig. 14.16 Classification of behavior for separated cases

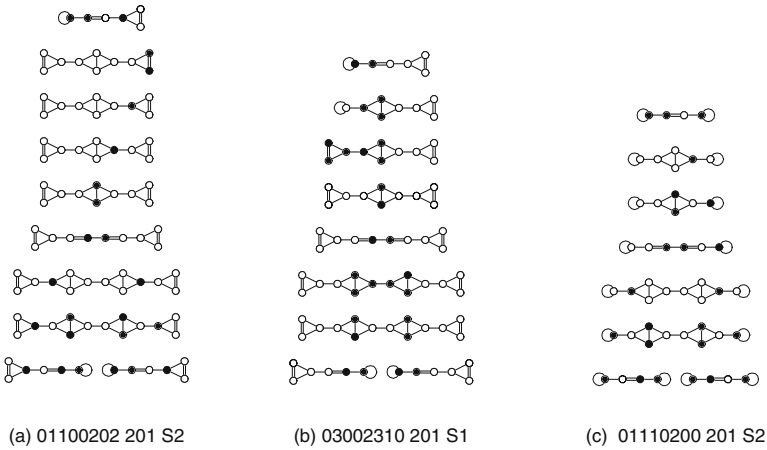

Fig. 14.17 Self-replication steps with two states, and corresponding rule sets

These graphs were generated in the course of graph evolution when large graphs were separated into many graphs.

Because the rules with two states described above do not break (some of the) symmetry of the initial graphs, many resultant graphs are symmetric when the graph is connected. However, each component of this symmetry can contain rich structures. Especially, as described above, when a graph is divided into sub-graphs, the components might be capable of self-replication.

In cellular automata, classification of behavior into four classes was proposed by Wolfram [24]. Among them, class 4 involves a mixture of order and randomness exhibiting complex behavior. Although we expect that the class 4 behavior will be found also in graph-rewriting automata, it is not yet found. One reason would be that simulation time steps are too small. Class 4 behavior can be characterized sometimes by interaction among locally stable structures. To examine such interaction, observation for a longer time is appropriate, and further analysis is required.

14.6 Conclusions

We proposed a framework called graph-rewriting automata for generating and modeling complex adaptive networks. It has the following advantages:

- It can express processes that include dynamic changes in the number of the elements and topology.
- It can deal naturally with processes in the closed space.

For rule description, it has the following features:

- Graph-rewriting is restricted as local.
- The rules are described uniformly.

Graph-rewriting automata's strong power of expression will provide a new tool to describe various complex processes. It is especially suitable to describe a development process in a closed space, where the process itself determines its boundary conditions. Thereby, the global structure and local states are coupled effectively. Self-replication is a typical example of such processes.

We have demonstrated that this framework can generate network evolution of various types by considering hand-coded rule sets, mechanically searched rule sets, and exhaustive trials. Using hand-coded rule sets, we can easily embed various logical structures. On the other hand, the space of the rule sets is too huge to explore. An evolutionary computation method was applied to generate rule sets for graph-rewriting automata automatically. In particular, self-replication has been addressed and many self-replicating systems (graphs and corresponding rule sets) were obtained. Many obtained graphs are symmetric and differ from hand-coded graphs. The replication processes differ from those of cellular automata in the sense that they use node division effectively, thereby simplifying the replication processes. We did not need to guide the search using a complicated fitness function; a simple one generated various self-replicating systems, suggesting the expressiveness of graph-rewriting automata for self-replication processes. In addition, an exhaustive trial was performed for simple cases with two states. A variety of development processes were found even with the limited states and simple analysis.

Our system has two restrictions for simplification as follows, which were introduced to make the structure and development process simple.

One restriction is the structural restriction. In this paper, we considered planar graphs with three link nodes. Planar restriction is relaxed by permitting non-planar initial states or by introducing new rewriting rules. The structure can be extended in many ways depending on the objects to be modeled in the graph-rewriting automata. For example, an additional rewriting rule for non-planar graphs was introduced in [20] to model von Neumann style self-replication.

The other restriction is in the updating process. Lateral inhibition of link rules and separate updating steps for node and link rules were assumed. These come mainly from the requirement to make the update process deterministic. We can exclude such exceptions by, e.g., asynchronous application of rules instead of synchronous

application to the whole system if we permit the stochastic development. Such extension is examined in [21].

The following are subjects for future work. First, more precise analysis of graph development is necessary to evaluate the properties of graphs quantitatively. For this purpose, we must develop a more elaborate visualization method because it is not easy to qualify the properties of an interesting development. Although our simulator is effective when the graph size is less than a few hundred, it is difficult to grasp the time series of overall graph development when the graph is much larger. Furthermore, there is room for improvement on our framework in two ways: refinement by further simplification, and enhancement by introducing, e.g., physical properties such as the distance between nodes or the physical environment. Finally, we are interested in examination of a subset (or a variant) of this framework that permits a reversible development processes.

Inheriting accumulated knowledge in cellular automata and complex networks, graph-rewriting automata will open a new dimension of study by introducing topological freedom to system description. It will cast new light on various subjects in science and technology, such as complex morphogenesis of living systems, self-assembling molecular systems, innovative nanoscale production methods, and fundamental physics.

References

1. Church, A.: An unsolvable problem of elementary number theory. American Journal of Mathematics **58**(2), 345–363 (1936)
2. Giavitto, J.-L., Spicher, A.: Topological rewriting and the geometrization of programming. Physica D **237**(9), 1302–1314 (2008)
3. Gross, T., Blasius, B.: Adaptive coevolutionary networks: a review. Journal of the Royal Society Interface **5**(20), 259–271 (2008)
4. Gruau, F., Eisenbeis, C., Maignan, L.: The foundation of self-developing blob machines for spacial computing. Physica D **237**(9), 1282–1301 (2008)
5. Holland, J. H.: Adaptation in Natural and Artificial Systems. University of Michigan Press (1975)
6. Ilachinski, A.: Cellular Automata, A Discrete Universe. World Scientific (2001)
7. Ilachinski, A., Halpern, P.: Structurally dynamic cellular automata. Complex Systems **1**(3), 503–527 (1987)
8. Kataoka, N.: Modified graph automata. In: Workshop Proc. of ALIFE IX, pp. 137–141 (2006)
9. Lindenmayer, A.: Mathematical models for cellular interaction in development, Parts I and II. Journal of Theoretical Biology **18**, 280–315 (1968)
10. Lohn, J. D., Reggia, J. A.: Automatic discovery of self-replicating structures in cellular automata. IEEE Transactions on Evolutionary Computation **1**(3), 165–178 (1997)
11. Minsky, M.: Computation: Finite and Infinite Machines. Prentice Hall, Englewood Cliffs, NJ (1967)
12. Prusinkiewicz, P., Lindenmayer, A.: The Algorithmic Beauty of Plants. Springer-Verlag, New York (1990)
13. Rozenberg, R. (ed.): Handbook of Graph Grammars and Computing by Graph Transformation, Vol. 1: Foundations. World Scientific (1997)
14. Salzberg, C., Sayama, H., Ikegami, T.: A tangled hierarchy of graph-constructing graphs. In: Proc. Ninth International Conference on the Simulation and Synthesis of Living Systems (Artificial Life IX), pp. 495–500, MIT Press, Cambridge, MA (2004)

15. Sayama, H.: Generative network automata: A generalized framework for modeling complex dynamical systems with autonomously varying topologies. In: Proc. 2007 IEEE Symposium on Artificial Life, pp. 214–221, IEEE Press, Los Alamitos, CA (2007)
16. Sipper, M.: Fifty years of research on self-replication: An overview. Artificial Life **4**(3) 237–257 (1998)
17. Smith, D. M. D., Onnela, J.-P., Lee, C. F., Fricker, M., Johnson, N. F.: Network automata and the functional dynamic network framework. arXive:physics/0701307v2 (2007)
18. Tomita, K., Kurokawa, H., Murata, S.: Graph automata: natural expression of self-reproduction. Physica D **171**(4), 197–210 (2002)
19. Tomita, K., Kurokawa, H., Murata, S.: Automatic generation of self-replicating patterns in graph automata. International Journal of Bifurcation and Chaos **16**(4), 1011–1018 (2006)
20. Tomita, K., Murata, S., Kurokawa, H.: Self-description for construction and computation on graph-rewriting automata. Artificial Life **13**, 383–396 (2007)
21. Tomita, K., Murata, S., Kurokawa, H.: Asynchronous graph-rewriting automata and simulation of synchronous execution. Lecture Notes in Computer Science **4648**, 865–876 (2007)
22. Turing, A. M.: On computable numbers, with an application to the Entscheidungsproblem. Proc. London Mathematical Society, Series 2, **42**(2) 230–265 (1936)
23. von Neumann, J.: Theory of Self-Reproducing Automata. University of Illinois Press, Urbana (1966)
24. Wolfram, S.: Cellular Automata and Complexity. Addison-Wesley, Boston, MA (1994)
25. Wolfram, S.: A New Kind of Science. Wolfram Media, Champaign, IL (2002)

Chapter 15
Generative Network Automata: A Generalized Framework for Modeling Adaptive Network Dynamics Using Graph Rewritings

Hiroki Sayama and Craig Laramee

Abstract A variety of modeling frameworks have been proposed and utilized in complex systems studies, including dynamical systems models that describe state transitions on a system of fixed topology, and self-organizing network models that describe topological transformations of a network with little attention paid to dynamical state changes. Earlier network models typically assumed that topological transformations are caused by exogenous factors, such as preferential attachment of new nodes and stochastic or targeted removal of existing nodes. However, many real-world complex systems exhibit both state transition and topology transformation simultaneously, and they evolve largely autonomously based on the system's own states and topologies. Here we show that, by using the concept of graph rewriting, both state transitions and autonomous topology transformations of complex systems can be seamlessly integrated and represented in a unified computational framework. We call this novel modeling framework "Generative Network Automata (GNA)". In this chapter, we introduce basic concepts of GNA, its working definition, its generality to represent other dynamical systems models, and some of our latest results of extensive computational experiments that exhaustively swept over possible rewriting rules of simple binary-state GNA. The results revealed several distinct types of the GNA dynamics.

15.1 Introduction

A variety of modeling frameworks have been proposed and utilized for research on the dynamics of complex systems [1–3]. A major class of modeling frameworks is that of dynamical systems models, including ordinary or partial differential equations and iterative maps [4], artificial neural networks [5, 6], random Boolean networks [7–9], and cellular automata [10, 11]. While they are capable of producing strikingly complex and even biological-like behaviors [12–16], these tools generally

H. Sayama (✉)
Collective Dynamics of Complex Systems Research Group, Department of Bioengineering, Binghamton University, State University of New York, Binghamton, NY 13902-6000, USA;
New England Complex Systems Institute, Cambridge, MA 02138, USA,
e-mail: sayama@binghamton.edu, sayama@necsi.edu

T. Gross, H. Sayama (eds.), *Adaptive Networks,* Understanding Complex Systems,
DOI 10.1007/978-3-642-01284-6_15,

assume a network made of a fixed number of components organized in a fixed topology. Their dynamics are considered as trajectories of system states in a confined phase space with time-invariant dimensions.

The recent surge of network theory in statistical physics has demonstrated yet another graph-theoretic approach to complex systems modeling [17–19]. It addresses the self-organization of network structure via local topological transformations such as random or preferential addition, modification and removal of components and their interactions (i.e., nodes and links). Among the most actively investigated issues in this field is how statistical properties of the entire network topology will be affected by additions (growth or augmentation) and removals (failures or attacks) of nodes and links, and in particular, how networks can be more robust against the latter [20–24]. Those additions and removals are typically assumed as perturbations coming from external sources, not incorporated into the dynamics of the network itself. They are also limited in that not much attention has been paid to dynamical state changes on the network. Researchers recently started investigating dynamical state changes on complex networks [25–30]. They are still largely focusing on fixed network topologies or topologies varied by exogenous perturbations.

When looking into real-world complex networks, however, one can find many instances of networks whose states and topologies "coevolve", i.e., they keep changing over the same time scales due to the system's own dynamics (Table 15.1). In these networks, state transitions of each component and topological transformations of networks are deeply coupled with each other. Understanding and describing the coevolution of states and topologies of networks is now recognized as one of the most important problems to address [21, 31]. Several theoretical models of coevo-

Table 15.1 Real-world examples of complex networks whose states and topologies change over the same time scales due to the network's own dynamics

Network	Nodes	Links	Example of node states	Example of node addition or removal	Example of topological changes
Organism	Cells	Cell adhesions, intercellular communications	Gene/protein activities	Cell division, cell death	Cell migration
Ecological community	Species	Ecological relationships (predation, symbiosis, etc.)	Population, intraspecific diversities	Speciation, invasion, extinction	Changes in ecological relationships via adaptation
Epidemiological network	Individuals	Physical contacts	Pathologic states	Death, quarantine	Reduction of physical contacts
Social network	Individuals	Social relationships, conversations, collaborations	Sociocultural states, political opinions, wealth	Entry to or withdrawal from community	Establishment or renouncement of relationships

lutionary networks have been proposed and studied most recently [32–36], yet each of these studies used different model formulations for different phenomena, with limited implications given for how these coevolutionary network models could be linked to other existing complex systems models.

Here we aim to address the above-mentioned lack of linkages between coevolutionary network models and other existing complex systems models by developing a more comprehensive formulation. Specifically, we show that, by using the concept of graph rewriting, both state transitions and autonomous topology transformations of complex systems can be seamlessly integrated and represented in a unified computational framework. We call this novel modeling framework "*Generative Network Automata (GNA)*" [37]. The name indicates the integration of knowledge accumulated in dynamical systems theory, network theory, and graph grammar theory.

In the following sections, we will introduce basic concept of graph rewriting, a working definition of GNA, its generality to represent other dynamical systems models, and some of our latest results of extensive computational experiments that exhaustively swept over possible rewriting rules of simple binary-state GNA. The results revealed several distinct types of the GNA dynamics.

15.2 About Graph Rewriting

The key characteristic of GNA is that it should have mechanisms for transformations of local network topologies as well as transitions of local states. Topological transformations may be modeled as a rewriting process of local network configurations. We will therefore adopt methods and techniques developed in graph grammar theory [38] to construct general formulations of GNA.

Graph grammars, studied since late 1960s in theoretical computer science [39–42], are an extension of formal generative grammars in computational linguistics to discuss similar rule-based generative processes of graphs, or networks. They recursively define a set of "valid" graph topologies that can be generated through repetitive applications of a given set of node and/or link replacement rules. A computational implementation of such processes is called a graph rewriting system, often used to simulate particular generative processes of network topology. Here the word "generative" means that the replacements are triggered by local topological features of the network itself, and not by external sources of perturbation as typically assumed in modern network theory.

A classic, and probably most widely known, example of graph rewriting systems is the Lindenmayer system, or L-system [43]. It is a simple rewriting system that can produce self-similar recursive structures in a sequential string (in this sense, the L-system remains within the range of classic formal grammars). What makes this system outstanding is that it comes with an interpretation that converts a resultant string into a tree-like topological structure, which may appear just like a natural tree if parameters are appropriately chosen. This example shows the capability of graph rewriting systems to describe the emergence of natural complex structures using a set of small local rules.

Although their relevance to biology was initially recognized [39, 44], applications of graph grammars have so far remained within computer science, such as pattern recognition, compiler design, and data type and process specification [38, 40–42], and their use has been not so common even within computer science due to unintuitive, complicated formulation and lack of software tools for modeling [45]. Moreover, most applications were primarily focused on context-free rewriting rules, and they rarely considered dynamical state transitions on networks. Recently, context-dependent graph grammars have been applied to describe reaction rules in artificial life/artificial chemistry, including models of self-replication [46–48], self-assembly [49], morphogenesis [50, 51] and dynamic state changes [51] of artifacts. However, none of them integrated graph grammars into complex systems modeling in a flexible, generalizable way so as to be readily applicable to networks studied in other domains.

To the best of our knowledge, our GNA framework is among the first to systematically integrate graph rewritings in the representation and computation of the dynamics of complex networks that involve both state transition and autonomous topological transformation. Our long-term goal is to develop a comprehensive theory of GNA and a set of analytical/computational tools that can be broadly applied to the modeling of various complex systems.

15.3 Definition of GNA

A working definition of GNA is a network made of dynamical nodes and directed links between them. Undirected links can also be represented by a pair of directed links symmetrically placed between nodes. Each node takes one of the (finitely or infinitely many) possible states defined by a node state set S. The links describe referential relationships between the nodes, specifying how the nodes affect each other in state transition and topological transformation. Each link may also take one of the possible states in a link state set S'. A configuration of GNA at a specific time t is a combination of states and topologies of the network, which is formally given by the following:

- V_t: A finite set of nodes of the network at time t. While usually assumed as time-invariant in conventional dynamical systems theory, this set can dynamically change in the GNA framework due to additions and removals of nodes.
- $C_t : V_t \to S$: A map from the node set to the node state set S. This describes the global state assignment on the network at time t. If local states are scalar numbers, this can be represented as a simple vector with its size potentially varying over time.
- $L_t : V_t \to \{V_t \times S'\}^*$: A map from the node set to a list of destinations of outgoing links and the states of these links, where S' is a link state set. This represents the global topology of the network at time t, which is also potentially varying over time.

States and topologies of GNA are updated through repetitive graph rewriting events, each of which consists of the following three steps:

1. Extraction of part of the GNA (subGNA) that will be subject to change.
2. Production of a new subGNA that will replace the subGNA selected above.
3. Embedding of the new subGNA into the rest of the whole GNA.

The temporal dynamics of GNA can therefore be formally defined by the following triplet $\langle E, R, I \rangle$:

- E: An extraction mechanism that determines which part of the GNA is selected for the updating. It is defined as a function that takes the whole GNA configuration and returns a specific subGNA in it to be replaced. It may be deterministic or stochastic.
- R: A replacement mechanism that produces a new subGNA from the subGNA selected by E and also specifies the correspondence of nodes between the old and new subGNAs. It is defined as a function that takes a subGNA configuration and returns a pair of a new subGNA configuration and a mapping between nodes in the old subGNA and nodes in the new subGNA. It may be deterministic or stochastic.
- I: An initial configuration of GNA.

There are a couple of other commonly used procedures needed to simulate GNA dynamics, such as the removal of the selected subGNA from the whole GNA and the re-connection of "bridge" links (i.e., links that were between the old subGNA and the rest of the GNA) when embedding the new subGNA. Because the workings of these procedures are fairly obvious, we omit detailed explanations for them. The above E, R, I are sufficient to uniquely define specific GNA models. The entire picture of a rewriting event is illustrated in Fig. 15.1, which visually shows how these mechanisms work together.

This rewriting process, in general, may not be applied synchronously to all nodes or subGNAs in a network, because simultaneous modifications of local network topologies at more than one places may cause conflicting results that are inconsistent with each other. This limitation will not apply though when there is no possibility of topological conflicts, e.g., when the rewriting rules are all context-free, or when GNA is used to simulate conventional dynamical networks that involve no topological changes.

We note that it is a unique feature of GNA that the mechanism of subgraph extraction is explicitly described in the formalism as an algorithm E, not implicitly assumed outside the grammatical rules like what other graph rewriting systems typically adopt (e.g. [51]). Such algorithmic specification allows more flexibility in representing diverse network evolution and less computational complexity in implementing their simulations, significantly broadening the areas of application. For example, the preferential attachment mechanism widely used in modern network theory to construct scale-free networks is hard to describe with pure graph grammars but can be easily written in algorithmic form in GNA, as demonstrated in the next section.

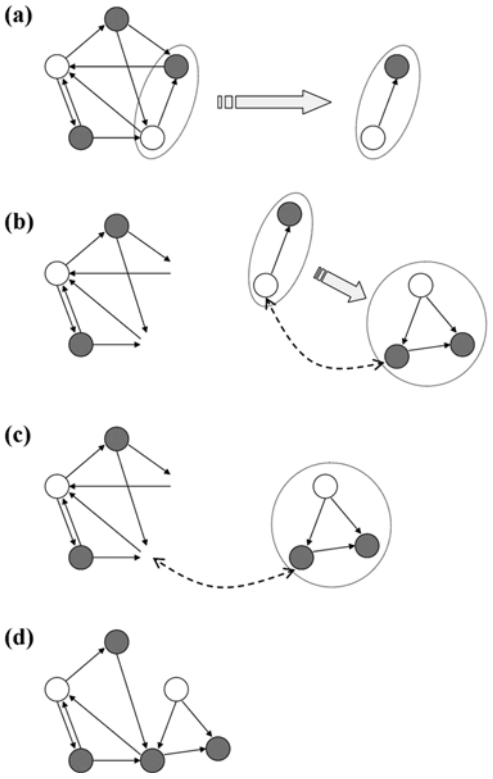

Fig. 15.1 GNA rewriting process. (**a**) The extraction mechanism E selects part of the GNA. (**b**) The replacement mechanism R produces a new subGNA as a replacement of the old subGNA and also specifies the correspondence of nodes between old and new subGNAs (*dashed line*). This process may involve both state transition of nodes and transformation of local topologies. The "bridge" links that used to exist between the old subGNA and the rest of the GNA remain unconnected and open. (**c**) The new subGNA produced by R is embedded into the rest of the GNA according to the node correspondence also specified by R. In this particular example, the *top gray node* in the old subGNA has no corresponding node in the new subGNA, so the bridge links that were connected to that node will be removed. (**d**) The updated configuration after this rewriting event

While the definition given above is one of the simplest possible formulations of GNA, it already has considerable complexity compared to conventional dynamical systems models. The possibility of temporal changes of V_t and L_t particularly makes it difficult to investigate its dynamical properties analytically. However, the updating process of GNA is algorithmically described and hence their dynamics can be experimented through computer simulation relatively easily. We have developed a package in Wolfram Research Mathematica for small-scale simulation and visualization of GNA with node states.[1] The results presented in this chapter were obtained using this package.

[1] The Mathematica package is still under active development but may be available upon request.

15.4 Generality of GNA

The GNA framework is highly general and flexible so that many existing dynamical network models can be represented and simulated within this framework.

For example, if R always conserves local network topologies and modifies states of nodes only, then the resulting GNA is a conventional dynamical network model, including cellular automata, artificial neural networks, and random Boolean networks (Fig. 15.2 a, b). A straightforward application of GNA typically comes with asynchronous updating schemes, as introduced in the previous section. Since asynchronous automata networks can emulate any synchronous automata networks [52], the GNA framework covers the whole class of dynamics that can be produced by conventional dynamical network models. Moreover, as mentioned earlier, synchronous updating schemes could also be implemented in GNA for this particular class of models because they involve no topological transformation.

On the other hand, many network growth models developed in modern network theory can also be represented as GNA if appropriate assumptions are implemented in the subGNA extraction mechanism E and if the replacement mechanism R causes no change in local states of nodes (Fig. 15.2 c).

15.5 Computational Exploration of Possible Dynamics of Simple Binary-State GNA

In this section we report our latest results of extensive computational experiments that exhaustively swept over possible rewriting rules of simple binary-state GNA. The results shown here were obtained with much less restricted rule sets than those assumed in our previous work [37].

15.5.1 Assumptions

There are infinitely many possible mechanisms for E and R because there are no theoretical upper bounds in terms of the size of the old subGNA selected by E (it could be infinitely large as the GNA grows) and the new subGNA produced by R (it could be arbitrarily large by the design of R). Making reasonable assumptions to restrict the possibility of mechanisms for E and R is critical to facilitate systematic study on the dynamics of GNA. Here we make the following assumptions (Fig. 15.3):

1. Node states are binary (0 or 1).
2. No link state is considered (i.e., links homogeneously take only one state and it will never change).
3. Links are undirected (i.e., every connection between nodes is represented by a pair of symmetrically placed directed links).

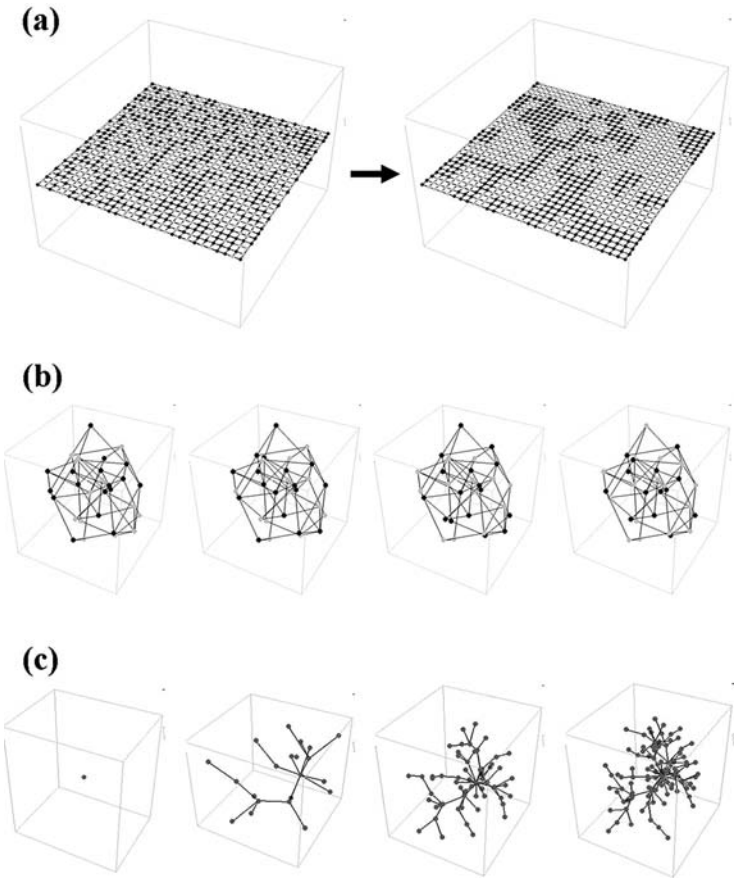

Fig. 15.2 Various dynamical network models simulated using GNA. These examples were represented in the same format of $\langle E, R, I \rangle$ (see text) and simulated using the same simulator package implemented in Mathematica. (**a**) Simulation of asynchronous 2-D binary cellular automata with von Neumann neighborhoods and local majority rules. Space size: 100×100. (**b**) Simulation of an asynchronous random Boolean network with $N = 30$ and $K = 2$. Time flows from left to right. Nodes of random Boolean networks are non-homogeneous, i.e., they obey different state-transition rules. Here each node's own state-transition rule is embedded as part of its state, and the replacement mechanism R refers to that information when calculating the next state of a node. (**c**) Simulation of a network growth model with the Barabási-Albert preferential attachment scheme. Time flows from left to right. Each new node is attached to the network with one link. The extraction mechanism E is implemented so that it determines the place of attachment preferentially based on the node degrees, which causes the formation of a scale-free network in the long run

4. The extraction mechanism E always selects a subGNA by
   a randomly picking one node u from the entire GNA (Fig. 15.3a),
   b taking all the destination nodes of its outgoing links $L_t(u)$ (Fig. 15.3b), and
   c producing a subGNA "induced" by these nodes $\{u\} \cup L_t(u)$, i.e., a subGNA that includes all these nodes as well as all the links present between them (Fig. 15.3c).

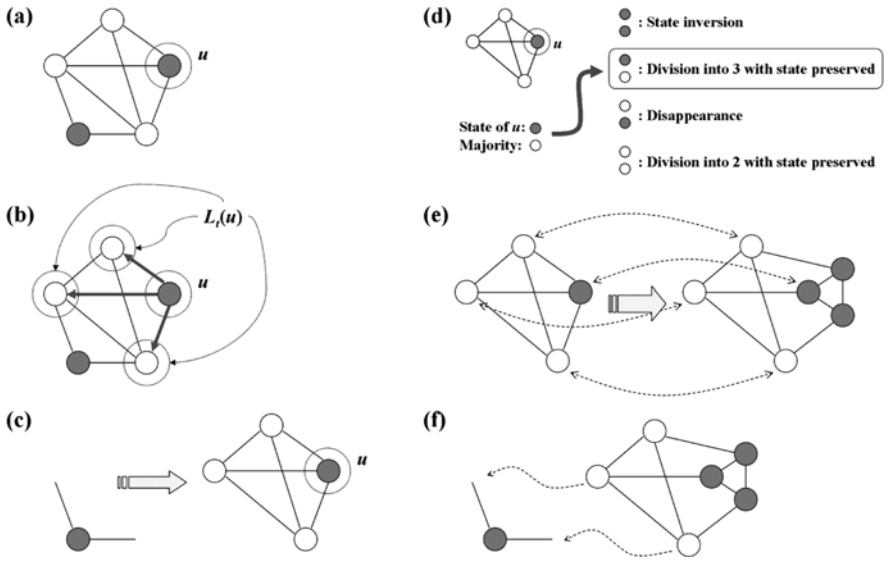

Fig. 15.3 Simplified GNA rewriting process used for the exhaustive sweep experiments. The extraction mechanism E (**a**) randomly picks one node u, (**b**) takes all the destination nodes of its outgoing links $L_t(u)$, and (**c**) produces a subGNA induced by those nodes $\{u\} \cup L_t(u)$. The replacement mechanism R (**d**) refers to the state of the central node u in the selected subGNA and the local majority state within it to determine what happens to the local configuration, (**e**) produces a new subGNA as well as the correspondence of nodes between the old and new subGNAs based on the choice made in (**d**), and then (**f**) embeds the new subGNA into the rest of the GNA

5. The replacement mechanism R only refers to the state of the central node u and the local majority state within the induced subGNA. If there are equal numbers of 0's and 1's within the subGNA, one of the two states is randomly chosen. This two-bit information will be used to determine what will happen to the local configuration (Fig. 15.3d). The following ten possible rewriting outcomes are made available (which are extended from [37]):

   (0) The central node u disappears.
   (1) Everything remains in the same condition.
   (2) The state of the central node u is inverted.
   (3) The central node u divides into two with the state preserved in both nodes.
   (4) The central node u divides into two with the state inverted in both nodes.
   (5) The central node u divides into two with the state inverted in one node.
   (6) The central node u divides into three with the state preserved in all three nodes.
   (7) The central node u divides into three with the state inverted in all of three nodes.
   (8) The central node u divides into three with the state inverted in two of three nodes.
   (9) The central node u divides into three with the state inverted in one of three nodes.

In cases where node division occurs, the links that were connected to the central node u is distributed as evenly as possible to its daughter nodes (Fig. 15.3e).

6. The initial condition I consists of a single node with state 0.

Note that the above model assumptions will always generate planar graphs in which the node degrees are bounded up to three when initiated with a single node. Therefore all the results shown in this chapter are topologically planar.

15.5.2 Methods

We carried out an exhaustive sweep of all the possible rewriting rules that satisfy the assumptions discussed above. Since the extraction mechanism E is uniquely defined, it is only the replacement mechanism R that can be varied. Here R is defined as a function that maps each of the four possible two-bit inputs to one of the ten possible actions. Therefore the number of all the possible R's is $10^{2^2} = 10{,}000$. To indicate a specific R, we will use its "rule number" $rn(R)$ that is defined by

$$rn(R) = a_{11} \times 10^3 + a_{10} \times 10^2 + a_{01} \times 10^1 + a_{00} \times 10^0, \qquad (15.1)$$

where a_{ij} is a numerical representation (numbers associated with each of the ten possible actions shown above) of the choice that R will make when the state of the central node u is i and the local majority state is j.

It should be noted that there are two different ways of counting time steps in asynchronous simulations. One is simply to count one rewriting event as one time step, which we call *computational time*. The other is to measure the progress of virtual time in a simulated world between discrete events by considering one rewriting event as taking $1/N_t$ of the unit of time, where N_t is the number of nodes at time t. This is based on the assumption that every node is updated once on average per unit of time, which is a reasonable and useful assumption especially when one wants to compare results of asynchronous simulations with those of synchronous ones. We call the latter notion of time *simulated time*. All the t's in this chapter represent simulated time.

We simulated the GNA dynamics for rn ranging from 0 to 9,999. For each rn five independent simulation runs were conducted and the average of their results were used. Each run continued until 500 rewriting events were simulated, or N_t exceeded 1,000, or N_t became 0, whichever was sooner.

During each run, we recorded time series of N_t by sampling its value in every half unit of simulated time. We then calculated its growth characteristics, estimated order of polynomial growth k and estimated rate of exponential growth r, by conducting nonlinear fitting of a hypothetical growth model to the time series data (explained later). In addition, after each simulation run, we measured the following quantities of the final GNA configuration:

- Number of nodes
- Number of links

- Average node degree
- Number of connected components
- Size of the largest connected component
- Average node state

If all the nodes disappear during the simulation run, the average node degree and the average node state are indeterminate.

15.5.3 Results

We first studied the growth characteristics of GNA and their differences between different rules. Figure 15.4 presents sample growth curves superposed in a single plot, showing temporal changes in number of nodes over simulated time. Several distinct types of growth patterns are already visible in this plot. Curves that go nearly flat along the t axis indicate that the GNA for these cases did not grow at all. Many other rules showed rapid exponential growth processes (dense bundle of sharply rising curves on the left). Between these two, there are relatively fewer intermediate cases that exhibit either slow, fluctuating growth, or even linear growth, which are qualitatively different from other growth curves.

We extracted the growth characteristics of each rule from its time series data by fitting to them a hypothetical growth model $N_t \sim (t+1)^k e^{rt}$ using the least squares method, where k and r are the estimated order of polynomial growth and the estimated rate of exponential growth, respectively. For each rule, these values were calculated with five independent simulation runs and then their averages were used for the analysis. We excluded rules in the form of "***0" or "0**2" (where "*" can be any single-digit number) that caused immediate node extinction and hence failure of nonlinear fitting. This filtering excluded 1,100 rules, leaving a total of 8,900 (out of 10,000) rules that were used in the following plots.

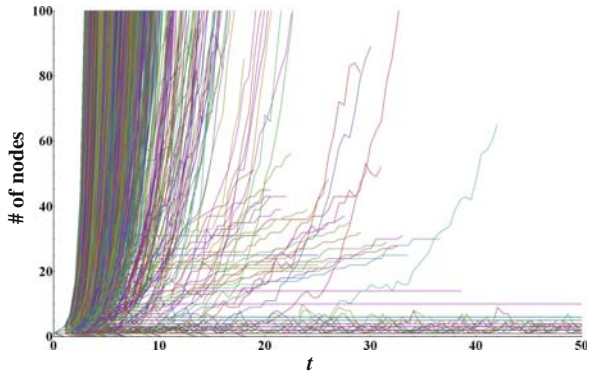

Fig. 15.4 Growth curves of randomly selected 10% of the 50,000 independent simulation runs (5 runs × 10,000 rules)

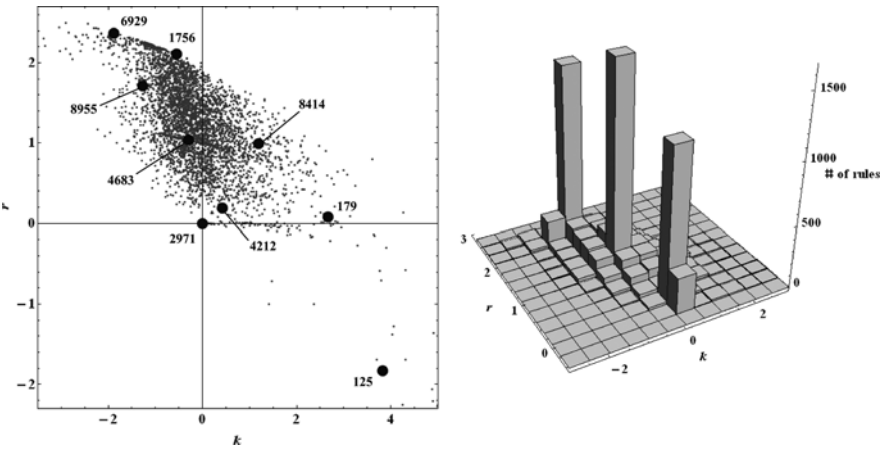

Fig. 15.5 *Left*: Distribution of growth characteristics, estimated order of polynomial growth k and estimated rate of exponential growth r, of the 8,900 GNA rules (excluding rules in the form of "***0" or "0**2" that caused immediate node extinction and hence failure of nonlinear fitting). Sample cases shown in Fig. 15.6 are indicated with *large black dots*, accompanied with the corresponding rule numbers. *Right*: 3-D histogram of growth characteristics in the parameter area $-3 < k < 3$ and $0 < r < 3$. It is clearly seen that there are three distinct peaks, which correspond to non-growers, exponential growers by binary node divisions, and exponential growers by tertiary node divisions

Figure 15.5 (left) shows the distribution of the growth characteristics (k and r) of the 8,900 GNA rules. The distribution is continuously spread mostly in the first and second quadrants, in which there are a couple of visually identifiable dense clusters. The slightly slanted linear cluster near the top of the second quadrant corresponds to rules that make GNA grow exponentially through continuous tertiary node divisions. The other slanted linear cluster located around $(k, r) = (0, 1)$ corresponds to rules that make GNA grow exponentially through continuous binary divisions. Between and around these two clusters there are many other rules that show intermediate exponential growth rates. A relatively thin linear cluster at $k > 0$ and $r \sim 0$ is considered of non-growing or polynomially growing GNA rules. Most of the GNA rules belong to one of these three clusters, as seen in the histogram on the right. Finally, the sparse distribution of rules in the fourth quadrant are the ones that lead to node extinction.

Figure 15.6 shows actual growth patterns of several rule samples (indicated by large black dots in Fig. 15.5), which confirms topological diversity generated even within this restricted set of binary-state GNA rules. The first five rows ($rn = 6{,}929$, 8,955, 1,756, 4,683 and 8,414) are the samples of exponentially growing rules. For $rn = 1{,}756$ and 4,683, every rewriting event exclusively causes tertiary and binary node divisions and forms planar and linear structures, respectively, where node states remain homogeneous and do not change at all. On the other hand, for $rn = 6{,}929$, 8,955 and 8,414, state-1 nodes appear at the beginning of simulation and the node states influence the network growth processes. Such interaction

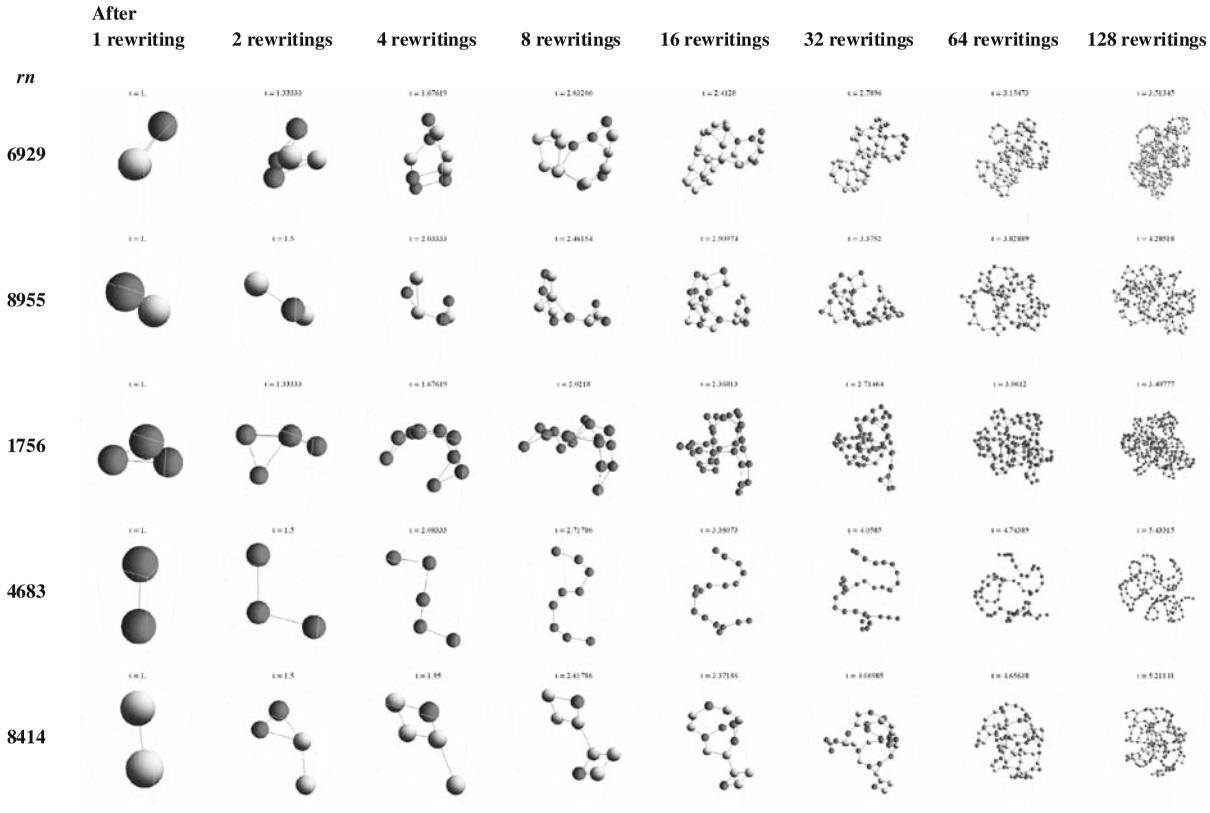

Fig. 15.6 Sample growth patterns of several GNA rules. Each row presents one specific simulation run for a particular GNA rule (indicated on the *left* by rn). Each image shows an actual GNA configuration after specific times of rewriting events. Note that the number of rewritings does not necessarily scale along the simulated time, which is given at the *top* of each image. *Dark gray dots* represent nodes in state 0, while *light gray* ones in state 1

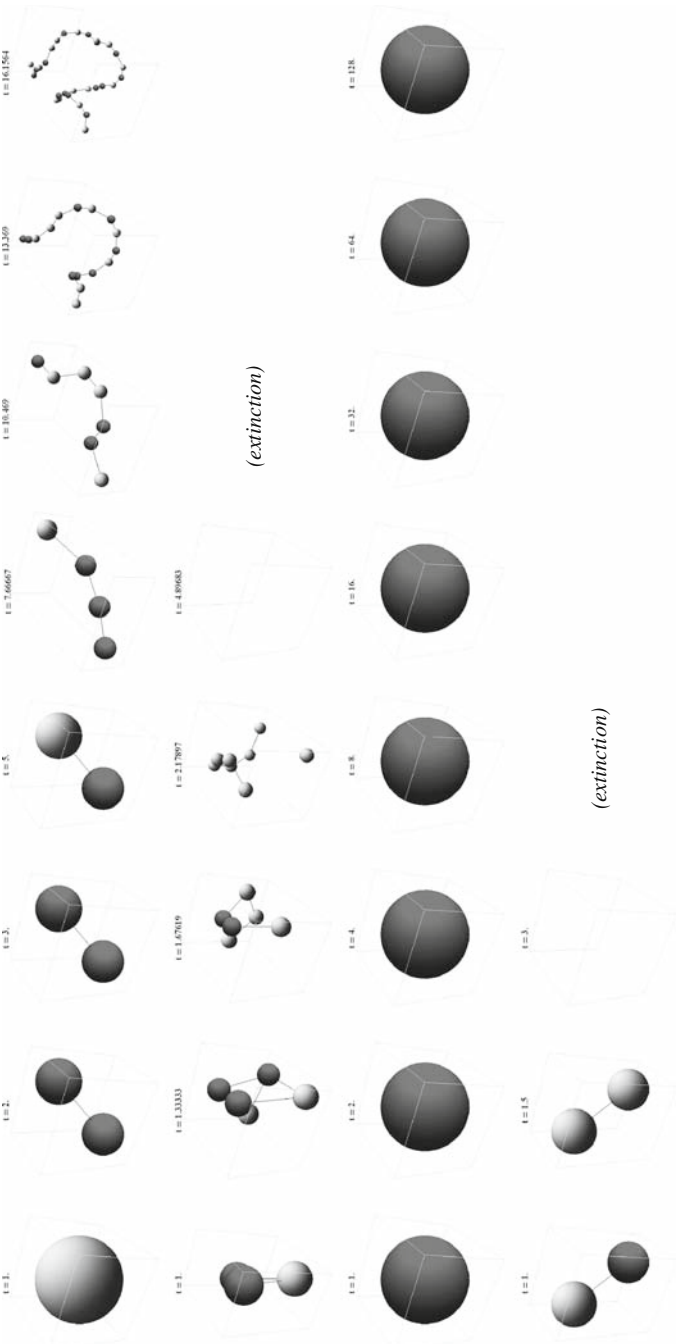

Fig. 15.6 (continued)

between node states and network topology results in a final GNA configuration with non-homogeneous node state distribution and a growth rate that is different from those of homogeneous network growth. The rest are the examples that do not show exponential growth, among which $rn = 4{,}212$ uniquely demonstrates a very slow growth of a linear structure driven by a complicated interaction between state-0 and state-1 nodes on it.

We also investigated the topological characteristics of the final GNA configurations obtained at the end of each simulation run. For this purpose, we additionally excluded rules that always ended up with node extinction, because average node degrees or states cannot be defined for such rules. As a result, we used 8,617 rules for the following analyses. Figure 15.7 shows the histograms of rule frequencies arranged in terms of six topological characteristics (described earlier) of the final

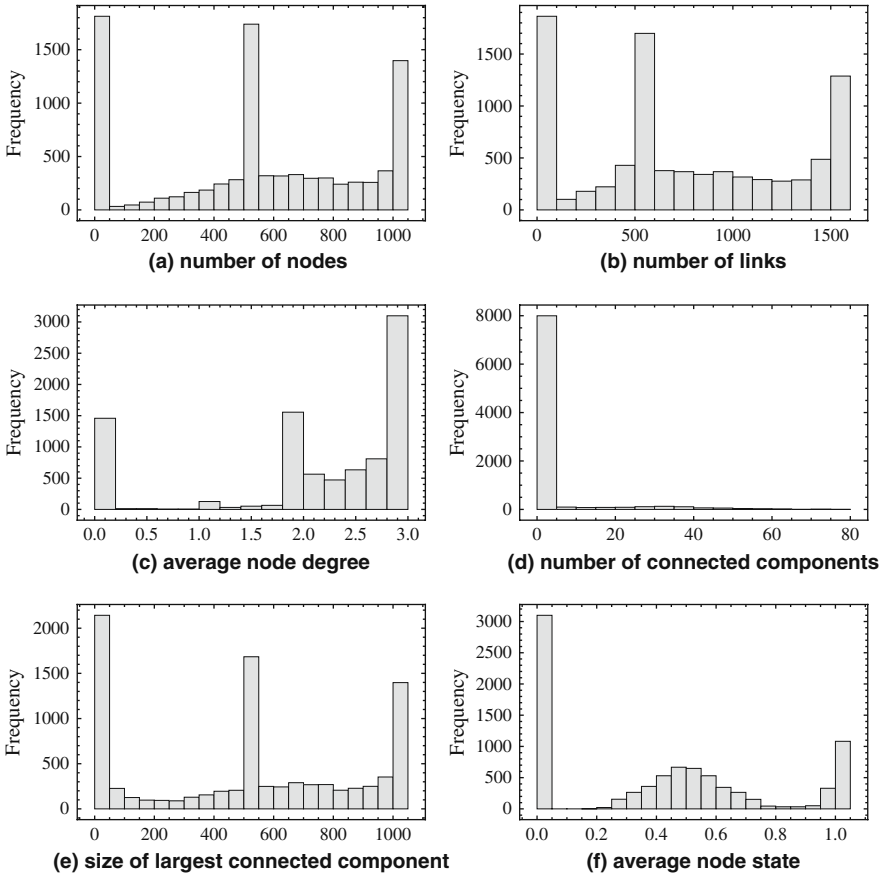

Fig. 15.7 Histograms of rule frequencies over six topological characteristics of the final GNA configurations. Each characteristic was calculated by averaging measurements obtained from five independent simulation runs for each rule. 8,617 GNA rules after filtering (see text) were used to produce these plots

GNA configuration. Three distinct peaks are commonly seen in (a), (b), (c) and (e) of these plots. These three peaks correspond to two types of exponential growers (by tertiary and binary node divisions) and non-growers. Between these peaks other cases distribute with relatively lower frequencies. Plot (d) indicates that most rules produce connected network structures only. In terms of the node state distribution, plot (f) shows that many GNA rules produce networks which are homogeneous regarding node states (represented by two peaks at 0.0 and 1.0) but other rules produce heterogeneous state distributions as well (represented by a gentle peak around 0.5). The distribution in (f) is asymmetric because we used a single node of state 0 as an initial condition for all the simulations.

Figure 15.8 is a scatter plot matrix made of $7 \times 7 = 49$ scatter plots, each of which visually shows correlation between two of the seven characteristics described above: number of nodes, number of links, average node degree, number of connected

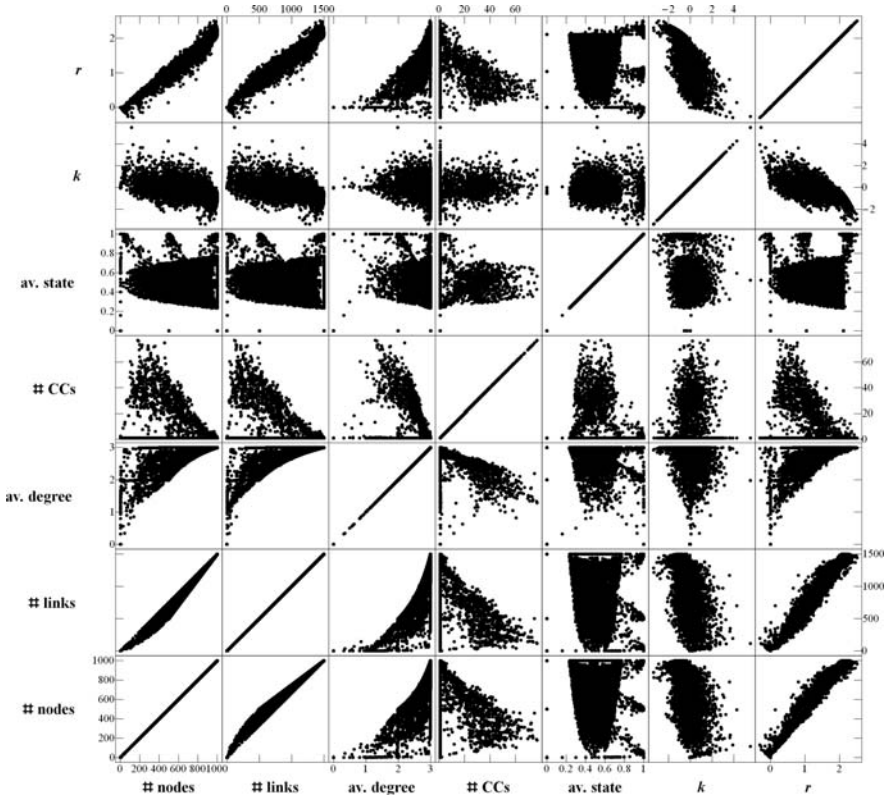

Fig. 15.8 Scatter plot matrix showing $7 \times 7 = 49$ scatter plots, each of which visually shows correlation between two of the following seven characteristics of GNA. From *left* (*bottom*) to *right* (*top*): number of nodes, number of links, average node degree, number of connected components, average node state, estimated order of polynomial growth k, and estimated rate of exponential growth r

components, average node state, estimated order of polynomial growth k, and estimated rate of exponential growth r. The size of largest connected components was not included because it is strongly correlated with the number of nodes as most of the networks were well connected (see Fig. 15.7d, as well as (a) and (e)). This matrix gives several interesting observations. There is a simple correlation between number of nodes, number of links and average node degree for obvious reasons, as already reported in our previous work [37]. More importantly, average node states have significant impacts on other properties of GNA, as seen in the fifth column/row of the matrix. For networks whose node states are homogeneous (i.e., average node state ~ 0 or 1), there is always only one local situation possible: a node of state 0 (or 1) surrounded by nodes of the same state. For such a network to remain in homogeneous states while staying away from node extinction, there are only three possible outcomes (tertiary division with state preserved, binary division with state preserved, or absolutely no change). This necessarily results in only three values possible for number of nodes, number of links and estimated rate of exponential growth, for average node state ~ 0 or 1. It is also notable that the largest numbers of connected components are achieved when the average node states take intermediate values. This suggests that node states play a critical role in determining when and where a node should disappear to cut the network and increase the number of connected components. Without such state-driven control of node disappearance, the nodes would easily become extinct.

Finally, we conducted principal component analysis (PCA) on the distribution of results in a seven-dimensional vector space created by the seven characteristics used in Fig. 15.8. Data were rescaled before the analysis so that the standard deviation was one in each dimension. As a result, we extracted four important dimensions in the data distribution (Table 15.2). The primary dimension is strongly correlated with number of nodes, number of links, average node degree, and estimated rate of exponential growth r, which may be understood as a factor relevant to general topological growth. The secondary dimension is strongly correlated to number of connected components, average node state, and estimated order of polynomial growth k, which may be understood as a factor related to node disappearances caused by state changes. Note that the basis vector of this dimension happened to

Table 15.2 Results of principal component analysis (PCA) applied to the same data shown in Fig. 15.8. Components and eigenvalues in bold face indicate four important dimensions

		Eigenvector						
Component	Eigenvalue	# of nodes	# of links	Av. node degree	# of CCs	Av. node state	k	r
1	**4.014**	0.490	0.485	0.441	−0.087	0.082	−0.265	0.495
2	**1.203**	−0.021	0.005	−0.269	−0.642	−0.603	−0.388	0.034
3	**0.895**	0.122	0.108	0.028	0.584	−0.763	0.204	0.085
4	**0.718**	0.105	0.121	0.192	−0.484	−0.109	0.831	−0.018
5	0.151	−0.234	−0.383	0.828	−0.071	−0.186	−0.177	−0.207
6	0.019	0.490	−0.768	−0.101	−0.018	0.015	0.073	0.392
7	0.001	−0.662	−0.034	0.004	−0.002	−0.002	0.102	0.741

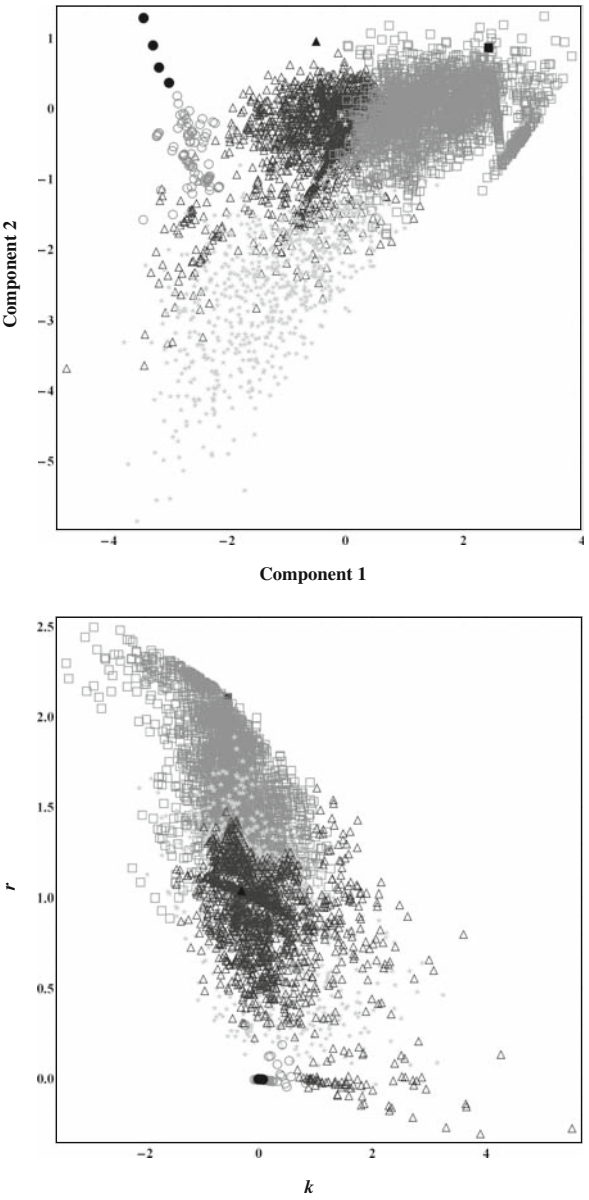

Fig. 15.9 Results of hierarchical clustering of the data distribution conducted in a dimension-reduced vector space. *Top*: Clusters projected to a two-dimensional space using the primary and secondary dimensions detected by PCA. *Bottom*: Same results mapped in the *k*-*r* space in the same way as in Fig. 15.5. Numbers of rules in these clusters are as follows: *Filled circle* 1,103, *filled triangle* 1,000, *filled square* 1,000, *open circle* 412, *open triangle* 1,812, *open square* 2,529, and *star* 761

be taken in opposite direction to its correlated characteristics, so the lower value in this dimension means greater number of connected components, higher average node state, and higher order of polynomial growth.

We further applied Ward's minimum-variance hierarchical clustering algorithm to the data distribution in a vector space whose dimensions were reduced from seven to four according to the results of PCA. The clustering results were split into seven clusters as shown in Fig. 15.9, where the top plot presents the results in a two-dimensional space using the primary and secondary dimensions detected by PCA, whereas the bottom plot maps the same results in the k-r space in the same way as in Fig. 15.5.

Rules in each cluster were manually sampled and inspected in further detail to see what kind of common dynamics exist within each type, which revealed the following: The first three clusters, filled circles (1,103 rules), filled triangles (1,000 rules) and filled squares (1,000 rules), share exactly the same growth characteristics within each cluster so that they appear as a point in the k-r plot (Fig. 15.9, bottom). Specifically, the filled circles are non-growers without state changes or with regular state alterations between 0 and 1 (e.g., rn =2,971), while the filled triangles and the filled squares are exponential growers without state changes, growing solely by binary (e.g., rn =4,683) and tertiary (e.g., rn =1,756) node divisions, respectively. The other three clusters denoted by open markers involve active node state changes that influence their growth patterns. Specifically, the open circles (412 rules) show very slow or even no growth (e.g., rn = 4,212), while the open triangles (1,812 rules) and the open squares (2,529 rules) show exponential-like growth predominantly by binary (e.g., rn = 8,414) and tertiary (e.g., rn = 6,929 and 8,955) node divisions, respectively. Finally, the cluster denoted by light gray stars (761 rules) involve active node state changes and frequent node disappearances, typically producing more than one connected components (e.g., $rn = 179$).

These results altogether demonstrate the diversities of potential dynamics of simple GNAs, in both topology and temporal evolution. Of particular importance compared to other network growth models is the possibility of interaction between network topology and node state distribution, which is key to nontrivial dynamics observed in the types that involve active node state changes.

15.6 Conclusion

We proposed Generative Network Automata as a new generalized framework for the modeling of complex dynamical networks, with which one can uniformly describe both state transitions and autonomous topological transformations using repetitive graph rewritings. We explored possible dynamics of simple binary-state GNA and observed several distinct types of topologies and growth patterns that emerged from local rewriting rules, where dynamic state changes were coupled with topological changes in some types.

The work presented here had a couple of limitations that must be noted. One was that we employed several restrictions on possible rule sets to keep the search space small. For example, we assumed that the extraction mechanism E randomly picks a node from the network, which avoided the computationally inefficient subgraph-isomorphism problem that would need to be solved for other types of extraction mechanisms that look for particular topological features. The other limitation was the small network size. We experimented with GNAs whose size was up to 1,000 nodes, which is significantly smaller than many real-world complex networks being investigated today. We realize that, to enable unrestricted GNA modeling and simulation at a significantly larger scale, several technical issues will need to be addressed in a computationally efficient way, including:

1. How to represent and rewrite large GNA configurations
2. How to extract subGNAs that match given patterns from a large GNA configuration
3. How to keep track of statistical/dynamical properties of GNAs during simulation with minimum computational overheads
4. How to embed complex GNAs in a 2-D or 3-D visualization space in a visually meaningful manner
5. How to derive the optimal rule set that best explains the network evolution given by experimental data

Some of these problems apparently involve intractable computational complexity if exact solutions are sought.[2] We are therefore working to develop computationally practical solutions to these problems by using appropriate approximations and heuristics.

We hope that GNA will help formulate many distinct complex systems in the same "format", enabling one to compare those systems systematically, to identify their commonness and uniqueness, and to actively exchange knowledge between different fields beyond disciplinary boundaries. We anticipate several areas of immediate applications, including (a) ecology and epidemiology modeling where organisms and pathogens actively reshape their habitat structure (e.g., niche construction, effects of host survivability in epidemiological networks), (b) social network modeling where individual states and behaviors modify the network topology (e.g., evolution of social ties, self-organization of collective knowledge among people), and (c) biologically inspired engineering design where local rewriting rules can be exploited as a means to indirectly control the emergent dynamics of artifacts that develop and self-organize over time.

References

1. Bar-Yam, Y. (1997) *Dynamics of Complex Systems*. Westview Press.
2. Wiggins, S. (2003) *Introduction to Applied Nonlinear Dynamical Systems and Chaos*, 2nd Ed. Springer.

[2] The subgraph-isomorphism problem is known to be NP-complete.

3. Boccara, N. (2004) *Modeling Complex Systems*. Springer-Verlag.
4. Strogatz, S. H. (1994) *Nonlinear Dynamics and Chaos*. Westview Press.
5. McCulloch, W. S. and Pitts, W. (1943) A logical calculus of the ideas immanent in nervous activity. *Bull. Math. Biophys.* 5:115–133.
6. Hopfield, J. J. (1982) Neural networks and physical systems with emergent collective computational abilities. *PNAS* 79:2554–2558.
7. Kauffman, S. A. (1969) Metabolic stability and epigenesis in randomly constructed genetic nets. *J. Theor. Biol.* 22:437–467.
8. Derrida, B. and Pomeau, Y. (1986) Random networks of automata: A simple annealed approximation. *Europhys. Lett.* 1:45–49.
9. Kauffman, S. A. (1993) *The Origins of Order*. Oxford University Press, Oxford.
10. Wolfram, S. (1984) Universality and complexity in cellular automata. *Physica D* 10:1–35.
11. Ilachinski, A. (2001) *Cellular Automata: A Discrete Universe*. World Scientific.
12. May, R. M. (1976) Simple mathematical models with very complicated dynamics. *Nature* 261:459–467.
13. Berlekamp, E. R., Conway, J. H., and Guy, R. K. (1982) *Winning Ways for Your Mathematical Plays Vol. 2: Games in Particular*, Chapter 25: "What is Life?". Academic Press.
14. Pearson, J. E. (1993) Complex patterns in a simple system. *Science* 261:189–192.
15. Sayama, H. (1999) A new structurally dissolvable self-reproducing loop evolving in a simple cellular automata space. *Artificial Life* 5:343–365.
16. Salzberg, C. and Sayama, H. (2004) Complex genetic evolution of artificial self-replicators in cellular automata. *Complexity* 10(2): 33–39.
17. Watts, D. J. and Strogatz, S. H. (1998) Collective dynamics of 'small-world' networks. *Nature* 393:440–442.
18. Strogatz, S. H. (2001) Exploring complex networks. *Nature* 410:268–276.
19. Newman, M., Barabási, A.-L. and Watts, D. J., eds. (2006) *The Structure and Dynamics of Networks*. Princeton University Press.
20. Albert, R., Jeong, H. and Barabási, A.-L. (2000) Error and attack tolerance of complex networks. *Nature* 406:378–382.
21. Albert, R. and Barabási, A.-L. (2002) Statistical mechanics of complex networks. *Rev. Mod. Phys.* 74:47–97.
22. Shargel, B., Sayama, H., Epstein, I. R. and Bar-Yam, Y. (2003) Optimization of robustness and connectivity in complex networks. *Phys. Rev. Lett.* 90:068701.
23. da Fontoura Costa, L. (2004) Reinforcing the resilience of complex networks. *Phys. Rev. E* 69:066127.
24. Beygelzimer, A., Grinstein, G. M., Linsker, R. and Rish, I. (2005) Improving network robustness by edge modification. *Physica A* 357:593–612.
25. Bar-Yam, Y. and Epstein, I. R. (2004) Response of complex networks to stimuli. *PNAS* 101:4341–4345.
26. Motter, A. E. (2004) Cascade control and defense in complex networks. *Phys. Rev. E* 93:098701.
27. de Aguiar, M. A. M. and Bar-Yam, Y. (2005) Spectral analysis and the dynamic response of complex networks. *Phys. Rev. E* 71:016106.
28. Zhou, H. and Lipowsky, R. (2005) Dynamic pattern evolution on scale-free networks. *PNAS* 102:10052–10057.
29. Tomassini, M. (2006) Generalized automata networks. In Yacoubi, S. E., Chopard, B. & Bandini, S., eds., *Cellular Automata: Proceedings of the 7th International Conference on Cellular Automata for Research and Industry (ACRI 2006)*, pp. 14–28. Springer-Verlag.
30. Motter, A. E., Matías, M. A., Kurths, J. and Ott, E., eds. (2006) *Special Issue: Dynamics on Complex Networks and Applications, Physica D* 224.
31. Gross, T. and Blasius, B. (2008) Adaptive coevolutionary networks: a review. *J. R. Soc. Interface* 5:259–271.
32. Holme, P. and Ghoshal, G. (2006) Dynamics of networking agents competing for high centrality and low degree. *Phys. Rev. Lett.* 96:098701.

33. Holme, P. and Newman, M. E. J. (2006) Nonequilibrium phase transition in the coevolution of networks and opinions. *Phys. Rev. E* 74:056108.
34. Gross, T., D'Lima, C. J. D. and Blasius, B. (2006) Epidemic dynamics on an adaptive network. *Phys. Rev. Lett.* 96:208701.
35. Pacheco, J. M., Traulsen, A. and Nowak, M. A. (2006) Coevolution of strategy and structure in complex networks with dynamical linking. *Phys. Rev. Lett.* 97:258103.
36. Palla, G., Barabási, A.-L. and Vicsek, T. (2007) Quantifying social group evolution. *Nature* 446:664–667.
37. Sayama, H. (2007) Generative network automata: A generalized framework for modeling complex dynamical systems with autonomously varying topologies. *Proceedings of The First IEEE Symposium on Artificial Life (IEEE-CI-ALife '07)*, IEEE, pp.214–221.
38. Rozenberg, G., ed. (1997) *Handbook of Graph Grammars and Computing by Graph Transformation Volume 1: Foundations*. World Scientific.
39. Claus, V., Ehrig, H. and Rozenberg, G., eds. (1979) *Proceedings of the International Workshop on Graph-Grammars and Their Application to Computer Science and Biology*, October 30–November 3, 1978, Bad Honnef, Germany. Lecture Notes in Computer Science 73, Springer-Verlag.
40. Ehrig, H., Nagl, M. and Rozenberg, G., eds. (1983) *Proceedings of the Second International Workshop on Graph-Grammars and Their Application to Computer Science*, October 4–8, 1982, Haus Ohrbeck, Germany. Lecture Notes in Computer Science 153, Springer-Verlag.
41. Ehrig, H., Nagl, M., Rozenberg, G. and Rosenfeld, A., eds. (1987) *Proceedings of the Third International Workshop on Graph-Grammars and Their Application to Computer Science*, December 2–6, 1986, Warrenton, VA. Lecture Notes in Computer Science 291, Springer-Verlag.
42. Ehrig, H., Kreowski, H.-J. and Rozenberg, G., eds. (1991) *Proceedings of the Fourth International Workshop on Graph-Grammars and Their Application to Computer Science*, March 5–9, 1990, Bremen, Germany. Lecture Notes in Computer Science 532, Springer-Verlag.
43. Lindenmayer, A. (1968) Mathematical models for cellular interaction in development I. Filaments with one-sided inputs. *J. Theor. Biol.* 18:280–289.
44. Doi, H. (1984) Graph-theoretical analysis of cleavage pattern: Graph developmental system and its application to cleavage pattern of ascidian egg. *Development, Growth & Differentiation* 26:49-60.
45. Blostein, D., Fahmy, H. and Grbavec, A. (1996) Issues in the practical use of graph rewriting. In *Proceedings of the Fifth International Workshop on Graph Grammars and Their Application to Computer Science*, Lecture Notes in Computer Science 1073, Springer, pp. 38–55.
46. Tomita, K., Kurokawa, H. and Murata, S. (2002) Graph automata: Natural expression of self-replication. *Physica D* 171:197–210.
47. Hutton T. J. (2002) Evolvable self-replicating molecules in an artificial chemistry. *Artificial Life* 8:341–356.
48. Klavins, E. (2004) Universal self-replication using graph grammars. In *Proceedings of the 2004 International Conference on MEMS, NANO and Smart Systems (ICMENS 2004)*, pp. 198–204.
49. Klavins, E., Ghrist, R. and Lipsky, D. (2004) Graph grammars for self-assembling robotic systems. In *Proceedings of the 2004 IEEE International Conference on Robotics and Automation (ICRA'04)*, vol. 5, pp. 5293–5300.
50. Kniemeyer, O., Buck-Sorlin, G. H. and Kurth, W. (2004) A graph grammar approach to artificial life. *Artificial Life* 10:413–431.
51. Kurth, W., Kniemeyer, O. and Buck-Sorlin, G. H. (2005) Relational growth grammars – A graph rewriting approach to dynamical systems with a dynamical structure. In *Proceedings of the 2004 International Workshop on Unconventional Programming Paradigms (UPP 2004)* Lecture Notes in Computer Science 3566, Springer, pp. 56–72.
52. Nehaniv, C. L. (2004) Asynchronous automata networks can emulate any synchronous automata network. *Intl. J. Algebra & Computation* 14:719–739.